Use of Sensors for Fire Detection and Monitoring

by

Noah Ryder

A thesis
presented to the University of Waterloo
in fulfillment of the
thesis requirement for the degree of
Doctor of Philosophy
in
Mechanical and Mechatronics Engineering

Waterloo, Ontario, Canada, 2019

© Noah Ryder 2019

Examining Committee Membership

The following served on the Examining Committee for this thesis. The decision of the Examining Committee is by majority vote.

External Examiner:	Bart Merci Professor, Dept. of Flow, Heat, and Combustion Mechanics University of Gent
Supervisor:	Elizabeth Weckman Professor, Dept. of Mechanical and Mechatronics Engineering University of Waterloo
Internal Members:	Cecile Devaud Professor, Dept. of Mechanical and Mechatronics Engineering University of Waterloo
	Patricia Nevia Professor, Dept. of Mechanical and Mechatronics Engineering University of Waterloo
Internal-External Member:	Stacey Scott Professor, Dept. of Systems Design Engineering University of Waterloo

Author's Declaration

I hereby declare that I am the sole author of this thesis. This is a true copy of the thesis, including any required final revisions, as accepted by my examiners.

I understand that my thesis may be made electronically available to the public.

Abstract

The ultimate goal of placing fire detection systems in buildings and structures is to allow for the rapid detection of fire and accurate prediction of ensuing fire behavior. Through a-priori prediction of how a fire might evolve, relevant information can be delivered to the appropriate stakeholders. In the near-term, development of detection systems which detect fire events more quickly, with better discrimination against nuisance and false alarms, and allow real-time monitoring of the state of a fire is a critical interim step. If we are able to detect fires earlier than is presently possible, loss of life, injuries and property damage may be drastically reduced. In addition, if earlier detection is simultaneously paired with collection of better information on the spatial location of the fire, and its stage of development, this information can be delivered to emergency first responders. Emergency response planning and actions can then be targeted such that appropriate resources are applied earlier in a fire situation. This will further reduce the potential for loss of life and injury to both occupants and first responders, as well capital losses due to fire.

The advent of building monitoring systems affords excellent potential to improve upon current fire detection protocols. Building systems incorporate a large quantity of different sensors for a variety of uses. Currently, most building sensors are focused primarily on the parameters necessary to optimize building efficiency and on intrusion detection, but they are installed at much higher density than standard fire detectors and the density is increasing as greater efficiencies in cost and quicker return on investment can be achieved. While most of these sensors are presently chosen to fulfill building management purposes, there is significant opportunity to integrate some of the existing sensors, or to develop new sensors of similar type, for applications in systems for rapid fire detection, real-time fire monitoring, and potentially fire forecasting.

Leveraging building environmental and other sensors for this expanded use, however, requires further knowledge about the characteristics of fires, from ignition to full growth, specifically with regards to those physical characteristics which might be measured by any new fire detection sensor suites.

One of the biggest challenges associated with development of new fire detection systems is their associated cost and the reluctance on the part of building owners, insurers, and other parties to invest in detection systems when fire is such a rare event. Thus while there has been research into improved fire detection technology, there has been limited advancement in detection system design. Ultimately, the limiting factors around potential use of building monitoring sensors for this purpose will relate to determination of optimal

sensor response to various signals generated by a developing fire and optimal sensor density in terms of cost versus position of sensors relative to potential fire sources. One of the best chances for improved fire detection, as well as potentially for reduced nuisance alarms and enhanced fire monitoring, is to first take advantage of the signals transmitted by building sensors and assess their potential for use in fire detection.

Therefore the objectives of this research were to characterize fire and non-fire environments using a range of sensor technologies to determine potential characterization parameters and to evaluate background and nuisance sensor response using the same sensor technologies; to identify candidate sensors and develop an idealized sensor block; and finally to develop algorithms for fire state determination.

Approximately 125 experiments were performed in a range of environments ranging from a $1m^3$ box to full-scale experiments in a two-story structure. Temperature, relative humidity, and luminosity were measured during all experiments, while heat flux and heat release rate were additionally measured during the full-scale experiments.

The research shows that fire signals measured using non-fire sensors could be distinguished from background and nuisance signals indicating their potential for use in improved fire state determination. The data collected, in particular with regards to luminosity and relative humidity, has not been previously reported in the literature and thus provides new information that may be leveraged for incipient fire detection and monitoring.

Furthermore a novel learning algorithm, hierarchical temporal memory, a real-time continuous learning algorithm yielded promising results for fire state determination. Real-time data streaming of the sensor data paired with the hierarchical temporal memory yielded the ability to rapidly identify fire anomalies.

Acknowledgements

I would like to thank all the people who made this thesis possible. I would like to thank my wife and children who have supported and encouraged me during this effort even when it meant not being able to spend time with them. Without their continued love, support, and occasional prodding I would never have been able to finish this.

I would like to thank everyone at the UW Fire Lab for your assistance. You went out of your way to help me incorporate my sensors into your experiments and showed me the ropes of the lab. Matt, Njegos, and Pat thanks for everything.

My advisor, Elizabeth Weckman, has provided guidance and insight throughout the whole process, including down what turned out to be two dead end streets of research. As they say, third times the charm. For your patience with a part-time student trying to keep too many balls in the air, thank you.

Table of Contents

List of Figures **xv**

List of Tables **xxxv**

Nomenclature **xxxvii**

1 Introduction **1**

1.1 State of the Art 2

1.2 Scientific Objectives 4

1.3 Outline 4

2 Literature Review **7**

2.1 Compartment Fire Behavior and Fire Dynamics 7

2.1.1 Qualitative Description of a Compartment Fire 8

2.1.2 Energy Release and Heat Transfer 10

2.1.3 Plumes, Flame Heights, and Ceiling Jets 11

2.1.4 Smoldering and Flaming Combustion 13

2.2 Basics of Fire Detection and Monitoring 20

2.2.1 Detectors 22

2.2.2 Multi-criteria Detection 29

2.3 The Potential in Environmental Building Sensors 31

2.4 Detection and Monitoring Algorithms 34
2.4.1 Continuous Learning Algorithm 35
2.5 Conclusions and Summary of Knowledge Gaps 38

3 Commercial Sensors **41**
3.1 Commercial Sensor Selection 41
3.2 EDS Sensor Characterization 44
3.2.1 Small Scale - Oven Temperature Testing 44
3.2.2 Small Scale - Box Testing 50
3.3 Large Scale Experimental Design 61
3.3.1 Experimental Facility 62
3.3.2 Nuisance Sources 69
3.3.3 Fire Sources 69
3.4 Results and Analysis 70
3.4.1 Temperature 70
3.4.2 Relative Humidity 72
3.4.3 Light Intensity 79
3.5 Conclusions 82

4 Fire State Determination (FSD) Sensor Block Development **85**
4.1 FSD Sensor Selection 85
4.1.1 Sensor Block Components 87
4.2 FSD Sensor Characterization 95
4.2.1 Temperature and Humidity Sensor Response 95
4.2.2 Light Sensor Response 96
4.2.3 Gas Sensor Static Response 96
4.2.4 Gas Sensor Dynamic Response 99
4.3 Experimental Design 102

4.3.1 Instrumentation and Methodology . . . 104
4.3.2 Fuel Load . . . 106
4.4 Results and Analysis . . . 108
4.4.1 Mass Loss and Heat Release Rate . . . 109
4.4.2 Species Production . . . 112
4.4.3 Compartment Temperature and Humidity . . . 114
4.4.4 Heat Flux and Light Intensity . . . 116
4.4.5 Combined Results . . . 120
4.5 Background Data Collection . . . 122
4.6 Conclusions . . . 122

5 Fire State Determination and Algorithm Development 127
5.1 Hierarchical Temporal Memory Algorithm . . . 128
5.2 Algorithm Results and Discussion . . . 132
5.3 Impact of Sensor Location . . . 145
5.4 Conclusions . . . 145

6 Summary of Conclusions and Future Work 149
6.1 Conclusions . . . 149
6.2 Future Work . . . 151

References 155

Appendices 165

A Experimental Details 167

B Sensor Block 175

C HRR **181**

C.1 Burn Room Experimental Results 181

C.2 Living Room Full-Scale Results 581

D Programming **585**

D.1 Arduino Programming 586

D.2 Linux Programming 592

D.3 HTM Programming 596

D.3.1 analyze.py 596

D.3.2 data.py 599

D.3.3 main.py 616

D.3.4 nupicanomalyoutput.py 622

D.3.5 plotter.py 632

E CutSheets **637**

List of Figures

2.1 Stages of Fire Growth, modified from[12] 9
2.2 Conceptual Stages of Fire Growth (with permission) [13] 10
2.3 Schematic of candle flame. [37] 16
2.4 Sample building energy consumption map [94] 33
2.5 Fire, sensors, and modeling relationship 36

3.1 EDS Sensor Block 43
3.2 Screen capture of real time monitoring from multiple THLP sensors during two fire experiments 43
3.3 Location and orientation of EDS sensors and thermocouples in oven . . . 45
3.4 Zoomed in temperatures from EDS sensors and thermocouple during early heating period 47
3.5 THLP and Thermocouple data from oven test 48
3.6 Temperature and ΔT between thermocouples and sensor 49
3.7 Interior of cube with EDS sensors 51
3.8 Normalized Humidity and Temperature results from Ethanol pool fire small-scale test 53
3.9 Normalized Light, Humidity, and Temperature results from Heptane pool fire box test 55
3.10 Variation in light intensity from Heptane pool fire box tests 56
3.11 Variation in normalized light intensity from Heptane pool fire box tests . . 57
3.12 Average light intensity observed over box tests 59

3.13 Relative humidity variation by sensor location 60
3.14 Exterior of Burn Structure 63
3.15 General layout of burn structure 64
3.16 Burn room showing fire brick floor, opening, and fiber insulation 65
3.17 Sectional view of burn room 66
3.18 Burn room and location of EDS sensors 67
3.19 EDS Sensors Experimental Matrix 68
3.20 Comparison of temperature by fire size and type, THLP-03 71
3.21 Comparison of temperature EMA by sensor location: ceiling (THLP-02), wall (THLP-03), and floor (THLP-09) 73
3.22 Comparison of EMA temperature rate of change by sensor location: ceiling (THLP-02), wall (THLP-03), and floor (THLP-09) 74
3.23 Comparison of relative humidity by fire size and type, THLP-03 76
3.24 Comparison of relative humidity by sensor location 77
3.25 Comparison of relative humidity by sensor location 78
3.26 Comparison of EMA relative humidity rate of change by sensor location: ceiling (THLP-02), wall (THLP-03), and floor (THLP-09) 80
3.27 Variation in light from flame flickering 81
3.28 Image light analysis (intensity and color) for Figure 3.27 (a) and (g) . . . 81
3.29 Light Intensity for identical fire sizes ($10kW$) at various distances from the sensor 83
3.30 Comparison of measured light intensity vs. theoretical light intensity . . . 84

4.1 Yun Microcontroller Schematic (www.arduino.cc/en/Guide/ArduinoYun) 88
4.2 Light sensors utilized in sensor block 90
4.3 TCS34725 Block Diagram 90
4.4 Temperature and Relative Humidity sensor utilized in sensor block 91
4.5 Example Sensor Block 95
4.6 Example Light Meter vs. Light Sensor Comparison 97

4.7 Sensors in LOI Chamber 98
4.8 CO_2 and CO sensor calibration curves 100
4.9 Layout of burn facility 103
4.10 Interior of Burn Structure Showing Load Cells 107
4.11 Interior of Burn Structure Showing Fuel Load 108
4.12 Development of Sofa Fire 110
4.13 Comparison of Heat Release Rate for Test 2-4 111
4.14 HRR, O_2, and CO Concentration for Test 8 113
4.15 Sofas and chairs post-fire 114
4.16 Temperature in burn room at TC tree #2, Test 8, ground is Z=0m 115
4.17 Temperature Measured at FSD sensor 01 for Tests 2-4 117
4.18 RH Measured at FSD sensor 01 for Tests 2-4 118
4.19 Measured Heat Flux for Tests 2-4 119
4.20 Measured Heat Release Rate, Light Intensity, and Heat Flux for Test 4 . . 120
4.21 Heat Release Rate, O_2 and CO Concentration, Heat Flux and Light Intensity for Test 4 121
4.22 Background long term temperature, RH, and lux measurements in an office setting 123
4.23 Background long term temperature, RH, and lux ROC measurements in an office setting 124

5.1 HTM primary functional steps [95] 129
5.2 Application of HTM methodology to multiple inputs [95] 131
5.3 Example initial algorithm training (dark grey), raw data (blue line), and anomaly score (green, yellow, or red "flag") for RH, Temperature, and Light Intensity 133
5.4 Long-term background data over a period of 3.5 months. Showing raw data and anamoly scores. 136
5.5 Example temperature, humidity, and light data shown with the HTM anomaly likelihood. 137

5.6 Example temperature, humidity, and light ROC data shown with the HTM anomaly likelihood. 138
5.7 Test 4 THLP-03 overall anomaly likelihood computed from individual sensor anomaly likelihoods. 139
5.8 Temperature, humidity, and light data from Test 20. The first anomaly identified for each sensor using the HTM algorithm is marked with a diamond. 141
5.9 Comparison of RH raw data and anomaly scoring by sensor location for the same test fire. 146
5.10 Comparison of lux raw data and anomaly scoring by sensor location for the same test fire. 147

B.1 Sensor Block 175
B.2 Sensor Block 176
B.3 Sensor Block 177
B.4 Sensor Block 178
B.5 Sensor Block 179

C.1 Sensor Locations 182
C.2 Test 06 THLP 01 183
C.3 Test 06 THLP 02 184
C.4 Test 06 THLP 03 185
C.5 Test 06 THLP 04 186
C.6 Test 06 THLP 05 187
C.7 Test 06 THLP 07 188
C.8 Test 06 THLP 08 189
C.9 Test 07 THLP 03 190
C.10 Test 07 THLP 04 191
C.11 Test 07 THLP 05 192
C.12 Test 07 THLP 07 193
C.13 Test 07 THLP 08 194

C.14 Test 08 THLP 03 195
C.15 Test 08 THLP 04 196
C.16 Test 08 THLP 05 197
C.17 Test 08 THLP 07 198
C.18 Test 08 THLP 08 199
C.19 Test 09 THLP 03 200
C.20 Test 09 THLP 04 201
C.21 Test 09 THLP 05 202
C.22 Test 09 THLP 07 203
C.23 Test 09 THLP 08 204
C.24 Test 10 THLP 03 205
C.25 Test 10 THLP 04 206
C.26 Test 10 THLP 05 207
C.27 Test 10 THLP 07 208
C.28 Test 10 THLP 08 209
C.29 Test 11 THLP 03 210
C.30 Test 11 THLP 04 211
C.31 Test 11 THLP 05 212
C.32 Test 11 THLP 07 213
C.33 Test 11 THLP 08 214
C.34 Test 12 THLP 03 215
C.35 Test 12 THLP 04 216
C.36 Test 12 THLP 05 217
C.37 Test 12 THLP 07 218
C.38 Test 12 THLP 08 219
C.39 Test 13 THLP 03 220
C.40 Test 13 THLP 04 221

C.41 Test 13 THLP 05 222
C.42 Test 13 THLP 07 223
C.43 Test 13 THLP 08 224
C.44 Test 14 THLP 03 225
C.45 Test 14 THLP 04 226
C.46 Test 14 THLP 05 227
C.47 Test 14 THLP 07 228
C.48 Test 14 THLP 08 229
C.49 Test 15 THLP 03 230
C.50 Test 15 THLP 04 231
C.51 Test 15 THLP 05 232
C.52 Test 15 THLP 07 233
C.53 Test 15 THLP 08 234
C.54 Test 17 THLP 03 235
C.55 Test 17 THLP 04 236
C.56 Test 17 THLP 05 237
C.57 Test 17 THLP 07 238
C.58 Test 17 THLP 08 239
C.59 Test 18 THLP 03 240
C.60 Test 18 THLP 04 241
C.61 Test 18 THLP 05 242
C.62 Test 18 THLP 07 243
C.63 Test 18 THLP 08 244
C.64 Test 19 THLP 01 245
C.65 Test 19 THLP 02 246
C.66 Test 19 THLP 03 247
C.67 Test 19 THLP 04 248

C.68 Test 19 THLP 05 249
C.69 Test 19 THLP 07 250
C.70 Test 19 THLP 08 251
C.71 Test 20 THLP 01 252
C.72 Test 20 THLP 02 253
C.73 Test 20 THLP 03 254
C.74 Test 20 THLP 04 255
C.75 Test 20 THLP 05 256
C.76 Test 20 THLP 07 257
C.77 Test 20 THLP 08 258
C.78 Test 21 THLP 01 259
C.79 Test 21 THLP 02 260
C.80 Test 21 THLP 03 261
C.81 Test 21 THLP 04 262
C.82 Test 21 THLP 05 263
C.83 Test 21 THLP 07 264
C.84 Test 21 THLP 08 265
C.85 Test 22 THLP 01 266
C.86 Test 22 THLP 02 267
C.87 Test 22 THLP 03 268
C.88 Test 22 THLP 04 269
C.89 Test 22 THLP 05 270
C.90 Test 22 THLP 07 271
C.91 Test 22 THLP 08 272
C.92 Test 24 THLP 01 273
C.93 Test 24 THLP 02 274
C.94 Test 24 THLP 03 275

C.95 Test 24 THLP 04 276
C.96 Test 24 THLP 05 277
C.97 Test 24 THLP 07 278
C.98 Test 24 THLP 08 279
C.99 Test 28 THLP 01 280
C.100 Test 28 THLP 02 281
C.101 Test 28 THLP 03 282
C.102 Test 28 THLP 04 283
C.103 Test 28 THLP 05 284
C.104 Test 28 THLP 07 285
C.105 Test 28 THLP 08 286
C.106 Test 33 THLP 01 287
C.107 Test 33 THLP 02 288
C.108 Test 33 THLP 03 289
C.109 Test 34 THLP 01 290
C.110 Test 34 THLP 02 291
C.111 Test 34 THLP 03 292
C.112 Test 34 THLP 04 293
C.113 Test 34 THLP 05 294
C.114 Test 34 THLP 07 295
C.115 Test 34 THLP 08 296
C.116 Test 34 THLP 09 297
C.117 Test 35 THLP 01 298
C.118 Test 35 THLP 02 299
C.119 Test 35 THLP 03 300
C.120 Test 35 THLP 04 301
C.121 Test 35 THLP 05 302

C.122 Test 35 THLP 07 303
C.123 Test 35 THLP 08 304
C.124 Test 35 THLP 09 305
C.125 Test 36 THLP 01 306
C.126 Test 36 THLP 02 307
C.127 Test 36 THLP 03 308
C.128 Test 36 THLP 04 309
C.129 Test 36 THLP 05 310
C.130 Test 36 THLP 08 311
C.131 Test 36 THLP 09 312
C.132 Test 37 THLP 01 313
C.133 Test 37 THLP 02 314
C.134 Test 37 THLP 04 315
C.135 Test 37 THLP 05 316
C.136 Test 37 THLP 07 317
C.137 Test 37 THLP 08 318
C.138 Test 37 THLP 09 319
C.139 Test 38 THLP 01 320
C.140 Test 38 THLP 02 321
C.141 Test 38 THLP 03 322
C.142 Test 38 THLP 04 323
C.143 Test 38 THLP 05 324
C.144 Test 38 THLP 07 325
C.145 Test 38 THLP 08 326
C.146 Test 38 THLP 09 327
C.147 Test 42 THLP 01 328
C.148 Test 42 THLP 02 329

C.149 Test 42 THLP 03 330
C.150 Test 42 THLP 04 331
C.151 Test 42 THLP 05 332
C.152 Test 42 THLP 07 333
C.153 Test 42 THLP 08 334
C.154 Test 42 THLP 09 335
C.155 Test 43 THLP 01 336
C.156 Test 43 THLP 02 337
C.157 Test 43 THLP 03 338
C.158 Test 43 THLP 04 339
C.159 Test 43 THLP 05 340
C.160 Test 43 THLP 07 341
C.161 Test 43 THLP 08 342
C.162 Test 43 THLP 09 343
C.163 Test 44 THLP 01 344
C.164 Test 44 THLP 02 345
C.165 Test 44 THLP 03 346
C.166 Test 44 THLP 04 347
C.167 Test 44 THLP 05 348
C.168 Test 44 THLP 07 349
C.169 Test 44 THLP 08 350
C.170 Test 44 THLP 09 351
C.171 Test 45 THLP 01 352
C.172 Test 45 THLP 03 353
C.173 Test 45 THLP 04 354
C.174 Test 45 THLP 05 355
C.175 Test 45 THLP 07 356

C.176 Test 46 THLP 01 357
C.177 Test 46 THLP 02 358
C.178 Test 46 THLP 04 359
C.179 Test 46 THLP 05 360
C.180 Test 46 THLP 08 361
C.181 Test 46 THLP 09 362
C.182 Test 47 THLP 01 363
C.183 Test 47 THLP 02 364
C.184 Test 47 THLP 03 365
C.185 Test 47 THLP 04 366
C.186 Test 47 THLP 05 367
C.187 Test 47 THLP 08 368
C.188 Test 47 THLP 09 369
C.189 Test 48 THLP 01 370
C.190 Test 48 THLP 02 371
C.191 Test 48 THLP 03 372
C.192 Test 48 THLP 04 373
C.193 Test 48 THLP 05 374
C.194 Test 48 THLP 08 375
C.195 Test 48 THLP 09 376
C.196 Test 49 THLP 01 377
C.197 Test 49 THLP 02 378
C.198 Test 49 THLP 03 379
C.199 Test 49 THLP 04 380
C.200 Test 49 THLP 05 381
C.201 Test 49 THLP 08 382
C.202 Test 49 THLP 09 383

C.203 Test 50 THLP 01 384
C.204 Test 50 THLP 02 385
C.205 Test 50 THLP 03 386
C.206 Test 50 THLP 04 387
C.207 Test 50 THLP 05 388
C.208 Test 50 THLP 08 389
C.209 Test 50 THLP 09 390
C.210 Test 51 THLP 01 391
C.211 Test 51 THLP 02 392
C.212 Test 51 THLP 03 393
C.213 Test 51 THLP 04 394
C.214 Test 51 THLP 05 395
C.215 Test 51 THLP 08 396
C.216 Test 51 THLP 09 397
C.217 Test 52 THLP 01 398
C.218 Test 52 THLP 02 399
C.219 Test 52 THLP 03 400
C.220 Test 52 THLP 04 401
C.221 Test 52 THLP 05 402
C.222 Test 52 THLP 08 403
C.223 Test 52 THLP 09 404
C.224 Test 53 THLP 01 405
C.225 Test 53 THLP 02 406
C.226 Test 53 THLP 03 407
C.227 Test 53 THLP 04 408
C.228 Test 53 THLP 05 409
C.229 Test 53 THLP 08 410

C.230 Test 53 THLP 09 411
C.231 Test 54 THLP 01 412
C.232 Test 54 THLP 02 413
C.233 Test 54 THLP 03 414
C.234 Test 54 THLP 04 415
C.235 Test 54 THLP 05 416
C.236 Test 54 THLP 08 417
C.237 Test 54 THLP 09 418
C.238 Test 55 THLP 01 419
C.239 Test 55 THLP 02 420
C.240 Test 55 THLP 03 421
C.241 Test 55 THLP 04 422
C.242 Test 55 THLP 05 423
C.243 Test 55 THLP 08 424
C.244 Test 55 THLP 09 425
C.245 Test 56 THLP 01 426
C.246 Test 56 THLP 02 427
C.247 Test 56 THLP 03 428
C.248 Test 56 THLP 04 429
C.249 Test 56 THLP 05 430
C.250 Test 56 THLP 08 431
C.251 Test 56 THLP 09 432
C.252 Test 57 THLP 01 433
C.253 Test 57 THLP 02 434
C.254 Test 57 THLP 03 435
C.255 Test 57 THLP 04 436
C.256 Test 57 THLP 05 437

C.257 Test 57 THLP 08 438
C.258 Test 57 THLP 09 439
C.259 Test 58 THLP 01 440
C.260 Test 58 THLP 02 441
C.261 Test 58 THLP 03 442
C.262 Test 58 THLP 04 443
C.263 Test 58 THLP 05 444
C.264 Test 58 THLP 08 445
C.265 Test 58 THLP 09 446
C.266 Test 59 THLP 01 447
C.267 Test 59 THLP 02 448
C.268 Test 59 THLP 03 449
C.269 Test 59 THLP 04 450
C.270 Test 59 THLP 05 451
C.271 Test 59 THLP 08 452
C.272 Test 59 THLP 09 453
C.273 Test 60 THLP 01 454
C.274 Test 60 THLP 02 455
C.275 Test 60 THLP 03 456
C.276 Test 60 THLP 04 457
C.277 Test 60 THLP 05 458
C.278 Test 60 THLP 08 459
C.279 Test 60 THLP 09 460
C.280 Test 61 THLP 01 461
C.281 Test 61 THLP 02 462
C.282 Test 61 THLP 03 463
C.283 Test 61 THLP 04 464

C.284 Test 61 THLP 05 465
C.285 Test 61 THLP 08 466
C.286 Test 61 THLP 09 467
C.287 Test 62 THLP 01 468
C.288 Test 62 THLP 02 469
C.289 Test 62 THLP 03 470
C.290 Test 62 THLP 04 471
C.291 Test 62 THLP 05 472
C.292 Test 62 THLP 08 473
C.293 Test 62 THLP 09 474
C.294 Test 63 THLP 01 475
C.295 Test 63 THLP 02 476
C.296 Test 63 THLP 03 477
C.297 Test 63 THLP 04 478
C.298 Test 63 THLP 05 479
C.299 Test 63 THLP 08 480
C.300 Test 63 THLP 09 481
C.301 Test 66 THLP 01 482
C.302 Test 66 THLP 02 483
C.303 Test 66 THLP 03 484
C.304 Test 66 THLP 04 485
C.305 Test 66 THLP 05 486
C.306 Test 66 THLP 08 487
C.307 Test 66 THLP 09 488
C.308 Test 67 THLP 01 489
C.309 Test 67 THLP 02 490
C.310 Test 67 THLP 03 491

C.311 Test 67 THLP 04 492
C.312 Test 67 THLP 05 493
C.313 Test 67 THLP 08 494
C.314 Test 67 THLP 09 495
C.315 Test 68 THLP 01 496
C.316 Test 68 THLP 02 497
C.317 Test 68 THLP 03 498
C.318 Test 68 THLP 04 499
C.319 Test 68 THLP 05 500
C.320 Test 68 THLP 08 501
C.321 Test 68 THLP 09 502
C.322 Test 69 THLP 01 503
C.323 Test 69 THLP 02 504
C.324 Test 69 THLP 03 505
C.325 Test 69 THLP 04 506
C.326 Test 69 THLP 05 507
C.327 Test 69 THLP 08 508
C.328 Test 69 THLP 09 509
C.329 Test 73 THLP 01 510
C.330 Test 73 THLP 02 511
C.331 Test 73 THLP 03 512
C.332 Test 73 THLP 04 513
C.333 Test 73 THLP 05 514
C.334 Test 73 THLP 08 515
C.335 Test 73 THLP 09 516
C.336 Test 74 THLP 01 517
C.337 Test 74 THLP 02 518

C.338 Test 74 THLP 03 519
C.339 Test 74 THLP 04 520
C.340 Test 74 THLP 05 521
C.341 Test 74 THLP 08 522
C.342 Test 74 THLP 09 523
C.343 Test 75 THLP 01 524
C.344 Test 75 THLP 02 525
C.345 Test 75 THLP 03 526
C.346 Test 75 THLP 04 527
C.347 Test 75 THLP 05 528
C.348 Test 75 THLP 08 529
C.349 Test 75 THLP 09 530
C.350 Test 76 THLP 01 531
C.351 Test 76 THLP 02 532
C.352 Test 76 THLP 03 533
C.353 Test 76 THLP 04 534
C.354 Test 76 THLP 05 535
C.355 Test 76 THLP 08 536
C.356 Test 76 THLP 09 537
C.357 Test 77 THLP 02 538
C.358 Test 77 THLP 03 539
C.359 Test 77 THLP 04 540
C.360 Test 77 THLP 05 541
C.361 Test 77 THLP 08 542
C.362 Test 77 THLP 09 543
C.363 Test 78 THLP 02 544
C.364 Test 78 THLP 03 545

C.365 Test 78 THLP 04 546
C.366 Test 78 THLP 05 547
C.367 Test 78 THLP 08 548
C.368 Test 78 THLP 09 549
C.369 Test 79 THLP 02 550
C.370 Test 79 THLP 03 551
C.371 Test 79 THLP 04 552
C.372 Test 79 THLP 05 553
C.373 Test 79 THLP 08 554
C.374 Test 79 THLP 09 555
C.375 Test 80 THLP 02 556
C.376 Test 80 THLP 03 557
C.377 Test 80 THLP 04 558
C.378 Test 80 THLP 05 559
C.379 Test 80 THLP 08 560
C.380 Test 80 THLP 09 561
C.381 Test 81 THLP 02 562
C.382 Test 81 THLP 03 563
C.383 Test 81 THLP 04 564
C.384 Test 81 THLP 05 565
C.385 Test 81 THLP 08 566
C.386 Test 81 THLP 09 567
C.387 Test 82 THLP 02 568
C.388 Test 82 THLP 03 569
C.389 Test 82 THLP 04 570
C.390 Test 82 THLP 05 571
C.391 Test 82 THLP 08 572

C.392 Test 82 THLP 09 573
C.393 Test 83 THLP 02 574
C.394 Test 83 THLP 03 575
C.395 Test 83 THLP 04 576
C.396 Test 83 THLP 05 577
C.397 Test 83 THLP 08 578
C.398 Test 83 THLP 09 579
C.399 Heat Release Rate, O_2 and CO Concentration, Relative Humidity, and Light Intensity for Test 2 582
C.400 Heat Release Rate, O_2 and CO Concentration, Relative Humidity, and Light Intensity for Test 3 583
C.401 Heat Release Rate, O_2 and CO Concentration, Heat Flux and Light Intensity for Test 4 584

D.1 Block Diagram of Arduino/Linux Interface. 586

List of Tables

2.1 Primary plume correlations 13

2.2 Yield of CO as a function of ventilation (kg_{CO}/kg_{fuel})[40] 19

2.3 Maximum Theoretical Product Yields by Fuel [27] 19

2.4 Summary of Detector Characteristics [70] 29

3.1 Information and operational limits of the EDS Sensor Blocks 44

3.2 Orientation of Sensors in Oven Testing 45

3.3 Location of Sensors in Box Testing, all dimensions given from upper rear left corner of box 51

3.4 Light intensity vs distance 82

4.1 Expected Environmental Changes during Fire and Nuisance Exposures ("X" indicates large changes expected, "x" indicates minor changes expected, while "-" entry indicates an unknown influence) 86

4.2 Information and operational limits of the light sensors used in this study . 89

4.3 Information and operational limits of the gas sensors used in this study . . 92

4.4 Calibration coefficients for gas sensors used in this study 99

4.5 Sofa Fuel Component Weight (kg) 107

4.6 Summary of Measured Parameters 110

5.1 Summary of selected experiments for this analysis 134

5.2 ROC Thresholds 140

5.3 Comparison of anomalies detected using HTM and ROC thresholds 142
5.4 Alarm Time Comparison for Test 20. 144

Nomenclature, Symbols, and Terminology

Notation

A_T	Internal surface area of walls, ceiling, excludes ventilation openings [m^2]
A_W	Area of ventilation openings [m^2]
b	Plume radius [m]
D	Pool or fire diameter [m]
D_m	Specific optical density
c_p	Specific heat [kJ/kg· K]
F_{1-2}	View factor between object 1 and 2 [dimensionless]
g	Gravitational constant, 9.81 [m/s^2]
h	Convective heat transfer coefficient [$kW/m^2 \cdot K$]
I	Intensity of radiation (light)
k	Thermal conductivity [W/m·K]
K	Emission coefficient [m^{-1}]
l	Flame height [m]
L_V	Latent heat of vaporization
$\dot{m}$"	Mass rate [kg/s]
$\dot{Q}$	Heat or energy release rate [kW]
$\dot{Q}*$	Dimensionless heat or energy release rate [dimensionless]
$\dot{q}$"	Heat flux [kW/m^2]
r	Stoichiometric ratio [dimensionless]
T	Temperature [K;°C]
t	Time [s]
u	Velocity [m/s]
z	Distance (height in fire plume) [m]

Greek Symbols

α	Thermal diffusivity ($k\rho C$) [m^2/s]
χ	Combustion efficiency [dimensionless]
ΔH_c	Heat of combustion [kJ/g]
ϵ	Emissivity [dimensionless]
κ	Absorption coefficient [dimensionless]
ϕ	Global equivalence ratio [dimensionless]
ρ	Density [kg/m^3]
σ	Stefan-Boltzman constant, 5.7 x 10^{-8} [$W/m^2 \cdot K^4$]

Superscripts

$\dot{}$	Signifies a rate of change
$'$	Single prime, signifies per unit length
$''$	Double prime, signifies per unit area
$'''$	Triple prime, signifies per unit volume

Chapter 1

Introduction

The total cost of fire in North America is significant. In the U.S. alone, it has been estimated to be as high as $350 billion USD or 2.5% of the U.S. gross domestic product (including monetary equivalents for deaths and injuries) [1]. This cost is despite significant advancements in fire detection and protection, coupled with changes in human behaviour, specifically a drastic reduction in smoking. Fires are pervasive, yet rare and uncertain events; the probability of a fire occurring in any given structure during its lifetime is relatively low. When a fire does occur though, its unforeseeable nature and potential for rapid growth means that timely sensing and continuous transfer of useful information are key for effective mitigation and response. The greater the delay in sensing a fire, and the weaker the interpretation of signals from a developing fire, the larger the potential loss. Thus early detection and a clear understanding of a fire signature can reduce both loss of life and property damage. In order to advance the state of fire detection and response, then, typical fire signatures, as discerned by a wide range of sensor typologies, must be better characterized and understood.

The present research focuses on developing new understanding of the signals that accrue from building monitoring sensors during fire events. Since these sensors are typically installed at a much greater density than traditional fire sensors, they present significant potential for use, not only in detecting fire events, but also for monitoring and mapping the continued evolution of a fire during the critical first minutes after ignition. Thus, it is of considerable interest to understand how they can be utilized to sense a fire, how such information might be accurately deciphered and communicated for early fire detection, determination and monitoring of the fire state, and thus aid in emergency response. Therefore, this research begins with a detailed evaluation of the responses of a broad range of sensors to a set of early fire conditions. This phase of the investigation is designed to

gain better understanding of early fire signatures, which have not previously been systematically characterized during evolving fire situations, particularly in the cooler lower layer of a compartment. Results from these experiments will provide detailed temporal and spatial information related to the fire state in both controlled calibration experiments as well as less controlled structural fires and nuisance exposures.

The knowledge gained will then be utilized to develop representative parameter sets that may be indicative of a fire and to show the spatial variations in these measured parameters. For example the response of light and relative humidity sensors to provide qualitative assessments of fire size and show changes in the fire state. Additionally it will be necessary to collect an extensive background data set to define "normal" conditions in a variety of locations since information on non-fire conditions are equally critical to the determination of sensor signals when attempting to successfully identify a fire. The information can be further leveraged in a number of ways including the development of optimal sensor combinations that might be used to better detect and monitor particular stages of a fire, the identification of potential sensors and technologies that could be utilized in new multi-criteria fire detection and monitoring platforms for a wide range of applications, as well as the development of fire state determination algorithms.

1.1 State of the Art

The present state of the art in fire state determination is focused on the detection of fire events using a number of characteristic parameters chosen based on the governing physics that drive fire development. As discussed in Chapter 2, fire signatures are typically defined using concentrations of one or more products of combustion, changes in temperature conditions, and heat flux from the fire. For most commercial applications, the detection of a fire is linked to a subset of expected characteristics of the fire signature. Point source detectors, such as smoke and heat detectors, and sprinklers, rely on the conveyance of heat or products of combustion to a detector location usally near the ceiling for detection to occur. They are therefore inherently linked to the fire heat release rate, the fire plume and ceiling jet dynamics, and the space in which the fire and detectors are interacting. Light dependent sensors (heat flux, IR, UV, video) in contrast are integral, line-of-sight sensors that rely primarily on the fire heat release rate and flame emissivity. Regardless of the parameter of interest, both temporal and spatial variations of that parameter will be present within a space of interest, and subsequently will have an impact on the observed detector response as well.

There are countless sensors that exist in the marketplace and that are implemented for

a variety of uses. This work does not purport to fully review the potential of all available sensors; instead, it specifically addresses the characteristics and response of those sensors frequently leveraged in building information systems. The majority of these sensors are most frequently utilized for a single primary purpose not related to fire detection but instead, related to safety, security and environmental monitoring. Due to their required functions, they most often rely on the following specific sensor technologies based on need and location:

- Motion Sensors: these sensors detect motion in a space and are often interfaced with the lighting control system. If no motion is detected over a prescribed period of time, the lighting in the observed space is reduced. In addition, motion sensors are utilized to sense motion in areas that should not be occupied at certain times and are therefore commonplace for security applications.

- Humidity Sensors: relative humidity is monitored to ensure that an appropriate level is being maintained throughout the monitored space. Depending on the purpose of the space, the target level may vary. Humidity levels may be monitored and controlled for occupant comfort, to ensure that mold and mildew do not form, to ensure that products are properly conditioned, or for a variety of other reasons.

- Temperature Sensors: temperature is monitored in individual spaces and compared with the set point for the local system or with facility wide settings. Heating and cooling can then be provided as needed to each given area. Often the temperature and humidity are evaluated together in order to provide an optimal comfort setting for occupants or alternately to keep the space set at the desired levels for the storage of commodities.

- Ambient Light Sensor: light intensity may be measured throughout the day and supplemental or task lighting may be adjusted based on the quantity of ambient light. Changes in observed ambient light will adjust the quantity of supplied light. The target light levels will vary based on the area and target tasks that are being conducted.

A single sensing unit in a building monitoring system may consist of sensors of only a single type or it may contain mixtures of the above types of sensors. In general, however, increasingly greater numbers of individual sensors are being installed together in larger, integrated, single sensor blocks due to considerations of cost, space and power efficiency. In either case, the advent of indoor environment monitoring has led to significant advancements in sensor development and integration for overall management of a building

environment. If further directed by appropriate research efforts, such as that proposed here, additional advancements in these technologies may lead to adoption of next generation building monitoring systems for fire detection and monitoring as well. This challenge forms the motivation for the present research.

1.2 Scientific Objectives

This research has several primary research objectives:

- to identify fundamental physical characteristics of a fire for which sensors may provide useful information during the various stages of a fire. For this, the fundamental characteristics of the fire volume of interest must be temporally and spatially resolved to a higher degree than is currently available and then interpreted and clearly related to the variable being monitored by each sensor.
- to obtain new information on the sensor response to changes in each of the chosen variables and to discern whether these are brought about by the evolution of the fire or by potential nuisance sources. Once this information has been collected, it can then be evaluated to determine how a given sensor might perceive a fire or a non-fire condition.
- to identify candidate sensors and develop an idealized sensor block for use in fire state determination.
- to develop candidate continuous learning algorithms that can be paired with detailed data to conceive new methodologies for fire state determination and monitoring.

1.3 Outline

The thesis is composed of five additional chapters. Chapter 2 provides a literature review that covers that basics of fire dynamics, an overview of sensor technology, fire characterizations, and learning algorithms. Chapter 3 discusses initial testing performed with commercial sensors in a 1 m^3 box and large-scale testing of fire state variables during incipient fires. Chapter 4 covers the selection of sensors for the fire state determination sensor block, FSD sensor block characterization, and design and results of a series of large-scale fire tests conducted to collect detailed data of fire state progression during realistic

fires. Chapter 5 discusses the development of a hierarchical temporal memory continuous learning algorithm and the anomaly predictions of the algorithm when applied to the test results. Finally Chapter 6 provides a summary of the research conclusions, guidance on the selection and placement of sensors, and suggestions for future work.

Chapter 2

Literature Review

The prompt detection of fire is a critical component to effective emergency response and the minimization of loss of life and property. Thus the detection of fires is typically focused on determination of one or more parameters deemed characteristic to an evolving fire, whether light, heat or combustion products. In order to understand how the detection of fire is accomplished and what gaps exist in the present state of the art it is useful to provide a brief review of fire dynamics, parameters and technologies used for fire detection, sensor response to fire environments, and finally an overview of some of the algorithms that can be used to process sensor signals. Thus the following chapter provides a brief summary of the research in each of these areas and identifies gaps in the current knowledge, specifically with regards to the use of "non-fire" sensors and detection algorithms for characterization of a fire environment. The exploration of these topics form the foundation for the present research.

2.1 Compartment Fire Behavior and Fire Dynamics

Fire is a self-sustaining chemical reaction involving the release of heat, light, and products of combustion. Based on this understanding, in 1974 Custer et al. promoted the concept of a fire signature as being *"any product of a fire which changes ambient conditions and thus has potential use in fire detection"* [2]. Fire signatures are therefore defined by basic parameters which relate to the complex physical and chemical interactions that drive fire development. While the fundamentals underlying the concept of fire signatures have not changed since Custer, significant work has gone into attempting to determine what characteristics constitute an optimal fire signature and how to adequately capture, distinguish,

and measure these characteristics for a wide variety of purposes [3–8]. In order to gain an understanding of how these signatures are generated it is necessary to have a basic understanding of fire behavior, specifically in a compartment.

2.1.1 Qualitative Description of a Compartment Fire

This section provides only a brief summary of the overall concepts of fire growth within a compartment as this has been well documented elsewhere [9–11]. Additional information on the physical and chemical aspects of fire and compartment effects are briefly discussed in later sections.

A fire begins after the successful ignition of a material. Once initiated, it may follow one of two broad paths: one towards fire growth; the other towards self-extinguishment. The actual development of the fire will be largely dependent on the ventilation, fuel load and arrangement, as well as the enclosure geometry. If the fire does not self-extinguish during the early stages of development, then, as shown in Figure 2.1 it will grow. During the initial growth period, the fire is most often fuel-limited as there is abundant oxygen available in the compartment volume to mix with fuel vapours and sustain the combustion processes. The fire is then typically limited to the burning of a single item and the fire size is limited by the size of the fuel surface and how quickly the flame is able to spread across the surface. As the fire increases in size, additional fuels may become involved and if sufficient oxygen is available, the fire will continue to develop and may progress through a transition stage, normally referred to as flashover. After this point, it is considered that all of the fuel in the compartment is involved and the fire is considered to be fully-developed (or fully-involved).

Eventually the fire will decay as the quantity of fuel or available oxygen is reduced, Figure 2.1. If the environment becomes oxygen deficient at any point in this progression of fire development, instead of following the curve illustrated in Figure 2.1, the fire will become under-ventilated and potentially extinguish unless more air is introduced into the compartment. On the other hand, if sufficient oxygen is available throughout the duration of the fire, after it becomes fully developed it will burn for a period of time dependent on the total fuel load in the compartment and then begin to decay as the fuel is consumed. This will continue until all of the fuel is consumed or the fire is no longer able to sustain itself.

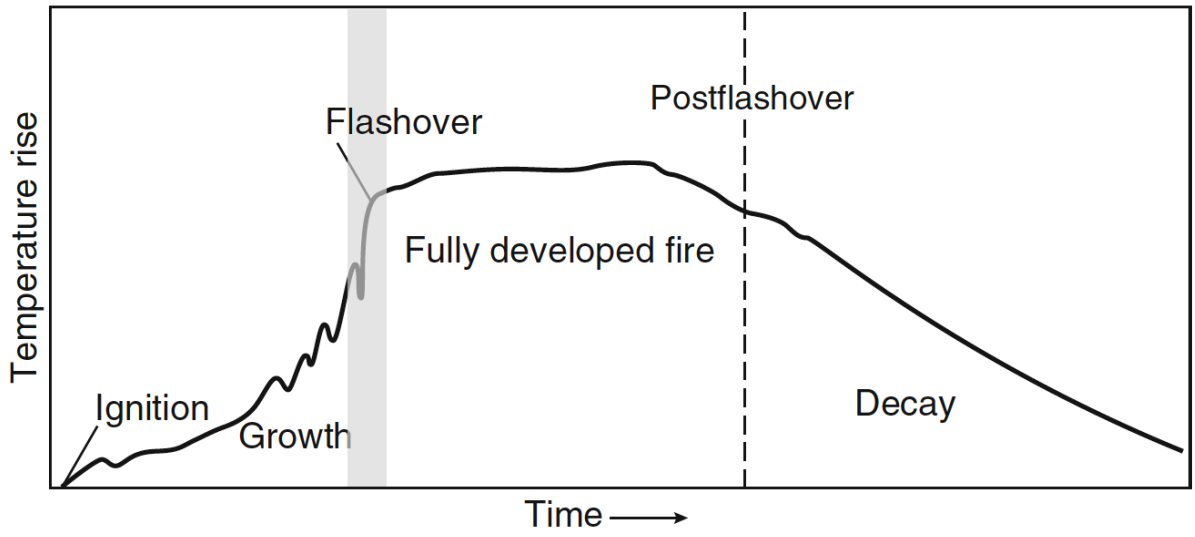


Figure 2.1: Stages of Fire Growth, modified from[12]

During the course of fire development, the hot gases form a buoyant plume and rise until they impinge on, and spread along, the ceiling forming a so-called ceiling jet which grows until it encounters the compartment walls. Due to collection of the hot gases along the ceiling, a hot layer begins to form and the smoke fills down from the ceiling of the compartment, Figure 2.2. In enclosures typical of single rooms, the fire may spread to other items in the room via a combination of direct heat transfer from the flames coupled with radiation from the descending hot layer. On the other hand, if the compartment environment is suitably large (an atrium, stadium, warehouse, etc.), the fire may behave more as an unconfined fire.

In the context of the fire development curve illustrated in Figure 2.1, most research into fire detection has been focused on development of sensors that operate based on reaching a threshold value of one of the readily observable characteristics of the fire plume, such as the quantity of smoke, CO concentration, temperature and velocity, during the early stages of fire growth. Very little work has been directed towards following the characteristics of the fire plume from its inception through to the later stages of the fire shown in Figure 2.1.

The following sections provide a more in-depth review of the physics of development of a compartment fire, outline common correlations for various fire and fire plume characteristics that have been developed based on experimental work, and describe work that has been done relating to detection of fires in compartments.



Figure 2.2: Conceptual Stages of Fire Growth (with permission) [13]

2.1.2 Energy Release and Heat Transfer

Rate of energy release, or heat release rate (HRR) from a fire, $\dot{Q}$, has been deemed by Babrauskas to be *"the single most important variable in characterizing the flammability of products and their consequent fire hazard"* [14]. The rate of energy released during the combustion process is dependent on the mass rate of burning of the fuel, $\dot{m}$", the fuel heat of combustion, ΔH_c, and the area of fuel involved in the fire, A, Equation (2.1).

$$\dot{Q} = \chi \dot{m}" \Delta H_c A \tag{2.1}$$

The value of total heat release rate from a fire is often segregated into two components, the radiative heat release rate and the convective heat release rate. Equation (2.1) can be applied to calculate either of these components by utilizing either the radiative or convective heat of combustion values developed by Tewarson [15, 16] and later compiled by others [17].

Additionally the combustion efficiency, χ, may be evaluated using either the local mixture fraction (calculated for the region local to the fire plume) or the global equivalence ratio (ϕ) averaged throughout the full test compartment. Equation (2.2) compares the mass ratio of fuel to air (oxygen) available in the entire compartment to the stoichiometric ratio which is the ratio that would be required locally for complete combustion of a given type of fuel.

$$\phi = \frac{m_{fuel}/m_{oxygen}}{(m_{fuel}/m_{oxygen})_{stoich}} \tag{2.2}$$

The equivalence ratio greatly impacts the combustion process. This is reflected in the mass rate of burning of the fuel, $\dot{m}$". As ϕ exceeds 1, indicating oxygen limited combustion,

the mass burning rate decreases while conversely when ϕ is less than 1 the excess air absorbs heat thus reducing the total energy available to continue the evaporation and combustion of fuel. As a result $\dot{m}$" is theoretically highest at the stoichiometric ratio, ϕ=1.

The energy released by the fire is transmitted via convection, conduction, and radiation to the surroundings. Different modes of heat transfer dominate at different stages of the fire. Conduction governs the heat transfer through the burning material as well as the transfer of heat through the surrounding enclosure surfaces, Equation (2.3). Convective heat transfer, the transfer of heat between two flowing fluids or a flowing fluid and a solid, dominates when room temperatures are low, Equation (2.4). As the fire progresses and a hot layer begins to form, radiative heat transfer as given by Equation (2.5), begins to take over as the dominant mode and is transmitted from the hot upper layer to the fuel surface [18] increasing $\dot{m}$" and A resulting in an increase in $\dot{Q}$".

$$\dot{q}"_{con} = \frac{k}{L}(T_1 - T_2) \tag{2.3}$$

$$\dot{q}"_{cnv} = h(T_1 - T_2) \tag{2.4}$$

$$\dot{q}"_{rad} = \epsilon\sigma F_{1-2}(T_1^4 - T_2^4) \tag{2.5}$$

This process is largely a surface area driven phenomena with the area of the fire driving $\dot{Q}$ which in turn impacts flame height, the formation of the plume, and the formation of the hot gas layer. The following section discusses the concept of the fire plume and ceiling jet as they are driving forces for fire detection.

2.1.3 Plumes, Flame Heights, and Ceiling Jets

A typical compartment fire scenario involves a burning fuel which is generating products of combustion. The fuel type and configuration, combustion efficiency, and the mode of combustion are crucial variables in defining the heat release rate and thus generation of products of combustion. The heat release rate is critical as it serves as the basis for much of the plume and ceiling jet theory.

The basis for our present understanding of fire plumes was developed nearly 70 years ago [19] and has served as a foundation for much of the ensuing fire plume research that has taken place in the intervening years [3, 20–22]. The basic mathematical model describing

the development of the buoyant fire plume is based on an axisymmetric point source model [19, 23–25]. A number of assumptions allow for the development of simplified analytical solutions [26]. These include:

1. The energy source (fire) may be treated as a point source;
2. The energy generated during combustion remains within the plume;
3. The plume driving force is buoyancy;
4. The density differences are weak within the plume and the Boussinesq approximation may be adopted;
5. The velocity and temperature profiles are constant at a specific location of Z with respect to time and radius; and
6. The horizontal entrainment velocity, v, is a fixed multiple, α, of the buoyancy driven vertical flow, u.

It further assumes that the hot plume gases rise until they come into contact with a ceiling in the case of a compartment fire or alternately until buoyancy in the plume is too weak to overcome drag in the case of a free fire. Karlsson [26] and Beyler [27] provide detailed reviews of plume and ceiling jet theory and a derivation of the ideal plume yielding ΔT as a function of height and HRR is provided by [26] and summarized in (2.6).

$$\Delta T = 5 \left[\frac{T_\infty}{g {c_p}^2 {\rho_\infty}^2} \right]^{1/3} \dot{Q}^{2/3} Z^{-5/3} \tag{2.6}$$

. McCaffrey [28] defined three basic regions of the fire including the plume:

1. Thermal plume;
2. Intermittent flame region (representing the flame height, L); and
3. Continuous flame region

L has been defined as the height at which the flame is visible 50% of the time [29] and a number of empirical correlations have been derived based on this definition which McCaffrey [28] has compiled and shown to be relatively consistent.

Development of the turbulent plume from a diffusion flame is driven by the physical and chemical processes that occur in the flame regions. Therefore these processes drive the plume velocity, u_0, plume temperature, T_0, plume radius, b, and plume mass flow rate, $\dot{m}_p$. Based on this, Zukowski [20], Heskestad [29], McCaffrey [28], and others have developed plume correlations based on fire heat release rate and height above the fuel surface derived from experimental measurements, Table 2.1. It is this behavior that fundamentally drives the parameters that are typically observed for fire detection purposes.

Table 2.1: Primary plume correlations

	ΔT	u	$\dot{m}_p$
(Zukowski)	$13.74\left[\frac{\dot{Q}^{2/5}}{Z}\right]^{5/3}$	$0.59\left[\frac{\dot{Q}}{Z}\right]^{1/3}$	$\dot{m}_p = 0.071\dot{Q}^{1/3} \cdot Z^{5/3}$
(Heskestad)	$25\left[\frac{\dot{Q}^{2/5}}{Z-Z_0}\right]^{5/3}$	$1.0\left[\frac{\dot{Q}}{Z-Z_0}\right]^{1/3}$	$\dot{m}_p = 0.071\dot{Q}^{1/3} \cdot (Z-Z_0)^{5/3} + 0.00192\dot{Q}_C$
(McCaffrey)	$2.27\left[\frac{\dot{Q}^{2/5}}{Z}\right]^{5/3}$	$1.1\left[\frac{\dot{Q}}{Z}\right]^{1/3}$	

As can be seen from the tabulated correlations, the basic relationship arrived at by each researcher is of the same basic form: ΔT is a function of $\dot{Q}^{2/3}Z^{-5/3}$; u is a function of $\dot{Q}^{1/3}Z^{-1/3}$; and $\dot{m}_p$ is a function of $\dot{Q}^{1/3}Z^{5/3}$. Further, these experimental results match well with the theoretically derived values obtained by Quintiere [26] and shown previously.

As discussed earlier, once the plume forms it will rise and expand until it dissipates or impinges on a ceiling. In the event of the plume impinging on the ceiling a boundary layer will be formed along the ceiling typically known as a ceiling jet. The ceiling jet directly relates to fire detection as it serves as the transport mechanism to deliver the products of combustion to the sensor. Before discussing details of the ceiling jet further, Section 2.2, it is necessary to better describe the various modes of combustion and their impact on the products of combustion that form the hot gas plume. This is the subject of the next section.

2.1.4 Smoldering and Flaming Combustion

As discussed above the products of combustion are typically what are being monitored by fire detection systems and the quantity and composition of the products of combustion will vary based on the mode of combustion.

In general, combustion involves a large series of complex chemical reactions; however, the process can be simplified by recognizing that there are three primary processes involved.

The first is pyrolysis of the fuel. This is then followed by oxidation of the resulting fuel and/or decomposition products in either the solid or gaseous phase [30]. Each process varies in the quantity of heat and smoke, defined by Gross et al [31] as the *"gaseous products of burning organic materials in which small solid and liquid particles are also dispersed"*, produced and thus resulting in different fire signatures. The properties will change based on $\dot{Q}$, ϕ, and the local equivalence ratio. When the oxidation takes place in the solid phase, smoldering is dominant, while oxidation in the gaseous phase results predominantly in flaming combustion [30].

In both cases, the first phase may involve pyrolysis, the thermal decomposition of the material due to an external heat source. The process of pyrolysis can result in charring, melting, and vaporization of the original fuel. If the material is exposed to sufficient external heat flux it may transition into either a smoldering or a flaming scenario. The basic reactions and potential products are shown below.

Pyrolysis:

$$\text{Fuel (solid)} + \text{Heat} \Rightarrow \text{Pyrolyzate (gas)} + \text{Char (solid)} + \text{Ash (solid)}$$

Heterogeneous oxidation:

$$\text{Char (solid)} + \text{O}_2\text{ (gas)} \Rightarrow \text{Heat} + \text{CO}_2 + \text{H}_2\text{O} + \text{other gases} + \text{Ash (solid)}$$

Gas-phase oxidation:

$$\text{Pyrolyzate (gas)} + \text{O}_2\text{ (gas)} \Rightarrow \text{Heat} + \text{CO}_2 + \text{H}_2\text{O} + \text{other gases}$$

Smoldering Combustion

Smoldering is the slowest of the self-sustaining combustion reactions and primarily occurs in porous char forming materials. Polyurethane foam, cigarettes, and cellulosic products are some of the most common materials which may undergo smoldering combustion.

In smoldering combustion, the reaction rate is very slow and dominated by the available oxygen, resulting in a low heat release rate, visibly flameless combustion process typically characterized by temperatures in the range of 450°C to 700°C and low flame spread rates on the order of 1 mm/min [9]. Although the process, and therefore flame spread rates, may be increased if oxidizer is forced through the material due to wind or ventilation, in reality smoldering fires can be incipient for hours before transitioning to flaming conditions or alternately extinguishment.

It has been reported that the efficiency of smoldering combustion, χ_{eff}, is typically on the order of 33% [32]. Therefore, the products of combustion from a smoldering fire vary significantly from those from a flaming fire. Both the production rate and the chemical species vary. The CO/CO_2 ratio which is linked to the combustion efficiency is ~ 0.4 for smoldering reactions but ~ 0.1 for flaming reactions [33]. A smoldering fire typically will produce increased yields of volatile organic compound's (VOC's), polycyclic aromatic hydrocarbons (PAH's), and particulates, however this is countered by the reduced production rate in comparison to flaming fires. The aerosol and particulate sizes typically associated with smoldering conditions are 1.5-3µm which is larger than those observed during the pyrolysis, .75-1.6µm, or during flaming combustion, .01-1µm, conditions [3, 34, 35].

In summary, smoldering fires have relatively low heat release rates and comparitively low temperatures which result in weak buoyant plumes. Further, the combined chemical and particulate signature created by the fire is different than that created by a flaming fire. Thus the characteristics of a smoldering reaction and the associated time scales mean that detection of smoldering events is primarily driven by species production and that the effectiveness of other detection methods (i.e. those associated with temperature) may be limited.

Flaming Combustion

Flaming combustion is the most common type of accidental fire and the mode of combustion that is most recognizable to people. It is also the mode of combustion that drives the HRR, flame height, and plume dynamics discussed previously and yields the three characteristics of a fire: heat, light, and products of combustion that are used for detection. In this section a brief summary of flaming combustion is provided primarily as it relates to issues relating to detection.

Faraday in his famous 1861 Christmas lectures stated *"there is not a law under which any part of the universe is governed which does not come into play, and is touched upon in the chemistry of a candle"* [36]. Though delivered to children and using a candle as the source of discussion, Figure 2.3, Faraday's lectures provide good insight into the structure of, and mechanisms driving, diffusion flames in general.

In examining Figure 2.3 [36], it can be observed that a diffusion flame consists of a fuel rich region where fuel is being driven off of the fuel surface, enclosed by a reaction zone (the flame), with an outer oxidizer rich region where oxidizer is entrained. The flame is a reaction zone where the fuel and oxidizer mix to within their flammable limits by diffusion, combustion occurs, and the maximum temperature is achieved. While much of the fuel and

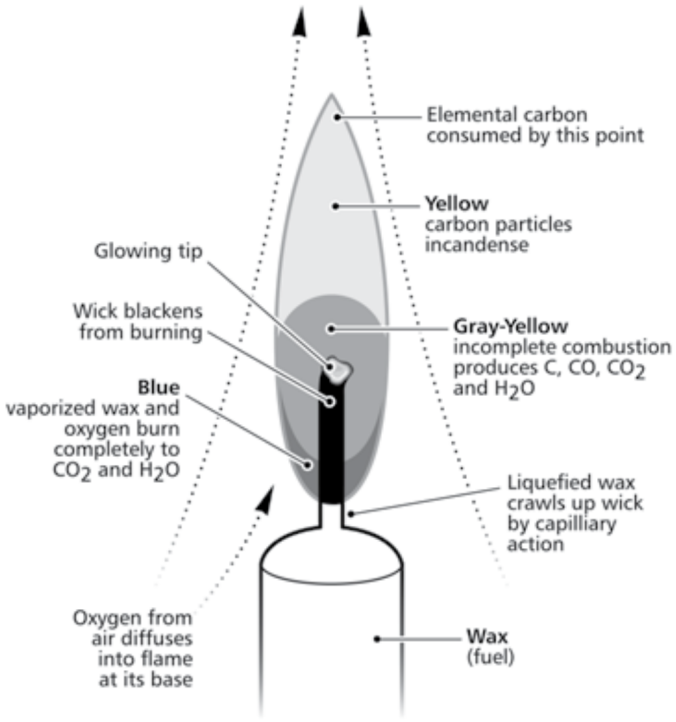


Figure 2.3: Schematic of candle flame. [37]

oxidizer can be consumed in the reaction zone, unburned reactants can also leak through the primary reaction zone and burn in the outer regions of the flame.

In a typical diffusion flame, the fuel reacts with oxygen supplied by the environment to form CO_2, H_2O, heat, light, and additional products of combustion. A candle is a useful example of a diffusion flame as the flame regions are laminar and therefore more readily observable than in larger turbulent diffusion flames which typically occur when flame heights exceed 0.33m [10].

In the small blue region near the base of the candle flame, Figure 2.3, the reaction is effectively complete yielding only CO_2 and H_2O. Above this region is a yellow-gray region in which more complex fuel molecules are "cracked" into simpler fuel chains and into carbonaceous substances just prior to entering the broad reacting zones. Coagulation, the combining of smaller liquid particles into larger particles, and agglomeration, the combining of multiple particles to form a chain or complex particulate structure, also occur and decrease the particle number while increasing the average particle size. Unburnt fuel cools this portion of the reaction zone resulting in incomplete combustion and the formation of

C, CO, and other products of combustion. In the final region, characterized by a yellow flame, unburnt carbonaceous particles are oxidized, increase in temperature and begin to incandesce. It is worth noting that while most of the changes in the flame are chemical in nature (i.e. the degradation of fuel), incandescence is a physical change [10, 36]. For simple laminar diffusion flames the majority of soot is consumed prior to the end of the reaction zone and thus the flame height is similar to the sooting height. For turbulent flames this relationship breaks down as soot is able to escape the flaming regions as the reaction fronts "tear" or are "stretched" [10]. For heavily sooting fuels or for underventilated conditions, the soot will not be fully oxidized within the reaction zone and so will escape in the fire plume and may be measured in the plume or ceiling jet.

Flaming zones produce peak temperatures in the range of 1500-2000 K, visible light, and smoke particles that are typically smaller, on the order of .01-1m, than those generated from smoldering combustion [3]. Due to the elevated temperatures, the gases rise and cooler air is entrained and a characteristic flame shape evolves as the products of combustion are convected away and new oxygen is provided to the flaming region. The diffusion flame zones in the fire, therefore, are recognizable by their yellow/orange coloration, heat and light generated, and smoke produced. These characteristics are key aspects that form the focus in fire detection, as discussed later.

Given the variability that exists in the products arising from the combustion processes in fires, and the fact that it is largely the products of combustion that pose the greatest hazard, it is of value to examine in more depth the ways in which the products of combustion can be characterized and what parameters are central to the detection of a fire. This discussion follows.

Products of Combustion

The products generated during various fire events have been examined in order to determine the impact of ventilation, fire type, and fuel on the products generated [2, 6, 18, 38, 39]. In particular, a strong focus has been placed on understanding the formation of gaseous products of combustion that directly contribute to a hazardous environment (i.e. CO, CO_2, NO_x, and other toxic compounds). A general relationship has been provided for gas phase oxidation of a wide range of carbon based fuels that fit the general molecular form shown in Equation (2.7) [3] and for which the stoichiometric amount of air is provided by Φ.

$$C_\alpha H_\beta O_\Gamma N_\delta X_\epsilon S_\tau + \frac{1}{\Phi}(O_2 + 3.76N_2) = \alpha CO_2 + \frac{\beta - \epsilon}{2} H_2O + \epsilon HX + \tau SO_2 + 3.76(\Phi + \frac{\delta}{2})N_2 \quad (2.7)$$

In Equation (2.7) "X" may represent fluorine, chlorine, or bromine and the stoichiometric amount of air designated as Φ, where $\Phi^{-1} = [\alpha + (\beta - \epsilon)/4 + \eta - \gamma/2]$.

In practice, the diffusion flames in fires do not behave in the idealized manner described above. Laminar diffusion processes can still exist in small local regions, but the mixing, and thus local stoichiometric ratio and resultant combustion reactions, occur on a temporally and spatially fluctuating basis. Therefore, while the "instantaneous" reaction kinetics and products of combustion still are present, clear delineation of fuel, air and flaming zones no longer exists so the reaction processes are averaged with the variation in flame position in space and time. Limited O_2 results in poor combustion efficiency with a decrease in peak temperatures and increase in soot yields outside of the flame region. These factors then have distinct ramifications in terms of the specific yields of the various products of combustion.

One key factor in determining yields of combustion products is the equivalence ratio. Recall that Equation (2.2) defined a global equivalence ratio for a compartment fire situation. While Φ may be measured globally it is not necessarily representative of the differences that exist in the local fuel/air ratios that define the flame. For a typical hydrocarbon fuel under stoichiometric (ideal) conditions CO_2 and H_2O will be produced. Under well-ventilated conditions, CO and soot can be produced due to poor mixing and heat losses from the presence of excess air. For a given fuel as the local equivalence ratio becomes greater than 1 (under-ventilated conditions), an increase in soot, unburned HC compounds, and CO production is observed. If the fuel contains chlorine, fluorine, bromine, or other compounds, related combustion products such as HCN, HCl, HF, or HBr will also be produced.

Table 2.2 provides a comparison of CO yields for well ventilated versus under-ventilated fires as determined using the global equivalence ratio while Table 2.3 summarizes the maximum theoretical yields for a selection of fuels burning under stoichiometric conditions. It should be noted that yields are the quantities of a compound produced at the fire source normalized by the quantity of fuel burned, whereas species concentration is the amount of species in a unit measure of smoke which can be expressed as either a mass or volume concentration. As such, CO concentration, typically in parts per million, and smoke are two of the primary parameters, in addition to temperature, that are widely used in the detection of fires.

Table 2.2: Yield of CO as a function of ventilation (kg_{CO}/kg_{fuel})[40]

Material	Well-Ventilated Fires	Under-Ventilated Fires
Methane (gas)	Not Reported	0.175
Propane (gas)	0.005	0.229
Propylene (gas)	0.020	0.200
Hexane (liquid)	0.011	0.195
Toluene (liquid)	0.066	0.107
Methanol (liquid)	0.001	0.236
Isopropanol (liquid)	0.002	0.168
Acetone (liquid)	0.003	0.304
Pine (solid)	0.004	0.138
PMMA (solid)	0.010	0.189
Pine (solid)	0.004	0.138
Flexible PU Foams	0.010-0.042	Not Reported
Rigid PU Foams	0.025-0.051	Not Reported

Table 2.3: Maximum Theoretical Product Yields by Fuel [27]

		Maximum Theoretical Yields (%)				
Fuel	Chemical Formula	k_{CO}	k_{CO_2}	k_{O_2}	k_{H_2O}	1/r
Acetone	C_3H_6O	2.50	3.93	3.81	1.60	9.45
Ethanol	C_2H_5OH	2.65	4.15	4.54	2.54	8.94
Hexane	C_6H_14	2.27	3.57	4.10	1.71	15.1
Isopropanol	C_3H_7OH	2.33	3.67	4.00	2.00	10.3
Methanol	CH_3OH	2.75	4.31	4.69	3.53	6.43
Methane	CH_4	10.94	17.19	25.00	14.06	17.2
Propane	C_3H_8	4.34	6.82	8.27	3.73	15.6
Propene	C_3H_6	4.76	7.48	8.17	3.07	14.7
PMMA	$C_5H_8O_2$	1.40	2.20	1.92	0.72	8.23
Toluene	C_7H_8	2.32	3.64	3.40	0.85	13.4
PU Foam	$CH_{1.74}O_{0.323}N_{0.0698}$	7.05	11.05	10.25	3.95	8.78
Wood (Spruce)	$CH_{3.584}O_{1.55}$	1.73	2.73	2.23	2.00	3.87

Once the initial products of combustion have formed and left the reaction region, the plume becomes of interest as it acts as the transport mechanism for the continued dispersion of the products and the characteristics of the smoke at a given location will impact the ability for a detector to operate. As the smoke produced currently acts as the primary means of fire detection, a discussion on fire detection and monitoring follows.

2.2 Basics of Fire Detection and Monitoring

The primary goal of fire detection devices and systems is to detect a fire as soon as possible after it ignites, so that the fire is sufficiently small to be controlled and egress for any occupants is possible. Such early detection of fires is critical to occupants in ensuring that they are able to safely egress from the area, but it is equally critical to alert personnel that there is a fire.

The identification of light, heat, or smoke singularly or in combination has formed the foundation of fire detection for over one hundred years. George Darby patented the first electric heat detector in 1902, which relied on a stick of butter to act as the buffer between conductors and subsequently yielded to more advanced mechanisms.[1] Twenty years later Heinrich Greinacher laid the theoretical groundwork for what much later became the ionization smoke detector with further work continuing until the mid 1960's when a single station photoelectric detector was developed and was adopted for general commercial use [41]. In more recent years, additional technologies have been used to observe the visual characteristics of flames, such as IR/UV detectors or video detection systems, however they are not widespread commercially.

Compartment fire characterization has been examined by a number of researchers [3, 4, 26, 41–45] and these characterizations have largely been focused on determination of the characteristic heat release rates, temperature, smoke production, and radiation associated with a fire as these characteristics are directly linked to development of a hazard from the fire. When an unwanted fire does occur, it is desirable to detect the onset of the fire at the earliest possible time. In order to accomplish this the focus has been on identifying characteristics of fires that can be detected after ignition has occurred and the fire has grown to a detectable size, where the threshold value set to define a detectable size may differ depending on the technology used in a given sensor system. As a point of reference in this respect, it is convenient to recall the conceptual fire growth curve provided in Figure 2.2.

[1] https://patents.google.com/patent/GB190225805A/en?oq=GB190225805A

Traditionally, fires have been detected using technologies which were readily suited for the determination of a threshold value of parameters, such as the temperature produced or products of combustion, that were believed to be representative of an incipient fire signature relatively soon after ignition (15kW$< Q <$100kW). Much of the work on fire characterization focused on determination of the characteristic products of combustion and heat released during the very early stages of the fire [4, 5, 11, 15, 46]. Therefore, these are also the variables that have most often been measured, directly or indirectly, in attempts to detect fires.

After identification of the parameters to be sensed, the placement of the detectors also becomes important. They must be located in such a way as to be effective with respect to anticipated fire location, fire characteristics and anticipated sensor response, while simultaneously being spaced to balance overall system cost.

One of the significant challenges with this approach is that no two accidental fires are identical. Thus, it proves difficult to generalize characteristics and threshold values for the heat or products of combustion across the full spectrum of potential fire exposures. This is further complicated when combined with the random location of a fire with regards to the detector location. In practice, the resultant uncertainties in response are assumed to be alleviated through the testing and approval process which uses a set of defined exposure criteria.

The inherent assumption in doing this is that, when installed, the sensors will be sufficiently spaced such that exposure conditions similar to those used in the test will eventually be experienced by the sensor during the course of the fire, whether early in fire development or at a later time. This may not however be the most efficient manner of detection and furthermore often times fire sensors may not be present at all. As a result, there is a gap in the ability to detect fires that requires exploration to determine what other parameters and associated sensors may be useful. In particular, the measurement of light, a primary characteristic of fires, has largely been ignored for fire detection purposes.

Despite the existence of a range of commercial fire detection technologies, the full time dependent physical signatures produced by fires have not been systematically characterized, especially with regards to their variations in space within a compartment and for determining those best for use in early fire detection and ongoing monitoring of a fire event. For example, many signals such as visible, ultraviolet, and infrared light are produced by fires along with the commonly detected heat and products of combustion, yet only limited work has been performed towards examining specific details of the light signatures produced from a fire relative to ambient light levels [47–49].

The primary focus of most of detector the work was on incremental improvement of

standard fire sensors with respect to detection times and signal thresholds and minimization of nuisance alarms rather than on the use of non-traditional fire signatures or sensing technologies to develop new technologies and systems for improved early fire detection and ongoing fire monitoring. With this perspective, the following sections summarize and, where appropriate, revisit existing work on fire signatures, as well as detector design and detection methods.

2.2.1 Detectors

The basic combustion processes and plume behavior that govern the generation and movement of smoke and heat from a developing fire are linked directly to the ability of smoke and heat detectors to accurately detect the fire. The following section briefly discusses the current state of fire detection for each of the three main categories of detectors: smoke/heat detectors, gaseous detectors, and light detectors.

Temperature and smoke based sensors rely on the plume and ceiling jet for activation. The buoyancy driven plume causes the products of combustion to rise and impinge on the ceiling forming a ceiling jet, which is the means for transporting heated gases and particulates to the detector location. As a result, a number of studies have examined the response of smoke and heat detectors (and similar sensors) to fire driven flows [2, 3, 7, 22, 35, 50–57] in order to provide insight and guidance on detectors. In general when the detectors addressed in the studies are in close proximity to a fire they show adequate response, however there remain a wide range of cases in which nuisance alarms are possible as well as cases in which a detector is not present or the spacing does not allow for an effective response time. Plume driven sensors are challenged in that their proximity to the fire is a primary driving force for the response and anything that may interfere with plume or ceiling jet dynamics will impact their activation. Thus the dependency on the plume is both a positive and negative defining characteristic of these types of sensor.

Measured characteristics of the fire and thermal plume have been used as the basis of design for, and evaluation of, thermal and smoke detection systems. For example, Alperts correlations for maximum ceiling jet velocity and temperature have been widely used for estimating the time to detection in design of both smoke and heat detectors[22]. Alpert expanded initial work performed by Morton [19] on plumes using a variety of ceiling heights and fuels including heptane sprays, ethanol pans, cardboard boxes, and pallets. He took measurements of the plume temperature and velocity and developed the empirical correlations outlined in Table 2.1. Despite their widespread use, his experiments were limited in the range of fire sizes evaluated, only examined smoke flow under “infinite”

smooth flat ceilings, minimized the impact of ventilation on the fire and fire compartment, and relied on relatively steady state (HRR) fires. Furthermore Alpert did not perform any testing with detector-fire placement ratios (r/H) <0.15, and thus assumed uniform conditions in this region.

In fact, many of the existing correlations make similar assumptions regarding well ventilated fire behavior and spatially uniform fire plumes with a fixed steady HRR [58]. The assumption regarding ventilation may be appropriate as typically during the incipient stages of a fire, when detection is desired, the space is well ventilated so the impact of ventilation on the combustion products may be limited. However, the use of a single $\dot{Q}$ and physical location obviously constitutes a significant over-simplification and averaging of fire characteristics relative to what will happen in a real fire situation. Instead, a fire grows in size spatially and with respect to heat release rate, as can be noted by the relative influence of $\dot{Q}$ on both the temperature and velocity of the plume, per Equation (2.8) based on derivations from ideal plume theory as well as experimental measurements [22, 50, 51, 58].

$$\Delta T_m \sim \dot{Q}^{2/3} Z^{-5/3}, U_m \sim \dot{Q}^{1/3} Z^{-1/3} \tag{2.8}$$

Detector design correlations based on the evolution of heat release rate in a growing fire have been proposed as a tool to better determine ideal detector spacing [52]; however, in practice this method has proven to be of limited value as results vary widely and change significantly across the range of normally expected changes in the fire heat release rate or other ambient conditions.

In summary, time-dependent fire growth and detector response characteristics are both critical in identifying the presence of a fire and monitoring its development over time since each play a role in driving detector response. Nonetheless, the early empirical relationships such as those proposed by Alpert [22] and others remain the primary means of predicting detector activation outside of the use of computational fluid dynamics (CFD). Clearly if it is desired to better monitor the fire state by moving beyond the alarm/no alarm signal threshold that is the present status-quo, the dynamic conditions in the fire environment and the corresponding detector response must be more broadly characterized and understood.

Smoke and Heat Detectors

Smoke detectors are relatively new technology [41]; however, they have seen wide-scale adoption. They are the most commonly installed fire detection devices as they are relatively

low cost, are easy to install and have been shown to reliably detect fires when in they are in the vicinity, however their installation may be limited outside of residential spaces, in particular when buildings are fully sprinklered. Successful detection of fire with a smoke detector relies on the assumption that a fire will produce smoke. Further, it is assumed that when a sufficient quantity of hot gases or sufficient accumulation of smoke particulates have been transported to the sensing chamber of a detection device, they will be observed and this is indicative of a fire.

There are two fundamental technologies leveraged by smoke detectors to detect the presence of products of combustion. These include two methods of photoelectric detection and one ionization detection method. NFPA 72, "National Fire Alarm Code" provides the following descriptions of the general types of smoke detectors :

1. *Ionization smoke detection* is the principle of using a small amount of radioactive material to ionize the air between two differentially charged electrodes to sense the presence of smoke particles. Smoke particles entering the ionization volume decrease the conductance of the air by reducing ion mobility. The reduced conductance signal is processed and used to convey an alarm condition when it meets preset criteria.

2. *Photoelectric light obscuration smoke detection* is the principle of using a light source and a photosensitive sensor onto which the principal portion of the source emission is focused. When smoke particles enter the light path, some of the light is scattered and some is absorbed, thereby reducing the light reaching the receiving sensor. The light reduction signal is processed and used to convey an alarm condition when it meets preset criteria.

3. *Photoelectric light scattering smoke detection* is the principle of using a light source and a photosensitive sensor arranged so that the rays from the light source do not normally fall onto the photosensitive sensor. When smoke particles enter the light path, some of the light is scattered by reflection and refraction onto the sensor. The light signal is processed and used to convey an alarm condition when it meets preset criteria.

The response of detectors, whether ionization or photoelectric, is a function not only of the particle sizes in the smoke, but also of the particle density and visual characteristics. Therefore, a given class of detectors may be more suitable for detection of fires that are predominated by one mode of combustion over another. For example, recall that smoldering fires can produce smoke where the average particle size is approximately 10 times larger than the particulate generated from flaming fires, but the particles from smoldering fires

are light in color and absorb little light [3, 43, 59]. Such differences in the smoke, as well as the temperature of the particles, and aging due to length of time from smoke production to location of detection with consequent agglomeration, can lead to the formation of larger particles [60, 61] which will also alter the ability of a given type of sensor to detect the smoke.

Ionization detectors typically respond more quickly to the smaller particulates generated by flaming fires while photoelectric detectors typically respond more quickly to the larger particles produced by smoldering fires [62]. Ionization detectors are sensitive to temperature, pressure, gaseous composition, and relative humidity. Fluctuations in these can cause false alarms [35, 63]. Similarly, dust particulates, water vapor (steam), or other materials in the air reaching an ionization detector can cause changes in the conductance of the sensor similar to those generated by the presence of smoke. This will again lead to potential false alarms. Also the particulates generated during the cooking process (toast, meats, frying, etc.) often are between 0.1-1.0 μm in diameter. Since this falls in the range of greatest sensitivity for ionization detectors, these present a third factor that could lead to false alarms with this family of detectors.

Optically based detectors (photoelectric smoke detectors) tend to respond more quickly to larger particulate sizes and therefore respond more quickly to smoldering fires. They are less sensitive to changes in ambient conditions [64] and more resistant to nuisance alarms from cooking smoke. Photoelectric detectors, however, respond most efficiently to particulate sizes from 1.0-10.0 μm in diameter and thus they can be delayed in responding to flaming fires. Non-fire generated particulates of similar diameters to those of a smoldering source can cause nuisance alarms from photoelectric detectors [35, 63]. Recent research has pursued improving photoelectric detection technologies to detect the presence of smaller particulates and/or to reduce the potential for nuisance alarms by introducing multiple scattering angles, modifying the wavelength of light used, and increasing the number and intensity of the wavelengths of light that are transmitted from the source to the sensor [64]. Nonetheless, detection is still based upon determination that the signal has passed a set threshold and once triggered they do not continue to monitor the state of the fire.

Underwriters' Laboratories defines a heat detector as *"a heat-detecting type of automatic fire detector which is an integral assembly of heat-responsive elements and non-coded electrical contacts, which function automatically under conditions of increased air temperature"*[65]. Heat detectors are typically spot type devices that respond to temperature changes in the environment around the sensing element. Most heat detectors respond when they sense a fixed temperature threshold and/or a defined rate of rise in temperature due to thermal energy convected from the fire plume to their location. Heat detectors typically have a low rate of nuisance alarms, but since the activation mechanism is based

on temperature, it often results in a delayed response in comparison to smoke detectors [21, 66].

Since current heat and smoke detectors are all point source detectors, their ability to perform is greatly dependent on the specific configuration of the sensing element as well as the position of the sensor relative to the fire plume and ceiling jet. If the ceiling jet is inhibited in reaching the detector, activation will be delayed or may not occur. Detectors are tested for listing purposed but this solely ensures that they meet certain response criteria when exposed to a specified set of controlled test conditions. In reality, an actual fire may be significantly larger or smaller than the test conditions, and will interact in real time with ventilation conditions in the fire compartment. As a result, a real fire will certainly have different heat release rate, particulate distribution and growth characteristics than the design fire, all of which will have drastic effects on detector response in the real fire situation. Furthermore, positive detection of a real fire depends significantly on the type and distribution of detectors, since the observed signal at a given detector will vary widely based on the relative position of that detector to the fire.

In fully sprinklered buildings for example, where fire detection systems may not exist, the first notice of a fire may be through activation of a sprinkler system as it responds to the heated gases in the fire plume. Depending on the speed of sprinkler activation, the fire may have grown significantly before it is detected and before occupants or fire response personnel are actually notified that it is even present. Although these, and other buildings, may not have formal fire detection systems, they do now contain other distributed sensing systems which may be leveraged to improve detection of fires and even monitor the overall fire and building environment until response personnel arrive. As a result, the topic of response and application of these sensors in fire detection is wide open for exploration.

Light Sensing Flame Detection

Some work has been performed on light sensing detectors, however this work has been limited to studies based on infrared and ultraviolet, with no examination of the visible light spectrum. Typical flame detectors optically sense either the ultraviolet (UV) or infrared (IR) radiation which emanates almost instantaneously from the flames of a growing fire. The radiation travels in straight lines in all directions from the fire source and while its intensity naturally decays as a function of the inverse radius squared, $1/r^2$, the light signal may be further attenuated if it has to travel through smoke or may be blocked entirely by obstacles in the path of the beam. Therefore, in order for a light detector to function, the detector must be able to "see" the flame directly. As a consequence, they are subject to false alarms from nuisance background sources of light [67]. On the other hand, because

they are based on transmission of light, these detectors often exhibit the fastest detection times of any type of fire detector.

Infrared detectors consist of a filter and lens system that is designed to screen out unwanted wavelengths and to focus the incoming energy at the desired wavelengths onto an infrared sensitive photovoltaic or photoresistive cell. Detectors can be designed to respond to the total IR signal from the flame alone or alternately, the IR signal sensor can be combined with a circuit that senses the frequency of flame flicker, which usually lies in the range of 5 to 30Hz. IR detectors are sensitive to solar radiation and other none fire sources of infrared light as well as being subject to interference from various gases..

The ultraviolet component of flame radiation is also used for fire detection, however as their operating wavelength is in the 0.11 to 0.30 μm region they are susceptible to detection of light from welding and various artificial light sources. Similar to IR detectors, they may also be subject to interference from various gases which can interfere with the transmission of light in the UV spectrum.

In addition to the technical limitations, both UV and IR optical flame detection systems also tend to be costly and therefore are primarily used in industrial applications but have not been adopted for commercial or residential use.

Video fire detection (VFD) systems that use a sequence of captured images paired with detection algorithms have also been developed. Cetin [68] provides a comprehensive review of video fire detection that encompasses technologies which have been developed for both the visible and IR/UV spectra. In general, video fire detection systems work by extracting moving portions from a series of images and examining the movement for patterns characteristic of flame flickering using Markov and other frequency domain techniques [68]. If they could be employed in a reliable manner, a major advantage of video and other light sensing devices is that they can respond to a fire very quickly relative to point sensors which are subject to a smoke transport delay time. However, Cetin et al. [68] concluded from their review that *"Due to noise, shadows, illumination changes, and other visual artifacts in recorded video sequences, developing a reliable video detection system is a challenge to the image processing and computer vision community. With todays technology, it is not possible to have a fully reliable VFD system without a human operator."*

Thus the conclusion with regards to light sensing devices is that they have potential for rapid fire detection, however they have not been widely employed and visible light sensors (luminosity) have been largely ignored to date.

Species Detection

As described above gases are produced throughout the entirety of the combustion process regardless of combustion efficiency. As a result, if a specific gas signature associated with a fire is known that signature may be used for fire detection purposes. The detection of species can be potentially advantageous in situations where the volume of production of solid particulates is limited (i.e. smoldering or slow growth fires). While gas detection in fire tests is commonly achieved using a variety of continuous-sampling analyzers which can offer excellent accuracy and dynamic response, they are typically limited to a single gas species, their application can be restricted due to the high cost of the individual analyzers and they are have not been generally adopted and put into use in non experimental conditions.

Recently however, developments in electronic gas sensors have broadened their range of applicability for fire gas analysis [69] though they have not been widely used for these purposes yet.

Historically the concentrations of CO, CO_2, and O_2 have been examined using a variety of continuous sampling methods that are not practical for commercial installations. Pfister [70] measured a range of gases using a variety of different detector technologies and concluded that the gases produced during the fire could successfully be measured using a variety of sensors, therefore the potential for a species based fire detector was possible. Jackson et al. [71] performed a set of experiments examining six different types of fires based on British Standard BS5445 and came to similar conclusions as Pfister. More recent studies have aimed at refining the idea of a "fire signature" [3, 72]. For this, they have focused on species production during the combustion of different fuel types and the ability to detect a fire based on one or more gaseous combustion products.

In most of these studies, while the intent was to measure target gas concentrations as functions of time, gases were only measured at a single location using complex and expensive gas analyzers so most data was not available in real-time. Thus, while the research shows that certain measured species may be used for fire detection, current technology typically allows confirmation of detection of that species only after the conclusion of testing. Based on these limitations and cost, it is not practical to use many of the existing analyzers for real world fire detection. The exception may be electronic gas sensors since they are relatively inexpensive, can accurately detect a range of gases and thus have been incorporated into a broad range of end-use products such as handheld detectors. To date, however investigations into the application of electronic gas detectors for fire applications have been limited [73] and there are no commercial fire sensors on the market that leverage these sensors, with the exception of some commercial CO detectors that are primarily intended for CO detection in non-fire conditions.

2.2.2 Multi-criteria Detection

Discrete detectors for heat or smoke have been widely used in commercial, residential, and industrial settings. Based on information outlined above, Table 2.4 presents a comparative summary of the general characteristics of these sensors.

Table 2.4: Summary of Detector Characteristics [70]

Detector Type	Response Speed	False Alarm Rate	Typical Applications
Heat	Slow	Low	Confined Spaces
Smoke	Fast	Medium	Open Covered or Confined Spaces
Flame (Light)	Very Fast	High	Open
Species	Fast	Low	Open Covered or Confined Spaces

Response speed and false alarm rates are relative, but are not indicative of specific speeds or rates.

While the individual sensors in Table 2.4 are ranked according to their relative performance in the various categories, it must be noted that all have shown a high degree of susceptibility to nuisance alarms in real use. In particular, the nuisance alarms tend to be caused by aerosols, dusts, non-fire or cooking generated particulates, welding or heat producing operations, humidity and steam, and other sources that are viewed similarly by the detectors as products of combustion. Pfister [70] summarized comprehensive statistics taken from Switzerland which indicated that the false alarm rate for single parameter sensors was nearly 95% of all alarms over a 5-year period. In contrast, after a trial implementation of multi-criteria detectors, the false alarm rate decreased to nearly 50% during the 18 months studied.

The notion of multi-criteria detection is that an alarm is generated based on information over and above the measured amplitude of the signal from a single sensor. As a result, multi-criteria detectors have been developed with associated signal processing algorithms that try to minimize the problem of nuisance alarms. In these systems, sensor signals will be processed using algorithms that examine the signal amplitude, signal time derivative (rate of change), and the frequency of changes for each sensor and across various combinations of sensors. Many studies have performed work examining the use of multiple sensors for fire detection. Some of the earliest work on multi-criteria detection focused on simply combining traditional smoke detectors with CO detectors or other sensors in an effort to reduce nuisance alarms. For example, Milke indicated that the addition of a CO detector could reduce false alarm rates in smoke detectors significantly, however detailed quantitative comparisons were not provided [42, 74, 75]. Such combination detectors were shown to improve overall fire detection rate as well as a reduce the rate of nuisance

alarms. The combinations were then further enhanced via incorporation of signal processing algorithms and development of neural networks, fuzzy logic, Markov Models and other "intelligent" algorithms intended to reduce false alarms while still ensuring timely detection [42, 44, 47, 63, 70, 76–79].

Consistent testing and field experience show that multi-criteria fire detection systems can outperform typical systems consisting of a single sensor [42, 44, 47, 63, 70, 76–79]. The performance improvements are exhibited through successful detection of a wider variety of fire phenomena while simultaneously reducing the number of unwanted alarms [80]. On the other hand, these systems have not significantly reduced the time to detection of a fire, largely because the time to detection still strongly depends on the location of the sensor with regards to the fire. Use of combinations of point sensors means that even the new systems and algorithms used to interpret the sensor data are still based on traditional plume and ceiling jet dynamics as the driving force for transport of soot or heat to the sensor element.

Two potential avenues could lead towards development of improved multi-criteria fire detection systems. The first is essentially an expansion of the multi-criteria approach which combines use of multiple sensors and the concept of sensor fusion. Here, the data from each individual sensor is combined using software and the combined signals are analyzed and interpreted to determine the presence of a fire based on criteria related to the response of more than one of the sensors in the package. While far from proven in real fire situations, in theory this approach could lead to more accurate fire detection through improved discrimination of fire signatures from nuisance signals by incorporation of data from multiple sensors in the decision making process.

The second approach to improved detection relies on the incorporation of intelligent detection algorithms into the sensor data analysis process. Artificial Intelligence (AI) methods (neural nets, fuzzy logic, Markov Models, hierarchical temporal memory) are employed to learn about the environment in which the sensor is placed in order to make better predictive decisions about the presence, or lack of, a fire. While again largely untested in real fire situations, the notion is that enhanced knowledge about the environment will establish a baseline condition from which to make improved decisions during detection of fires.

Additional research is required to advance any of these options. Successful development of detection systems using either of the above strategies requires simultaneous collection and advanced analysis of reliable data from multiple sensor types. In practice, this requires development of combinations of several relatively low cost sensors into a single detector package, development of appropriate systems consisting of sets of low cost sensors tailored to measure a single important fire detection parameter, or the leveraging of existing sensors

that may be used for fire purposes when paired with appropriate algorithms. In support of decision-making and AI algorithms, it is also necessary to systematically characterize key parameters and define fire signatures unique to the evolving environment during a fire. Such determinations will advance current knowledge and methodologies for fire state determination. These must then be aligned with response times and signal levels from a variety of sensors to identify technologies for use in any next-generation multi-criteria fire detection systems.

To date, some developments have been made with regards to detection and fire state determination. Yet, it has been pointed out in state-of-the-art research reviews in each of the last 3 decades that there are various gaps in the existing knowledge base [2, 64, 81–84]. The identified gaps revolve around several key areas: limitations in the current state of the art in fire sensing technology, understanding of physical characteristics and sensor response to those parameters during incipient fire growth, lack of understanding of the variation in signals based on sensor placement, lack of knowledge of regarding non-fire sensor response to fire conditions, and appropriate algorithms for interpretation of gathered sensor data. These gaps provide ample opportunity to advance science in the areas of fire characterization, non-fire sensor signatures, detection algorithms, and multi-criteria sensing systems. This forms a focus of the present research.

2.3 The Potential in Environmental Building Sensors

Fire detection technology for residential, industrial, and commercial environments has remained relatively static as discussed above. On the other hand, the rapidly increasing drive for energy efficiency and sustainability in these environments has driven development of new energy monitoring sensors, building materials, construction techniques, and architecture that focus on energy conservation in order to meet the needs of more energy conscious consumers and owners.

Optimization and improvement in the energy performance of buildings and structures has been shown to be essential and effective in reducing energy consumption and increasing building comfort. To this end, the evaluation of the thermal environment in the structure requires the knowledge of four physical parameters: air humidity, air temperature, mean radiant temperature and air velocity [85]. These sensors are then utilized to best degree in the sensor-rich environment that characterizes a Building Environmental Monitoring System (BEMS), so that a wide range of cost effective new sensors and sensor analysis approaches have also recently become available to potentially leverage for a multitude of purposes. At the same time, the potential benefits to energy conservation of increased

sensing resolution in office buildings has been investigated using computer simulation [86] and it has been shown that increased sensor density can lead to optimization of comfort or energy consumption , or tailoring of conditions to specific rooms or regions [87]. This increased density of BEMS sensors has then led to increased demand for cheaper sensors. Decreasing cost of such sensor networks is in turn increasing the adoption rate. The parameters and their observation, along with other parameters of interest such as light intensity, intuitively lend themselves to use in fire state determination as well [85]. So while currently the BEMS sensors are primarily focused towards energy efficiency and security, the ability to leverage their availability presents a great opportunity for fire state determination. Prior to pursuing these for fire detection, however, work must first be done to understand building sensor response to fire environments and then to work towards optimization of sensor distribution for best fire detection performance. Following this, an appropriate set of combined BEMS and fire sensors could be identified to advance next generation fire detection applications.

In BEMS when light, temperature, and humidity parameters are captured and analyzed on a continuous basis, it has been shown that the environment can be observed and understood from an energy usage perspective and changes can be made to the building operation in response to the observed conditions. For example, lighting and room conditioning may be decreased to lower energy consumption based on areas identified as unoccupied. In the latest BEMS integrations, sensors have been added directly into each light fixture, thus enabling the development of a detailed energy consumption map, Figure 2.4. Moving forward, the ability to leverage these sensors and create maps that could serve as a framework for presenting more complete data sets for fire state determination would be groundbreaking with regards to increased temporal and spatial knowledge of the fire environment.

Monitoring of building systems and conditions via a system of controls and sensors that make up a BEMS [85] is also driving improvements in wireless sensor networks (WSN) within existing infrastructure, creating the opportunity for monitoring and control of any structure through a distributed network of sensors. The increasing number of communication protocols (ModBus, M-Bus, Ethernet, Cellular, ZigBee, WiFi, BACnet, and others [88–92]) being implemented into sensors and communications demonstrates the rapid development of these systems. At the same time, however, there is also a lack of uniformity in development and adoption of a universal standard for sensor to sensor and sensor to base communications. This suggests that, even with the current state of adoption of BEMS, similar complications will need to be overcome during conception of new systems intended for potentially different life safety applications.

Computer simulations, nodal energy models, and CFD are often utilized during the initial design and evaluation of the performance of building systems. These tools are

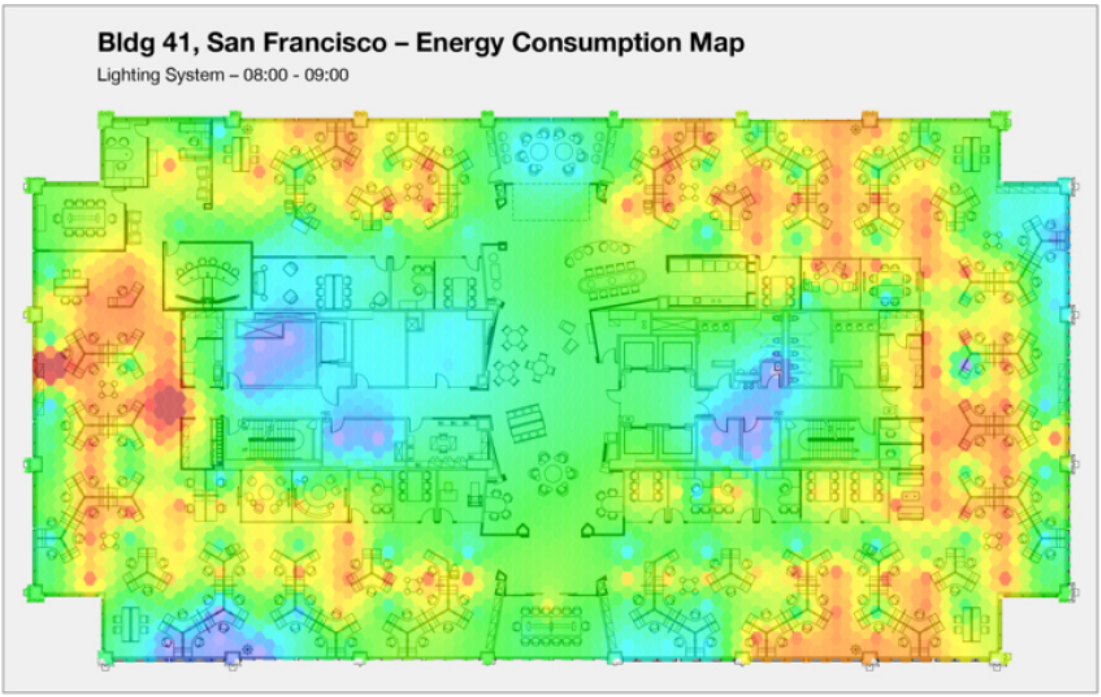


Figure 2.4: Sample building energy consumption map [94]

rarely used after the building is occupied during continuing operations. More recently however, this is beginning to change due to emerging methodologies that facilitate seeding such models with real time data gathered from installed sensor networks. This, paired with condition assessments and decision making logic, greatly enhances the overall utility and performance of BEMS. The process, known as Dynamic Data-Driven Simulation and Analysis (DDDSA), has not been widely utilized in the past due to the significant quantities of high fidelity data required in order to make well-informed decisions [93]. The increased usage of coupled BEM and WSN systems; however, could well enable use of DDDSA to transition from a purely theoretical exercise into paradigm shifting, real-world applications such as faster than real time fire forecasting, structural integrity assessments, and occupant egress assessments.

Thus, while the building industry at large has begun to study and implement WNS and BEMS for environmental and energy control and monitoring functions, there has been little published research done with regards to evaluation of the use of similar technologies for advanced fire detection purposes. In order to evaluate the potential for building sensors to be leveraged for fire detection purposes the response of the sensors to a fire environment

needs to be characterized and appropriate algorithms need to be developed to properly evaluate the data in order to yield useful information.

2.4 Detection and Monitoring Algorithms

As discussed above BEMS provide a data rich environment; however once the sensor response to the fire environment is collected it must be understood and analyzed to make it useful. This process requires that appropriate algorithms be developed for data processing and information transfer. Such algorithms may be largely broken down into rule-based systems and data-driven systems. The anticipated outcomes of rule-based systems are defined by user-imposed sets of rules and logic statements (if-then). These can often contain limiting assumptions about system behaviour which, in turn can result in reduced performance and can be difficult to modify if there are changes to the underlying structure of the data that is being analyzed. While rule-based systems can be simple and efficient for implementing basic logic arguments ("if this than that"), as a system becomes more inherently complex, the rule structure can become less flexible and increasingly hard to decipher, and may need to contain numerous exceptions to the rules to account for the introduction of new data [95].

Alternatively, data-driven systems use a different approach that relies primarily on the definition of relevant data and leaves the "rule-making" up to the machine through a learning process that relies on the raw data that is believed to hold at least the majority of relevant information related to system behaviour. Once a set of key features of a system have been defined (i.e. increase in temperature and humidity), the formulas that use these features to predict system outcomes are learned automatically by the algorithm. For this to work, typically the algorithm needs to have access to a multitude of data samples covering ranges of system behaviour and labeled with the desired outcomes, so that it can properly adapt to, and develop the appropriate relationships. Essentially, the algorithms learn what combination of sensor signals and information constitutes a fire by being "exposed" to large data-sets of fire and non-fire scenarios and identifying patterns that represent fires while also recognizing signals that are representative of non-fire conditions, including potential nuisance sources. The relationship between the actual fire state, the observed state, and the modeled state is shown in Figure 2.5, where the modeled state ideally is representative of the actual state but relies on the sensor data to make that interpretation.

The largest set of studies that examined various data for inclusion in such next generation fire detection algorithms was conducted under the auspices of the US Navy [47, 49, 96]. However, these studies still focused primarily on use of standard gas component analysis,

temperature, thermal imaging, and visual signals for the detection of the fire. Using a large data set that was collected, they applied several data classification schemes, namely Principle Component Analysis, Hierarchical Cluster Analysis, and Probabilistic Neural networks [76, 97, 98] in order to categorize the various signals and develop methods to detect a fire whilst minimizing false alarms. In other work, the approach has been to adopt a maximum value for each parameter of interest with a cascading system whereby threshold values are set for flaming, smoldering, nuisance, and ambient conditions. If the minimum threshold values are not met for each sensor signal in a given system, the detection algorithm cascades down to the next possible fire state [98].

The adaptive learning that is possible through application of machine learning techniques allow algorithms to be continuously modified as additional information is gained about a range of conditions (i.e. normal operation, false alarm, actual event) or a range of characteristics of different fire states. Additionally as sensors are added or removed from the system the algorithm can be trained to adapt to these changes. This is potentially extremely powerful in the present context since data can then be obtained from numerous real-world locations over time and constantly integrated into the algorithms to improve the FSD response.

To capitalize on the potential of data-driven methods for fir state determination (FSD), appropriate learning algorithms have to be determined and implemented for use with the sensor data discussed above. Some of these are discussed in the following sections.

2.4.1 Continuous Learning Algorithm

This section outlines the concept of continuous learning algorithms for the identification of anomalies and linking them to potential presence of a fire. In this context, an anomaly is defined as a point in time where the observed behavior of the system, as represented by the data, is unusual and significantly different from past behavior. The anomaly may be temporal if the value is within the norm regarding magnitude but occurs at a time outside of the typical times when a similar observation would be made. Alternately, it may be spatial if the observed value falls outside of the normal range for a given location. Either situation indicates a condition that requires more investigation to determine whether it is representative of a fire. This type of approach is being used more regularly for BEMS and other uses [85, 95]. For comprehensive FSD, it is desired to be able to leverage the increasing number of sensors and real-time data that is available in building environments and use it in an algorithm designed to detect signal anomalies that relate to a fire.

Although not commonly used in fire safety applications, in more general terms the use of

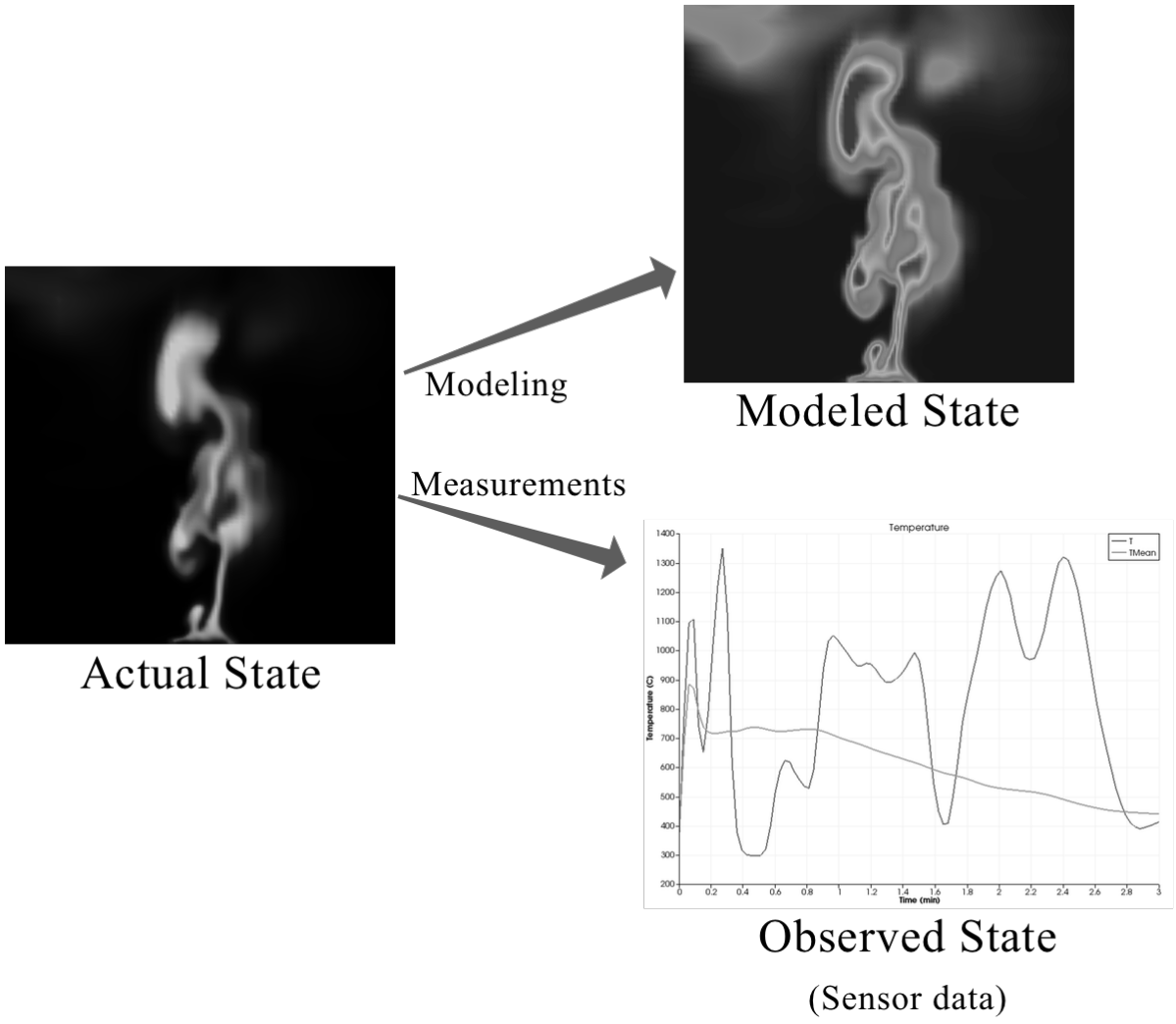


Figure 2.5: Fire, sensors, and modeling relationship

continuous data-streams to identify anomalies have very practical and useful applications, especially if additional information on the quality of the data or size of the event is also available. The detection of an anomaly in a real-time data stream is particularly challenging though as the system must be designed to collect and process the data and output a meaningful decision in real-time, rather than making repeated passes through existing data sets to come to an informed decision. In the case of FSD for either fire detection or monitoring, the first challenge relates to the quantity and complexity of data that has to be collected from an entire network of sensors. Due to this, there is also little, if any, opportunity for human intervention during the process. As a result, a FSD system will optimally have to operate in an unsupervised environment in which there is no necessity for manual manipulation of any of the sensor parameters. For this, then, a number of network and machine learning algorithms suited specifically to unsupervised anomaly detection were examined.

The first category of potential models investigated were those based on neural networks and machine learning. Most neural network and machine learning models need to be trained in "batch" mode, which requires copious amounts of relevant data to be available at the beginning of the training process [99]. Further, the systems are often trained against this data while they are off-line in order to minimize error. For real-time anomaly detection in a system where the inputs may be changing both temporally and spatially this approach is sub-optimal. The preferred approach would not rely on a large initial data set, which in the case of fires is not available, and further, would have the ability to train the system "live" and continuously in time and space. In order to accomplish this, the system and sensors that compose it must be able to continuously learn about their environment and appropriately modify the statistics regarding observations about that space in order to continue to make accurate predictions about the fire state.

Chandola et al.[100, 101] surveyed and summarized numerous anomaly detection algorithms and fit them into three primary categories:

- Sequence-based anomaly detection: Detecting anomalous sequences from a database of test sequences.
- Contiguous subsequence-based anomaly detection: Detecting anomalous contiguous subsequences within a long sequence.
- Pattern frequency-based anomaly detection: Detecting patterns in a test sequence with anomalous frequency of occurrence.

Based on the definitions of each category, the sequence-based anomaly detection category seems to fit best with fire detection. Many of the models that fit into this category

(Markovian, Hidden Markov, Window based, Neural Network, and Kernel based) have been used previously for multi-criteria fire detection, albeit not in a continuous learning format [99, 102, 103].

Rose-Pehrsson et al. [47] describes using a Neural network with multiple sensors to accurately detect a fire while minimizing nuisance sources, however the algorithm was fed data, and was not readily adaptable to dynamic data sets and was not able to account for temporal changes in signals.

Cui et al. [104] discussed a number of methods for continuous learning and evaluated their ability to accurately detect anomalies when provided with a changing data stream. The paper covers hierarchical temporal memory, autoregressive integrated moving average, feedforward neural networks, online sequential extreme learning machine, recurrent neural networks, and echo-state networks, as applied to sequence prediction problems with both artificial and real-world data. Cui concluded that the hierarchical temporal memory (HTM) model achieved comparable accuracy to other state-of-the-art algorithms while offering numerous additional benefits stating: *"The model exhibits properties that are critical for sequence learning, including continuous online learning, the ability to handle multiple predictions and branching sequences with high order statistics, robustness to sensor noise and fault tolerance, and good performance without task-specific hyper- parameters tuning."*

It must be cautioned however, that while learning algorithms are presently an area of significant research across many disciplines, most of this research lies well outside of applications to fire state determination. As such, there is a need to further explore and ensure the applicability of various emerging data-driven approaches to fire state determination and to identify, if possible, an optimal approach on which to base future detection systems.

2.5 Conclusions and Summary of Knowledge Gaps

The literature review has indicated that there are a number of areas in which additional knowledge is required in order to advance the state of the art in fire state determination. These gaps in existing knowledge establish the need and provide an opportunity to explore the topics examined in this research. The key knowledge gaps that have been identified are summarized as follows:

1. Characterization of the fire environment using "non-standard" fire sensors

2. Characterization of "background" signals for comparison with those observed in the fire environment

3. Analysis of fire growth based on sensor signals

4. Appropriate algorithms for detection using sensor data

5. Integration of building or other sensors into fire detection/monitoring systems

Based on these identified gaps the present research focuses on several key areas

1. Identification and detailed measurement of fire characterization parameters

2. Testing of existing building and comfort sensing units in fire environments and evaluation of observed parameters

3. Determination of sensors that work for development of an ideal multi-use sensor block and development of block

4. Testing of the developed sensor block in various fire environments to obtain new data related to focus areas 1 and 2

5. Development of potential algorithms for fire state determination

These topics are explored in the following chapters beginning with an evaluation of commercial sensors to determine whether they are suitably able to characterize a fire environment and provide information regarding the fire state.

Chapter 3

Commercial Sensors

From the literature review it is clear that while BEMS systems have gained increasing use in commercial, industrial and residential applications, there exists a limited quantity of information on the potential for integration and usage of commercial environmental and comfort sensors into present fire detection paradigms. The overall density of environmental and comfort sensors far exceeds that of standard fire detection devices and thus may be useful in the early detection and monitoring of the fire state. However, there exists a fundamental lack of understanding of how the sensors respond, and what if any useful information may be obtained from them, in a fire environment.

The first objective of this phase of the research was to identify suitable candidate commercial sensors or sensor packages for testing and to evaluate the characteristics of their response under controlled environments and fire scenarios in order to establish information related to detection range, accuracy, and response time (lag) in each situation. The following sections discuss the commercial sensors that were selected followed by the results of the commercial sensor testing.

3.1 Commercial Sensor Selection

A great number of sensors exist and an ever increasing number are entering the market as the decreasing price and ubiquity of building and environment monitoring systems make market conditions ripe for their use in a wide variety of applications. Individual or corporate desire to learn more about home and workplace environments and to reduce operating costs, as well as the rise of a "maker" mentality, has helped drive an increase in both the

availability and range of commercial sensors on the market while simultaneously lowering the price. Available sensors range in size, form factor, parameters measured, suitability for use in different spaces, as well as their level of integration into a system. For the purposes of this study, it was initially desired to utilize commercial sensors that were readily available, had an installed user base (to ensure that they were representative of at least a subset of the installed market), and provided access to the data from the sensor blocks in a suitable format for analysis.

Selection of a sensor for use in a particular space is influenced by a number of factors, including the type of space and its function, the foot print and ceiling height of the space, and the specific sensed parameters of interest. Wall switch sensors are typically used for smaller rooms, ceiling sensors typically cover larger areas, while corner/wall sensors are often chosen for corridors or areas with high L/D ratios. Depending on the type of sensor and usage, the same sensor may be appropriate for multiple applications. Thus, ideally the chosen sensors would also be ones that could be installed in each of these locations.

While there were a variety of sensor block products (XBEE, Simms, Embedded Data Systems, and others) that were investigated for use, the sensor blocks chosen for this study were off-the-shelf sensor blocks developed by Embedded Data Systems (EDS) and shown in Figure 3.1. These blocks contain sensors to measure temperature, humidity, light intensity, and pressure (THLP) simultaneously and are able to transmit the signal and data wirelessly via proprietary software to a computer in real time. The sensors communicate over the 2.4GHz band to an EDS Meshnet controller which transmits and receives data from each sensor block over a closed wireless network. Each sensor block acts as a repeater in the mesh network which helps to ensure a strong communication signal between each sensor block, the controller, and the receiving computer. A typical screen shot from the sensor block is shown in Figure 3.2. As illustrated, all of the information from the sensors could be monitored live on a computer screen during testing, and could also be downloaded in csv format for more detailed analysis. The product and company had an installed user base and an active community forum for discussion. Furthermore, the sensor blocks were relatively inexpensive (<$100) and thus could be installed in numerous locations and tested to failure in fire environments but also readily replaced if required.



(a) Outside of EDS Block

(b) EDS PCB

Figure 3.1: EDS Sensor Block

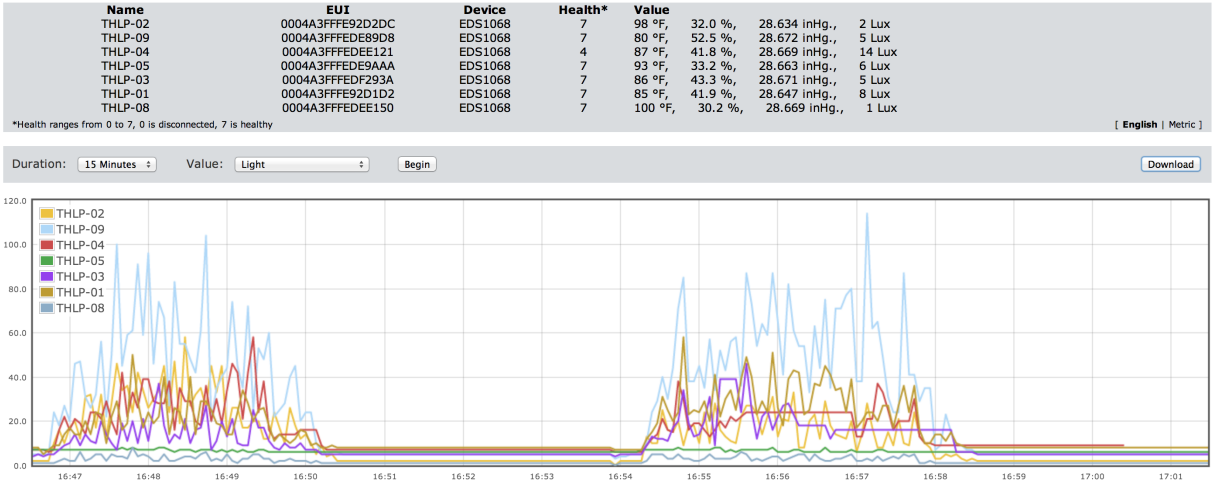


Figure 3.2: Screen capture of real time monitoring from multiple THLP sensors during two fire experiments

The EDS sensor blocks and their accompanying software allowed for a high degree of customization regarding data collection. The communication protocols and infrastructure are built in and the ability to communicate wirelessly with one or more sensor blocks

greatly simplified the data transmission, collection, and sensor installation process and ensured that data could be collected throughout a test up until the time of potential sensor failure.

3.2 EDS Sensor Characterization

After acquisition, the EDS sensor blocks were subjected to a series of tests to characterize their response to a range of conditions in various environments. In particular, the aim of these tests was to establish speed and accuracy of each sensor response to the parameter(s) that they measure. The operational limits and basic sensor information is provided in Table 3.1 as received by the manufacturer with full details provided in Appendix E.

Table 3.1: Information and operational limits of the EDS Sensor Blocks

	Minimum	**Typical**	**Maximum**	**Units**
Temperature Range	-40	-	125	$^{\circ}C$
Temperature Accuracy	-0.5	± 0.25	+0.5	$^{\circ}C$
Temperature Resolution	-	0.0625	-	$^{\circ}C$
Relative Humidity Accuracy	-3	-	+3	%RH
Operating Humidity	0	-	90	%RH
Pressure Range	300	-	1,100	hPa/Millibar
Pressure Accuracy	-2.5	± 1	+2.5	hPa/Millibar
Light Measurement Range	0	-	65,535	Lux
Light Sensitivity	-20	-	+20	%

3.2.1 Small Scale - Oven Temperature Testing

The first phase of testing of the sensor reponse was conducted in a Cole Parmer StableTemp Oven to evaluate the thermal response, repeatability and accuracy of temperature values measured using the environmental sensors in comparison with thermocouple measurements. Seven EDS sensors were placed on a rack in the middle of the oven with their sensing elements oriented in various configurations. Some sensors were placed either up (i.e. with the sensor face in the -Z orientation simulating a ceiling mount) or down, and others were either open (the mounting plate was removed) or closed as shown in Figure 3.3. When viewing the results Figure 3.5, a sensor designated as THLP-08 OU would indicate

that **T**emperature**H**umidity**L**ight**P**ressure Sensor 08 was oriented in the Open and Up orientation. Table 3.2 provides a description of the orientation of each sensor block in the oven testing. THLP-06 was kept outside of the oven as a control sensor block.

Table 3.2: Orientation of Sensors in Oven Testing

	Open/Closed	**Orientation**
THLP-01	Open	Up
THLP-02	Closed	Down
THLP-03	Open	Down
THLP-04	Open	Up
THLP-05	Closed	Down
THLP-07	Open	Down
THLP-08	Open	Up

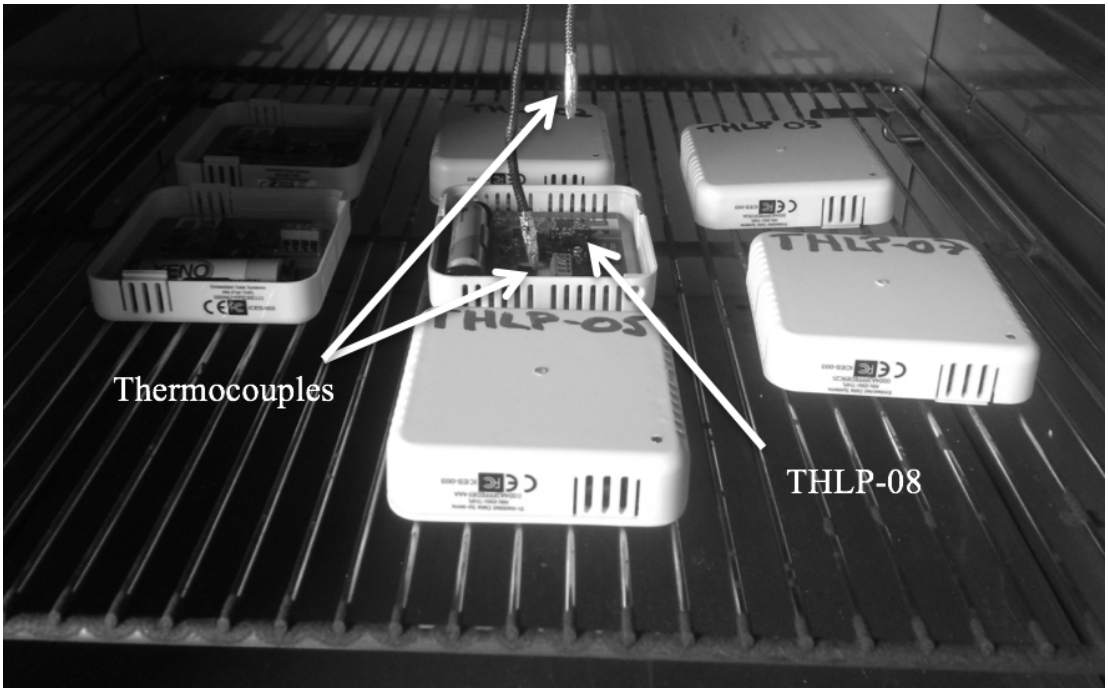


Figure 3.3: Location and orientation of EDS sensors and thermocouples in oven

The oven was sealed but contained sufficient venting to prevent a pressure buildup and

no light was created during this oven experiment, so temperature was the primary variable to be measured. Thus, signals from the temperature sensors in a number of EDS blocks were examined to determine the response and lag time of the temperature sensors in a controlled thermal environment.

The oven temperature controller was set to heat the oven to a maximum of 55°C. The EDS sensors were placed in the oven and set to measure the oven the temperature as it increased. Thermocouples were placed in the oven centered above THLP-08, the central sensor in Figure 3.3, to monitor the temperature and compare with the signals from the EDS sensors. The lowest thermocouple was placed within the open sensor housing adjacent to the embedded EDS temperature sensor in order to get an accurate reading of the temperature at that sensor. Additional thermocouples were spaced vertically in increments of 2.5 above the sensor block to record the overall oven temperature throughout the test. A final thermocouple was placed adjacent to the oven thermal controller in order to verify the temperature observed at the controller and shown on the external oven display.

Figure 3.4 depicts measured temperatures during the early stage of the oven heating. At 120 seconds the oven was turned on and the thermocouple adjacent to THLP-08 began to respond to the resulting temperature increase in approximately 35 seconds, while the EDS sensors begin to observe the change after approximately 55 seconds. The observed rate of rise is also different for a number of the EDS sensors in comparison to the thermocouple, such that a simple time shift does not account for the temperature differences. The EDS sensors that were "closed", namely THLP-02 and THLP-05, exhibited a thermal lag that is primarily associated with the mounting plate and the resulting delayed entry into the sensor block. When these sensors were configured with the mounting plate removed they exhibited identical behavior to the other EDS sensors. In all cases there was some observed lag in temperature observed, which is discussed below. This lag is assumed to be due to several factors including different thermal measuring techniques, the size and location of the sensor on the EDS boards, and the thermal mass associated with the EDS unit itself in comparison to the thermocouple.

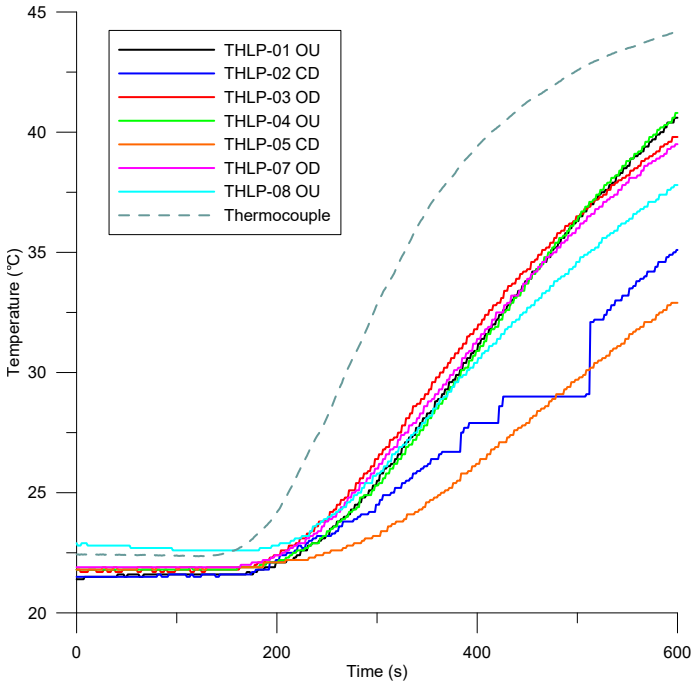


Figure 3.4: Zoomed in temperatures from EDS sensors and thermocouple during early heating period

Two minutes of baseline data was obtained prior to turning the oven on, after which the oven temperature increased at an approximate rate of 10°C per minute, as measured by the thermocouple at the oven thermal controller. The temperature rate of rise at the location of the EDS sensors was measured as 1°C per minute during the first minute of heating and then increased in a linear fashion to approximately 5°C per minute during the 3rd minute of heating. It continued increasing at this rate until hitting an inflection point at approximately 90% of the maximum temperature at which point the rate of rise decreased significantly until a near steady-state temperature was observed.

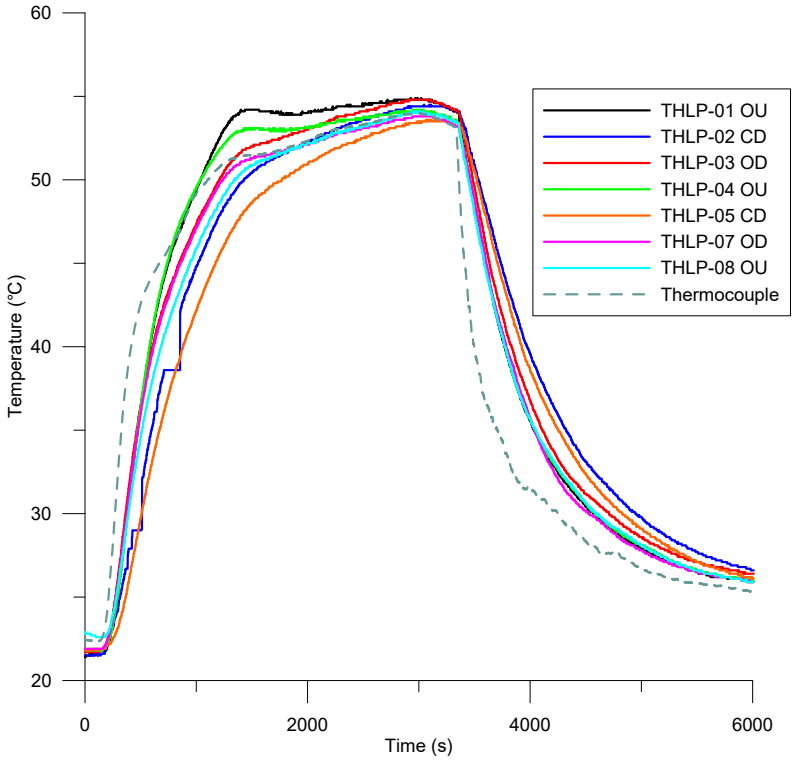


Figure 3.5: THLP and Thermocouple data from oven test

Temperature time traces from each THLP sensor and the thermocouple placed in the enclosure of EDS sensor THLP-08 are compared in Figure 3.5. As can be observed, the trends in the data measured by the EDS sensors are similar to those seen in the thermocouple data, though a lag in response is observed between all of the EDS sensors and the thermocouple. This lag occurs for all sensors regardless of orientation and appears to be further affected by whether the sensor mounting plate is in place.

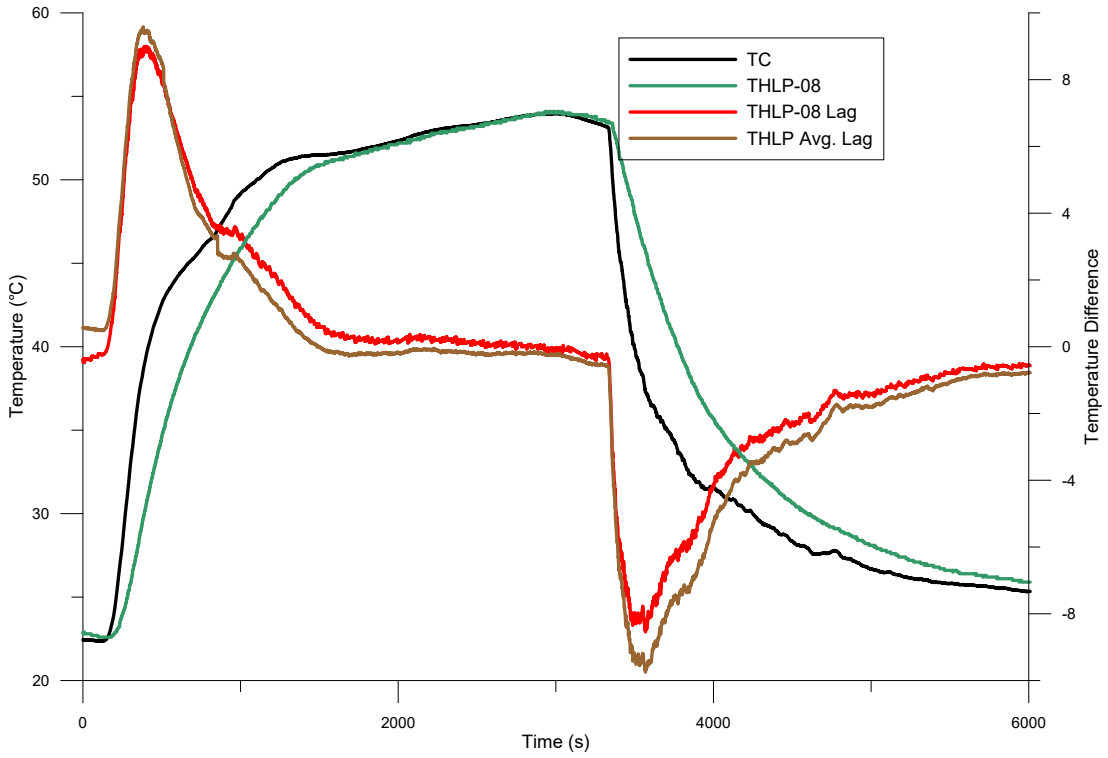


Figure 3.6: Temperature and ΔT between thermocouples and sensor

Figure 3.6 shows the time traces of measured temperatures from THLP-08 and the thermocouple inside the THLP-08 sensor enclosure. This data is overlaid with plots of the calculated difference between the temperature measured by EDS sensor THLP-08 and the thermocouple inside the THLP-08 sensor enclosure, as well as the calculated temperature differences between the average of the values of temperature measured by all EDS sensors in the oven and that measured by the same thermocouple. As can be observed from the figure, temperature differences are magnified during the rapid ramp up and cool down periods of the oven, with a maximum difference of approximately 25% (8°C) observed during the ramp up period. The lag data based on the average of the sensor temperatures exhibit several noticeable differences from the lag seen between the THLP-08 sensor and

thermocouple. This further supports the conclusion that sensor orientation and sensor to sensor variation play a role in the measured values. The data also indicates that the accuracy of the temperature values measured by the sensors is quite high when compared to the thermocouple measurements, as the steady state temperatures measured by the EDS sensors converge to the same value as measured by the thermocouple after some period of time. The 55°C oven set point was nominally the temperature observed at each sensor at steady state as well as at the thermocouple. Though not plotted here, the precision and repeatability of measurements are also high for similar tests.

The preliminary data indicated that the thermal sensors included in the EDS sensor blocks exhibit a fair degree of responsiveness to changes in ambient temperature. On initial examination at least, the orientation of the sensor/sensor enclosure combination has an impact on responsiveness, with the Closed Down oriented sensors demonstrating the greatest lag in response to changes in temperature. This served as the justification for additional testing, and at a larger scale, aimed toward determination of potential impacts, if any, of the enclosure/sensor orientations on fire detection and monitoring for the temperature and other embedded sensors. It is important to note that during a fire, in particular the growth stage, that the conditions in the space will not be steady state and that sensor lag may play a critical role. However, the initial response of the sensors do not show a significant delay from that of the TC and then follow a similar, albeit delayed response.

3.2.2 Small Scale - Box Testing

Building from the oven testing, a number of small scale experiments were performed in a $1m^3$ cubic test enclosure built from oriented strand board. The test enclosure is depicted in Figure 3.7 and Table 3.3 contains a summary of test conditions in terms of illustrating the sensor orientation and position. This testing examined the signals and response of the various sensors to several different fire sources intended to represent a variety of incipient fires and also allowed for parameters in addition to temperature to be examined.

The fuel packages used in this evaluation included a set of tea light candles (varying from 1-4 burning simultaneously) meant to represent a matrix of distributed very small flickering flames, a 0.00785 m^2 ($\sim$3.25 kW) pool of ethanol typical of a low sooting, low luminosity fire just after ignition, and a 0.00785 m^2 ($\sim$4 kW) pool of heptane typical of a more heavily sooting, luminous fire source soon after ignition.

Table 3.3: Location of Sensors in Box Testing, all dimensions given from upper rear left corner of box

	Horizontal (+X)	**Horizontal (+Y)**	**Vertical (-Z)**
THLP-03	50 cm	50 cm	0 cm
THLP-04	0 cm	0 cm	0 cm
THLP-05	100 cm	100 cm	0 cm
THLP-07	100 cm	20 cm	25 cm
THLP-08	0 cm	35 cm	50 cm

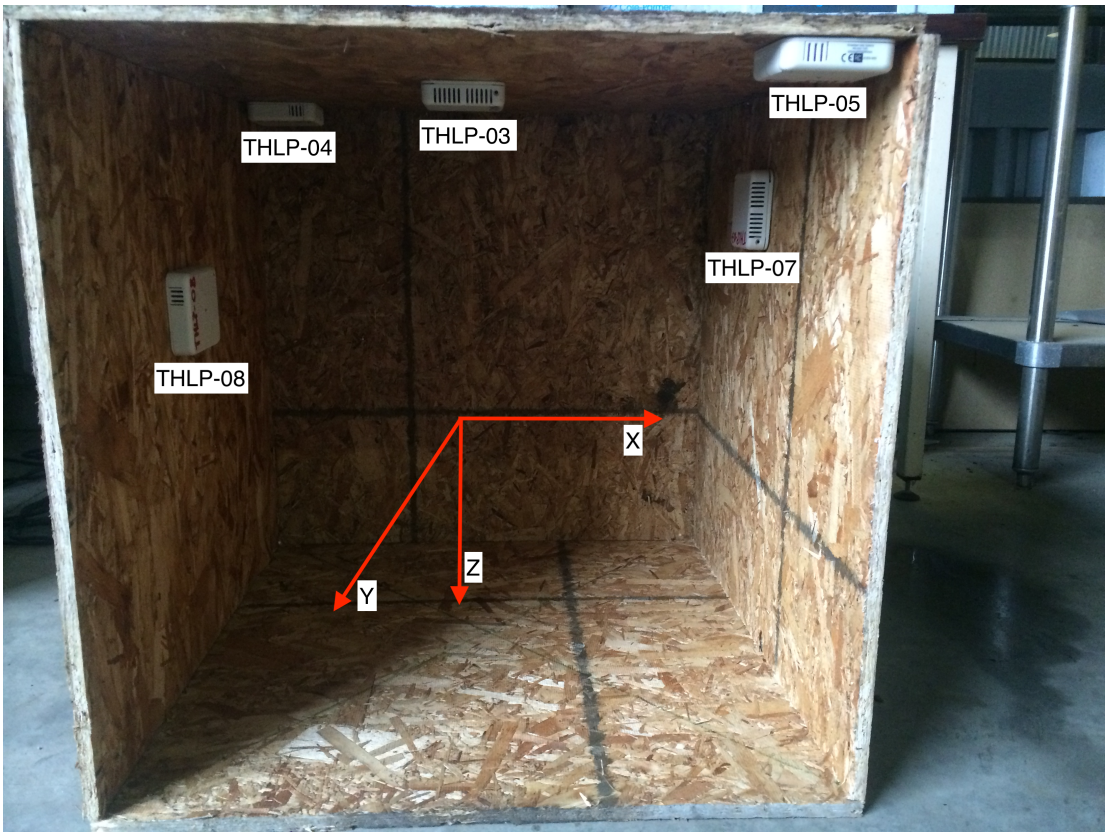


Figure 3.7: Interior of cube with EDS sensors

The tea light fires produced very nominal changes in the observed conditions in the enclosure, with slight rises in temperature and humidity observed over an extended duration

(30+ minutes). The change in conditions observed likely represent a reasonable lower limit of sensitivity of the sensors to fires the size of a candle flame and a slowly increasing change of environment as might be expected for a smoldering or small continuous flaming fire. The ethanol and heptane pool fires however produced more interesting results as discussed below.

Ethanol Fires

The ethanol pool fires produced interesting, and somewhat unexpected responses in both the thermal and humidity signals, while, as anticipated, the light sensor registered an almost non-observable increase in signal level from 0 lux to a maximum of 20 lux. The observed minimal increase in light level was expected as ethanol is extremely clean burning and produces only a faint blue flame with minimal luminosity. On the other hand, the temperature and humidity data merit some additional discussion.

The fire was ignited at 215 seconds into the recorded data and, as can be observed in Figure 3.8, the THLP-08 temperature and humidity sensors immediately began to respond and measure noticeable changes in temperature and humidity levels in the compartment. In particular, measured values of humidity increased very quickly and the sensor indicated 100% relative humidity in less than 30 seconds after ignition. Temperature data also increased but at a much slower rate than captured by the relative humidity sensor and reached a peak of 85°C. At approximately 430 seconds into the test, vertical line shown on Figure 3.8, the compartment was opened to allow some air entrainment. This led to the initial significant drop in humidity seen in the plot. The door was fully removed 45 seconds later, resulting in a subsequently more gradual decrease in the humidity time trace. This venting was initially done so as to limit the peak temperatures that would be seen by the sensors in the compartment during initial testing. Due to the interesting results, repeat tests were conducted and yielded nearly identical results.

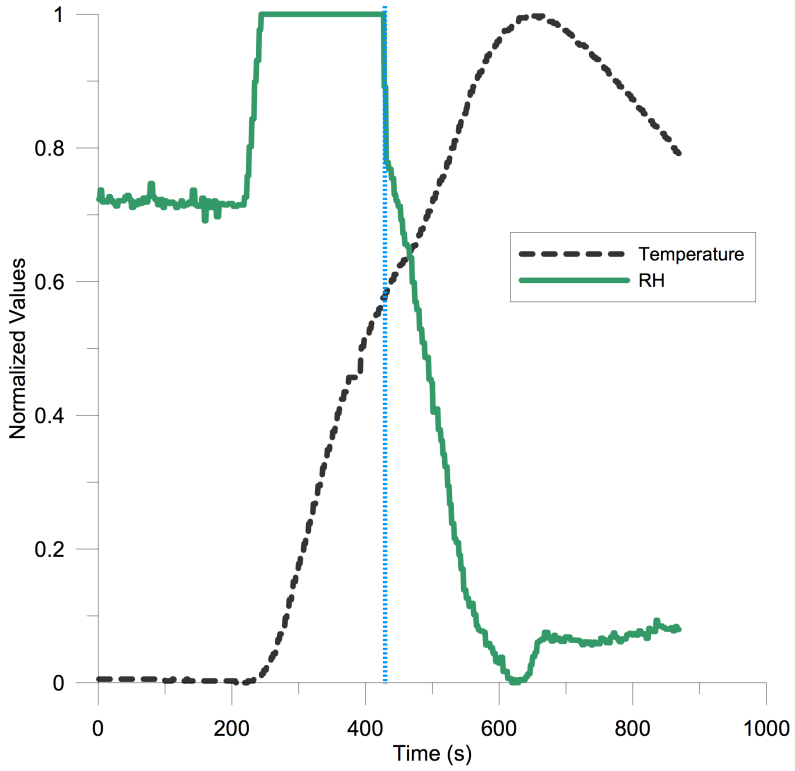


Figure 3.8: Normalized Humidity and Temperature results from Ethanol pool fire small-scale test

The initial increase in relative humidity after ignition is to be expected, as the combustion of ethanol under well ventilated conditions primarily produces H_2O and CO_2. Early in the fire and without ventilation in the compartment, the water vapor produced by combustion drives the observed increase in relative humidity since heating of the compartment environment is not sufficient to counteract the water being produced by the combustion process. When the door is opened, combustion products escape from the volume and fresh exterior air is entrained into the compartment and mixes with the combustion products. Simultaneously, the fire continues to burn and produce heat which dries out the volume, resulting in a reduction in relative humidity to values below the ambient conditions mea-

sured at the start of the test. The fact that these observations, and thus processes, are repeatable is of interest since the rate of change of relative humidity is significantly higher than the rate of change of temperature early in the fire and thus may provide a good initial indicator of an environmental change that is indicative of a fire. Further, it may be possible to scale and use the data related to decreasing relative humidity to indicate dynamic changes in the ventilation conditions in a fire compartment (i.e. a window or door opening as a result of breakage or human/mechanical intervention) during a fire as well.

Heptane Pool Fires

The heptane pool fire tests resulted in very similar observations as those from the ethanol tests with respect to signals from both temperature and humidity sensors. As would be expected, there are differences in the observed light levels from fires of ethanol versus heptane. Differences and similarities in the EDS sensor signals from the two fires can be seen through comparison of the representative data for THLP-08 for heptane presented in Figure 3.9 relative to that for ethanol in Figure 3.8. As in the ethanol fires, the humidity data sensed in the compartment with the heptane fire rapidly increases to 100% right after ignition while values of temperature increase much more gradually. The humidity signal again drops rapidly when the compartment door is initially opened and ventilation is allowed, while measured peak temperatures continue to increase slowly until the fuel burns out.

Values of light intensity from the luminous heptane fires are presented as functions of time in Figure 3.10 for five sensors located in different positions in the compartment. Peak values approached 300 lux, 15 times higher than those measured from the ethanol fires. This is due to the much higher soot yield in heptane fires when compared to ethanol fuelled fires. The presence of soot results in a higher radiative fraction and therefore a much more luminous flame.

As can be observed in Figure 3.9 and Figure 3.10, the EDS light sensors register the increase in light intensity from the heptane fire instantaneously after ignition of the fuel and prior to the response of either the humidity sensor or temperature sensors to the presence of a fire. This is consistent with the fact that electromagnetic (EM) waves travel very quickly, so under normal circumstances, detection of changes in EM radiation should only be limited by detector response time. From this testing, as well as through separate examination of their response, the EDS light sensors appears to register changes in intensity effectively instantaneously. This rapid response, with associated ability to support very high sampling frequencies, facilitates observation of the unsteadiness of the flame which is indicated by the variations in sensor output values shown in Figures 3.9 and 3.10.

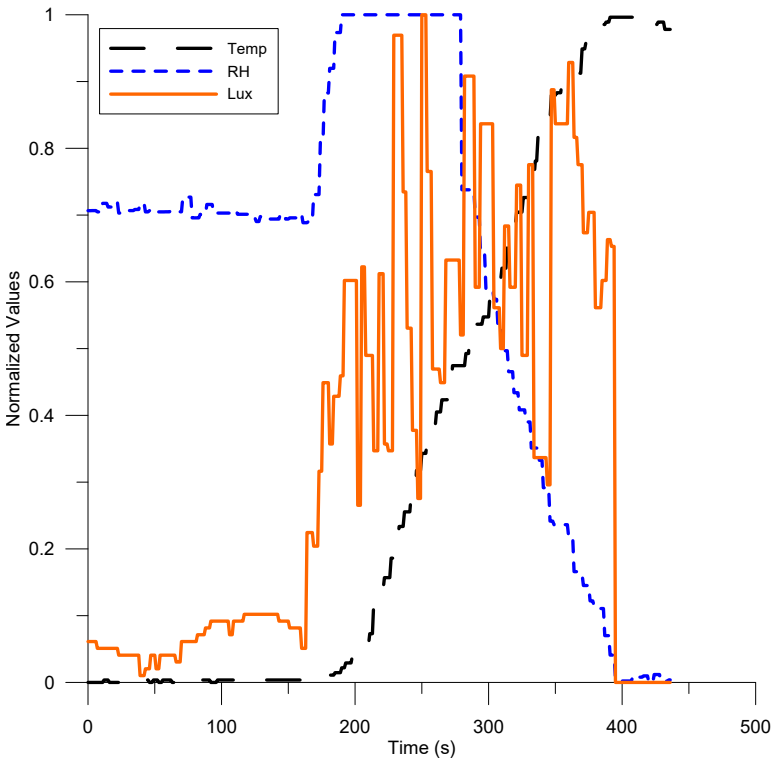


Figure 3.9: Normalized Light, Humidity, and Temperature results from Heptane pool fire box test

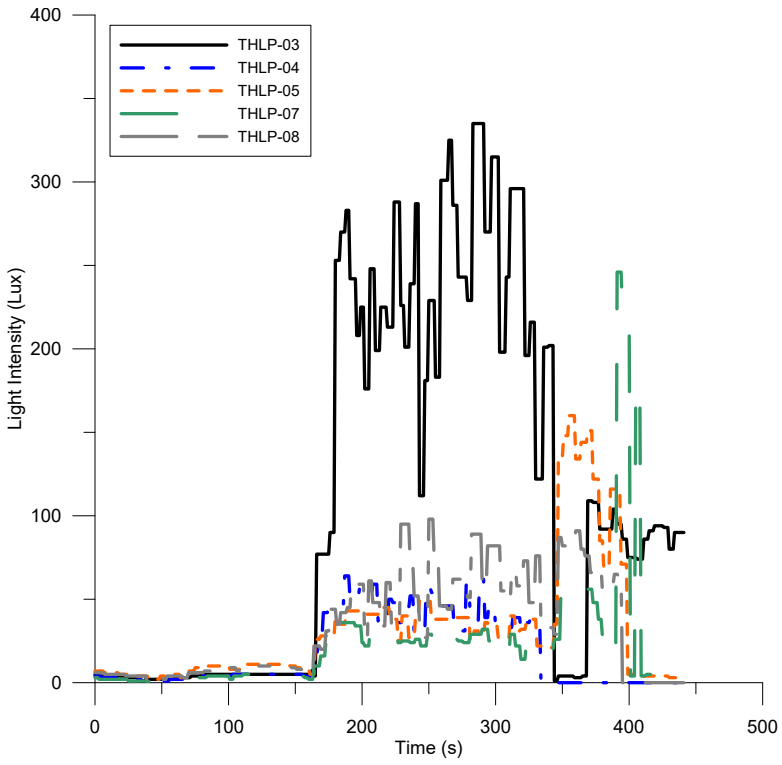


Figure 3.10: Variation in light intensity from Heptane pool fire box tests

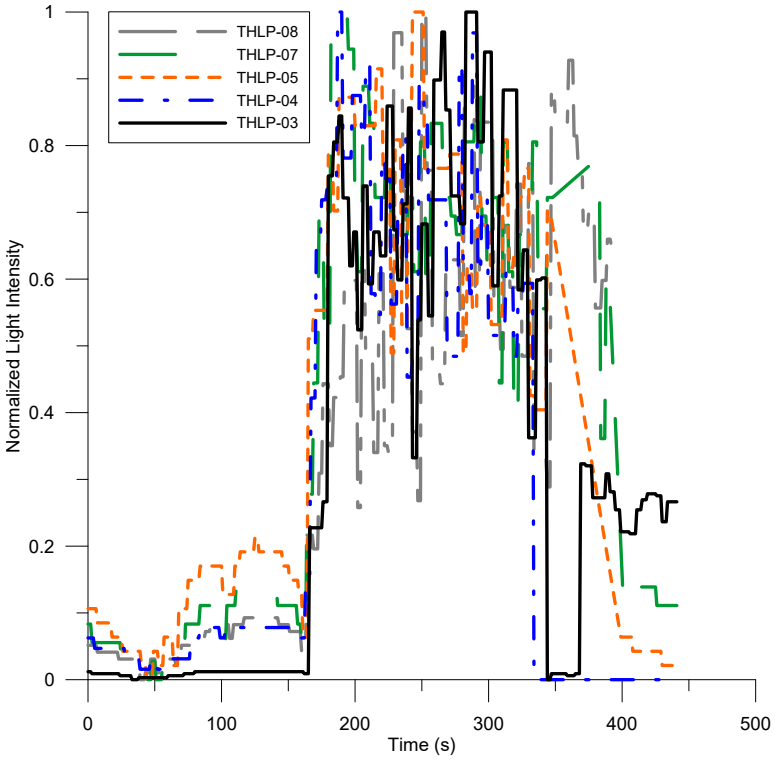


Figure 3.11: Variation in normalized light intensity from Heptane pool fire box tests

As may be observed in Figure 3.10 and Figure 3.11, the measured light intensity can vary significantly depending on the location of the sensor within the box. This is because the light sensors are integrating sensors and therefore measure the cumulative light that reaches the sensing element from any source, which includes not only direct light from the fire but also any reflected light from any other surfaces within a direct line of sight of the sensor itself. For example, sensor THLP-03 measured the highest light intensity in these tests. This is because it was mounted on the ceiling above the fire so that the full fire and any light reflected onto the floor of the compartment was within the field of view. Sensors THLP-04 and THLP-05 placed in the corners and thus further from the plume and fire source measured lower levels of light intensity while THLP-07 and THLP-08 which were located lower down on the wall were oriented tangential to the fire plume and similarly observed reduced light intensity levels. Independent of location, however, due to their virtually instantaneous signal response, each sensor immediately records the change in light level due to ignition of the fire, as well as conveying very similar trends in the unsteadiness of light levels thereafter. Also of note was that sensors located in similar positions and thus affording nominally the same field of view yielded similar intensity levels as shown in Figure 3.12. In fact, when the light intensity values are normalized according to Equation (3.1), the trends in response are nearly identical as illustrated in Figure 3.11.

$$I' = \frac{I_i - I_{min}}{I_{max} - I_{min}} \tag{3.1}$$

It is of interest to further examine the measured values of relative humidity sensed by the EDS sensor blocks located at various positions within the compartment as well. These are summarized in Figure 3.13 which shows the variations in relative humidity signals observed depending on location of the sensor. While most sensors did begin to detect the initial increase in relative humidity in the box at approximately the same time and thereafter registered values that increased quickly to 100% relative humidity, the sensor located at the rear of the box, THLP-04, signalled only a very small initial increase in relative humidity with subsequent values that never reached 100%.

Although not plotted here, temperatures measured by sensor THLP-04 also are significantly lower than those detected by the EDS sensor blocks at the other locations. Through post test analysis, the apparent damping of the relative humidity and temperature signals from THLP-04 was determined to be due to the orientation and placement of the sensor block. Time varying compartment air could not readily enter the sensor casing, so changes in ambient conditions were not registered, impacting determination of both temperature and relative humidity. A similar damped response was observed for all of the tests conducted in the box. In contrast, the light sensor in THLP-04 measured similar lux levels to

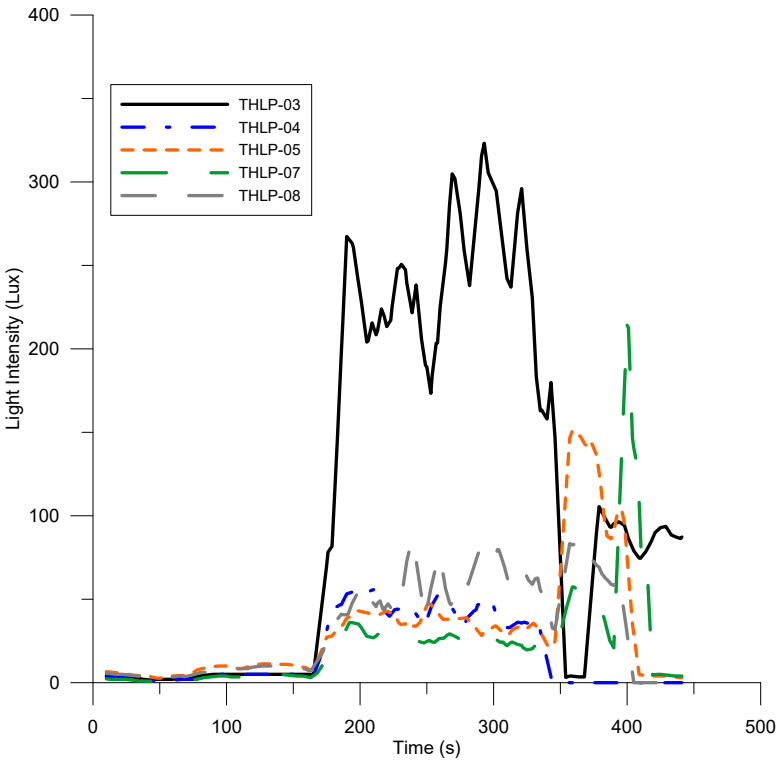


Figure 3.12: Average light intensity observed over box tests

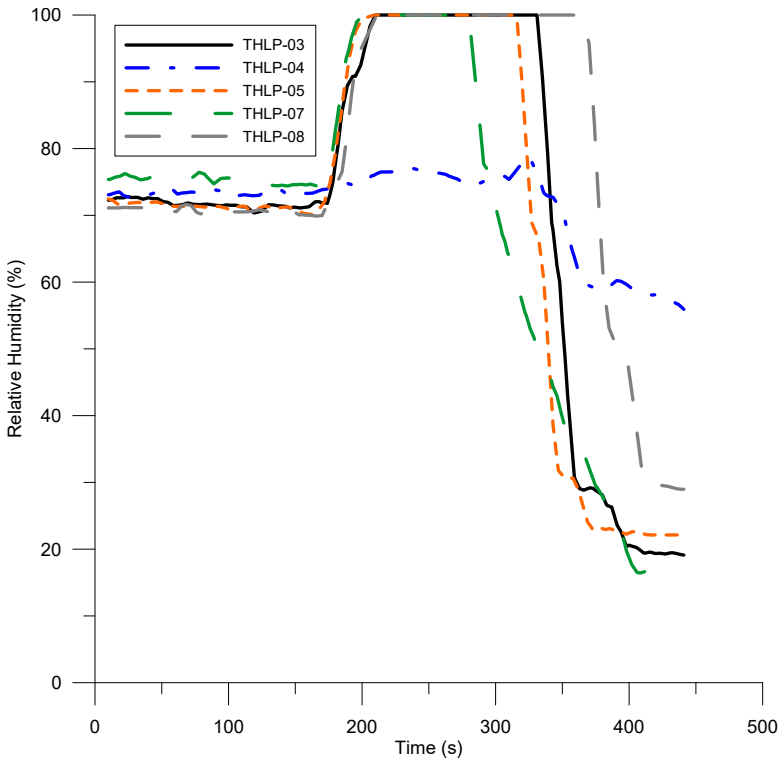


Figure 3.13: Relative humidity variation by sensor location

those seen by the other sensors, because despite sensor location and orientation, THLP-04 still had a direct view of the fire such that there was no significant impact on measured values of light intensity.

Repetitions of the box testing yielded similar results across tests for each parameter of interest. Figure 3.12 shows light intensity data averaged across 5 repeat box tests. This provides a very comparable trace to the single test trace shown in Figure 3.10. Similar results were also obtained from temperature and relative humidity signals, showing the high degree of repeatability in the testing, but perhaps more importantly in the observed sensor response.

In summary, the reduced scale testing conducted in the oven and the $1m^3$ box demonstrated that the EDS sensors were capable of observing changes as a result of being in a fire environment. The $1m^3$ box testing further demonstrated that the sensors were capable of observing fires as small as a tea light candle. While the responses of various sensors were nominal in some cases, the experiments proved the capability of the sensors to detect changing compartment conditions. The temperature, humidity, and light intensity sensors all responded rapidly to variations in ambient conditions, although the light sensor consistently provided the most rapid response. Further, the relative humidity showed interesting results in the initial stages as the relative humidity signal increased dramatically after the fire was ignited and also changed as ventilation conditions in the compartment were varied. Overall, the observations suggest that the combination of sensor responses may be of interest for establishing the presence of a fire and potentially providing on-going information regarding the fire state. As a result, this first stage of reduced scale testing supported further exploration of the use of the EDS sensors for fire detection through a series of larger scale realistic fire tests. This is the subject of the next section.

3.3 Large Scale Experimental Design

As discussed above, results obtained through reduced scale testing led to the decision to explore the response of the various sensors to fires established in a large scale test environment for different fuels and a range of heat release rates. In addition, the response of the sensors to a range of background signals and typical nuisance sources was investigated. Many of the tests were designed to explore the lower limits of sensor response, intended to determine their behaviour in situations representative of incipient or early stage fire development, or to better understand their ability to distinguish between low level signals and surrounding noise. In each test as well, multiple sensor blocks were utilized, providing

an extensive data set for analysis, and from which to gain insight into the potential of EDS type sensor blocks for fire detection.

3.3.1 Experimental Facility

The experiments were conducted in the University of Waterloo burn facility, a two-story steel structure designed to accommodate large scale fire experiments and shown in Figure 3.14. The structure is fire hardened and has has a 120 m^2 floor area per storey and a total structure volume of approximately 290 m^3 with interior floor plan (wall configuration) depicted in Figure 3.15 for each floor. For these experiments, an interior burn room was built on the bottom level of the house as depicted in Figures 3.17 and 3.18.

It was built with wood stud walls covered in gypsum wall board. Non-combustible fiber insulation was installed in the burn room to provide additional fire resistance at the ceiling and fire bricks similarly provided fire resistance to the floor, Figure 3.16. Spray foam was used to seal cracks throughout to ensure minimal leakage through the walls and ceiling.



Figure 3.14: Exterior of Burn Structure

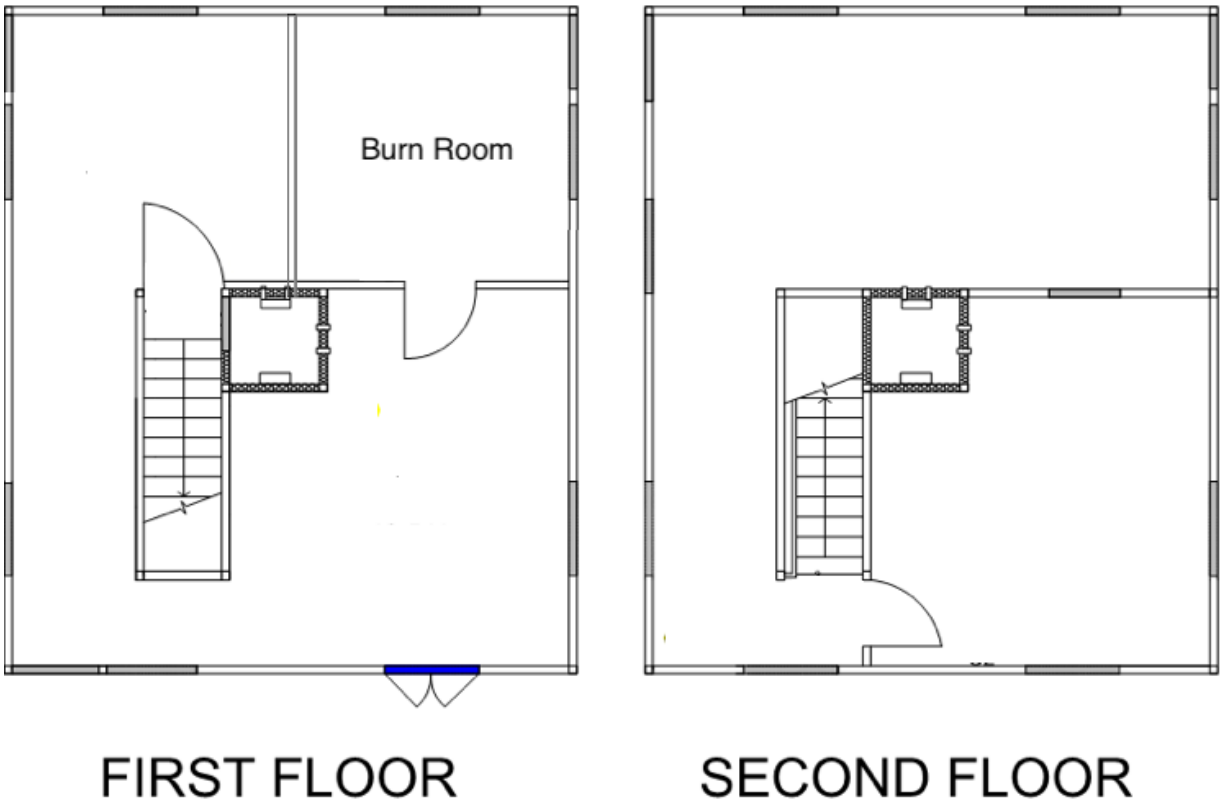


Figure 3.15: General layout of burn structure

All the fires were initiated in the burn room which is shown in cross-section in Figure 3.17. The room was outfitted with EDS sensors as shown in Figure 3.18. Sensors were located at three different heights within the room, THLP-09 at floor level, three sensors at 48" from the floor (THLP-01,-03 and -04) representative of sensors installed at switch height, and three mounted to the ceiling (THLP-02,-08 and -07). In addition there was a sensor located on the ceiling immediately outside of the burn room, THLP-05. For a number of tests smoke detectors were installed in the space to determine the smoke detector activation time as compared to the sensor response as well.



(a) Burn room door

(b) Burn room interior

Figure 3.16: Burn room showing fire brick floor, opening, and fiber insulation

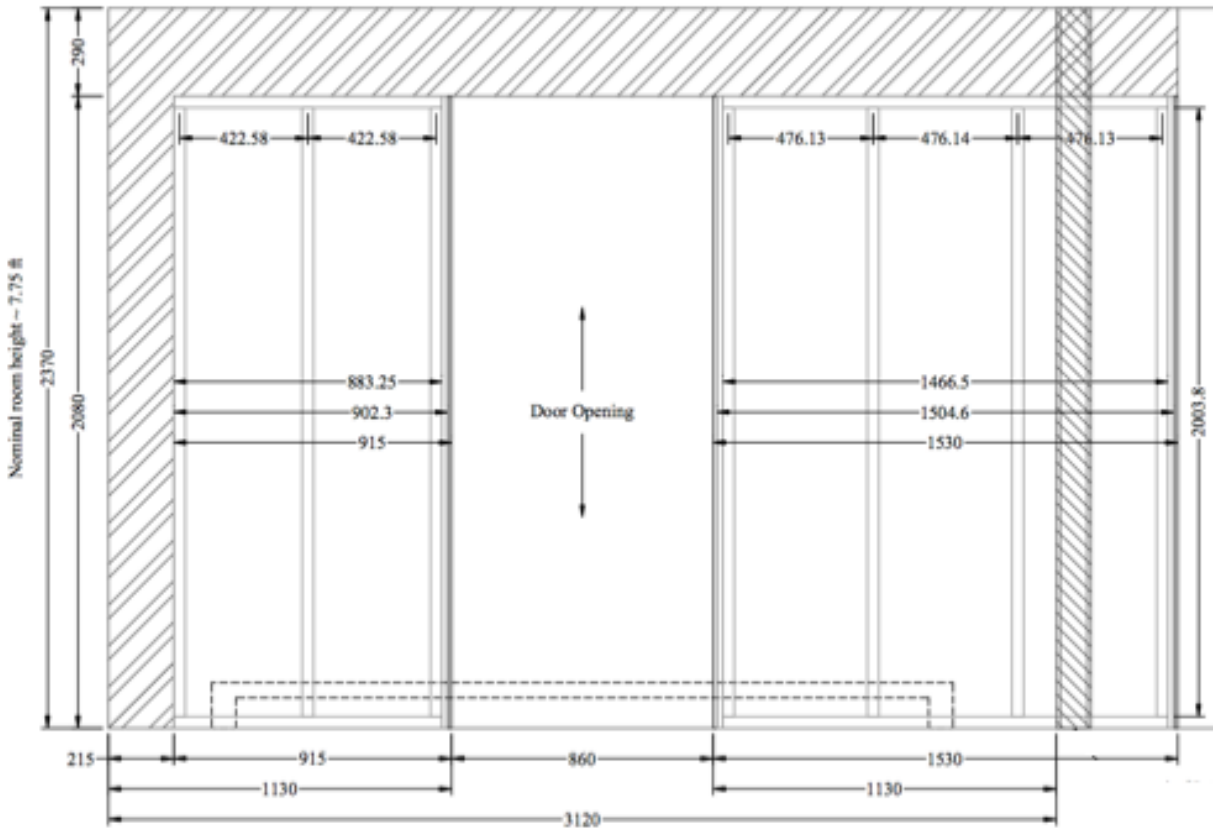


Figure 3.17: Sectional view of burn room

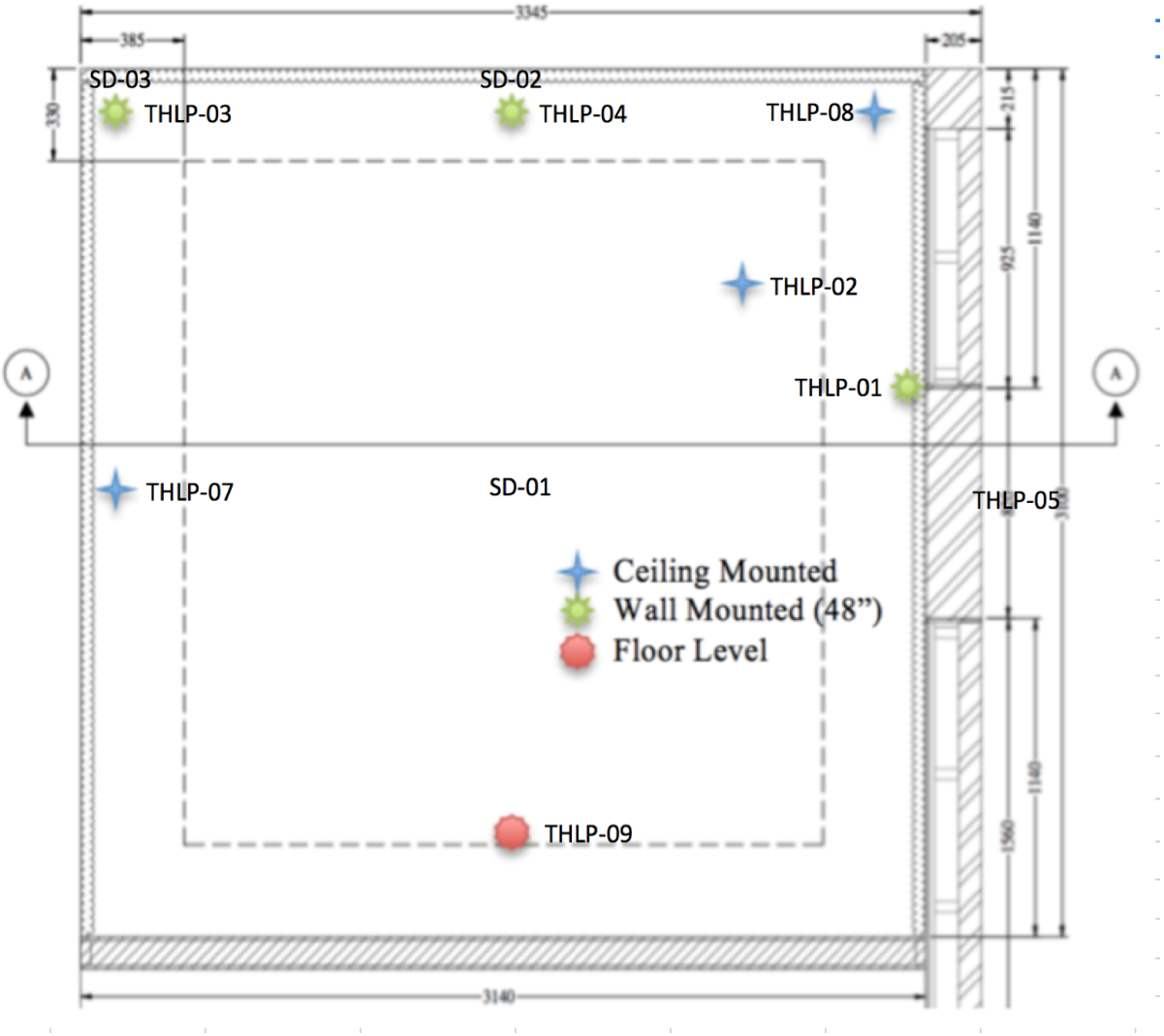


Figure 3.18: Burn room and location of EDS sensors

The experimental matrix that was developed for these tests is shown in Figure 3.19. It consisted of long term background tests of sensor response in a kitchen, a bathroom with a shower, a general office area and a lab space, as well as 100 individual tests targeted towards characterization of the various sensors. These are discussed further below.

	Pool Size (Liquid Fuels)			
	32 mm	75 mm	100 mm	200 mm
Ethanol				
Heptane				
Ethanol/Heptane($1/R^2$) Testing [3]				

	Gaseous Fuels		
	Slow t^2 ($0.00293\ kW/s^2$)	Medium t^2 ($0.01172\ kW/s^2$)	Fast t^2 ($0.0469\ kW/s^2$)
Propane (0.0041 kg/kg)			

	Solid Fuels
Shredded Paper (Tamped, smouldering)	
Crumpled Paper	
$^1/_4$ Wood Crib	
$^1/_4$ OSB Crib	
$^1/_2$ Wood Crib	
Polyurethane Foam (Flaming)	
Polyurethane Foam (Smouldering)	

	Nuisance
Steam (boiling water)	
Flashing Lights	
Electric Heater	
Hot Plate	
Cutting Torch	
Burnt Toast	

	Long Term Background
Kitchen	
Bathroom (w/shower)	
General office area	
Lab space	

Figure 3.19: EDS Sensors Experimental Matrix

3.3.2 Nuisance Sources

A range of nuisance sources were included in the test series to determine the response of the sensor blocks to typical potential nuisance sources. While traditional nuisance sources include items that may create particulates, aerosols, or other products that might produce a false alarm, the range of potential nuisance sources expands when humidity, light, or other parameters are introduced. As such the traditional nuisance sources were expanded to include sources of steam, constant and flickering light sources, heat sources (space heater or stove top), a cutting torch, burnt toast and other potential nuisance fire sources, such as smoldering newsprint.

3.3.3 Fire Sources

Fires were fuelled by liquid, gaseous and solid fuels. Four sizes of pool fire, having diameters of 0.032, 0.075, 0.1 and 0.2 m, were fueled by either ethanol (non-radiating), heptane (radiating) and an ethanol/heptane mixture. An adjustable propane torch was used to generate fire sizes that approximated slow, medium and fast t-squared fire growth rates. Shredded paper, crumpled paper, 1/4 and 1/2 size UL wood cribs (scaled in length, width, and height), a 1/4 scale OSB crib, as well as flaming and smoldering polyurethane foam blocks were also utilized.

The heat release rates of the fires examined varied widely depending on the fuel utilized, but in general for pool fires as well as for the wood crib and foam fires, it was representative of incipient and very early growth fires. Utilizing Equation (3.2) and the properties for heptane ($\dot{m}$"=0.101 kg/m^2s, $\Delta H_{C,eff} = 44.6Mj/kg.k$, and $k\beta = 1.1$ [17]), heat release rates were calculated to range from approximately 200 W, corresponding to the smallest heptane pool fire of diameter $\sim$ 32mm, to a maximum of nearly 100 kW, corresponding to the largest heptane fire, of pool diameter of $\sim$200mm.

$$\dot{Q} = \Delta H_{C,eff} \dot{m}" A(1 - e^{-k\beta D}) \tag{3.2}$$

Specific heat release rates for wood crib, polyurethane foam smoldering and paper fires were not measured.

3.4 Results and Analysis

For each of the approximately 100 experiments results were obtained for light, temperature, and humidity at each sensor location for each test outlined in the experimental matrix, Figure 3.19. The range of tests and variety of sensor locations allowed for extensive spatially specific data to be collected on each fire environment within the compartment.

Plots showing representative comparisons of signals for each of the measured parameters are provided in the following sections, while the remainder of the results are presented in Appendix A. As expected, differences exist in the magnitude of the measured values of the various parameters observed both spatially and as a result of changes in the fire size and fuel.

3.4.1 Temperature

Representative temperature data measured by sensor THLP-03 situated 48" above the floor for liquid fuelled fires is provided in Figure 3.20 for a range of fire sizes (fuel types, pan size and fuel volume).

Since the burn house is unconditioned, each test begins with a slightly different ambient temperature, but the increase in temperature registered by the sensor over the duration of the liquid fuel fires is nominally 5 °C, a relatively small increase. As expected, the measured temperature increases are directly linked to the burning duration (fuel volume) of the fires, in addition to the pool size, with larger pools and fuel volumes, resulting in more elevated temperatures even midway down in the compartment. The larger, solid fuels, in particular the 1/4 size wood crib, resulted in a significantly higher temperature increase, approximately 30 °C, at the location of the sensor as they burned approximately 5-10x as long as the liquid fuels.

For a given fuel and pool diameter the location of the sensor impacted the observed rise in temperature. Figure 3.21 provides a comparison of an exponential moving average (EMA) for ceiling, wall, and floor mounted sensors for a 20cm pan of heptane centered in the burn room. The (EMA) provides more weight to newer data in the set, according to Equation 3.3. Here P is the present value observed by the sensor, α is the smoothing factor, and N is the number of time periods. The sensors located on the ceiling show the greatest change in temperature, followed by those on the wall, and lastly the sensor located at the floor. This behavior is consistent with expected temperature gradients within the fire room.

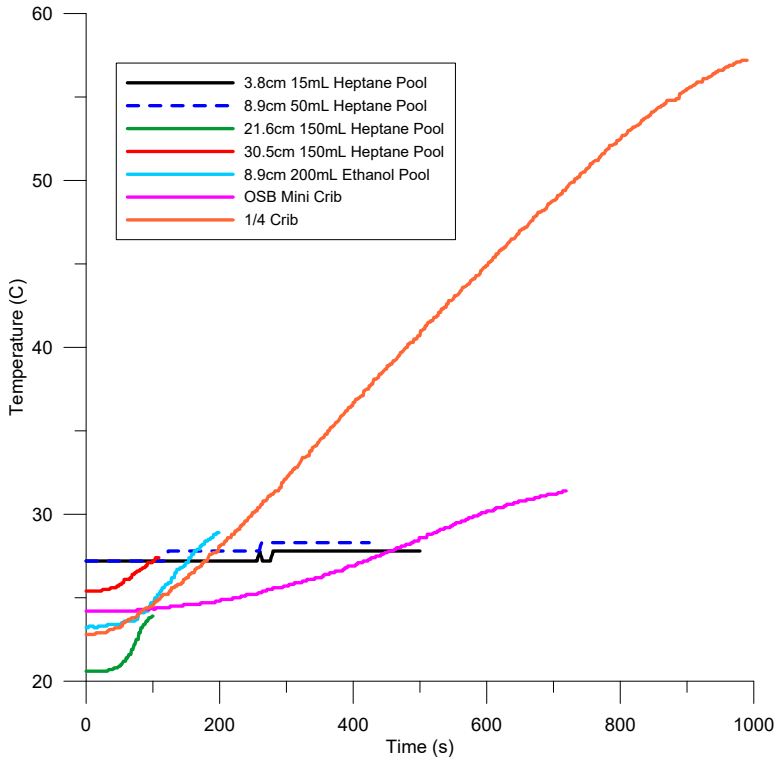


Figure 3.20: Comparison of temperature by fire size and type, THLP-03

$$EMA_t = (P * \alpha) + (EMA_{t-1} * (1 - \alpha))$$
$$\alpha = \frac{2}{1 + N} \tag{3.3}$$

Use of the EMA method to smooth the sensor data is advantageous, as when values change rapidly then the present value enables this change to be observed and potentially responded to in a more timely fashion. The number of time periods evaluated can be varied to examine the impact of averaging with fewer time periods, resulting in more weight being placed on the present value. In this case $N = 10$ with an associated time period of 1s, consistent with moving averages used for forward predictions of trends.

As can be observed in Figure 3.22 the temperature rate of rise at the ceiling mounted sensor, THLP-02, ranged from nominally 0 °C/s during non-fire and transport times to 0.15 °C/s. Similar rates were observed for other ceiling mounted sensor locations, however,as shown in the plot, rates of rise at other sensor locations varied significantly from those measured at the ceiling. Specifically, the rates of change of temperature at sensors located on the wall at standard switch height as well as at receptacle height were significantly lower but similar to one another. Thus, regardless of location, a temperature difference was observed with the initial change being observed at nominally the same time, similarly while the rate of change varied based on location in all measured locations the rate exceeded the baseline observed rate of change threshold.

3.4.2 Relative Humidity

A representative relative humidity data set for liquid fuelled fires with a range of fire sizes is provided in Figure 3.23 for a single, ceiling mounted sensor location. Each data set is presented from the time of ignition until combustion ceased. In general, with the exception of the smallest pool size, the relative humidity increases after ignition, rises to a maximum and then decreases for the remainder of the duration of the fire. This behavior is consistent with that observed in the reduced scale testing in which the relative humidity rose initially and then declined in the space as the air was subsequently dried out from additional heat produced by the fire and/or replaced with lower humidity ambient air. The rise in relative humidity in the large scale environment resulted in a maximum relative humidity of approximately 85%, whereas in the reduced scale testing the air was saturated at 100% relative humidity for some time prior to its eventual decline. Given the response of this sensor across fire sizes, it is anticipated that a fire established over a larger quantity of fuel

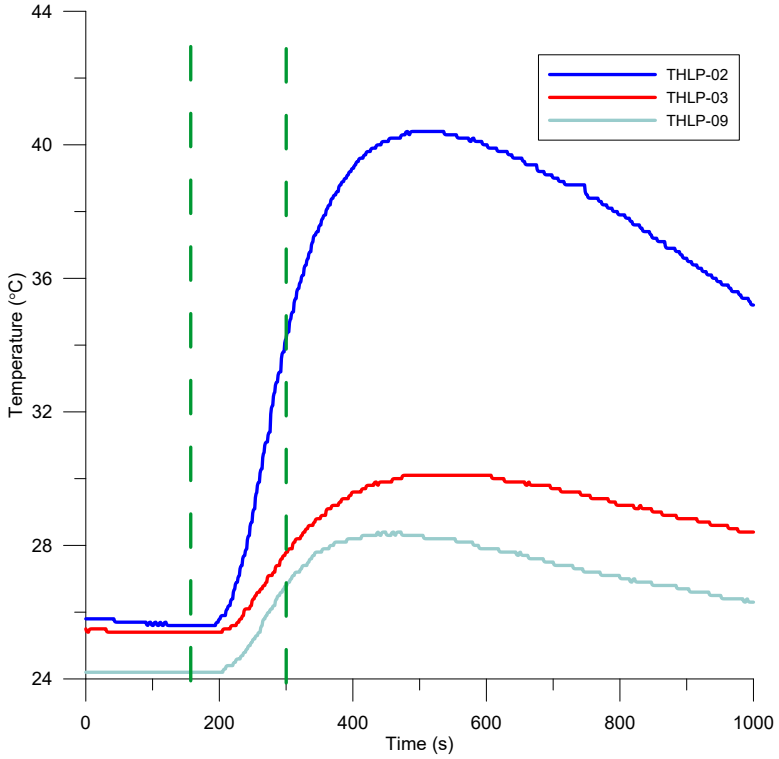


Figure 3.21: Comparison of temperature EMA by sensor location: ceiling (THLP-02), wall (THLP-03), and floor (THLP-09)

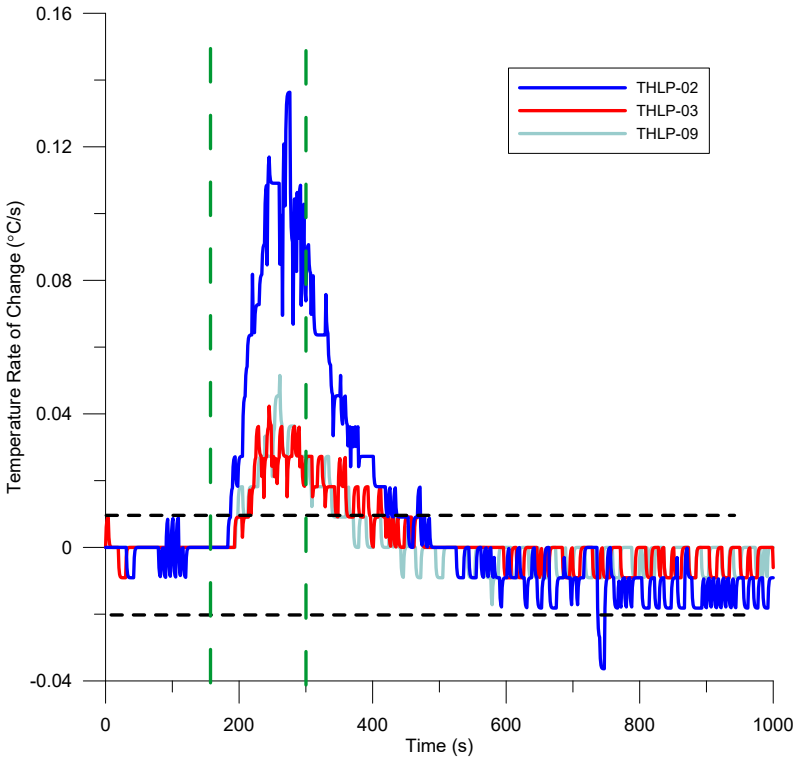


Figure 3.22: Comparison of EMA temperature rate of change by sensor location: ceiling (THLP-02), wall (THLP-03), and floor (THLP-09)

may lead to increased humidity levels as well. The observed change in humidity occurred more quickly and with a greater rate of change than that measured by the temperature sensor in the same location.

Amongst the fuels tested for a given fire diameter, the heptane fires yielded the largest increase in humidity in the space, however for a given pan size the ethanol produced a larger relative rise in comparison to the heptane. This is to be expected as ethanol has relatively more H than C, Equation 3.4, in comparison to heptane, Equation 3.5 and thus for an equivalent quantity of O_2 ethanol will produce nominally 50% more H_2O than heptane. The results across the range of fuel surface areas are consistent with the idea that fires with the highest HRR will lead to the largest increases in relative humidity over the course of the fire.

$$C_2H_6 + 3O_2 \rightarrow 11CO_2 + 3H_2O \tag{3.4}$$

$$C_7H_{16} + 11O_2 \rightarrow 7CO_2 + 8H_2O \tag{3.5}$$

Figure 3.24 provides a comparison of relative humidity data collected during a fire involving 150 ml heptane in a 20cm diameter diameter pool. The data include signals from ceiling, wall, and floor mounted sensors (Figure 3.18), each averaged using the same EMA approach as discussed in the section on temperature above. For a given fuel and pool diameter, it is clear that the location of the sensor impacted the observed relative humidity. Similar to the response observed for temperature above, it can be noted from the zoomed in version of the data in Figure 3.25, that those sensors located on the ceiling typically responded a few seconds earlier than those on the wall or at floor level as would be expected by a parameter that is largely driven by plume dynamics. However, it is worth observing that the greatest rate of change of humidity was not observed on the ceiling but at THLP-03 on the wall at the rear of the structure in contrast to the observed peak rate of change of temperature which occurred at the ceiling location and also that THLP-05, located just outside the room responded relatively quickly and this response is believed to be due to the gases exiting the fire compartment.

An examination of the rate of change of the RH based on the EMA sensor signals, is shown in Figure 3.26. During pre and post fire conditions ($180 < t_{fire} < 300$), the rate of change in relative humidity varies minimally between -0.2 to 0.2%, however once the fire ignites the rate of change varies significantly in particular for the sensors located on the wall and ceiling. While the signals from only one sensor mounted on each of the wall, ceiling, and floor are presented for clarity, similar results were observed for the other sensors as well. The sensor monitoring conditions at the floor was largely unaffected by changes in

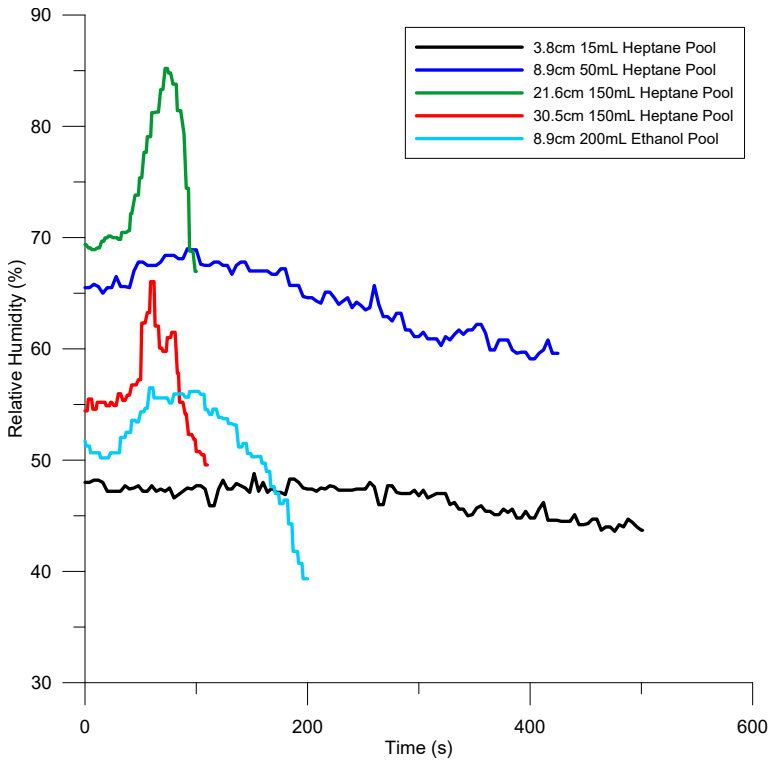


Figure 3.23: Comparison of relative humidity by fire size and type, THLP-03

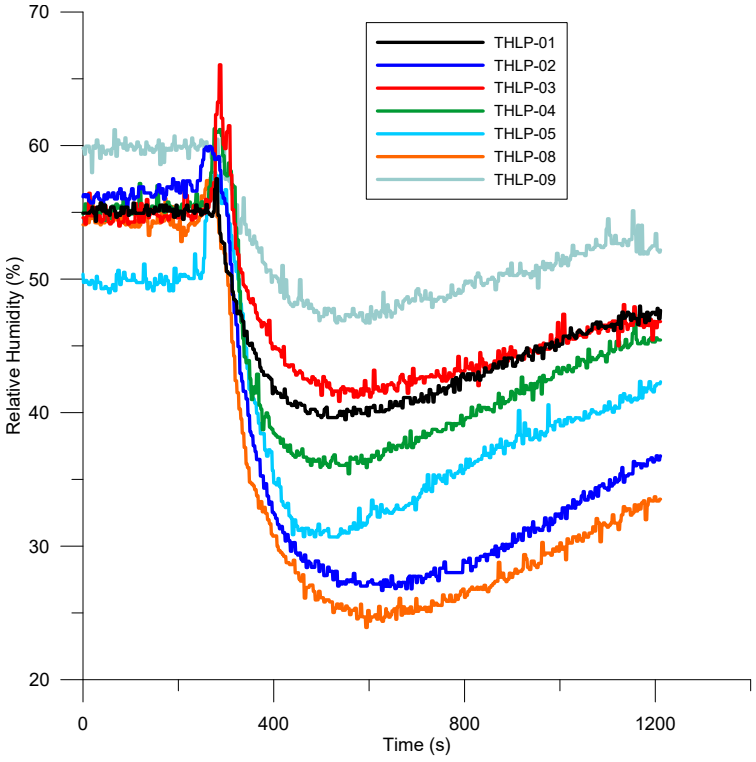


Figure 3.24: Comparison of relative humidity by sensor location

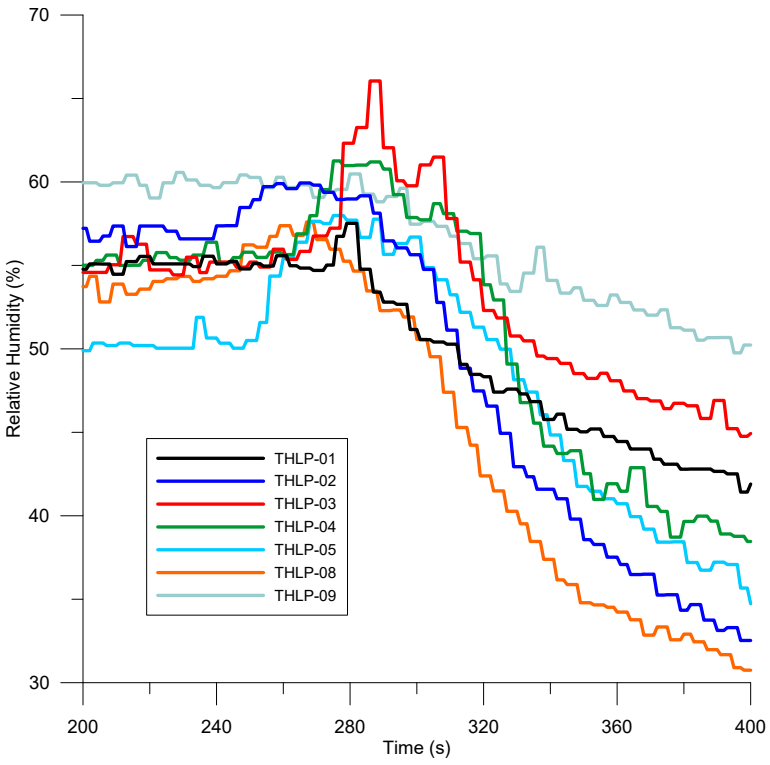


Figure 3.25: Comparison of relative humidity by sensor location

relative humidity based on the observed rate of change; however, it must be pointed out that the overall relative humidity at the floor was reduced throughout the duration of the fire, Figure 3.24, although at a slower rate than for some of the other sensor locations.

Based on the observations, the relative humidity continued to decline for a period of time after the fire was extinguished. The degree to which this occurred varied based on the size of the pool fire and its burning duration. As is discussed in Chapter 3.4.1, the temperature continues to rise at the sensor locations for some period of time after the fire dies down and this dynamic is partially responsible for the continued "drying out" of the space. For the test shown, despite the decrease to values lower than pretest, by approximately 1800 seconds after ignition the relative humidity returns to pre-fire levels at all sensor locations. Those sensors located on the walls and floor, which did not decrease as significantly after the fire, returned in a shorter time frame, though the rate of change of relative humidity was similar. Similar behavior was observed for other tests as well.

Based on the data obtained and analysis above, the value of relative humidity alone may not be suitable for determination of a fire condition as it can vary significantly. On the other hand, the rate of change in relative humidity is observed to increase rapidly to values exceeding 0.2%/s within 15 seconds after ignition of the fires tested. Therefore, the rate of change of relative humidity, either in isolation or in combination with the measured relative humidity, should be considered as a viable parameter to evaluate with regards to fire state determination.

3.4.3 Light Intensity

In the small-scale testing, it was observed that the flickering of the flames of the various fires resulted in changes in the light intensity that was measured by the sensors. Figure 3.27 shows a series of images of a ∼210 W heptane fire in a 3.3 cm pan over a period of 1.5 seconds (0.25 second increments between photos). From the images, it can be observed that there is a significant difference in the light intensity in the space as a result of the unsteadiness of the flame. When analyzed using image processing software, as shown in Figure 3.28 the image light analysis and color breakdown show significant differences between captured images as would be expected from Figure 3.27.

It was observed, as expected, that differing levels of light were measured at the light sensors throughout the burn room for a given fire. This prompted a systematic study to capture the effects on the light intensity of distance between the fire and sensor. For this, a series of 9 cm diameter, 15mL heptane pool fires were ignited and allowed to burn to completion, approximately 3 minutes each. The fires were placed at distances from

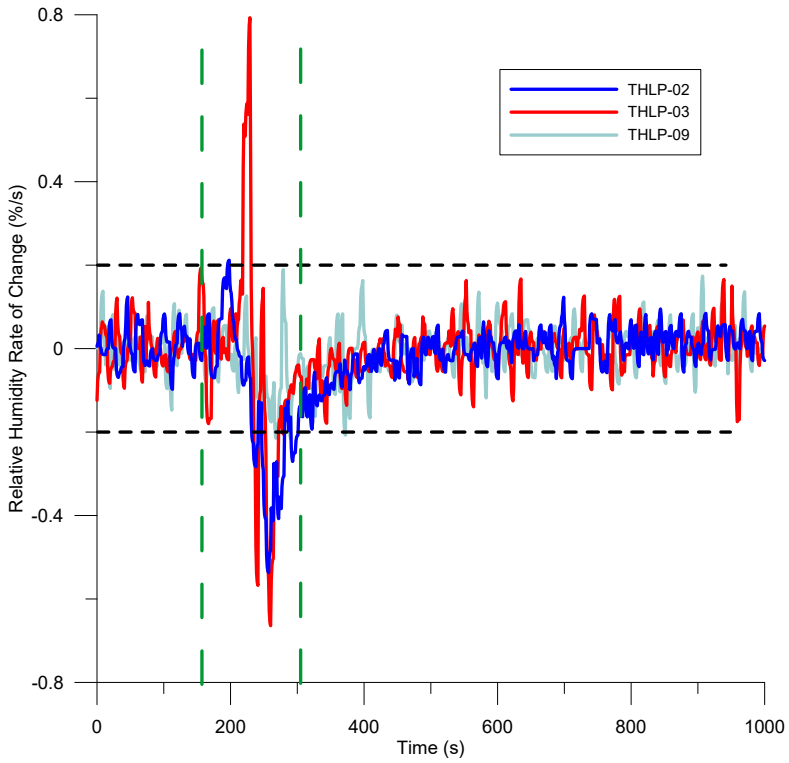
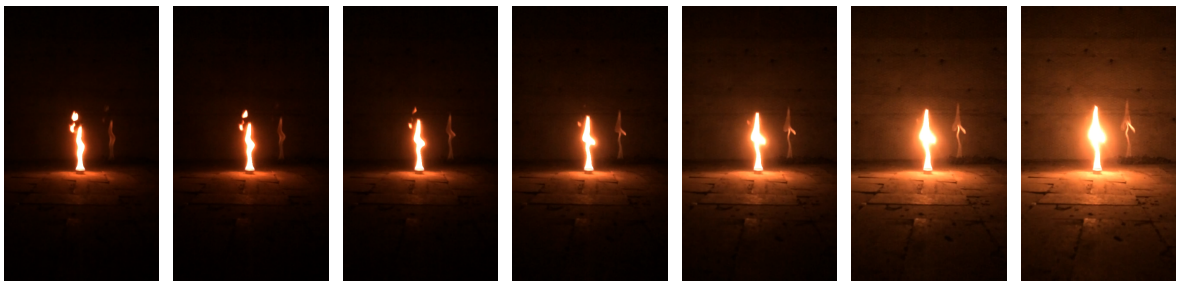


Figure 3.26: Comparison of EMA relative humidity rate of change by sensor location: ceiling (THLP-02), wall (THLP-03), and floor (THLP-09)



(a) 0.00s (b) 0.25s (c) 0.50s (d) 0.75s (e) 1.00s (f) 1.25s (g) 1.50s

Figure 3.27: Variation in light from flame flickering

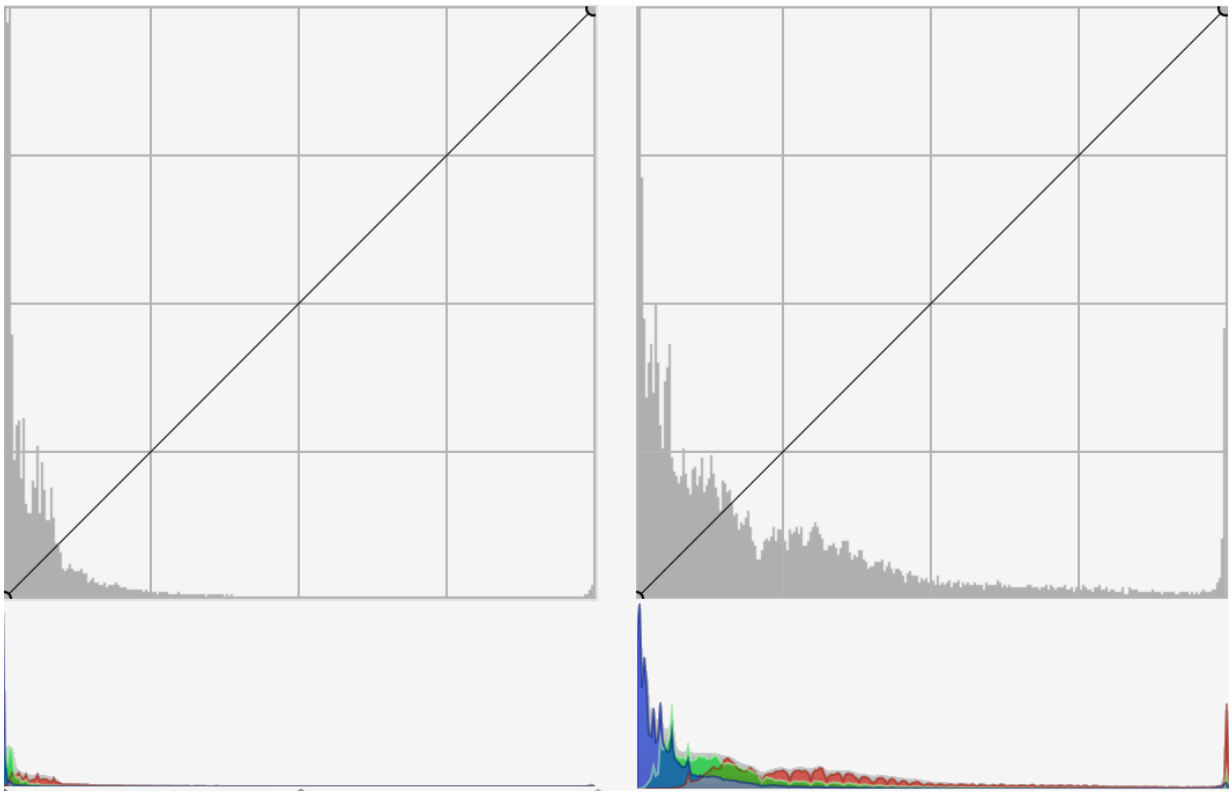


Figure 3.28: Image light analysis (intensity and color) for Figure 3.27 (a) and (g)

20cm-200cm from THLP-09, located at the floor. The measured light intensity was found to be approximately inversely proportional to the distance of the fire from the source, as illustrated in Figure 3.29 and summarized in Table 3.4. This matches the expected behavior of light decay as a function of $1/r^2$.

Plotting of the average light intensity values as a function of distance matches well with theory. The "theoretical" light intensity of the source was estimated using a light intensity meter located at 20cm from the source and then the decay was evaluated according to Equation (3.6) which produced the measured vs theoretical comparison shown in Figure 3.30. The measured vs. theoretical intensity (illuminance) shows a high degree of linearity, though it is slightly biased towards the measured intensity at the lower light and slightly biased towards the theoretical at high levels. Nonetheless the R^2 value exceeds 0.997 indicating a high goodness of fit for the linear regression.

$$E = \frac{I}{r^2} \tag{3.6}$$

Table 3.4: Light intensity vs distance

Distance(cm)	20	30	40	60	80	100	120	140	160	180	200
Peak Lux	757	450	266	128	105	78	72	62	53	35	32
Avg. Lux	600	310	171	100	80	62	48	43	38	34	32

3.5 Conclusions

The results of the testing indicate that the parameters measured using the EDS sensors can be used to reliably identify the changes in an environment as a result of a fire. This behavior was observed at both small and medium scale environments and fires as small as 10 kW could reliably be detected with the tested sensors. In sprinklered environments where no other detection method may be present incipient fire detection may be detected well before sprinkler activation. The relatively small size of the fires and the ability to identify the presence of the source indicates a strong potential for these types of sensors to be leveraged for fire detection purposes. The sensor performance with small fires, representative of incipient growth fires, provided the basis for continuing the research and examining the sensor performance relative to background and noise signals and in larger scale fires, as well as to expand the range of sensors evaluated to better capture the fire environment and explore additional sensors that are being integrated into current technology.

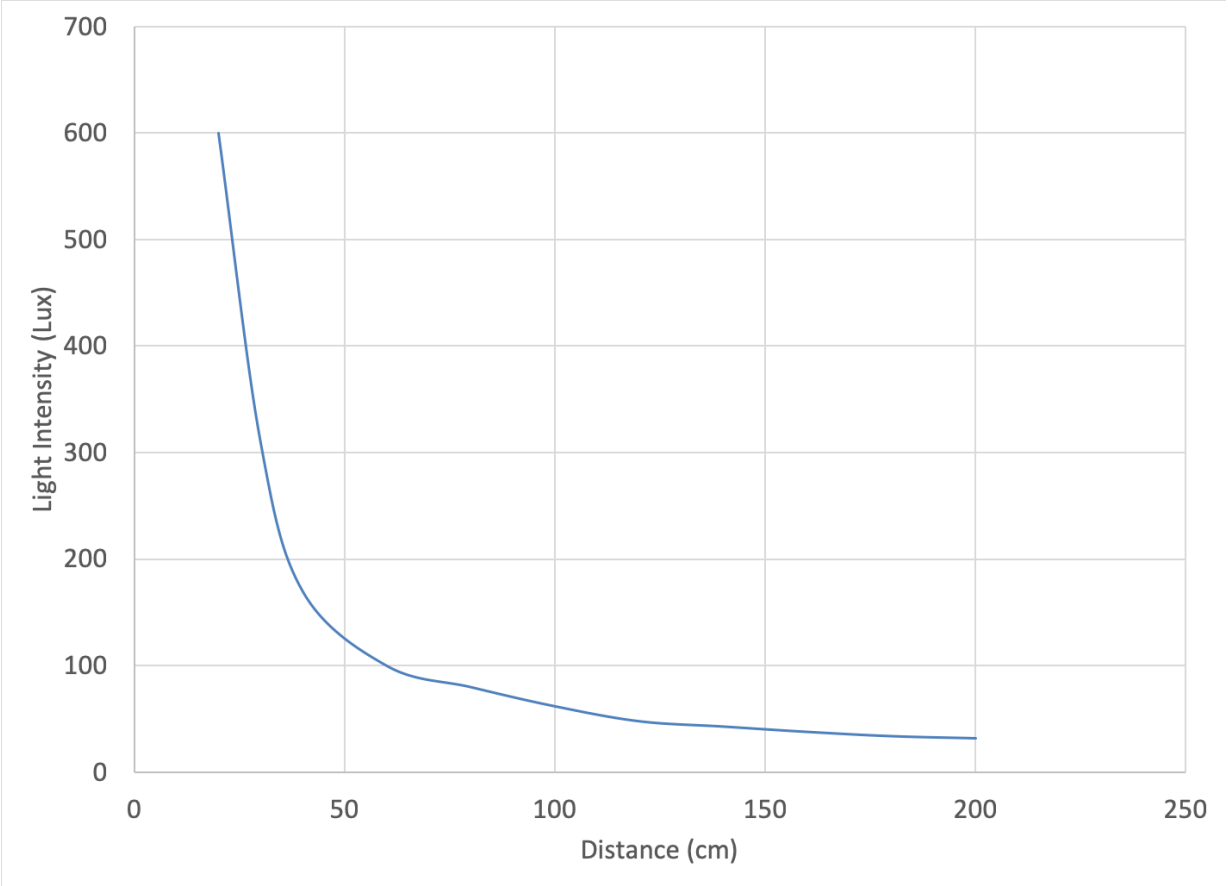


Figure 3.29: Light Intensity for identical fire sizes ($10kW$) at various distances from the sensor

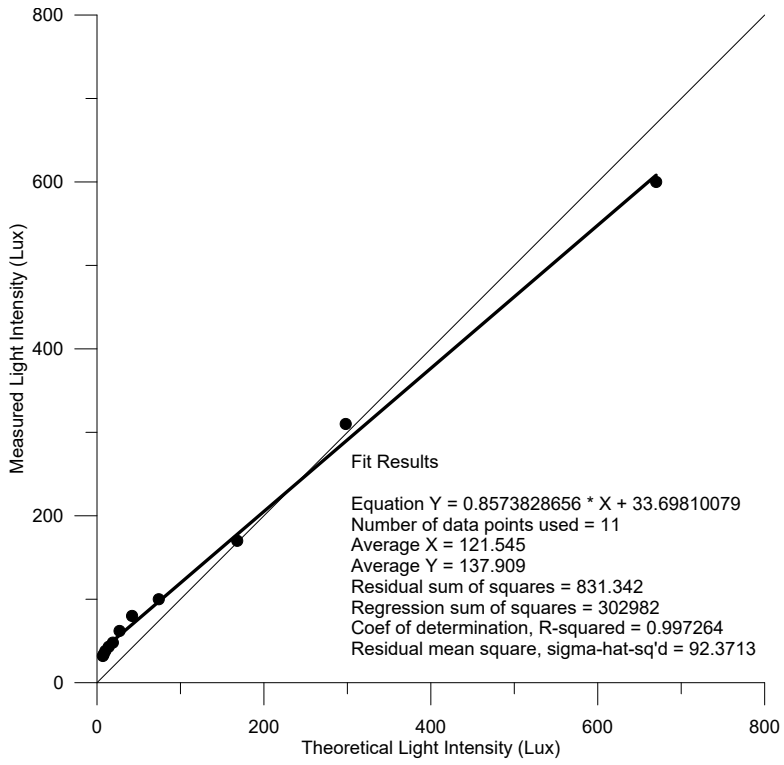


Figure 3.30: Comparison of measured light intensity vs. theoretical light intensity

Chapter 4

Fire State Determination (FSD) Sensor Block Development

4.1 FSD Sensor Selection

Based on the initial success of the off-the-shelf sensor units it was determined that there was the potential to utilize similar sensor components to develop novel units for fire state determination (FSD). Therefore, this second phase of the research set out to combine sensors into a new FSD sensor block that could be used to distinguish, capture and recognize signals from fires during the different stages of fire growth. From the literature review and initial experimental results, it was determined that a range of different conditions and sensor signal magnitudes might be observed in a room in which a fire is present. Therefore, the sets of parameters that were expected to be observed during different types of fires and nuisance sources, as well as the qualitative magnitude of the anticipated changes, were compiled and are provided in Table 4.1.

From the compilation, together with assessment of readily available sensor types, it was decided to utilize the base set of sensors contained in the off-the-shelf sensor units and expand these capabilities by adding gas sensors. A custom sensor block was designed that incorporated temperature, light, humidity, motion, oxygen, carbon monoxide, and hydrocarbon sensors. The sensors were connected to a wireless Arduino micro-controller and powered by a rechargeable lithium-ion battery pack. The micro-controller captured the sensor signals and transmitted them in real-time to a live web database. Specifics of the controller, as well as the various sensor components, are discussed in the following sections.

Table 4.1: Expected Environmental Changes during Fire and Nuisance Exposures ("X" indicates large changes expected, "x" indicates minor changes expected, while "-" entry indicates an unknown influence)

	Fires			**Nuisance Sources**			
	Incipient Fire	**Developed Fire**	**Smoldering Fire**	**Steam**	**Heater**	**Burnt Toast**	**Torch**
Temperature	x	X	-	x	x	-	-
Light Intensity	x	X	-	-	-	x	x
Humidity	X	X	x	X	x	-	-
Light Wavelength	x	X	X	-	x	-	-
Light Color	x	X	-	-	x	-	-
CO Concentration	x	X	X	-	-	-	-
CO_2 Concentration	X	X	-	-	-	x	-
Heat Flux	x	X	-	-	x	-	-
Motion	x	X	-	-	x	-	-
Sound	x	X	-	-	x	-	-
Pressure	x	X	-	-	x	-	-

While Table 4.1 highlights a selection of environmental parameters that might be expected to undergo a change during a fire in a compartment, sensors that could distinguish changes in temperature, light, and humidity were included as they had already been demonstrated to be suitable for fire detection. CO sensors were added to aid in discerning flaming vs smoldering fires while additional sensors to measure light wavelength and color were added to complement the light intensity sensor signals to aid in differentiating between fire and non-fire light sources. Finally CO_2 sensors were added to complement the humidity sensor to better capture and identify incipient fire conditions.

4.1.1 Sensor Block Components

Micro-controller

One of the key components in design of the new sensor block for fire detection was selection of the platform for data acquisition and control. The platform needed to be reliable, flexible, and allow for sufficient data channels and processing speeds. The Arduino platform fulfilled the hardware requirements and has been widely integrated into a range of applications. An Arduino Yun was selected as the micro-controller platform for the sensor block. Arduino provides a robust and well documented platform that integrates directly with analog and digital sensors. The Yun programming is standard and utilizes an Atmel ATmega32U4 processor. It also has an additional processor, an Atheros AR9331, that allows for Linux and the OpenWrt wireless stack to be run direct from the microprocessor without any additional hardware or software components. The OpenWrt capability enables real-time wireless communication to a computer ensuring that data would be captured at least up until the point of sensor/board failure due to fire exposure. Additional details on the Yun configuration and scripting are provided in Appendix D while additional information and specifications for the Arduino board may be found in Appendix E. While not the primary driver for the choice of platform, the relatively low cost of the Arduino board allowed for a greater number of sensor blocks to be built. This also facilitated the decision to treat each sensor block as "disposable", thereby providing minimal hardening of the sensor blocks against the harsh conditions encountered in the fire experiments.

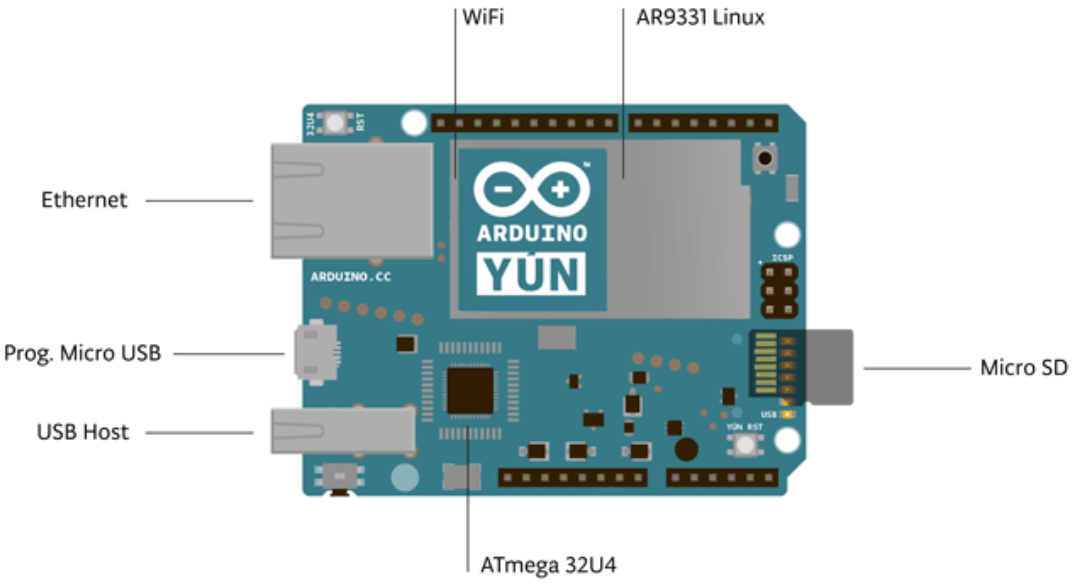


Figure 4.1: Yun Microcontroller Schematic (www.arduino.cc/en/Guide/ArduinoYun)

With the control system chosen, specific sensors had to be selected to monitor the various light, temperature, humidity, gas and motion signals from the fire. Each is described in more detail in the sections below.

Light Sensors

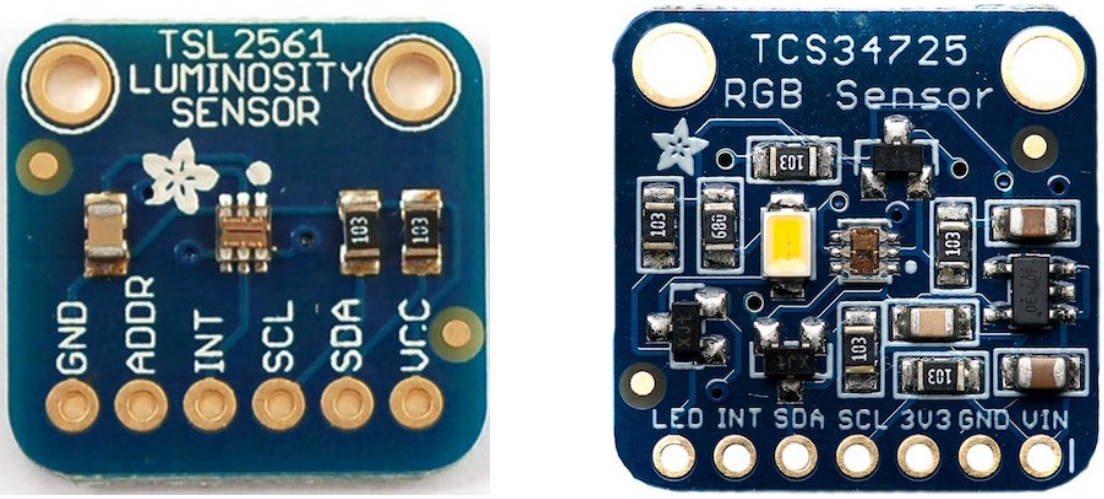
Two different light sensor boards were integrated into the sensor block, models TSL2561 and TCS34725. Figure 4.2 and Table 4.2 provide information on each sensor, additional information and specifications on the sensors may be found in Appendix E. The TSL2561 luminosity sensor was chosen for the sensor block since it is a high resolution, wide range, digital light sensor that appeared well suited for use in the potentially wide range of light situations that might be encountered in various fire situations and stages of growth. The sensor is an integrating light sensor that easily interfaces to the Arduino system. It contains light sensing components that have much better precision than is obtained from CdS photocells used in many similar sensor systems. The sensor contains both infrared and

full spectrum light sensing diodes which allows for infrared, full-spectrum or human-visible light signals to be evaluated to examine which of the spectra might show the greatest response and least noise when observing a fire versus ambient or nuisance sources. An additional benefit is that the incident Lux levels can be calculated and the sensor can be dynamically configured for different gain/timing ranges to detect light ranges from 0.1 - 40,000 Lux which provides the flexibility for detection of light emission from incipient through to well established fire plumes.

The TSL2561 luminosity sensor was coupled with the complementary TCS34725 RGB colour light sensor to more completely determine the luminous signatures arising from different fire and nuisance scenarios. As shown schematically in Figure 4.3, the TCS34725 returns the colour of light signature as red, green, blue (RGB) and clear light sensing values via color sensing photodiodes. Whereas the TSL2561 sensor includes an IR light sensor, the TCS34725 sensor includes an integrated IR blocking filter to minimize the IR spectral component of the incoming light. This filter ensures a more accurate measurement of RGB color in the visible spectrum and thus better simulates the range and expected human response to light. The TCS34725 is seen as a good complement to the TSL2561 luminosity sensor above as it focuses on the visible light spectrum and light color which is anticipated to vary when a fire is compared to typical light sources. With the two sensors combined, the color of the light can be differentiated while the Lux levels across the spectrum are simultaneously measured, allowing for a complete characterization of the incident light from the various fire and nuisance situations.

Table 4.2: Information and operational limits of the light sensors used in this study

	TSL2561	TCS34725
PCB Manufacturer	*Adafruit*	*Adafruit*
Operating range	0.1–40,000 lux	3,800,000:1 Dynamic Range
Operating temperature	-30–80°C	-40–85°C
Response time	<15 s (t_{90})	2 s (t_{90})



(a) TSL2561 Light Sensor (b) TCS34725 RGB Sensor

Figure 4.2: Light sensors utilized in sensor block

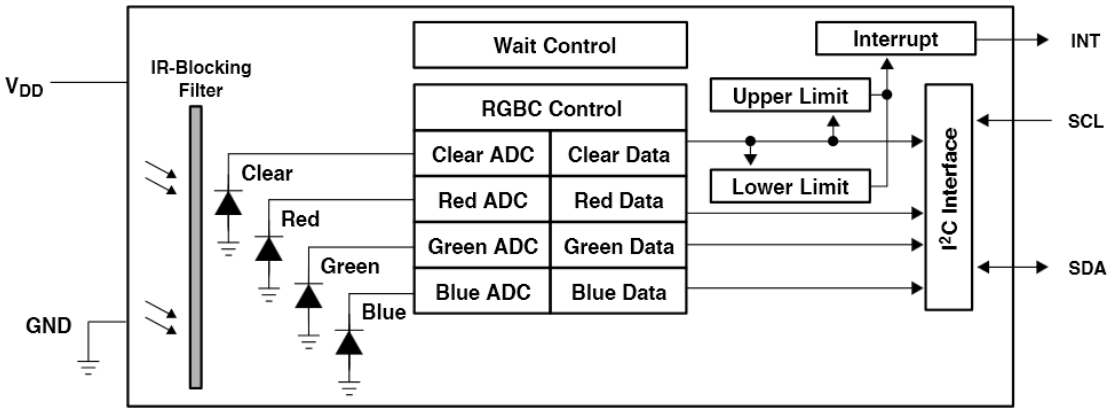


Figure 4.3: TCS34725 Block Diagram

Temperature and Humidity Sensors

With the light sensors chosen, the next requirement was to find appropriate sensors to measure temperature and relative humidity from the fire situations. The HTU21D-F, Figure 4.4, digital, I2C relative humidity and temperature sensor was chosen. A summary of the sensor specifications follows with additional information and specifications provided

in Appendix E. Each sensor is individually calibrated and tested at the factory and therefore provides calibrated, linearized digital output signals with resolution that can be varied from 8/12bit up to 12/14bit for relative humidity/temperature respectively. A PTFE filter/membrane is installed integral to the sensor housing to protect the sensors against water, dust and particulate contamination without affecting the response time. The sensor is rated to provide temperature measurements over a range of -40°C to 125°C, where the upper limit may be slightly low for the present use but was considered to be high enough to capture changes in the output signals during the incipient and early growth stages of the fire. For relative humidity, the sensor provides measurements from 0-100% with an accuracy of 2% @25°C over the majority of the measurement range. The sensor output is referenced to ambient temperatures of 25°C so when used in environments with different ambient temperatures, a correction factor, C_{temp}, of -0.15 %RH/°C must be applied to the output signal. Thus, the correction for exposure to elevated temperatures yields a significant increase in RH so when used in temperature varying fire environments, the measured relative humidity signals had to be temperature compensated according to Equation (4.1). The RH compensation factor was programmed into the Arduino framework and thus all output from the sensor provided corrected RH measurements.

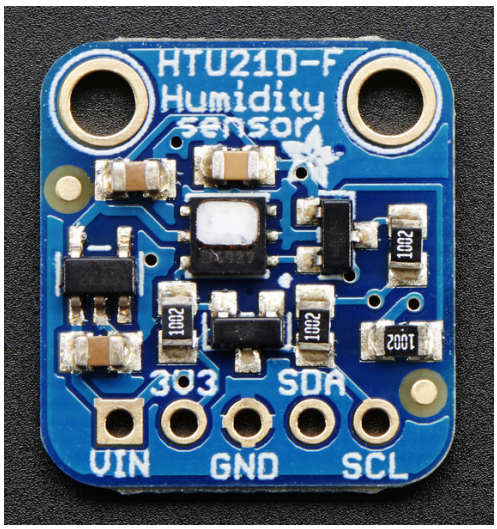


Figure 4.4: Temperature and Relative Humidity sensor utilized in sensor block

$$RH_{compensated} = RH_{actualT} + (25 - T_{actual}) * C_{temp} \tag{4.1}$$

Gas Sensors

There are a wide range of chemical sensors available that can be used to measure gas concentration based on specific chemical or physical processes, such as optical phenomena, electrical and electrochemical interactions, and mass accumulation. Once it was decided to measure concentrations of O_2, CO_2, and CO to distinguish different types of fire and chart fire development in this study, a number of inexpensive electrochemical devices were selected. The key characteristics of each of the chosen sensors are summarized in Table 4.3. All sensors were supplied on customized printed circuit boards (PCBs) designed to simplify power requirements and data acquisition, and facilitate sensor interface with the Arduino microcontroller. A brief description of each sensor is provided below; additional information and specifications may be found in Appendix E.

Table 4.3: Information and operational limits of the gas sensors used in this study

	O_2	CO	C_xH_y	CO_2
Name	ME2-O2-Φ20	MQ-7	MQ-4	MG-811
PCB Manufacturer	*Seeed*	*DFRobot*	*DFRobot*	*DFRobot*
Operating range	0–25 vol%	20–2000 ppm	20–5000 ppm	350–10,000 ppm
Operating temperature	-20–50°C	-20–50°C	-20–50°C	-40–75°C
Operating humidity	0–99%	<95%	<95%	0–99%
Response time	<15 s (t_{90})	∼30 s (t_{90})	∼30 s (t_{90})	5 s ($t_{63.2}$)

The ME2-O2-Φ20 oxygen sensor is an amperometric electrochemical device utilized to measure oxygen concentration. It is made up of four main components: a capillary diffusion barrier, cathode, oxygen ion conductor, and anode. A small sample of gas is able to enter the sensor through the diffusion barrier and interface with the cathode. When an external voltage is applied to the sensor, any oxygen molecules present in the gas sample undergo a reduction reaction, forming oxygen ions. The oxygen ions then pass from the cathode to the anode via the oxygen ion conductor, which is situated between the cathode and anode. Once the oxygen ions reach the anode, an oxidation reaction re-forms oxygen molecules. The sensor can be calibrated to measure oxygen concentration in the gas mixture since as the concentration increases, the electrochemical current increases resulting in a higher analog voltage output from the sensor.

The MQ-7 carbon monoxide sensor is a SnO_2 based semi-conductor sensor used to detect carbon monoxide concentration that operates off of an alternating voltage. As the

voltage cycles through a low temperature condition (corresponding to 1.5 V), the CO concentration is measured as the conductivity of the semiconductor increases with increasing CO concentration. Then,as the sensor is heated to elevated temperatures (corresponding to 5.0 V) any gases that adsorbed onto the sensor surface at the lower voltage (temperature setpoint) are cleaned and the cycle continues. Changes in conductivity at the low temperature (low voltage condition) provide the output signal which can then be calibrated and converted back into the concentration of CO in the gas sample in contact with the sensor surface. The sensor consists of two electrodes separated by an electrolyte. A periodic triangular voltage wave is applied to each of the two electrodes in turn. When CO is present in a gas sample that passes through the sensor, the CO molecules and their ions move toward the negatively polarized electrode. When the voltage is reversed, CO and its ions move in the opposite direction, forming a series of peaks and valleys in a current-voltage plot. The amplitudes of these correspond to the concentration of CO present in the sample.

The MQ-4 sensor is a semiconductor sensor for hydrocarbon gases which, like the MQ-7 described above is based on an SnO_2 semiconductor sensing element. Instead of the alternating voltage used for the MQ-7 CO sensor, for measurement of hydrocarbons (methane, propane, butane, etc) the sensor is supplied with a stable 5.0 V signal to maintain the heater at the required measurement temperature. The load resistance is then adjusted to set the required sensitivity of the sensor depending on the gas to be sensed. Changes in conductivity provide the output signal which can then be calibrated and converted back into the concentration of hydrocarbon in the gas sample in contact with the sensor surface. It is important to note that the sensor is not able to distinguish between various hydrocarbons, but rather provides an integral measure of whatever comes in contact with the sensing element.

The MG-811 carbon dioxide sensor is a potentiometric solid electrolyte sensor used to measure carbon dioxide concentration. The voltaic cell uses a solid electrolyte, a reference electrode, and a working electrode. The reference electrode is independent of the gas that is being tested as it is sealed in a column with a control gas that is electrochemically reversible. The working electrode is exposed to the gas of interest. Once the gas molecules come in contact with the working electrode, specific reactions take place which lead to creation of chemical potentials at each electrode-electrolyte interface and the gradient in potential across the electrodes results in an overall drop in electrical potential, which is measured as an electromotive force, and output as an analog voltage. Again the voltage signal can be calibrated to an output concentration of CO_2 gas. This is particularly important with solid electrolyte based electrochemical devices as they will tend to operate faster in high temperature conditions such as those encountered during fires, since the solid electrolytes have higher conductivity at higher temperatures and thus the electrode reactions occur at

a faster rate.

Motion Sensors

The final sensor that was installed in the sensor block was a passive infrared (PIR) motion sensor which is normally used to capture changes in motion within a monitored space. PIRs are pyroelectric sensors which detect levels of infrared radiation. The higher the temperature of an object in the field of view of a motion sensor, the greater the radiation emitted from the object, and thus received by the PIR sensor. The PIR sensor in a motion detector is split into two halves and wired so that the signals on each half cancel each other out under non-motion conditions (i.e. there are identical signatures on each half). If one half of the sensor sees more or less IR radiation than the other (i.e. an emitting body enters the field of view on one side or the other), the output will swing high or low indicative of motion. Since it has previously been observed that the temperature gradient between smoke and ambient air or flaming and non-flaming conditions is often sufficient to trigger a motion detector, it was deemed useful to integrate a PIR sensor into the final sensor block.

FSD Sensor Housing

With the individual sensors chosen, the housing for the FSD sensor block was designed and then 3D printed. This allowed for rapid customization of the sensor block and housing and ensured that all components including power and data transmission elements could efficiently be contained in a single unit while maintaining functionality. The final housing was nominally a 8 cm cube which included ports for recharging the 3.8V lithium-ion batteries, a micro-usb connection to the Arduino board, and a power port in the event that the unit needed to be powered by an external power source. Figure 4.5 shows an assembled sensor block in which the PIR, light guides, and several gas sensors are visible. The light guides (clear plastic posts visible in Figure 4.5) were introduced to help collect and focus the light onto the light sensor surfaces as the sensors were embedded in the housing and it was noted that the received light was greatly reduced in comparison to a sensor in the open. The addition of the light guides resolved this issue. Additional photos and details of the sensor block housing and contents may be found in Appendix B.

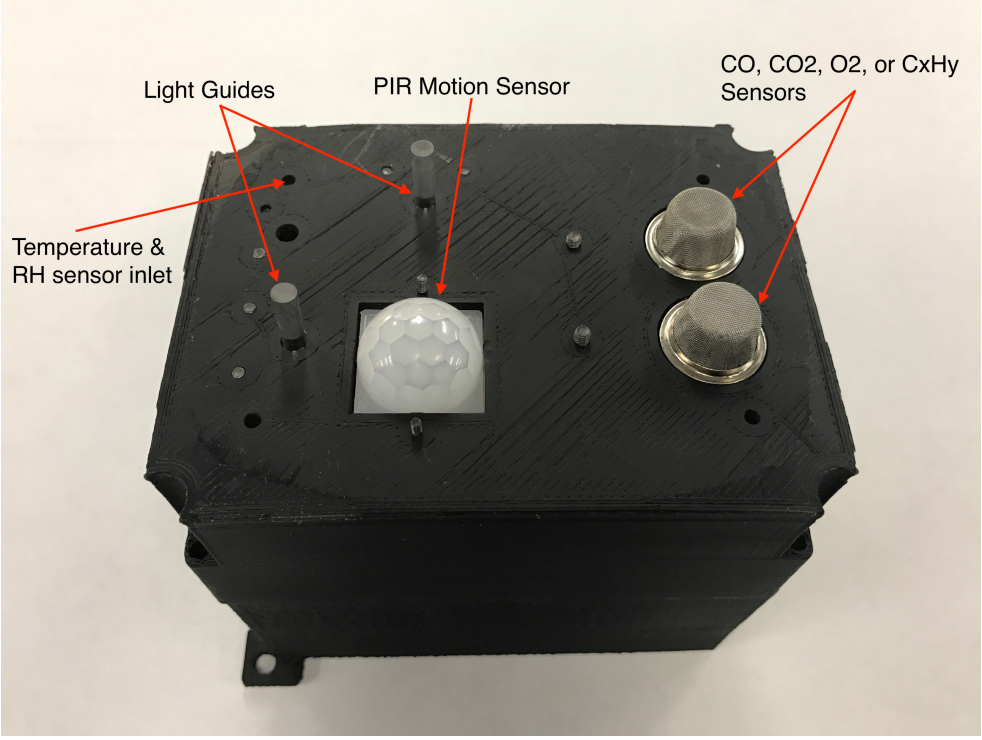


Figure 4.5: Example Sensor Block

4.2 FSD Sensor Characterization

For each of the sensors identified in Section 4.1.1, and prior to incorporation into the sensor block housing, a characterization of the sensors was performed. Temperature and humidity sensors were characterized in an oven, light sensors were characterized using a known light intensity at a fixed distance, and gas sensors were characterized using a limited oxygen index (LOI) system. Each of the characteristic sensor responses is discussed briefly in the sections below.

4.2.1 Temperature and Humidity Sensor Response

The HTU21D-F temperature and humidity sensor response was characterized in a 35 liter MicroClimate benchtop test chamber. The chamber was able to provide RH from 5%-95% and temperatures from -50-190°C. Sensors were introduced into the oven at nominally

25°C, the temperature at which the sensors are calibrated from the factory, and the temperature was increased to 100°C over approximately a 10 minute period in a near linear fashion. During this time the RH was simultaneously increased from 10% to 65%. Data was collected every second from the sensors and both temperature and RH showed sensor response aligned with the cut sheet, Appendix B after temperature correction of the RH measurement following Equation 4.1. The final RH measurement from the sensor was approximately 76% at 100°C, consistent with an actual RH of 65% at a temperature of 100°C. Each sensor installed in a FSD block was tested in the chamber prior to installation to ensure accurate and functioning sensors prior to testing.

4.2.2 Light Sensor Response

The TSL2561 and TCS34725 light sensors were characterized against a white light source with a known intensity as measured using a NIST calibrated Extech LT300 light meter. The light source was placed a fixed distance (varied between 15 and 30cm) from the meter and the intensity was measured in an otherwise unlit room with a background light intensity of 2 lux. The light meter was then removed and the light sensors were located the same distance from the light source. For each sensor the observed intensity (lux) was within 5% of that measured by the light meter, Figure 4.6. Response time for each sensor was effectively instantaneous and tracked in real-time with changing intensity of the light source. The light source was able to provide stable calibrated light intensities up to 25,000 lux. While the sensors also are able to measure IR and RGB color, these outputs were not characterized.

4.2.3 Gas Sensor Static Response

A limiting oxygen index (LOI) system was used for initial characterization and calibration of the O_2, CO_2, and CO sensors. By mounting each sensor into the apparatus and using a calibrated gas mixture containing a known concentration of each target gas, it was possible to evaluate the static and dynamic characteristics of the electronic gas sensors.

A calibration curve of the sensor static response (i) was developed tying the sensor output signal (Y_i) to the mole fraction of the target gas, (X_i). Variable-area flowmeters with a range of 1–10 L/min and an accuracy of $\pm$ 0.3 L/min were installed in both gas lines of the LOI apparatus. Gas sensors were hung inside the LOI test chimney, Figure 4.7, with the sensor power and communications wire exiting the top of the chimney. For evaluation of the static response, the sensors were exposed to each reference gas mixture until their output signal reached a steady state value.

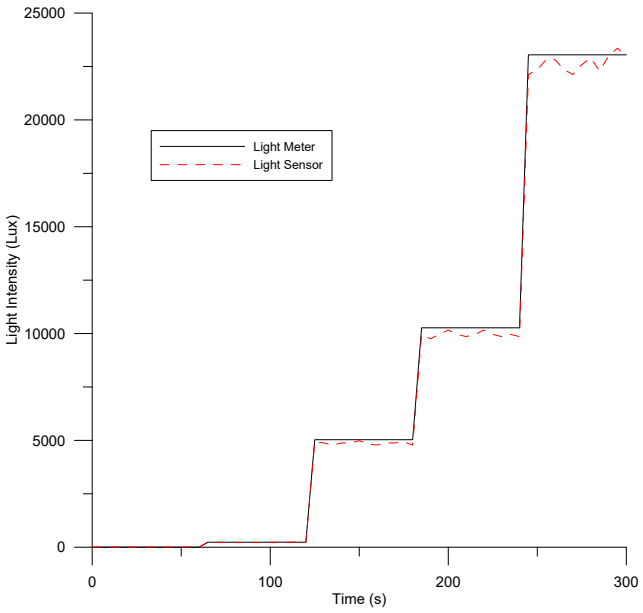


Figure 4.6: Example Light Meter vs. Light Sensor Comparison

For the O_2 sensors, several points on the calibration curve were determined by exposing the sensors to varying O_2 concentrations obtained by adjusting the volumetric flow rates in the O_2 and N_2 lines of the LOI while also maintaining a total flow rate of 10.6 L/min and a gauge pressure of 68.95 kPa (10 psig) in both lines.

For calibration of the CO_2 and CO sensors, custom gas mixtures containing known mole fractions of those gases were required for each point on the respective calibration curves. Since the electronic gas sensors used in this study were known to exhibit good linearity ($\Delta Y_i/\Delta X_i$ is constant over the sensor's range), Appendix B , a two-point calibration scheme was used. Low calibration points were determined using the ambient values of the target gas (400 ppm CO_2 and 5 ppm CO respectively) while custom gas mixtures were used for high calibration points, specifically 10100 $\pm$ 200 ppm CO_2 (N_2 balance) and 1992 $\pm$ 40 ppm CO (N_2 balance) gas mixtures. During calibration, the O_2 line was closed and the calibration gas was run past the sensors through the N_2 line at a flow rate of 10.6 L/min and a gauge pressure of 68.95 kPa.

With the gas temperature held constant, the accuracy of the LOI analyzer can be verified using the following equation, derived from the ideal gas law:

$$X_{O_2} = \left(1 + 1.069 \frac{\dot{V}_{N_2}}{\dot{V}_{O_2}}\right)^{-1} \tag{4.2}$$

where $\dot{V}_i$ is the volume flow rate of gas i measured by the flowmeters, M_i is the molar mass of gas i, and $\sqrt{M_{O_2}/M_{N_2}} = 1.069$.

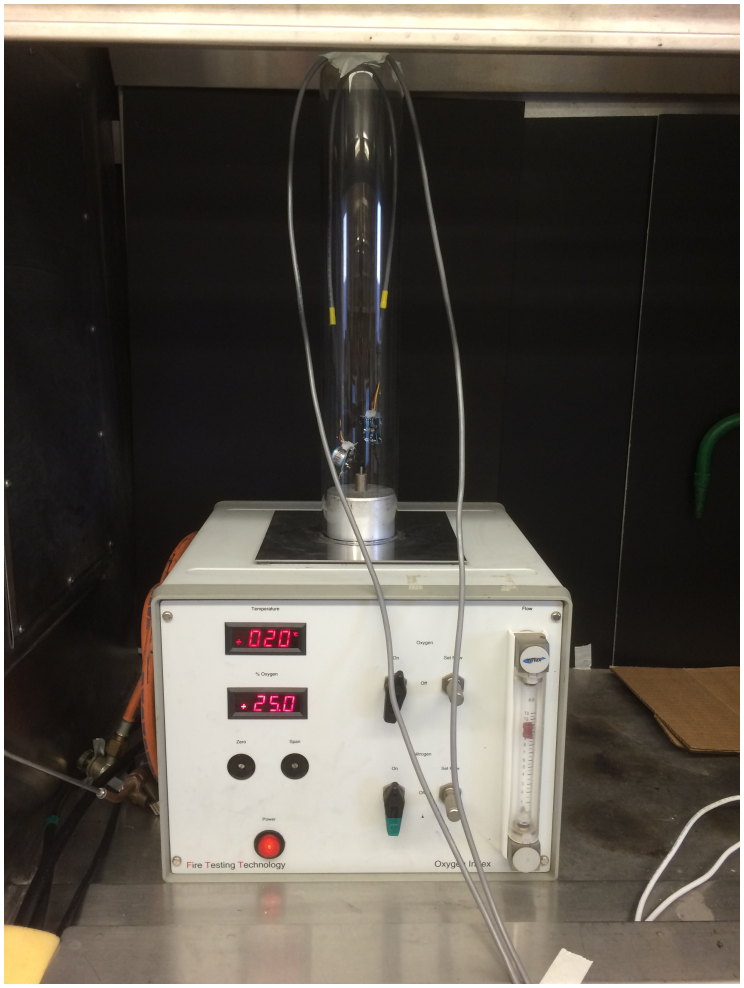


Figure 4.7: Sensors in LOI Chamber

In practice, the O_2 sensors tended to reach steady state in less than a minute, while CO_2 and CO sensors could take as long as 20 minutes to reach steady state (although

the apparent initial response was instantaneous). It should be noted that after "burn in" the response time for the CO_2 and CO sensors appeared to be much quicker. From these results, an example of which is shown in Figures 4.8a and 4.8b, representative calibration curves were established in the form given by Equation 4.3:

$$X_i = a_i Y_i + b_i \tag{4.3}$$

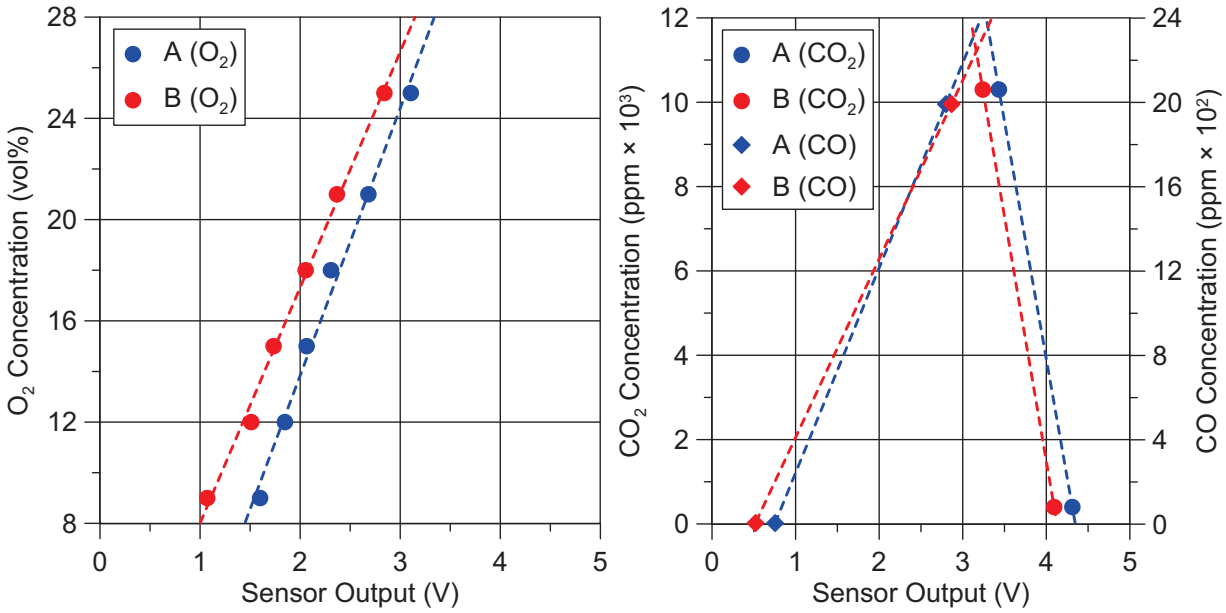
where the coefficients a_i and b_i are summarized in Table 4.4. Similar calibrations were performed and used in the analysis of the output data from all the sensors involved in the study.

Table 4.4: Calibration coefficients for gas sensors used in this study

Sensor ID	Gas	Output Units	a_i	b_i	Baseline (V)
A	O_2	vol%	10.07	-2.18	2.392
B	O_2	vol%	9.31	-1.31	2.368
C	O_2	vol%	12.58	-10.79	2.563
D	O_2	vol%	8.58	0.53	2.112
E	O_2	vol%	11.48	-8.75	2.732
F	O_2	vol%	7.63	2.18	2.167
A	CO_2	ppm	-12375	52499	4.21
B	CO_2	ppm	-11250	46525	4.10
C	CO_2	ppm	-13718	59884	4.34
D	CO_2	ppm	-7945	34605	4.31
E	CO_2	ppm	-19063	80585	4.21
F	CO_2	ppm	-8577	37325	4.31
A	CO	ppm	971.7	-728.4	0.755
B	CO	ppm	846.6	-435.4	0.520
C	CO	ppm	1058.7	-794.0	0.755
D	CO	ppm	875.8	-468.8	0.541
E	CO	ppm	1131.1	-806.0	0.717
F	CO	ppm	930.7	-518.7	0.562

4.2.4 Gas Sensor Dynamic Response

The sensor specifications (Table 4.3) provided by the manufacturer indicate that the t_{90} response time for the CO_2 and CO sensors should be less than 30 seconds; however, obser-



(a) O_2 sensor calibration curves

(b) CO and CO_2 sensor calibration curves

Figure 4.8: CO_2 and CO sensor calibration curves

vations made during static response calibrations alluded to a much slower initial response. To this end, the response of each sensor was assessed by imposing a step change in the target gas, and applying a first-order dynamic response correction. To achieve a step change with the LOI, the target gas mixture was first allowed to flow through the LOI with the chimney in position but no sensors installed. Once the target gas flow and mole fraction were set, the chimney was removed, the sensors affixed inside, and then the chimney with sensors was placed back into position on the LOI at a recorded time t_{ON}. The dynamic response of the O_2 sensors was assessed in a 15% mixture of O_2 by volume; the custom gas mixtures described above were used for the CO_2 and CO sensors.

In the following equations, y_i and Y_i are the raw signal output and the corrected signal of sensor i respectively; note that Y_i is used in Equation 4.3 to determine the value of the target gas X_i in units of vol% or ppm. The first order response model is given by:

$$\tau_i \frac{\mathrm{d}y_i}{\mathrm{d}t} + y_i = k_i Y_i \ , \tag{4.4}$$

where τ_i and k_i are the time constant and gain of sensor i respectively. Given a step input from the baseline voltage B_i to the reference voltage A_i, and an initial condition of

$y_i(t=0) = k_i B_i$, the solution to Equation 4.4 for the "modeled" signal $y_{i,m}$ is:

$$y_{i,m} = k_i \left[A_i + (B_i - A_i) \cdot \exp\left(\frac{t_{ON} - t}{\tau_i} \right) \right] \quad . \tag{4.5}$$

The time constant τ_i was determined for each sensor by minimizing the sum of the square of the residual terms $(y_i - y_{i,m})$ over the domain of the step input. For the O_2 sensors the time constant was quite small, with an average value of 10 s. In contrast, the time constant for CO_2 and CO sensors was significantly greater, with average values of 70 s and 159 s respectively. These time constants are exceptionally large, and when used to correct data, will have an effect of increasing the apparent rate of change. It should be noted that, despite the large response times, the apparent response was instantaneous for all sensors. Furthermore, the gain was negligible for all three sensors ($k_i = 1$). With the time constants determined, and $\mathrm{d}y_i/\mathrm{d}t$ computed using a noise-robust numerical differentiation scheme [73], the corrected signal Y_i was then computed from Equation 4.4.

Additional Considerations

Each gas sensor used in this research produces an analog output signal between 0 and 5 V. The signals are acquired using 10-bit analog channels (i.e. 1024 unique values), so the resolution of each output signal is approximately 4.9 mV. Applying the calibration curves (Figures 4.8a–4.8b), the resolutions of the gas sensors as configured are therefore approximately 0.05% for O_2, 50 ppm for CO_2, and 5 ppm for CO. This resolution is suitable for evaluating trends in the concentrations of these gases during the tests conducted; however, it was found that some smoothing of the analog data was required.

Sensor stability is qualitatively very good with two important considerations. First, the CO_2 sensors require that a nominal amount of target gas (approximately 350 ppm, typical of ambient levels) is present in order to produce a stable response. Based on normal ambient CO_2 concentrations, and the anticipated test conditions, this does not pose a problem for the FSD sensor block. Even when the level is high enough, though, the CO_2 sensors occasionally fail to produce stable baseline readings in ambient conditions. This is most often found to be due to a defective sensor, which indicates that it is critical to test and calibrate these sensors prior to use.

The second consideration is that the gas sensors used in this study have an initial warm-up period of anywhere from an hour (O_2 sensors) to as long as two days in the case of CO_2 and CO sensors. Therefore, all of the sensors were connected to a reliable power source for a period of several days, without interruption, before they were conditioned, calibrated

and used in testing. Once the warm-up period was complete the sensors performed well and remained stable throughout the entirety of the experimental test duration.

4.3 Experimental Design

As described in Chapter 3, the fire tests were conducted in the University of Waterloo Live Fire Research Facility "Burn House", a two-story steel structure designed to accommodate large scale fire experiments. The structure is fire hardened, with a 120 m^2 floor area on each story and a total structure volume of approximately 290 m^3. The interior wall configuration can be varied based on the specific set of experiments being conducted so that for the large fire experiments described below, the building is outfitted with interior steel stud walls covered in gypsum wall board throughout the lower floor. An additional layer of concrete board is installed on those areas of the walls and ceiling directly exposed to fire. Non-combustible fiber insulation is installed in the burn room to provide additional fire resistance at the ceiling; this also reduced heat losses through the ceiling to the upper levels of the house. A series of cement board platforms are installed on the floor to provide fire resistance, as well as facilitate running, and provide protection for, instrumentation lines that pass through the burn room to the central data acquisition system. Spray foam was again used to seal cracks throughout.

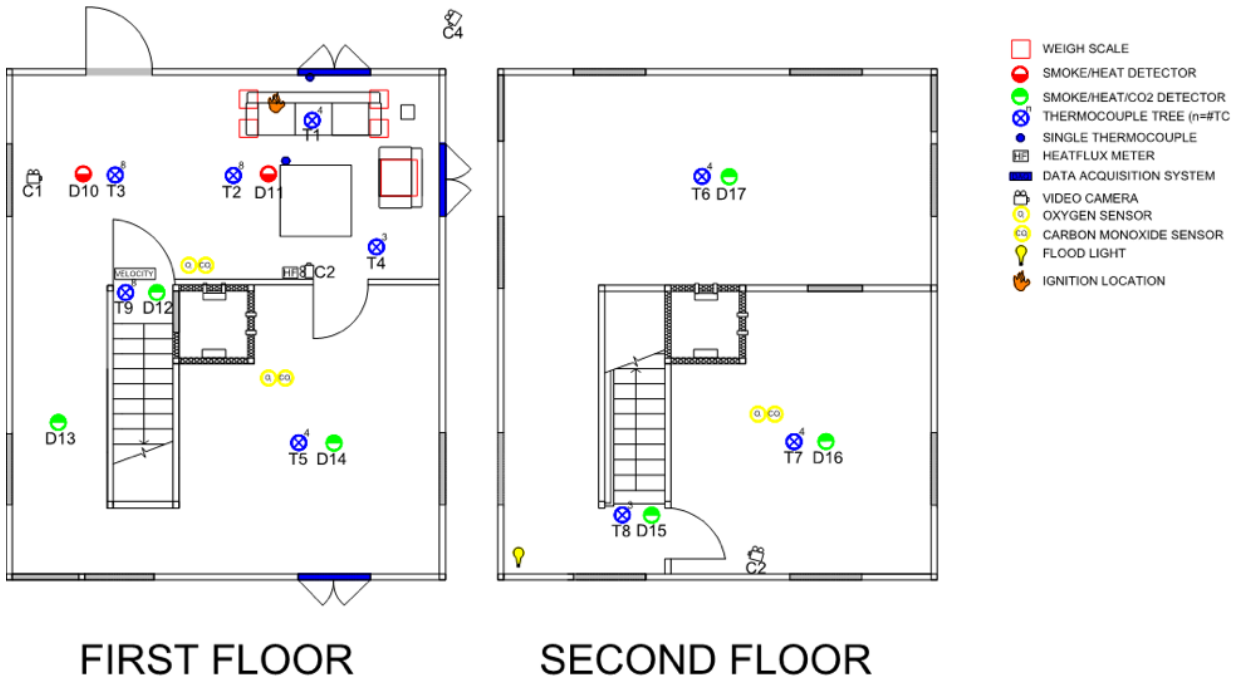


Figure 4.9: Layout of burn facility

4.3.1 Instrumentation and Methodology

The Burn House was instrumented with a variety of sensors in order to evaluate the fire growth, thermal development, and tenability within the structure. The positioning and types of the instrumentation at the various locations in the burn house is shown in Figure 4.9.

Temperature and Gas Measurements

Nine thermocouple trees, each containing an array of thermocouples spaced vertically from floor to just below the ceiling of the room (in total 50 individual thermocouples in the nine arrays), were positioned throughout the rooms, hallways, and stairs of the experimental facility. These are designated as T1 through T9 in Figure 4.9. The thermocouples were 24 gauge Type K, with ceramic fibre insulation and a braided Inconel jacket. All thermocouple output was measured and recorded using a National Instruments (NI) Fieldpoint data acquisition system (with built-in cold junction compensation) at a sampling rate of approximately 1 Hz. Temperature readings are considered to be accurate to 0.4% of the measured temperature.

Gas sampling for oxygen and carbon monoxide concentrations was conducted at three locations; in the living room, in the kitchen, and in the small bedroom as shown in Figure 4.9 using an independent Arduino interface as the data acquisition system. In each case, oxygen and carbon monoxide sensors were mounted together at a height of 0.6 m from the floor. This elevation was used for two reasons; first, it is representative of the minimum height required for occupants to be able to escape the structure; and second, it was the elevation of the seat of the sofa and therefore concentrations measured at this position represent gas concentrations at the base height of the fire.

All sensors were calibrated at the start of the experiments, and any sensor damaged during an experiment was replaced prior to the next experiment.

The velocity of gases through the stairwell door was measured at the base of the stairs on the first story using a vertical rake of eight sensors located 0.15 m (6 in) in from the right side of the doorway and spaced 0.20 m apart. Each sensor consisted of a high temperature bi-directional probe connected to a differential pressure transducer, installed at the same height as the probe to which it was connected, as well as a thermocouple to measure gas temperature at that height. From these measurements, and given calibration coefficients for each pressure transducer and bi-directional probe, gas velocity was calculated using

Bernoulli's principle for incompressible flow. All transducer signals for velocity measurement were recorded with the same NI DAQ system, and at the same sampling frequency, used to acquire the thermocouple signals.

Mass Loss and Heat Flux

High precision load cells were used to measure the time-varying mass of both the sofa and the armchair throughout the duration of the tests. A set of four 60 kg capacity load cells were used to monitor the mass of the sofa (one under each foot) and a single 150 kg capacity weigh scale was used for the armchair. The load cells were calibrated prior to each experiment, and had an accuracy of 10 g. To protect from thermal damage the load cells were shielded by a protective layer of drywall over a thin wood frame placed between the cells and the furniture items. Sofa and armchair mass was monitored and the analog output of each was recorded with the NI system.

A water-cooled Gardon heat flux gauge was installed with its exposed face flush with the wall facing the sofa at a height of 0.6 m from the ground. The heat flux gauge was positioned to have a clear view of the developing fire. During a test, it measured the total incident heat flux from the fire, the surroundings, and hot gases within the living room. The voltage output of the Gardon gauge was recorded with the NI system and a calibration coefficient was applied during post processing to derive the values of heat flux over time.

Commercial Smoke and CO Sensors

Off-the-shelf commercial smoke detectors were installed at various locations throughout the structure, representative of the typical installation locations in residential buildings. The detectors were used to measure the smoke detector response time at each installed location for each of the fires. All of the detectors consisted of a combined smoke and heat detector. Devices on the second floor were additionally equipped with a carbon monoxide detector. The detectors were connected to a fire alarm control panel to record the activation times for each of the devices.

Video

A series of day/night surveillance cameras were installed throughout the burn house. The cameras were positioned to monitor the fire growth and spread, as well as the smoke development through the building. The cameras feeds were recorded by a digital video recorder located outside the burn house.

Fire State Determination Blocks

In addition to the individual sensors and data acquisition equipment described above, the new FSD blocks were located throughout the experimental facility. Locations of the FSD blocks varied based on the specific experiment; however, in general a block was located adjacent to Camera 1 (C1), a block was located at floor level at the same location, a block was located on the ceiling in the hallway (D13), and finally a block was located at the top of the stairs on the second floor (D15).

4.3.2 Fuel Load

A total of nine tests were conducted using identical fuel arrangements as shown in Figure 4.9. Three distinct furniture fuel compositions were used, with three repeat tests done for each sofa type (A, B, C). For each test, the fire load consisted of a three-seat upholstered sofa, an upholstered armchair, a hard wood coffee table, and a hard wood side table. Two types of textile were used for the furniture upholstery; a fabric constructed with natural fiber and a fabric constructed from polyester. The mass of the frame, foam, fabric, and other items were all recorded for each sofa and chair during construction. A breakdown of the weight of each main component is provided in Table 4.5 for each sofa, along with post-fire mass and total mass loss. This mass breakdown is important as it directly relates to the potential energy available, in particular the mass of the foam which was the key contributor to the heat release rate of each fire.

The fires were initiated with #4 wood crib consistent with British Standard 5852 [105]. The crib was placed on the end of the sofa furthest from the chair and was positioned against the rear cushion, Figure 4.9. After ignition the fire was allowed to progress without interference.

In each test the entire mass of fabric and foam on the sofas was consumed, while the remaining sofa components and furniture showed only minor indications of involvement in the fire: some surface charring was observed on the upholstered chair and coffee table. Despite the charring, there was no observation of flaming combustion or indication of mass loss on either table or on the armchair. For purposes of analysis it is assumed that there was no secondary fire in these experiments, and therefore that the temperature, species and smoke distributions in the burn room developed solely from the sofa fire.

Table 4.5: Sofa Fuel Component Weight (kg)

	Type	**Frame**	**Foam**	**Fabric**	**Misc.**	**Total**
Sofa 1	A	37.9	10.4	7.7	4.1	60.1
Sofa 2	A	38.1	10.5	7.5	4.0	60.1
Sofa 3	B	34.1	10.6	7.7	4.1	56.5
Sofa 4	C	34.4	8.4	5.7	4.1	52.5
Sofa 5	C	34.2	8.4	5.7	4.1	52.4
Sofa 6	C	37.8	8.5	5.7	4.1	55.2
Sofa 7	B	37.8	10.2	9.2	4.0	61.2
Sofa 8	A	37.4	10.1	9.2	3.9	60.6
Sofa 9	B	36.9	9.9	9.2	4.0	60.0



Figure 4.10: Interior of Burn Structure Showing Load Cells



Figure 4.11: Interior of Burn Structure Showing Fuel Load

4.4 Results and Analysis

In all nine of the tests, the sofa fires developed with an initial period of rapid growth, followed by an abrupt transition to decay; the fires would eventually extinguish completely within 20 minutes following ignition. In every case, both windows in the living room cracked, and the inner panes were observed to have broken away and the frames showed signs of thermal deformation. However, in no case did a window completely break out, and as such, no additional ventilation was provided to the fire beyond the leakage inherent in the structure. Accordingly, the fires behaved as would be expected of typical ventilation-limited fires, with no transition to flashover being observed. The repeatability in the test results for each type of furniture (A, B, C) allowed for comparison of a single data set for each type to be representative [106]. The following sections discuss the observations and analysis for the representative large scale tests.

4.4.1 Mass Loss and Heat Release Rate

A general progression of the fire development is shown in Figure 4.12, which was typical of the large fire tests. As can be seen, the fire progresses along the sofa and continues to grow in intensity as the sofa becomes more fully involved. During this period the smoke layer begins to form and descend increasing the room temperatures and reducing visibility in the space. As the growth continues the fire becomes ventilation limited, eventually burning out. To delve further into detail of fire development mass loss rates and related heat release rates were calculated and assessed.

Heat release rate (HRR) was computed using the measured mass loss rate of the sofa and an estimated value of average heat of combustion for the burning material, $\Delta H_{c,eff}$. Given the noise in the mass loss data caused by small fluctuations in the instantaneous mass recordings, a spline was fitted to the mass versus time data to achieve a representative mass loss profile for each test. The mass loss rate is then calculated from the time derivative of the spline of the measured mass data, and the heat release rate is determined from the mass loss rate multiplied by the assumed effective heat of combustion.

It was determined that the contribution of the frame and miscellaneous sofa components to the participating fire load was negligible, based on pre and post test weight comparisons and physical observations. As a result $\Delta H_{c_{eff}}$ was assumed to be 17.9 MJ/kg. This value has been shown to be consistent with large-scale sofa burns, as well as previous cone calorimeter testing, of similar polyurethane foam cushion material [107], though each material will ideally be tested to ensure that $\Delta H_{c_{eff}}$ utilized are correct. Throughout the course of the fire the mass loss rate varies. The maximum observed mass loss rate ($\dot{m}_p$) and the average observed mass loss rate ($\dot{m}_{avg}$) for each test are provided in Table 4.6 and the heat release rate ($\dot{Q}$) is calculated in accordance with Equation (4.6) where the derivative is numerically obtained using central difference from the spline fit curve.

$$\dot{Q} = \Delta H_{c_{eff}} \frac{\Delta m}{\Delta t} \tag{4.6}$$

The results show that there is some variation regarding the heat release rate and fire growth rate, however the rapid rate of fire growth resulted in the fire becoming oxygen deficient as observed by the measured and observed conditions.

Table 4.6 provides measured and calculated parameters related to the mass loss and HRR for each test. Incipient time, t_i, is defined as the time period after ignition but prior to the observation of a noticeable increase in HRR (or more specifically a noticeable increase in the mass loss rate). A t^2 fire growth rate coefficient was estimated based on a curve fit from times t_i to t_p where t_p is the time at which the peak heat release rate $\dot{Q}_p$ is believed

to have occured based on the maximum measured $\dot{m}_p$. The fires ranged from nominally slow growth (Test 3) to ultrafast (Test 8) based on the calculated α value and observed $\dot{Q}_p$. The integral of the HRR is calculated to determine the total energy released, Q. In general the tests of identical material resulted in very comparable weight normalized total heat release rate (±5%), however Type C (tests 3, 6, and 9) showed the greatest variation between the tests (-13% to +20% from calculated).

Table 4.6: Summary of Measured Parameters

	$\dot{\mathbf{m}}_p$ *(g/s)*	$\dot{\mathbf{m}}_{avg}$ *(g/s)*	$\Delta\mathbf{m}$ *kg*	α *(kW/s^2)*	$\mathbf{t}_i$ *s*	$\mathbf{t}_p$ *s*	$\dot{\mathbf{Q}}_p$ *kW*	$\mathbf{Q}$ *MJ*
Test 1 (Sofa 9, B)	247	27.1	15.5	0.08600	132	357	2632	395
Test 2 (Sofa 2, A)	146	27.4	26.1	0.08560	174	342	2416	393
Test 3 (Sofa 4, C)	68	16.6	19.4	0.00383	306	834	1067	350
Test 4 (Sofa 7, B)	129	24.2	25.2	0.03294	186	450	2296	430
Test 5 (Sofa 1, A)	464	19.4	16.5	0.21000	117	276	3531	391
Test 6 (Sofa 6, C)	597	20.9	20.5	0.03294	186	463	1897	290
Test 7 (Sofa 3, B)	302	15.3	20.5	0.10000	125	310	1897	400
Test 8 (Sofa 8, A)	887	20.6	16.7	0.22000	100	256	2609	430
Test 9 (Sofa 5, C)	302	20.0	22.5	0.02250	200	517	2333	400



Figure 4.12: Development of Sofa Fire

Figure 4.13 illustrates a representative set of time varying HRR plots determined during the test series for each sofa assembly type (A, B, C). The repeat tests for a given sofa type resulted in similar growth rates α and $\dot{Q}_p$ [106]. The different sofa types, on the other hand, yielded different results where sofa C exhibited a significantly slower growth, α, and lower $\dot{Q}_p$ but with a significantly longer burning duration as shown in Table 4.6 and illustrated as an example in Figure 4.13.

The calculated results are consistent with the measurements of heat release rate for similar furniture in free burning atmospheres completed by others. Similar fire experiments are documented in [107, 108], which show similar peak heat release rates greater than 3 MW

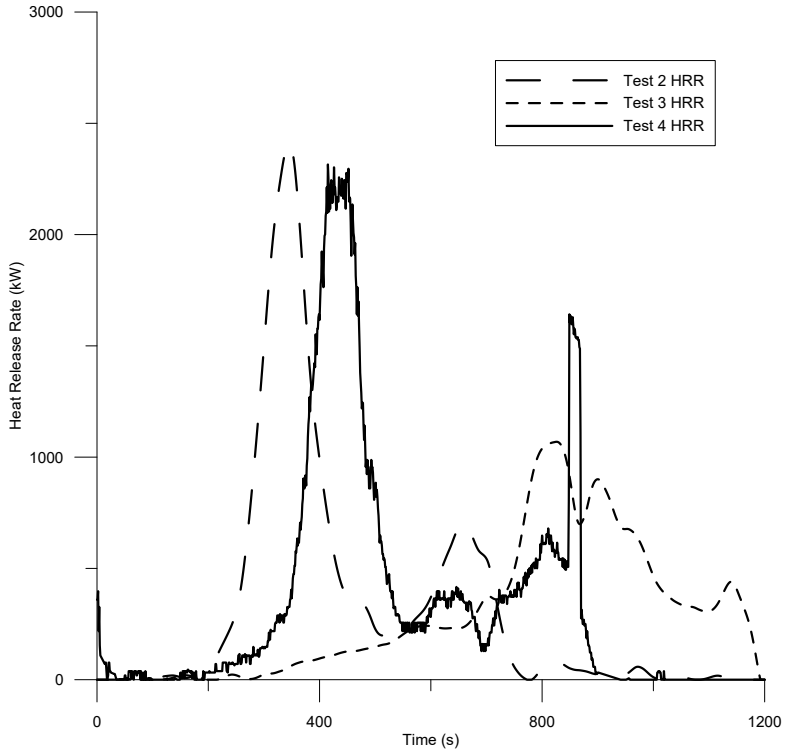


Figure 4.13: Comparison of Heat Release Rate for Test 2-4

for three seat sofas of similar mass to the current furniture. Given the similar construction type, mass, and fire growth rates of the furniture in this study, a similar peak heat release rate would be expected. In this case, the peak heat release is reduced, providing evidence that the fires became under-ventilated during the burning phase, resulting in reduced burning intensity and heat release. This is verified by the gas measurements taken during the experiments discussed below.

4.4.2 Species Production

Gas Concentration

O_2 and CO measurements were made throughout the experiments using the FSD sensor blocks. The results were largely consistent with expectations as shown in the results of Test 8, Figure 4.14. The oxygen in the burn room begins to decrease with increasing HRR and shortly thereafter the CO levels increase. As discussed earlier the CO sensors utilized in this study have a maximum range of 2500 ppm, which was reached in each of the fires. Thus while the CO concentration likely attained levels above those measured, which is reasonable to assume given that the O_2 concentration continued to decline in numerous experiments after the CO levels peaked, the observed increase in CO remains useful and informative as it lasts well beyond the incipient stage of the fire. In most cases, the upper detection limit of CO concentration was only exceeded at or near the measured peak heat release rate, once the fire was well developed, and thus the incipient and growth stages of the fire were well documented with regards to CO development, at least qualitatively.

It can be seen that the oxygen concentration in the first floor begins to decrease significantly immediately prior to the decrease in calculated heat release rate and the heat release rate declines rapidly as the oxygen concentration decreases beyond approximately 18%. This is very close to the limiting oxygen concentration (LOI) for flexible polyurethane foam (the primary component burning) and accordingly provides further rationale that the measured peak heat release rate occurred at the onset of an under-ventilated condition.

The oxygen concentrations continue to decline as the heat release rate decreases, and eventually, the fire self extinguishes. In each case, the fire on the sofa continued to burn for a period following the peak heat release rate and the majority of foam and fabric comprising the sofa was observed to have been consumed when the fire extinguished, while most of the wood framing material was left intact. While there was some thermal damage and charring to the adjacent furniture pieces, primarily the upholstered chair, there was

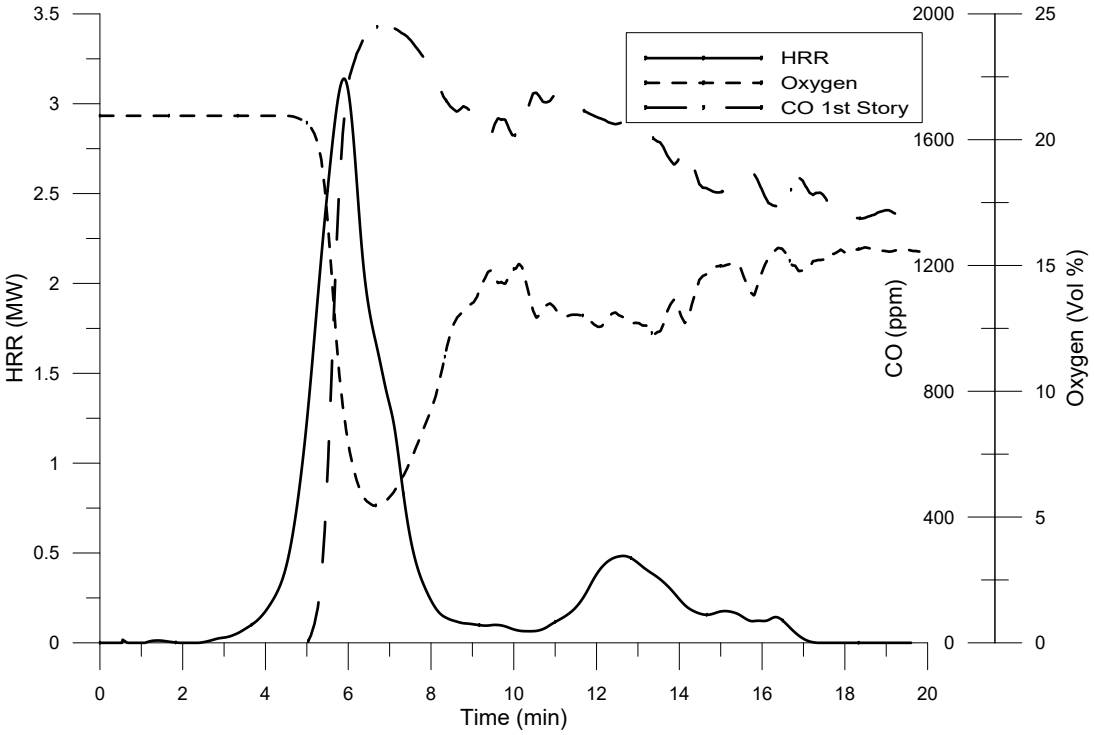


Figure 4.14: HRR, O_2, and CO Concentration for Test 8



(a) Sofas post-fire (b) Chairs post-fire

Figure 4.15: Sofas and chairs post-fire

not significant fire spread or damage to the other furniture items, Figure 4.15 and they were deemed not to have contributed significantly to the fire development.

4.4.3 Compartment Temperature and Humidity

Compartment temperature was measured using a series of thermocouple trees as well as via the sensor blocks. Relative humidity was measured using the sensor blocks. The compartment temperatures varied based on location in the burn house as well as a function of height within each room. Peak gas temperatures were observed to be in the vicinity of 900°C, Figure 4.16, while average upper layer temperatures were closer to 600°C in the burn room, consistent with temperatures usually illustrative of flashover, though flashover was not observed in any of the tests. Figure 4.16 shows the variation in temperature vs height in the burn room as a function of time and is illustrative of the typical variation observed throughout the tests, though the specific time resolved data varied for each test.

In general, the temperature follows similar trends to that of HRR. Peaks are observed at approximately the same times with typical temperature gradients existing as a function of height. Similarly RH begins to increase as HRR and temperature increase. As HRR begins to decline and room temperatures decrease, the RH similarly drops and continues to decline until it eventually returns to ambient conditions.

The initial rise in RH is understood to occur as the combustion gasses contain significant quantities of water which leads to a rise in the quantity of water vapor, and consequently

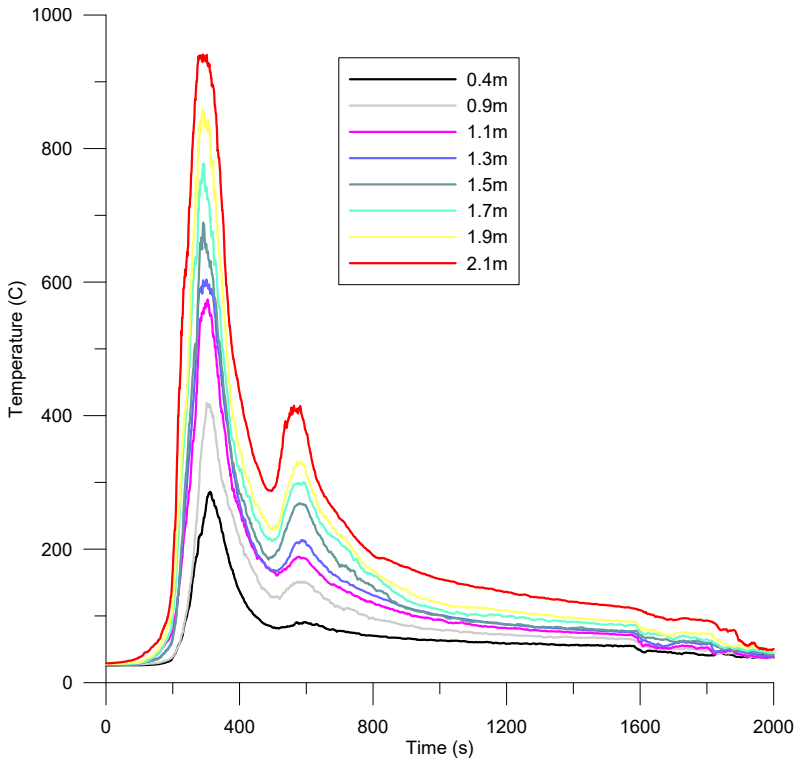


Figure 4.16: Temperature in burn room at TC tree #2, Test 8, ground is Z=0m

a rise in RH as the temperature is slowly increasing, Figure 4.18. As Q and temperature increase, the RH declines as RH is temperature dependent, an increase in T causes a decrease in RH for the same content of water vapor, Equation (4.7).

$$RH = 100\% * 10^{m\left[\frac{T_d}{T_d+T_n} - \frac{T_a}{T_a+T_n}\right]} \tag{4.7}$$

The relative humidity within the structure changed throughout the duration of the test as expected. The location of the sensors relative to the fire source (i.e. room of origin, adjacent room, or 2nd floor) as well as the specific fire fuel load impacted the specific trends.

4.4.4 Heat Flux and Light Intensity

Heat flux was measured opposite the couch with the face of the heat flux gauge flush to the wall. Thus initially the heat flux at the gauge is primarily direct radiation from the fire, however as the fire progresses there is additional flux from hot layer reradiation and descent of the plume. As shown in the representative data of Figure 4.19, the heat fluxes observed at the wall did not exceed the typical flashover criterion of 20 kW/m^2 during the test duration, reaching peak values of nominally 12 kW/m^2, 13 kW/m^2, and 6 kW/m^2 for Tests 2, 3, and 4, respectively. This is consistent with the fact that flashover was not observed during any of the tests and that the peak heat flux occurred at approximately the same time as peak HRR. Thus it is assumed that the wall heat flux was nominally the same or greater than that which would have been observed at floor level.

The light intensity observed during the tests at each of the FSD sensor blocks showed a rapid increase in lux that corresponded to the increase in the calculated heat release rate of the fire as well as the observed measured heat flux. This increase in lux intensity tracked with changes in HRR throughout the fire or until visual obscuration of the light sensor began to occur at which time the light intensity decreased. Of note is that the rise in light intensity tracked in real time with the HRR and peaked just before the peak HRR for test 4 before quickly declining, Figure 4.20. Similar trends were observed for the other tests with the lux levels increasing in proportion to the HRR. As the HRR increased, the generation of products of combustion similarly increased which resulted in a lowering of the smoke layer height and obscuration of the FDS sensor block. This decline is consistent with the smoke layer heights determined in [106] and may also be observed in the differences in measured values observed at the various the sensor locations. In Figure 4.20 it may be observed that Yun002, which was located at floor level in the burn room, illustrated a

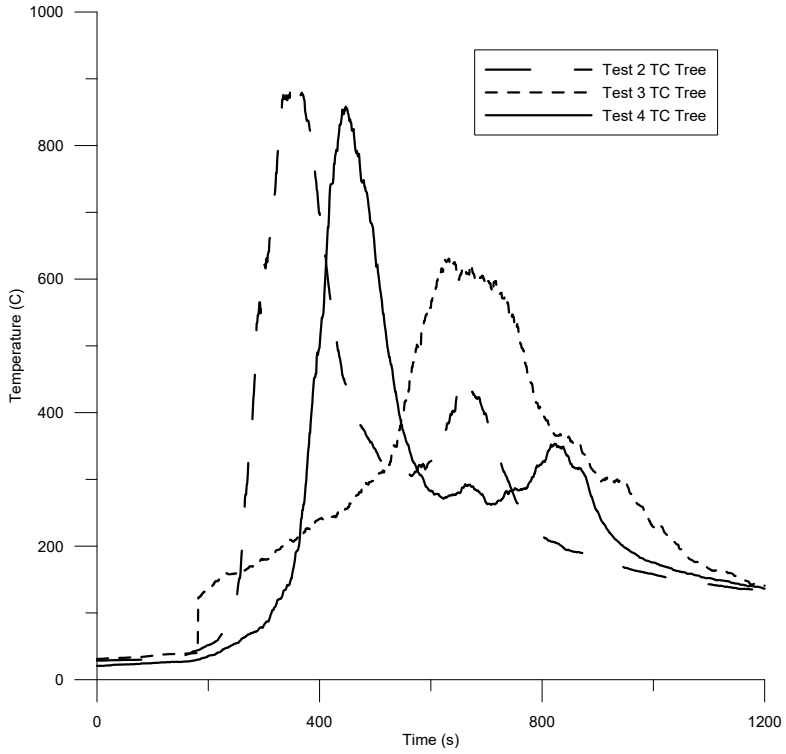


Figure 4.17: Temperature Measured at FSD sensor 01 for Tests 2-4

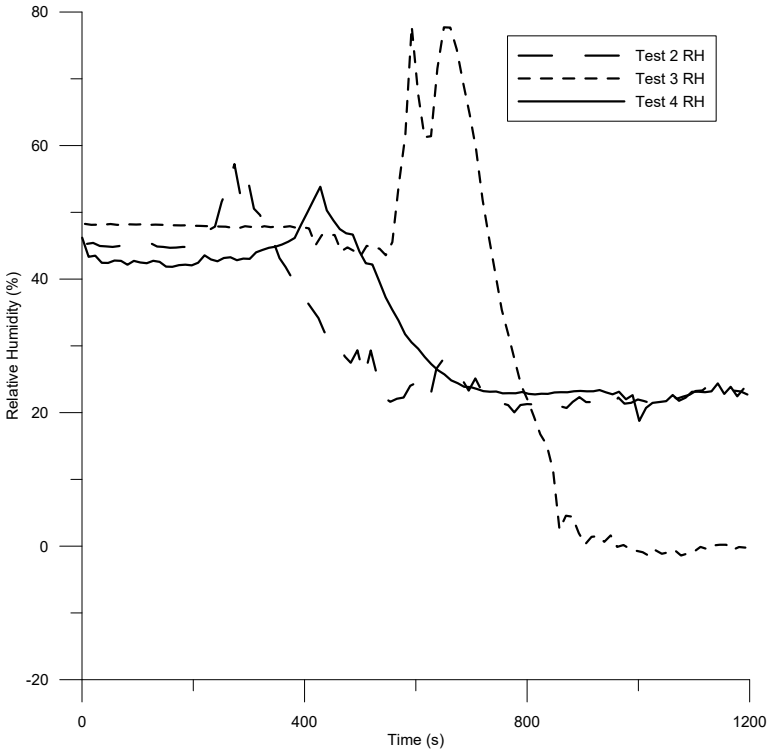


Figure 4.18: RH Measured at FSD sensor 01 for Tests 2-4

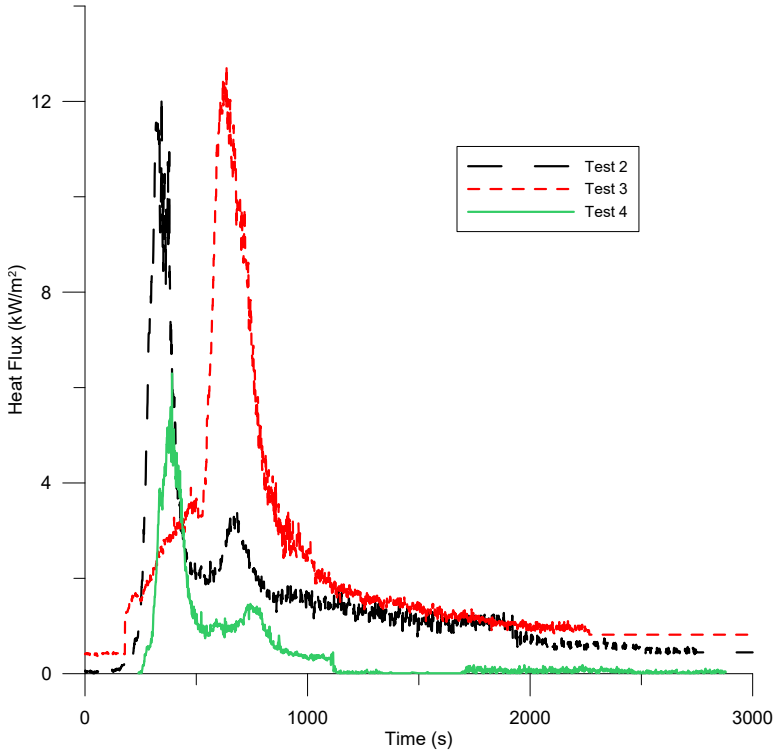


Figure 4.19: Measured Heat Flux for Tests 2-4

similar trend regarding response to that of Yun005 located at a height of 1m, however it showed a significantly reduced peak as would be expected based on its location with the compartment.

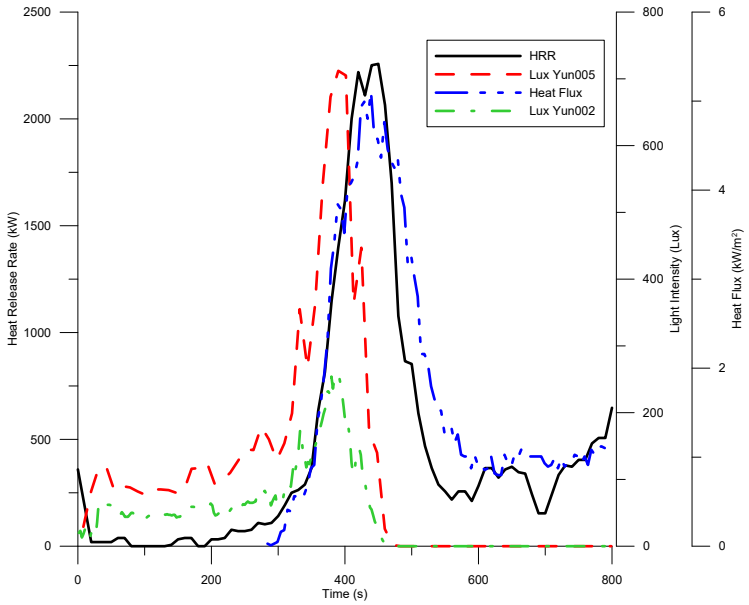


Figure 4.20: Measured Heat Release Rate, Light Intensity, and Heat Flux for Test 4

4.4.5 Combined Results

When examining the results from the various sensor response it is obvious that the FSD sensor block is able to detect and measure in a quantifiable way the progress of the fire. The O_2 and CO gas sensor readings tracked with HRR while the light intensity tracked with HRR and heat flux. Figure 4.21 illustrates the combined results for Test 4 from the FSD sensor block in conjunction with the measured heat flux and calculated HRR. As it has been shown in the previous sections that fires can be observed using the FSD sensor block for both small and larges-scale fires, it remains to be demonstrated how they respond and what they observe in non-fire conditions. To this end background non-fire data was collected and is discussed below.

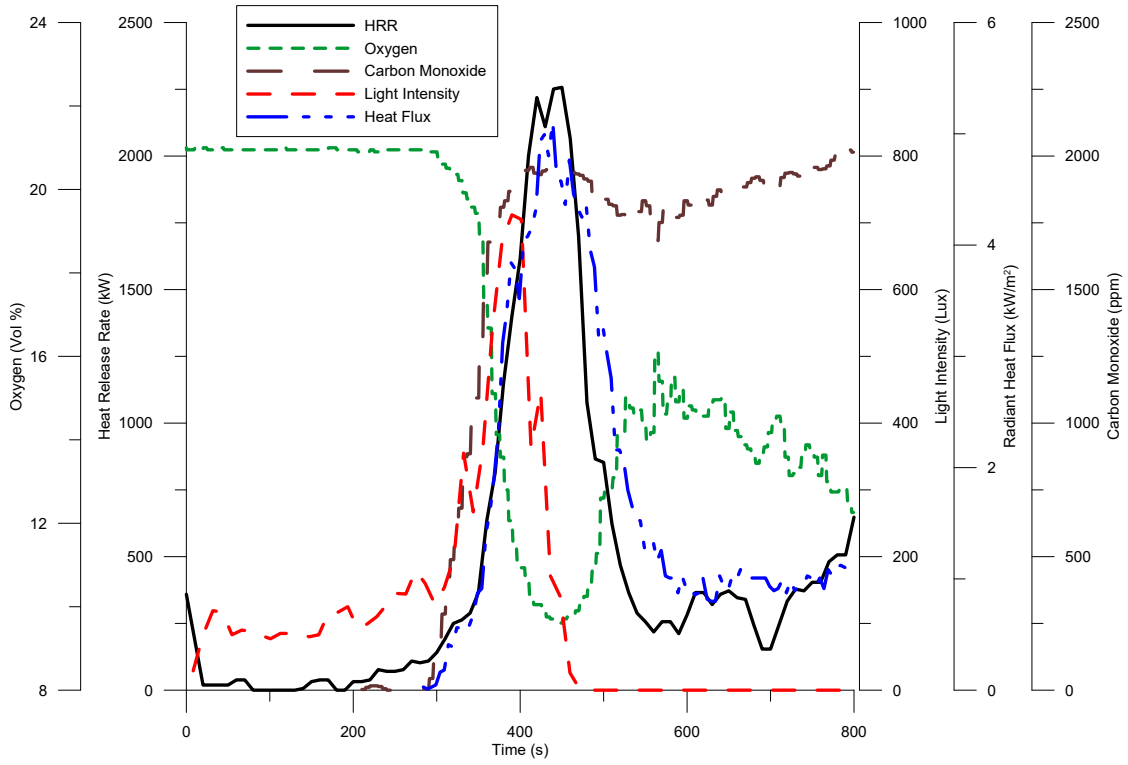


Figure 4.21: Heat Release Rate, O_2 and CO Concentration, Heat Flux and Light Intensity for Test 4

4.5 Background Data Collection

For fire state determination to be possible it is necessary to be able to detect and recognize changes in sensor response that are sufficiently different from normal that it is clear that a fire is present. While for some parameters this is straightforward and obvious, temperature for instance, other sensors may not have a clear and distinct response that can be linked directly to the presence of a fire.

As a result, background data was collected from a variety of locations over an extended period of time to establish non-fire conditions for comparison with the evaluated fire scenarios. This data was used in the algorithm development discussed in Chapter 5. Temperature, humidity, and light was measured in multiple locations for several months to evaluate the sensor response in non-fire conditions. Additionally CO was measured however, the background CO levels were negligible and there was no observable change in the background over the duration of the tests.

The non-fire background data indicates that while changes in parameters are observed, that the amplitudes, rate of change (ROC), and frequency of the signals are clearly differentiable from those observed during fire conditions.

A sample of the background data collected is provided in Figures 4.22 and 4.23 showing the raw data collected as well as the computed ROC data from an office setting. Similar data was also collected from multiple locations in a residential setting and showed similar results. As the intent of fire state determination is to quantitatively differentiate fire from non-fire conditions, this background data helps forms the basis for the algorithm development discussed in the following chapter by establishing a range of conditions that may be encountered in which the exposed FSD sensors will observe changes even when a fire is not present. This background data also supports the ROC thresholds that were established in Chapter 3.4 and which are utilized in Chapter 5.2.

4.6 Conclusions

The work performed in this phase of the research confirmed the findings from Chapter 3. Namely it was determined that characteristics of fires could reliably be determined using existing non-fire sensors. In all 9 large scale tests, a fire was recognized by the light, temperature, and relative humidity sensors. Furthermore when the sensors were in place the gaseous sensors also showed a clear response to the changing environment. When the signals generated during a fire were compared with nuisance and background signals they

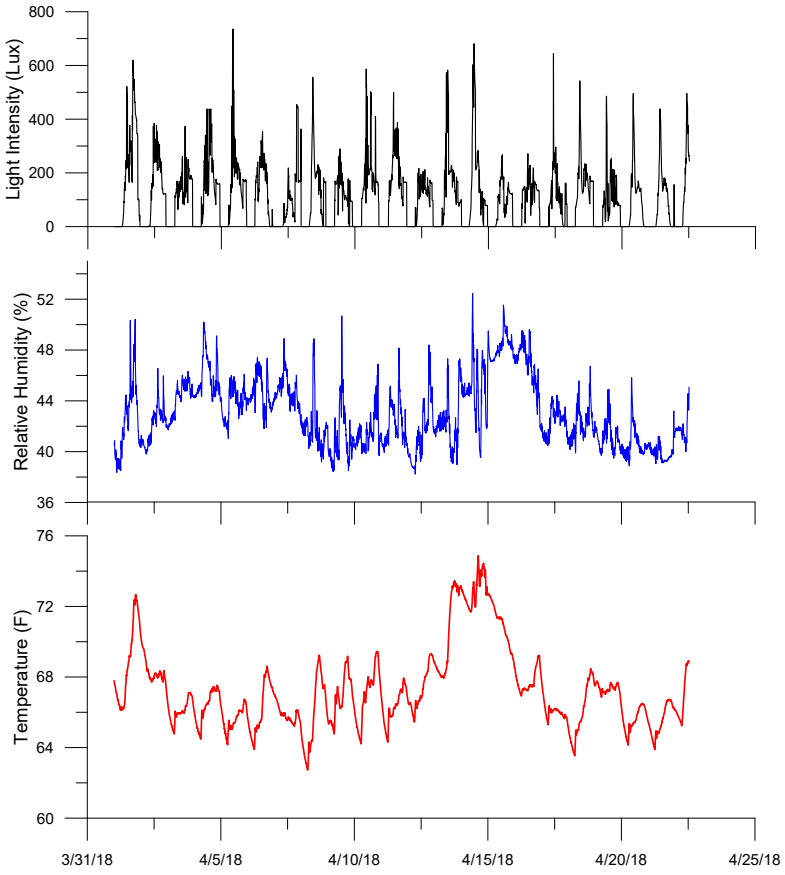


Figure 4.22: Background long term temperature, RH, and lux measurements in an office setting

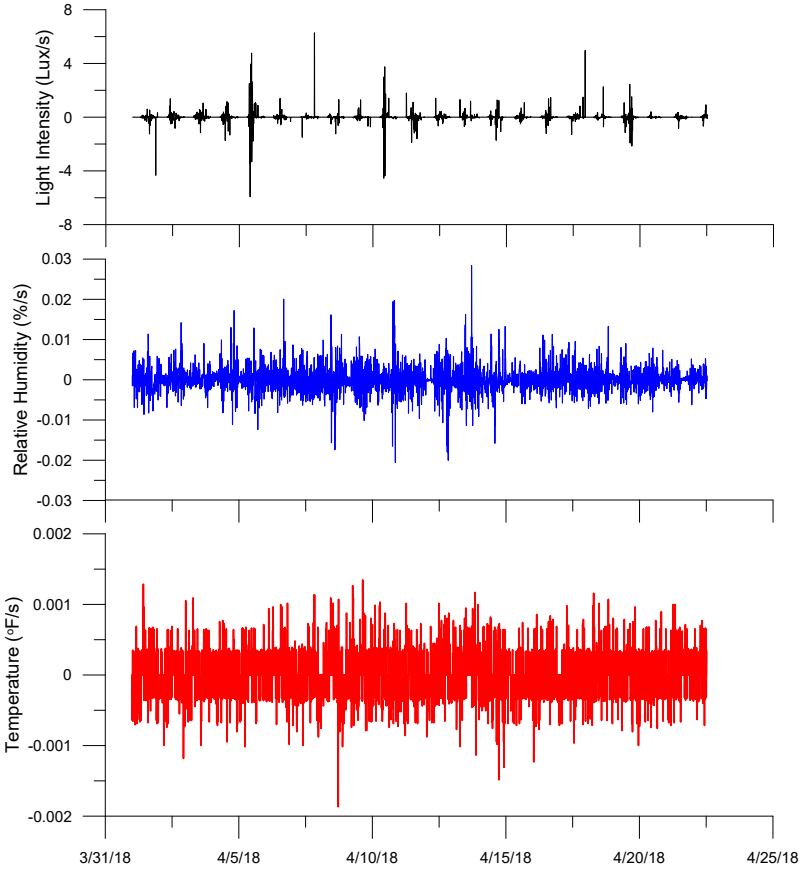


Figure 4.23: Background long term temperature, RH, and lux ROC measurements in an office setting

could be readily distinguished based on the observed rate of change as well as threshold values depending on the parameter of interest. Specifically, temperature and humidity data exhibited threshold values and rate of change data during a fire that was significantly different than background signals that were observed from long term background data collection. The light sensors exhibited quicker response and exceeded those observed for the background data, however at times the magnitude of the light was of the same order as that obtained from background depending on the sensor location.

It was also shown, as expected, that with a higher sensor density, both in terms of parameters measured as well as location, greater information could be obtained to support the detection and monitoring of fire. Finally it was demonstrated that over and above the simple binary response that forms the basis for most fire detection systems, that information on the fire state could be determined. While drawing specific conclusions about the size of the fire was not possible at this stage, the trends in fire growth were clearly observed and did track with the measured heat release rate. Thus, these results clearly show the potential for leveraging non-fire sensors for fire state determination as long as the data is available and appropriate algorithms for data handling can be put into place. These conclusions led to the next phase of the research, discussed in the following chapter, which focuses on the evaluation of a streaming continuous learning algorithm that can leverage the data streams from a series of sensors to provide information on anomalies that may be representative of a fire.

Chapter 5

Fire State Determination and Algorithm Development

Fire state determination (FSD) is predicated on the fact that at different stages during the growth of a fire the observed conditions are sufficiently different from the normal range of ambient conditions that a fire can be adequately detected and recognized. FSD requires the collection of relevant sensor data, the conversion of that data into actionable information, and ultimately the transmission of that information to stakeholders so that appropriate actions may be taken.

The prior chapters focused on determining the characteristics of compartment environments under fire and non-fire conditions based on signals from the various sensors in FSD sensor blocks. It was demonstrated that fires can readily be distinguished from non-fire conditions and furthermore that based on the non-fire conditions observed that they do not generate a false positive when examining the collected data. The next logical step is then to determine how to best leverage the data from these sensors for use in real time FSD protocols in an actual environment. A functioning FSD implementation would thus incorporate one or more sensor blocks and data signals as well as an algorithm to process the data and make a determination of the fire state. This formed the objective of this phase of the research.

This chapter is focused first on describing the steps taken towards the development of a potential FSD algorithm based on the combined sensor data discussed above. It then closes with a discussion of the possibility for the development of synthetic fire data generated from computational models that can extend real world test data for further algorithm training. This is viewed as a potential means for improvement and extension of the present research

towards development of next generation FSD methods.

5.1 Hierarchical Temporal Memory Algorithm

As discussed in Chapter 2 and as shown in Figure 2.5, a main goal of this phase of the research was to collect sets of sensor data and leverage it for Fire State Determination. With the development of appropriate algorithms and simulation tools, the observations of the actual fire state might also be extended to predict the anticipated fire behavior and/or to drive fire models to show in real time the on-going state of a fire or in faster than real time to predict what will happen in a future state of the fire.

This section outlines the development of the Hierarchical Temporal Memory (HTM) algorithm identified for FSD based on the sensor data outlined above. The data outlined in Chapter 4 is used with the normal steady stream of background data in a compartment environment, to determine whether anomalous signals are generated when a fire is present. In this context, an anomaly is defined as a point in time where the observed behavior of the system, as represented by the data, is unusual and significantly different from past behavior. As indicated previously, the anomaly may be temporal if the value is within the norm regarding magnitude but occurs at a time outside of the typical times when a similar observation would be made. Alternately, it may be spatial if the observed value falls outside of the normal range for a given location. Either situation indicates a condition that requires more investigation to determine whether it is representative of a fire. For comprehensive FSD, it is desired to be able to leverage the increasing number of sensors and real-time data that is available in building environments and use it in an algorithm designed to detect signal anomalies that relate to a fire.

In essence, for FSD then, an HTM algorithm has to be structured to identify and memorize recurring spatial patterns and, over time, recurring temporal sequences of such patterns, which can further be related to various states of a normal or, in contrast, a fire environment.

A key strength of utilizing HTM models in this application is that they have the ability to adapt to the changing statistics embodied in "live", potentially constantly changing streaming data sets. From a practical perspective, however, this can be challenging to accomplish in real-time, t and without an inherent ability to look ahead it is necessary to add capability to reliably determine whether the system behavior is outside of the norm prior to $t + 1$. As a result, while HTM models are continuously learning based on the input data streams, they do not directly provide an anomaly score and therefore must be interfaced to other algorithms for effective FSD.

Although multiple methods for anomaly prediction are available in the literature [99–101, 104, 109] one promising methodology for continuous data streaming anomaly detection for fire state determination was that developed by Ahmad et al., [95] in which an anomaly score and anomaly likelihood is computed from a set of input data. Ahmad [95] proposed the following requirements for such applications:

- Algorithm must make predictions online (using existing data from the stream)
- Algorithm must learn continuously without storing the entire data stream (though this may be likely)
- Algorithm must run unsupervised, without manual intervention
- Algorithm should predict anomalies as early as possible
- Algorithm should minimize false positive and false negative predictions.

The HTM implementation and anomaly detection scheme used in this work was developed specifically to meet these requirements and is modeled after that proposed by Ahmad [95].

The core HTM algorithm, shown in Figure 5.1, receives a stream of inputs, x_t, which are then transformed using an encoder [110] and spatial pooling process [104] to create a sparse binary representation of the input data, $a(x_t)$. The HTM sequence memory then models temporal patterns in $a(x_t)$, and outputs another sparse binary representation $\pi(x_t)$ that is a prediction for $a(x_{t+1})$.

Given a specific input, x_t, a series of internal state vectors $\pi(x_t)$ is compared to the observed input vector, $a(x_t)$. A raw anomaly score,s_t, is calculated based on the comparison of the vectors and an anomaly likelihood value, L_t, is computed to determine if the system is anomalous or not as shown schematically in Figure 5.1.

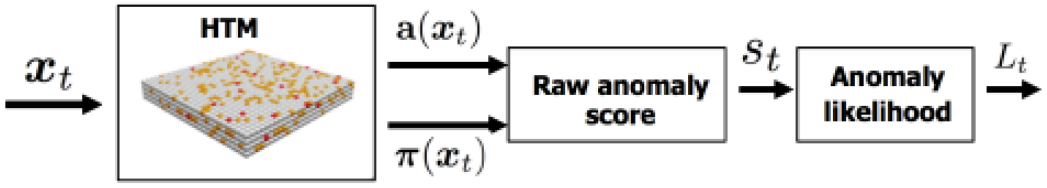


Figure 5.1: HTM primary functional steps [95]

$$s_t = 1 - \frac{\pi(x_{t-1}) \cdot a(x_t)}{|a(x_t)|} \tag{5.1}$$

Using Equation(5.1) the anomaly score is evaluated by comparing the deviation between predicted and observed input. If the current input is perfectly predicted the anomaly score will be 0, conversely if the input is completely under-predicted the anomaly score will be 1. Values between 0 and 1 represent various degrees of similarity between the observed value and the prediction. An advantage of coupling this anomaly detection approach with a continuous learning system based on HTM, is that if there is a shift in the system behavior it will result in a high anomaly score initially but will eventually adjust to 0 as the model learns and adapts the baseline sequences to any new "normal" conditions.

The value of anomaly likelihood, calculated using equation (5.2) is then a metric which defines how anomalous the current input is based on the memorized history of the HTM. The likelihood is calculated using a rolling normal distribution where the mean and variance are updated with each input with a window of the last W anomaly scores. As shown in equation (5.2) then, the anomaly likelihood is defined as the complement of the tail probability.

$$L_t = 1 - Q\left(\frac{\tilde{\mu}_t - \mu_t}{\sigma_t}\right) \tag{5.2}$$

where:

$$\tilde{\mu}_t = \frac{\sum_{i=0}^{W'-1} s_{t-1}}{W'} \tag{5.3}$$

W' is the range of the short term moving averages for the input where $W' \ll W$. User defined thresholds can be set to bound the values of anomaly likelihood. The detection of an anomaly can then be established by

$$\text{anomaly detected}_t \equiv L_t \geq 1 - \epsilon \tag{5.4}$$

which reflects how well the model is able to predict the behaviour in comparison to the recently measured signal history.

The above methodology outlines a combined HTM and anomaly detection process for a single data stream; however, for FSD it may be necessary or beneficial to extend the approach to allow for collection and analysis of multiple input streams. In this case, the same method can be used by developing a series of independent HTM models representing multiple sensors at a single location or in close proximity to each other, for instance in the same room.

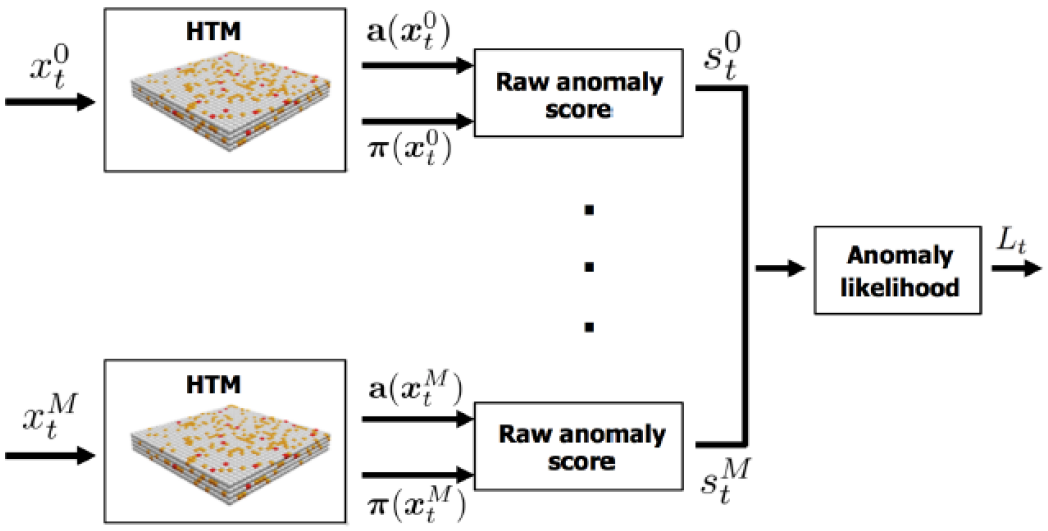


Figure 5.2: Application of HTM methodology to multiple inputs [95]

These are then used to evaluate both individual anomalies as well as in development of a global measure that aggregates the results from the individual models. This approach allows for a high degree of flexibility and robustness in the event that one (or a small number of) data stream(s) is irregular or for some reason removed from the system.

The above approach is implemented for analysis of a live input stream with results shown in Figures 5.3. This data set represents a 24 hr period in which the first 11 hours was background data and then a fire was initiated. In the initial stage (grey bar), the model is learning the patterns in the data set and it is not reporting an anomaly score as every new sequence in the input data is unfamiliar to the model, when that input is compared to the short history of learned sequences. After the data training process, during which the algorithm familiarizes itself with the actual patterns in the input data (blue line), only new and previously unseen patterns will trigger high anomaly scores (indicated by yellow or red "flags"). Changes in magnitude of a given signal, such as unusually high or low activity, will also cause the anomaly score to rise, causing a yellow or red flag to be shown. Typically, an anomaly score above 0.8 is a good indication that an unusual pattern has been detected in the input data stream. Figure 5.3 provides a zoomed window of the 24 hour period and it can be observed that an anomaly is detected from the raw data for all three measured parameters. Light intensity registers first due to the sensors instantaneous measurement, while the RH and temperature are delayed as the heat and humidity are

transported to the location of the sensor. Once the fire dies out the anomaly score returns to normal.

With the HTM algorithm developed and interfaced to an anomaly detection routine, the next step was to apply the new methods for analysis of the experimental fire data discussed in Chapters 3 and 4 to further assess its potential as the base algorithm for an effective FSD protocol.

5.2 Algorithm Results and Discussion

The experimental data streams collected from light, temperature, and humidity sensors were treated as live-streaming data sets and used as input for assessment of the HTM on the raw data stream, HTM on the processed rate of change data stream, and ROC threshold methodologies outlined above. First, the sensor data are examined individually using the HTM method. After the initial evaluations on the individual sensors, a multi-component HTM algorithm was utilized to evaluate the sensors as a system. Finally, the HTM analysis is also compared to the Rate of Change (ROC) analysis that leveraged the identified *post hoc* ROC thresholds discussed in Chapter 3.

The criteria for anomaly detection for each of the methods is as follows:

- HTM single sensor analysis: Anomaly Likelihood L_t >0.5
- HTM multi-component analysis: Combined System Likelihood L_t >0.8
- ROC threshold analysis: T > 0.02°C/s, or Humidity > 0.2 %/s, or Light > 2 lux/s

Thus for the HTM analysis regardless of the input data stream, either the raw data or the running rate of change, if the single or multi-sensor criteria is met it will be classified as an anomaly. For the ROC threshold analysis, if the ROC exceeds any of the defined thresholds it will be classified as anomalous.

The data from a subset of 20 experiments, including both small- and large-scale tests discussed in Chapters 3 and 4, were selected for the analysis as summarized in Table 5.1. The tests were chosen to cover both flaming and smoldering fires with a range of values of heat release rate. In addition, and as outlined in prior chapters, this data was deemed to provide an excellent test bed for the HTM algorithm since other methods of analysis clearly indicated that fire and non-fire scenarios could be discerned based on the sensor data from these experiments. Further, it was demonstrated that the data contained useful information

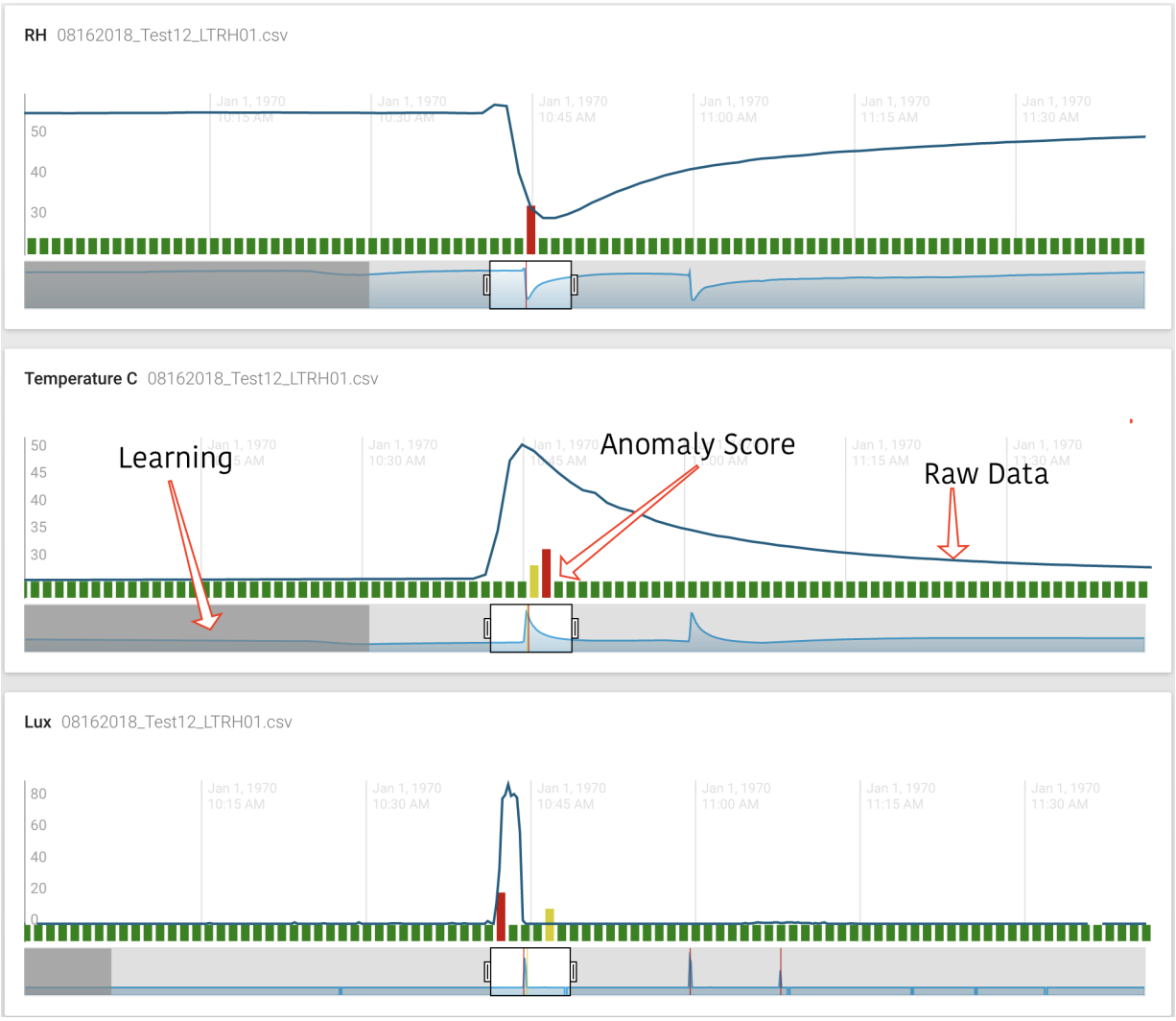


Figure 5.3: Example initial algorithm training (dark grey), raw data (blue line), and anomaly score (green, yellow, or red "flag") for RH, Temperature, and Light Intensity

on the fire state over and above the simple binary fire-non/fire signal provided by most standard detectors, a key attribute in determining the utility of new FSD algorithms as well. Since the intent of this initial evaluation was to assess the algorithm against positive, albeit mainly still relatively small, fire sources, data from the tests involving the smallest fire sources (< 3 kW) and nuisance sources were excluded at this stage.

Table 5.1: Summary of selected experiments for this analysis

No.	Type	Fuel	Burning Duration (s)	HRR (kW)
1	Flaming	Hay/Wood	485	Not Recorded
2	Flaming	100mL Heptane	60	3
3	Flaming	150mL Heptane	60	3
4	Flaming	150 mL Heptane	180	3
5	Flaming	150 mL Heptane	60	35
6	Flaming	100 mL Heptane	55	35
7	Flaming	100 mL Heptane	27	35
8	Flaming	150 mL Heptane	58	35
9	Flaming	100 mL Heptane	60	35
10	Flaming	100 mL Heptane	210	22
11	Flaming	100 mL Heptane	270	22
12	Flaming	100 mL Heptane	195	22
13	Flaming	100 mL Heptane	225	22
14	Flaming	100 mL Heptane	285	22
15	Flaming	150 mL Heptane	90	94
16	Flaming	100 mL Heptane	75	35
17	Flaming	100 mL Heptane	60	35
18	Smoldering	PU Foam	15	Not Recorded
19	Smoldering	PU Foam	90	Not Recorded
20	Flaming	Sofa	900	2300

As a first step in analysis of the new HTM algorithm, the background data discussed in Chapter 4.5 was used as input to evaluate whether anomalies would be detected in any individual sensor data during non-fire conditions in a space over a prolonged period of time. Figure 5.4 shows data collected from temperature, humidity, and light sensors over a period of 3.5 months for a single location, along with the corresponding anomaly likelihood values calculated by the HTM algorithm for each sensor. Similar to the figure above yellow flags indicate a potential anamoly while a red flag indicates an anomalous condition.

Note that the signals from each sensor are quite distinct and all change, but that for the most part they change with fairly regular patterns that the HTM algorithm learns over

time. During the 3.5 months a series of anomalies were detected on each sensor on an individual basis, however in no case did anomalies register at the same time across all of the sensors. Therefore an important benefit of leveraging multiple sensors can be observed in that at no time during the observational period would the combined system likelihood, L_t have indicated an anomaly that might have been representative of a fire.

Figure 5.5 shows a sample raw data stream for temperature, humidity, and light data from THLP-03, along with the HTM predicted anomaly likelihood. For experiment 4, Table 5.1, the data was for a small fire composed of 150 mL of Heptane in a 7cm pan located in the center of the compartment in the Burn House. THLP-03 was located on the wall of the compartment, 1.2 m above the floor, Figure 4.9. The elapsed time shown in Figure 5.5 is the time from ignition.

As shown in Figure 5.5 and using an anomaly threshold of 0.5, the HTM algorithm identified anomalies multiple times for each sensor. All the anomalies identified by the HTM algorithm occurred within the first two minutes of the test. Even though the temperature continued to increase and the humidity continued to decrease over the remainder of the test, the HTM algorithm did not identify this data as anomalous due to having learned the recent trends in the signal outputs based on the trends in the previous data in the data stream. Figure 5.6 shows the HTM anomaly scores that were determined using the ROC data for each sensor in Experiment 4 for comparison with raw sensor data scores in Figure 5.5.

To demonstrate the potential benefits of a combined anomaly likelihood for this system of sensors, Figure 5.7 shows the individual anomaly likelihood values, as well as the overall system anomaly likelihood $L_{t_{system}}$, for Test 4 and THLP-03 during the first 60 seconds of the experiment. At approximately 40 s after ignition, the anomaly likelihood of the relative humidity and light data both increased to near 0.4, a typical warning level, but did not rise to the 0.5 threshold used to identify anomalies in the data stream from an individual sensor. However, when the anomaly likelihoods of each sensor are combined, the system anomaly likelihood reaches the threshold of 0.8 used to indicate an anomaly in the system. Having anomaly likelihoods on two separate sensors in a system that rise to warning levels is unlikely in a non-anomalous instance, therefore the desired behavior in this case is to identify this as an anomaly, though not specifically a fire. The relative humidity and light data for THLP-03 in Test 4 both reached the individual sensor anomaly threshold of 0.5 prior to 40s. However, the system anomaly likelihood exceeding 0.8 provides a higher degree of certainty that Sensor Suite 3 is observing anomalous conditions. Thus a warning code could be provided at the time when the first sensor exceeds an anomalous value, which would then be followed by an alarm state.



Figure 5.4: Long-term background data over a period of 3.5 months. Showing raw data and anamoly scores.

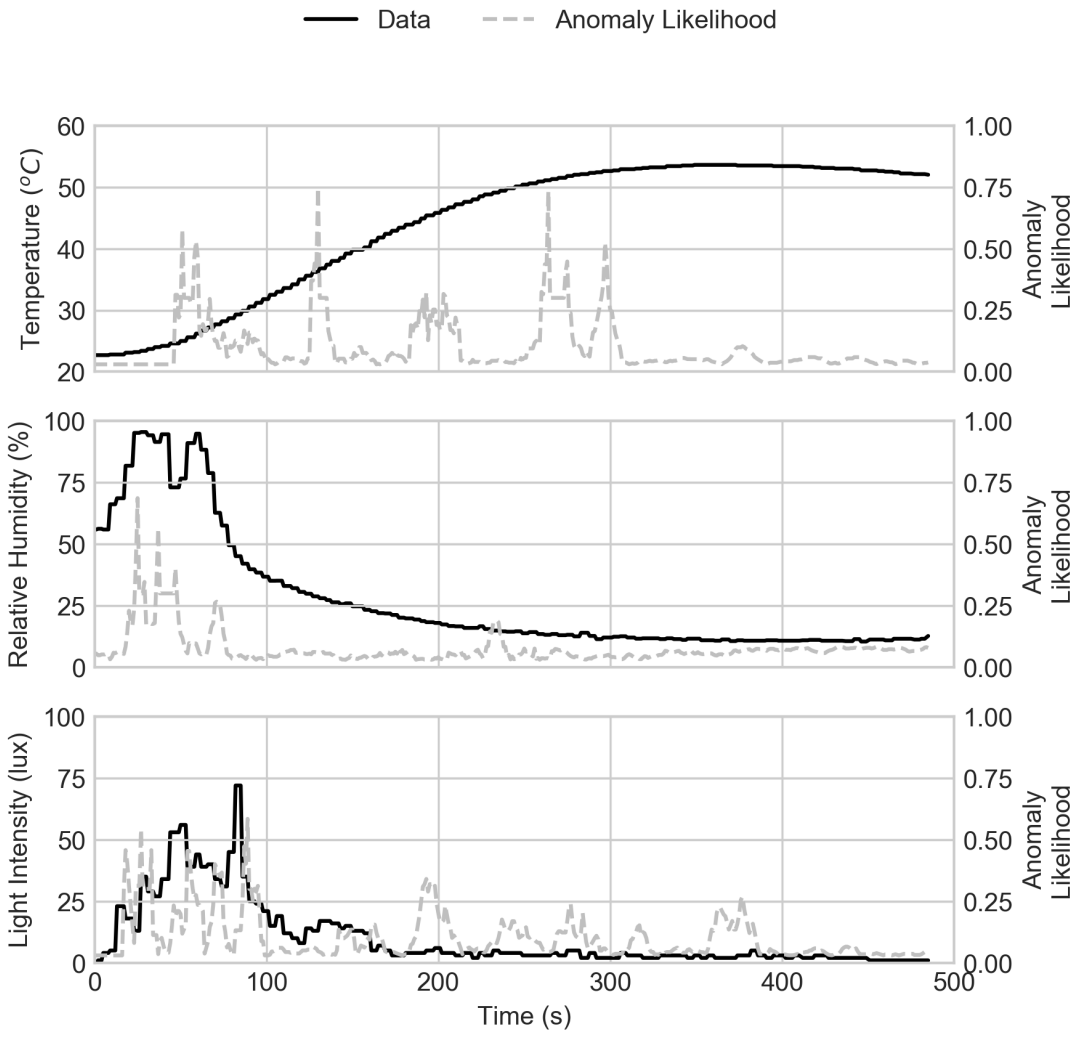


Figure 5.5: Example temperature, humidity, and light data shown with the HTM anomaly likelihood.

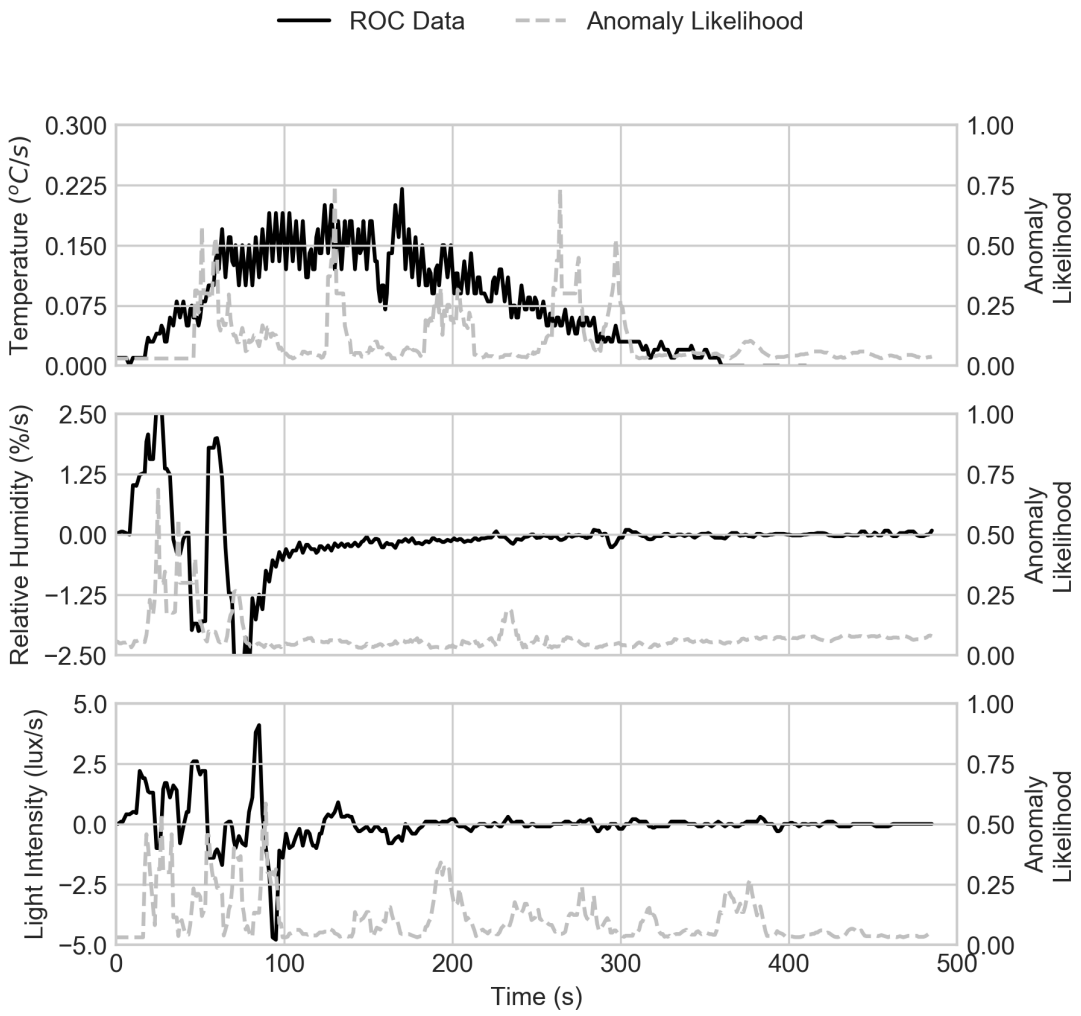


Figure 5.6: Example temperature, humidity, and light ROC data shown with the HTM anomaly likelihood.

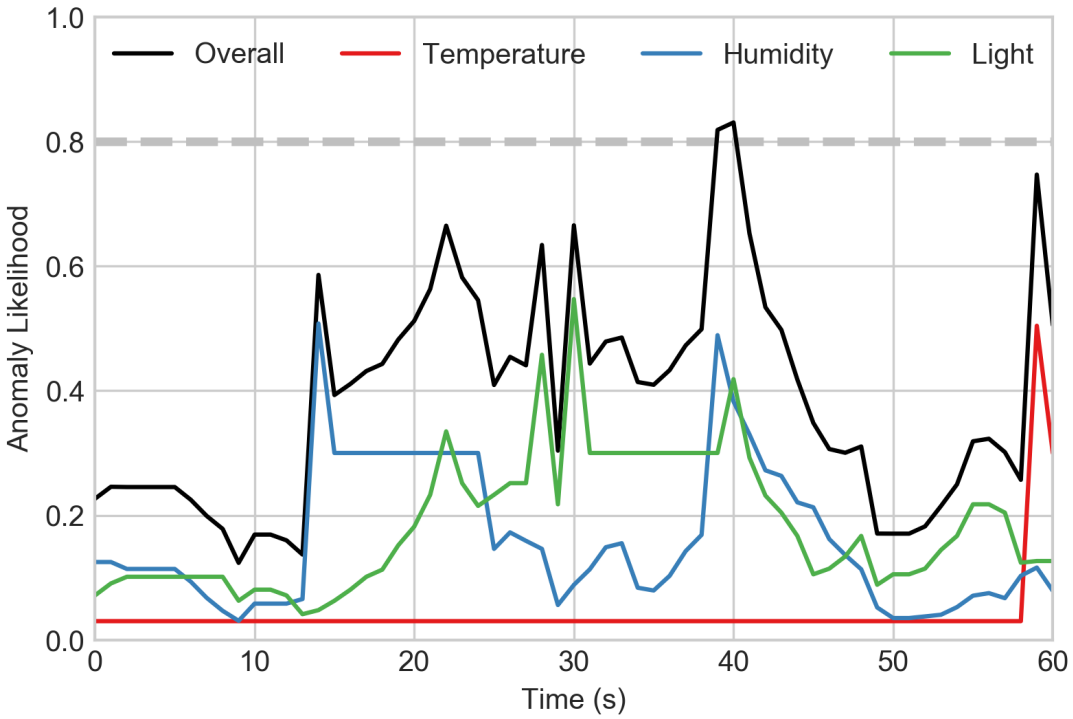


Figure 5.7: Test 4 THLP-03 overall anomaly likelihood computed from individual sensor anomaly likelihoods.

Test 20 in the HTM experiments, Table 5.1, was data captured from Test 5 of the large-scale test series as discussed in Chapter 4. Additionally the FSD sensor blocks developed in Chapter 5 were utilized in this analysis instead of the THLP sensors. Figure 5.8 shows the temperature, humidity, and light data from Yun-05. The sensors were located near "C1" on Figure 4.9 at a height of 100 cm above the floor. The times at which the HTM algorithm identified the first anomaly in the data stream for each sensor are marked with a diamond in Figure 5.8. While not immediately clear in the figure the anomalies occur when there appears to be a more severe rate of change for each measured parameter. From the fire test timeline, this corresponds to the onset of fire growth in the experiment thus clearly indicating that the algorithm could resolve differences in the environment due to the presence of a fire even in this larger test situation.

From the above discussion, it is clear that even despite differences in sensor blocks used for the experiments evaluated, the HTM algorithm was able to successfully identify anomalies in the various data streams as a result of changes within the environment resulting from both small and large HRR fires. Further, the same algorithm was used for all the fires evaluated in Table 5.1 This highlights another main feature with application of HTM algorithms in FSD - the algorithms are data agnostic as they do not require manual intervention to adjust to different applications or contexts.

As a basis of comparison to the HTM algorithm as applied to the raw sensor signals, the Rate of Change (ROC) data from the various sensors used in the experiments was determined. As shown previously in Chapter 3.4, the ROC data was consistently contained within narrow bands during non-fire conditions. Therefore, threshold values of ROC for each sensor were determined *post hoc* and are listed in Table 5.2. These threshold values were determined from ten point moving averages of the ROC for each sensor. A second version of the HTM algorithm, using the processed ROC data rather than raw sensor data but with the same anomaly detection routine, was then developed.

Table 5.2: ROC Thresholds

Sensor	Threshold
Temperature	± 0.02 °C/s
Humidity	± 0.2 %/s
Light	± 2 lux/s

Once the two HTM algorithms described above were developed and tested, they were applied to analyze the data from all relevant sensors in each of the 20 experiments listed in Table 5.1. Each test included between one and seven sensor suites so that in total, there were 124 data streams examined across the 20 selected tests. Each data stream consisted

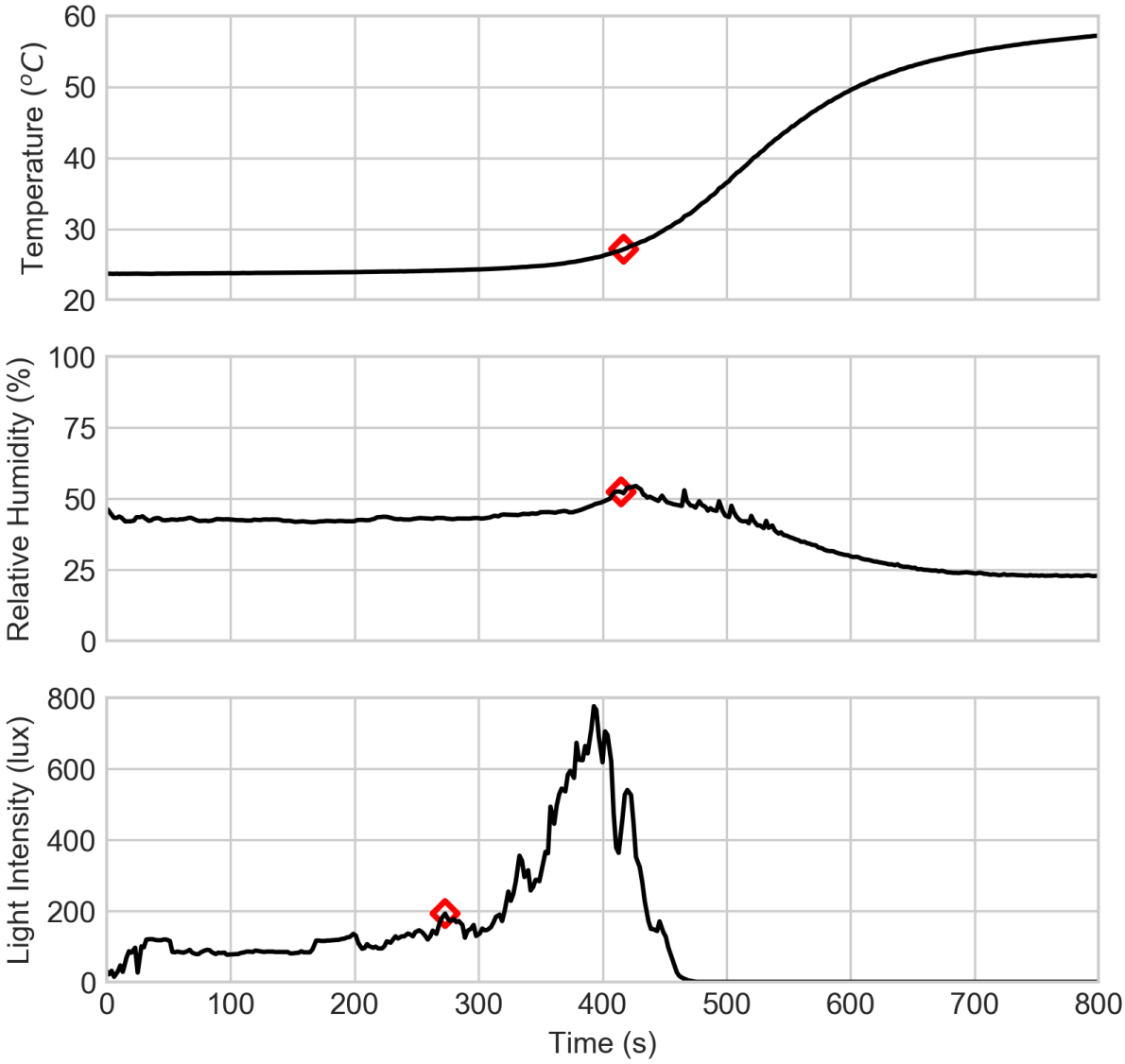


Figure 5.8: Temperature, humidity, and light data from Test 20. The first anomaly identified for each sensor using the HTM algorithm is marked with a diamond.

of temperature, light, and humidity data. All data streams contained data for at least two of those three sensor types. However, 18 of the data streams were for sensor suites located outside the fire compartment (see THLP-05 in Figure 4.9), therefore these were excluded

from further analysis and only those 106 sensor suites located within the compartment were examined. In addition, another 10 data streams were for smoldering fires that did not produce significant changes in the temperature, relative humidity, or light data. Overall, at least one anomaly was detected using the HTM algorithm to process raw signal inputs in 18 out of 20 tests. At least one anomaly was detected in 19 out of 20 tests with the HTM algorithm using the processed ROC data as input. Utilizing just the ROC threshold approach discussed in Chapter 3.4 and summarized in Table 5.2, resulted in the detection of at least one anomaly in all 20 tests.

Table 5.3 summarizes the number of anomalies identified using the HTM algorithm and the ROC thresholds listed in Table 5.2. Using the ROC thresholds, resulted in detection of anomalies in 92 of the 96 data streams (96%). In addition, in 15 of the 18 tests, the ROC threshold approach identified at least one anomaly on all detectors in the test. Although not the primary focus of this analysis, the ROC threshold approach also identified anomalies on Sensor Suite 5 (THLP-05) in 15 of 18 tests. Since sensor suite 5 was located outside of the Burn Room, this indicated that sensors that are remote from the fire may also be able to provide insight into the development of a fire or provide early warning. Nonetheless, while the ROC threshold method would appear very effective, the high rates of identifying anomalies with this approach are expected since the threshold values were determined aposteriori from the same data set as the one to which they are applied. Furthermore, while positive, the method is not conducive for a continuous learning environment and the thresholds would need to be established directly for each installed location which may not be practical. In addition, the wider applicability of these thresholds relative to sensor signals across a range of fire situations is completely unknown.

Table 5.3: Comparison of anomalies detected using HTM and ROC thresholds

Sensor	Anomaly Counts		
	HTM (Raw)	HTM (ROC)	ROC Thresholds
Temperature	9	21	64
Humidity	9	27	56
Light	30	65	77
System	30	49	-
Total Detections	37	77	92
	39%	80%	96%

The HTM algorithm identified anomalies in fewer of the data streams than was determined using ROC thresholds. Using the HTM algorithm with the raw sensor data resulted in detection of anomalies in 37 of the 96 data streams (39%). Using the processed ROC

data in the HTM algorithm significantly improved performance. With anomalies detected in 80% of the data streams. Specifically, the number of anomalies identified in the temperature and humidity data approximately doubled, while light anomaly detection values increased by approximately 40%.

Therefore, the present preliminary HTM algorithm which had no 'seed' data nor specific domain expertise in detecting a fire state was still able to detect anomalies in the sensor data from the fire tests in simulated "real-time" a high proportion of the time. The background data periods in the test data, where the HTM algorithm learned the normal background patterns in the data, were relatively short. It is anticipated that more extensive background data collection will enhance the pattern recognition capability of the algorithm consistent with other studies leveraging HTM. Consistent with the input data used, the anomalies that were detected earliest by the HTM algorithm tended to be in tests with larger fire sizes and more significant changes in the sensor data that could readily be discerned as anomalies. Improved performance in basic anomaly detection is therefore expected from the HTM algorithm as it is exposed to more data as well.

In addition to actual detection of an anomaly, another key requirement in effective FSD is optimization of the time, relative to initiation of the fire, at which an appropriate anomaly would be detected using any given algorithm. In this respect, using ROC sensor data rather than the raw sensor signals with the HTM algorithm reduced the time at which anomalies were detected by, on average, approximately 10 - 60 s. In data streams where both the HTM with ROC data and the ROC threshold approaches were used to identify anomalies, the time at which anomalies were identified with the ROC threshold approach was, on average, approximately 40 - 70 s faster again than the approach based on using ROC data as input to the HTM algorithm.

As an example of relative detection time using the HTM algorithm, Test 20 included spot-type smoke and heat alarms in the test compartment and Table 5.4 compares the anomaly detection times for the HTM algorithm with ROC data to the response times for the commercial smoke and heat detectors located nearby for this test. It is important to note before directly comparing these values, that the temperature, humidity, and light sensors were located near "C1" on Figure 4.9 at heights of 15 cm and 100 cm above the floor of the compartment, respectively for Sensor Suites 5 and 7. In contrast, a combination smoke and heat detector labeled "D10" Figure 4.9 was located approximately 2 m from the sensor suites on the ceiling of the compartment a location where the plume effects would be expected to result in far quicker detection. Using the HTM algorithm to detect anomalies based on the data stream consisting of temperature, humidity, and light ROC data, and combining the sensor anomaly information to determine the three sensor system response produced alarm times that were similar to those of the ceiling-mounted, spot-type heat

detector, despite the significant disadvantage in sensor location for the present detector. When light sensor data was evaluated by itself, it detected an anomaly earlier than found for the combined system response. Of course, also it would be expected to detect anomalies in temperature, humidity, and light ROC data considerably earlier if the same sensors were located on the ceiling. The ceiling mounted smoke alarms activated approximately 270 s faster than this initial HTM three sensor algorithm; however, again the smoke alarms were installed on the ceiling.

Therefore, while there was a delay in detection, even this preliminary the HTM approach did in fact work regardless of sensor location. In an environment in which no other sensor exists therefore this notification would occur well before sprinkler activation would take place.

Table 5.4: Alarm Time Comparison for Test 20.

Detector	Height (cm)	Alarm Time (s)		
		HTM System	Smoke Detector	Heat Detector
Yun 5	15	360	-	-
Yun 7	100	368	-	-
Detector 10	244	-	90	330

As well as timeliness of detection, the rate of generation of false positives (i.e. detection of a fire when there is none) and the rate of false negatives (i.e. detection of no fire when one exists) are important parameters for evaluating any method of fire state determination. False positive indications of a fire were not explicitly examined in this work; however, the results presented in Figure 5.4 show promise that the continuous learning features of the HTM algorithm are applicable to this domain, and can be used to minimize false positives even in changing environments. One simple approach to increase the number of anomalies detected by the HTM algorithm, and possibly reduce the detection times, would be to adjust the threshold value of the anomaly likelihood. The trade-off in this approach, however, is that this would also likely increase false positive fire indications, so these competing factors must be balanced to optimize the solution for a specific application. Another possibility is to apply a weighting to the various sensor data to lend preference to a specific variable in the model, in particular when a multivariate stream is being evaluated. Again, more research would be required to develop an appropriate strategy in this respect.

5.3 Impact of Sensor Location

While not examined in depth, and thus a key topic for future work, a brief comparison of HTM results based on sensor locations is presented. As it may not be known where sensors may be located, confirmation that the HTM is still able to readily detect anomalies is critical if the sensors and algorithm are to provide information on the fire state. Furthermore, quantification of the impact of the location on the observed signal and HTM processing is required.

When examining a specific test fire, test 15 Table 5.1, a comparison of the HTM results based on sensor location is presented in Figures 5.9 and 5.10. The figures show a repeat of the same test being performed 4 times.

This comparison shows that while there is a difference in the anomaly scoring and timing for each sensor for RH and light intensity, each of the sensors results in the detection of anomalies at nominally the same time in most cases. The raw data trends are similar in that a ROC was observed in all cases and at all locations and while the RH behavior was delayed in some cases the light was instantaneous at each location. Furthermore the differences fall in line with expected behavior in that the light sensors respond at the same time while the signals from RH and temperature at the wall and floor are delayed due to time taken for the fire plume and ceiling jet to reach those locations. Clearly, additional work is also required to optimize approaches in processing data from multiple sensors at various locations within a space.

5.4 Conclusions

Given the success of the ROC thresholds at identifying the fire state across a range of fire and nuisance sources [111], and the improved performance of the HTM algorithm with the ROC data, future work with the HTM algorithm could also incorporate a more complex data model such as combining the raw and ROC sensor data in determining the presence of a fire. This approach is expected to increase the number of anomaly detections and reduce the detection time, while still leveraging the ability of the HTM algorithm to adapt to changing environments more readily than would use of any simple threshold approach.

Another area for future improvement of the HTM algorithm for fire state determination relates to how the anomaly likelihoods of the individual sensors are combined. The approach taken in this work was intentionally kept simple in order to assess a proof of concept of anomaly detection with an HTM approach based on the available sensor data.

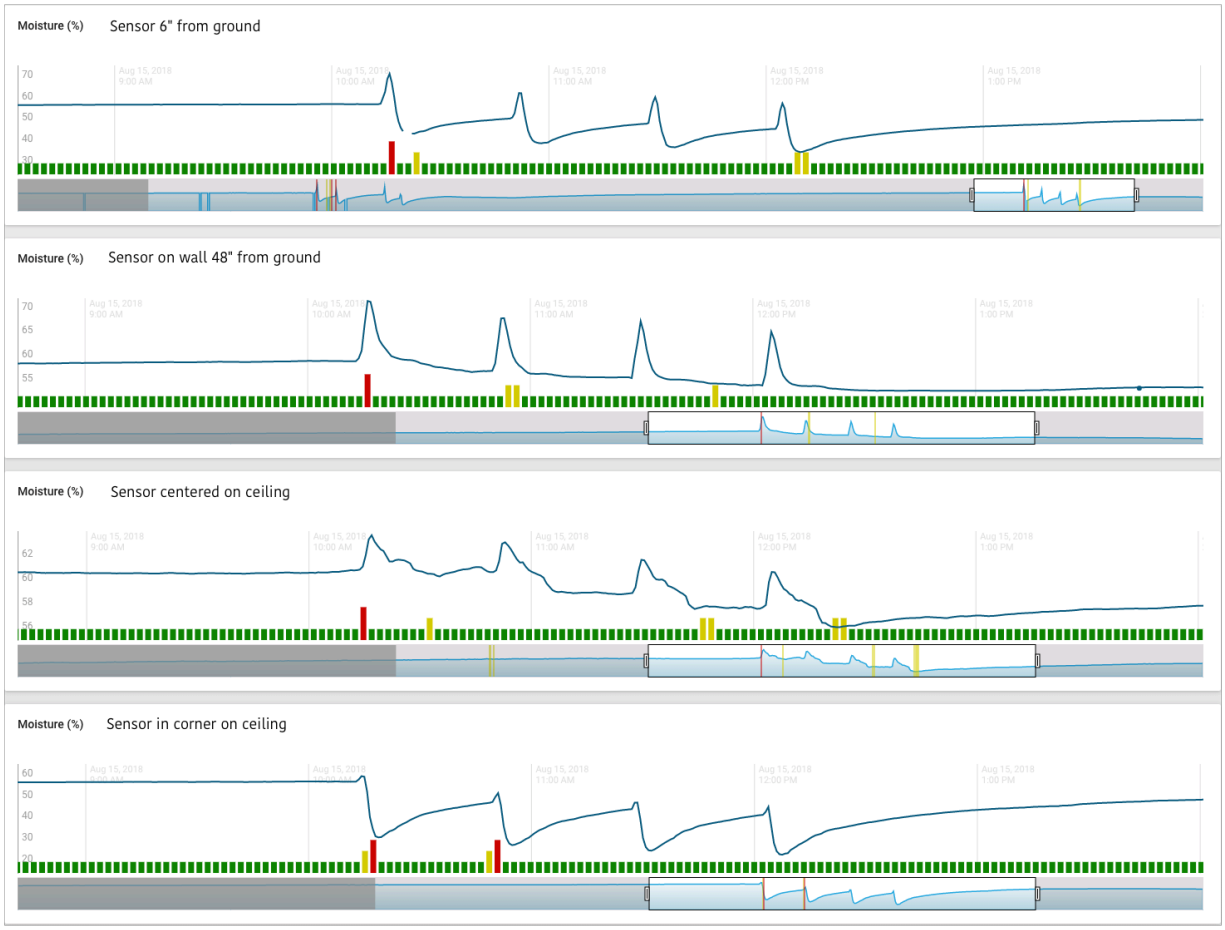


Figure 5.9: Comparison of RH raw data and anomaly scoring by sensor location for the same test fire.

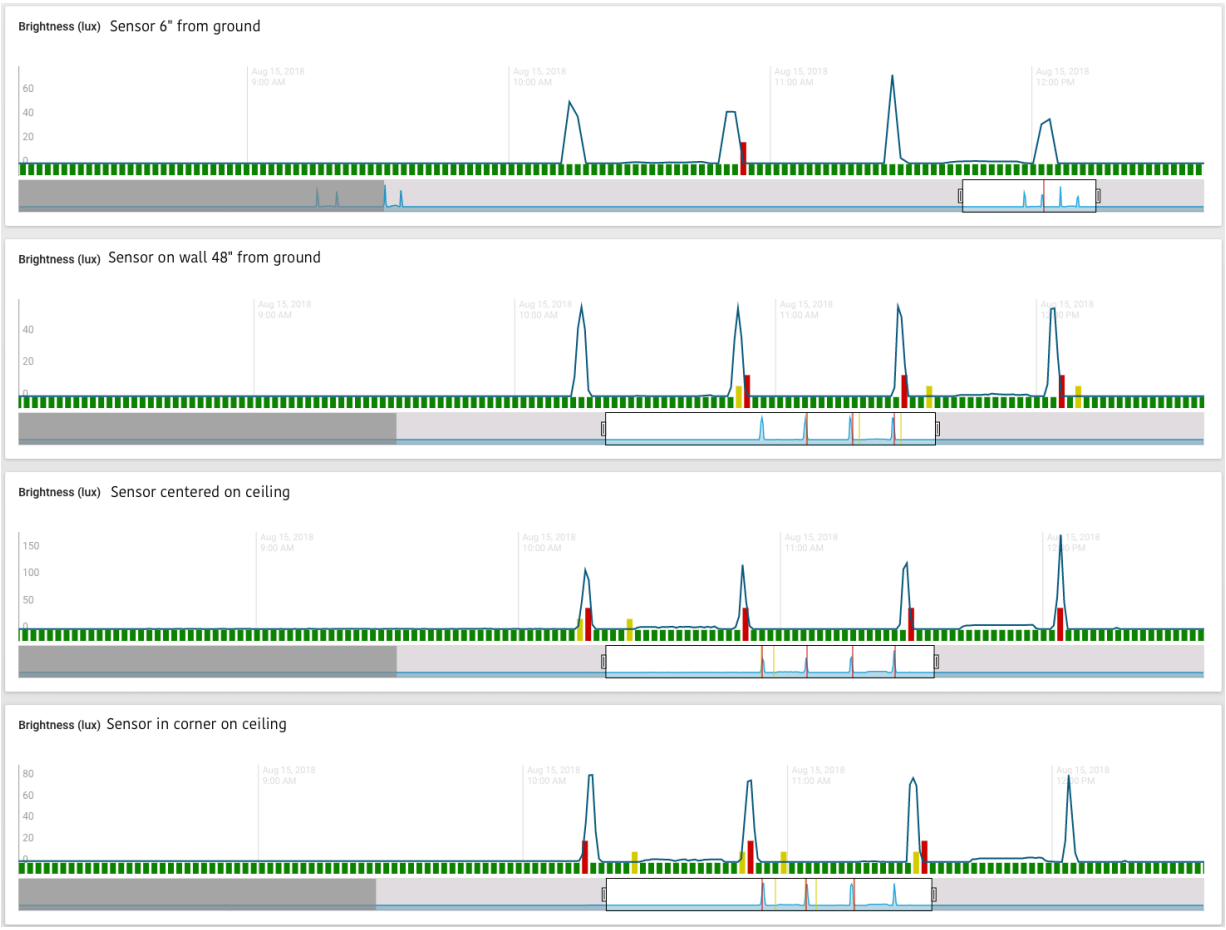


Figure 5.10: Comparison of lux raw data and anomaly scoring by sensor location for the same test fire.

As such, the anomaly likelihood detection scheme did not account for temporal delays in the anomaly likelihood of the individual sensor streams. The light sensor tends to respond to a changing environment much more rapidly than the temperature or humidity sensors. For example, an increase in fire growth rate in a compartment fire can result in an increase in light intensity, increased gas temperatures, and increased or decreased humidity levels. However, these changes in the sensor data, and the corresponding changes in the anomaly likelihood are not necessarily coincident in the data stream so more complex strategies could be devised to best combine information from varying sensor types for faster, yet reliable, determination of a fire.

Ahmad et al [95] proposed several alternative approaches that could be implemented in future versions of the present FSD algorithm. The first is one that uses a smooth temporal windowing mechanism to calculate the anomaly likelihood for a system of sensors where the spikes in anomaly likelihood are close in time but not exactly coincident. Another is one that is based on a scoring algorithm [95] with which it is possible to adjust the value to "reward" for early detection and "penalize" for later detection by assessing higher weights for early detection during an assessment window while reducing the weighting as time progresses. Similarly if a false positive is observed negative scores can be assigned. While the present simple method of assessing anomaly likelihoods in the individual sensor data was sufficient to prove the potential of HTM and anomaly detection approaches for FSD based on the sensor data that was collected during this research, implementing these more sophisticated approaches to synthesizing the anomaly likelihoods of a set of individual sensors should improve the overall performance of future, more advanced HTM algorithms for fire state determination.

Chapter 6

Summary of Conclusions and Future Work

6.1 Conclusions

While research has been performed on fire sensor response to fire and non-fire environments, very little work has been performed to examine the response of non-fire sensors to similar environments in order to determine what parameters may be readily observed by the sensors. However, the increase in BEMS and other non-fire sensors provides an excellent opportunity to leverage them for fire detection and monitoring purposes. In order to evaluate the potential, this research focused on the ability of various sensor technologies to observe conditions representing fire and non-fire conditions, the integration of multiple sensors into a sensor block, and the development and testing of potential algorithms that may be useful for fire state determination.

1. Identify potential characterization parameters

A series of small and medium scale experiments were conducted to identify the response of various building sensors to a range of fire and non-fire environments. The experiments involved a range of different fuels and nuisance sources. The experiments began with a $1m^3$ box and increased in size to a full-scale room in the University of Waterloo burn house. The experiments showed that across the range of fuels tested (heptane, ethanol, foam, etc.) that characteristics of fire such as relative humidity, temperature, and light intensity all were reliably determined using existing non-fire sensors. The fire signals measured using these sensors could be sufficiently distinguished from background and nuisance source signals, indicating their potential for fire detection and monitoring.

2. Identify candidate sensors, develop and test, an idealized sensor block.

Based on the findings of the preliminary work a sensor block was developed that utilized relative humidity, light, and temperature sensors similar to the commercial sensors and supplemented these with gaseous sensors to measure O_2, CO, and CO_2. The sensor blocks were designed to capture data from the full range of anticipated parameters and to transmit the data in a continuous streaming environment. The individual components of the sensor block were tested against known sources and then the sensor blocks were tested in a series of 9 full-scale living room fire experiments. The sensor response to the experiments showed that not only could the sensors distinguish fire from non-fire conditions but that the sensor response could provide additional information on the fire state. Light intensity showed the quickest response regardless of sensor location and tracked with HRR and the measured heat flux. Relative humidity and temperature exhibited increases in magnitude and in the observed rate of change, which was significantly different than that observed in non-fire conditions. The gas concentrations behaved as expected with O_2 decreasing as HRR increased and CO increasing as O_2 decreased. All sensor locations exhibited a clear response to fire conditions that demonstrated that information on the fire state could be determined. Finally it was shown that with a higher sensor density, both in terms of measured parameters and/or location that greater information could be obtained for fire state determination.

3. Development of algorithms for fire state determination.

Most fire detection systems provide binary feedback regarding the fire state, namely a fire or no-fire state. This limits the information that is transferred and also makes the detectors particularly susceptible to false alarms. As a result appropriate algorithms for fire state determination are required in order so that a fire can be adequately detected and recognized. As an initial step in this direction rate of change thresholds were determined *post hoc* for light intensity, relative humidity, and temperature based on the small and medium scale experiments. The thresholds established showed a high degree of success at identifying the fire state across a range of fire and nuisance sources, however this approach is limited in that it is not independent of the measured parameter or sensor location and thus its broader applicability outside of the tested environment may be limited. As a result a Hierarchical Temporal Memory (HTM) continuous learning algorithm for anomaly detection was developed to examine an approach that would allow for a wide range of parameters and sensor locations to be evaluated without any prior knowledge of the system or its installed environment.

The HTM approach examined background data to establish norms in the recurring spatial and temporal data patterns and when deviations occurred in these measured patterns

an increased anomaly score was produced. The HTM method applied to the raw data stream detected anomalies in nominally 40% of the streams evaluated, however applying the HTM method to the computed rate of change resulted in 80% of the data streams indicating an anomaly. The present HTM algorithm, with no initial "seed" data and with no domain expertise was able to detect and provide information on the changing fire state in "real-time" a high proportion of the time. By combining multiple parameters (light, temperature, and relative humidity) the anomaly likelihood can be refined to ensure fires may be detected while simultaneously not producing an anomaly based on a nuisance signal from a single parameter. The results of the HTM analysis indicate that the approach shows promise for fire detection and monitoring across a range of different fire sizes and sensor locations.

Finally, while the initial anomaly detection may indicate the onset of an event, the continuous data stream allows for continuous monitoring of the fire state as was demonstrated in the large scale experiments. The large experiments clearly showed that the light sensors trended with the measured heat flux and calculated heat release rate and that temperature and relative humidity changes were dynamic throughout the event indicating temporal and spatial information on the changing fire state is available throughout the fire event.

6.2 Future Work

This research produced new information regarding characterization of the fire environment, the parameters that may be leveraged to generate information on the fire state, and proposed the use of a learning algorithm for fires state determination. Nonetheless, there is additional work that can further knowledge in the field that is briefly discussed in this section.

1. Expanded fire environment characterization

As the results of this research indicate, light and relative humidity, in addition to the the classic parameters typically monitored in fire experiments, are readily able to detect a fire and provide information on the fire state. However, this research focused on a limited set of parameters and new sensors are being developed rapidly, each with its own range of operating conditions. Therefore, it is critical to evaluate a broader range of sensors, in particular those that are currently being implemented into BEMS systems, to determine their accuracy, response, and when or whether detection of a fire remains possible. This level of analysis can be performed in small or medium scale environments where the primary intent is to evaluate the sensors and their response in easily repeatable conditions. As

a supplement to this a broad range of long-term background data will prove useful for evaluation of non-fire environments to help clarify the range of each measured parameter in a variety of installed locations. Specifically the following topics are recommended for study:

- Evaluation of the response of a broader range of non-fire and commercial BEMS sensors to fire environments for the parameters examined in this work;
- Collection of background data using non-fire and commercial BEMS sensors for non-fire states; and
- Determination of additional parameters that may be leveraged (acoustic, vibration, electric or magnetic field, etc.) for fire detection independently or when combined with other parameters

2. Sensor location and selection

The characterization of an environment using sensors will depend heavily on the sensor itself and its intended use. While the parameters associated with fire detection are broadly known (light, heat, products of combustion) the response of a specific sensor is dependent on the sensor characteristics and location relative to the fire. While common sense, the greater the quantity of sensors integrated into the detection and monitoring system the more likely that the system will be able to reliably detect a fire, detect in a timely fashion, and reliably differentiate the signals from a nuisance source. This additionally valid for the placement of the sensors. Since most sensors are driven by plume dynamics sensors located at or near the ceiling are anticipated to respond quicker, however many BEMS sensors are located in other areas. Several topics are recommended for study:

- Evaluation of the impact of sensor location on response for a given fire exposure;
- Determination of quantitative information that can be ascertained about the fire and the environment if a sensor location is known;
- Determination of the minimal and optimal parameters that are required to accurately detect and monitor a fire; and
- Development of guidance on the use of non-fire sensors for research and application purposes.

3. Algorithm development

The concept of Fire State Determination (FSD) expands on the notion of fire detection to determine not only whether or not a fire is present but also to provide potential information on the fire size, location, and the dynamic nature of the fire. The interpretation of the data and conversion into information is an essential step in informing and making decisions and thus the optimal algorithms for FSD is an area of study in which additional research is needed. This initial work focused on establishing the potential for the HTM approach and demonstrated the potential benefits of a continuous learning algorithm that requires minimal initial information and does not require spatial awareness. Given the initial success additional work is justified to further explore the HTM approach and the integration of multiple parameters and perhaps other logical approaches to data handling that may supplement the HTM. Several key topics for exploration are:

- Detailed evaluation of the impact of sensor location on HTM anomaly prediction to determine where and for what parameters anomaly detection is significantly impaired or no longer possible;
- Exploration of the combination of rate of change threshold data with the HTM algorithm to reduce detection time and increase the successful fire detection rate;
- Continued exploration of multi-parameter HTM models and determination of optimal system likelihoods that represent fire conditions;
- Characterization and correction of the impact of temporal delays in a parameter on the calculated system likelihood; and
- Finally to explore weighting of the anomaly scoring to "penalize" for false or delayed anomalies while "rewarding" for earlier accurate detection.

References

[1] J Zhuang, V M Payyappalli, A Behrendt, and K Lukasiewicz. Total cost of fire in the united states, 2017.

[2] Custer, R. L. P. and R G Bright. Fire detection: The state-of-the-art. *NASA STI/Recon Technical Report N*, 75:10404, June 1974.

[3] W L Grosshandler. A review of measurements and candidate signatures for early fire detection. 1995.

[4] S P Nowlen. Enclosure environment characterization testing for the base line validation of computer fire simulation codes. 1987.

[5] M Janssens. *Fundamental thermophysical characteristics of wood and their role in enclosure fire growth*. PhD thesis, Rijksuniversiteit Te Gent, 1991.

[6] P Blomqvist and L Anders. Characterization of the combustion products in large-scale fire tests: comparison of three experimental configurations. *Fire and Materials*, 25(2):71–81, 2001.

[7] RW Bukowski. Large-scale laboratory fire tests of smoke detectors. *Fire detection for life safety*, 1977.

[8] Richard D Peacock and Vytenis Babrauskas. Analysis of large-scale fire test data. *Fire Safety Journal*, 17(5):387–414, January 1991.

[9] Dougal Drysdale. *An Introduction to Fire Dynamics*. Wiley, October 2011.

[10] James G Quintiere. *Fundamentals of fire phenomena*. Wiley, 2006.

[11] V Babrauskas. *Heat Release in Fires*. Interscience Communications, 1992.

[12] William D Walton, Philip H Thomas, and Yoshifumi Ohmiya. Estimating Temperatures in Compartment Fires. In *SFPE Handbook of Fire Protection Engineering*, pages 996–1023. Springer, New York, NY, New York, NY, 2016.

[13] G E Gorbett, J L Pharr, and S Rockwell. Fire dynamics, 2016.

[14] Vytenis Babrauskas. *Ignition Handbook*. Principles and applications to fire safety engineering, fire investigation, risk management and forensic science. Fire Science Publishers, 1 edition, June 2003.

[15] A Tewarson. Heat release rate in fires. *Fire and Materials*, 4(4):185–191, December 1980.

[16] A Tewarson and S Ogden. Fire behavior of polymethylmethacrylate. *Combustion and Flame*, 89(3-4):237–259, June 1992.

[17] P J DiNenno. *SFPE Handbook of Fire Protection Engineering*. National Fire Protection Association Quincy, MA, New York, NY, third edition, 2002.

[18] LY Cooper. Fire-Plume-Generated Ceiling Jet Characteristics and Convective Heat Transfer to Ceiling and Wall Surfaces in a Two-Layer Fire Environment: Uniform Temperature Ceiling and Walls. *Fire Science and Technology*, 1993.

[19] B R Morton, F R S Sir Geoffrey Taylor, and J S Turner. Turbulent gravitational convection from maintained and instantaneous sources. *Proc. R. Soc. Lond. A*, 234(1196):1–23, January 1956.

[20] E E Zukoski, Toshi Kubota, and Baki Cetegen. Entrainment in fire plumes. *Fire Safety Journal*, 3(3):107–121, February 1981.

[21] D D Evans. Ceiling jet flows. *SFPE handbook of fire protection engineering*, 1995.

[22] R L Alpert. Calculation of response time of ceiling-mounted fire detectors. *Fire Technology*, 8(3):181–195, August 1972.

[23] PH Thomas. On strong two-dimensional plumes. *Fire Safety Journal*, 34(1):47–53, 2000.

[24] Gunnar Heskestad and Michael A Delichatsios. The initial convective flow in fire. *Symposium (International) on Combustion*, 17(1):1113–1123, January 1979.

[25] Gunnar Heskestad. Rise of plume front from starting fires. *Fire Safety Journal*, 36(2):201–204, March 2001.

[26] Björn Karlsson and James G Quintiere. *Enclosure fire dynamics*. CRC, 2000.

[27] C L Beyler. Fire plumes and ceiling jets. *Fire Safety Journal*, 1986.

[28] Bernard J McCaffrey. Purely buoyant diffusion flames :. Technical report, National Bureau of Standards, Gaithersburg, MD, Gaithersburg, MD, 1979.

[29] Gunnar Heskestad. Fire Plumes, Flame Height, and Air Entrainment. In *SFPE Handbook of Fire Protection Engineering*, pages 396–428. Springer, New York, NY, New York, NY, 2016.

[30] Guillermo Rein. Smoldering Combustion. In *SFPE Handbook of Fire Protection Engineering*, pages 581–603. Springer, New York, NY, New York, NY, 2016.

[31] D Gross, J Loftus, and A Robertson. Method for Measuring Smoke from Burning Materials. In *Symposium on Fire Test Methods—Restraint & Smoke 1966*, pages 166–166–39. ASTM International, 100 Barr Harbor Drive, PO Box C700, West Conshohocken, PA 19428-2959, January 1967.

[32] T J Ohlemiller and W M Shaub. Products of wood smolder and their relation to wood-burning stoves, 1988.

[33] Guillermo Rein, Simon Cohen, and Albert Simeoni. Carbon emissions from smouldering peat in shallow and strong fronts. *Proceedings of the Combustion Institute*, 32(2):2489–2496, 2009.

[34] G Mulholland and T J Ohlemiller. Aerosol Characterization of a Smoldering Source. *Aerosol Science and Technology*, 1(1):59–71, October 2008.

[35] D Weinert, T G Cleary, G W Mulholland, and P Beever. Light Scattering Characteristics And Size Distribution Of Smoke And Nuisance Aerosols. *Fire Safety Science - Proceedings of the First International Symposium*, 7:209–220, 2003.

[36] Michael Faraday. A Course of Six Lectures on the Chemical History of a Candle; to which is added a Lecture on Platinum, 1861.

[37] Bill Hammack and Don DeCoste. *Michael Faraday's The Chemical History of a Candle*. With Guides to Lectures, Teaching Guides & Student Activities. Articulate Noise Books, 2016.

[38] Mohammed M. Khan, Archibald Tewarson, and Marcos Chaos. Combustion Characteristics of Materials and Generation of Fire Products. In *SFPE Handbook of Fire Protection Engineering*, pages 1143–1232. Springer New York, New York, NY, 2016.

[39] O Meland and L Lernvik. Detection Of Smoke: Full-Scale Tests With Flaming And Smouldering Fires. *Fire Safety Science - Proceedings of the First International Symposium*, 3:975–984, 1991.

[40] A Tewarson. Relationship Between Generation of CO and CO^2 and Toxicity of the Environments Created by Materials in Flaming and Nonflaming Fires and Effect of Fire Ventilation. In *Characterization and Toxicity of Smoke*, pages 23–23–11. ASTM International, 100 Barr Harbor Drive, PO Box C700, West Conshohocken, PA 19428-2959, January 1990.

[41] James A Milke. History of Smoke Detection:A Profile of How the Technology and Role of Smoke Detection Has Changed. Technical report, September 2010.

[42] James A Milke and Thomas J McAvoy. Analysis of signature patterns for discriminating fire detection with multiple sensors. *Fire Technology*, 31(2):120–136, 1995.

[43] WL Grosshandler. Towards the development of a universal fire emulator-detector evaluator. *Fire Safety Journal*, 1997.

[44] JA Milke. Using multiple sensors for discriminating fire detection. *Research Application Symposium*, 1999.

[45] K J Overholt and O A Ezekoye. Characterizing Heat Release Rates Using an Inverse Fire Modeling Technique - Springer. *Fire Technology*, 2012.

[46] Y He, A Fernando, and M Luo. Determination of interface height from measured parameter profile in enclosure fire experiment. *Fire Safety Journal*, 31(1):19–38, 1998.

[47] Susan L Rose-Pehrsson, Ronald E Shaffer, Sean J Hart, Frederick W Williams, Daniel T Gottuk, Brooke D Strehlen, and Scott A Hill. Multi-criteria fire detection systems using a probabilistic neural network. *Sensors and Actuators B: Chemical*, 69(3):325–335, October 2000.

[48] James A Lynch, Daniel T Gottuk, Susan L Rose-Pehrsson, Jeffrey C Owrutsky, Daniel A Steinhurst, Christian P Minor, Stephen C Wales, Frederick W Williams, and John P Farley. Volume Sensor Development Test Series 2 - Lighting Conditions, Camera Settings, and Spectral and Acoustic Signatures. November 2004.

[49] Susan L Rose-Pehrsson, Jeffrey C Owrutsky, Daniel T Gottuk, Justin A Geiman, and Frederick W Williams. Phase I: FY01 Investigative Study for the Advanced Volume Sensor. June 2003.

[50] Richard Bukowski. Smoke dectector design and smoke properties. Technical report, National Bureau of Standards, Gaithersburg, MD, Gaithersburg, MD, 1978.

[51] Richard W Bukowski, Richard D Peacock, Jason D Averill, Thomas G Cleary, Nelson P Bryner, and Paul A Reneke. Performance of Home Smoke Alarms, Analysis of the Response of Several Available Technologies in Residential Fire Settings. *Technical Note (NIST TN) - 1455*, 2003.

[52] T Cleary, M Anderson, and J Averill. Building and Fire Publications. In *Eighth International Conference on Liquid Atomization and Spray Systems, CA, USA, July 2000*, 1999.

[53] C Mealy, A Wolfe, and D Gottuk. Smoke Alarm Response and Tenability. *AUBE09: 14th International Conference*, 2009.

[54] F W Mowrer. An analysis of effective thermal properties of thermally thick materials. *Fire Safety Journal*, 40(5):395–410, 2005.

[55] EL Milarcik, SM Olenick, and RJ Roby. A Relative Time Analysis of the Performance of Residential Smoke Detection Technologies. *Fire Technology*, 44(4):337–349, 2008.

[56] J Milke and R Zevotek. Analysis of the response of smoke detectors to smoldering fires and nuisance sources. *Fire Technology*, 52(5):1235–1253, 2016.

[57] J R Qualey. Fire test comparisons of smoke detector response times. *Fire Technology*, 36(2):89–108, May 2000.

[58] FW Mowrer. Lag times associated with fire detection and suppression. *Fire Technology*, 26(3):244–265, 1990.

[59] B J Meacham. Factors affecting the early detection of fire in electronic equipment and cable installations. *Fire Technology*, 1993.

[60] SD Wolin, N L Ryder, F Leprince, JA Milke, FW Mowrer, and JL Torero. Measurements of smoke characteristics in HVAC ducts. *Fire Technology*, 37(4):363–395, 2001.

[61] CK Lee. Estimates of luminous flame radiation from fires. *Combustion and Flame*, 24:239–244, 1975.

[62] G W Mulholland. Smoke production and properties. *SFPE handbook of fire protection engineering*, 1995.

[63] Luis A Cestari, Clarence Worrell, and James A Milke. Advanced fire detection algorithms using data from the home smoke detector project. *Fire Safety Journal*, 40(1):1–28, February 2005.

[64] Zhigang Liu and Andrew K Kim. Review of Recent Developments in Fire Detection Technologies. *Journal of Fire Protection Engineering*, 13(2):129, 2003.

[65] UL - 521 Standard for Heat Detectors for Fire Protective Signaling Systems — Standards Catalog.

[66] David D Evans and David W Stroup. Methods to calculate the response time of heat and smoke detectors installed below large unobstructed ceilings. *Fire Technology*, 22(1):54–65, February 1986.

[67] Richard W Bukowski. Techniques for Fire Detection. In *NASA Workshop on Spacecraft Fire Safety*, pages 9–29, October 2017.

[68] A Enis Çetin, Bart Merci, Osman Günay, Behçet Uğur Töreyin, and Steven Verstockt. Camera-Based Techniques. In *Methods and Techniques for Fire Detection*, pages 3–46. Elsevier, 2016.

[69] D Gutmacher, U Hoefer, and J Wöllenstein. Gas sensor technologies for fire detection. *Sensors and Actuators B: Chemical*, 175:40–45, December 2012.

[70] G Pfister. Multisensor/Multicriteria Fire Detection: A New Trend Rapidly Becomes State of the Art. *Fire Technology*, 33(2):115–139, 1997.

[71] M A Jackson and I Robins. Gas sensing for fire detection: Measurements of CO, CO2, H2, O2, and smoke density in European standard fire tests. *Fire Safety Journal*, 22(2):181–205, January 1994.

[72] E Scorsone, A M Pisanelli, and K C Persaud. Development of an electronic nose for fire detection. *Sensors and Actuators B:*, 2006.

[73] Matthew J Didomizio, Noah L Ryder, and Elizabeth J Weckman. Electronic gas sensors in fire testing. In *14th International Conference and Exhibition on Fire Science and Engineering*, Nr Windsor, July 2016. Royal Holloway College.

[74] James A Milke. Monitoring Multiple Aspects of Fire Signatures for Discriminating Fire Detection - Springer. *Fire Technology*, 35(3):195–209, 1999.

[75] TJ McAvoy, J Milke, and TA Kunt. Using multivariate statistical methods to detect fires. *Fire Technology*, 32(1):6–24, 1996.

[76] Daniel T Gottuk, Michelle J Peatross, Richard J Roby, and Craig L Beyler. Advanced fire detection using multi-signature alarm algorithms. *Fire Safety Journal*, 37(4):381–394, June 2002.

[77] Daniel T Gottuk, Scott A Hill, Christopher F Schemel, and Brooke D Strehlen. Identification of Fire Signatures for Shipboard Multi-Criteria Fire Detection Systems. June 1999.

[78] JA Milke. Discriminating Fire Detection with Multiple Sensors and Neural Networks. *NFPRF, Fire Suppression and Detection Symp, Orlando, FL*, 1997.

[79] W W Jones. Development of a multi-criteria algorithm for fast and reliable fire detection. *International conference on automatic fire detection*, 2004.

[80] EWM Lee, RKK Yuen, SM Lo, KC Lam, and GH Yeoh. A novel artificial neural network fire model for prediction of thermal interface location in single compartment fire. *Fire Safety Journal*, 39(1):67–87, 2004.

[81] J A Milke. *Advances in Fire Detection and Suppression*. Fire Technology, 2001.

[82] R Bukowski. A history of NBS/NIST research on fire detectors. *NIST SPECIAL PUBLICATION SP*, 2001.

[83] H Luck. Remarks on the state of the art in automatic fire detection. *Fire Safety Journal*, 29(2-3):77–85, September 1997.

[84] Michael J Gollner. Detection and Suppression of Fires: A Cornerstone of Fire Protection Engineering. *Fire Technology*, 52(5):1193–1196, June 2016.

[85] Muhammad Waseem Ahmad, Monjur Mourshed, David Mundow, Mario Sisinni, and Yacine Rezgui. Building energy metering and environmental monitoring – A state-of-the-art review and directions for future research. *Energy and Buildings*, 120:85–102, May 2016.

[86] JKW Wong, H Li, and S W Wang. Intelligent building research: a review. *Automation in Construction*, 2005.

[87] Edward Arens Tom Webster Mingyu Shi Danni Wang. How the number and placement of sensors controlling room air distribution systems affect energy use and comfort. *Proceedings of the Second International Conference for Enhanced Building Operations*, pages 1–10, 2002.

[88] Yu-Chee Tseng, Meng-Shiuan Pan, and Yuen-Yung Tsai. Wireless Sensor Networks for Emergency Navigation. *Computer*, 39(7):55–62, July 2006.

[89] Jalpa Shah and Biswajit Mishra. Customized IoT Enabled Wireless Sensing and Monitoring Platform for Smart Buildings. *Procedia Technology*, 23:256–263, 2016.

[90] M Bahrepour, N Meratnia, and P J M Havinga. Automatic Fire Detection: A Survey from Wireless Sensor Network Perspective. 2008.

[91] Majid Bahrepour, Nirvana Meratnia, Paul J M Havinga, and M Havinga. Sensor Fusion-based Event Detection in Wireless Sensor Networks. In *6th Annual International Conference on Mobile and Ubiquitous Systems: Computing, Networking and Services*. IEEE, 2009.

[92] *Autonomous Sensors for Building Automation*, May 2011.

[93] W Jahn, G REIN, and J L Torero. Forecasting fire growth using an inverse zone modelling approach. *Fire Safety Journal*, 46(3):81–88, April 2011.

[94] Enlighted.com. https://www.enlightedinc.com/system-and-solutions/iot-applications/light/. Technical report.

[95] Subutai Ahmad, Alexander Lavin, Scott Purdy, and Zuha Agha. Unsupervised real-time anomaly detection for streaming data. *Neurocomputing*, June 2017.

[96] Susan Rose-Pehrsson, Frederick Williams, Jeffrey Owrutsky, Daniel Gottuk, Daniel Steinhurst, Christian Minor, Stephen Wales, and As Represented By The Secretary Of The Navy The Government Of The Us. Volume sensor: data fusion-based, multi-sensor system for advanced damage control. February 2008.

[97] Susan L Rose-Pehrsson, Christian P Minor, Daniel A Steinhurst, Jeffrey C Owrutsky, James A Lynch, Daniel T Gottuk, Stephen C Wales, John P Farley, and Frederick W Williams. Volume sensor for damage assessment and situational awareness. *Fire Safety Journal*, 41(4):301–310, June 2006.

[98] BCHR Hagen and JA Milke. The use of gaseous fire signatures as a mean to detect fires. *Fire Safety Journal*, 34(1):55–67, 2000.

[99] Yuwei Cui, Chetan Surpur, Subutai Ahmad, and Jeff Hawkins. A comparative study of HTM and other neural network models for online sequence learning with streaming data. In *2016 International Joint Conference on Neural Networks (IJCNN)*, pages 1530–1538. Numenta, Inc, United States, IEEE, October 2016.

[100] Varun Chandola, Arindam Banerjee, and Vipin Kumar. Anomaly detection: A survey. *ACM Computing Surveys (CSUR)*, 41(3):15–58, July 2009.

[101] V Chandola, A Banerjee, and V Kumar. Anomaly Detection for Discrete Sequences: A Survey. *IEEE Transactions on Knowledge and Data Engineering*, 24(5):823–839, 2012.

[102] Yuwei Cui, Subutai Ahmad, and Jeff Hawkins. Continuous Online Sequence Learning with an Unsupervised Neural Network Model. *Neural Computation*, 28(11):2474–2504, 2016.

[103] E Lee, P Lau, and K Yuen. Application of artificial neural network to building compartment design for fire safety. *Data Engineering and Automated Learning–IDEAL*, 2006.

[104] Yuwei Cui, Subutai Ahmad, and Jeff Hawkins. The HTM Spatial Pooler: a neocortical algorithm for online sparse distributed coding. *bioRxiv*, page 085035, February 2017.

[105] British Standards Institution. *Methods of Test for Assessment of the Ignitability of Upholstered Seating by Smouldering and Flaming Ignition Sources*. BS 5852. 1990.

[106] Peter Senez, Patrick Mulherin, and Elizabeth J Weckman. Repeatability of Underventilated Compartment Fire Testing with Complex Fuel Packages. In *FIre Materials*, pages 1–14, December 2017.

[107] V Babrauskas. Ignition of Wood: A Review of the State of the Art. *Journal of Fire Protection Engineering*, 12(3):163–189, August 2002.

[108] Alex Bwalya, Gary Lougheed, Ahmed Kashef, and Hamed Saber. Survey Results of Combustible Contents and Floor Areas in Canadian Multi-Family Dwellings. *Fire Technology*, 47(4):1121–1140, 2010.

[109] Victoria Hodge and Jim Austin. A Survey of Outlier Detection Methodologies. *Artificial Intelligence Review*, 22(2):85–126, 2004.

[110] Scott Purdy. Encoding Data for HTM Systems. *arXiv.org*, February 2016.

[111] N L Ryder and EJ Weckman. Multicriteria Detection: Leveraging Building Control and Comfort Sensors for Fire State Determination. In *16th International Conference on Automatic Fire Detection & Suppression, Detection, and Signaling Research and Applications Conference*, pages 341–348. AUBE/NFPA, September 2017.

Appendices

Appendix A

Experimental Details

Test Date	Test Location	Test Number	Fuel	Quantity	Ignition Time	Burn out Time	Burning Duration	Diameter or Equivalent (in)	Diameter or Equivalent (m)	Area (m^2)	HRR (kW)	$Q = m''\Delta H_{c,eff}(1 - e^{-k\beta D})A_{dike}$	Sensors	Experimental Notes
6/25/14	Oven	06-25-2014_01	NA	NA						0.00000				
7/7/14	Cube	07-07-2014_02	Ethanol	20g				1.5	0.0381	0.00114	0.448166		THLP-03, 04, 05, 07, 08	
7/7/14	Cube	07-07-2014_03	Heptane	10g				1.5	0.0381	0.00114	0.210788		THLP-03, 04, 05, 07, 08	
7/9/14	Burn Room		Hay & Wood						0					
7/9/14	Burn Room		Hay & Wood						0	0.00000				
7/10/14	Burn Room	07-10-2014_01	Ethanol	100mL				3.5	0.0889	0.00621	2.494937		THLP-03, 04, 05, 07, 08	
7/10/14	Burn Room	07-10-2014_02	Ethanol	200mL	14:03:00	14:06:20	0:03:20	3.5	0.0889	0.00621	2.494937		THLP-03, 04, 05, 07, 08	
7/10/14	Burn Room	07-10-2014_03	Heptane	100mL	15:14:00	15:15:12	0:01:12	3.5	0.0889	0.00621	2.604847		THLP-03, 04, 05, 07, 08	
7/10/14	Burn Room	07-10-2014_04	Heptane	150mL	15:46:00	15:47:50	0:01:50	3.5	0.0889	0.00621	2.604847		THLP-03, 04, 05, 07, 08	
7/10/14	Burn Room	07-10-2014_05	Crumpled Newsprint	150g	17:17:00	17:24:20	0:07:20		0	0.00000			THLP-03, 04, 05, 07, 08	
7/11/14	Burn Room	07-11-2014_01	Ethanol	150 mL	12:52:30	12:55:10	0:02:40		0	0.00000	0		THLP-03, 04, 05, 07, 08	
7/11/14	Burn Room	07-11-2014_02	Heptane	150 mL	14:01:00				0	0.00000	0		THLP-03, 04, 05, 07, 08	Doors closed to burn room to start doors open at 14:04:00
7/11/14	Burn Room	07-11-2014_03	Heptane	50 mL	15:34:30				0	0.00000	0		THLP-03, 04, 05, 07, 08	Windows closed to start test, open at 15:40:30
7/11/14	Burn Room	07-11-2014_04	Ethanol	50 mL					0	0.00000	0		THLP-03, 04, 05, 07, 08	
7/14/14	Burn Room	07-14-2014_01	Shredded Computer Paper	8" Can	13:04:15	13:05:00	0:00:45		0	0.00000			THLP-03, 04, 05, 07, 08	45 seconds of flaming and then transitioned to several minutes of smoldering
7/14/14	Burn Room	07-14-2014_02	Shredded Computer Paper	8" Can	13:09:00	13:09:45	0:00:45		0	0.00000			THLP-03, 04, 05, 07, 08	45 seconds of flaming and then transitioned to several minutes of smoldering
7/14/14	Burn Room	07-14-2014_03	OSB Mini Crib 5.5"		14:35:00	14:42:00	0:07:00		0	0.00000			THLP-03, 04, 05, 07, 08	Smoldering continued after flames extinguished. Crib made of 3/4" wide 1/2" thick strips. 2-3-3 configuration with 2 strips on bottom, 3 in middle, 3 on top. Making a 5.5" rectangle, 50 mL ethanol to

Test Date	Test Location	Test Number	Fuel	Quantity	Ignition Time	Burn out Time	Burning Duration	Diameter or Equivalent (in)	Diameter or Equivalent (m)	Area (m^2)	HRR (kW)	$Q = m''\Delta H_{c,eff}(1 - e^{-k\beta D})A_{dike}$	Sensors	Experimental Notes
7/14/14	Burn Room	07-14-2014_04	OSB Mini Crib 11"		15:38:00	15:50:00	0:12:00		0	0.00000			THLP-03, 04, 05, 07, 08	Smoldering continued after flames extinguished. 11" crib 3-3-3 configuration, 50 mL ethanol to start.
7/15/14	Burn Room	07-15-2014_01	1/4 Crib		15:39:00		##########		0	0.00000			THLP-01, 02, 03, 04, 05, 07, 08	1/4 crib made from 2x2" pieces with 100 mL as a base fuel. THLP-05 fell at 15:52:00 into test.
7/16/14	Burn Room	07-16-2014_01	Heptane	100 mL	13:10:30		##########	3.75	0.09525	0.00713	3.192867		THLP-01, 02, 03, 04, 05, 07, 08	
7/16/14	Burn Room	07-16-2014_02	Heptane	50 mL	13:41:30	13:48:25	0:06:55	3.75	0.09525	0.00713	3.192867		THLP-01, 02, 03, 04, 05, 07, 08	Video started at 13:41:03
7/16/14	Burn Room	07-16-2014_03	Heptane	150 mL	15:38:00	15:39:40	0:01:40	8.5	0.2159 0	0.03661 0.00000	34.86154 0		THLP-01, 02, 03, 04,	Video started at 15:38:30, IR
7/17/14	Burn Room	Test 01	Shredded Computer Paper		12:16:30		##########	8	0.2032	0.03243			THLP-01, 02, 03, 04, 05, 07, 08	Video started at 12:16:00
7/17/14	Burn Room	Test 02	1/4 Crib		13:27:30		##########		0	0.00000			THLP-01, 02, 03, 04, 05, 07, 08	Side window opened at 13:28:30. IR camera started at 13:27:00. Started with 75 mL of
7/18/14	Burn Room	Test 01	Tea Lights	1	11:00:00		##########		0	0.00000			THLP-01, 02, 03, 04, 05, 07, 08	IR camera started at 10:59:45
7/18/14	Burn Room	Test 02	Tea Lights	2	11:17:00		##########		0	0.00000			THLP-01, 02, 03, 04, 05, 07, 08	IR started at 11:16:45. Doors closed
7/18/14	Burn Room	Test 03	Tea Lights	4	11:29:00		##########		0	0.00000			THLP-01, 02, 03, 04, 05, 07, 08	IR at 11:29:15
7/18/14	Burn Room	Test 04	Heptane	15 mL	11:44:30		##########	1.5	0.0381	0.00114	0.210788		THLP-01, 02, 03, 04, 05, 07, 08	IR started at 11:44:15
7/18/14	Burn Room	Test 05	Heptane	15 mL	12:10:30	12:17:07	0:06:37	1.5	0.0381	0.00114	0.210788		THLP-01, 02, 03, 04, 05, 07, 08	IR started at 12:10:00, slow motion video captured as well
7/18/14	Burn Room	Test 06	Heptane	15 mL	12:32:15		##########	1.5	0.0381	0.00114	0.210788		THLP-01, 02, 03, 04, 05, 07, 08, 09	IR started at 12:31:45, addition of ground level sensor THLP-09
7/18/14	Burn Room	Test 07	Heptane	15 mL	15:24:00	15:32:20	0:08:20	1.5	0.0381	0.00114	0.210788		THLP-01, 02, 03, 04, 05, 07, 08, 09	Front window open, wind blew at 15:29:10 and flame oscillated significantly. IR started at 15:23:45, slow motion video captured as well.

Test Date	Test Location	Test Number	Fuel	Quantity	Ignition Time	Burn out Time	Burning Duration	Diameter or Equivalent (in)	Diameter or Equivalent (m)	Area (m^2)	HRR (kW)	$Q = m''\Delta H_{c,eff}(1 - e^{-k\beta D})A_{dike}$	Sensors	Experimental Notes
7/21/14	Burn Room	Test 01	Heptane	15 mL	13:03:00	13:09:20	0:06:20	1.5	0.0381	0.00114	0.210788		THLP-01, 02, 03, 04, 05, 07, 08, 09	Fire brick obstruction in place to block "view" of ground based sensor. 13.5" tall, 18" wide centered half way between sensor and flame. 22" from flame and 22" from sensor.
7/21/14	Burn Room	Test 02	Heptane	50 mL	13:11:00	13:18:05	0:07:05	3.5	0.0889	0.00621	2.604847		THLP-01, 02, 03, 04, 05, 07, 08, 09	Fire brick obstruction in place to block "view" of ground based sensor. 13.5" tall, 18" wide centered half way between sensor and flame. 22" from flame and 22" from sensor.
7/21/14	Burn Room	Test 03	Heptane	50 mL	14:35:00	14:41:45	0:06:45	3.5	0.0889	0.00621	2.604847		THLP-01, 02, 03, 04, 05, 07, 08, 09	Fire brick obstruction in place to block "view" of ground based sensor. 13.5" tall, 18" wide centered half way between sensor and flame. 22" from flame and 22" from sensor.
7/21/14	Burn Room	Test 04	Heptane	100 mL	14:53:05	14:54:22	0:01:17	8.5	0.2159	0.03661	34.86154		THLP-01, 02, 03, 04, 05, 07, 08, 09	Fire brick obstruction in place to block "view" of ground based sensor. 13.5" tall, 18" wide centered half way between sensor and flame. 22" from flame and 22" from sensor.
7/21/14	Burn Room	Test 05	Heptane	100 mL	15:06:33	15:07:46	0:01:13	8.5	0.2159	0.03661	34.86154		THLP-01, 02, 03, 04, 05, 07, 08, 09	Fire brick obstruction in place to block "view" of ground based sensor. 13.5" tall, 18" wide centered half way between sensor and flame. 22" from flame and 22" from sensor.

Test Date	Test Location	Test Number	Fuel	Quantity	Ignition Time	Burn out Time	Burning Duration	Diameter or Equivalent (in)	Diameter or Equivalent (m)	Area (m^2)	HRR (kW)	$Q = m''\Delta H_{c,eff}(1 - e^{-k\beta D})A_{dike}$	Sensors	Experimental Notes
7/21/14	Burn Room	Test 06	Heptane	150 mL	15:19:02	15:20:30	0:01:28	8.5	0.2159	0.03661	34.86154		THLP-01, 02, 03, 04, 05, 07, 08, 09	Fire brick obstruction in place to block on opposite of ground sensor. 22" from sensor.
7/21/14	Burn Room	Test 07	Heptane	100 mL	15:57:00	15:58:25	0:01:25	8.5	0.2159	0.03661	34.86154		THLP-01, 02, 03, 04, 05, 07, 08, 09	Fire brick obstruction in place to block on opposite of ground sensor. 22" from sensor.
7/21/14	Burn Room	Test 08	Heptane	50 mL	16:33:30		##########	3.5	0.0889	0.00621	2.604847		THLP-01, 02, 03, 04, 05, 07, 08, 09	Fire brick obstruction in place to block on opposite of ground sensor. 22" from sensor.
7/21/14	Burn Room	Test 09	Heptane	10 mL	16:42:30	16:45:10	0:02:40	1.5	0.0381	0.00114	0.210788		THLP-01, 02, 03, 04, 05, 07, 08, 09	Fire brick obstruction in place to block on opposite of ground sensor. 22" from sensor. Flame centered 3" from
7/21/14	Burn Room	Test 10	Heptane	10 mL	16:47:45	16:50:30	0:02:45	1.5	0.0381	0.00114	0.210788		THLP-01, 02, 03, 04, 05, 07, 08, 09	Fire centered in room
7/21/14	Burn Room	Test 11	Heptane	10 mL	16:53:30	16:57:10	0:03:40	1.5	0.0381	0.00114	0.210788		THLP-01, 02, 03, 04, 05, 07, 08, 09	Fire 30 cm from THLP-09
7/21/14	Burn Room	Test 12	Heptane	10 mL	16:59:00		##########	1.5	0.0381	0.00114	0.210788		THLP-01, 02, 03, 04, 05, 07, 08, 09	Fire 60 cm from THLP-09
7/21/14	Burn Room	Test 13	Heptane	10 mL	17:04:30	17:08:27	0:03:57	1.5	0.0381	0.00114	0.210788		THLP-01, 02, 03, 04, 05, 07, 08, 09	Fire 120 cm from THLP-09
7/25/14	Burn Room	Test 01	Water				0:00:00		0	0.00000			THLP-01, 02, 03, 04, 05, 07, 08, 09	Boiling of water began at 12:54:00, task light on during test.
8/1/14	Burn Room	Test 01	Heptane	15 mL	15:23:45	15:27:20	0:03:35	3.5	0.0889	0.00621	2.604847		THLP-01, 02, 03, 04, 05, 07, 08, 09	task light on during experiment
8/1/14	Burn Room	Test 02	Heptane	15 mL	15:30:15	15:33:25	0:03:10	3.5	0.0889	0.00621	2.604847		THLP-01, 02, 03, 04, 05, 07, 08, 09	THLP-09 moved to other side of burn room 130 cm from room center (mirrored from prior
8/1/14	Burn Room	Test 03	Heptane	15 mL	15:38:15	15:41:20	0:03:05	3.5	0.0889	0.00621	2.604847		THLP-01, 02, 03, 04, 05, 07, 08, 09	task light on during experiment. Fire 30cm from THLP-09
8/1/14	Burn Room	Test 04	Heptane	15 mL	15:44:15	15:47:20	0:03:05	3.5	0.0889	0.00621	2.604847		THLP-01, 02, 03, 04, 05, 07, 08, 09	task light on during experiment. Fire 60cm from THLP-09

Test Date	Test Location	Test Number	Fuel	Quantity	Ignition Time	Burn out Time	Burning Duration	Diameter or Equivalent (in)	Diameter or Equivalent (m)	Area (m^2)	HRR (kW)	$Q = m''\Delta H_{c,eff}(1 - e^{-k\beta D})A_{dike}$	Sensors	Experimental Notes
8/1/14	Burn Room	Test 05	Heptane	15 mL	15:55	15:57:30	0:02:30	3.5	0.0889	0.00621	2.604847		THLP-01, 02, 03, 04, 05, 07, 08, 09	task light on during experiment. Fire 120cm from THLP-09
8/1/14	Burn Room	Test 06	Heptane	50 mL	16:03:30	16:04:20	0:00:50	8.5	0.2159	0.03661	34.86154		THLP-01, 02, 03, 04, 05, 07, 08, 09	task light on during experiment. Fire 60cm from THLP-09
8/1/14	Burn Room	Test 07	Heptane	50 mL	16:06:45	16:07:25	0:00:40	8.5	0.2159	0.03661	34.86154		THLP-01, 02, 03, 04, 05, 07, 08, 09	task light on during experiment. Fire 120cm from THLP-09
8/5/14	Burn Room	Test 01	Heptane	15 mL	12:36:45	12:40:25	0:03:40	3.5	0.0889	0.00621	2.604847		THLP-01, 02, 03, 04, 05, 07, 08, 09	Fire 20cm from THLP-09
8/5/14	Burn Room	Test 02	Heptane	15 mL	12:42:45	12:45:30	0:02:45	3.5	0.0889	0.00621	2.604847		THLP-01, 02, 03, 04, 05, 07, 08, 09	Fire 40cm from THLP-09
8/5/14	Burn Room	Test 03	Heptane	15 mL	12:54:30	12:58:20	0:03:50	3.5	0.0889	0.00621	2.604847		THLP-01, 02, 03, 04, 05, 07, 08, 09	Fire 60cm from THLP-09
8/5/14	Burn Room	Test 04	Heptane	15 mL	12:59:15	13:02:30	0:03:15	3.5	0.0889	0.00621	2.604847		THLP-01, 02, 03, 04, 05, 07, 08, 09	Fire 80cm from THLP-09
8/5/14	Burn Room	Test 05	Heptane	15 mL	13:05:45	13:09:00	0:03:15	3.5	0.0889	0.00621	2.604847		THLP-01, 02, 03, 04, 05, 07, 08, 09	Fire 100cm from THLP-09
8/5/14	Burn Room	Test 06	Heptane	15 mL	13:10:30	13:13:05	0:02:35	3.5	0.0889	0.00621	2.604847		THLP-01, 02, 03, 04, 05, 07, 08, 09	Fire 120cm from THLP-09
8/5/14	Burn Room	Test 07	Heptane	15 mL	13:15:15	13:18:30	0:03:15	3.5	0.0889	0.00621	2.604847		THLP-01, 02, 03, 04, 05, 07, 08, 09	Fire 140cm from THLP-09
8/5/14	Burn Room	Test 08	Heptane	15 mL	13:46:00	13:49:35	0:03:35	3.5	0.0889	0.00621	2.604847		THLP-01, 02, 03, 04, 05, 07, 08, 09	Fire 160cm from THLP-09
8/5/14	Burn Room	Test 09	Heptane	15 mL	13:57:15	14:01:30	0:04:15	3.5	0.0889	0.00621	2.604847		THLP-01, 02, 03, 04, 05, 07, 08, 09	Fire 180cm from THLP-09
8/5/14	Burn Room	Test 10	Heptane	15 mL	14:02:00	14:05:00	0:03:00	3.5	0.0889	0.00621	2.604847		THLP-01, 02, 03, 04, 05, 07, 08, 09	Fire 200cm from THLP-09
8/5/14	Burn Room	Test 11	Heptane	15 mL	14:07:15	14:10:10	0:02:55	3.5	0.0889	0.00621	2.604847		THLP-01, 02, 03, 04, 05, 07, 08, 09	Fire diagonal from THLP-09 60cm down and right (i.e. $(60^2+60^2)^{0.5}$)
8/5/14	Burn Room	Test 12	Heptane	15 mL	14:14:00		##########	3.5	0.0889	0.00621	2.604847		THLP-01, 02, 03, 04, 05, 07, 08, 09	Fire diagonal from THLP-09 90cm down and right (i.e. $(90^2+90^2)^{0.5}$)
8/5/14	Burn Room	Test 13	Heptane	100 mL	14:22:30	14:26:18	0:03:48	7.25	0.18415	0.02663	21.99935		THLP-01, 02, 03, 04, 05, 07, 08, 09	Fire 40cm from THLP-09
8/5/14	Burn Room	Test 14	Heptane	100 mL	16:30:30	16:35:00	0:04:30	7.25	0.18415	0.02663	21.99935		THLP-01, 02, 03, 04, 05, 07, 08, 09	Fire 80cm from THLP-09

Test Date	Test Location	Test Number	Fuel	Quantity	Ignition Time	Burn out Time	Burning Duration	Diameter or Equivalent (in)	Diameter or Equivalent (m)	Area (m^2)	HRR (kW)	$Q = m''\Delta H_{c,eff}(1 - e^{-k\beta D})A_{dike}$	Sensors	Experimental Notes
8/5/14	Burn Room	Test 15	Heptane	100 mL	16:46:45	16:50:30	0:03:45	7.25	0.18415	0.02663	21.99935		THLP-01, 02, 03, 04, 05, 07, 08, 09	Fire 120cm from THLP-09
8/5/14	Burn Room	Test 16	Heptane	100 mL	16:54:15	16:58:30	0:04:15	7.25	0.18415	0.02663	21.99935		THLP-01, 02, 03, 04, 05, 07, 08, 09	Fire 160cm from THLP-09
8/5/14	Burn Room	Test 17	Heptane	100 mL	17:03:15	17:08:00	0:04:45	7.25	0.18415	0.02663	21.99935		THLP-01, 02, 03, 04, 05, 07, 08, 09	Fire 200cm from THLP-09
8/5/14	Burn Room	Test 18	Hot Plate		17:11:00		##########		0	0.00000			THLP-01, 02, 03, 04, 05, 07, 08, 09	
8/5/14	Burn Room	Test 19	Water		17:40:00		##########		0	0.00000			THLP-01, 02, 03, 04, 05, 07, 08, 09	hot plate with pan and water to examine response to steam and heat source. Kettle removed from hot plate at 18:07:00. IR video/images taken
8/5/14	Burn Room	Test 20	Propane		18:19:00	18:25:50	0:06:50		0	0.00000			THLP-01, 02, 03, 04, 05, 07, 08, 09	Propane Torch
8/5/14	Burn Room	Test 21	Heptane	150 mL	18:36:30	18:38:20	0:01:50	12	0.3048	0.07297	93.6291		THLP-01, 02, 03, 04, 05, 07, 08, 09	Pan elevated so base is 4.5" from ground, pan is 2.5" deep, centered in room.
8/5/14	Burn Room	Test 22	Heptane	100 mL	18:54:45	18:56:00	0:01:15	8.5	0.2159	0.03661	34.86154		THLP-01, 02, 03, 04, 05, 07, 08, 09	Fire 40cm from THLP-09
8/5/14	Burn Room	Test 23	Heptane	100 mL	18:58:00	18:59:30	0:01:30	8.5	0.2159	0.03661	34.86154		THLP-01, 02, 03, 04, 05, 07, 08, 09	Fire 90cm from THLP-09
8/5/14	Burn Room	Test 24	Heptane	100 mL	19:02:10	19:03:15	0:01:05	8.5	0.2159	0.03661	34.86154		THLP-01, 02, 03, 04, 05, 07, 08, 09	Fire 160cm from THLP-09
8/6/14	Burn Room	Test 01	Heptane	20 mL	16:36:50	16:40:50	0:04:00	3.5	0.0889	0.00621	2.604847		THLP-01, 02, 03, 04, 05, 07, 08, 09	Smoke detectors and CO detector added. SD01 16:38:10, SD02 16:39:15, SD03 did not activate, CO did not activate, no
8/6/14	Burn Room	Test 02	Heptane	20 mL	16:53:15	16:57:35	0:04:20	3.5	0.0889	0.00621	2.604847		THLP-01, 02, 03, 04, 05, 07, 08, 09	SD01 16:55:30, SD02 16:55:08, SD03 did not activate, CO did not
8/6/14	Burn Room	Test 03	Heptane	100 mL	17:02:05	17:06:10	0:04:05	7.25	0.18415	0.02663	21.99935		THLP-01, 02, 03, 04, 05, 07, 08, 09	SD01 17:03:20, SD02 17:03:22, SD03 17:03:21, CO

Test Date	Test Location	Test Number	Fuel	Quantity	Ignition Time	Burn out Time	Burning Duration	Diameter or Equivalent (in)	Diameter or Equivalent (m)	Area (m^2)	HRR (kW)	$Q = m''\Delta H_{c,eff}(1 - e^{-k\beta D})A_{dike}$	Sensors	Experimental Notes
8/6/14	Burn Room	Test 04	Heptane	15 mL	17:23:15	17:26:50	0:03:35	1.5	0.0381	0.00114	0.210788		THLP-01, 02, 03, 04, 05, 07, 08, 09	SD01 17:24:25, turned off at 17:26:35. SD02, SD03 did not activate, CO did not
8/6/14	Burn Room	Test 05	Mini OSB Crib	2x3x3 configuration	17:34:00	17:42:00	0:08:00		0	0.00000			THLP-01, 02, 03, 04, 05, 07, 08, 09	20 mL of heptane added to start fire. SD01 17:36:45, SD02 17:34:45, SD03 17:35:05 turning off and on, CO did not activate,
8/6/14	Burn Room	Test 06	PU Foam	4x4x1"	17:57:45	17:58:30	0:00:45		0	0.00000			THLP-01, 02, 03, 04, 05, 07, 08, 09	15 mL of heptane added to start fire. SD01 17:58:05, SD02
8/6/14	Burn Room	Test 07	PU Foam	4x4x3"	18:05:30	18:07:05	0:01:35		0	0.00000			THLP-01, 02, 03, 04, 05, 07, 08, 09	SD01 18:05:50, SD02 18:05:55, SD03 18:06:00, CO did not activate, peak reading 151 ppm. All SD

Appendix B

Sensor Block

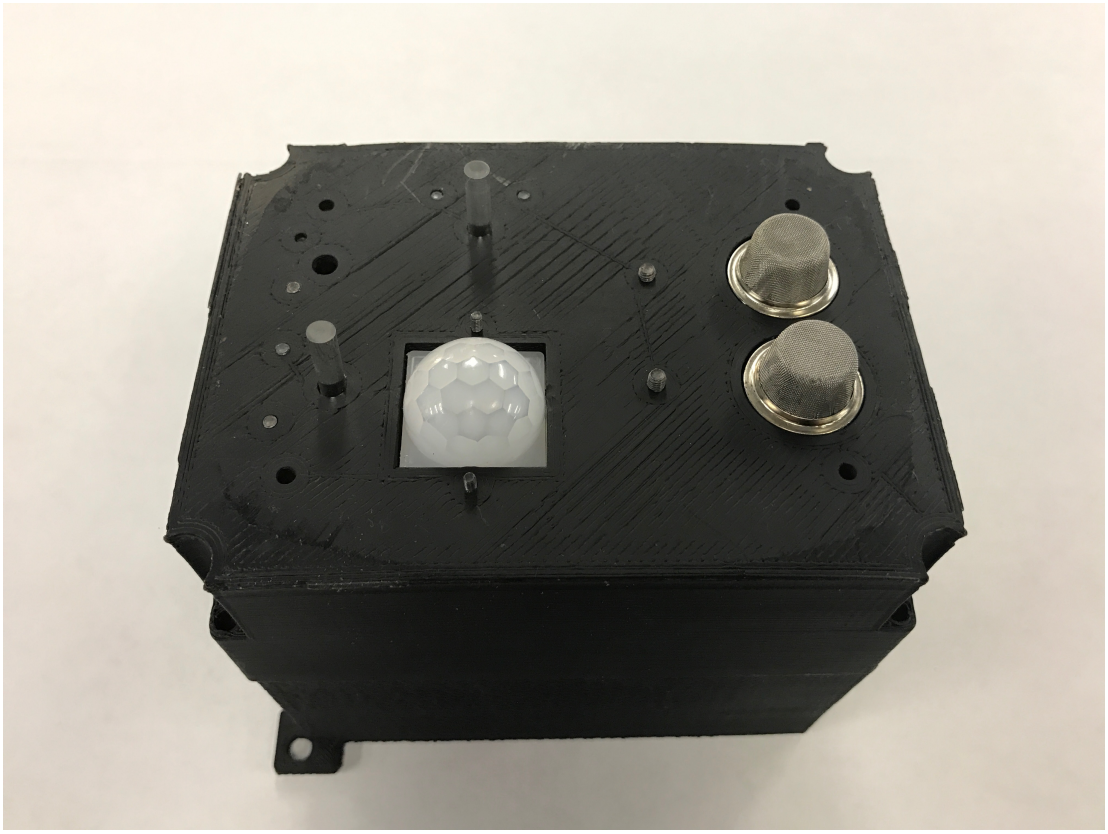


Figure B.1: Sensor Block

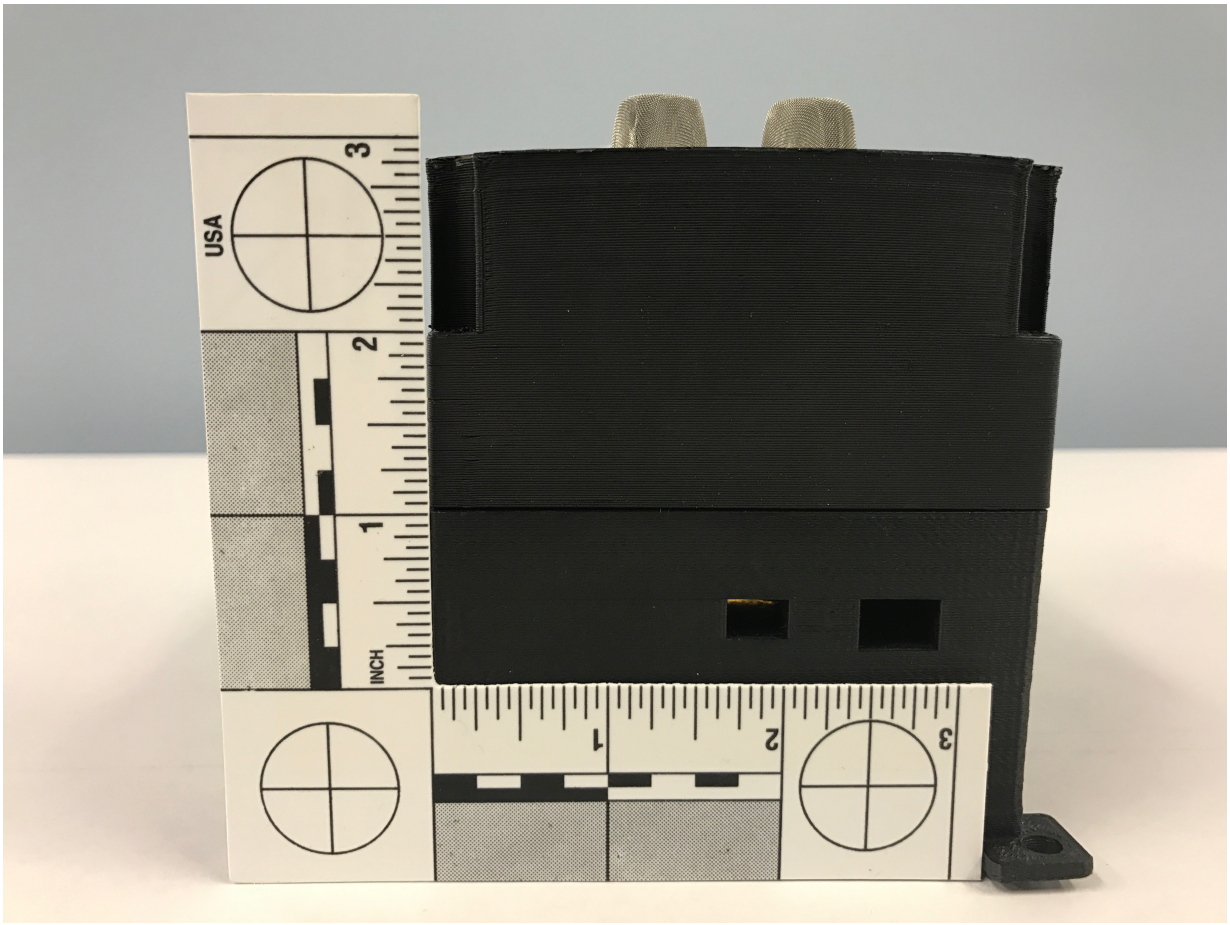


Figure B.2: Sensor Block

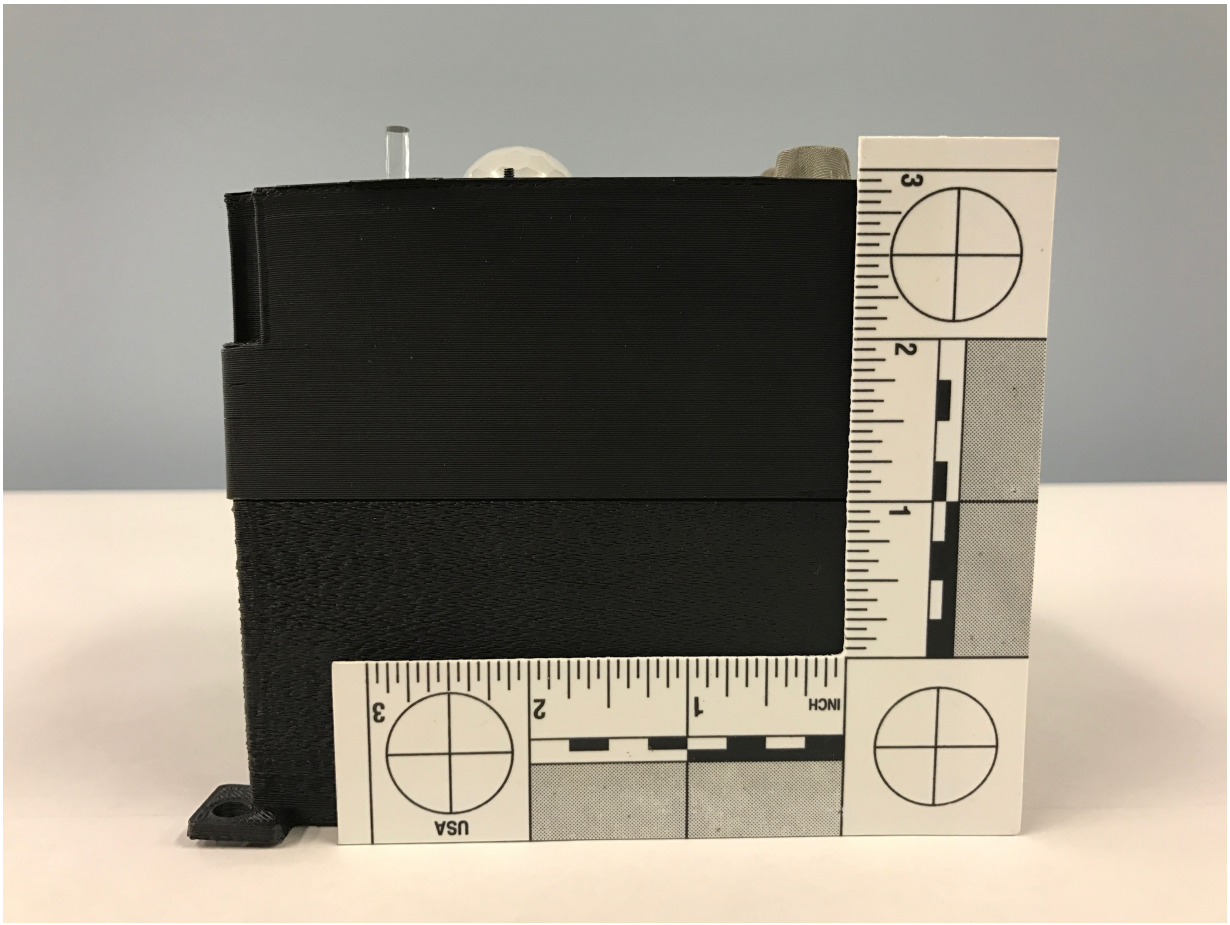


Figure B.3: Sensor Block

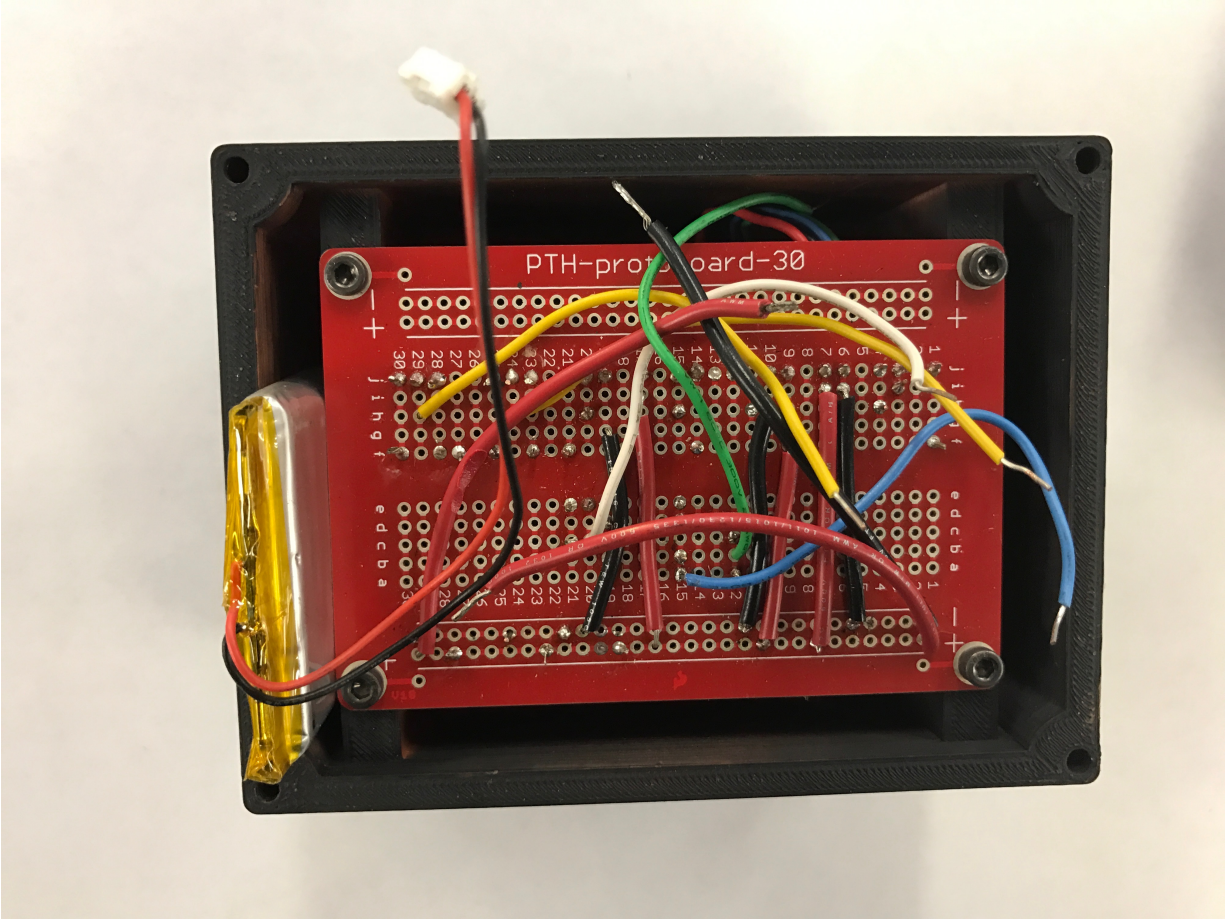


Figure B.4: Sensor Block

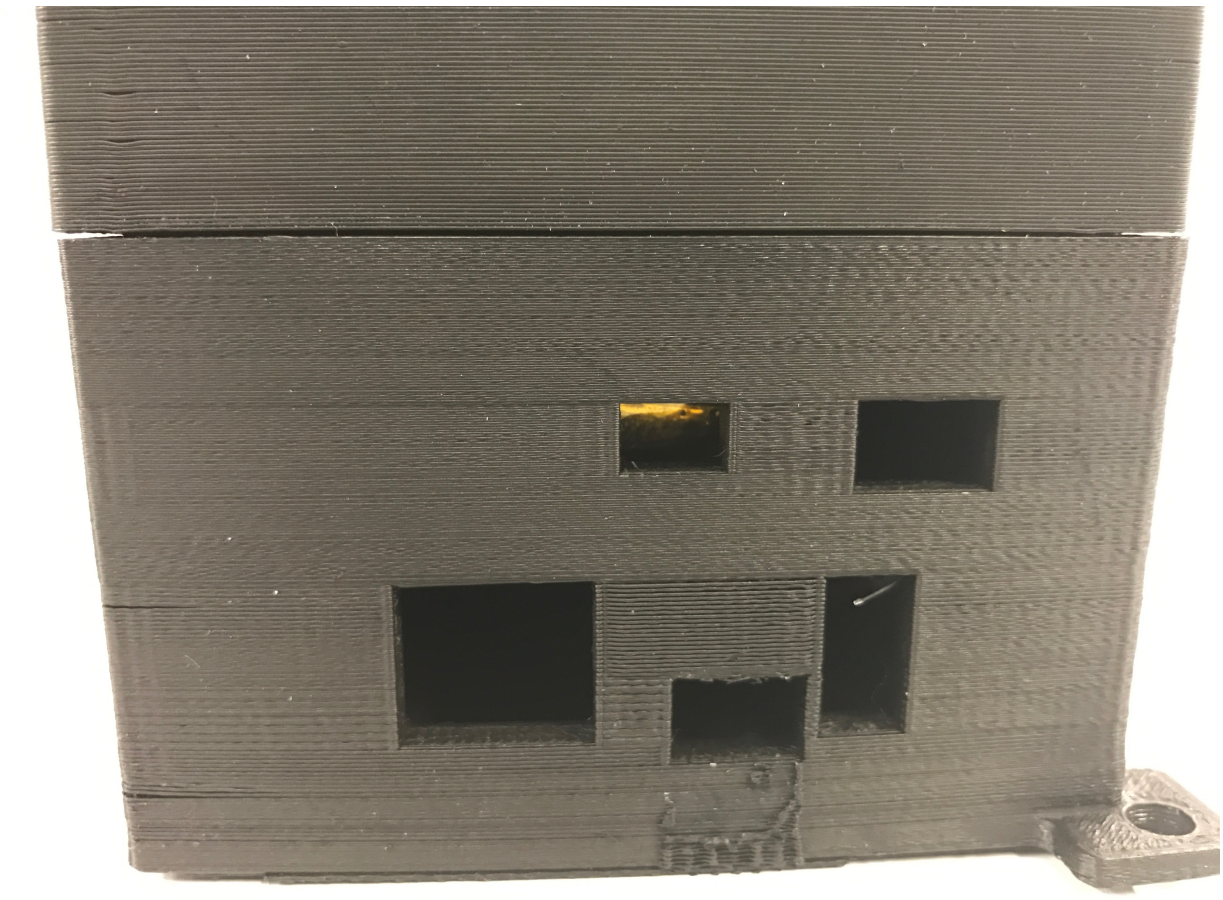


Figure B.5: Sensor Block

Appendix C

Experimental Results

C.1 Burn Room Experimental Results

The following section provides results for each sensor for each test conducted. The test details were provided in Appendix A and the sensor locations may be found in Figure C.1.

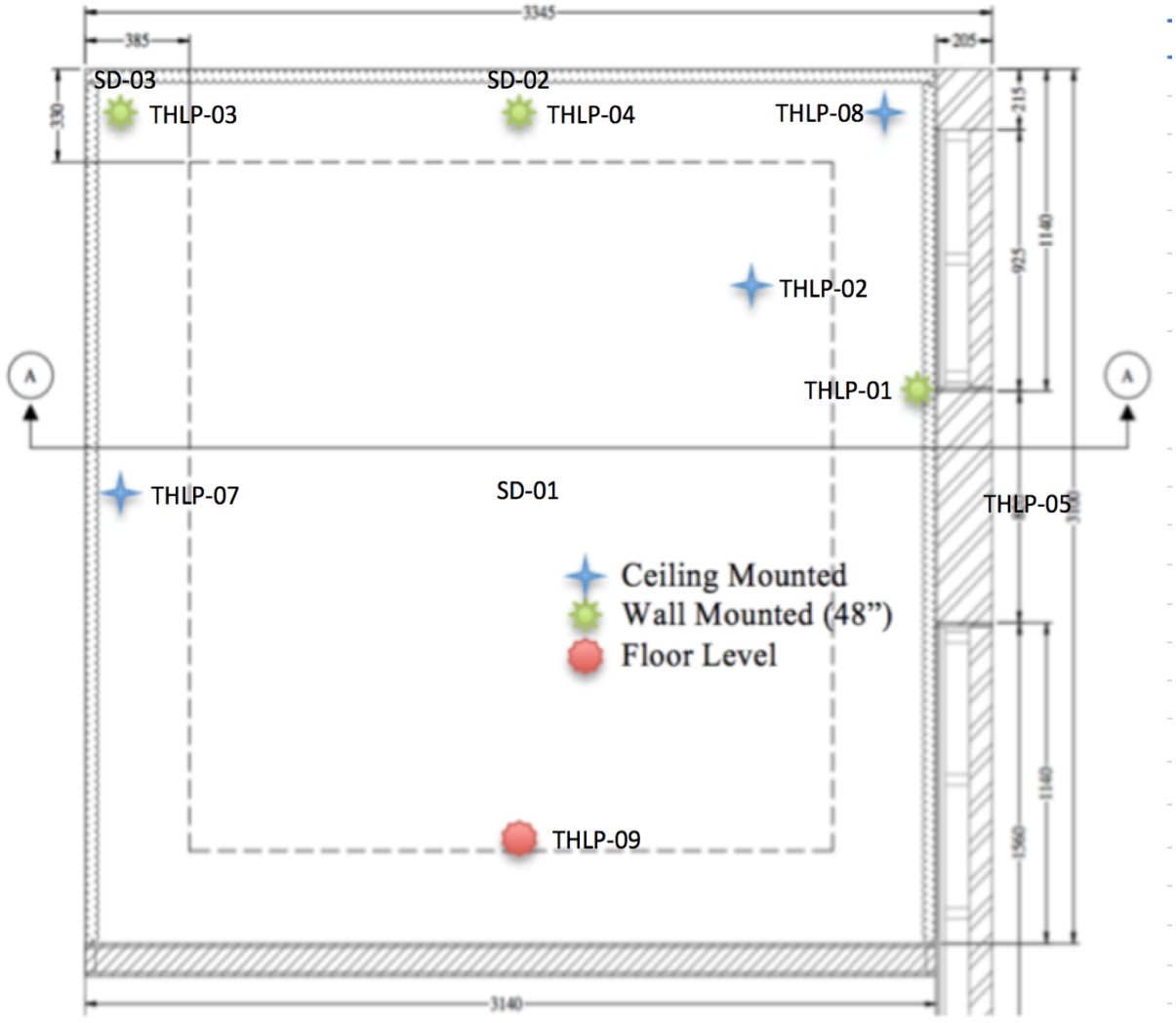


Figure C.1: Sensor Locations

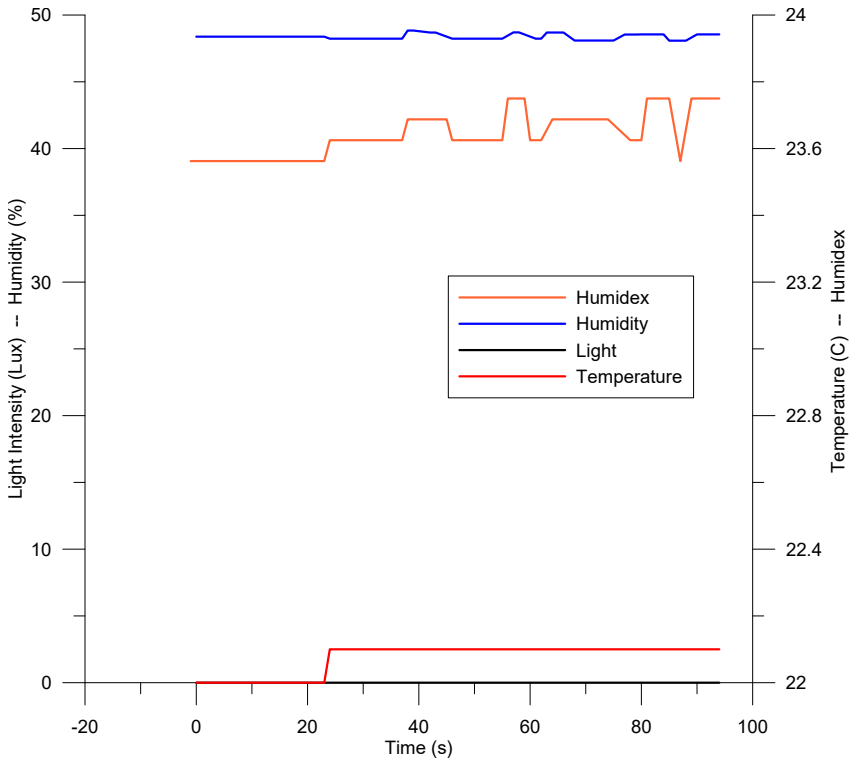


Figure C.2: Test 06 THLP 01

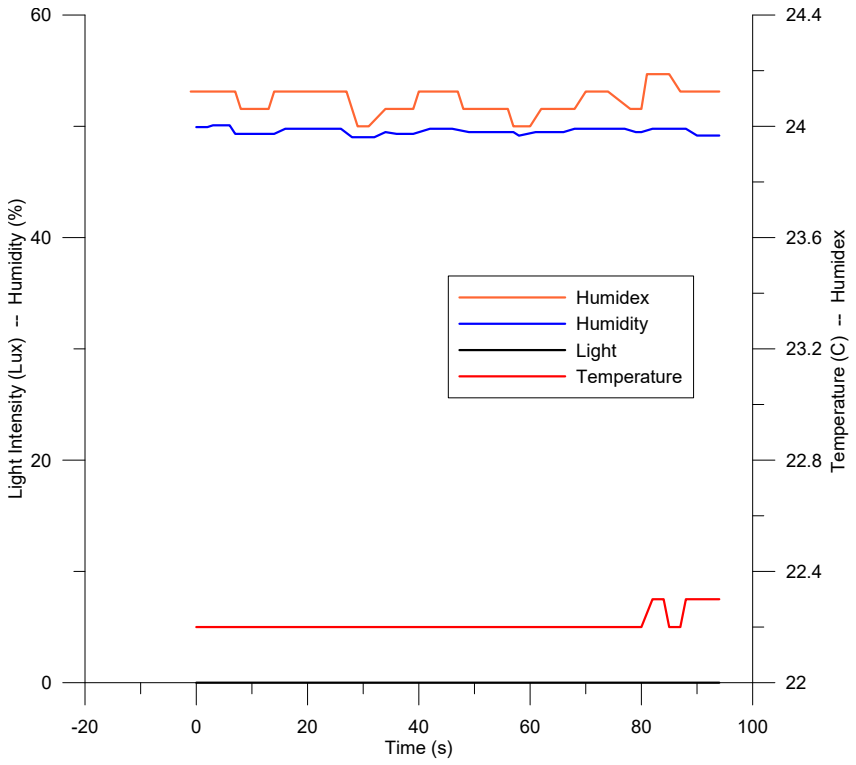


Figure C.3: Test 06 THLP 02

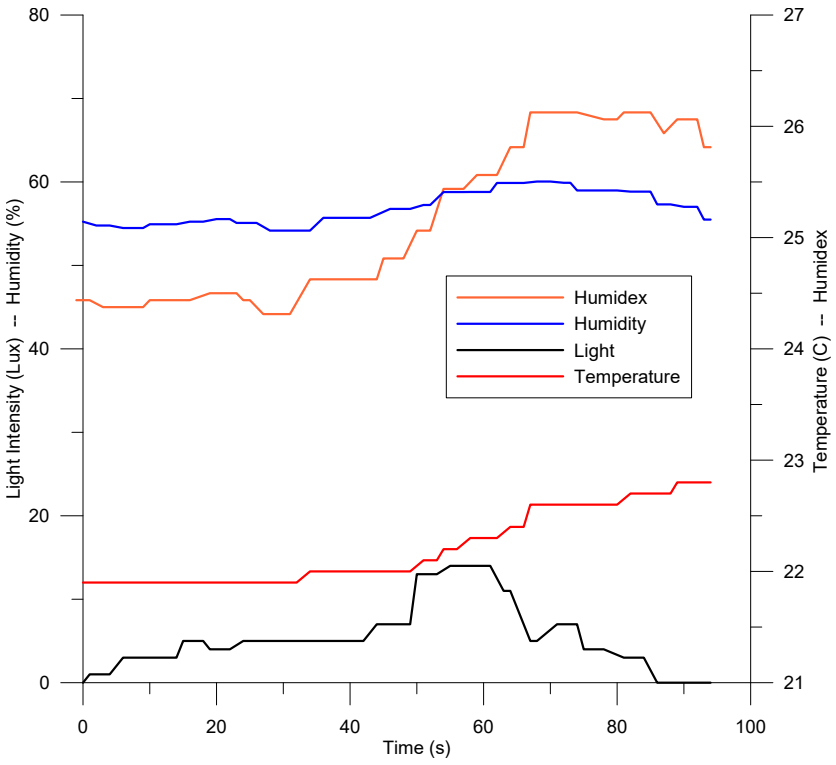


Figure C.4: Test 06 THLP 03

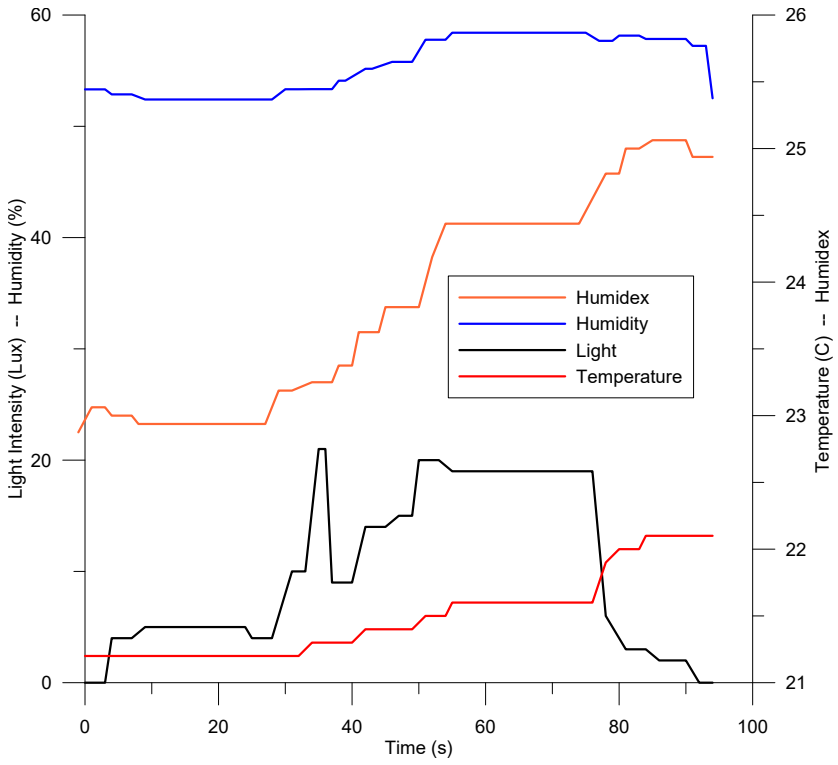


Figure C.5: Test 06 THLP 04

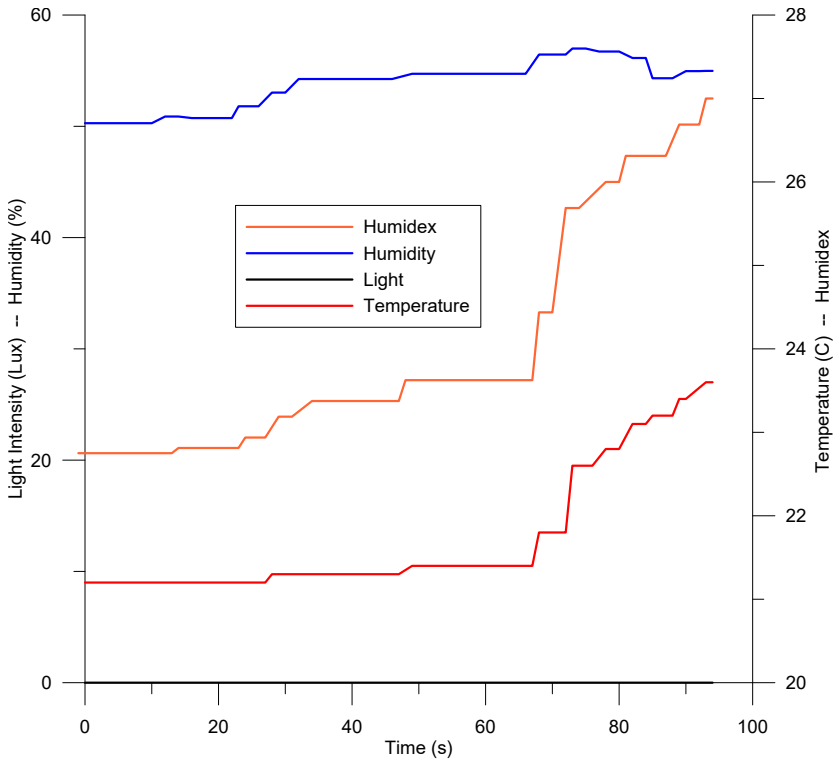


Figure C.6: Test 06 THLP 05

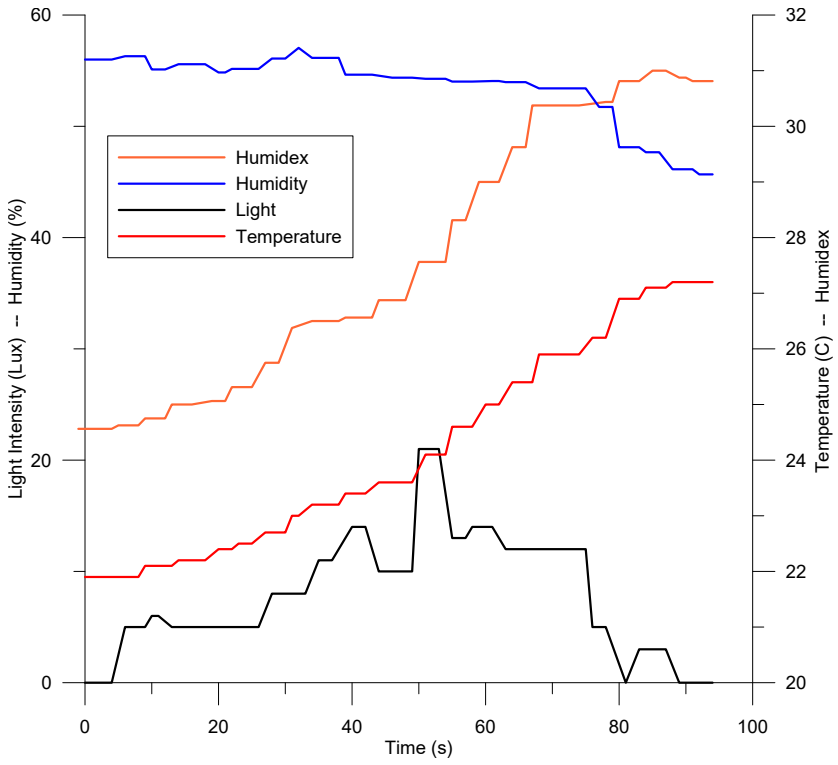


Figure C.7: Test 06 THLP 07

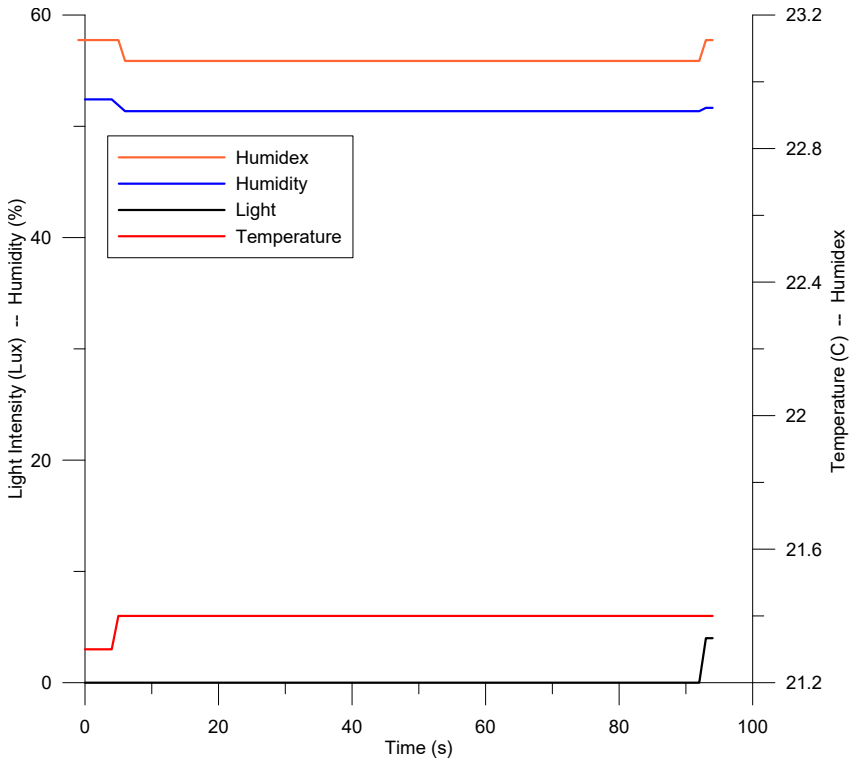


Figure C.8: Test 06 THLP 08

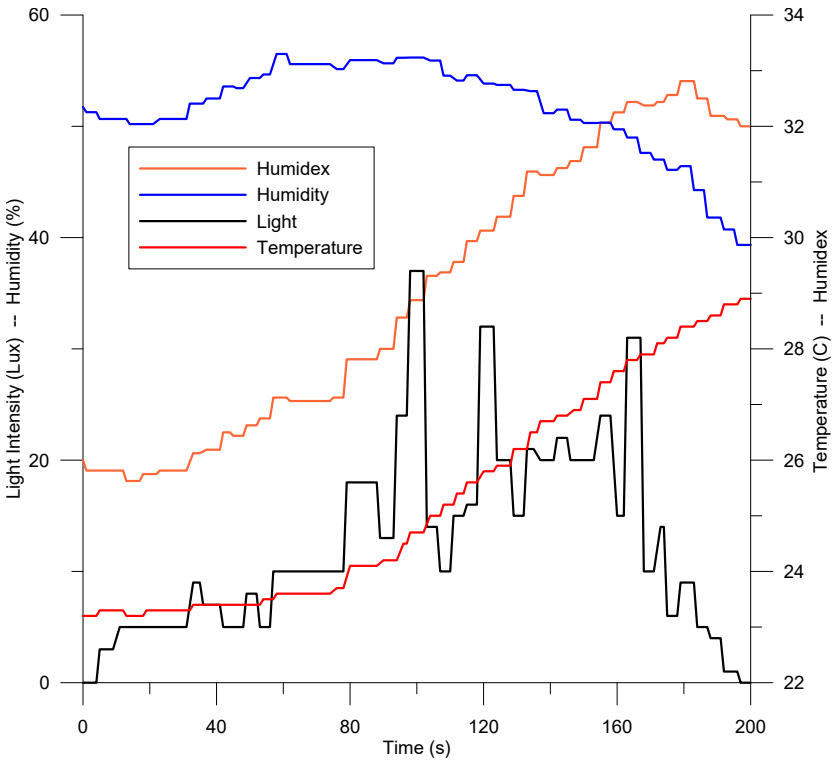


Figure C.9: Test 07 THLP 03

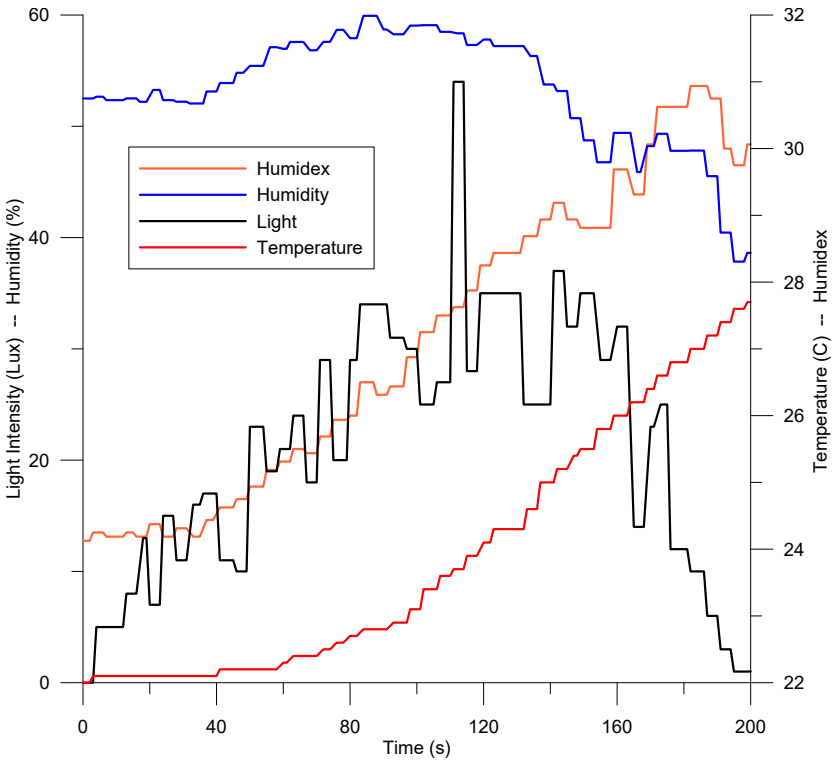


Figure C.10: Test 07 THLP 04

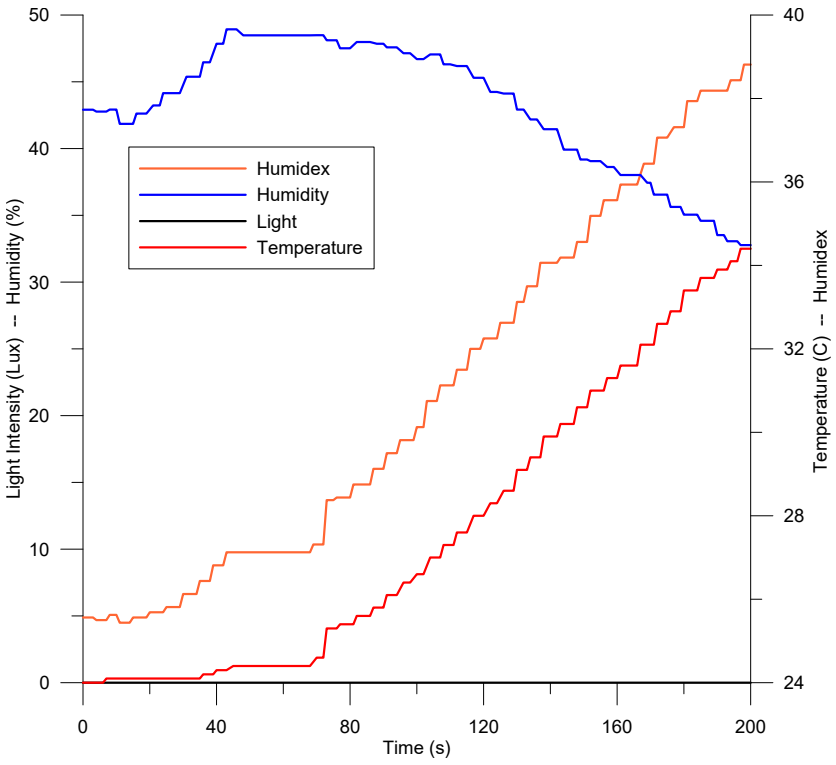


Figure C.11: Test 07 THLP 05

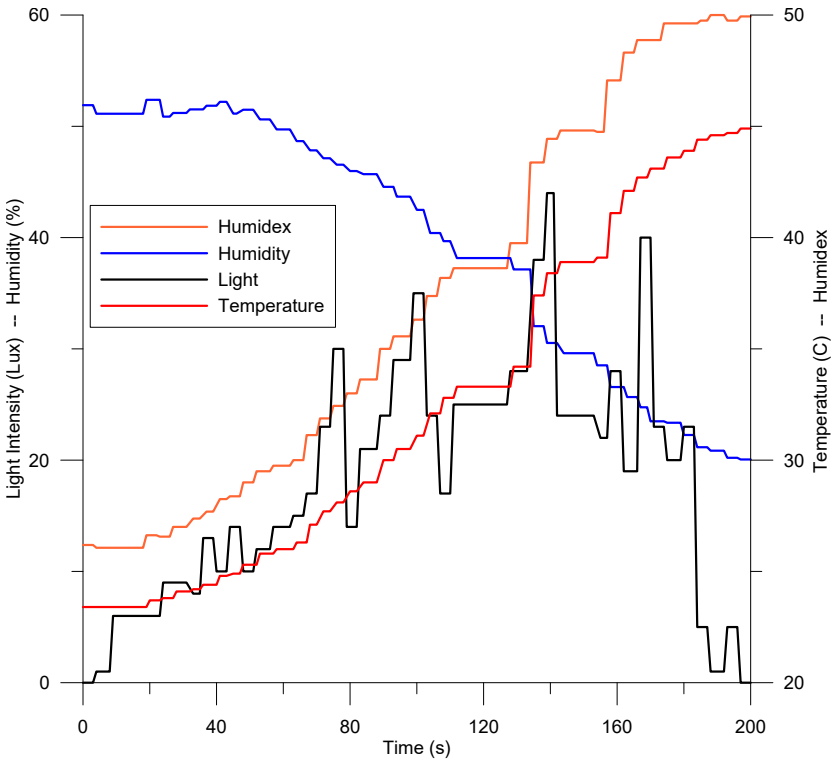


Figure C.12: Test 07 THLP 07

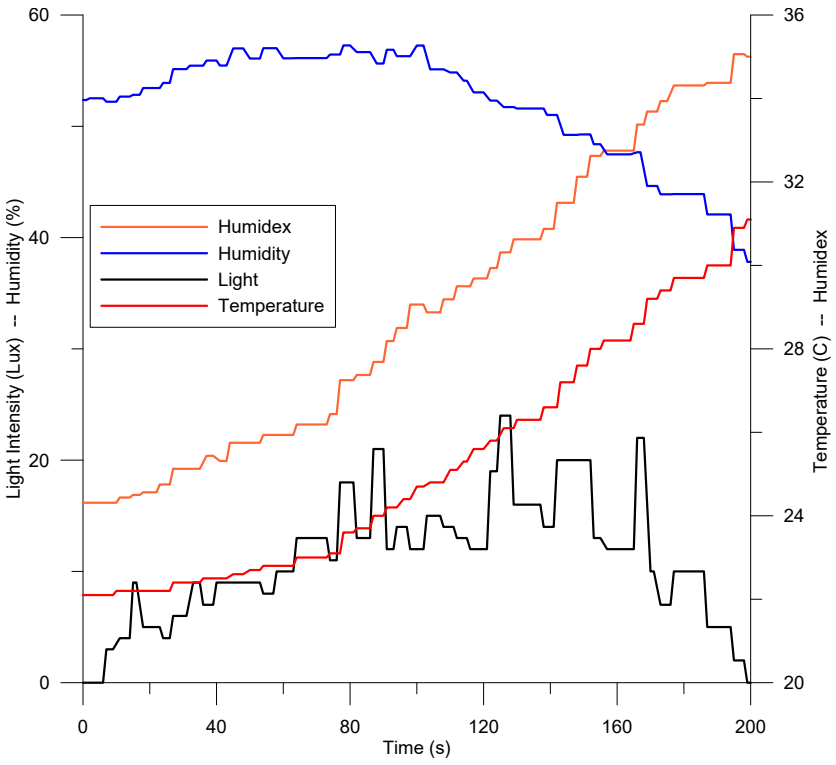


Figure C.13: Test 07 THLP 08

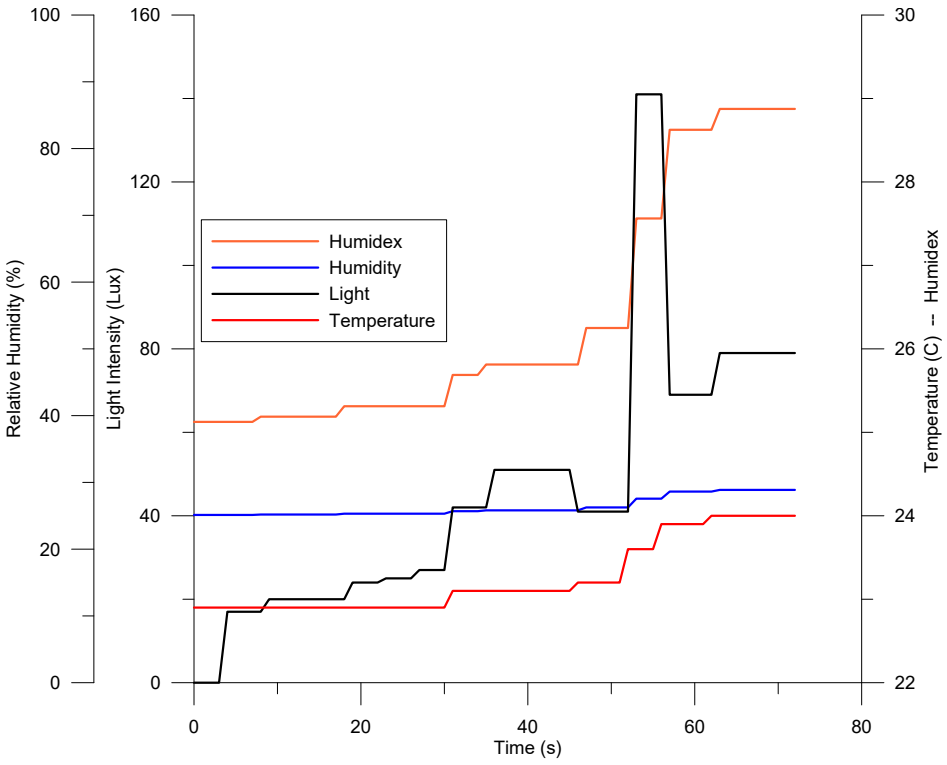


Figure C.14: Test 08 THLP 03

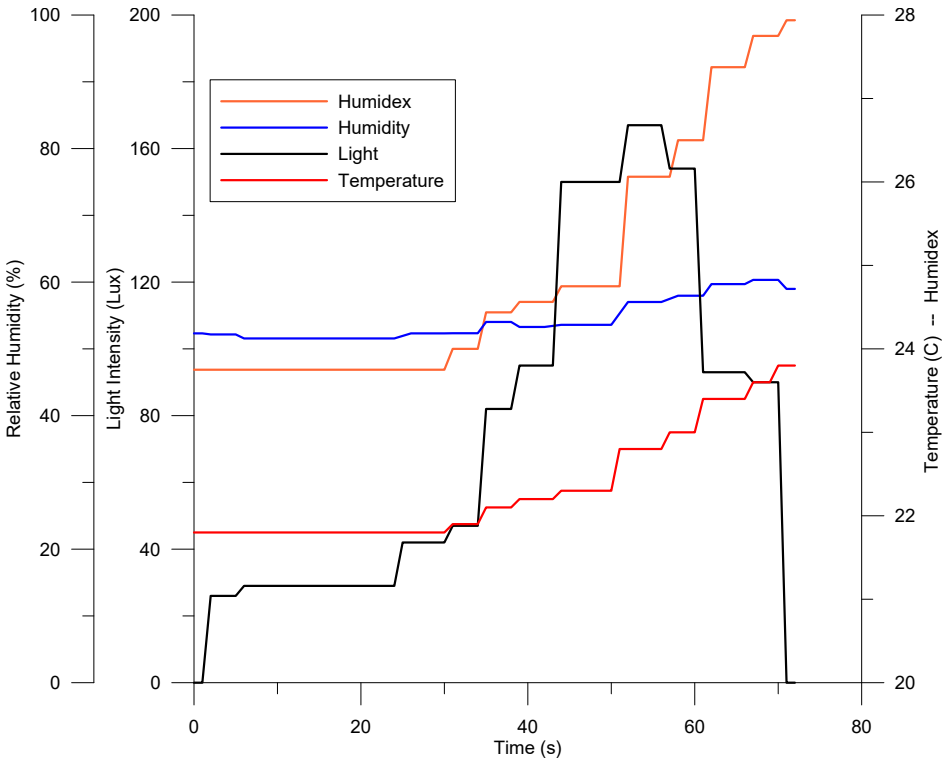


Figure C.15: Test 08 THLP 04

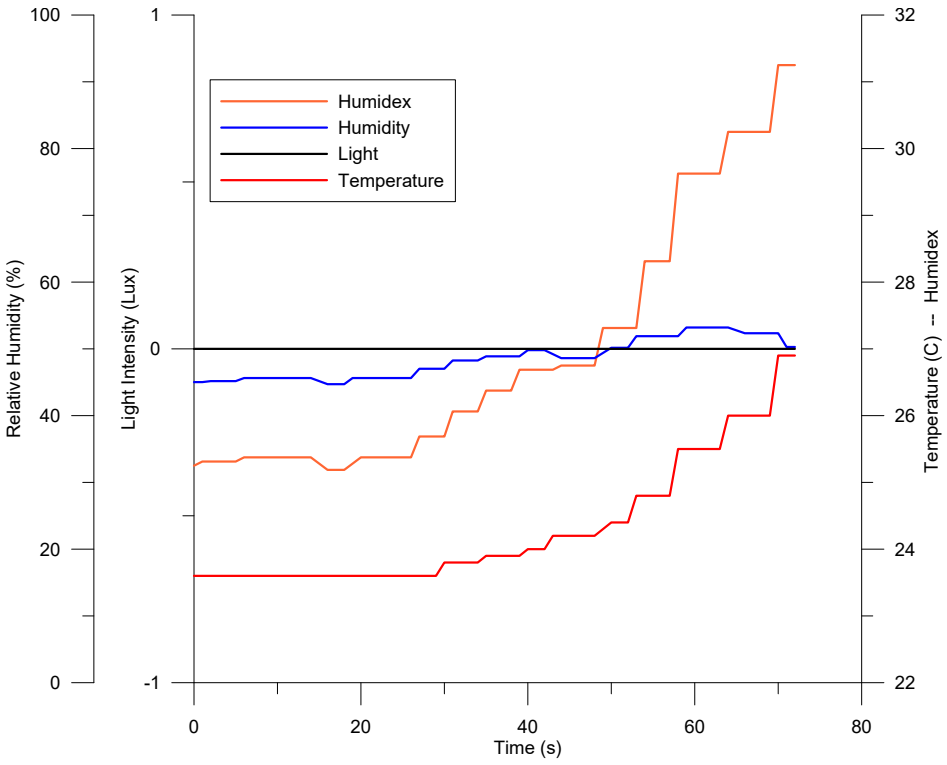


Figure C.16: Test 08 THLP 05

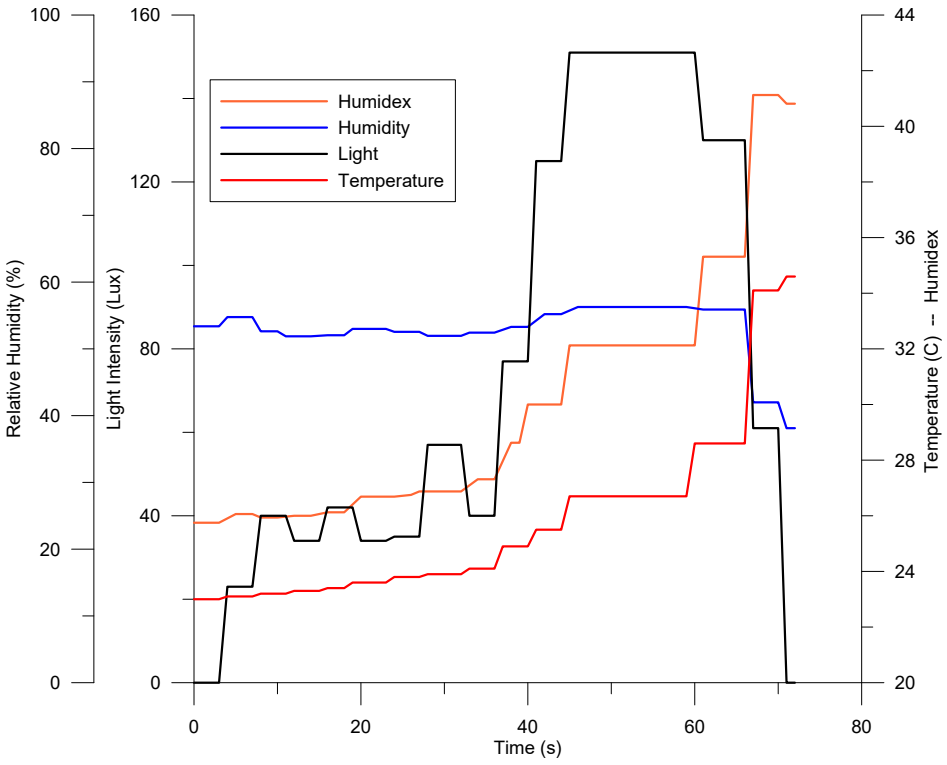


Figure C.17: Test 08 THLP 07

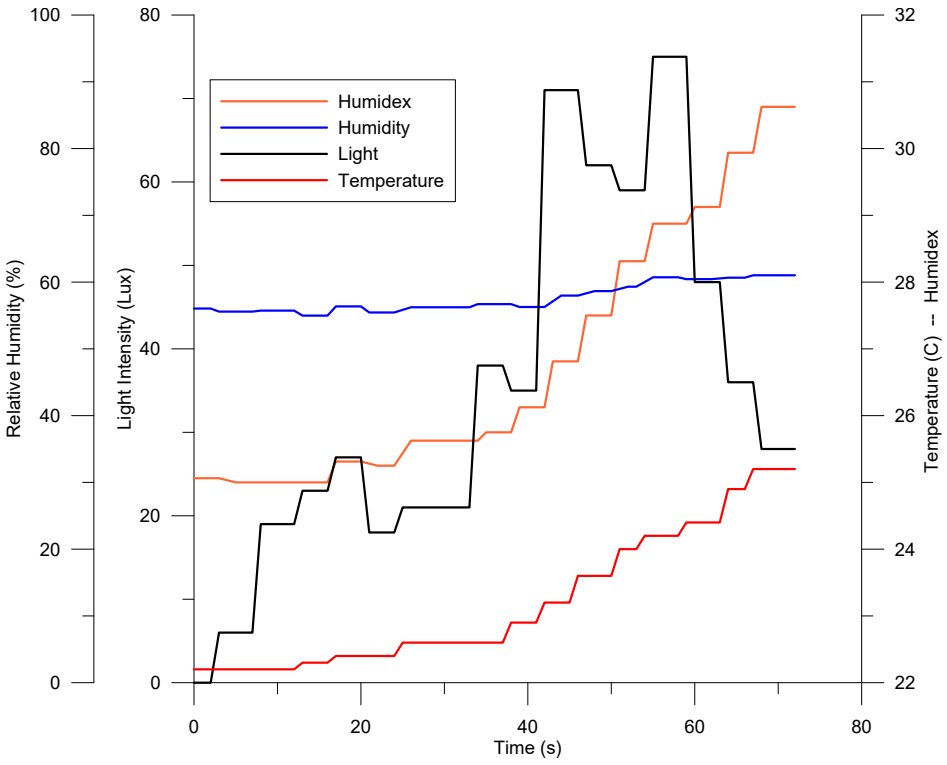


Figure C.18: Test 08 THLP 08

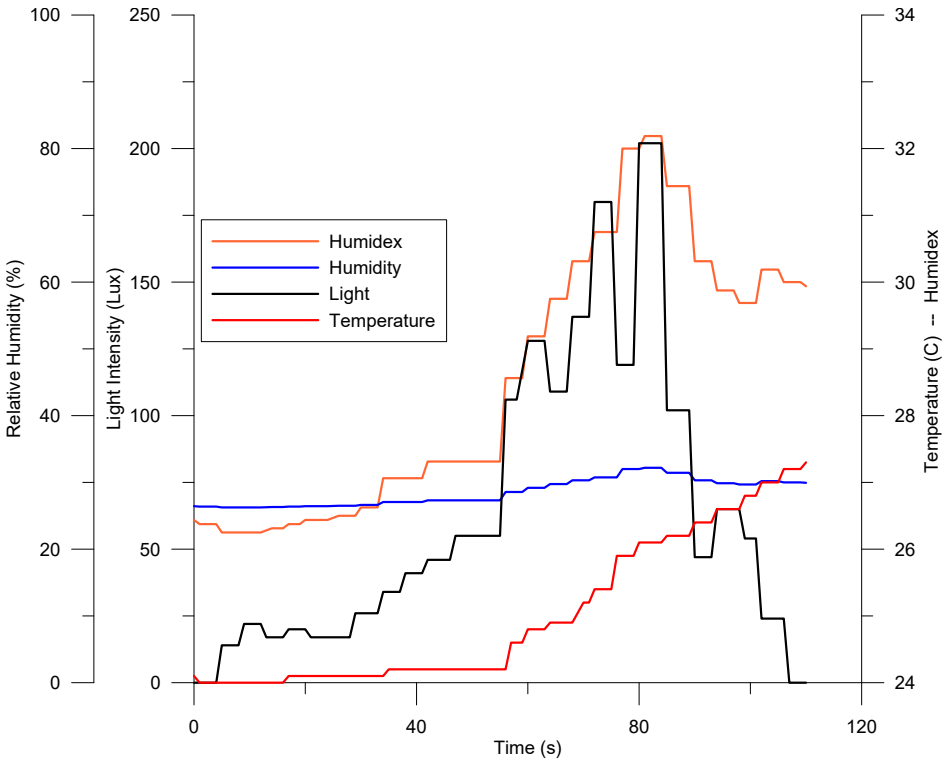


Figure C.19: Test 09 THLP 03

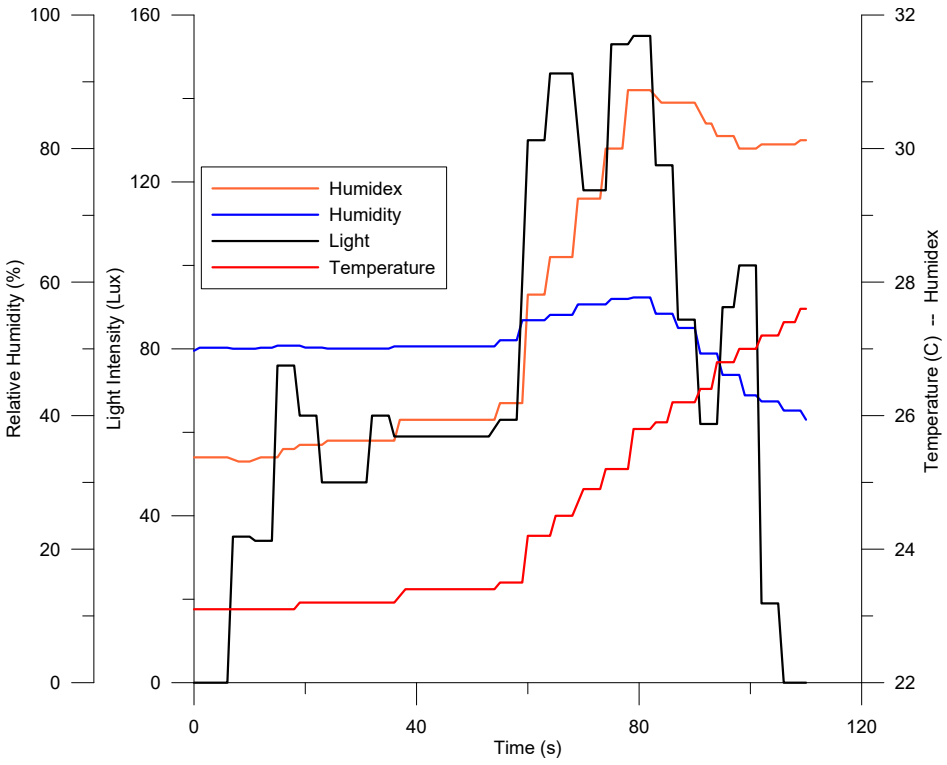


Figure C.20: Test 09 THLP 04

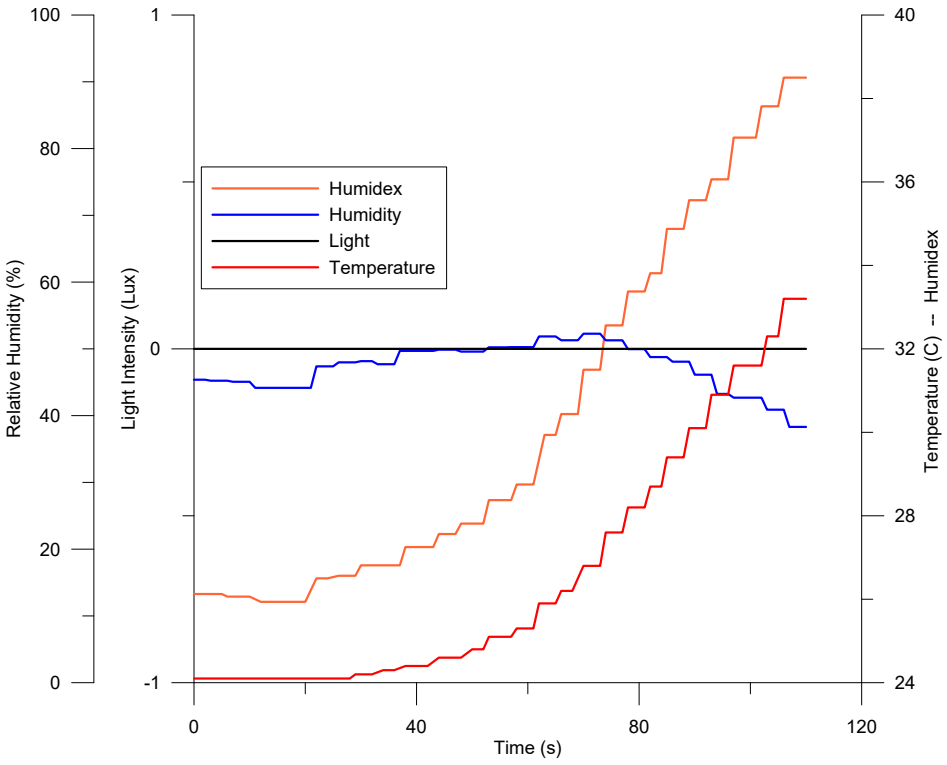


Figure C.21: Test 09 THLP 05

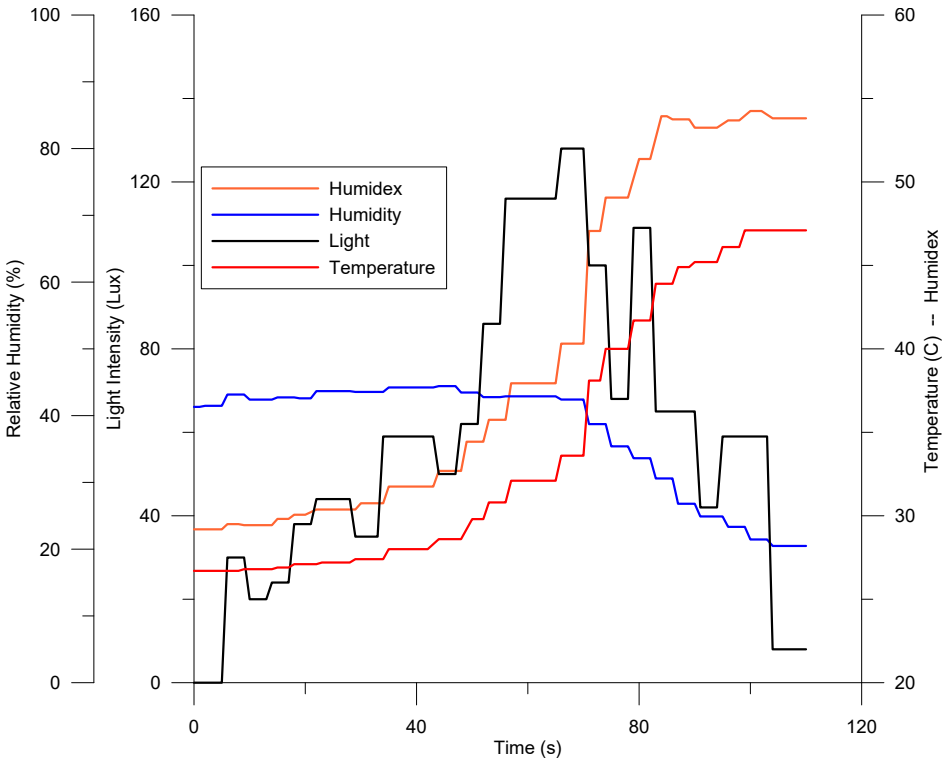


Figure C.22: Test 09 THLP 07

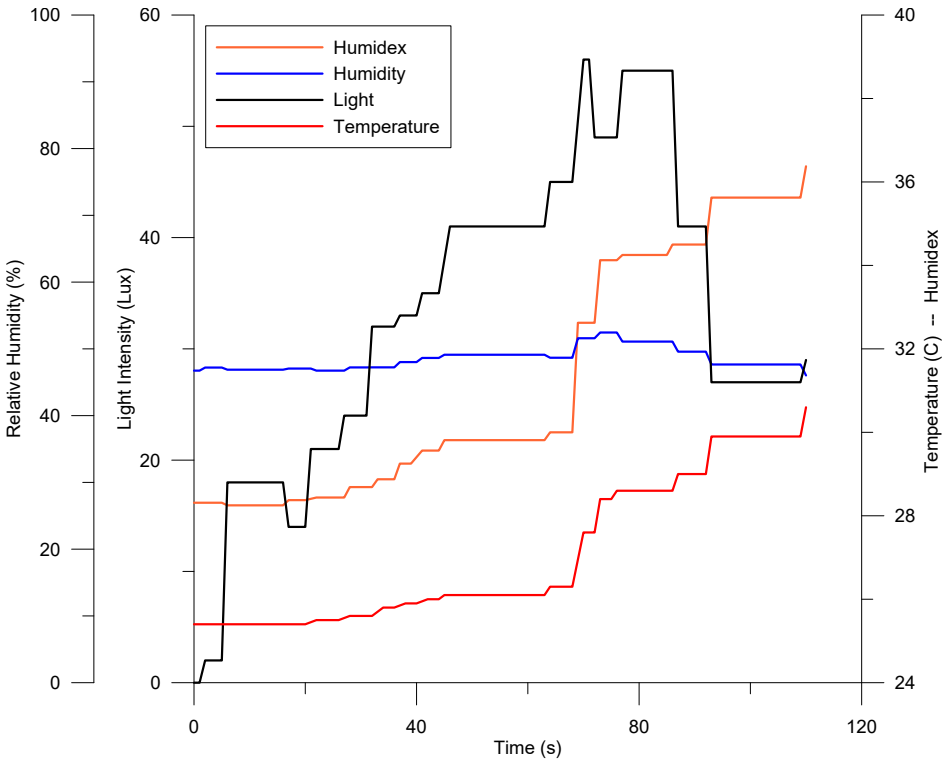


Figure C.23: Test 09 THLP 08

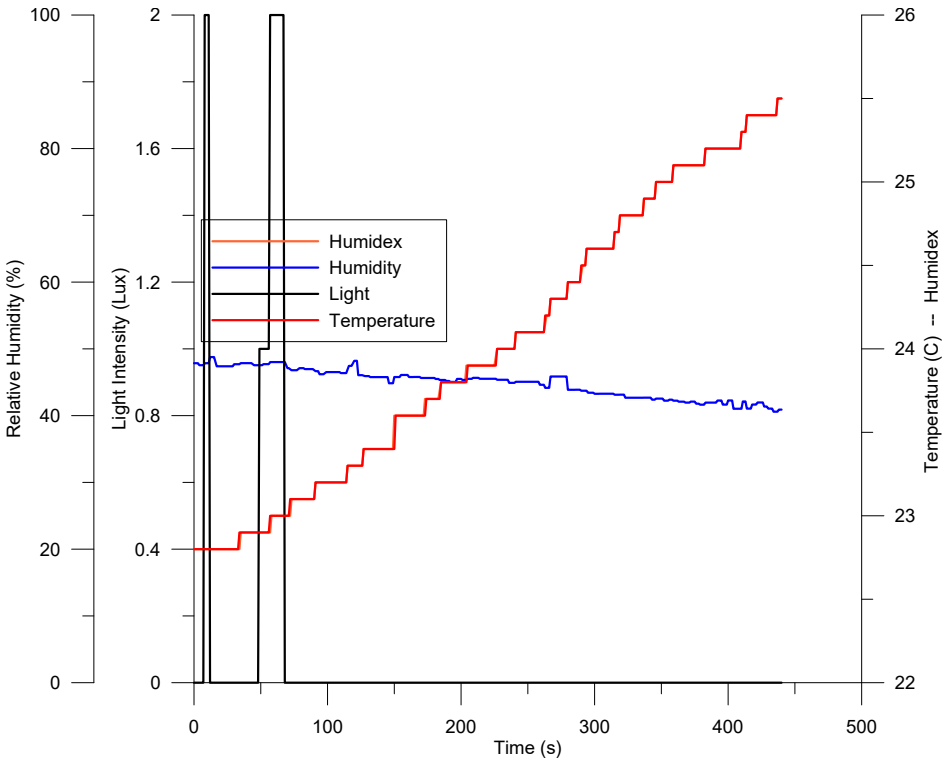


Figure C.24: Test 10 THLP 03

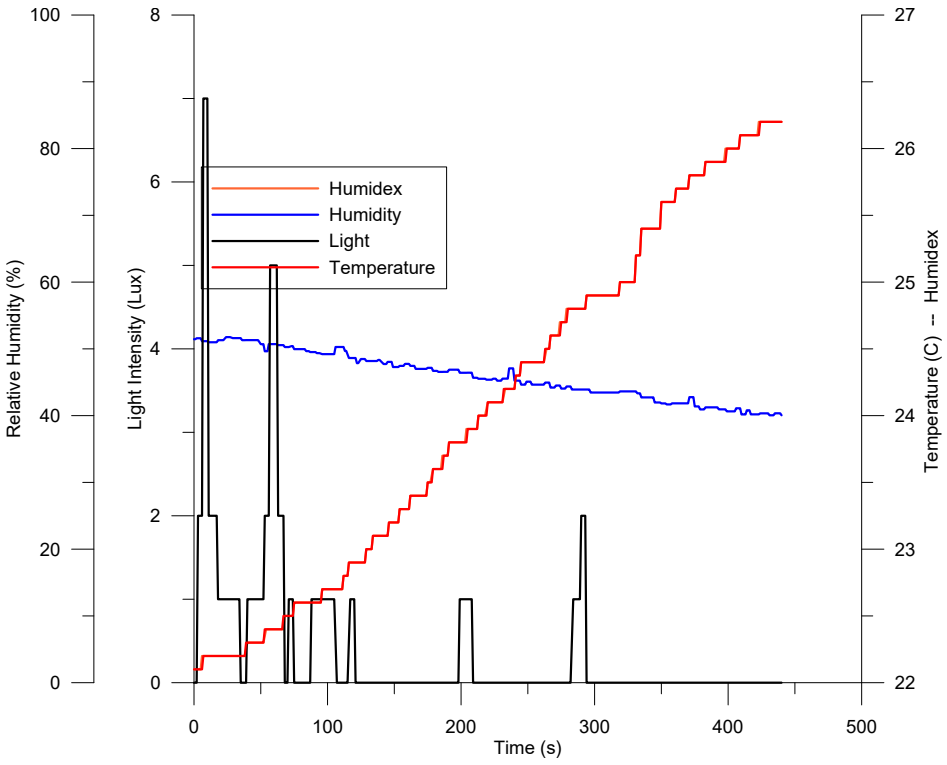


Figure C.25: Test 10 THLP 04

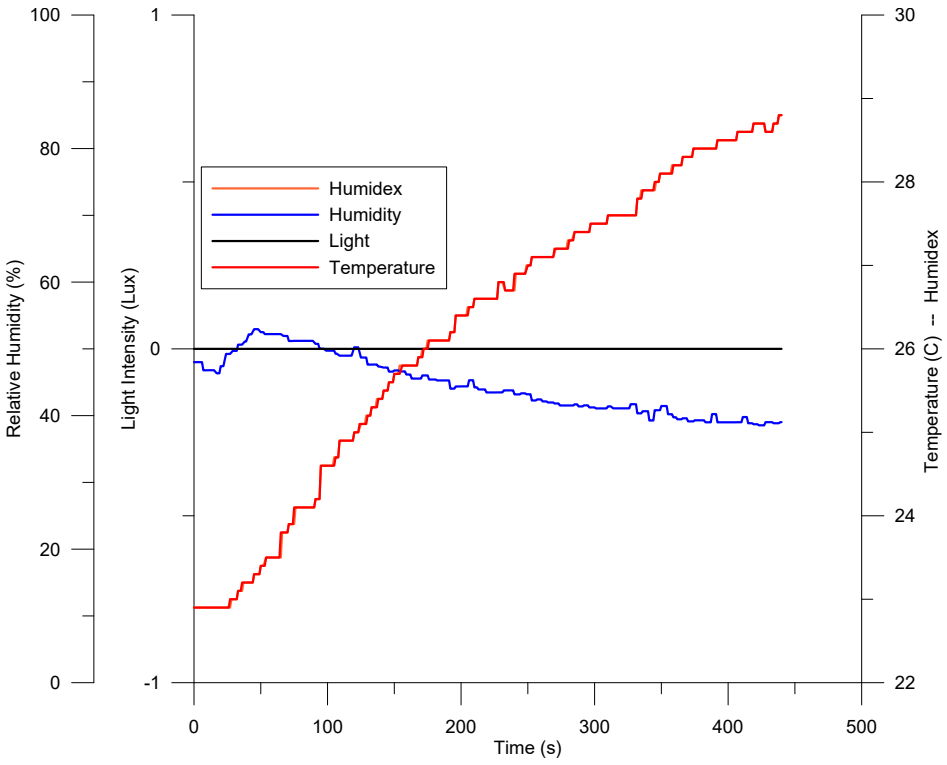


Figure C.26: Test 10 THLP 05

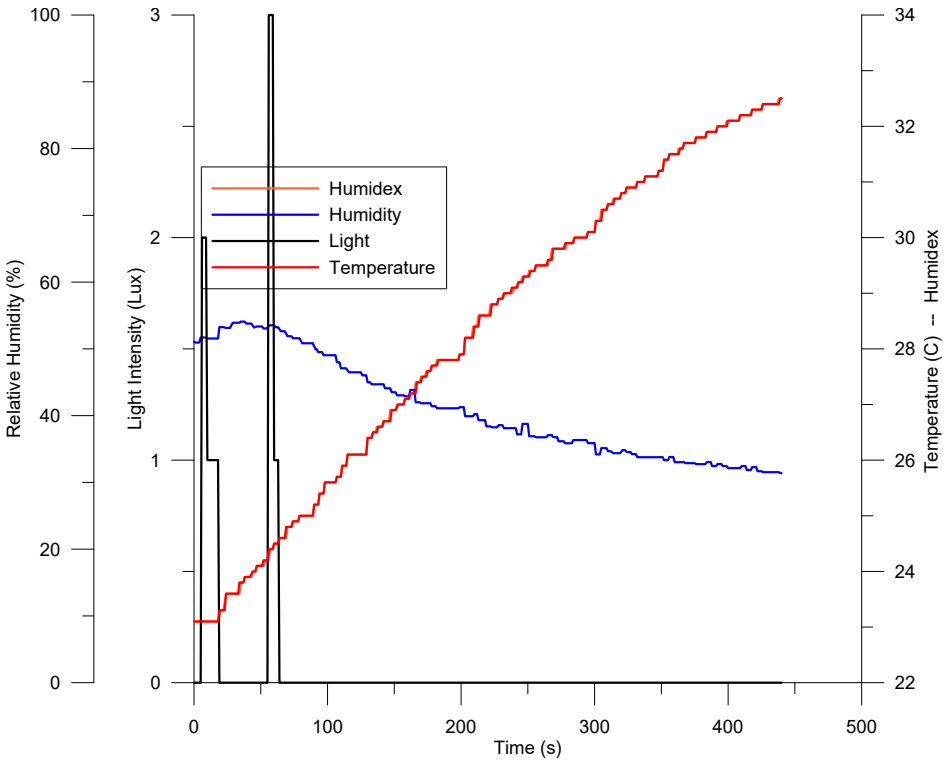


Figure C.27: Test 10 THLP 07

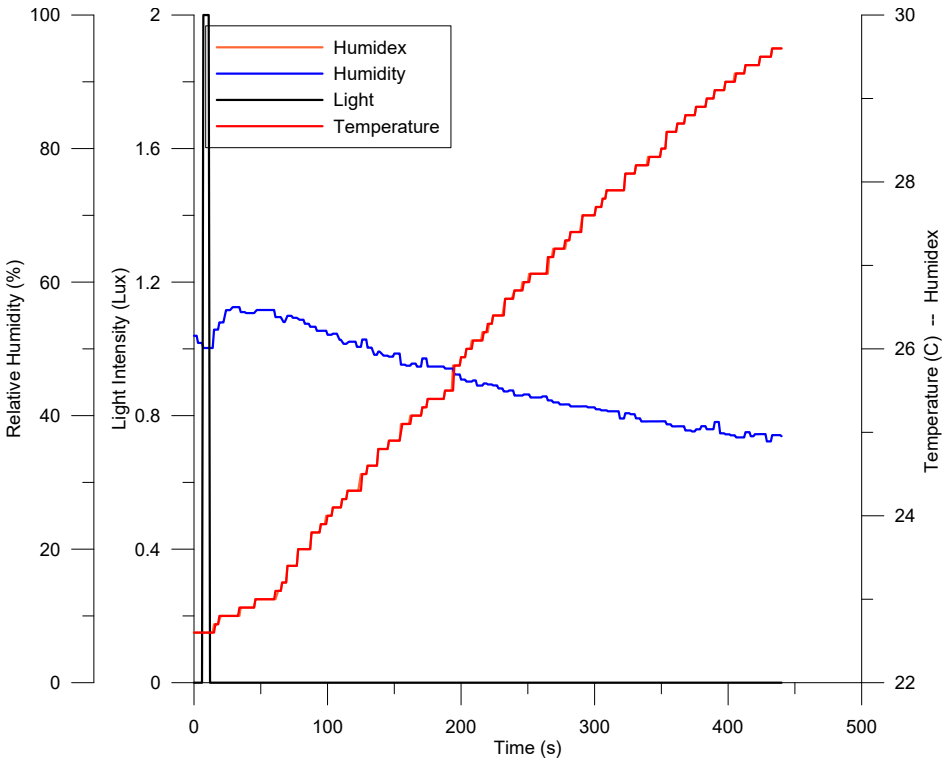


Figure C.28: Test 10 THLP 08

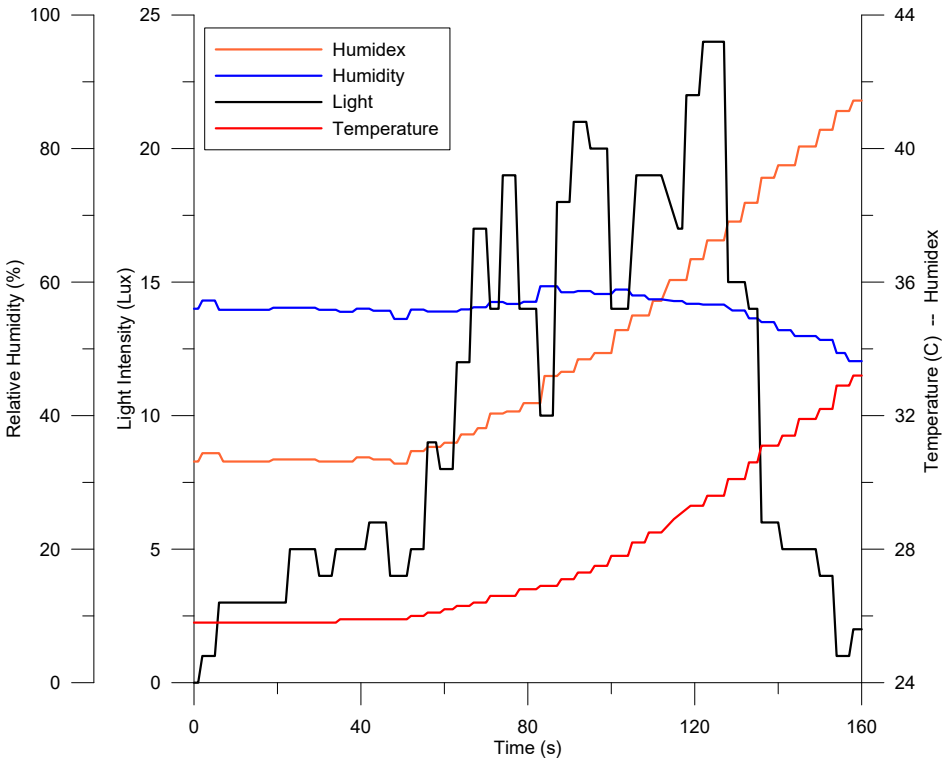


Figure C.29: Test 11 THLP 03

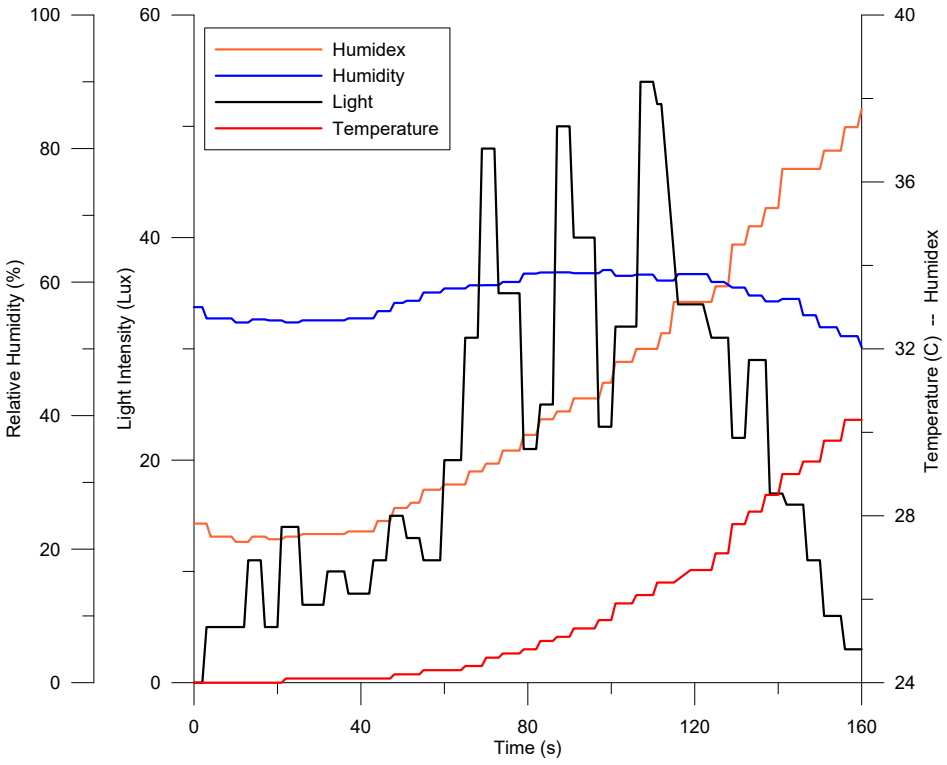


Figure C.30: Test 11 THLP 04

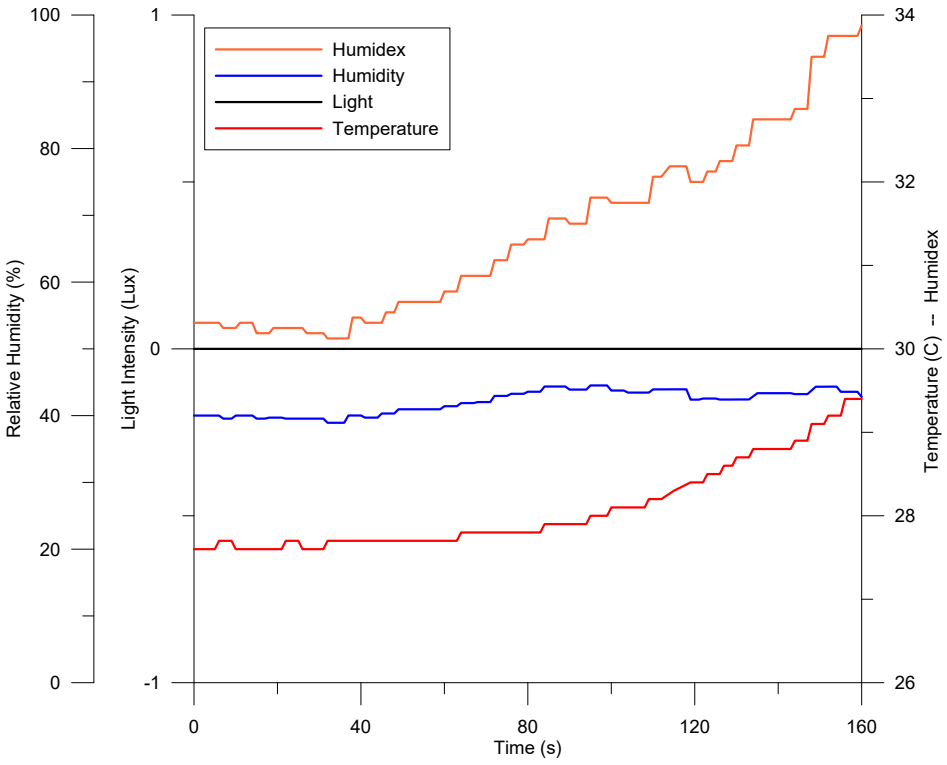


Figure C.31: Test 11 THLP 05

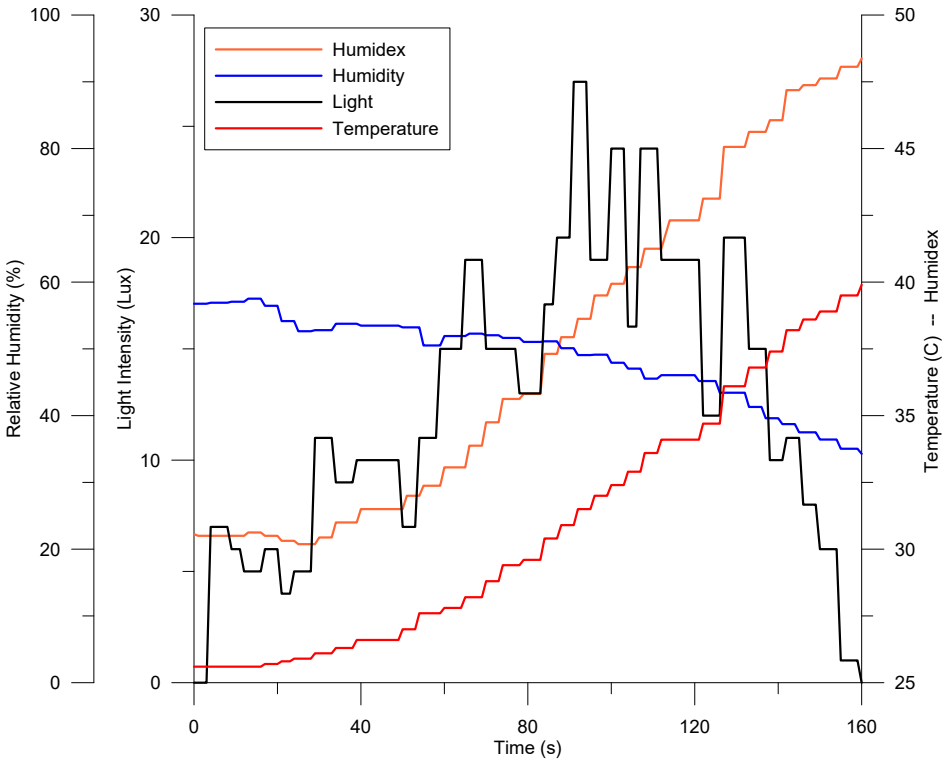


Figure C.32: Test 11 THLP 07

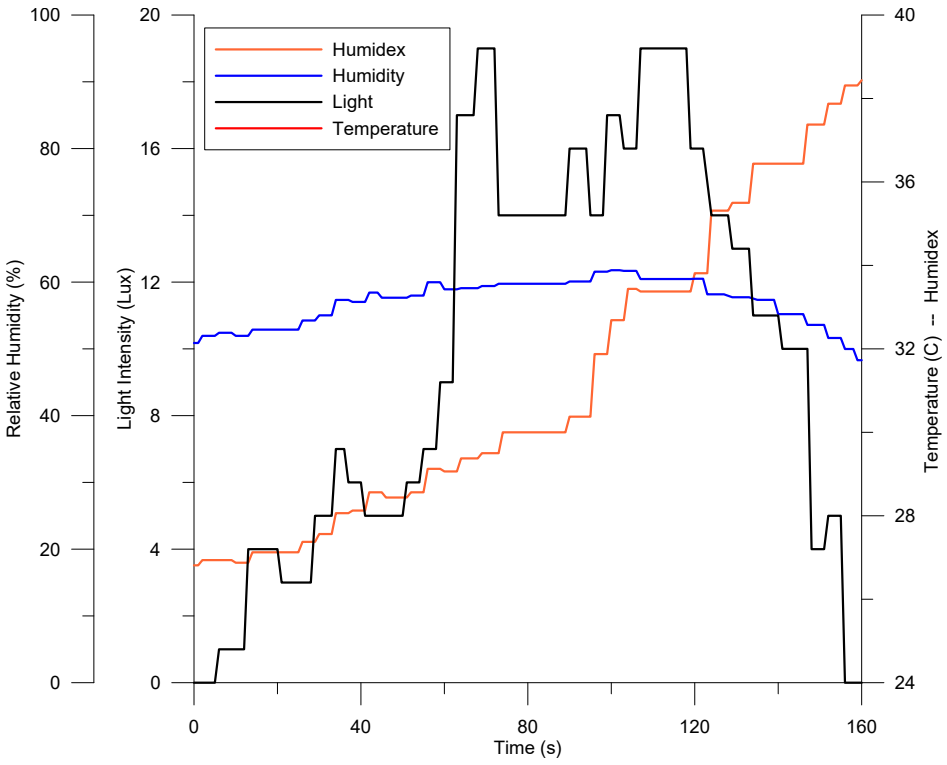


Figure C.33: Test 11 THLP 08

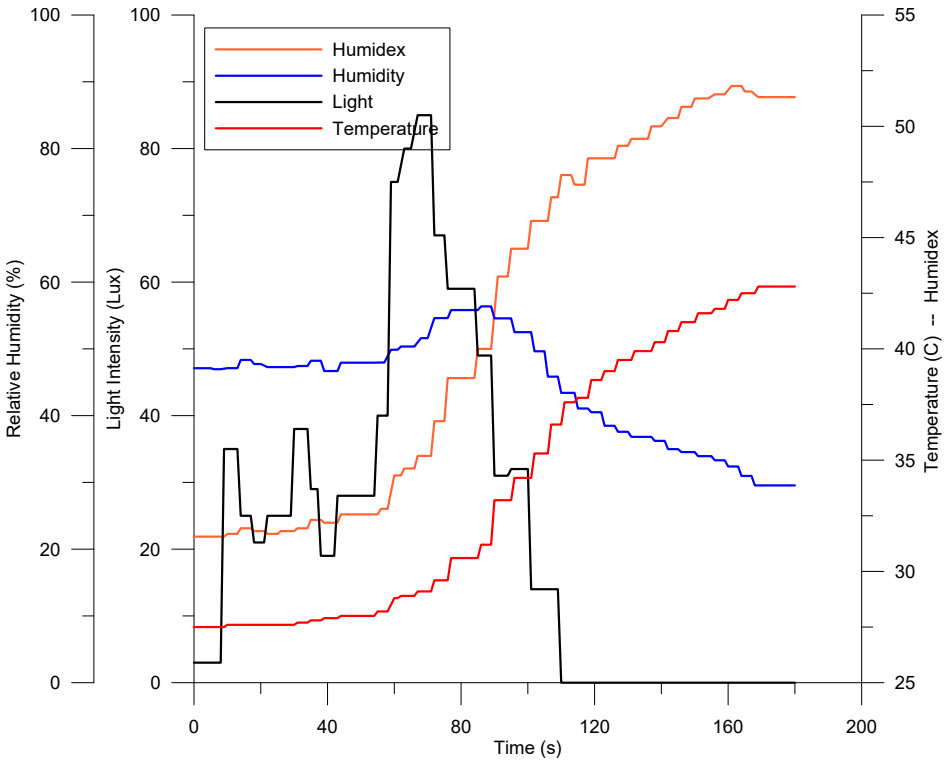


Figure C.34: Test 12 THLP 03

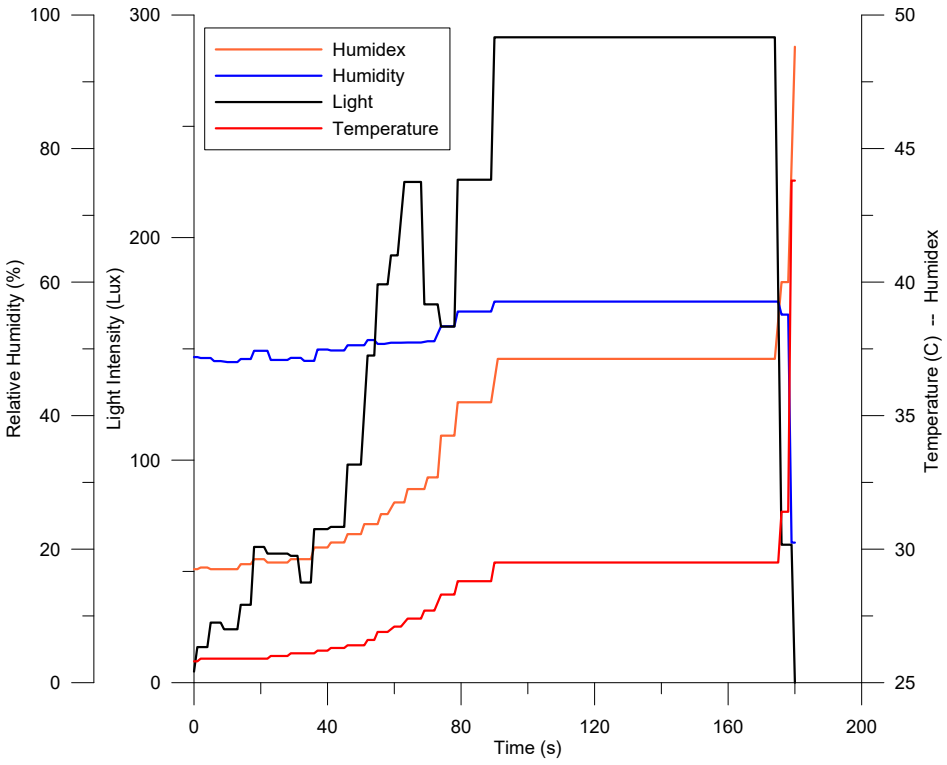


Figure C.35: Test 12 THLP 04

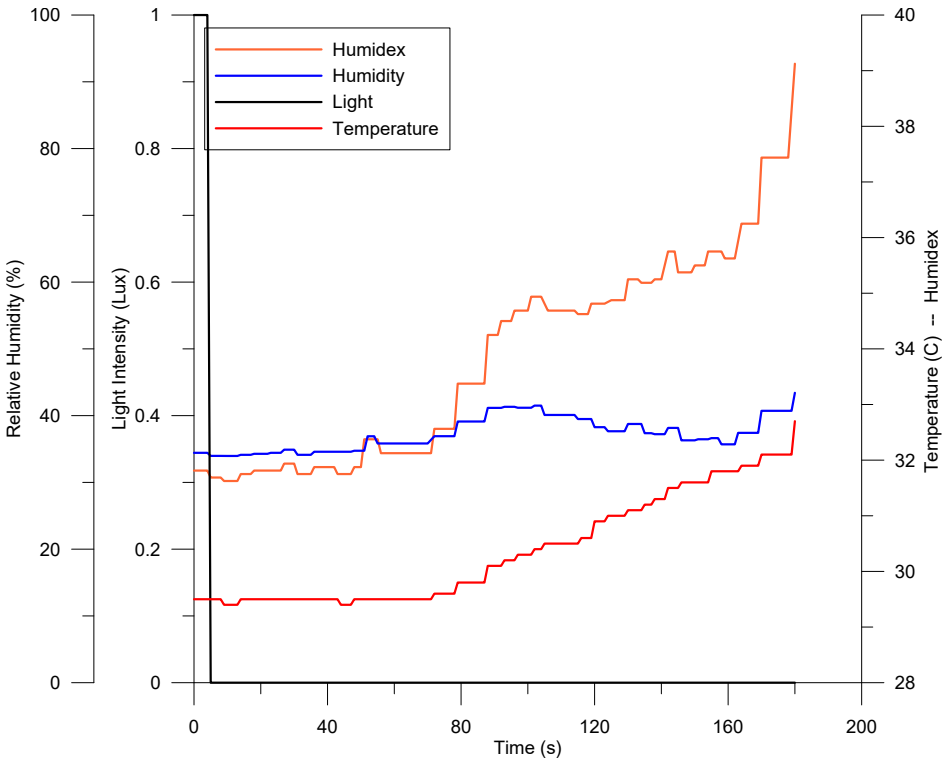


Figure C.36: Test 12 THLP 05

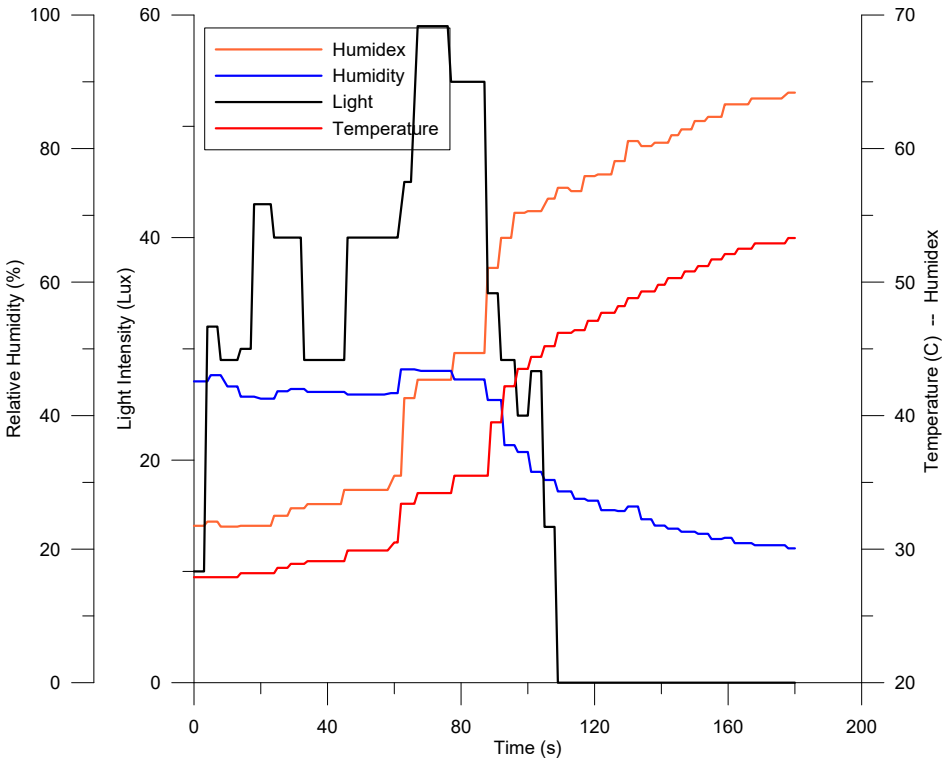


Figure C.37: Test 12 THLP 07

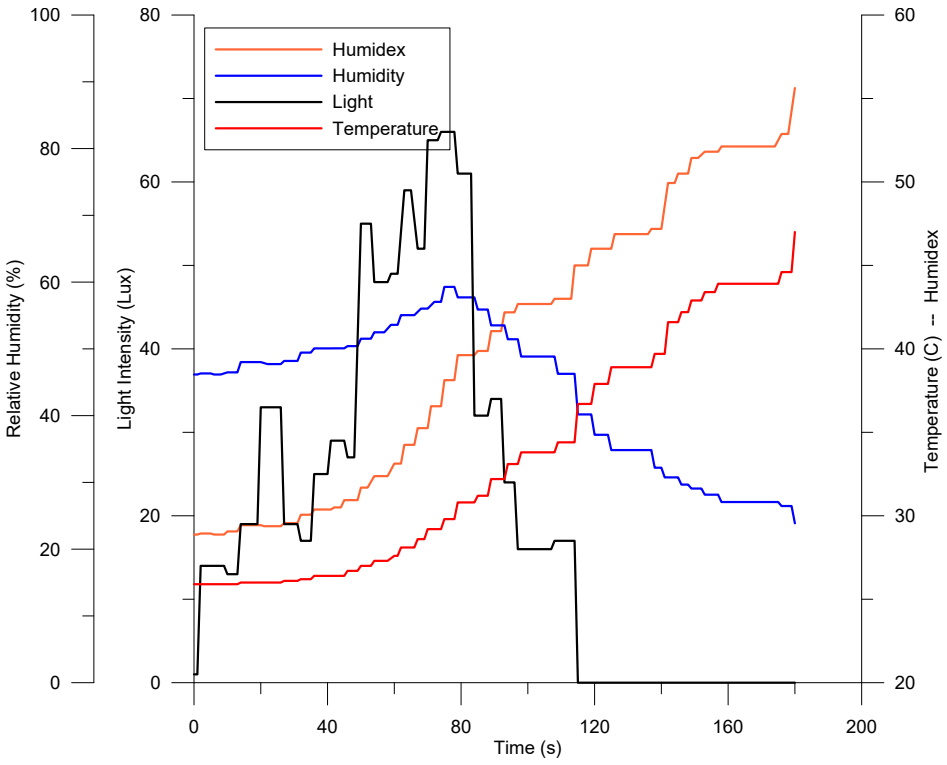


Figure C.38: Test 12 THLP 08

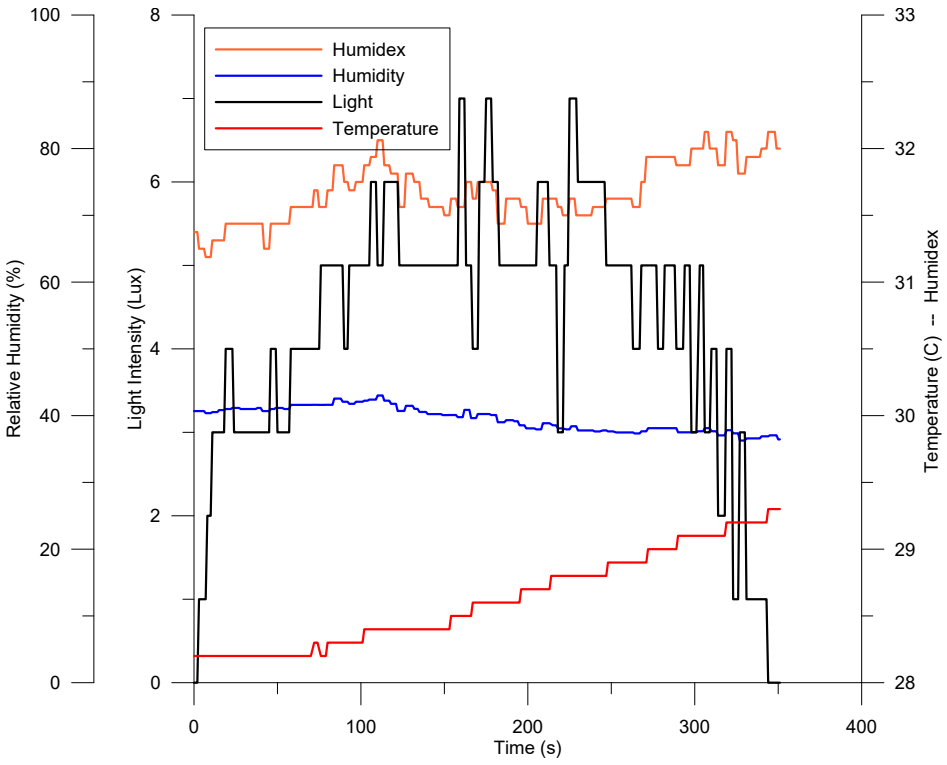


Figure C.39: Test 13 THLP 03

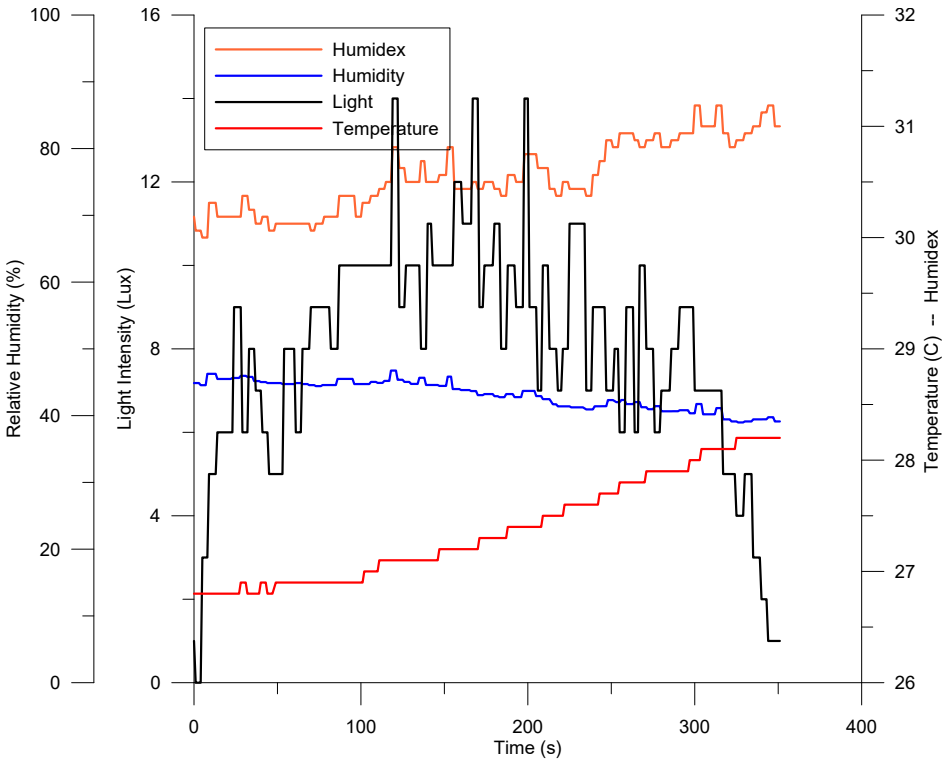


Figure C.40: Test 13 THLP 04

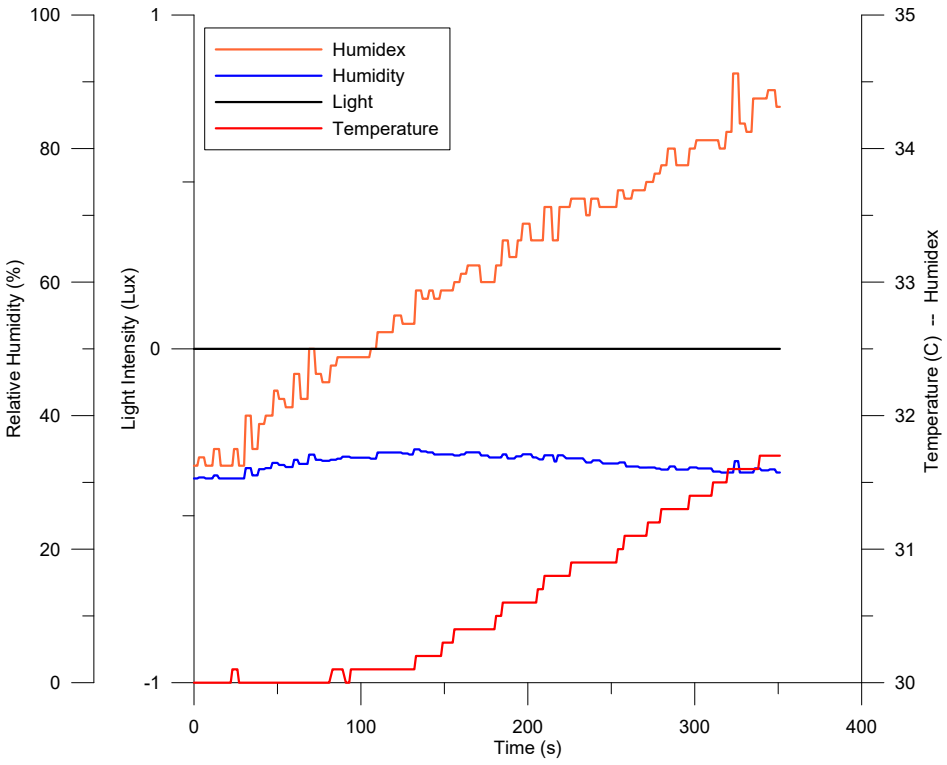


Figure C.41: Test 13 THLP 05

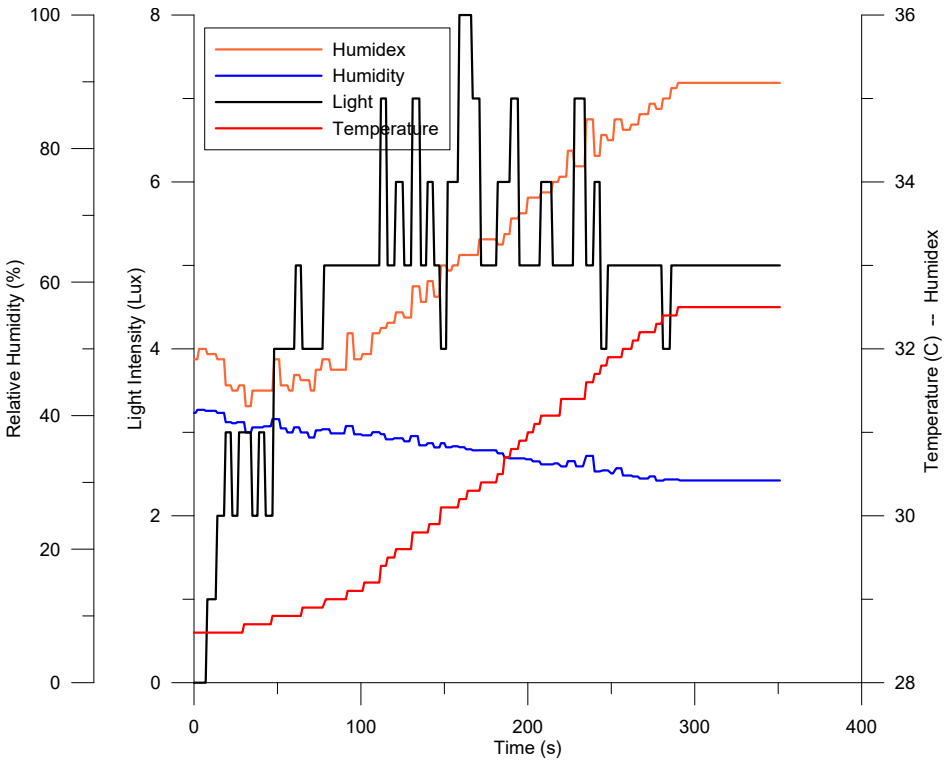


Figure C.42: Test 13 THLP 07

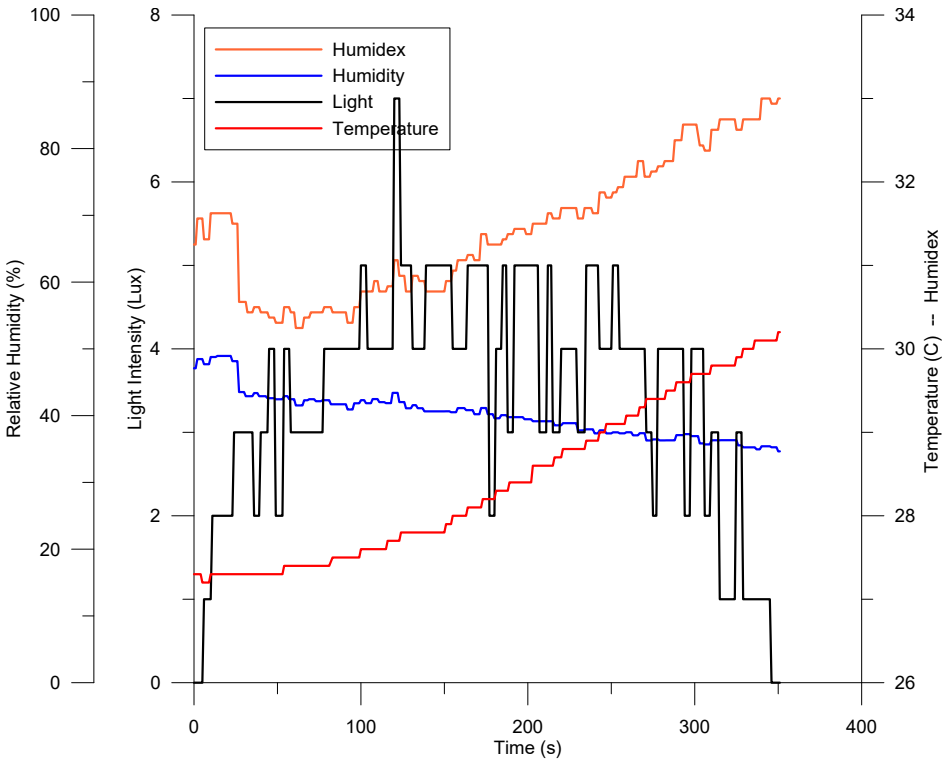


Figure C.43: Test 13 THLP 08

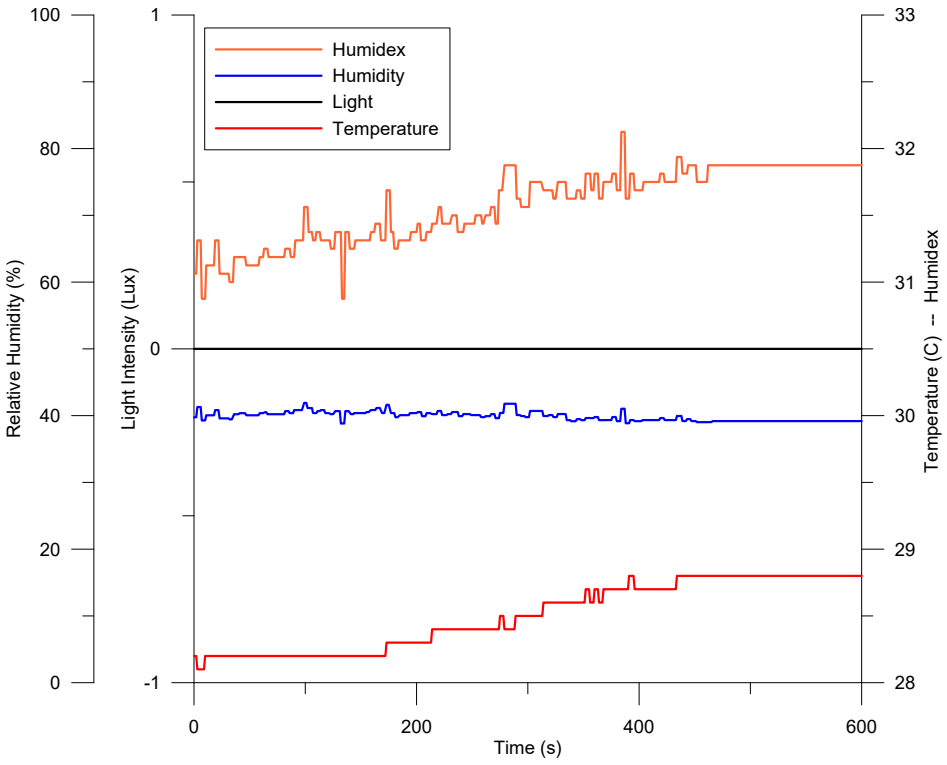


Figure C.44: Test 14 THLP 03

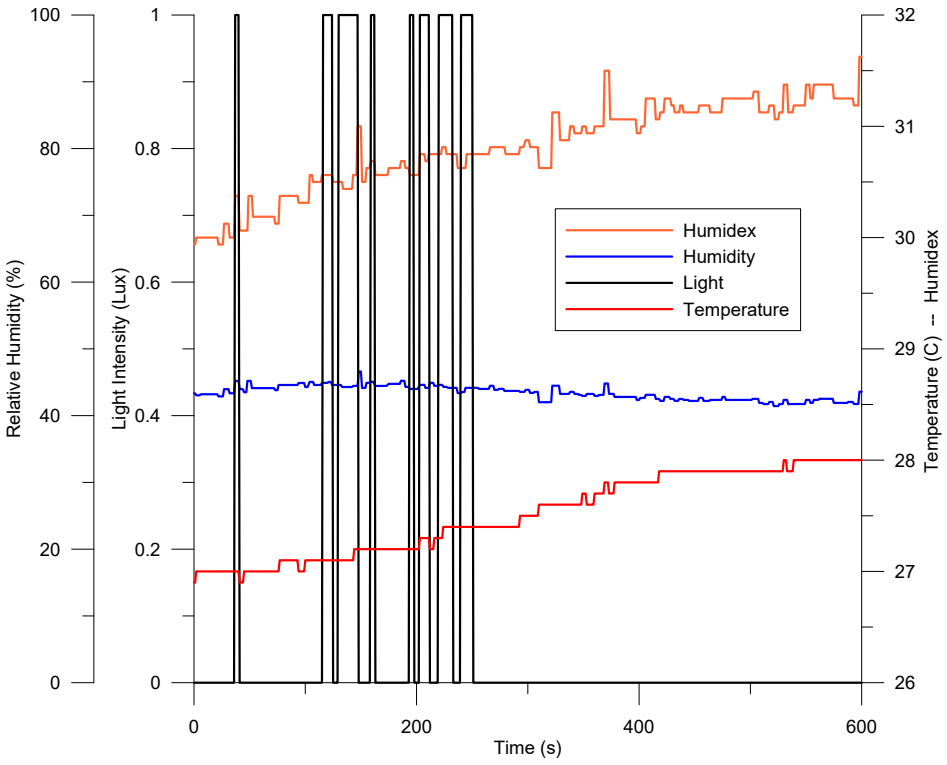


Figure C.45: Test 14 THLP 04

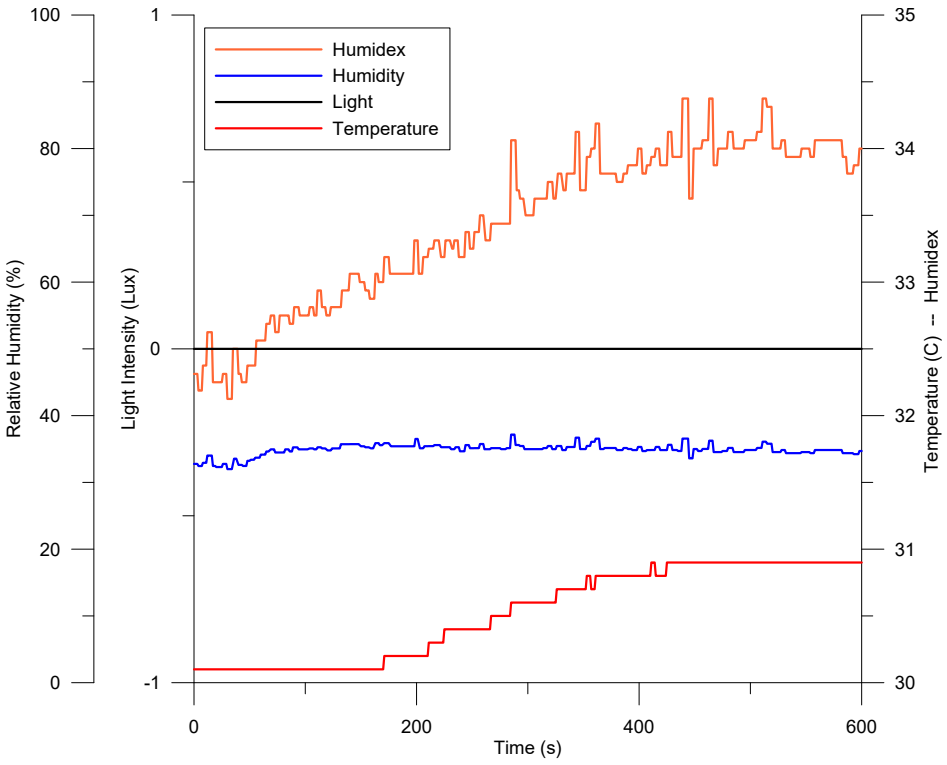


Figure C.46: Test 14 THLP 05

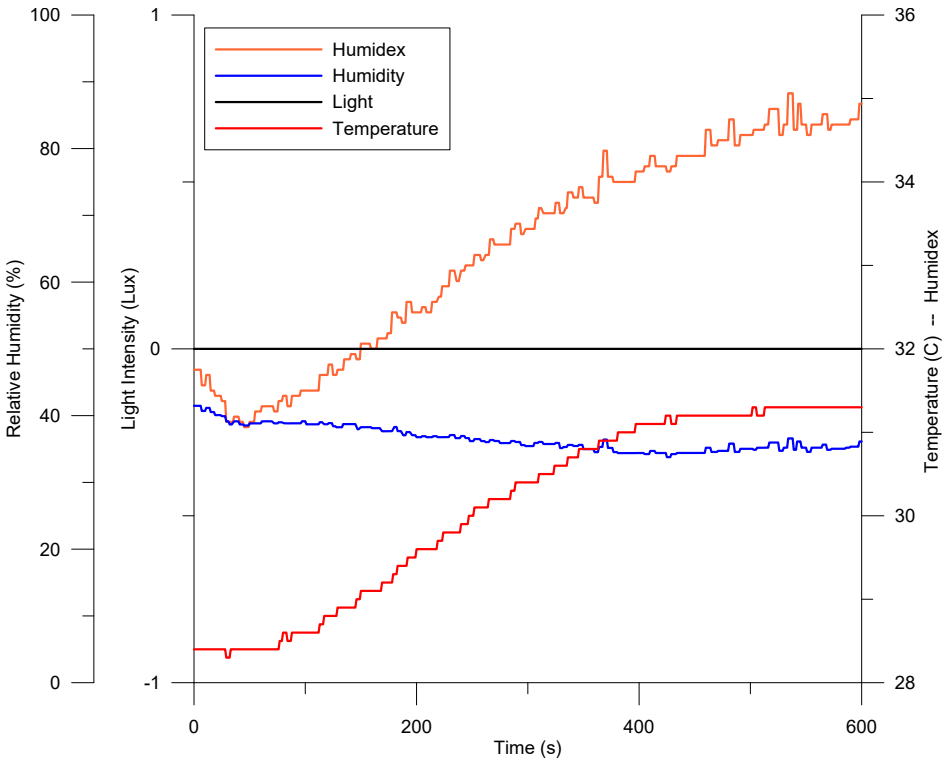


Figure C.47: Test 14 THLP 07

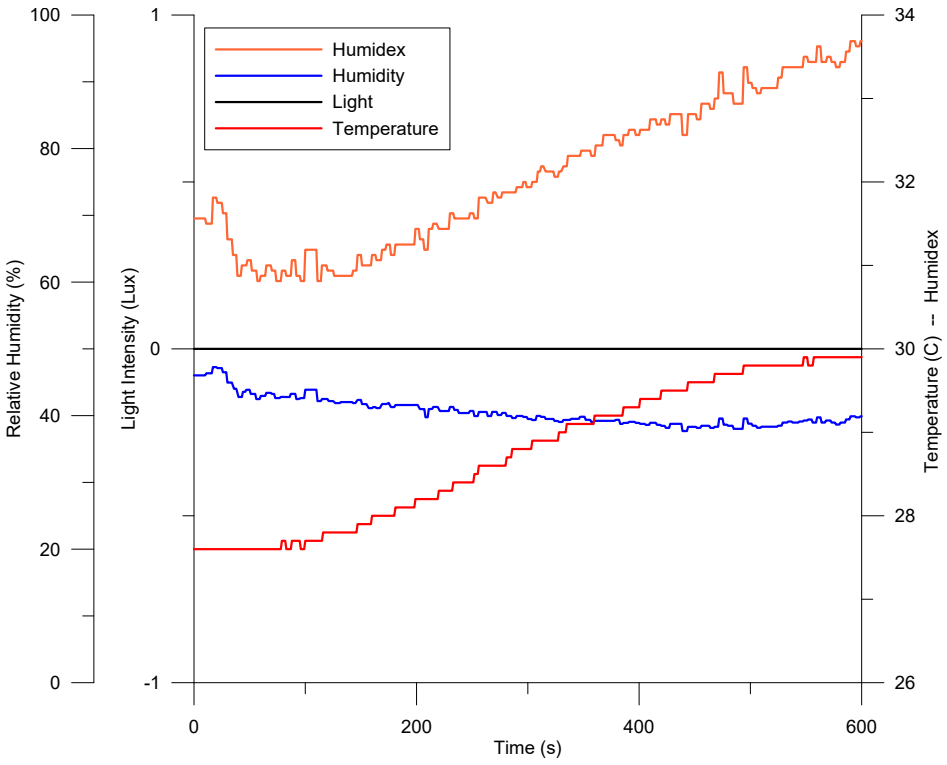


Figure C.48: Test 14 THLP 08

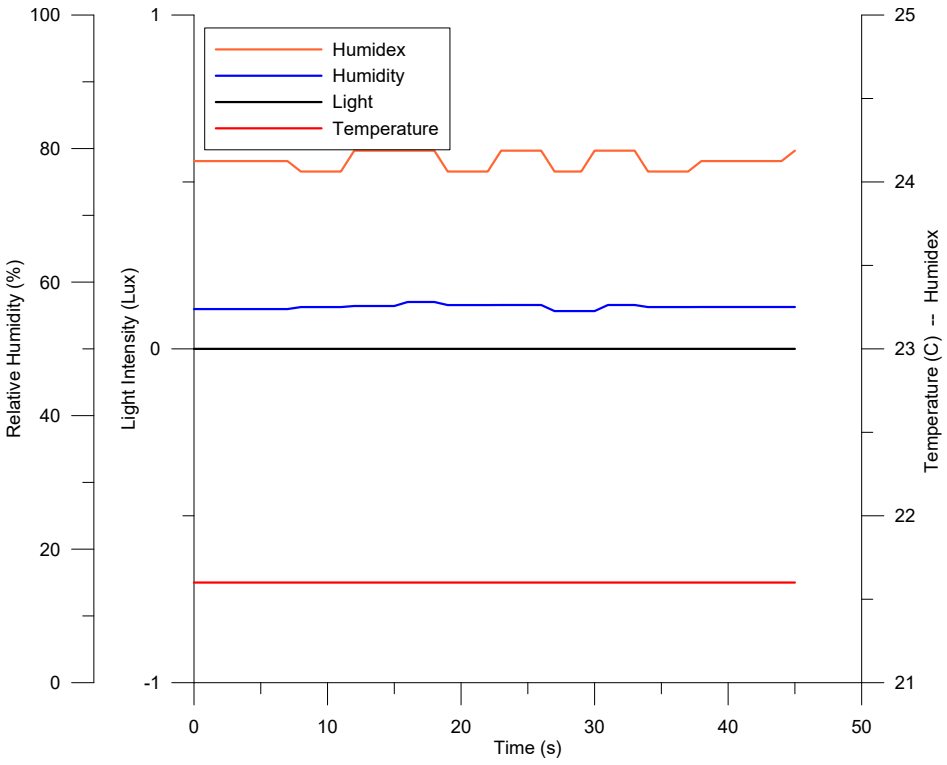


Figure C.49: Test 15 THLP 03

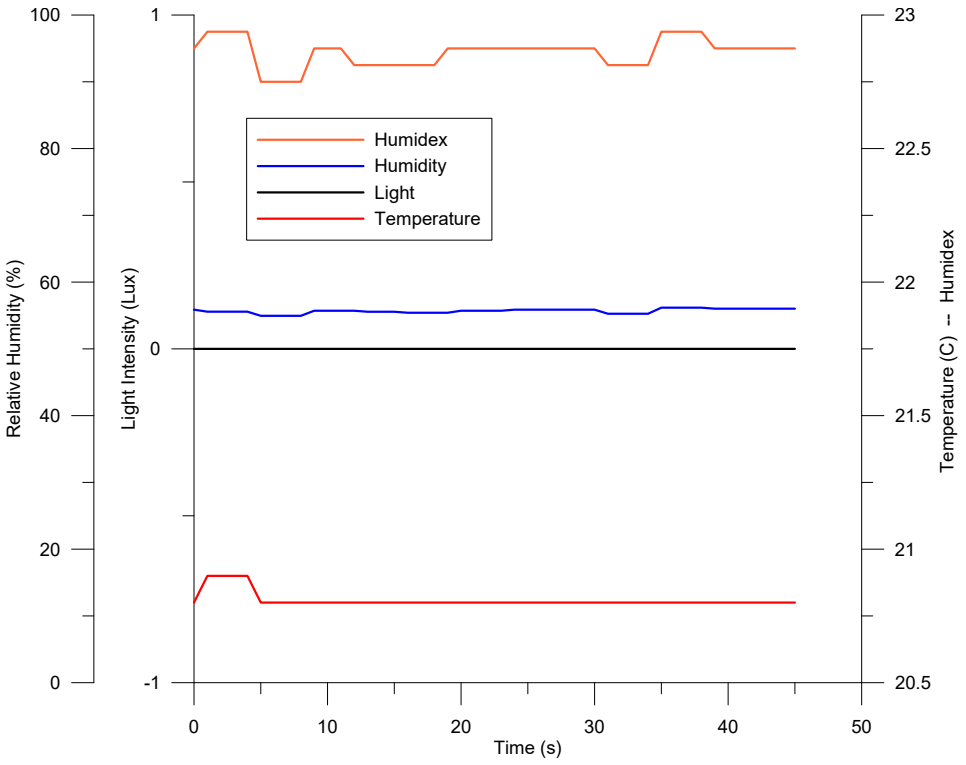


Figure C.50: Test 15 THLP 04

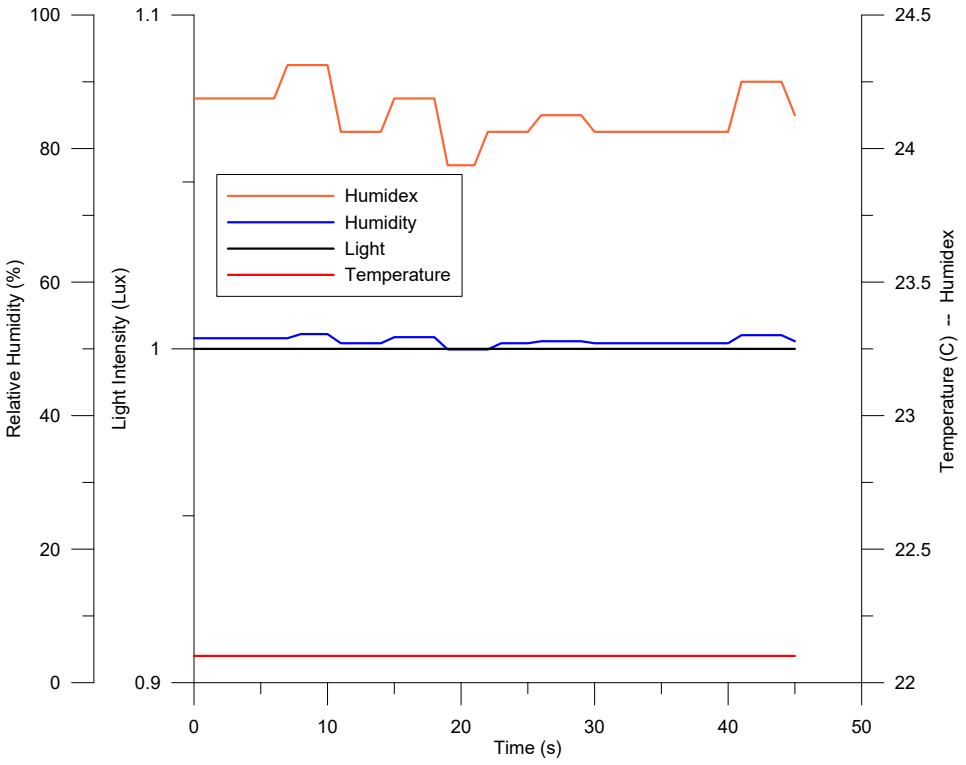


Figure C.51: Test 15 THLP 05

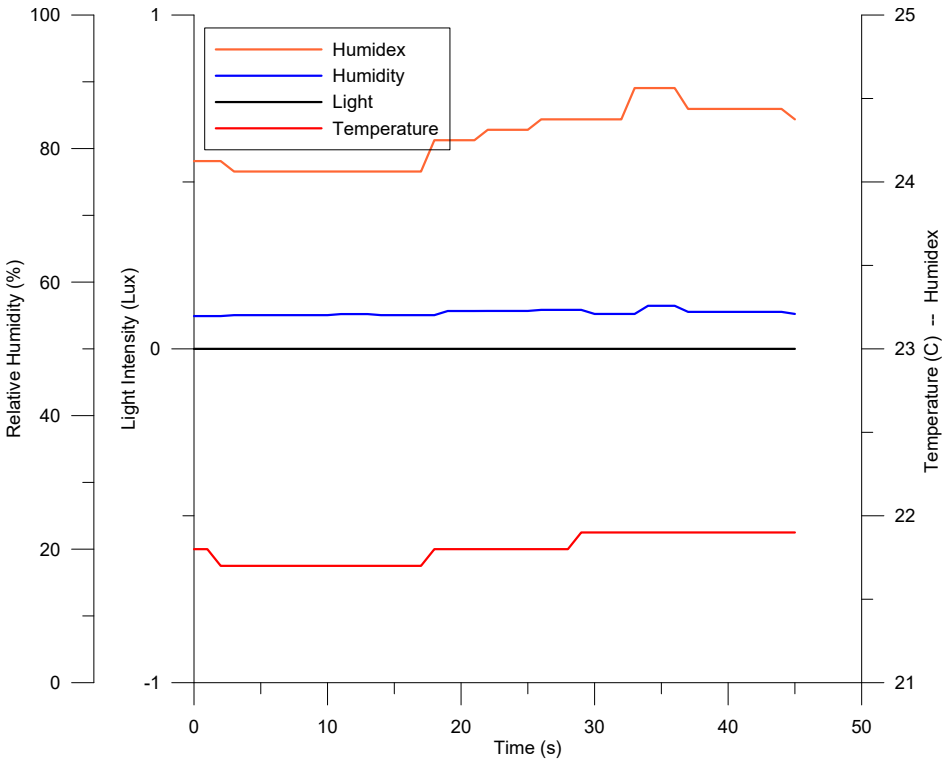


Figure C.52: Test 15 THLP 07

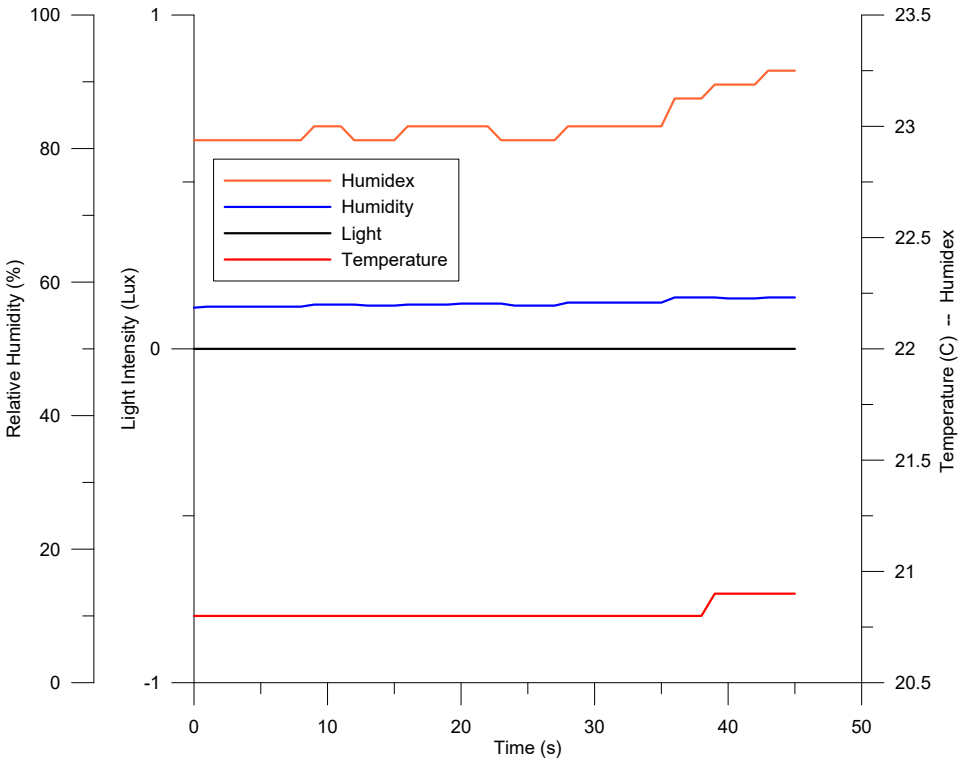


Figure C.53: Test 15 THLP 08

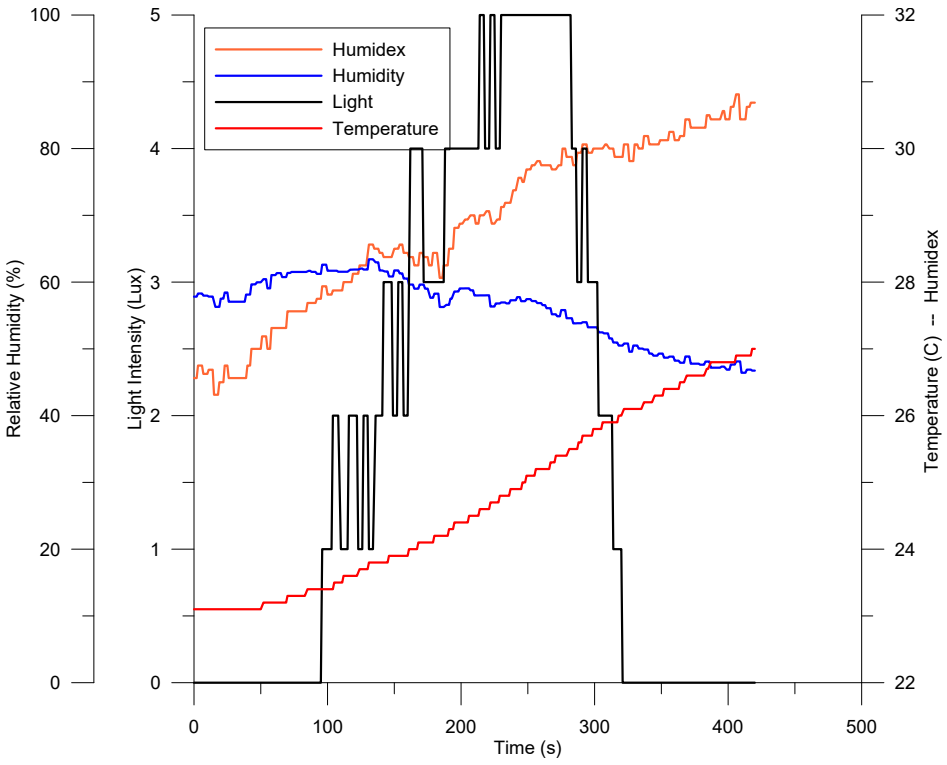


Figure C.54: Test 17 THLP 03

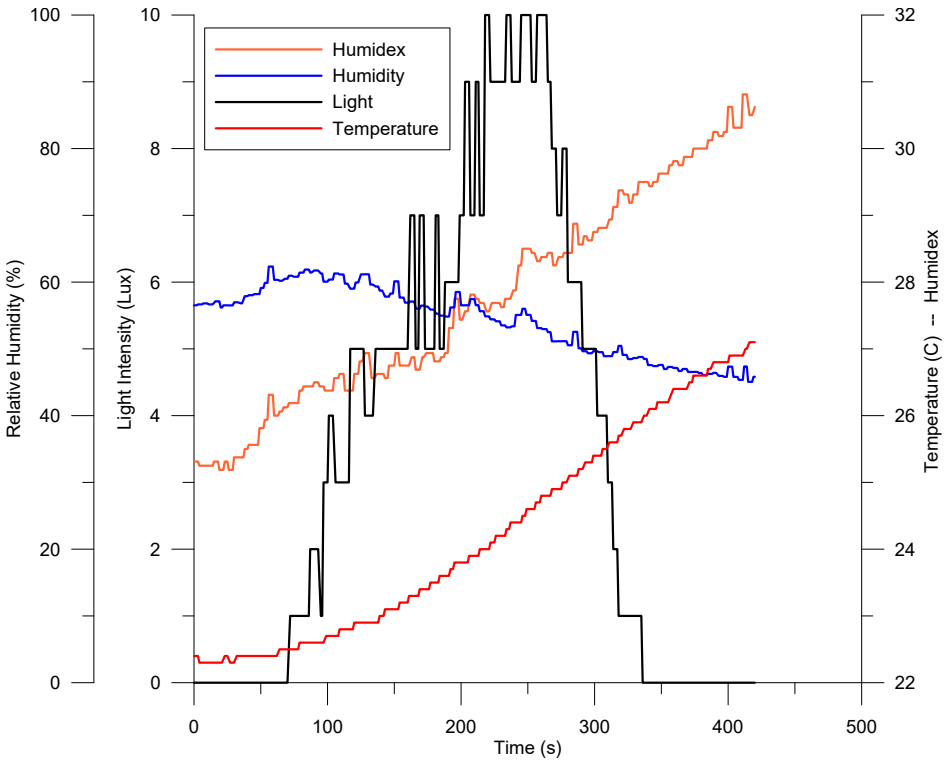


Figure C.55: Test 17 THLP 04

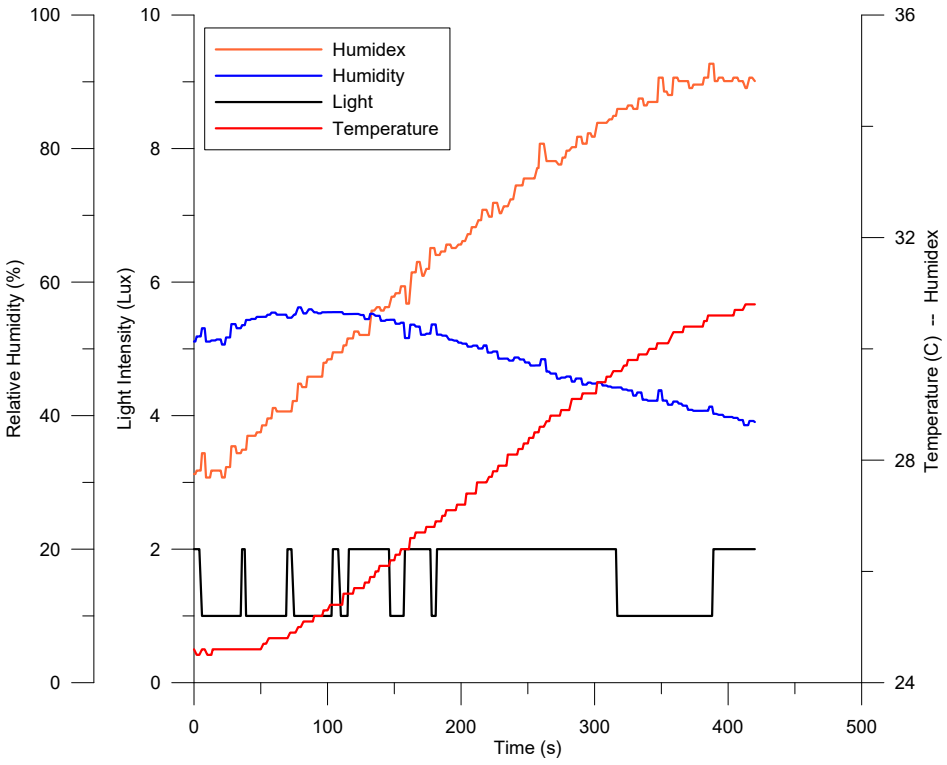


Figure C.56: Test 17 THLP 05

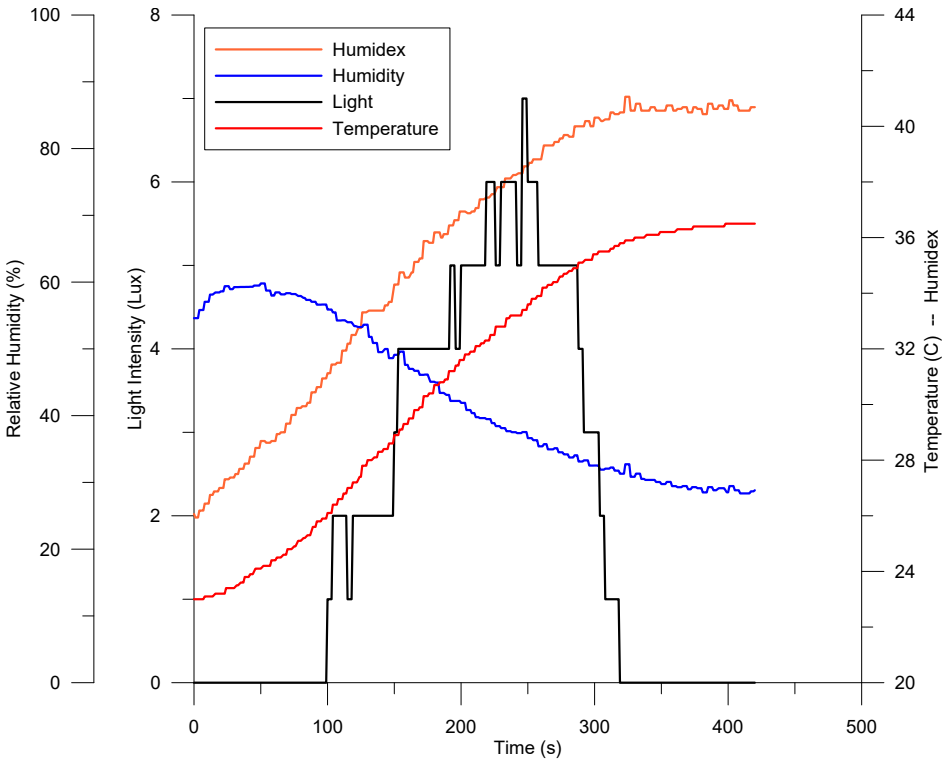


Figure C.57: Test 17 THLP 07

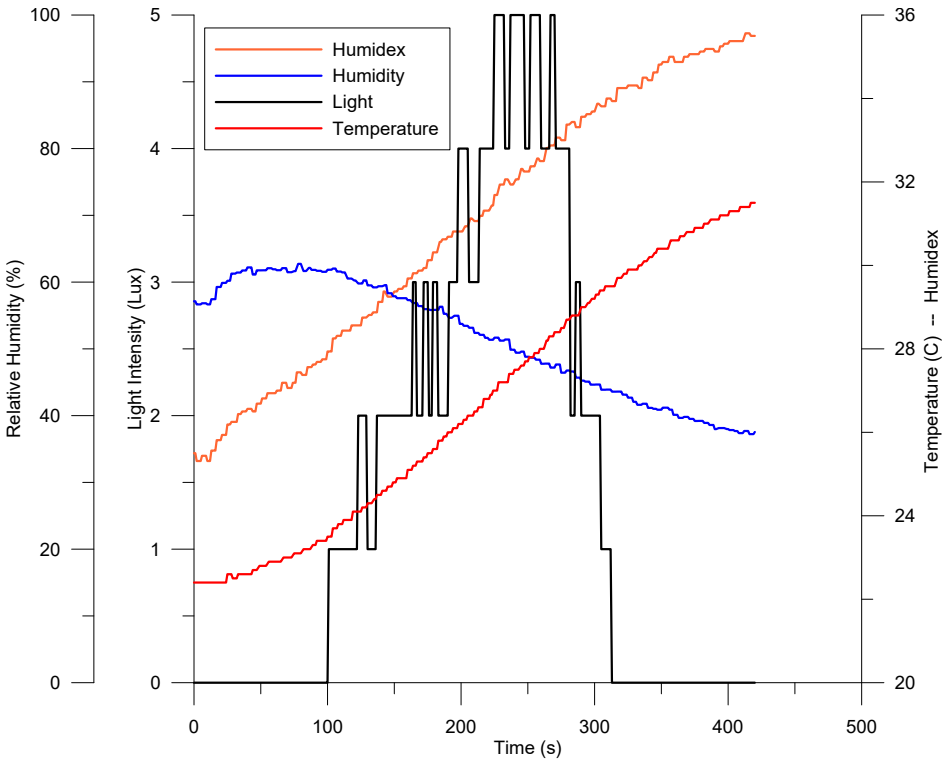


Figure C.58: Test 17 THLP 08

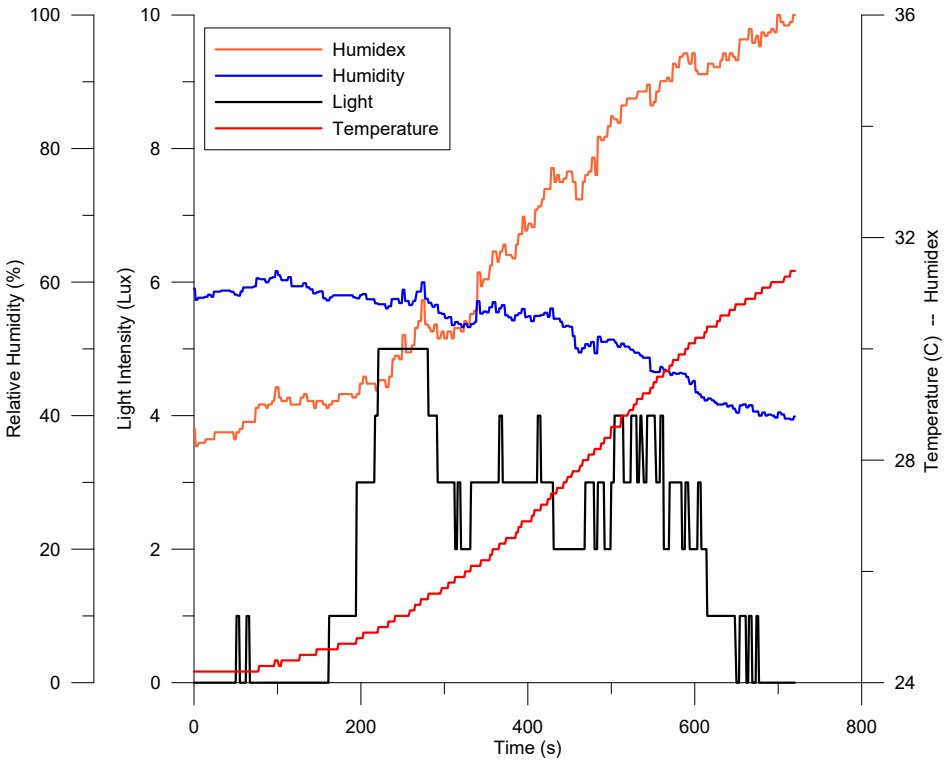


Figure C.59: Test 18 THLP 03

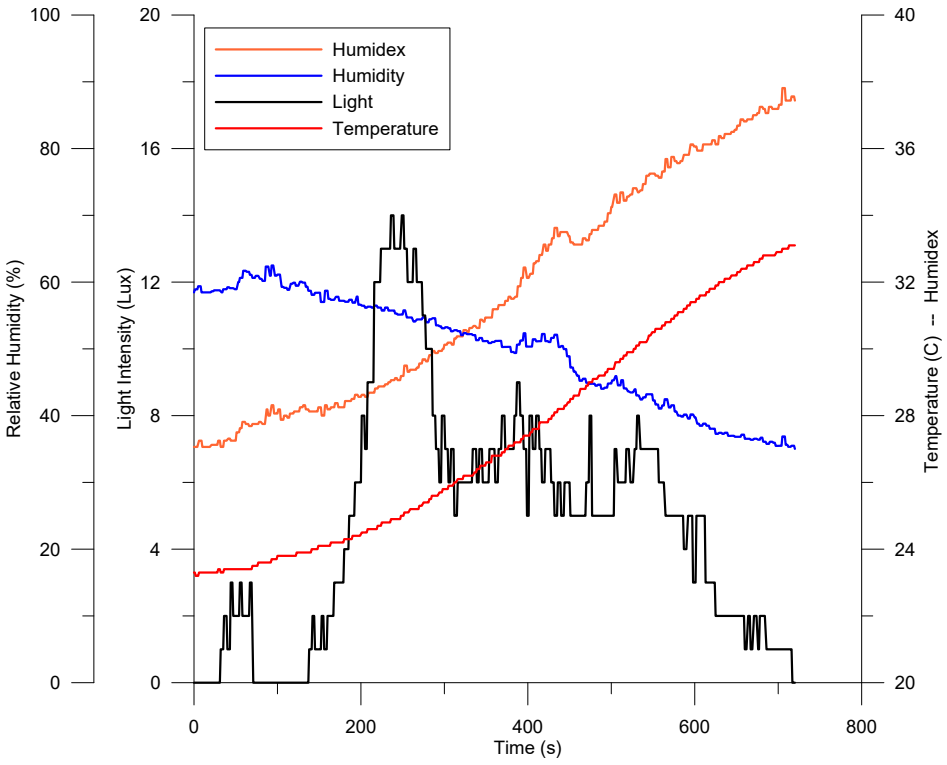


Figure C.60: Test 18 THLP 04

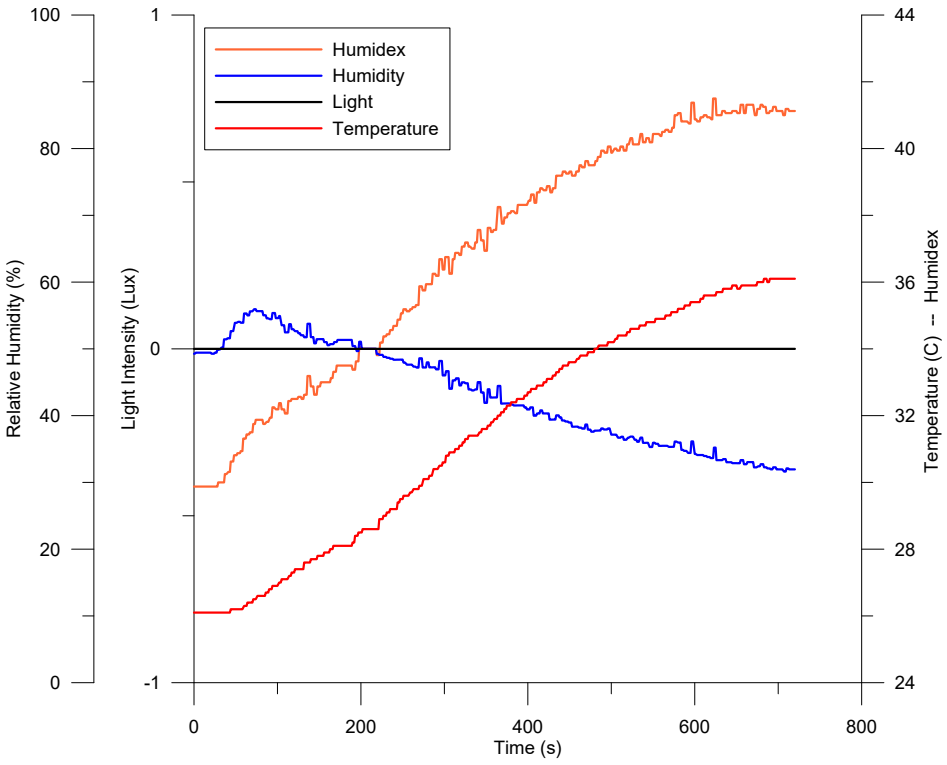


Figure C.61: Test 18 THLP 05

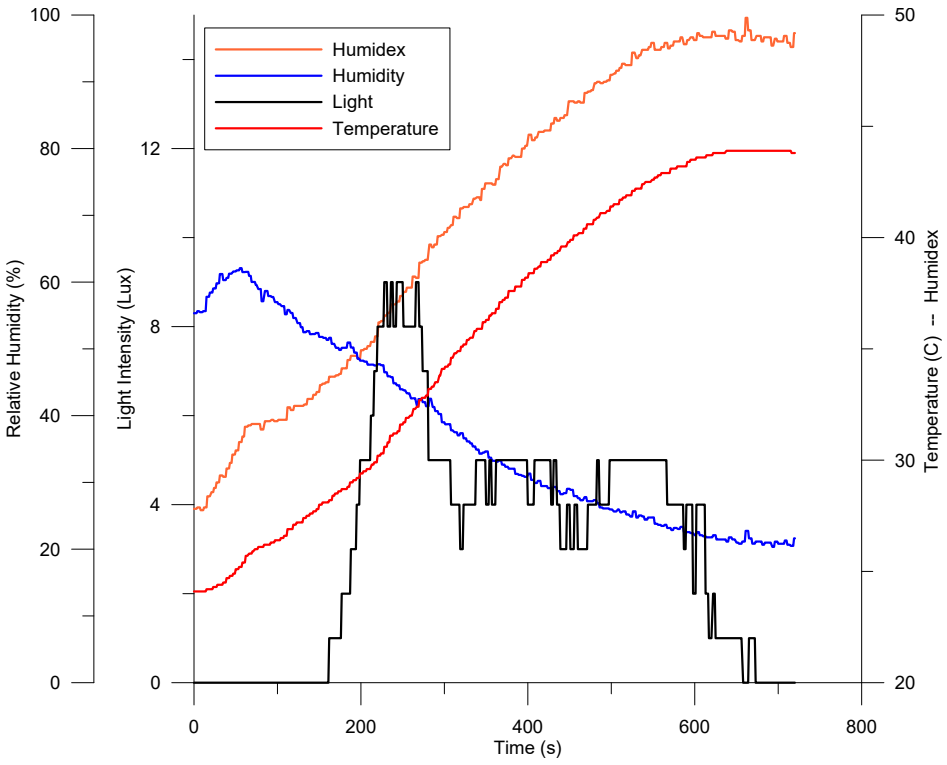


Figure C.62: Test 18 THLP 07

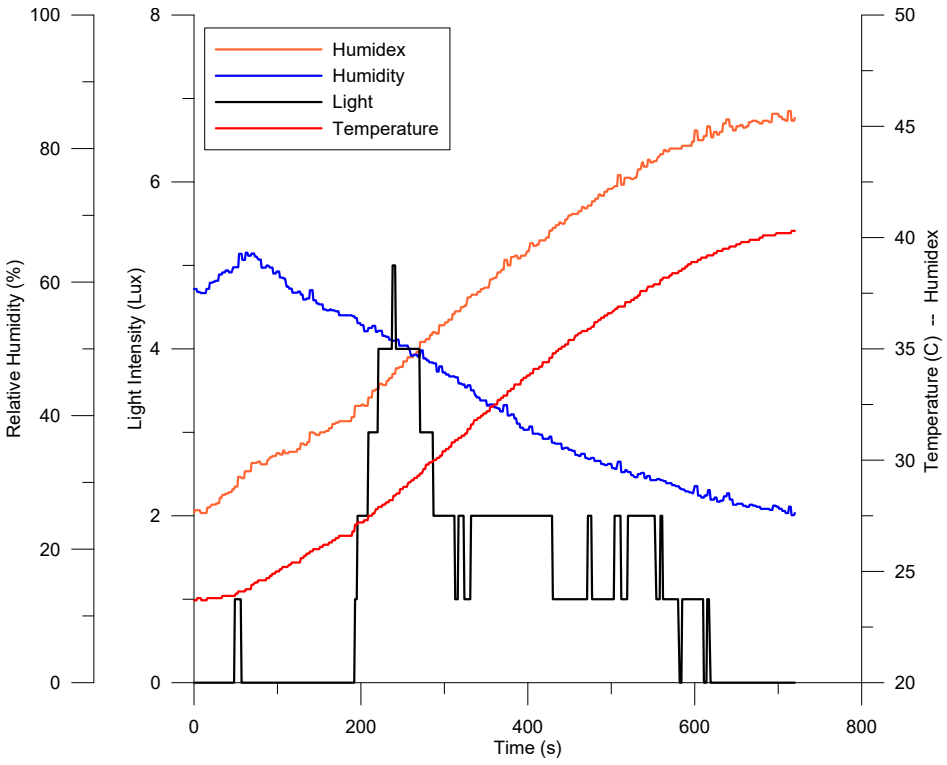


Figure C.63: Test 18 THLP 08

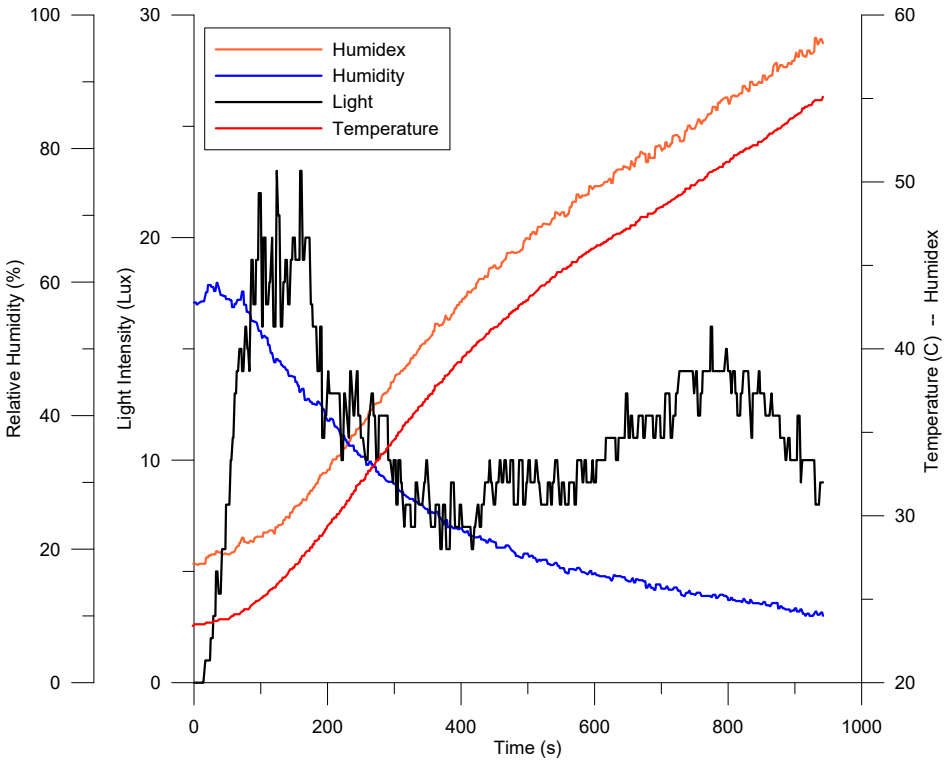


Figure C.64: Test 19 THLP 01

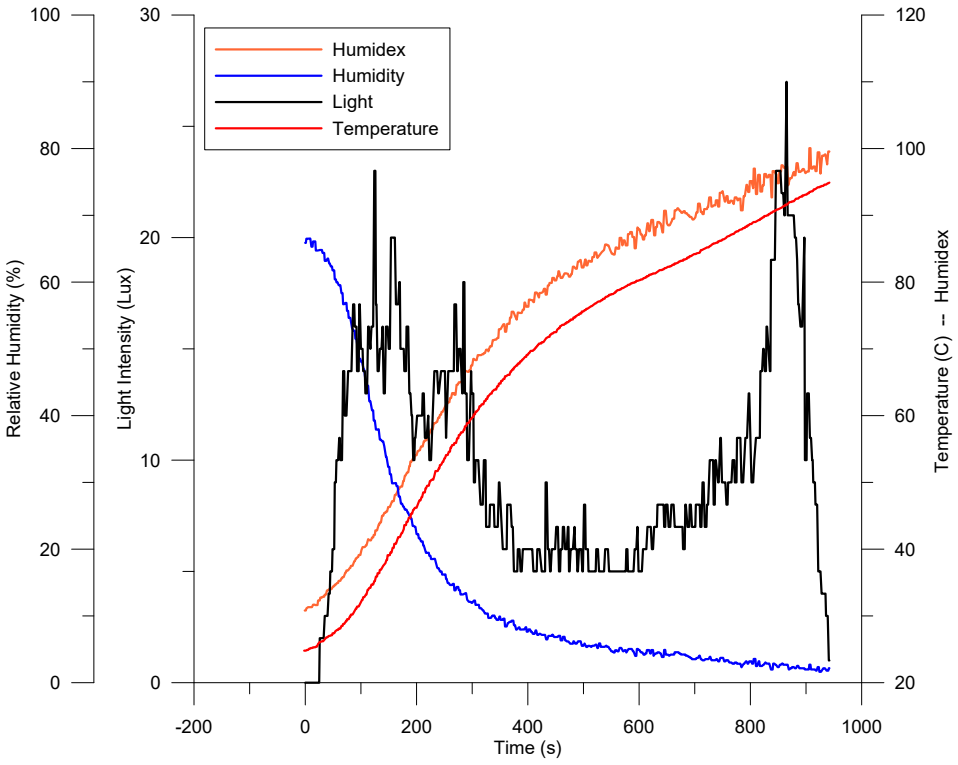


Figure C.65: Test 19 THLP 02

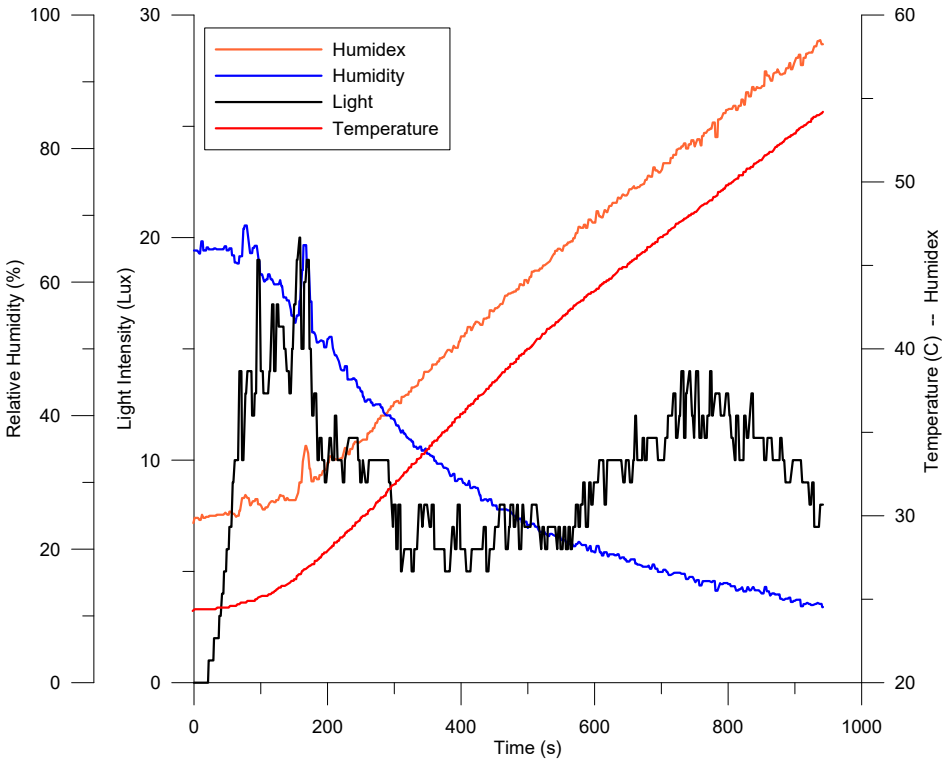


Figure C.66: Test 19 THLP 03

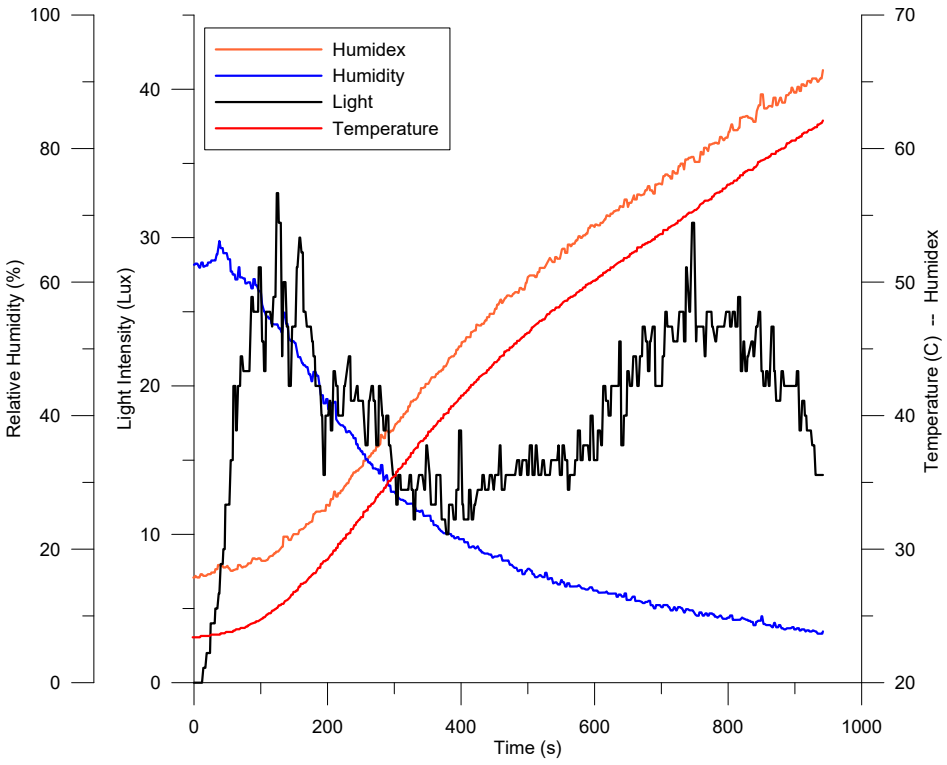


Figure C.67: Test 19 THLP 04

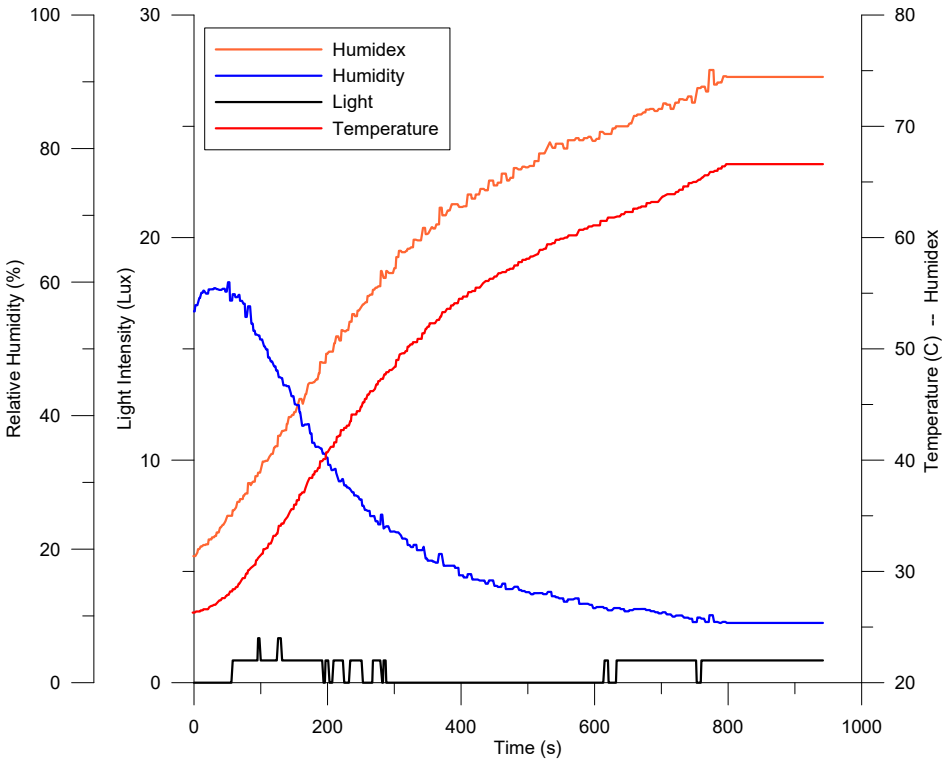


Figure C.68: Test 19 THLP 05

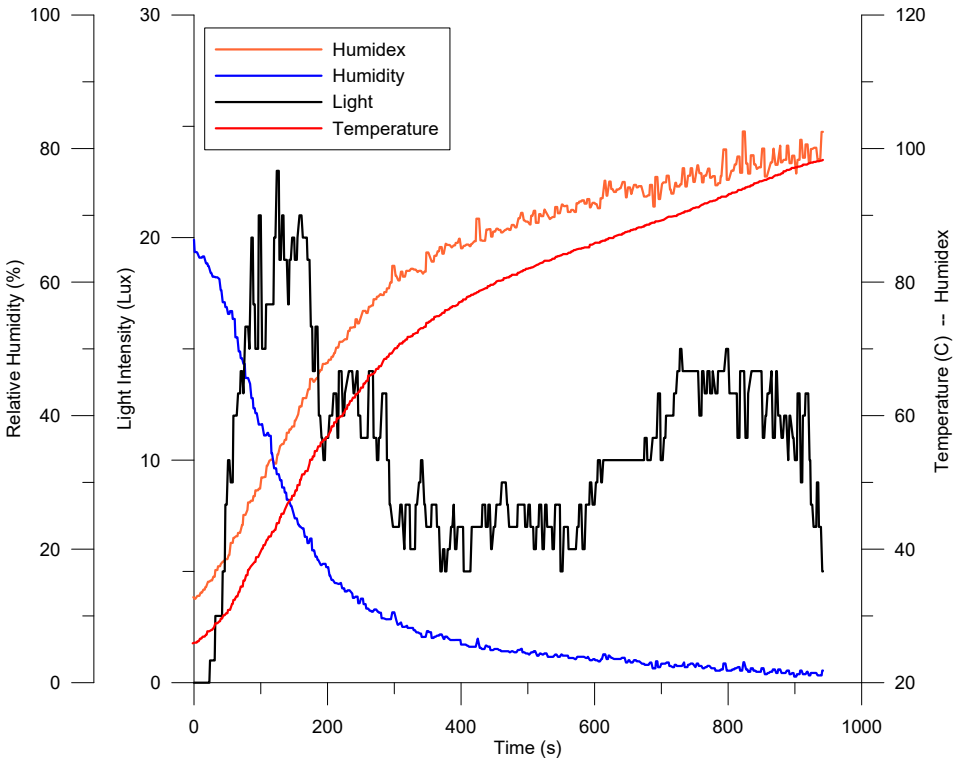


Figure C.69: Test 19 THLP 07

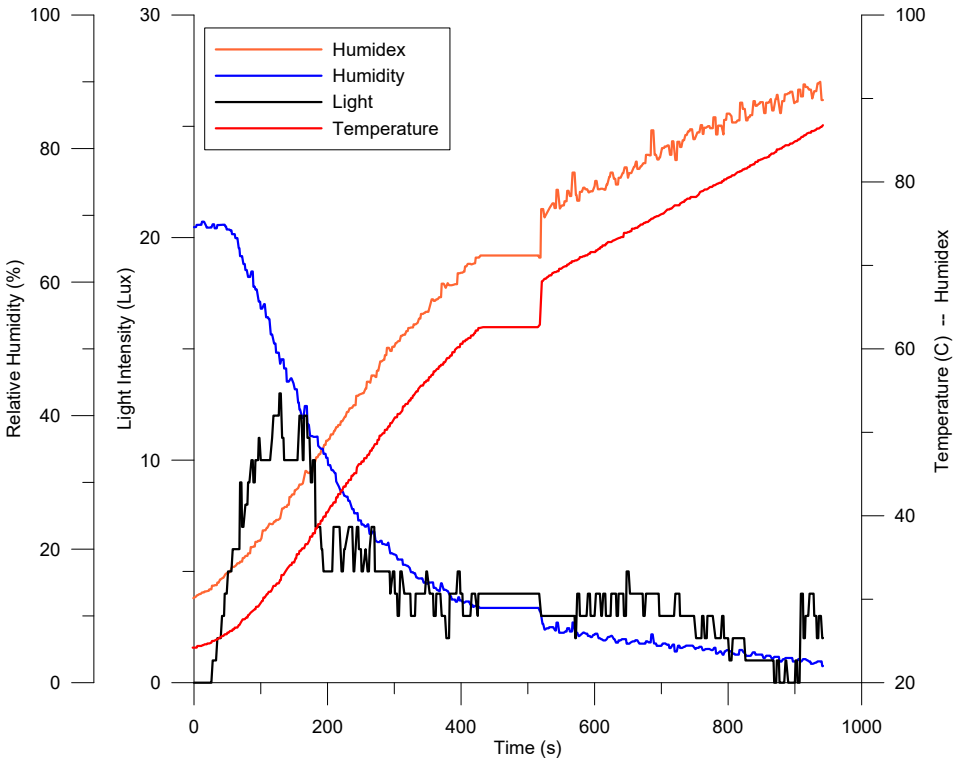


Figure C.70: Test 19 THLP 08

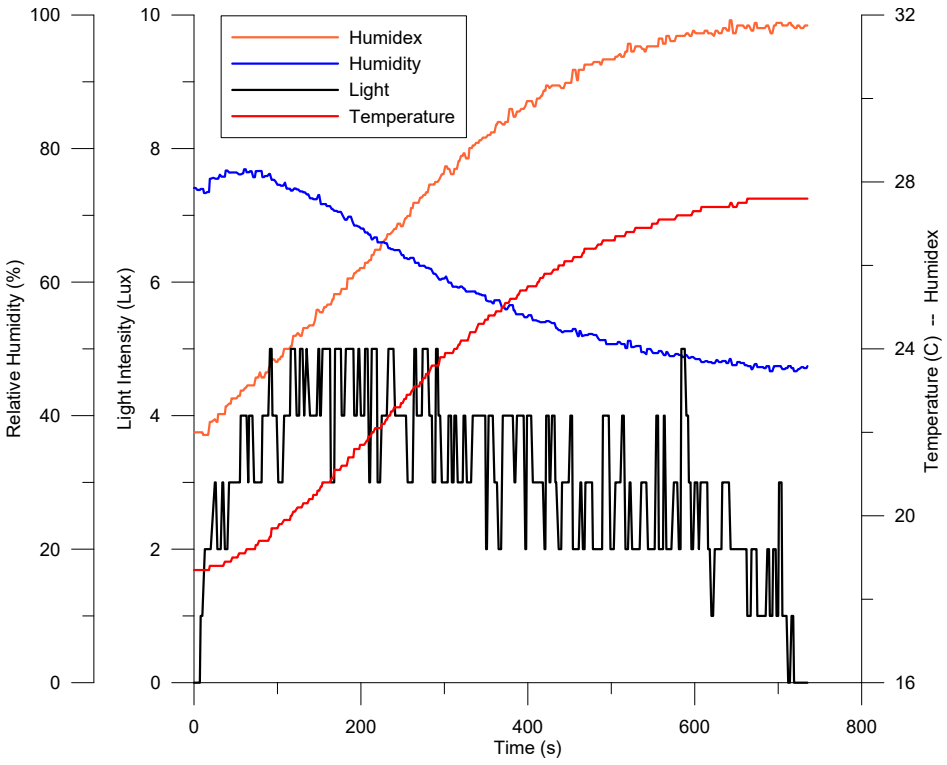


Figure C.71: Test 20 THLP 01

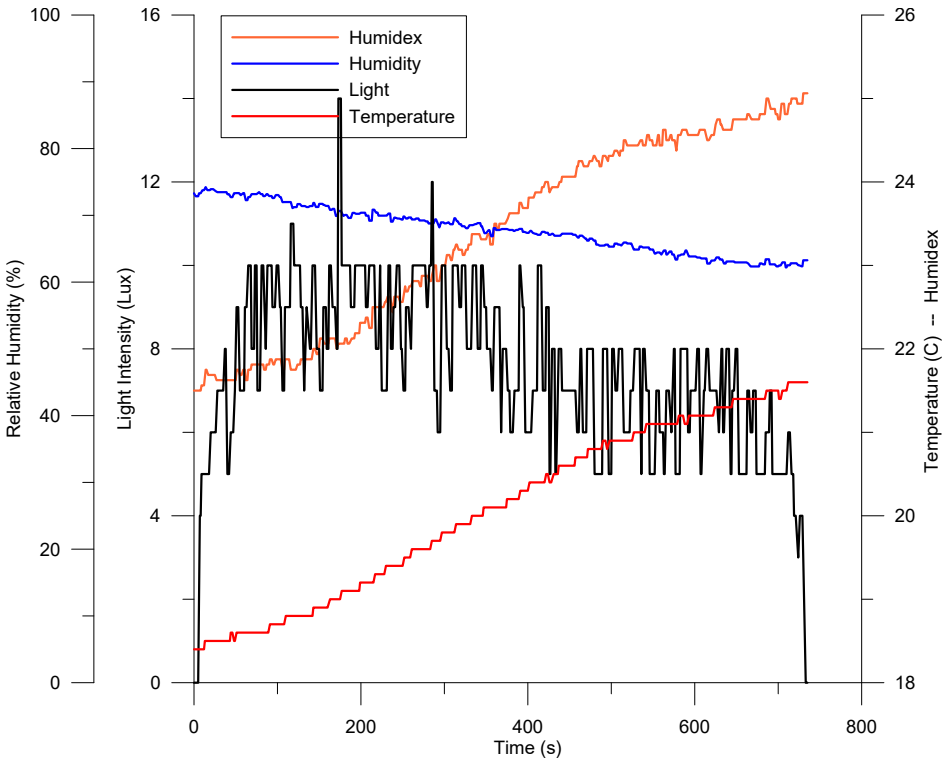


Figure C.72: Test 20 THLP 02

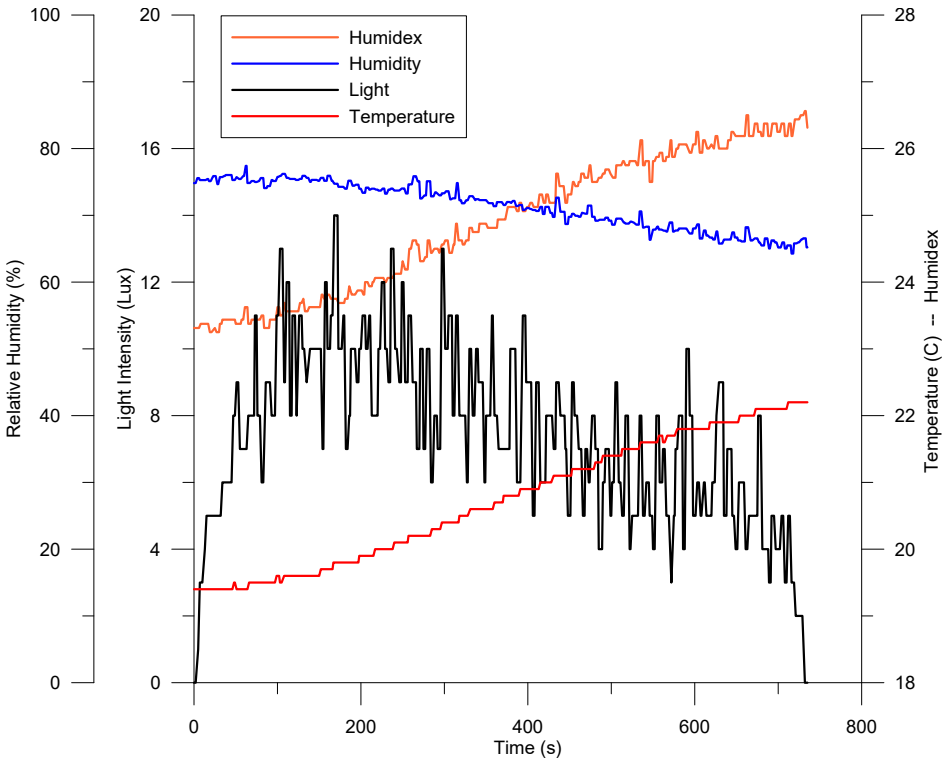


Figure C.73: Test 20 THLP 03

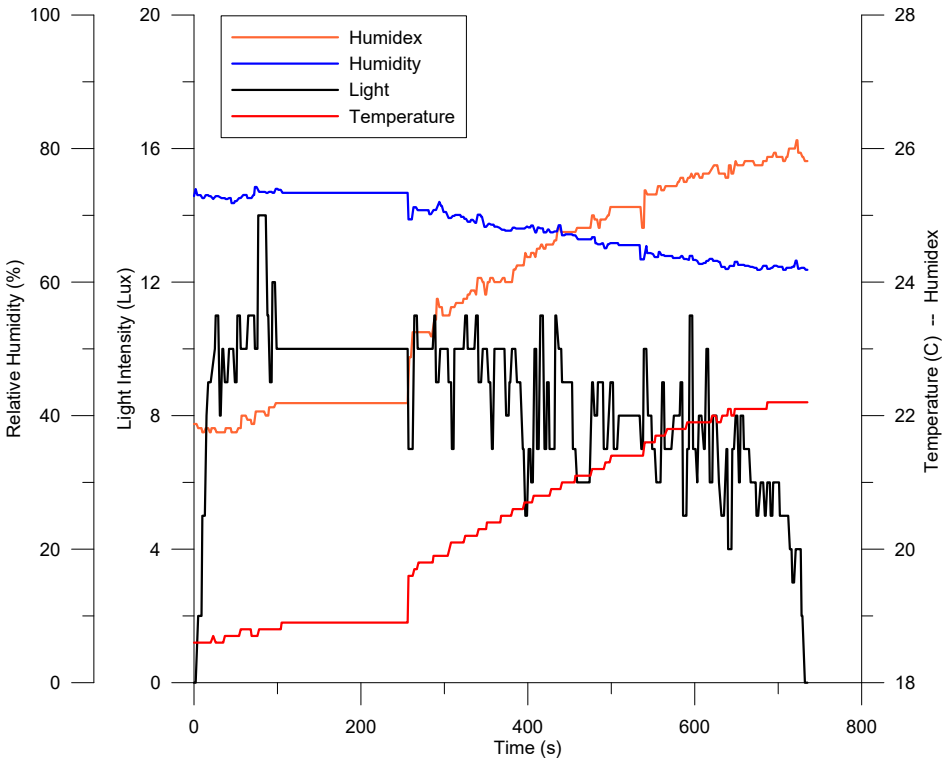


Figure C.74: Test 20 THLP 04

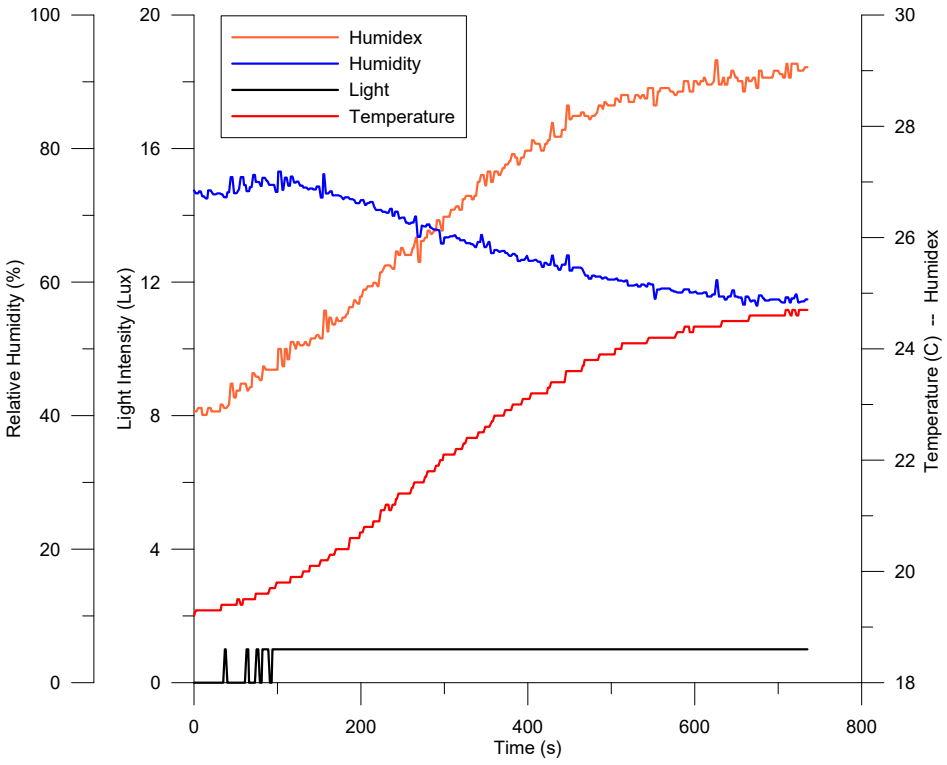


Figure C.75: Test 20 THLP 05

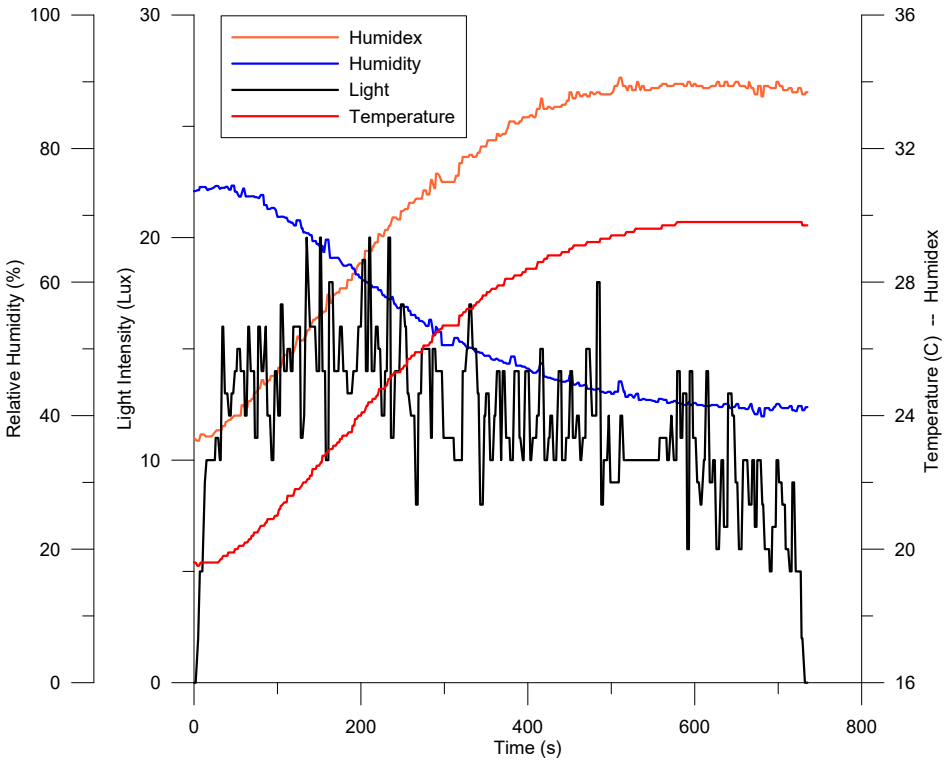


Figure C.76: Test 20 THLP 07

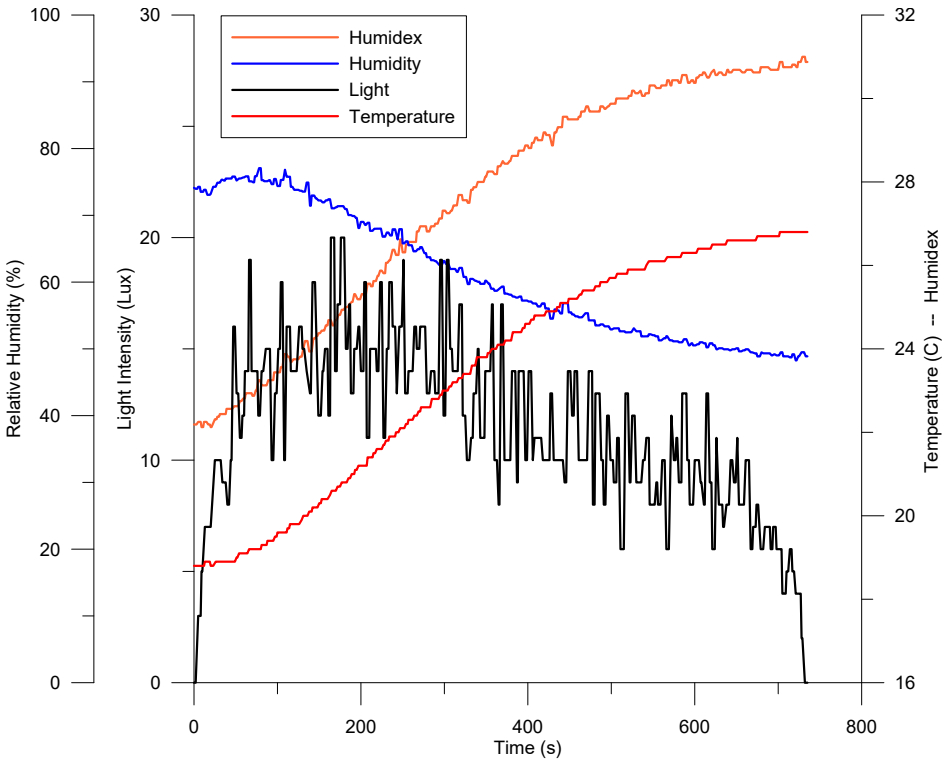


Figure C.77: Test 20 THLP 08

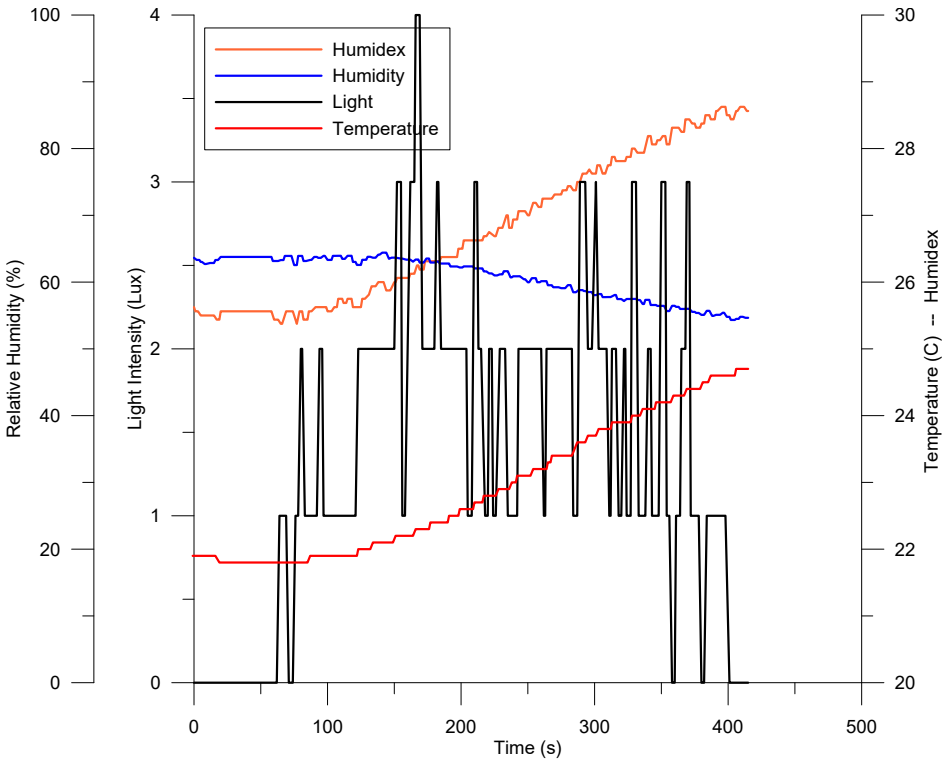


Figure C.78: Test 21 THLP 01

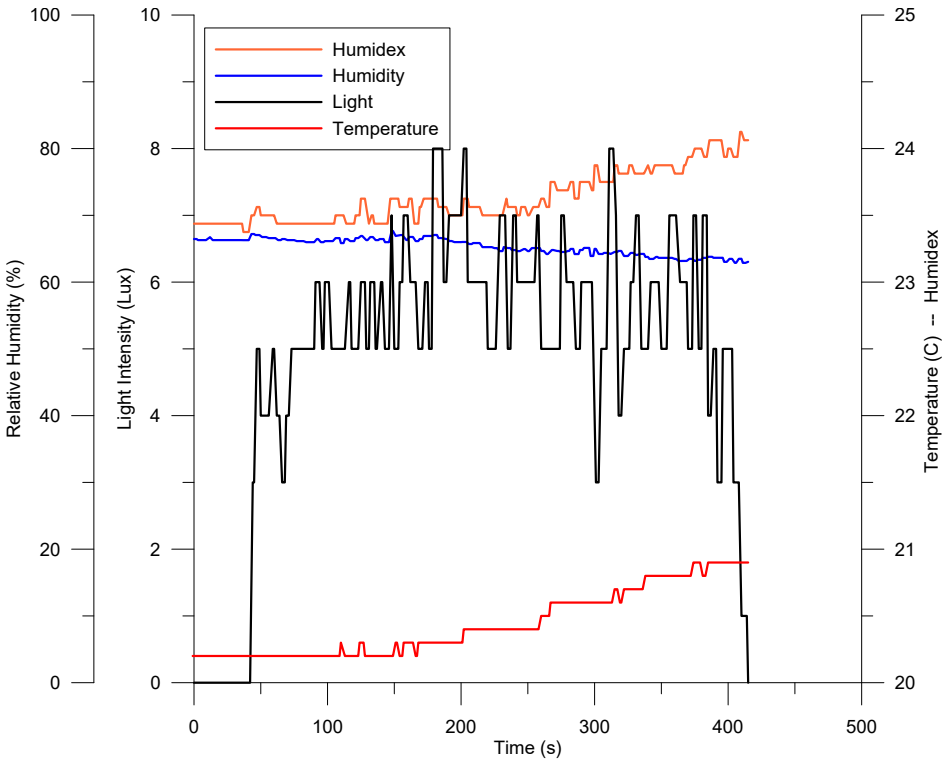


Figure C.79: Test 21 THLP 02

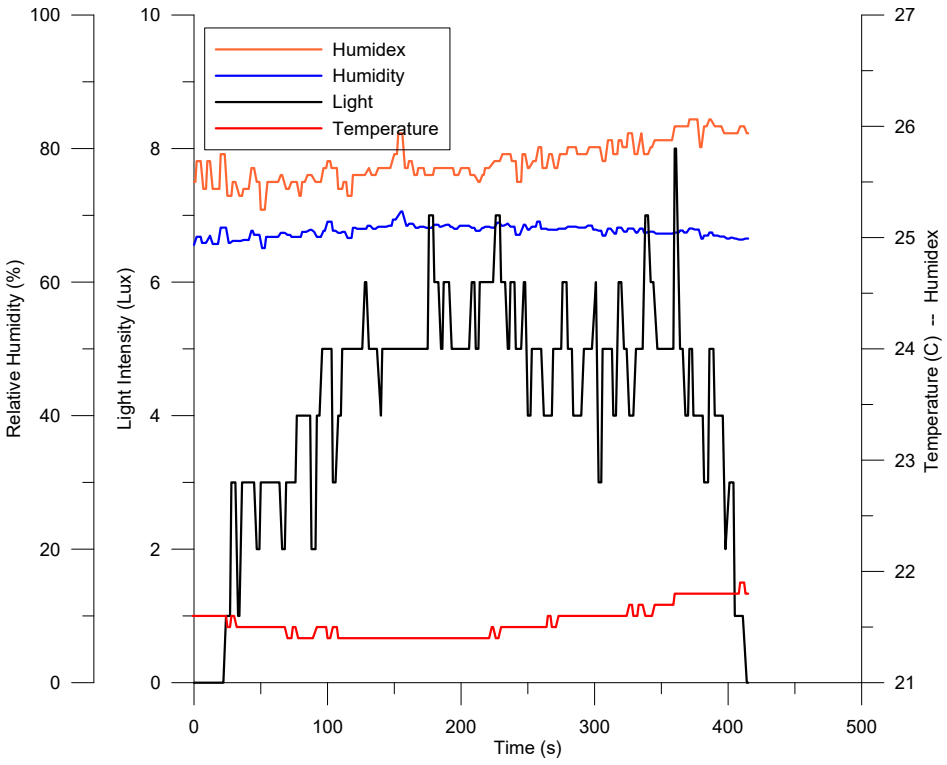


Figure C.80: Test 21 THLP 03

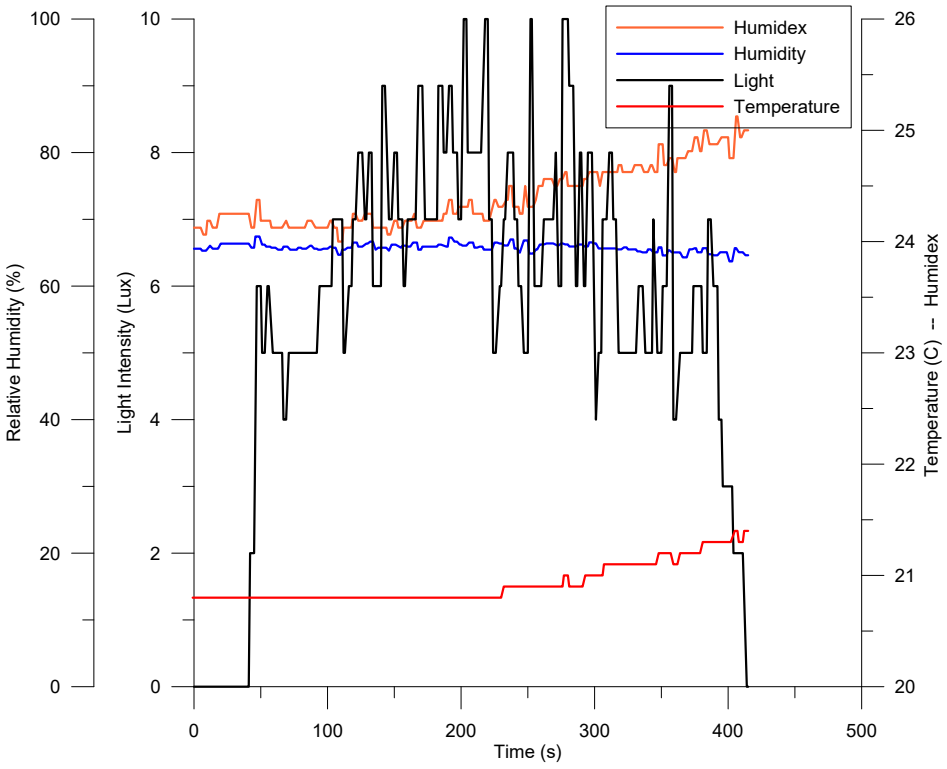


Figure C.81: Test 21 THLP 04

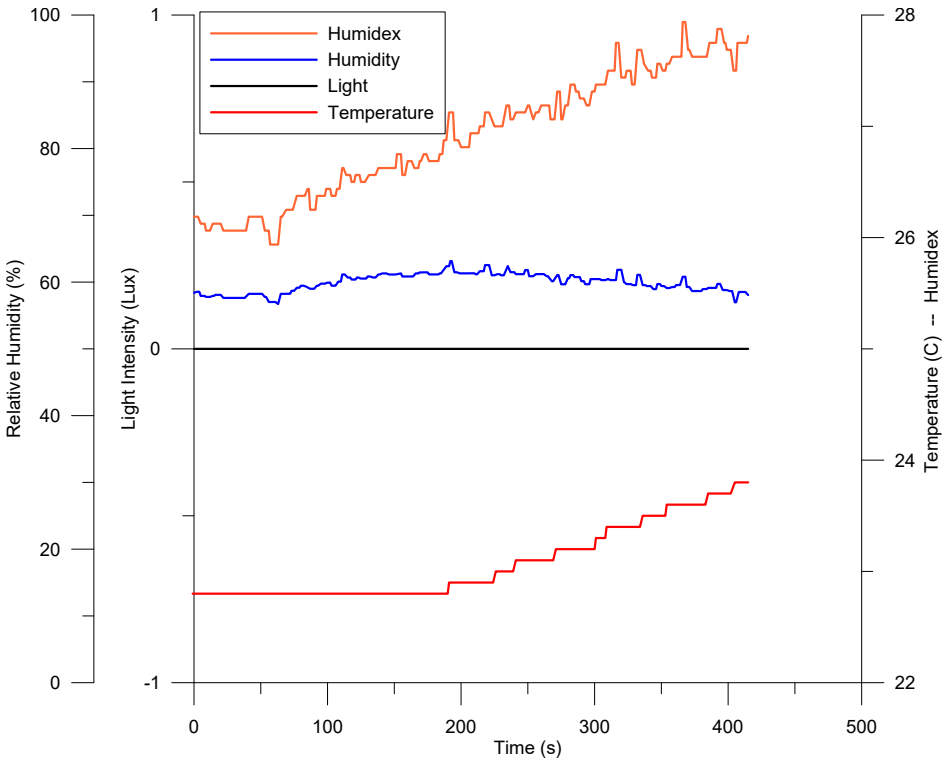


Figure C.82: Test 21 THLP 05

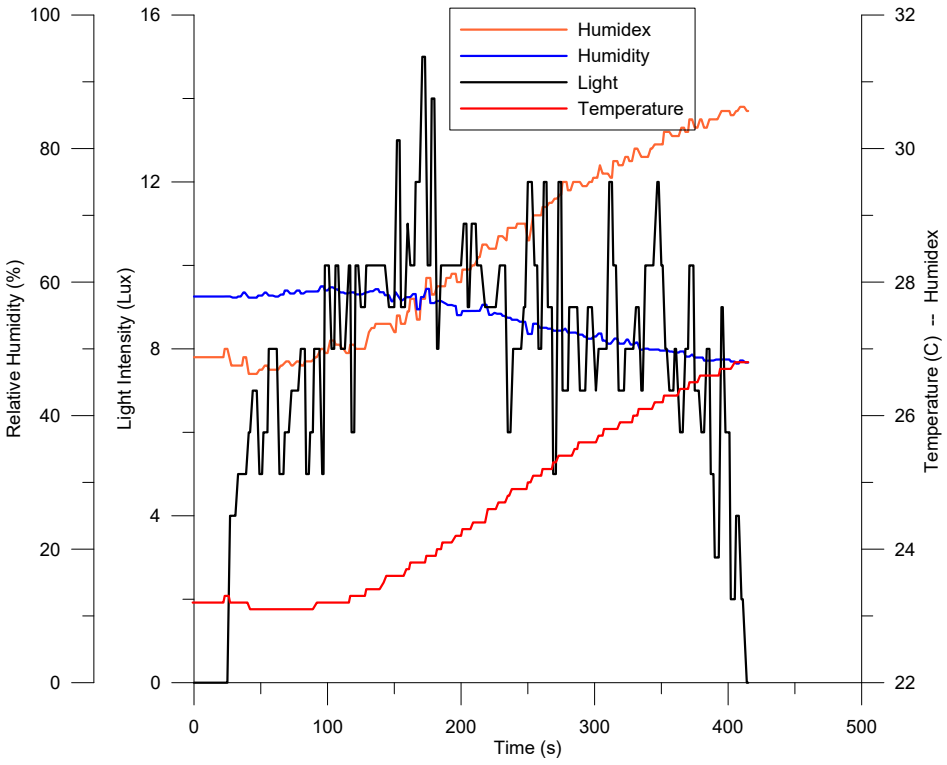


Figure C.83: Test 21 THLP 07

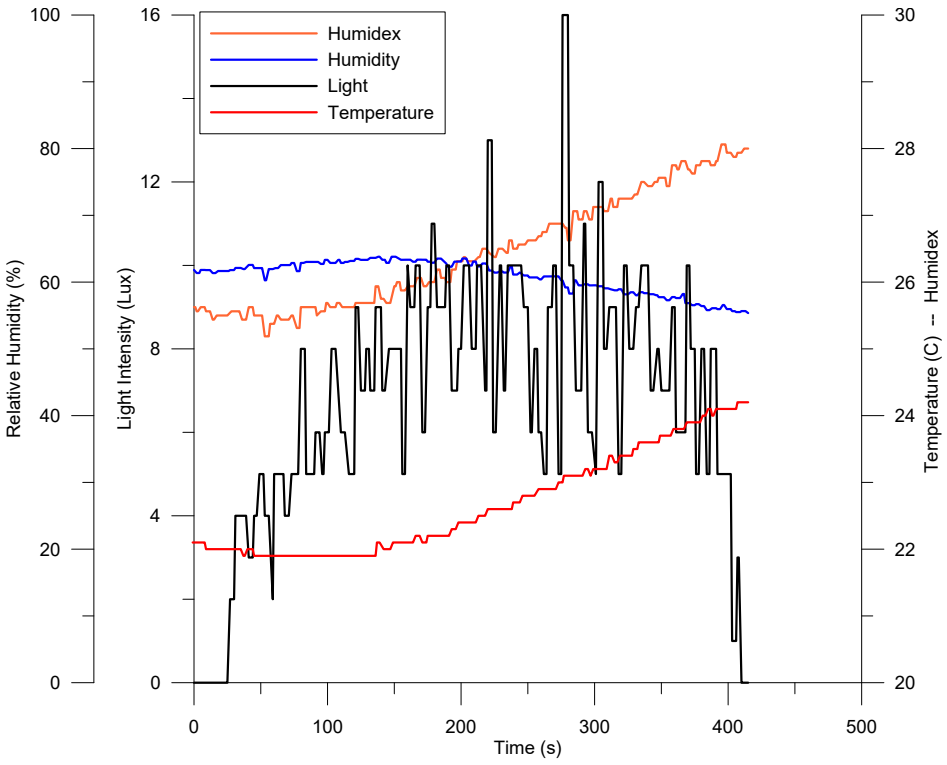


Figure C.84: Test 21 THLP 08

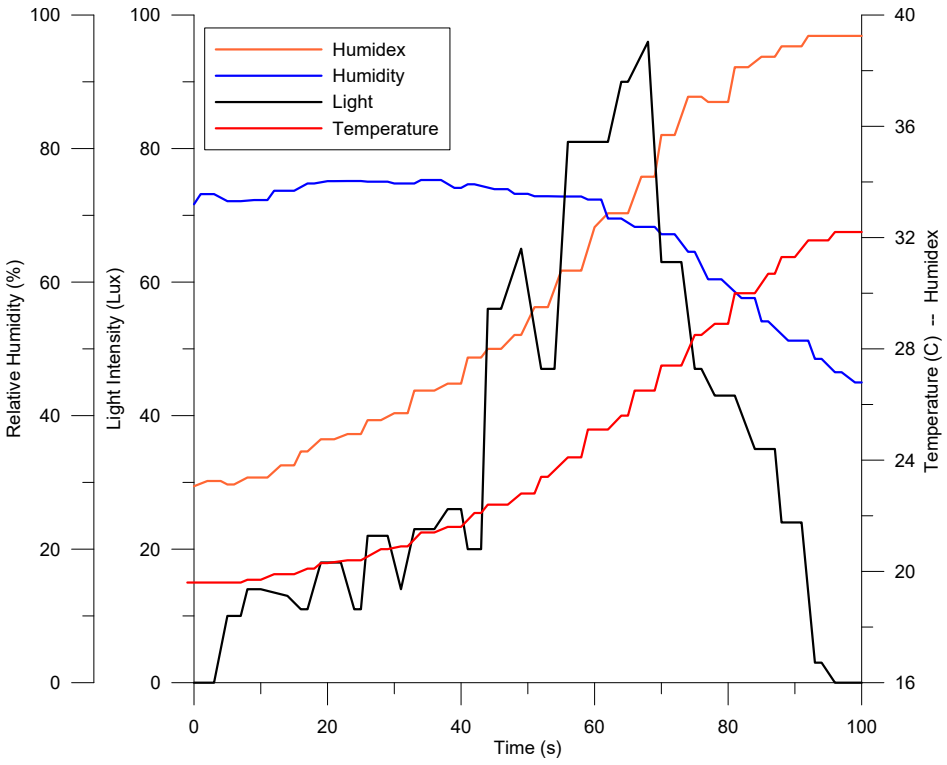


Figure C.85: Test 22 THLP 01

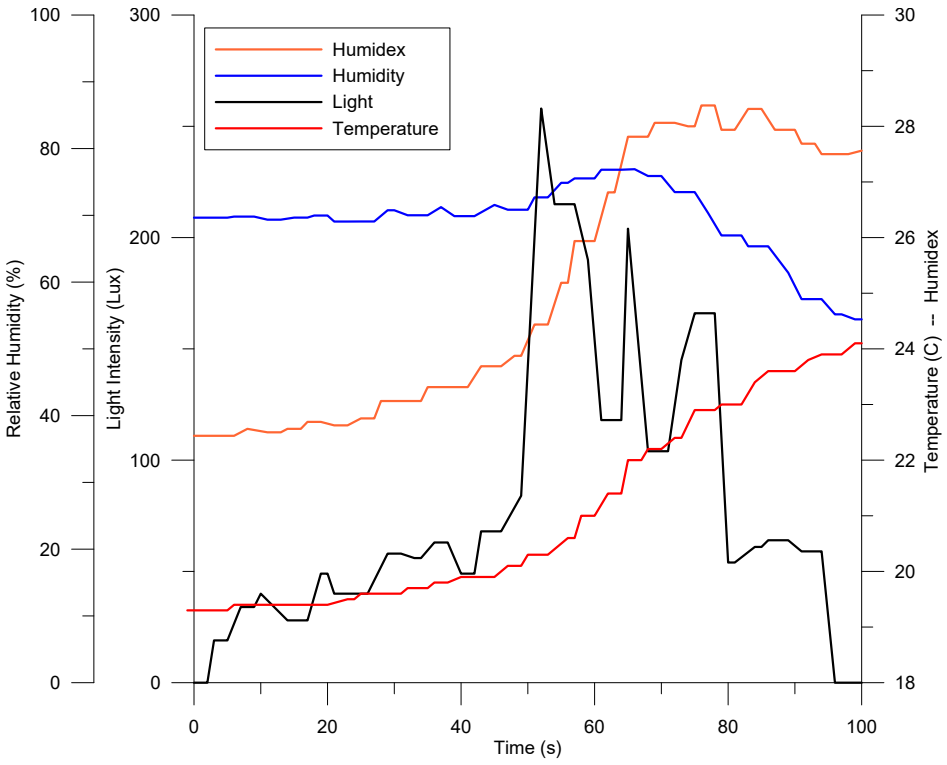


Figure C.86: Test 22 THLP 02

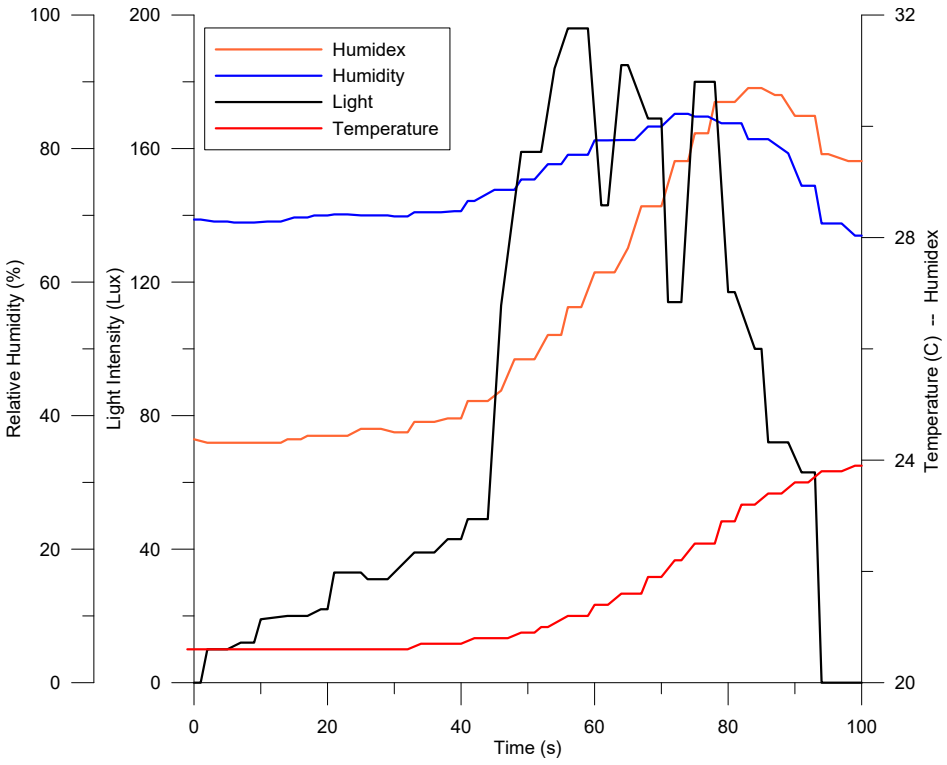


Figure C.87: Test 22 THLP 03

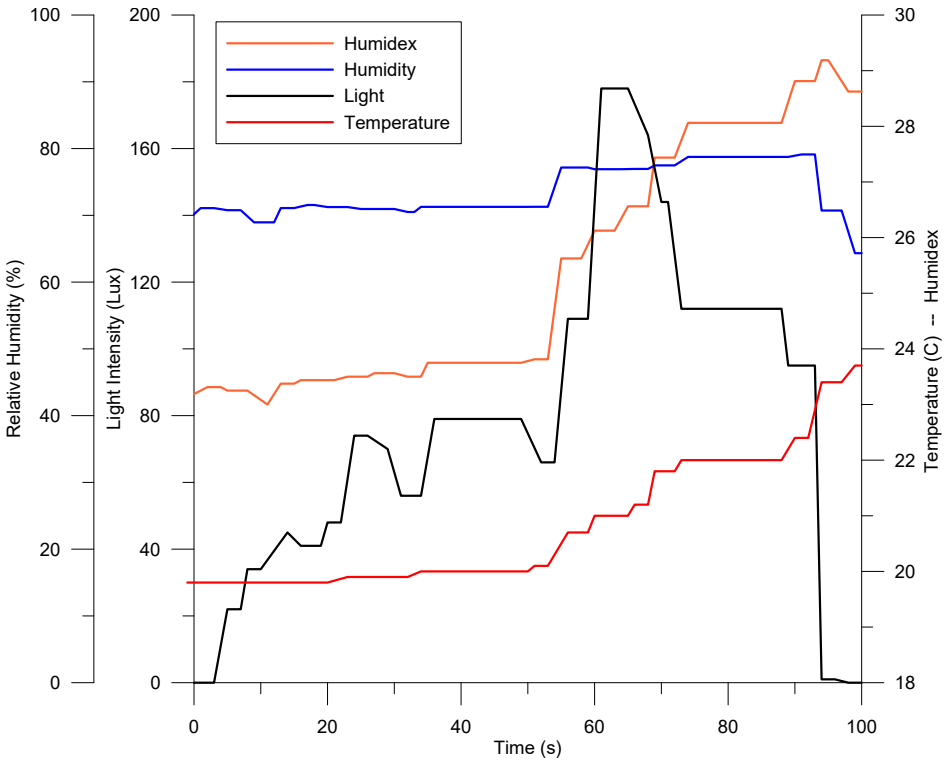


Figure C.88: Test 22 THLP 04

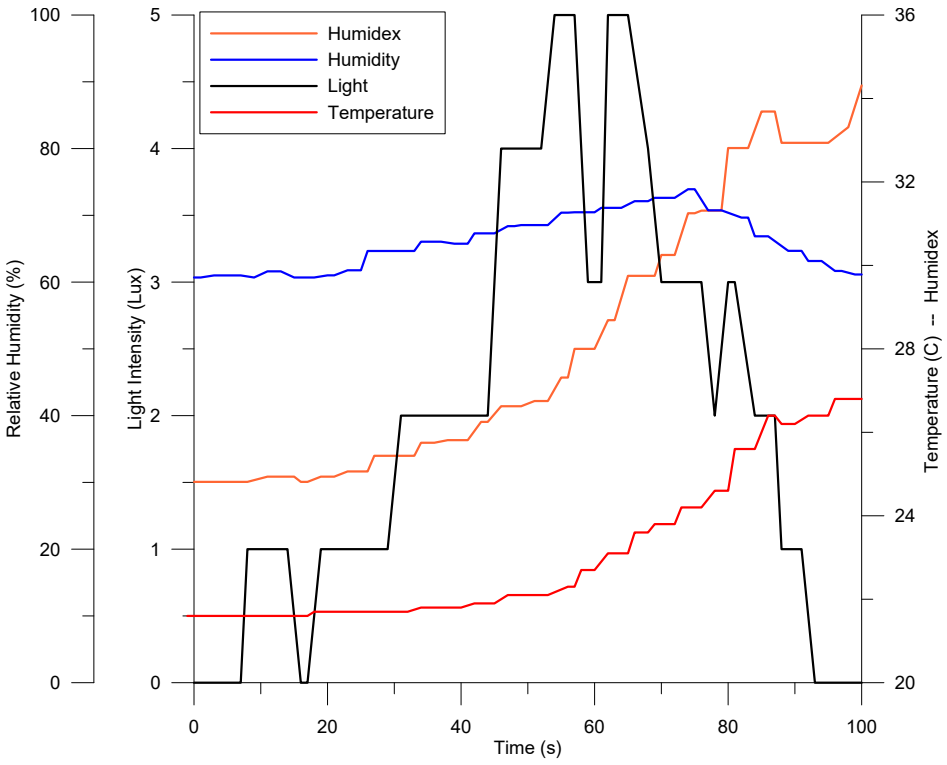


Figure C.89: Test 22 THLP 05

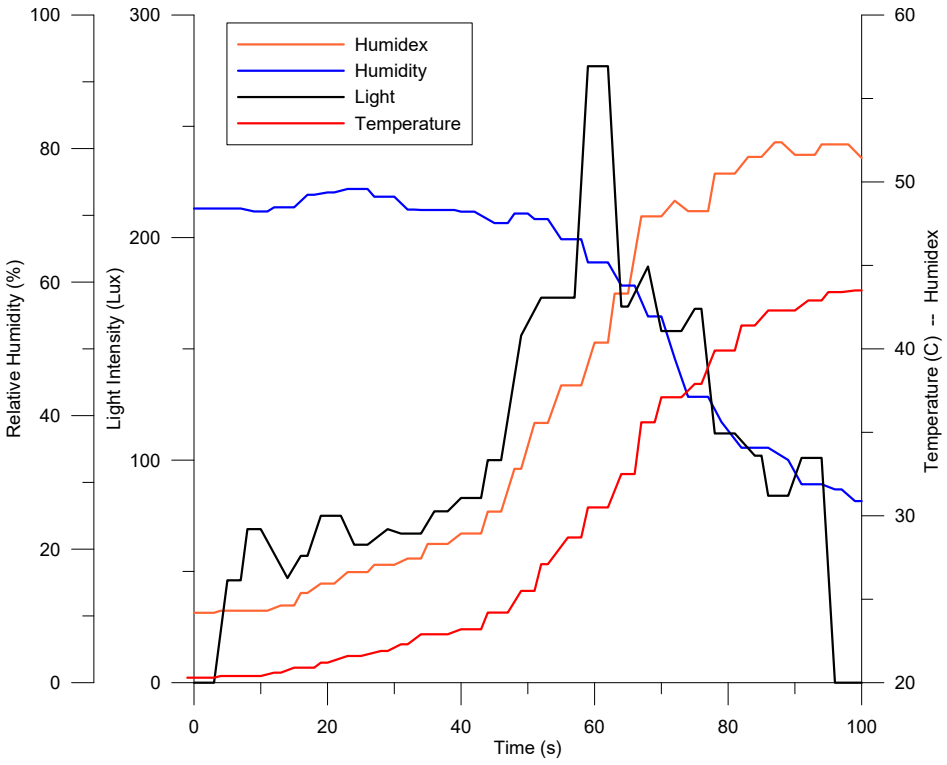


Figure C.90: Test 22 THLP 07

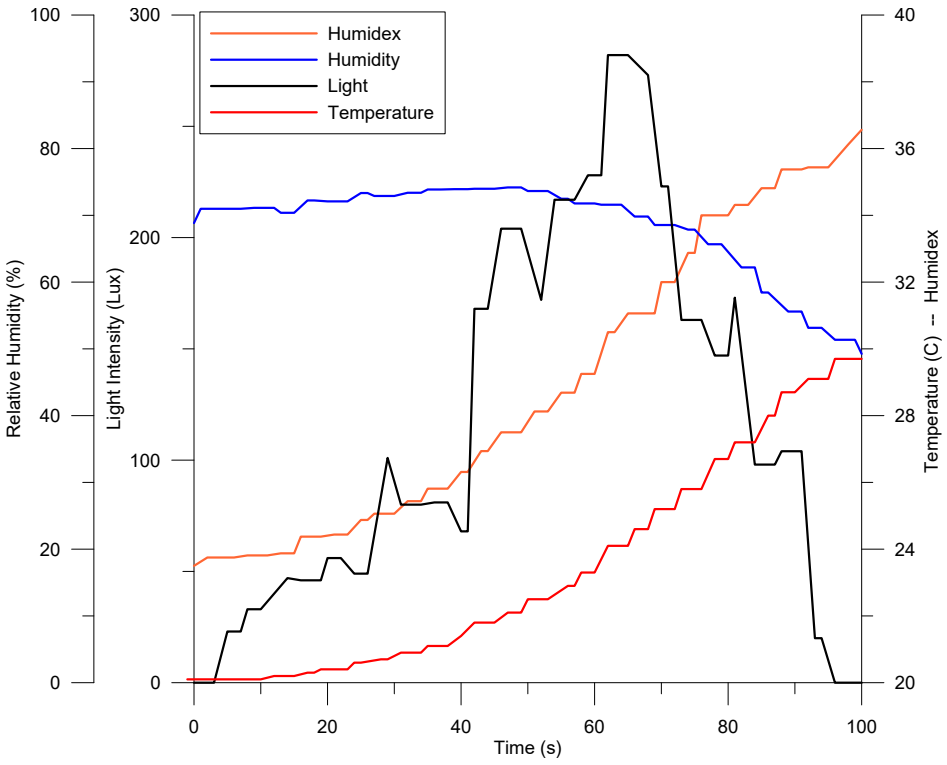


Figure C.91: Test 22 THLP 08

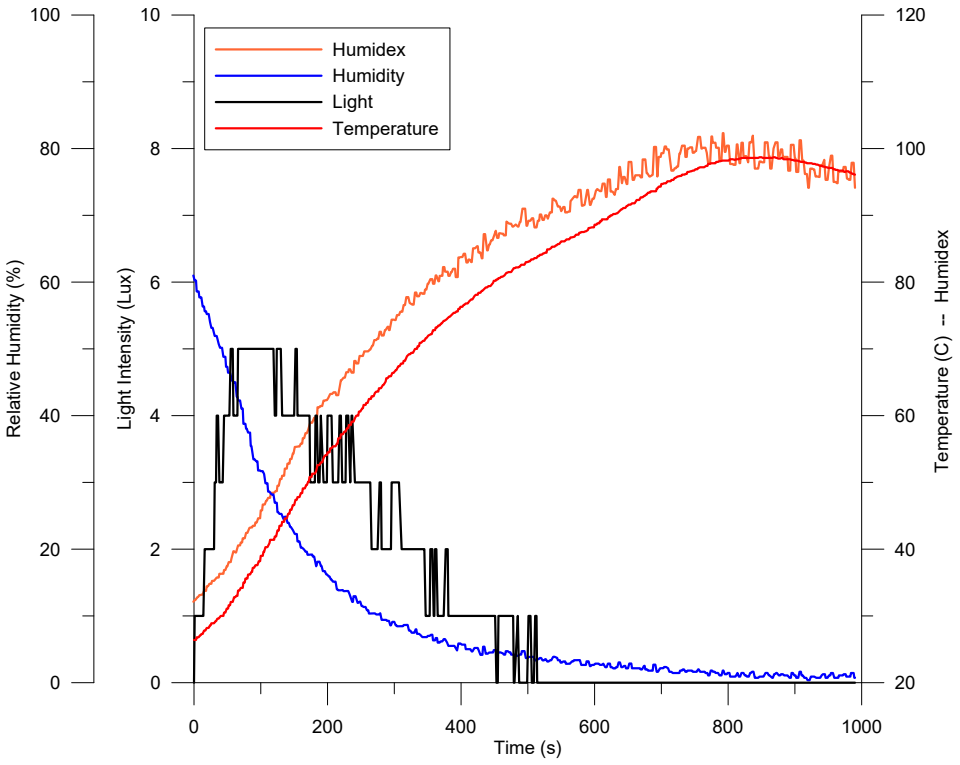


Figure C.92: Test 24 THLP 01

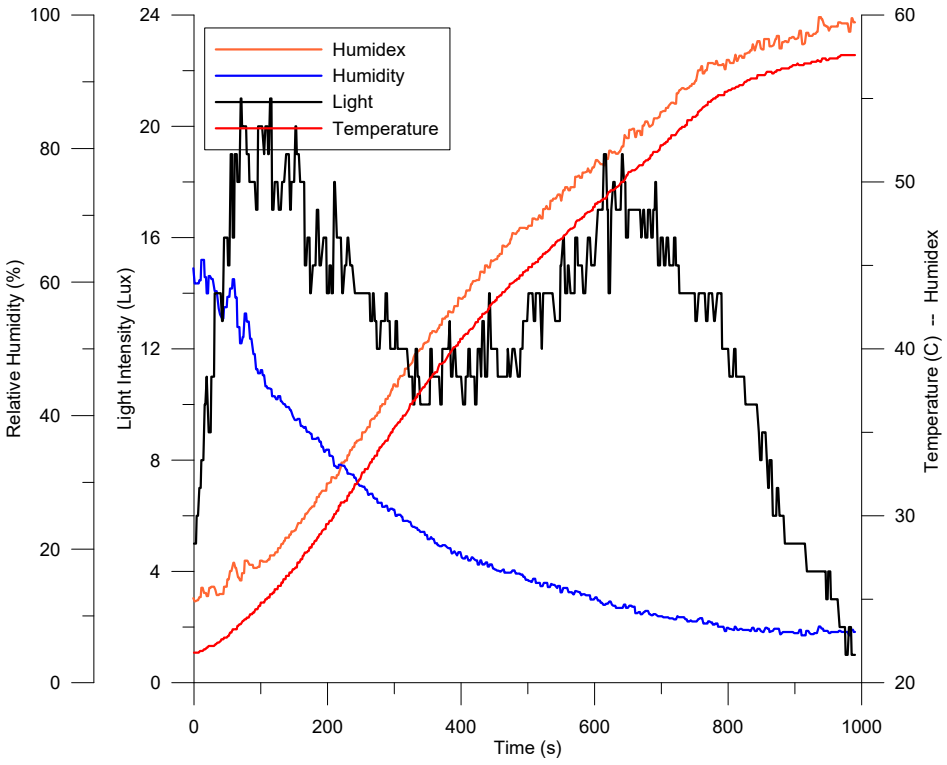


Figure C.93: Test 24 THLP 02

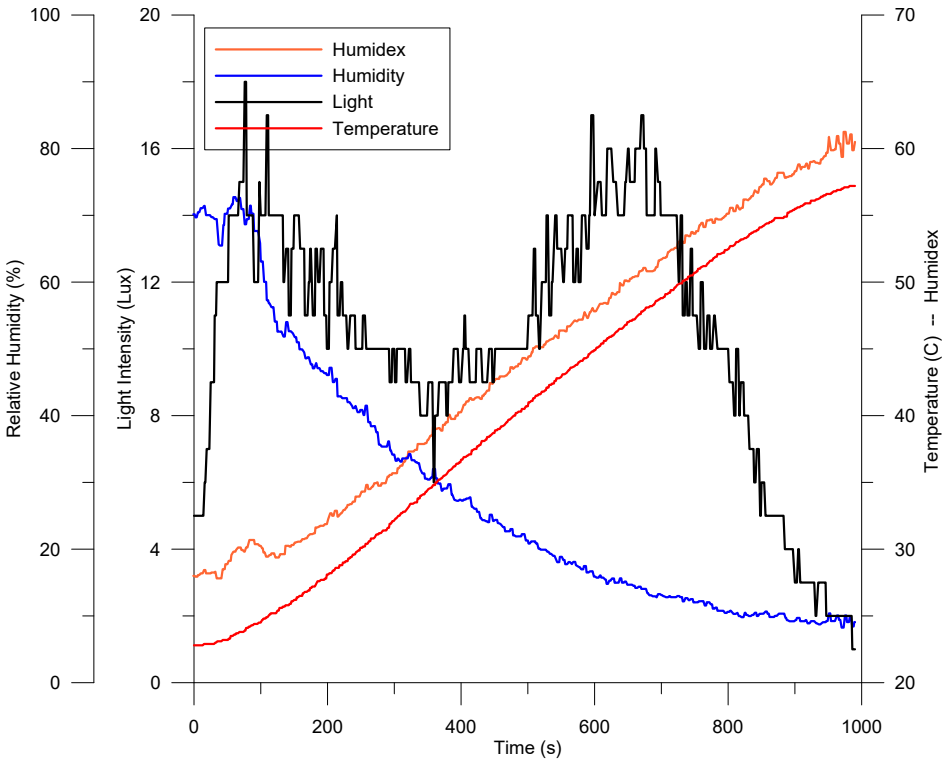


Figure C.94: Test 24 THLP 03

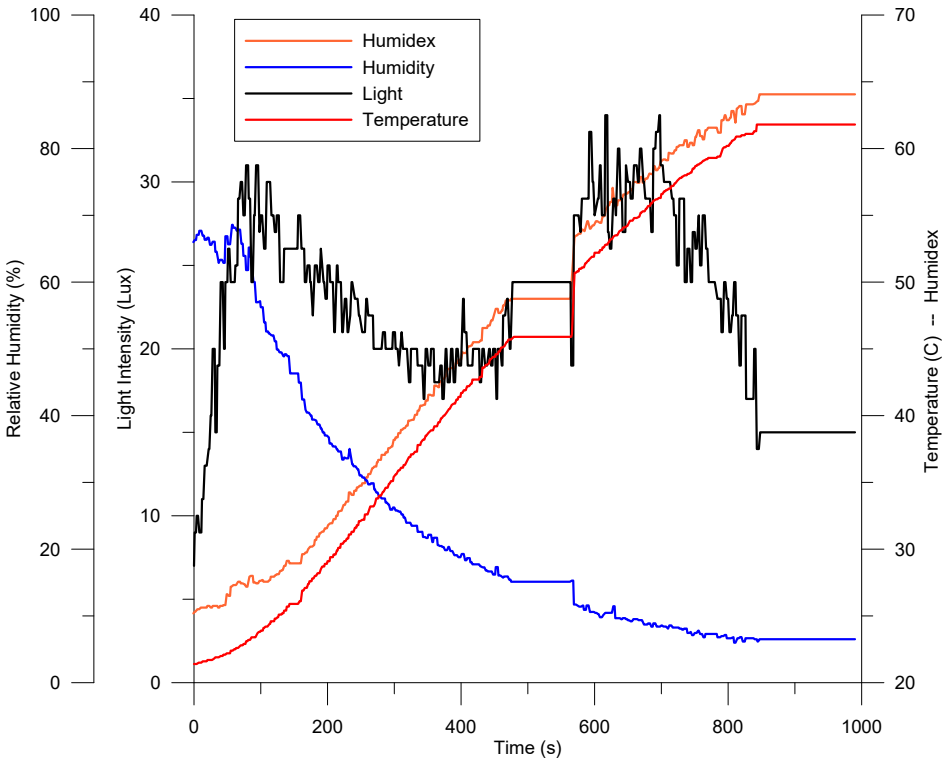


Figure C.95: Test 24 THLP 04

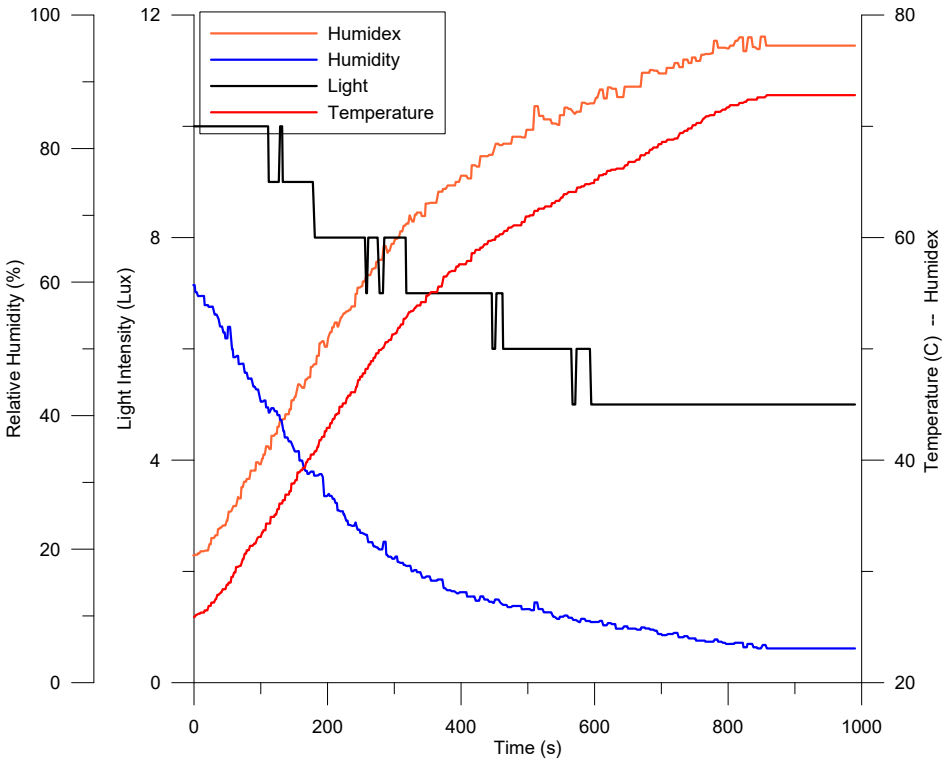


Figure C.96: Test 24 THLP 05

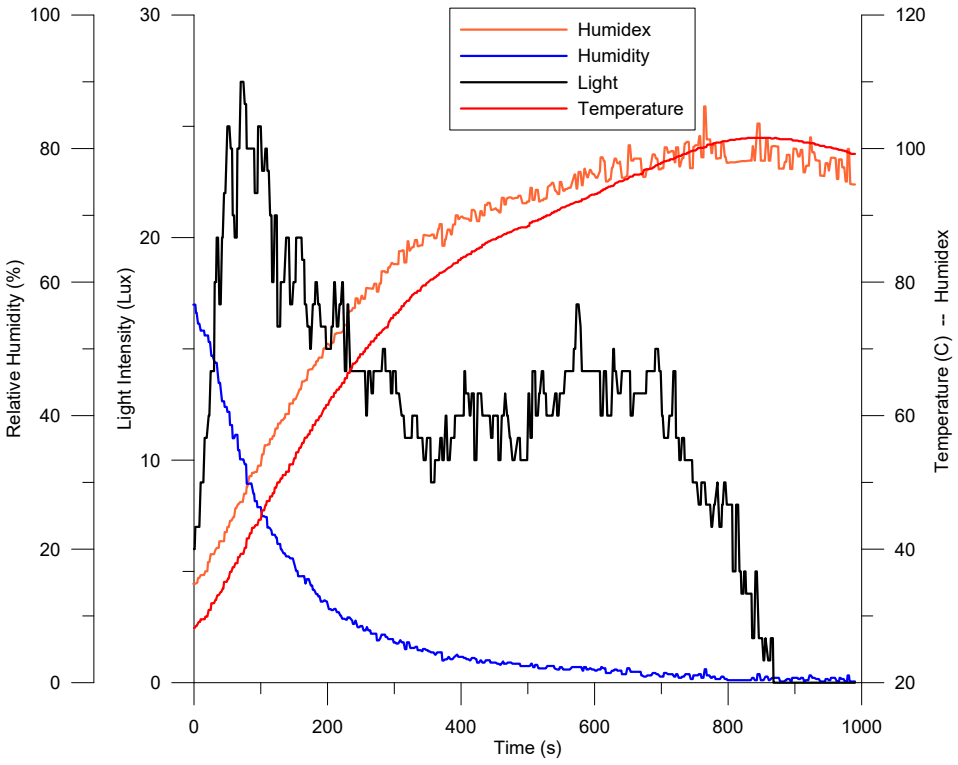


Figure C.97: Test 24 THLP 07

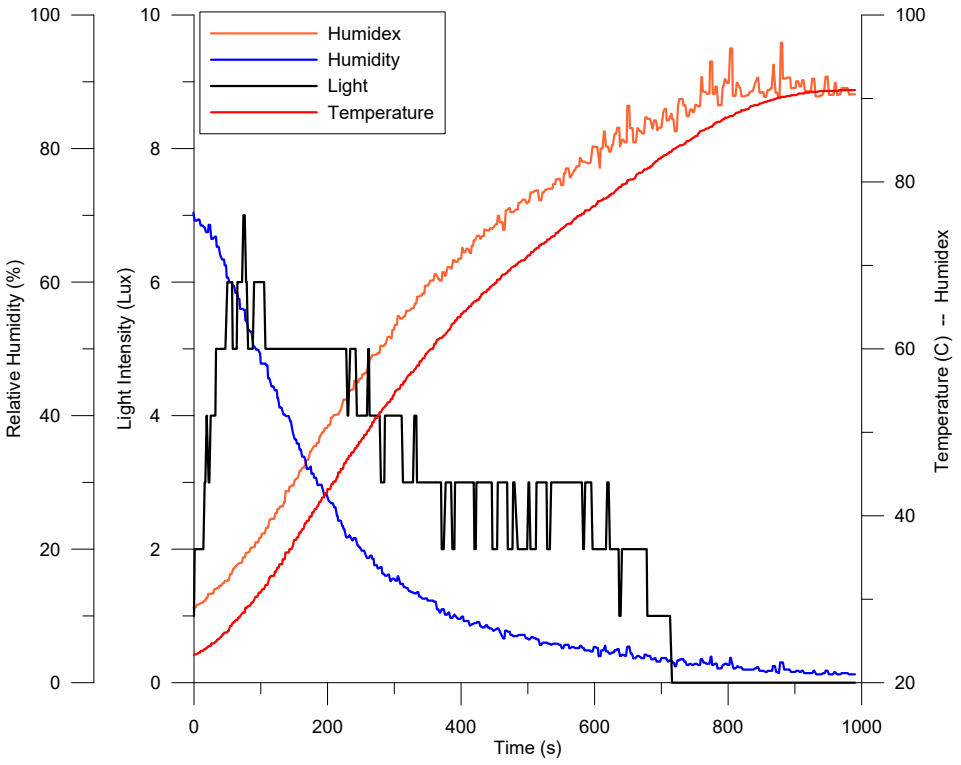


Figure C.98: Test 24 THLP 08

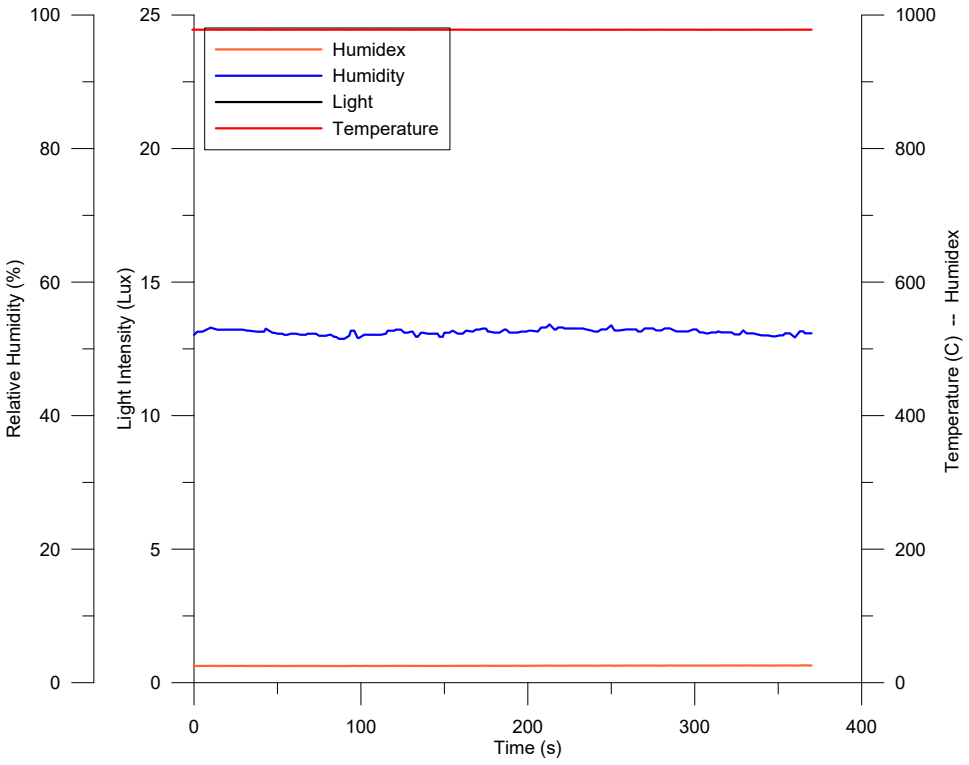


Figure C.99: Test 28 THLP 01

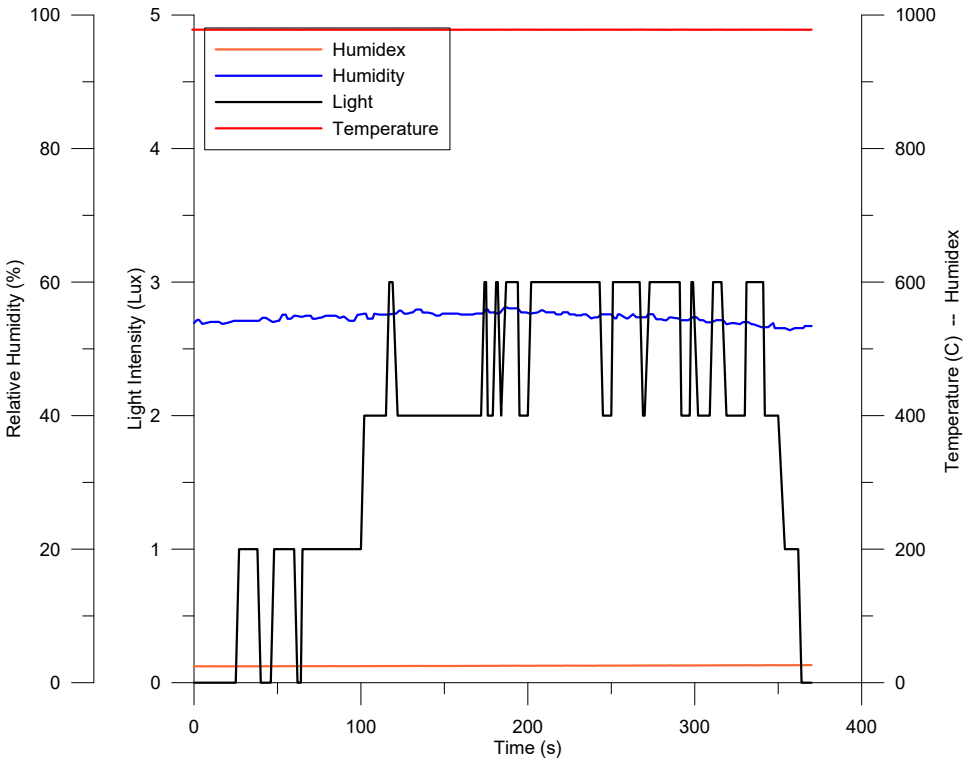


Figure C.100: Test 28 THLP 02

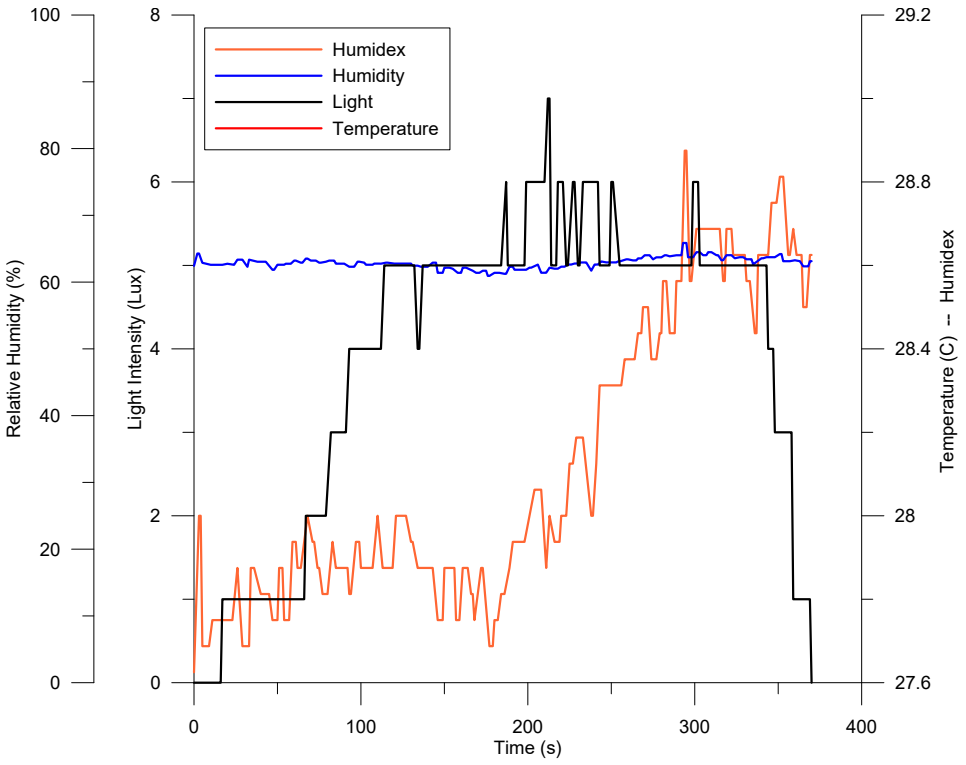


Figure C.101: Test 28 THLP 03

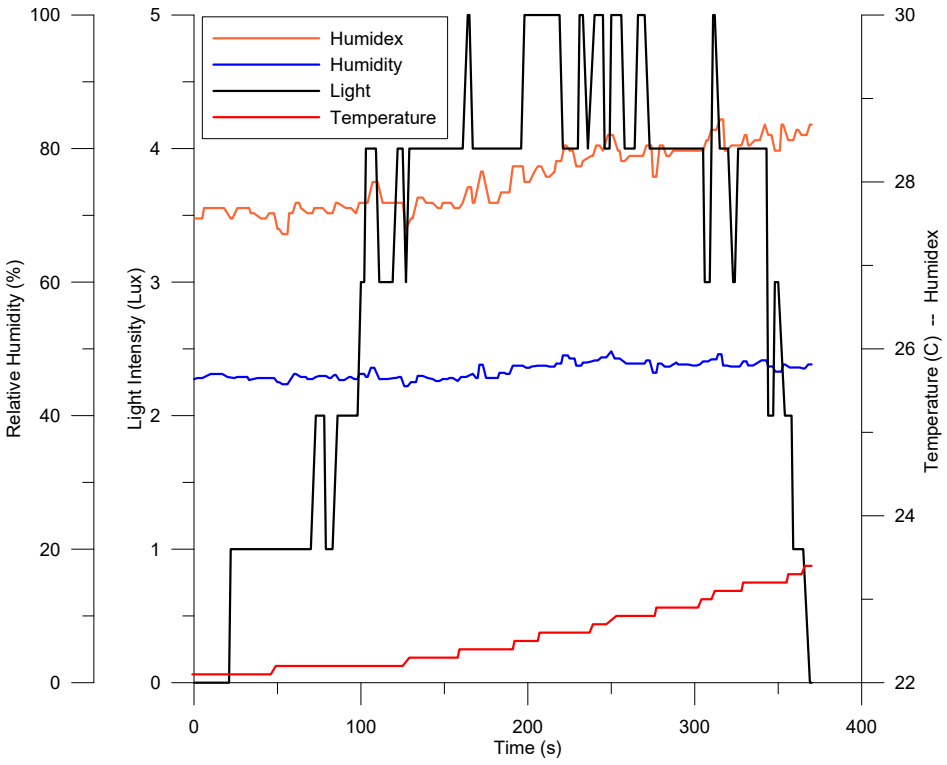


Figure C.102: Test 28 THLP 04

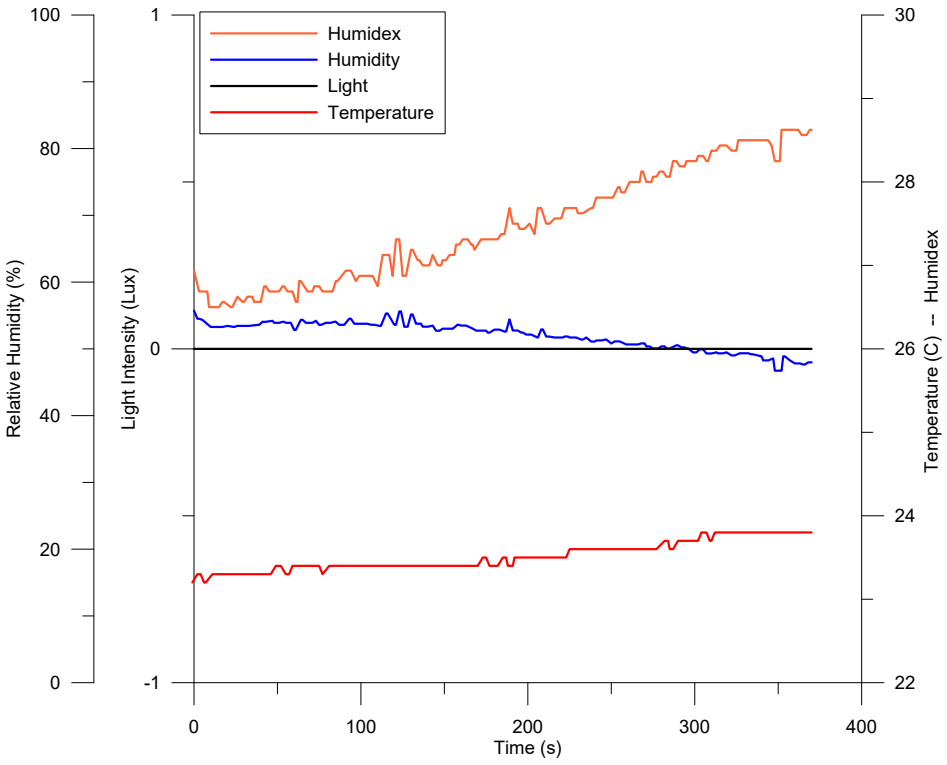


Figure C.103: Test 28 THLP 05

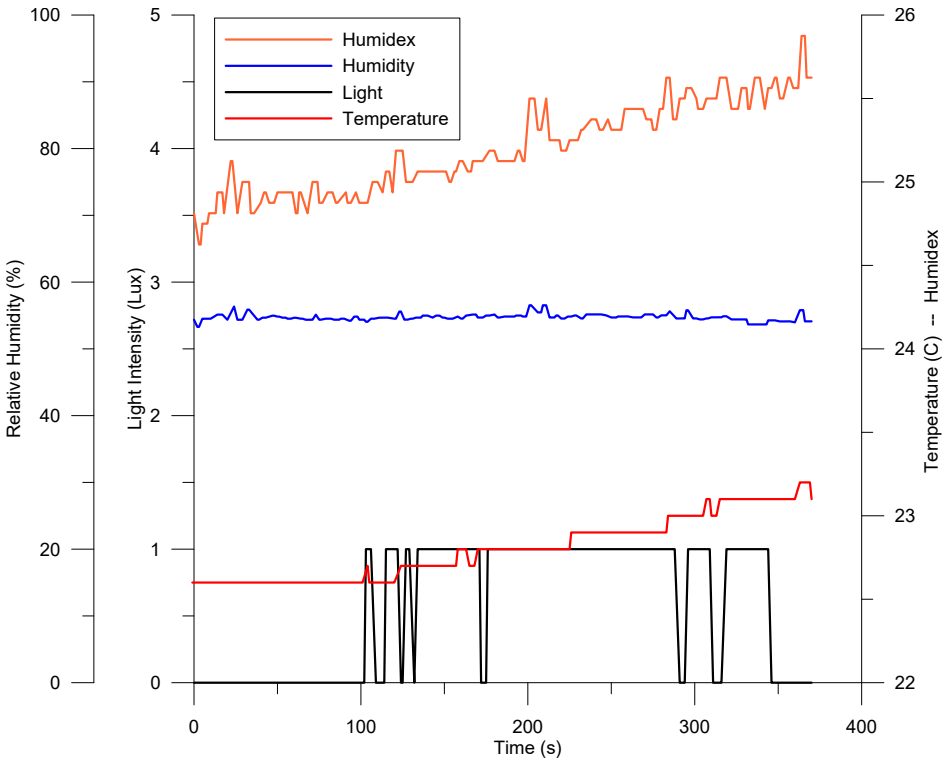


Figure C.104: Test 28 THLP 07

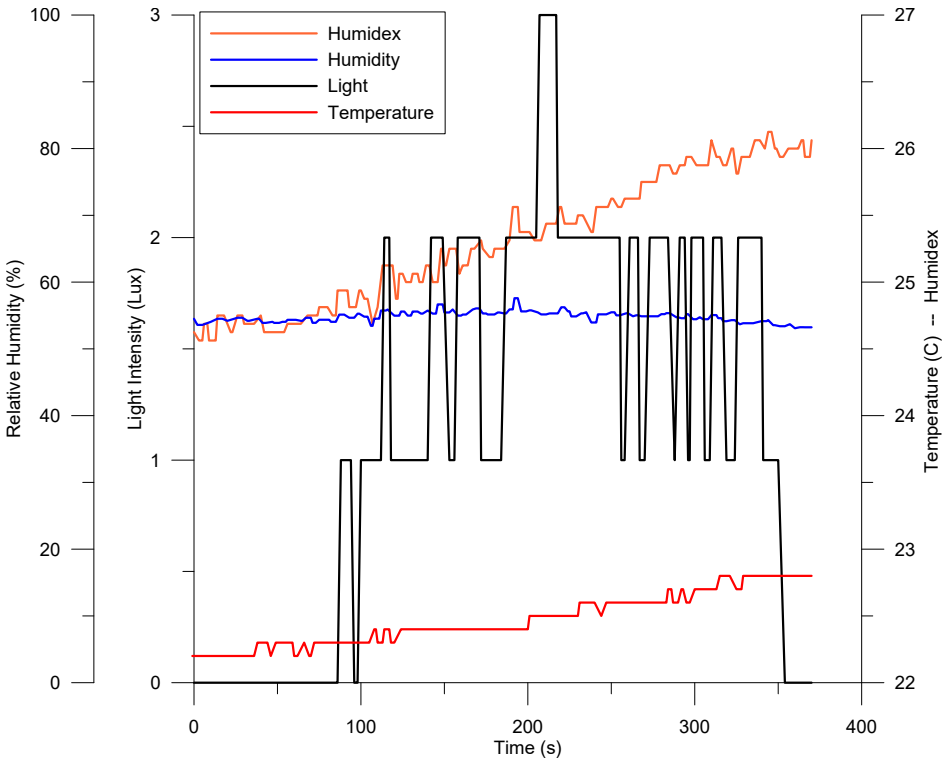


Figure C.105: Test 28 THLP 08

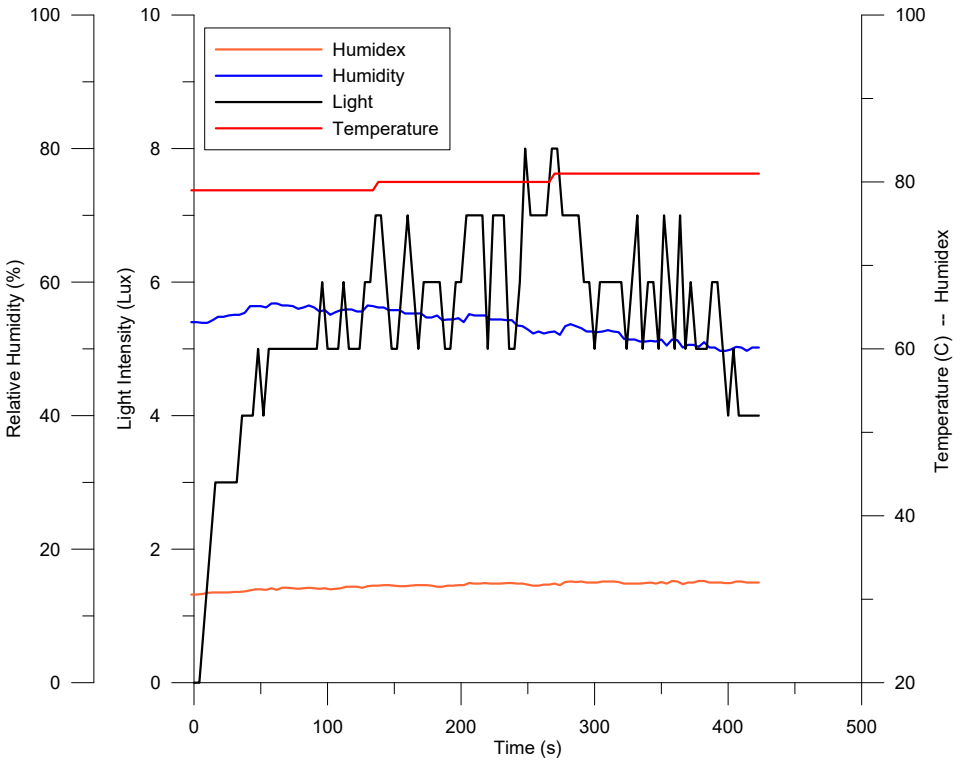


Figure C.106: Test 33 THLP 01

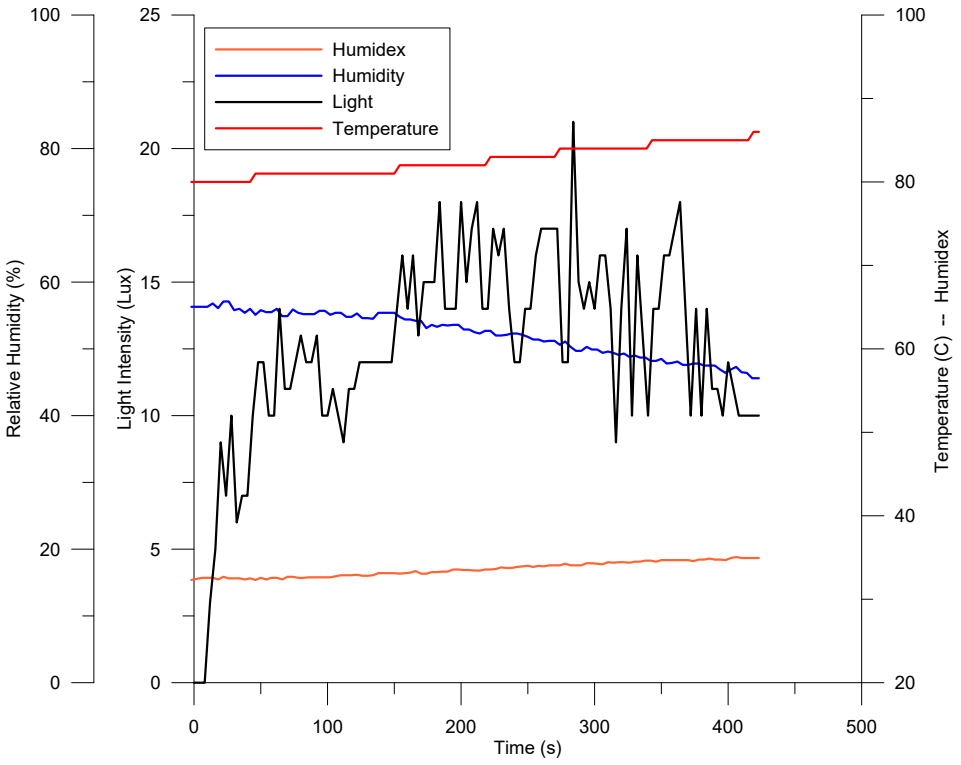


Figure C.107: Test 33 THLP 02

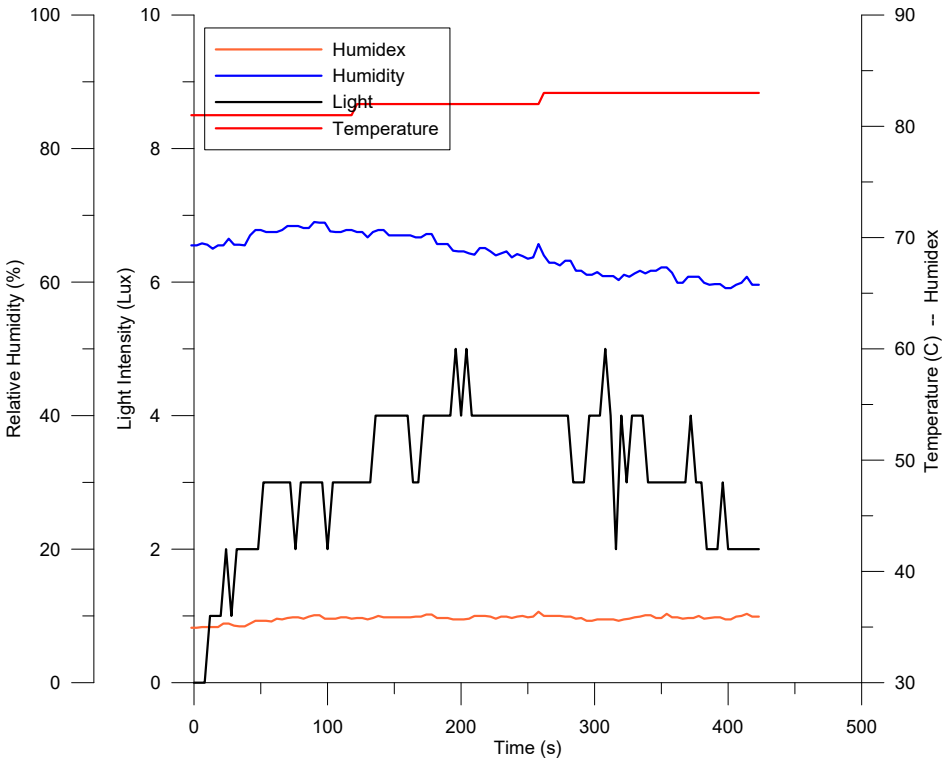


Figure C.108: Test 33 THLP 03

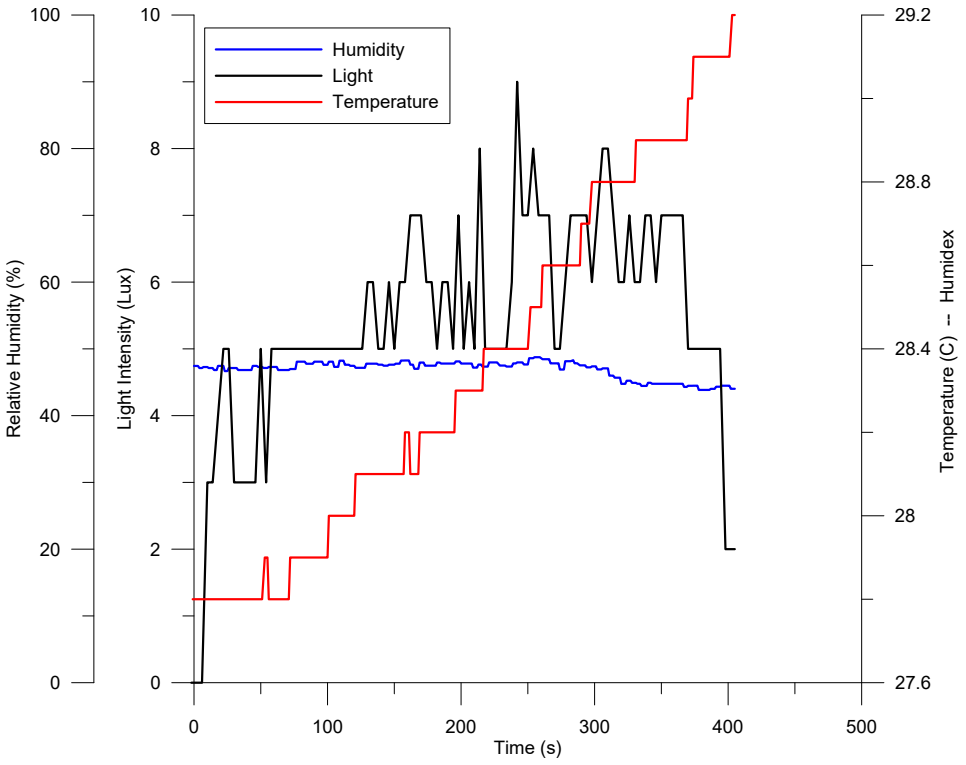


Figure C.109: Test 34 THLP 01

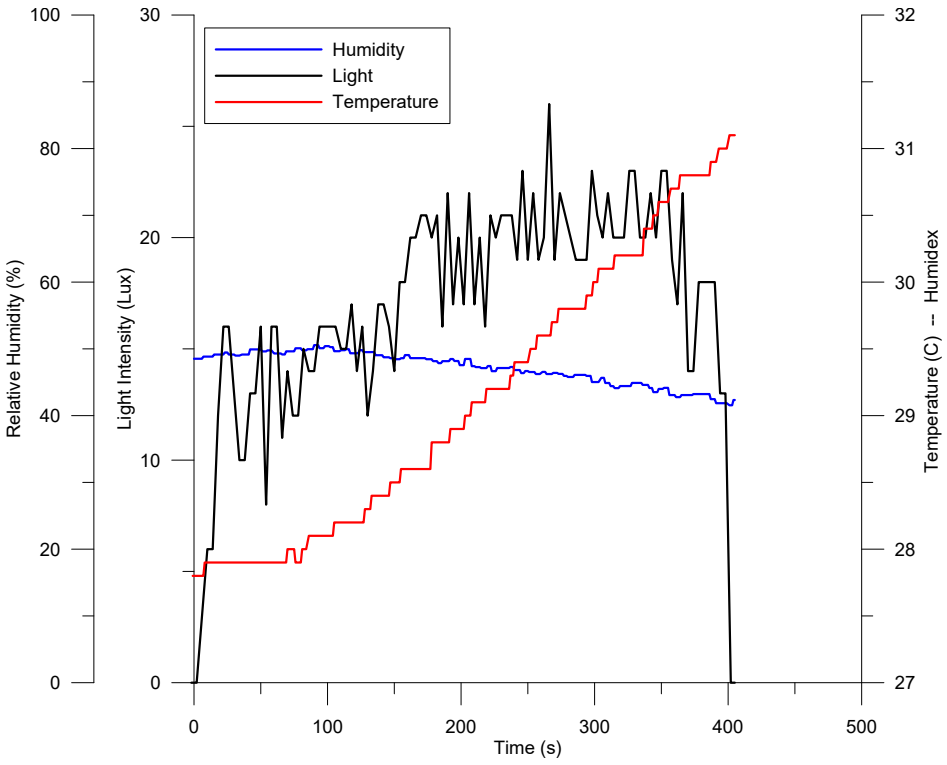


Figure C.110: Test 34 THLP 02

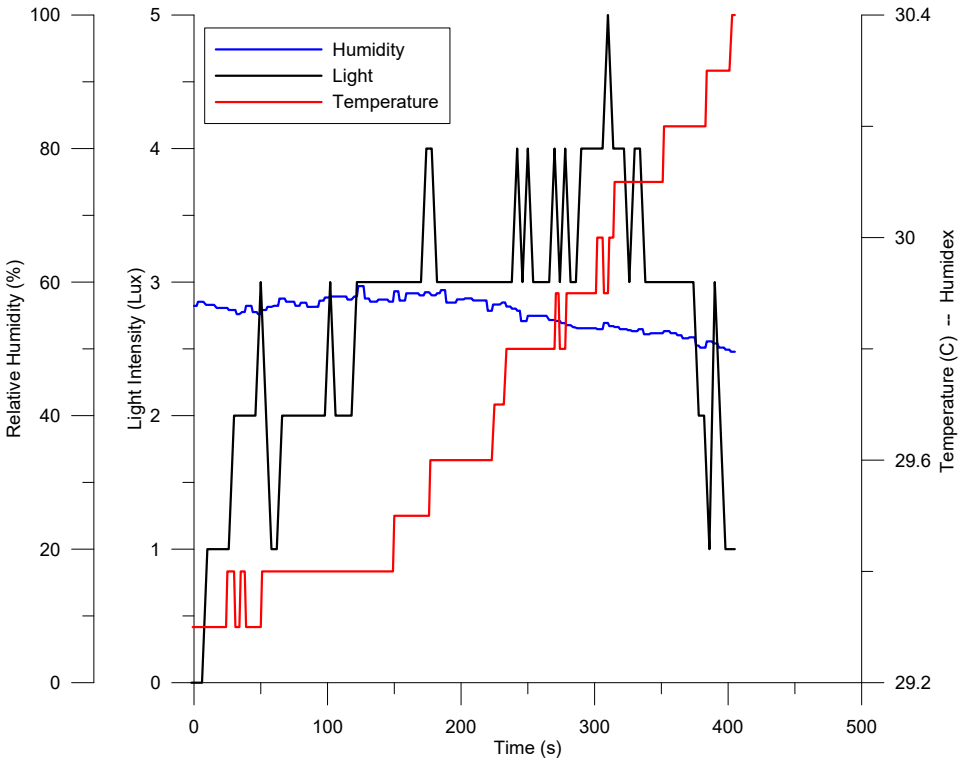


Figure C.111: Test 34 THLP 03

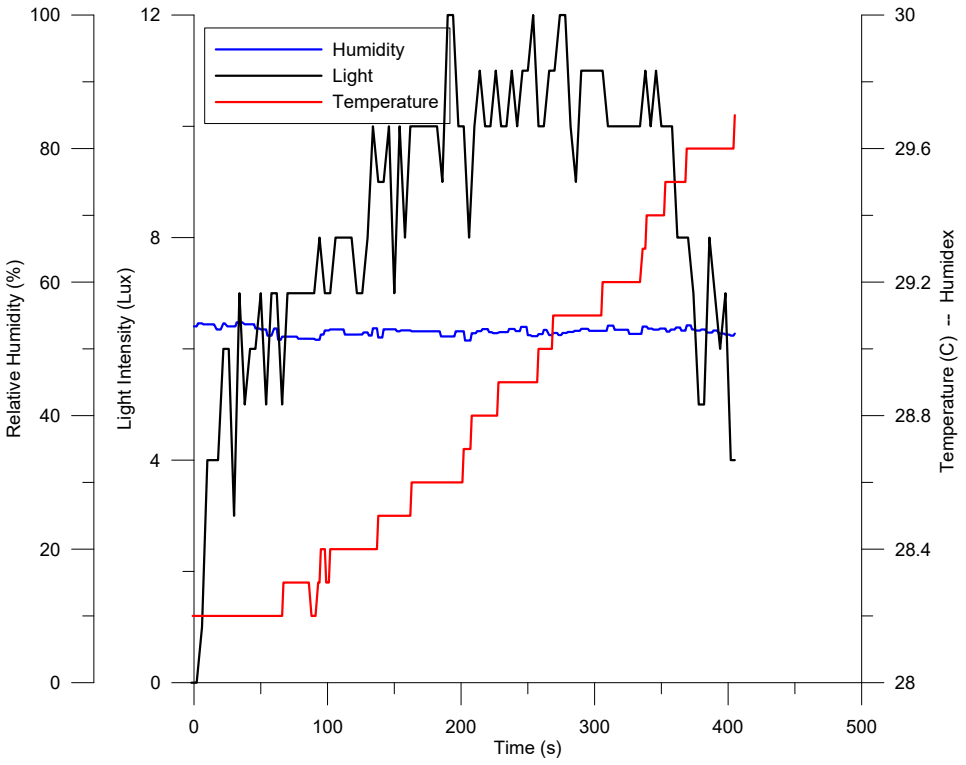


Figure C.112: Test 34 THLP 04

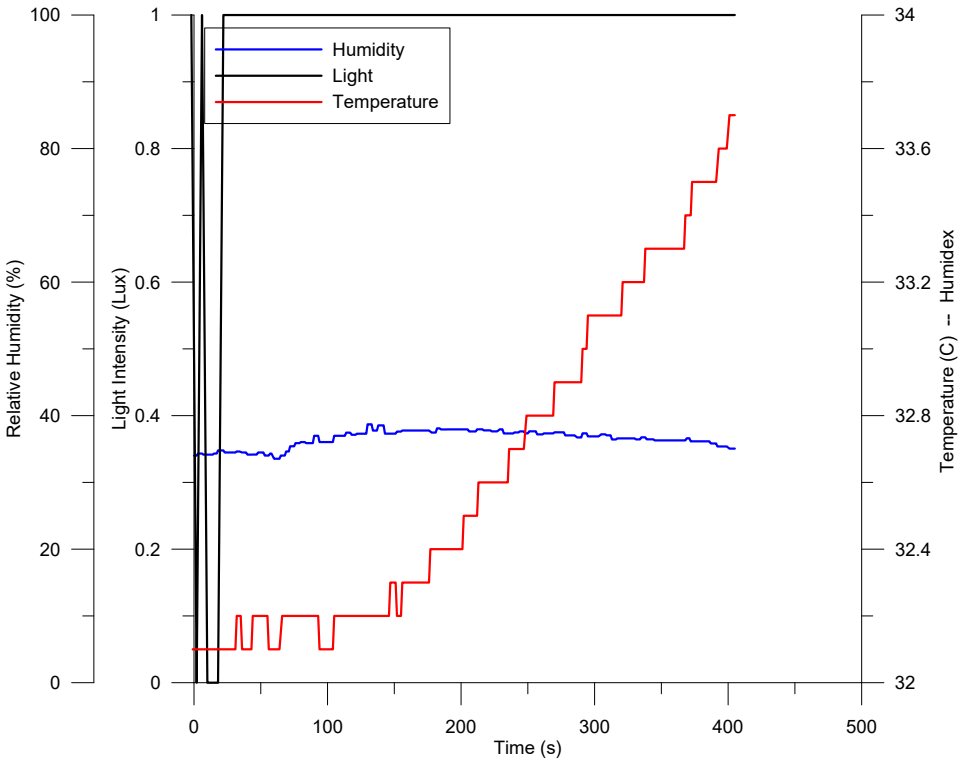


Figure C.113: Test 34 THLP 05

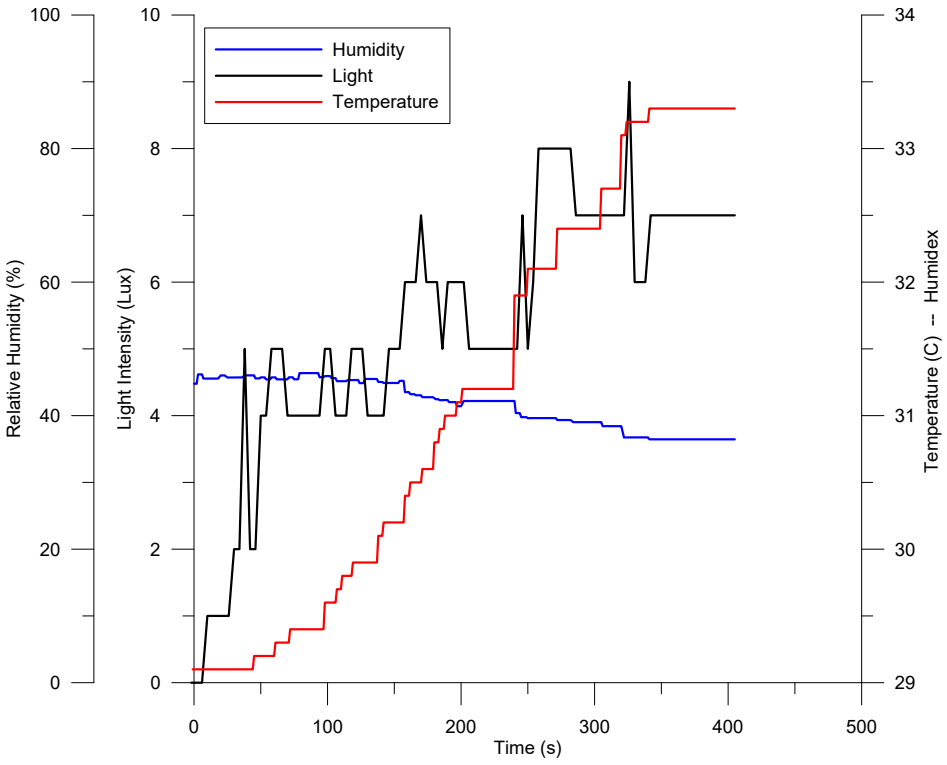


Figure C.114: Test 34 THLP 07

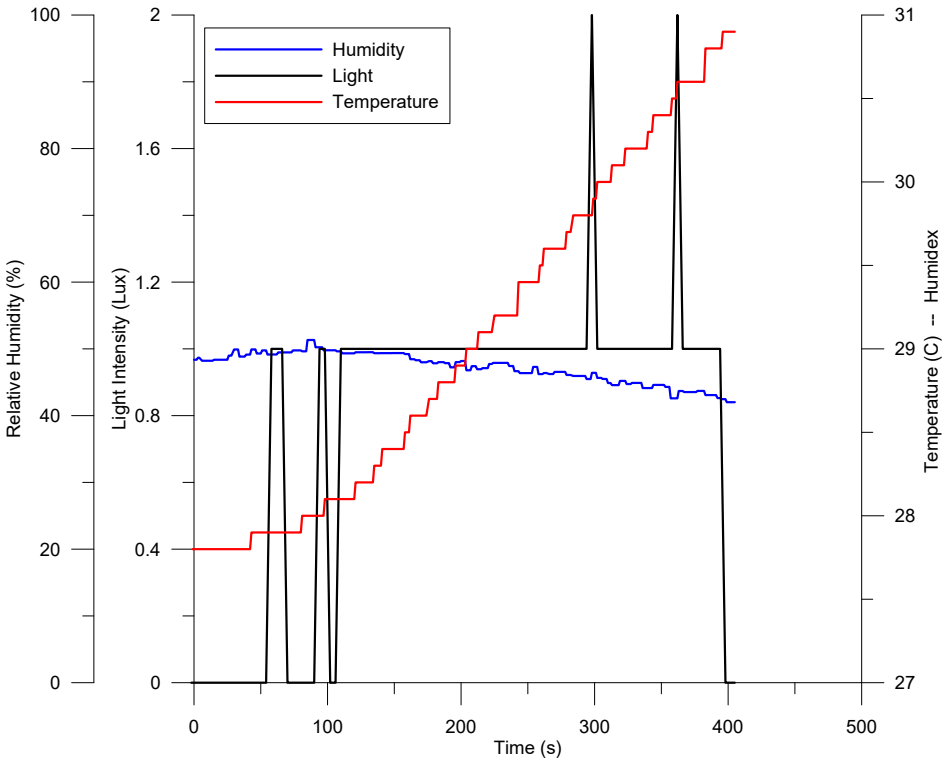


Figure C.115: Test 34 THLP 08

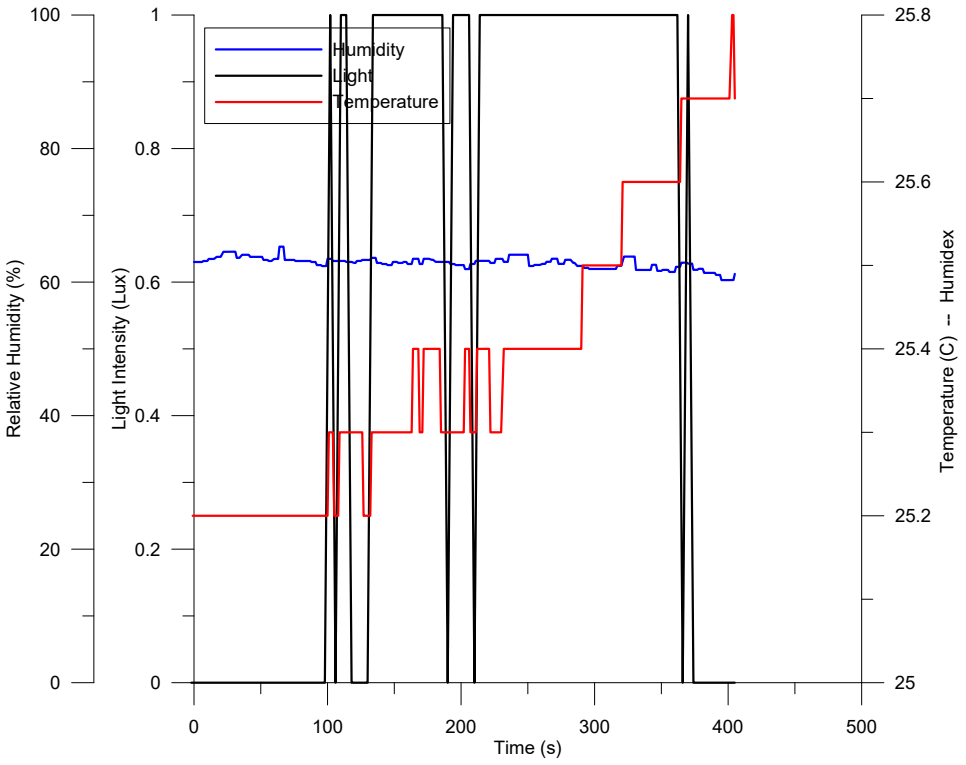


Figure C.116: Test 34 THLP 09

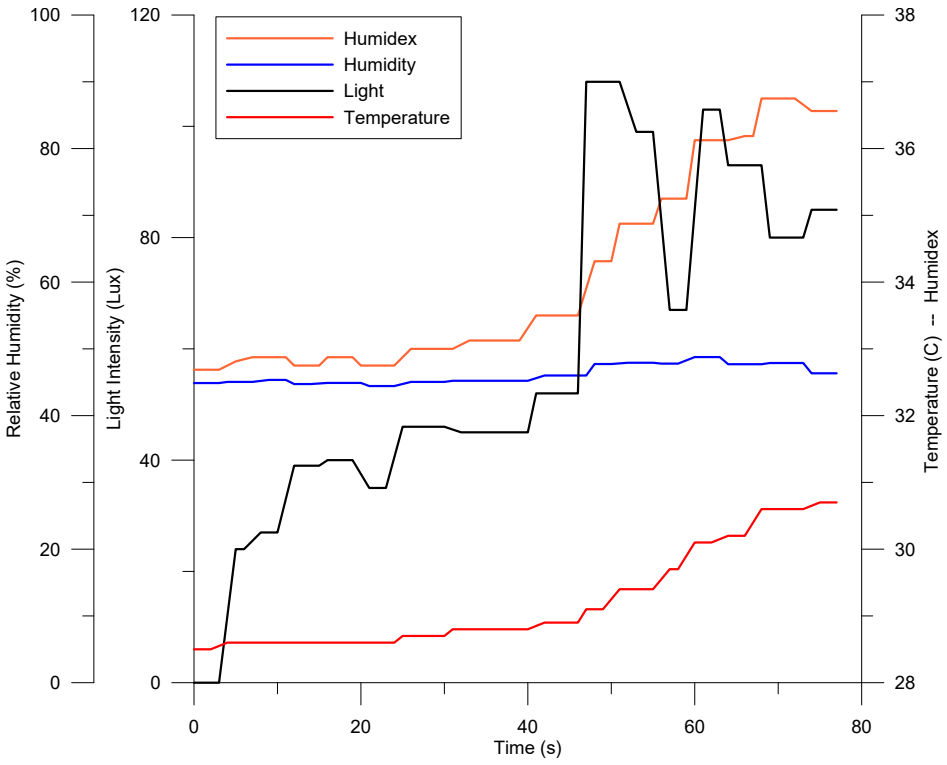


Figure C.117: Test 35 THLP 01

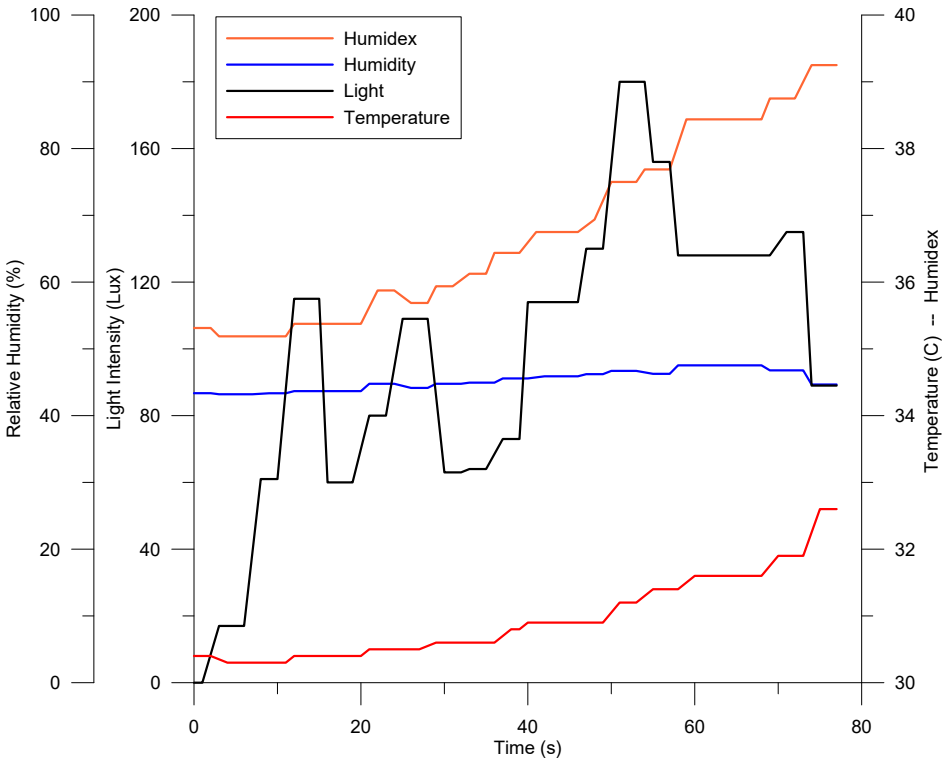


Figure C.118: Test 35 THLP 02

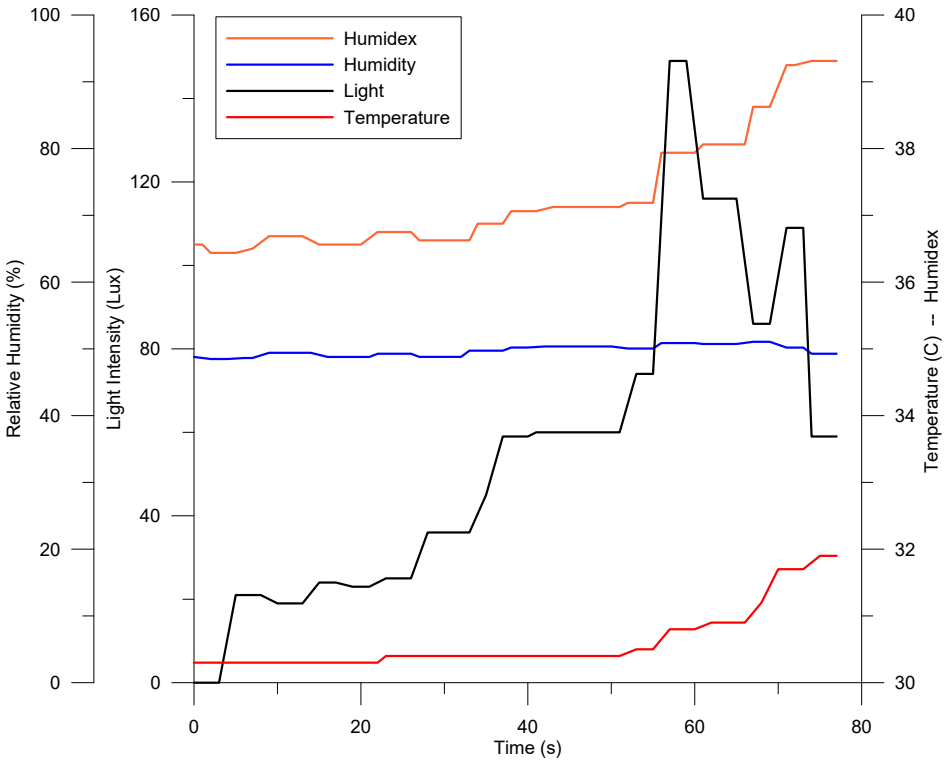


Figure C.119: Test 35 THLP 03

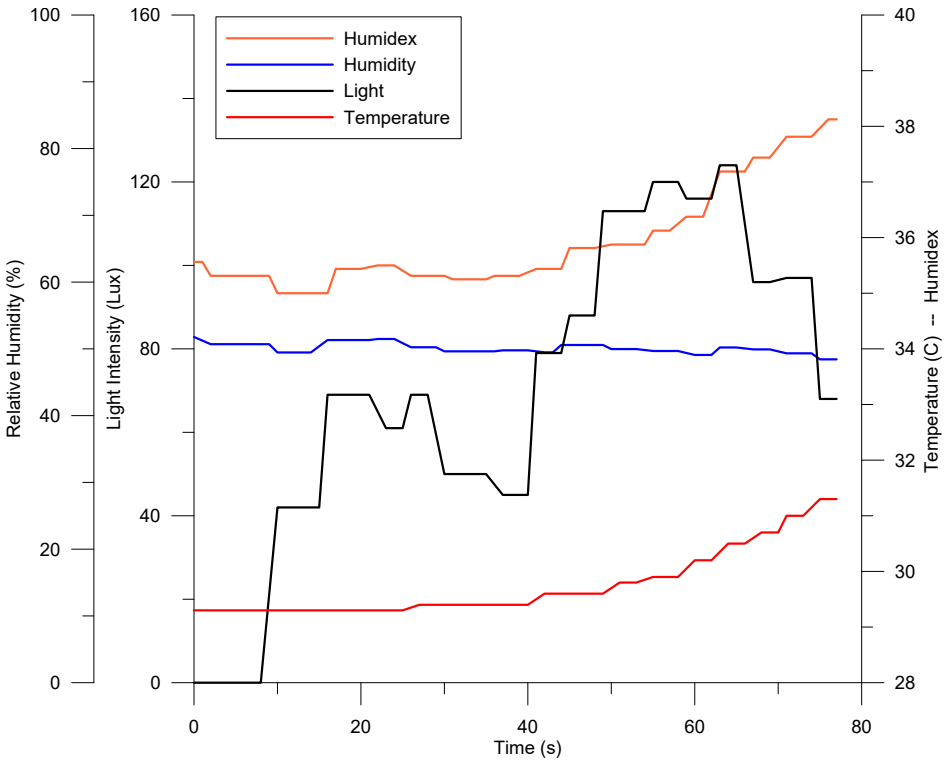


Figure C.120: Test 35 THLP 04

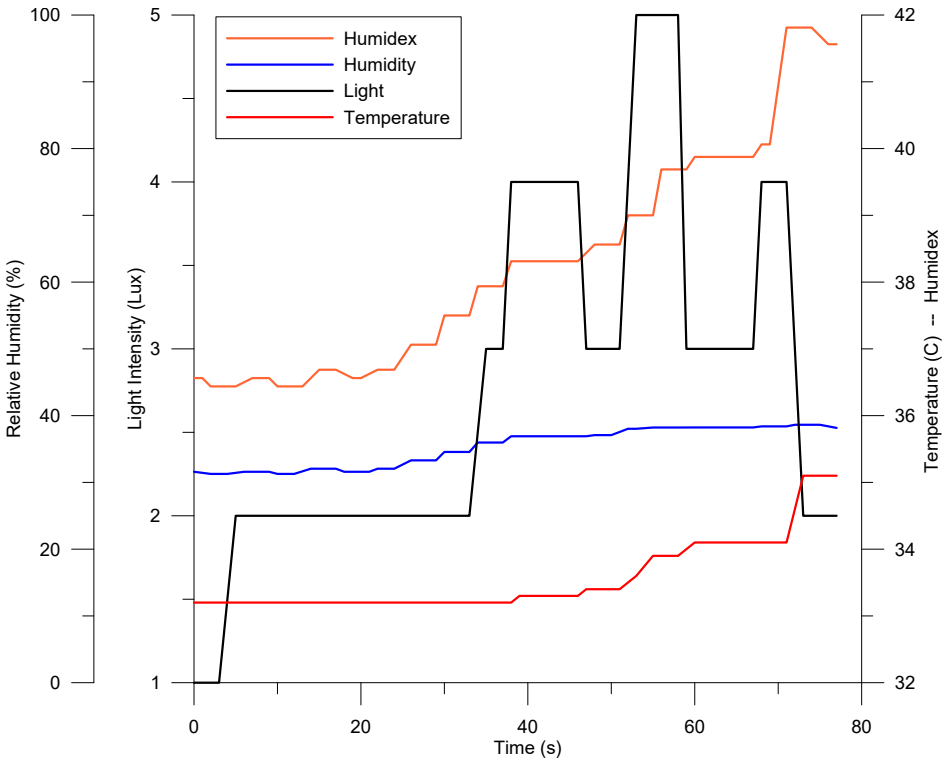


Figure C.121: Test 35 THLP 05

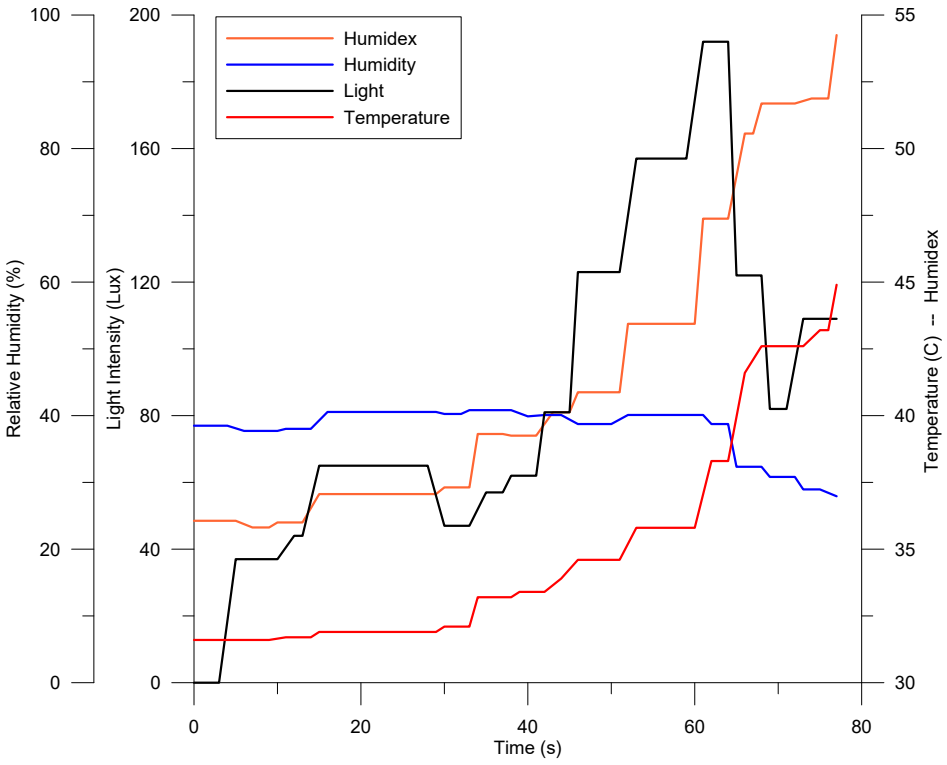


Figure C.122: Test 35 THLP 07

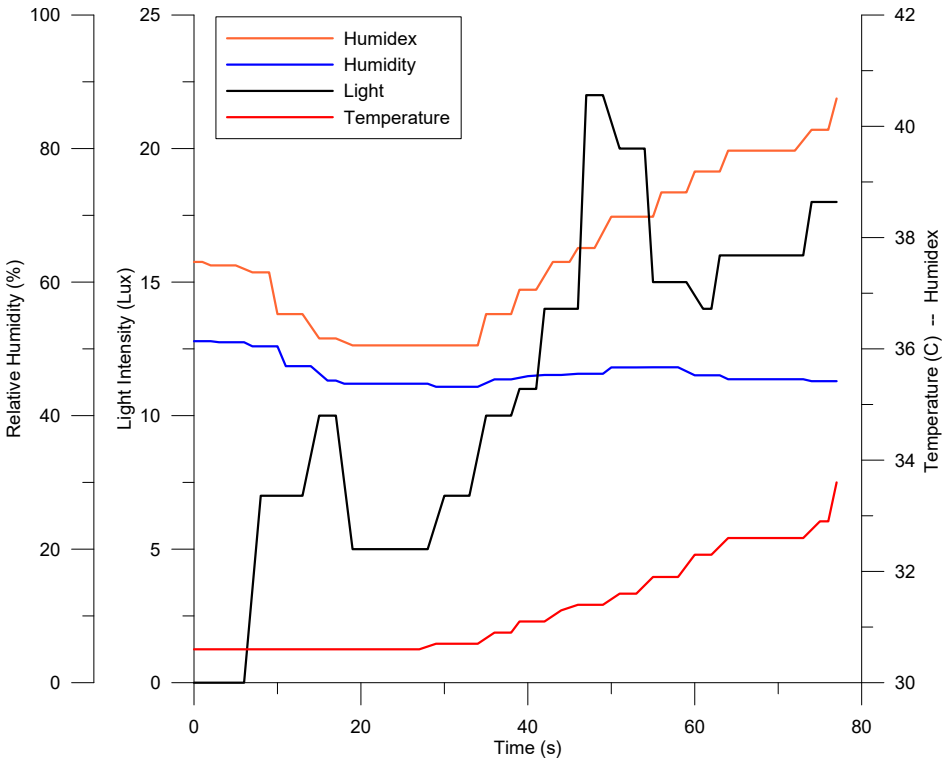


Figure C.123: Test 35 THLP 08

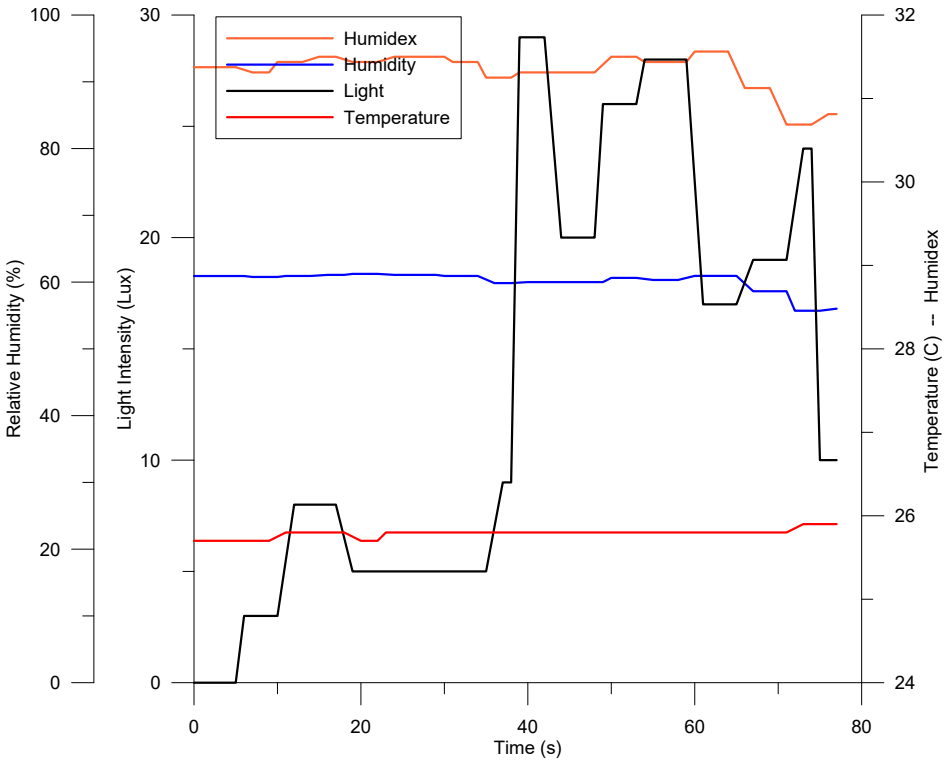


Figure C.124: Test 35 THLP 09

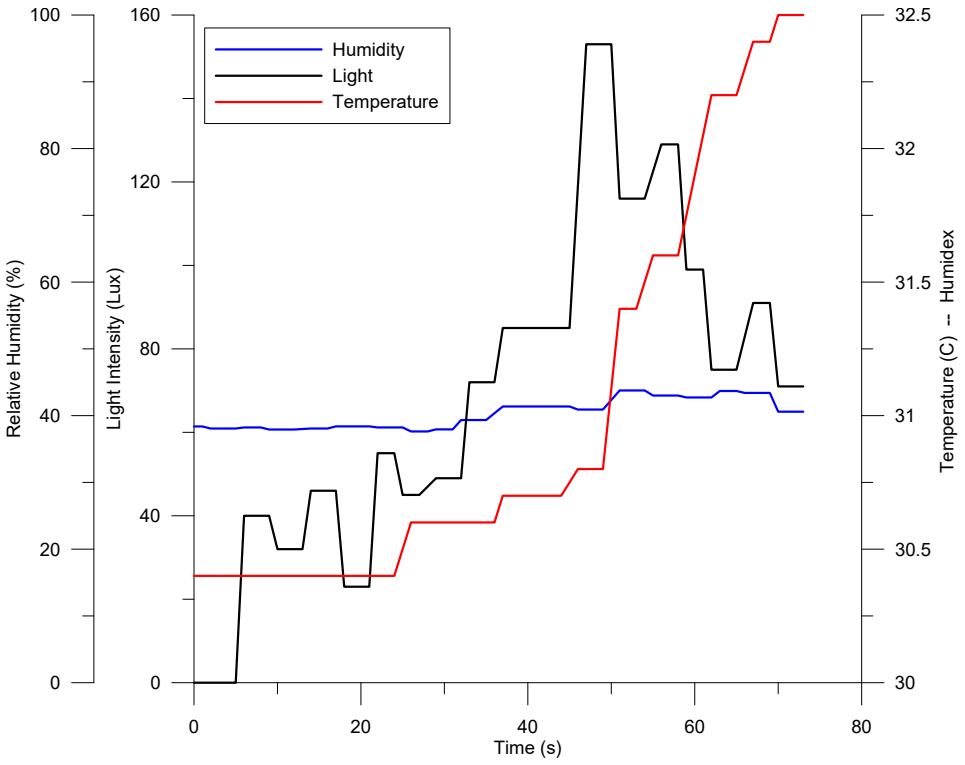


Figure C.125: Test 36 THLP 01

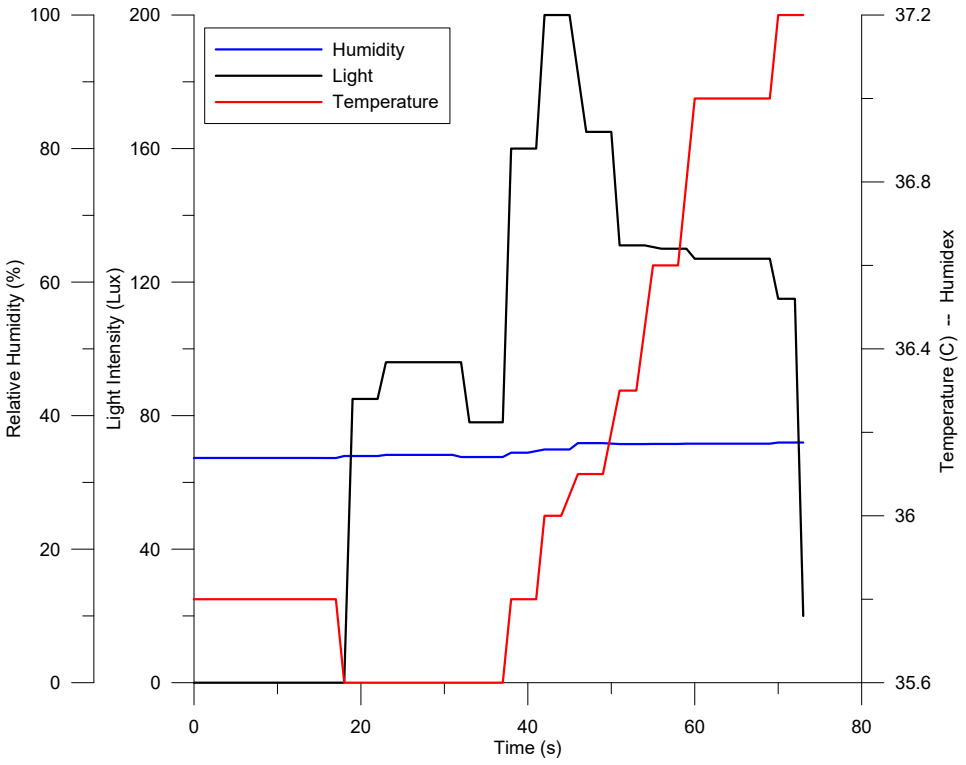


Figure C.126: Test 36 THLP 02

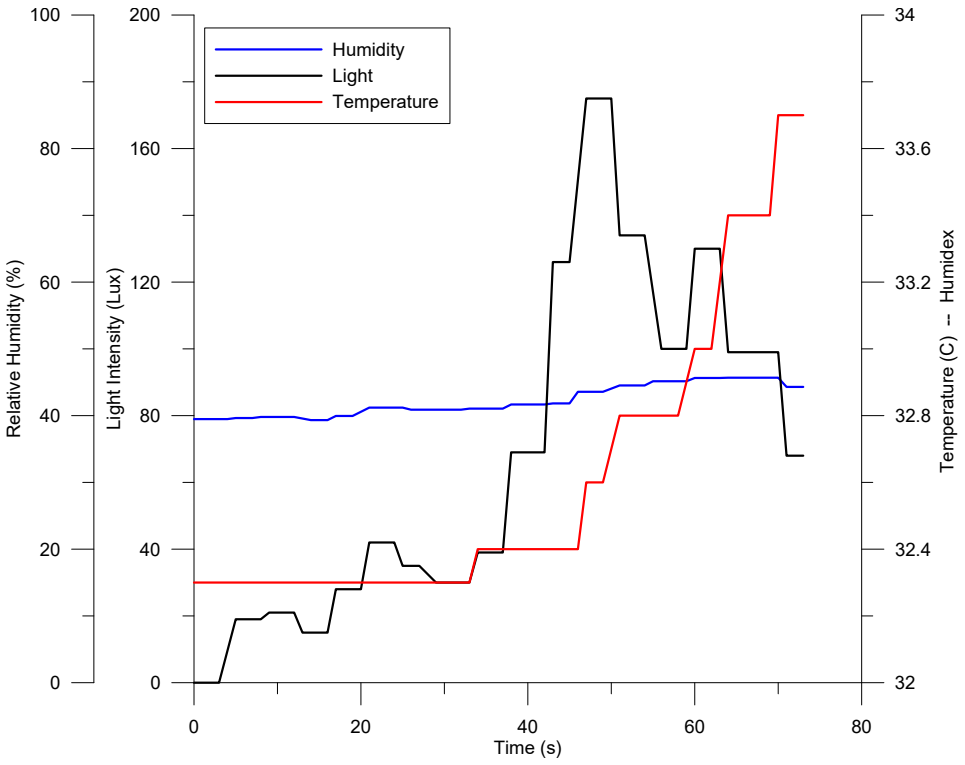


Figure C.127: Test 36 THLP 03

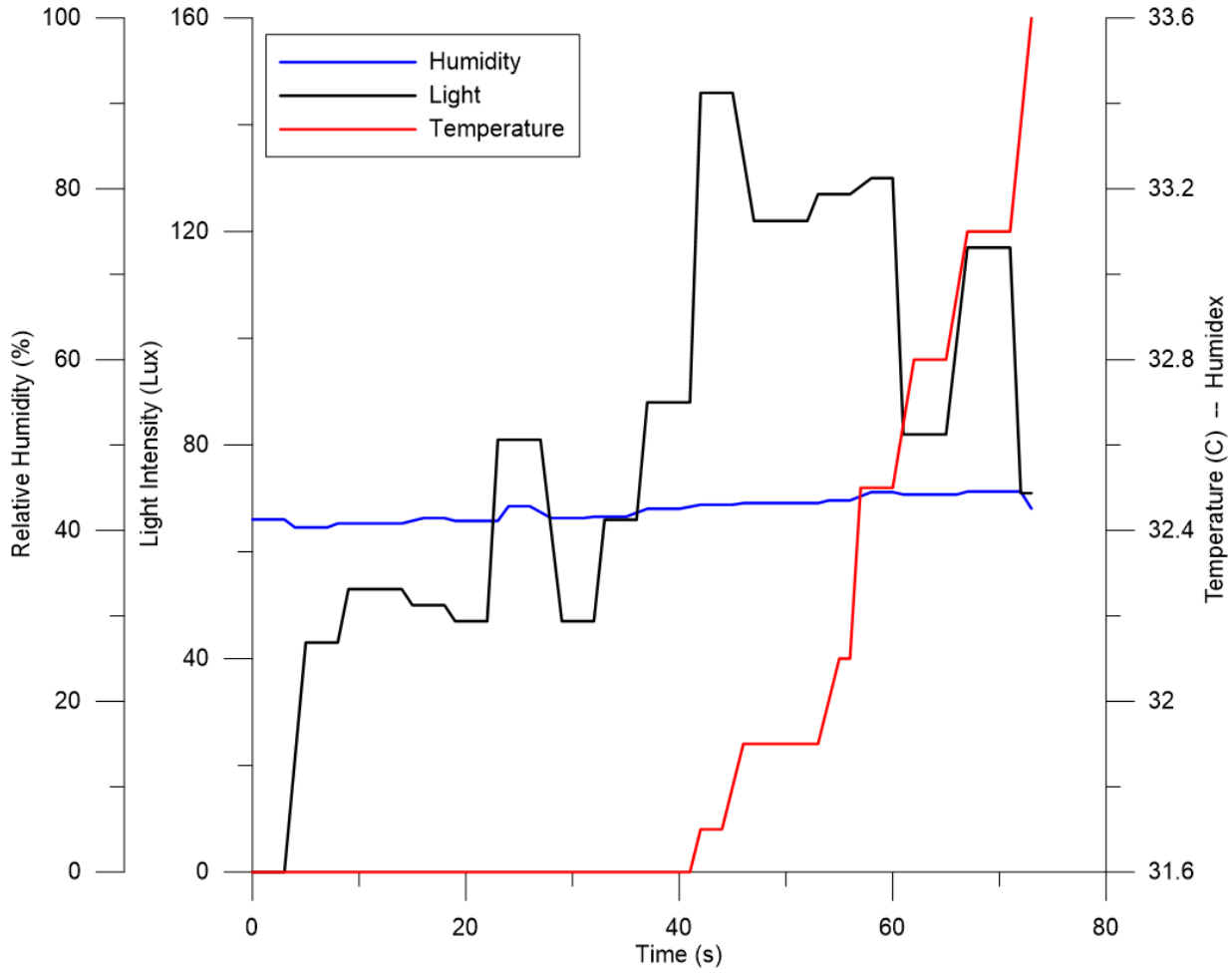


Figure C.128: Test 36 THLP 04

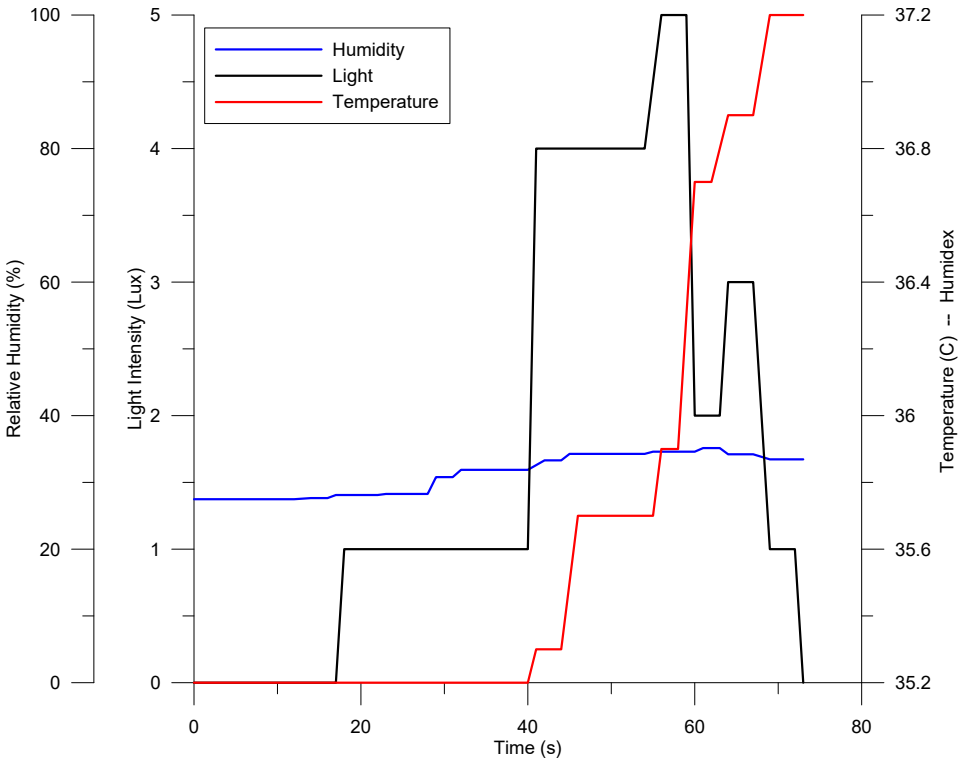


Figure C.129: Test 36 THLP 05

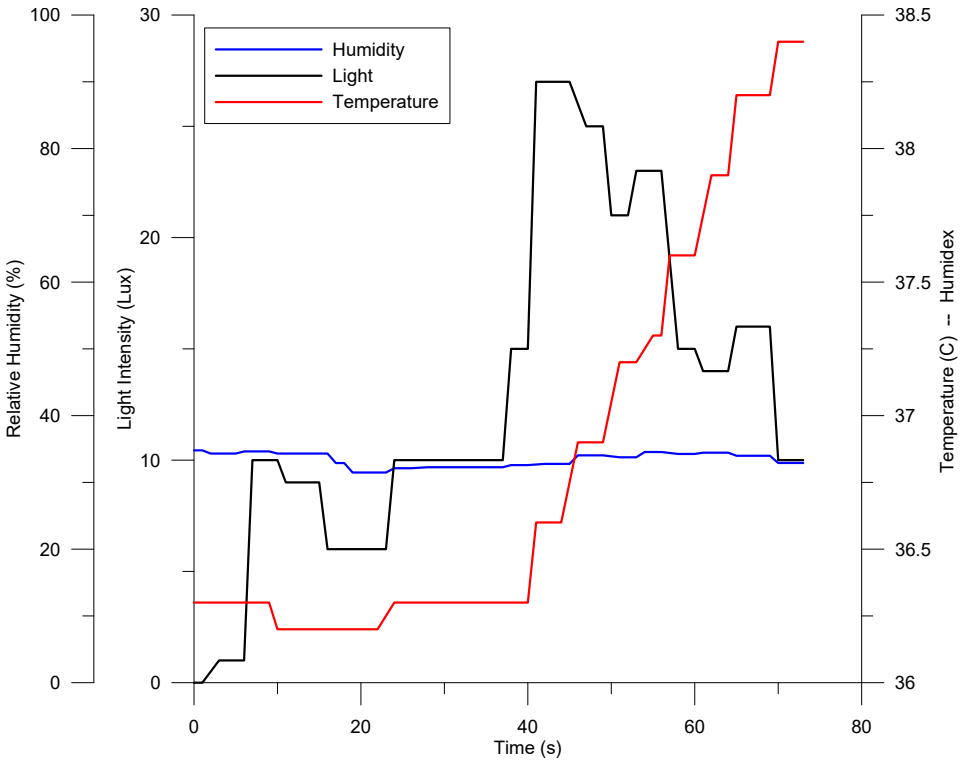


Figure C.130: Test 36 THLP 08

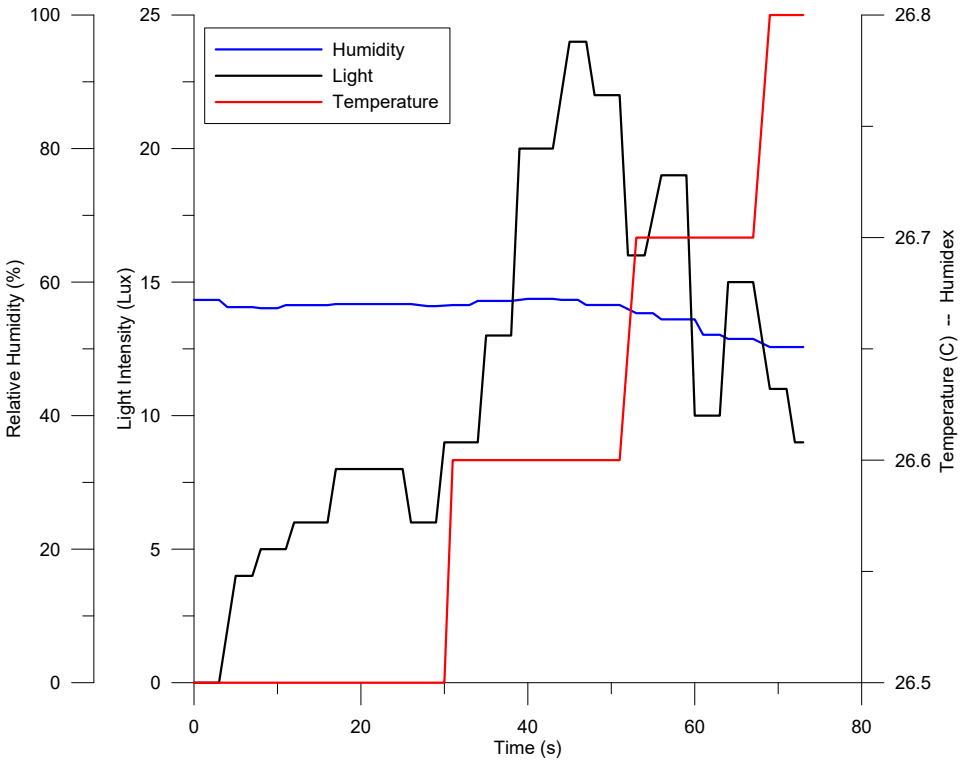


Figure C.131: Test 36 THLP 09

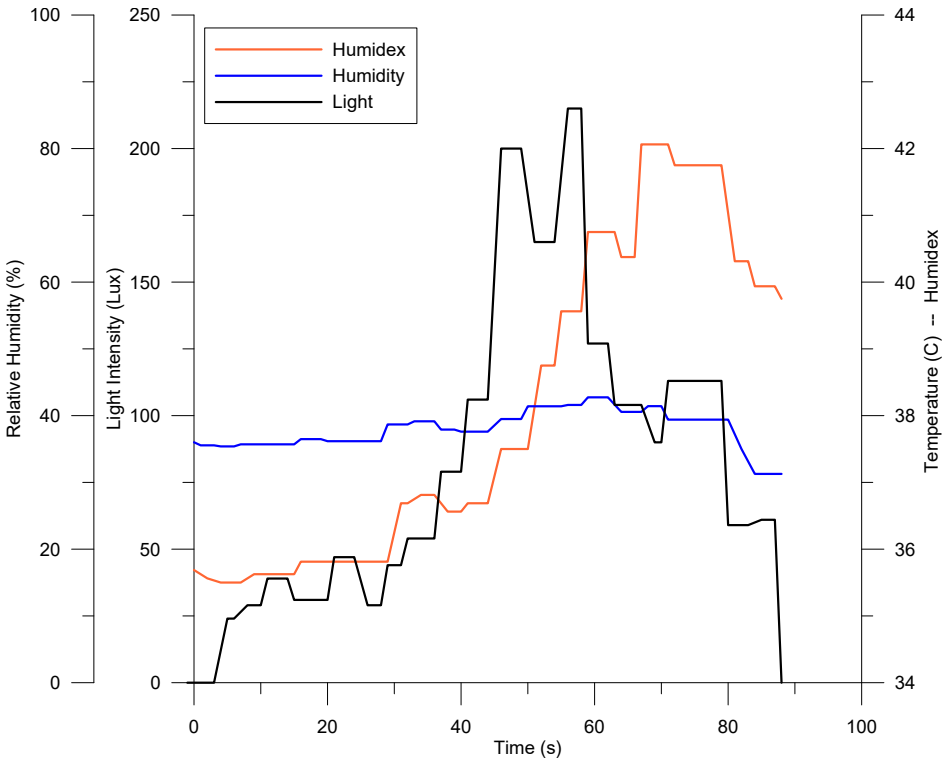


Figure C.132: Test 37 THLP 01

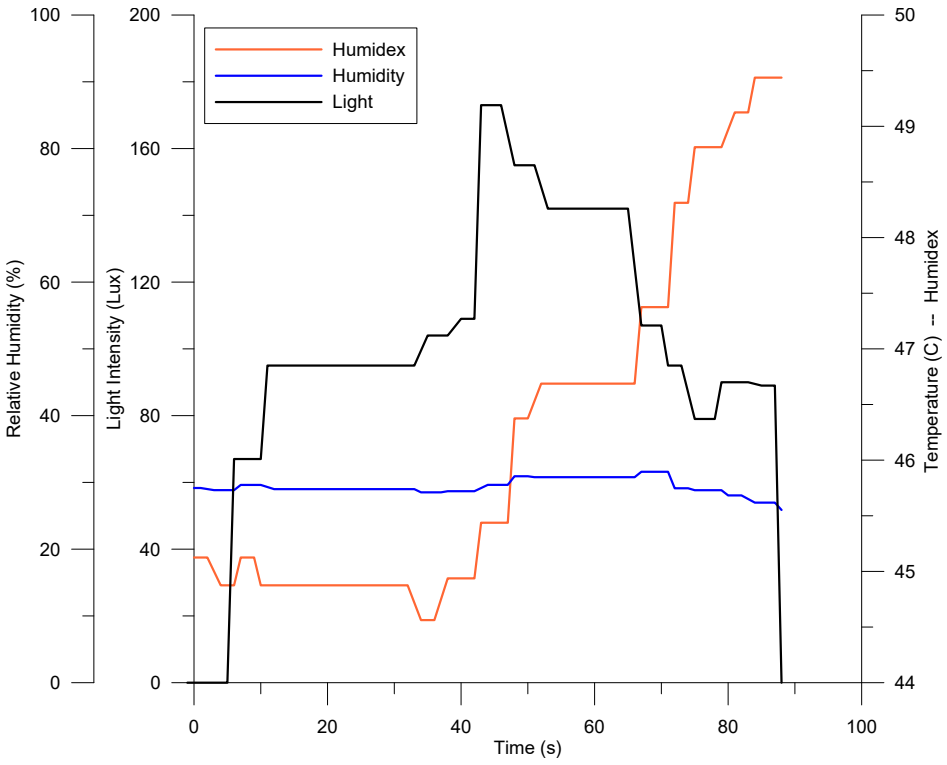


Figure C.133: Test 37 THLP 02

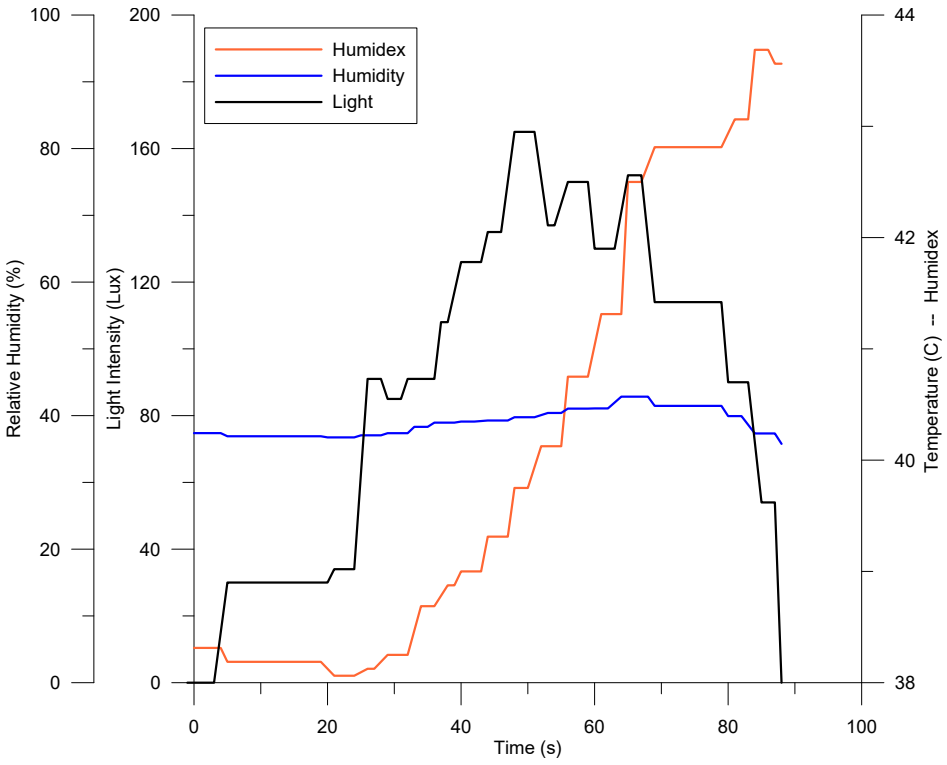


Figure C.134: Test 37 THLP 04

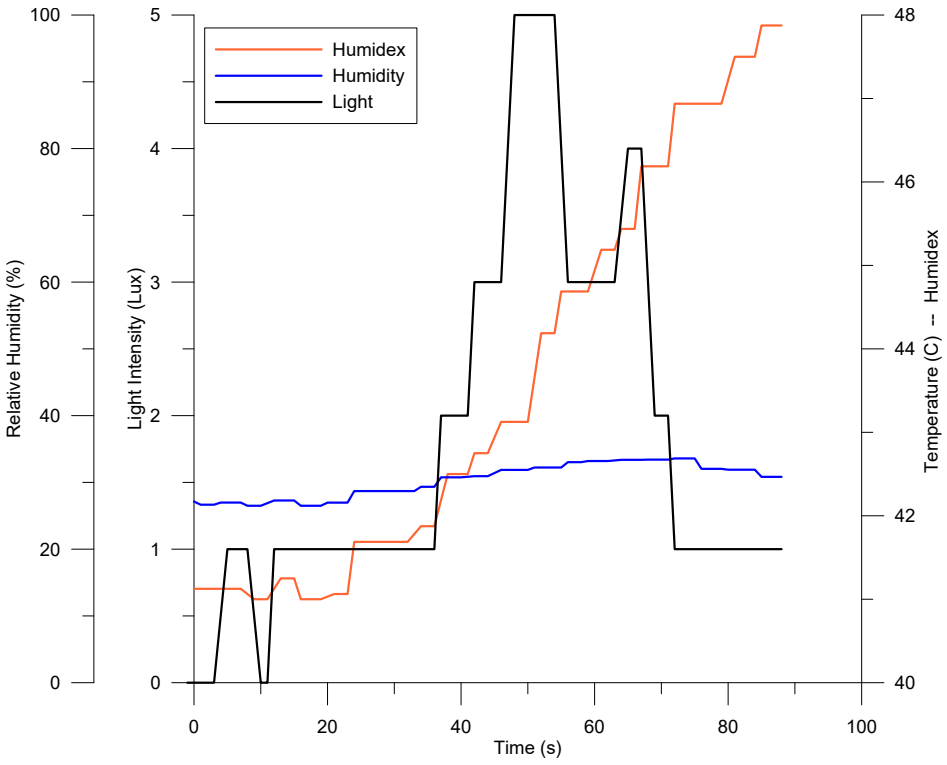


Figure C.135: Test 37 THLP 05

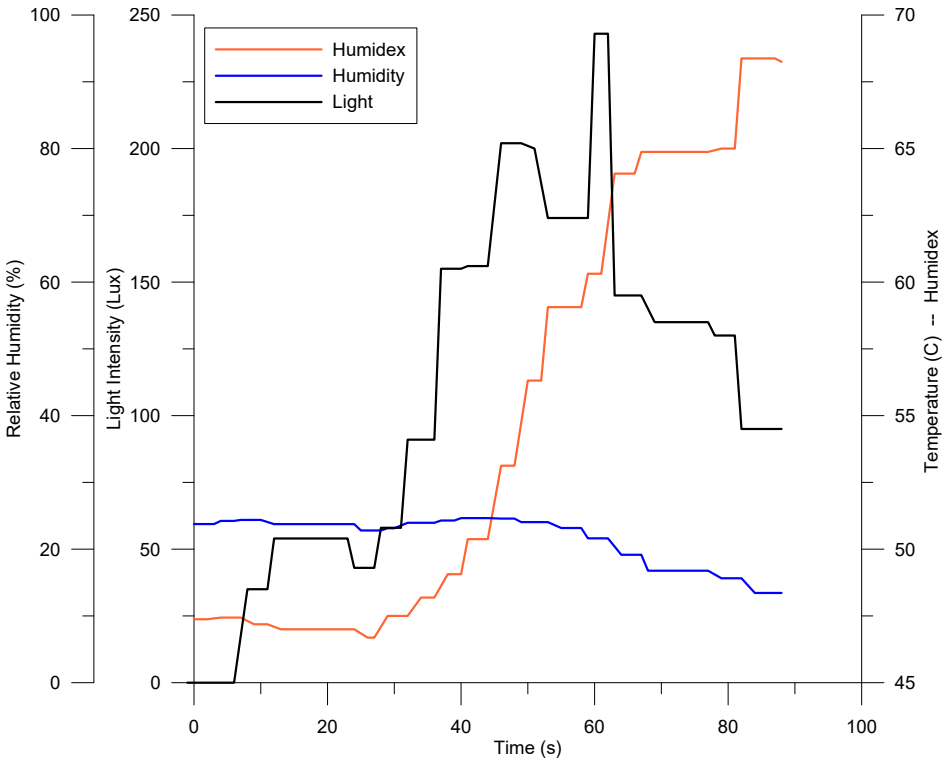


Figure C.136: Test 37 THLP 07

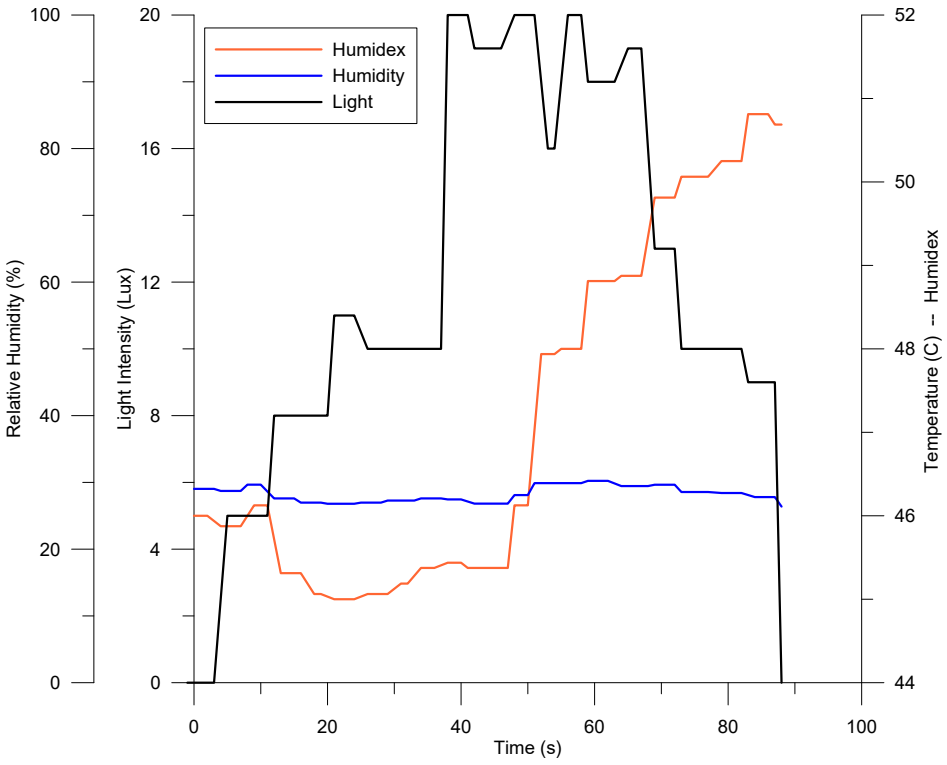


Figure C.137: Test 37 THLP 08

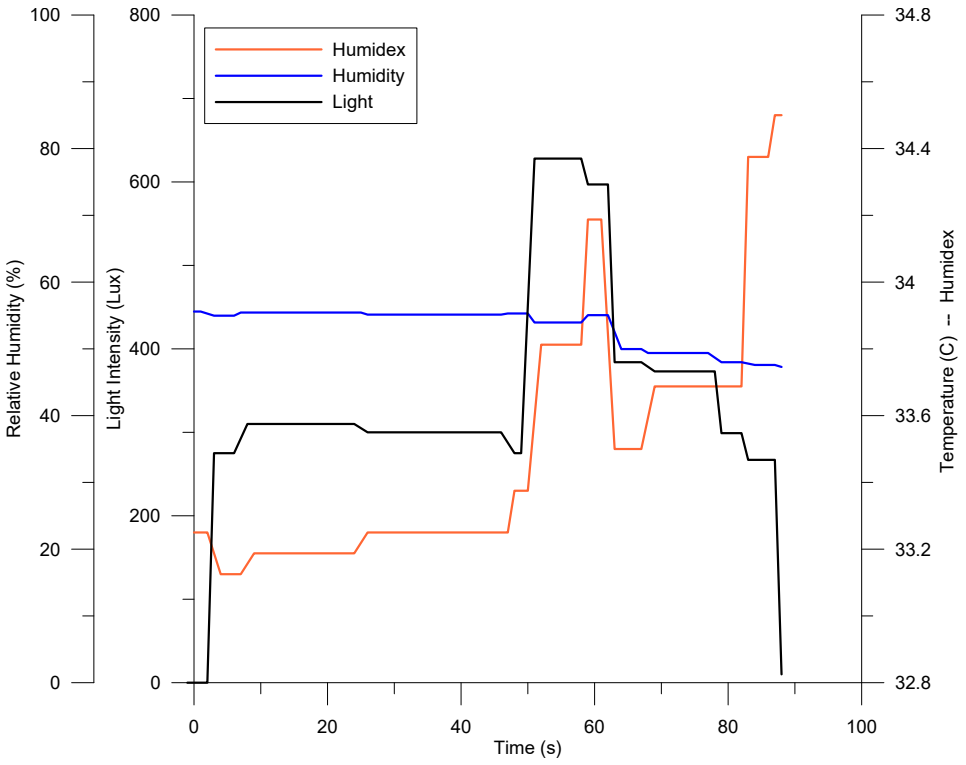


Figure C.138: Test 37 THLP 09

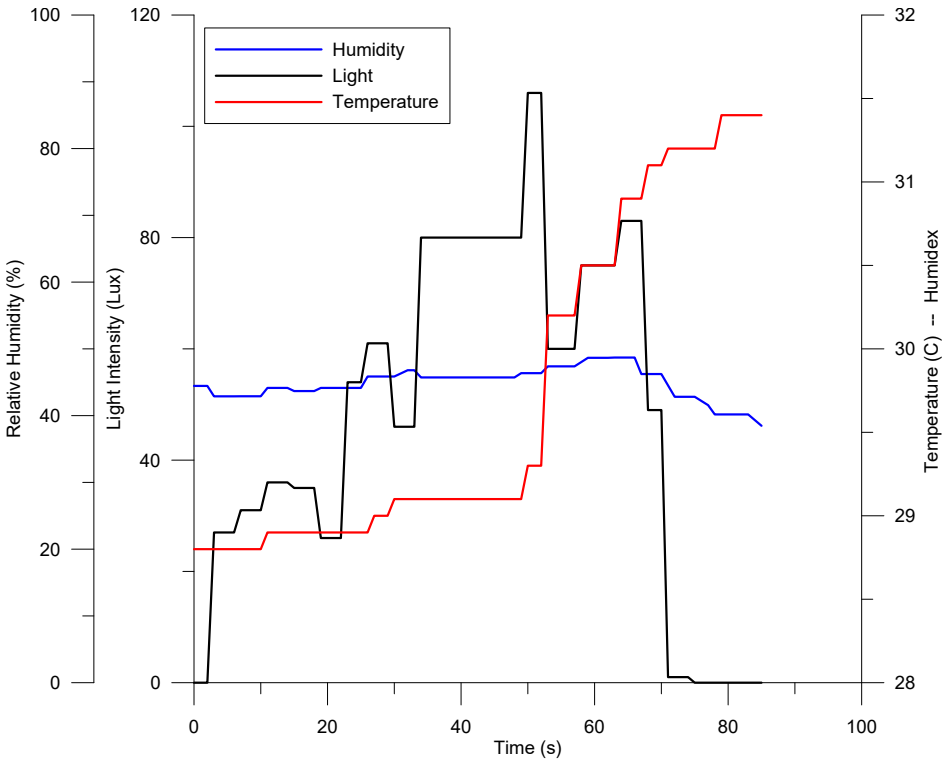


Figure C.139: Test 38 THLP 01

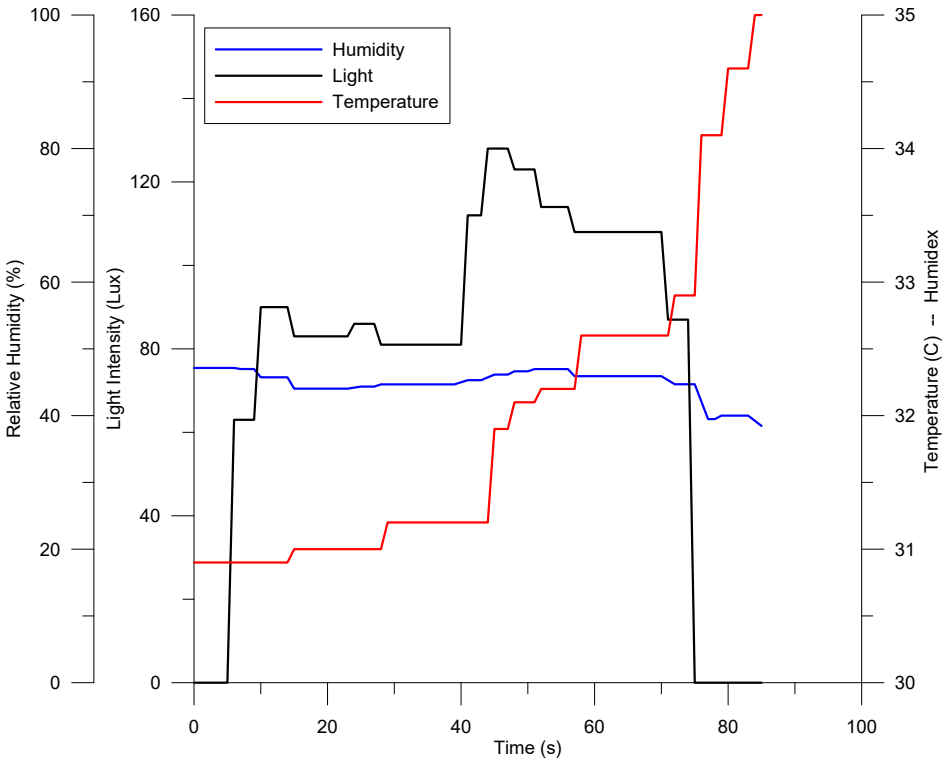


Figure C.140: Test 38 THLP 02

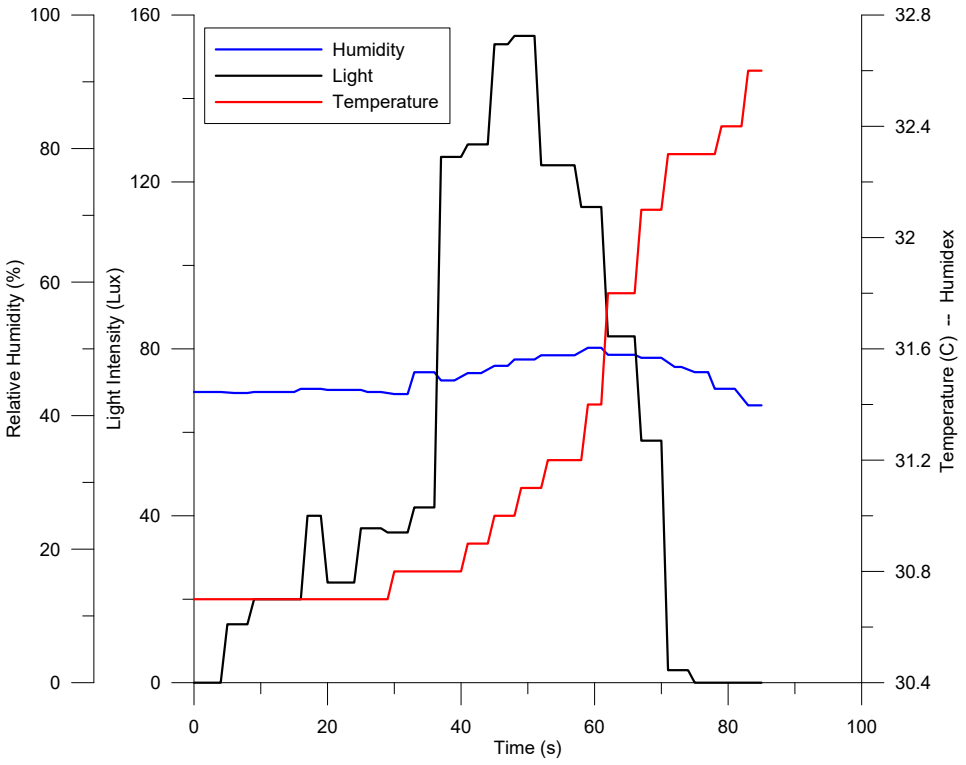


Figure C.141: Test 38 THLP 03

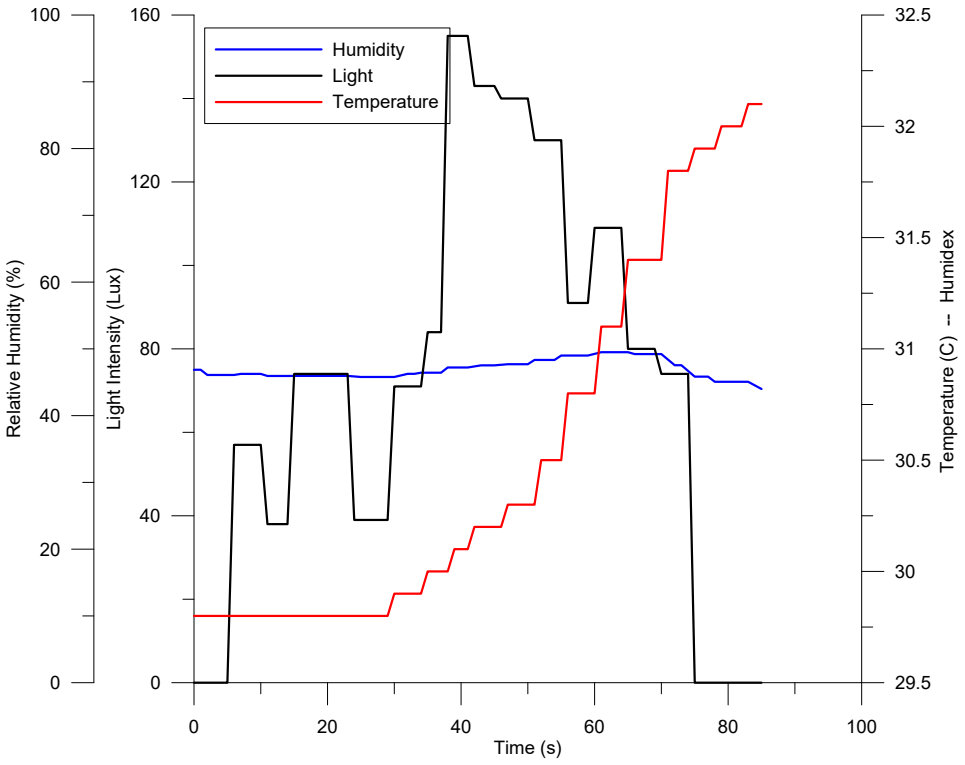


Figure C.142: Test 38 THLP 04

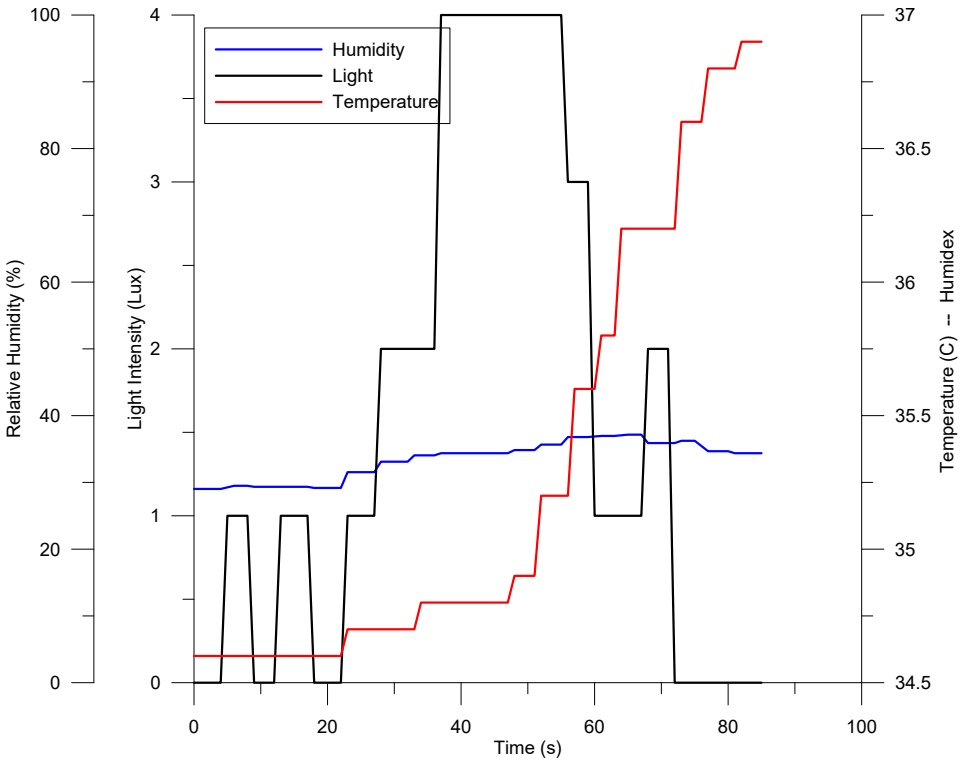


Figure C.143: Test 38 THLP 05

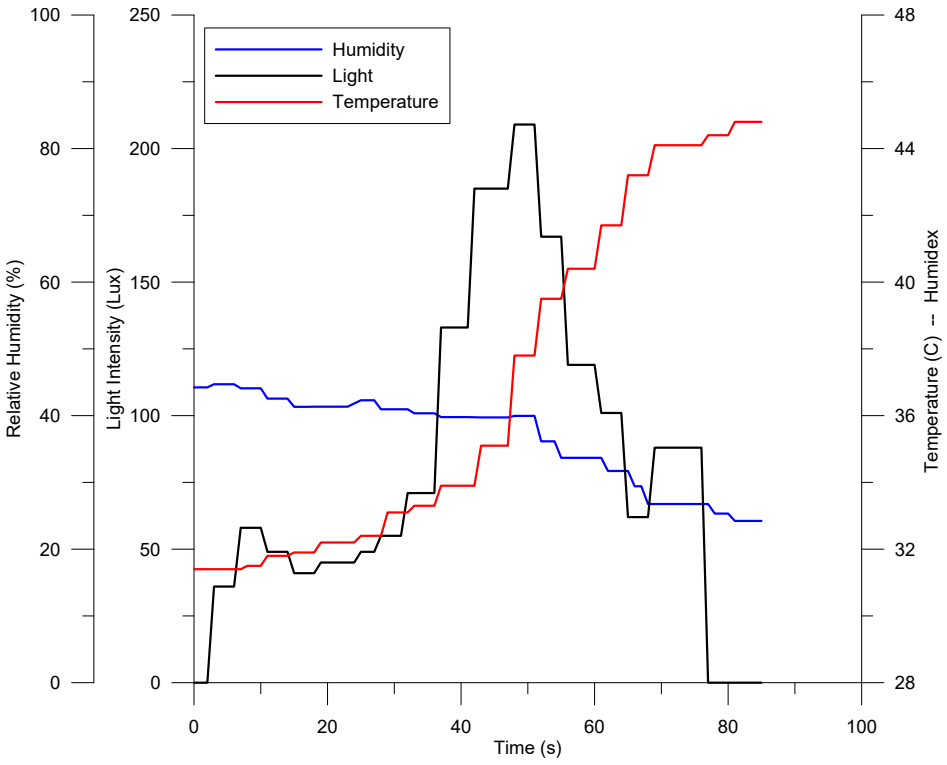


Figure C.144: Test 38 THLP 07

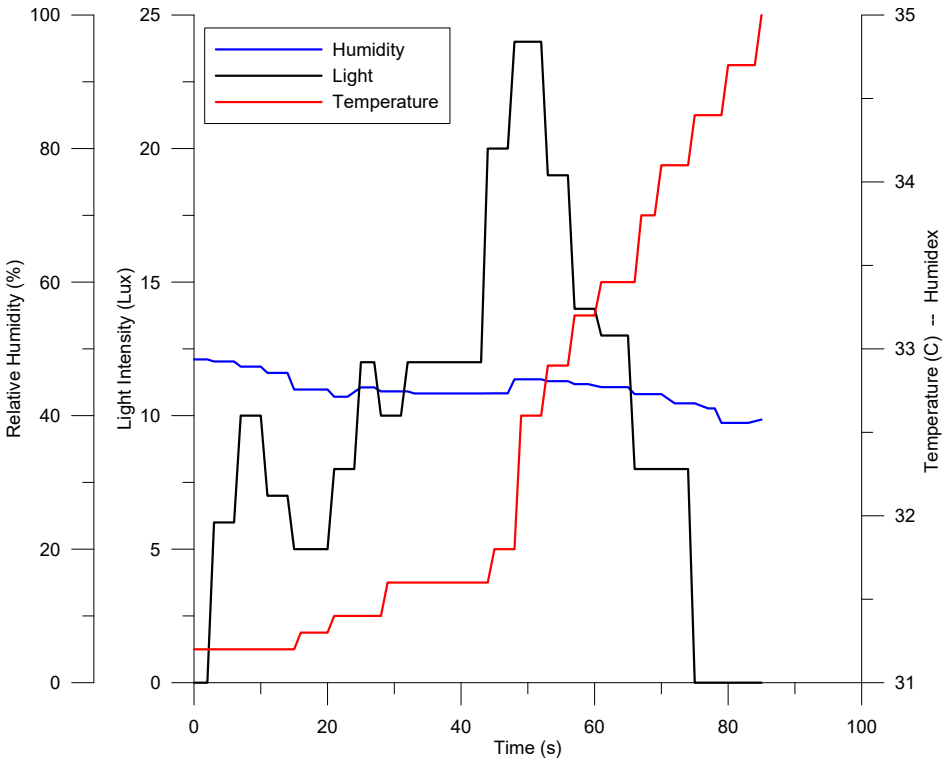


Figure C.145: Test 38 THLP 08

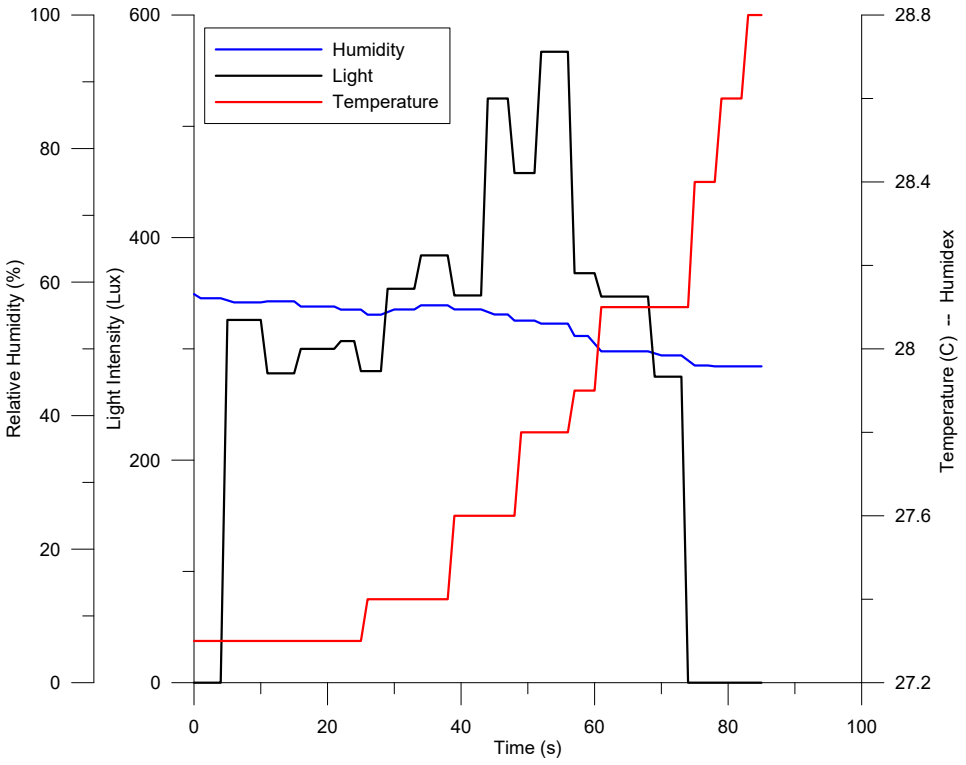


Figure C.146: Test 38 THLP 09

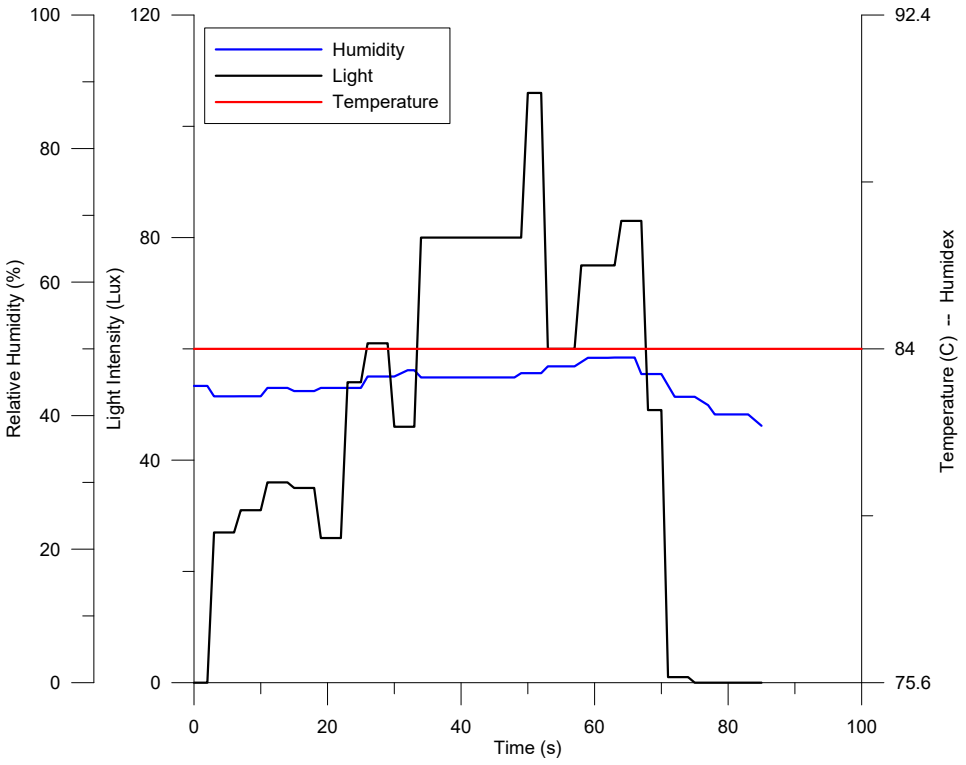


Figure C.147: Test 42 THLP 01

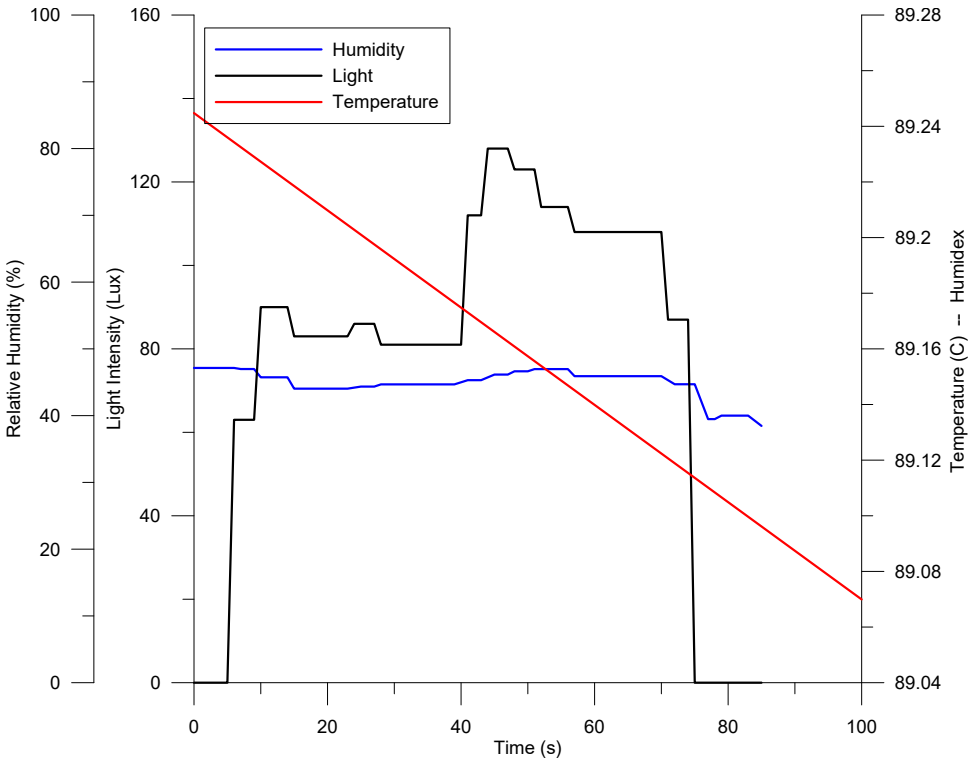


Figure C.148: Test 42 THLP 02

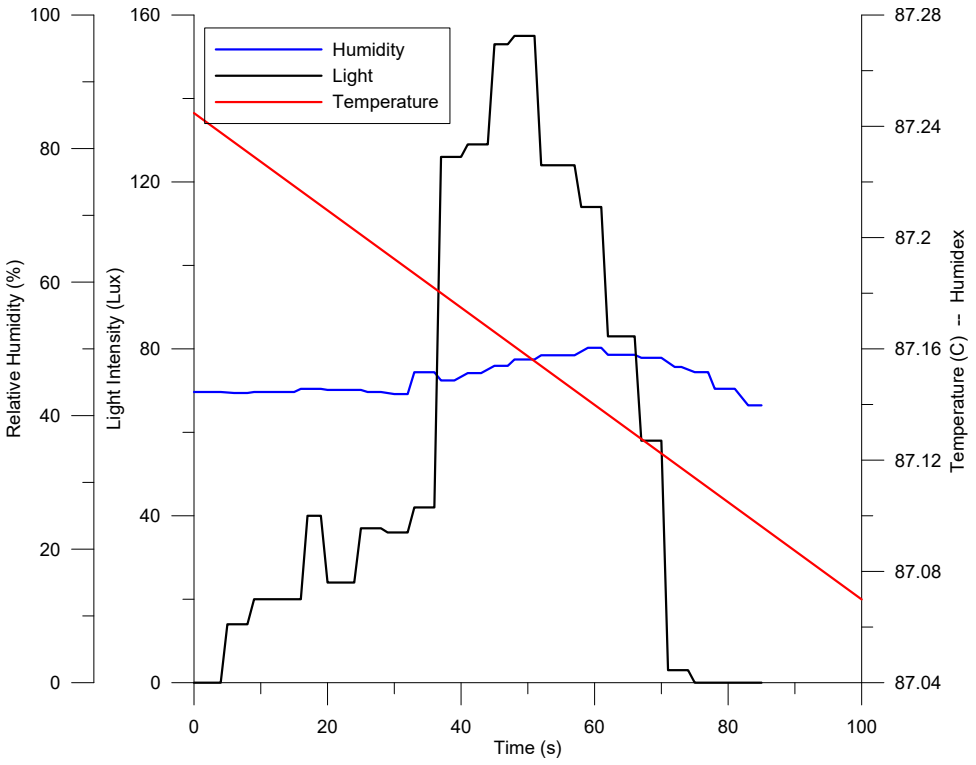


Figure C.149: Test 42 THLP 03

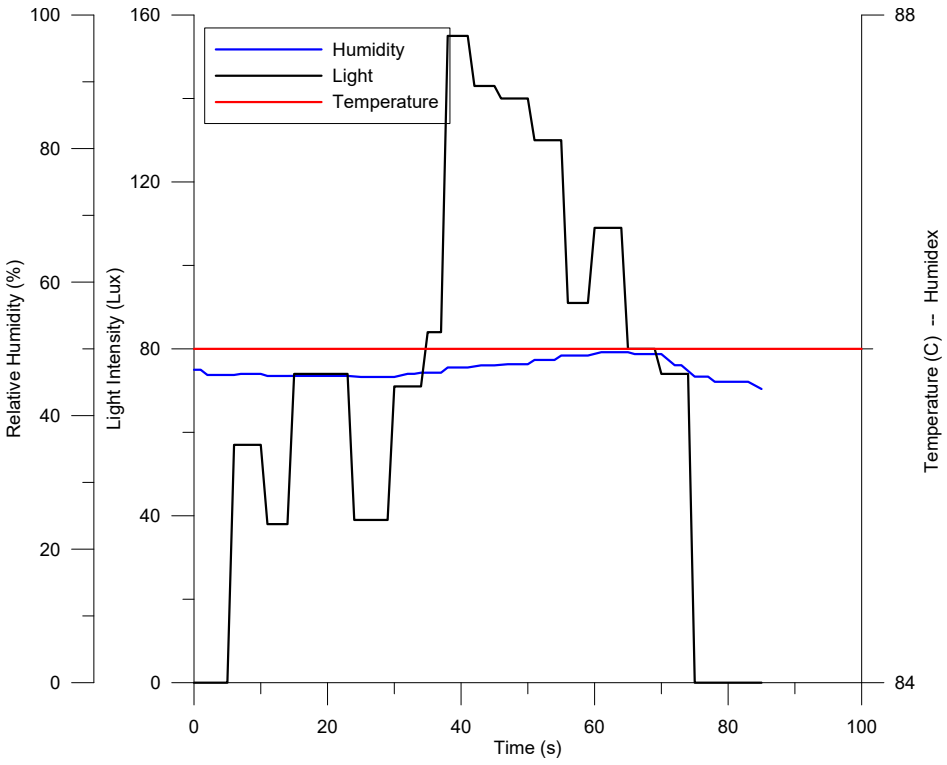


Figure C.150: Test 42 THLP 04

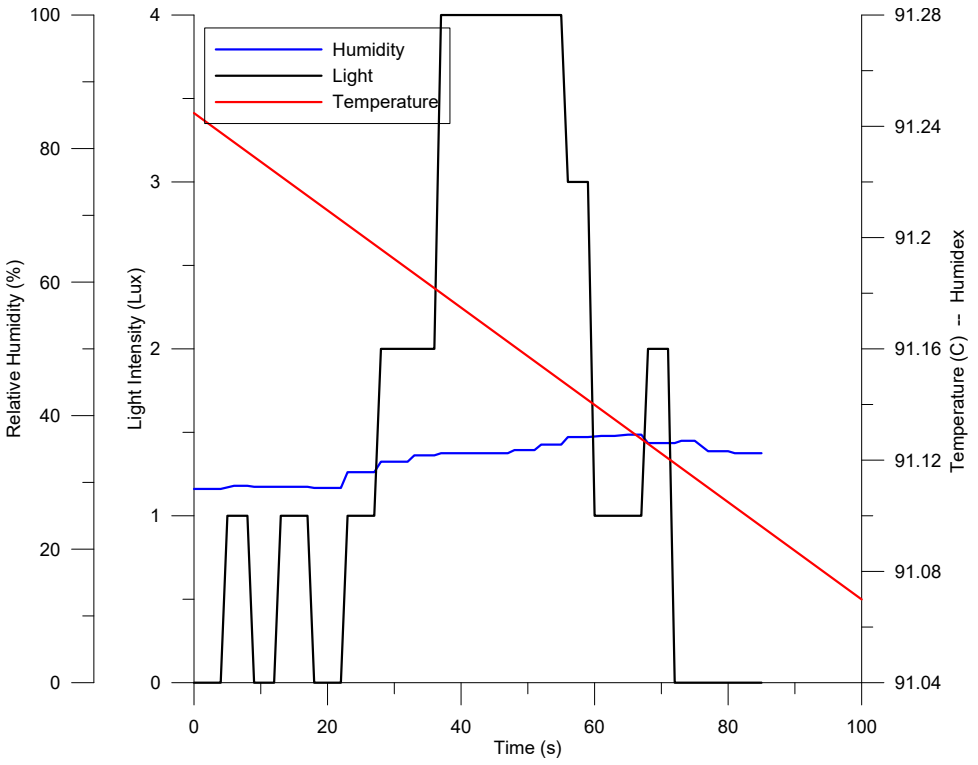


Figure C.151: Test 42 THLP 05

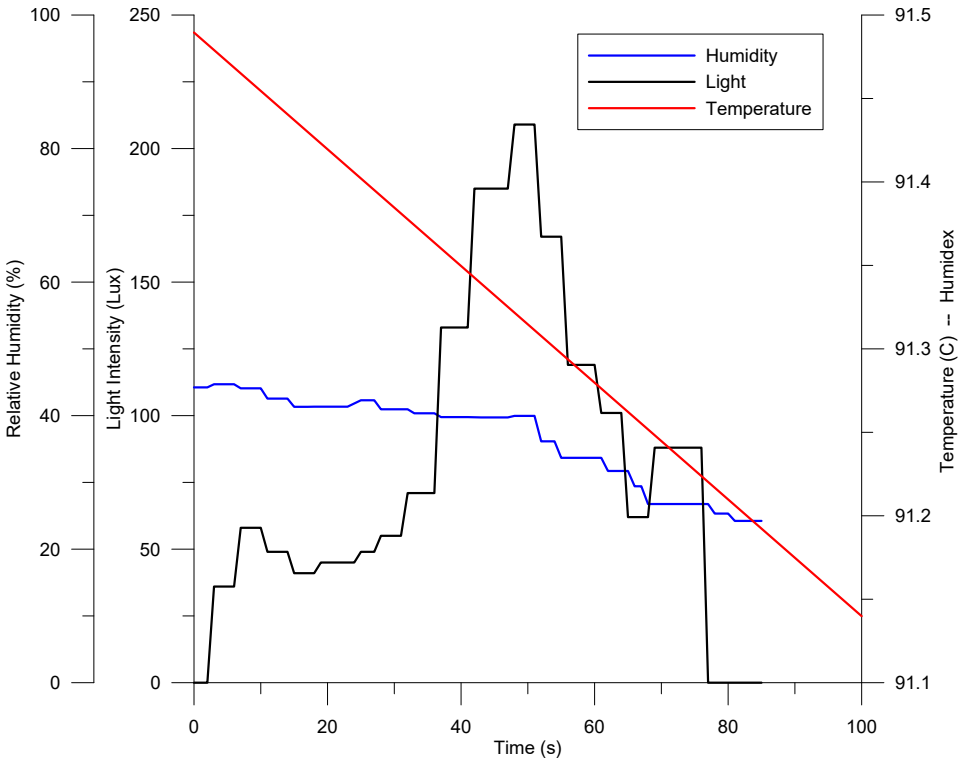


Figure C.152: Test 42 THLP 07

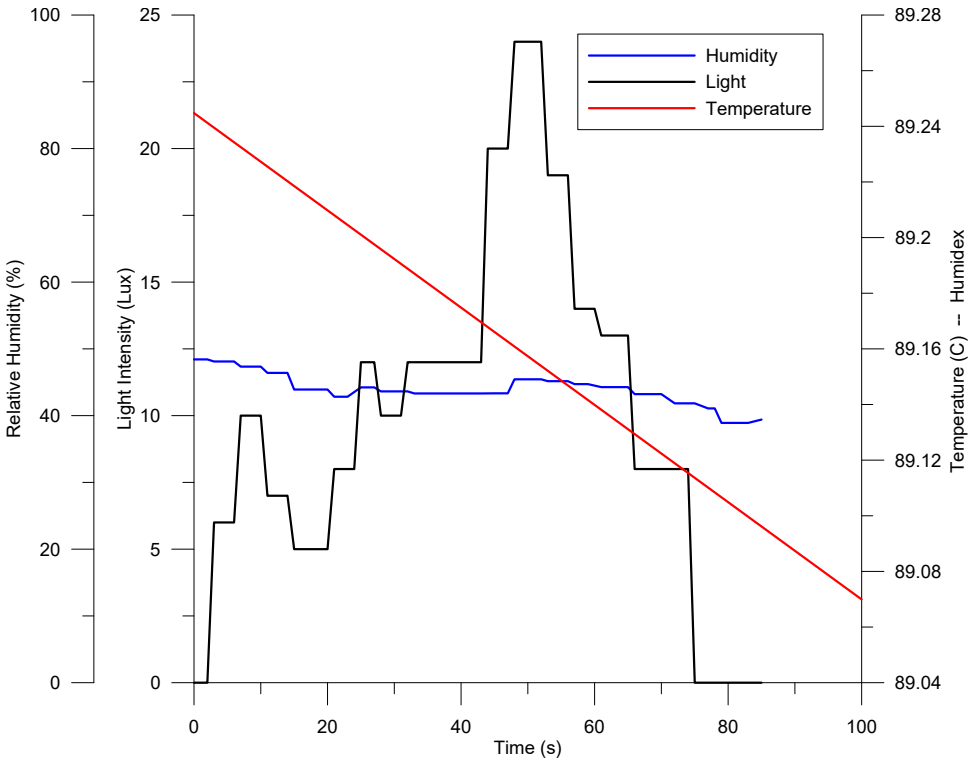


Figure C.153: Test 42 THLP 08

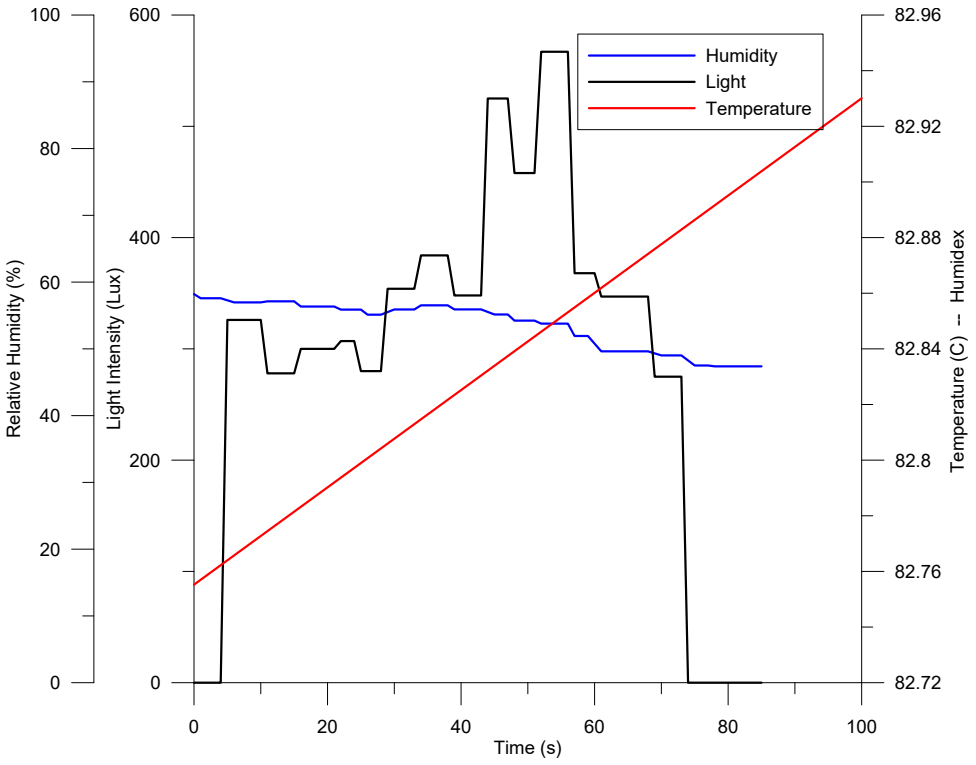


Figure C.154: Test 42 THLP 09

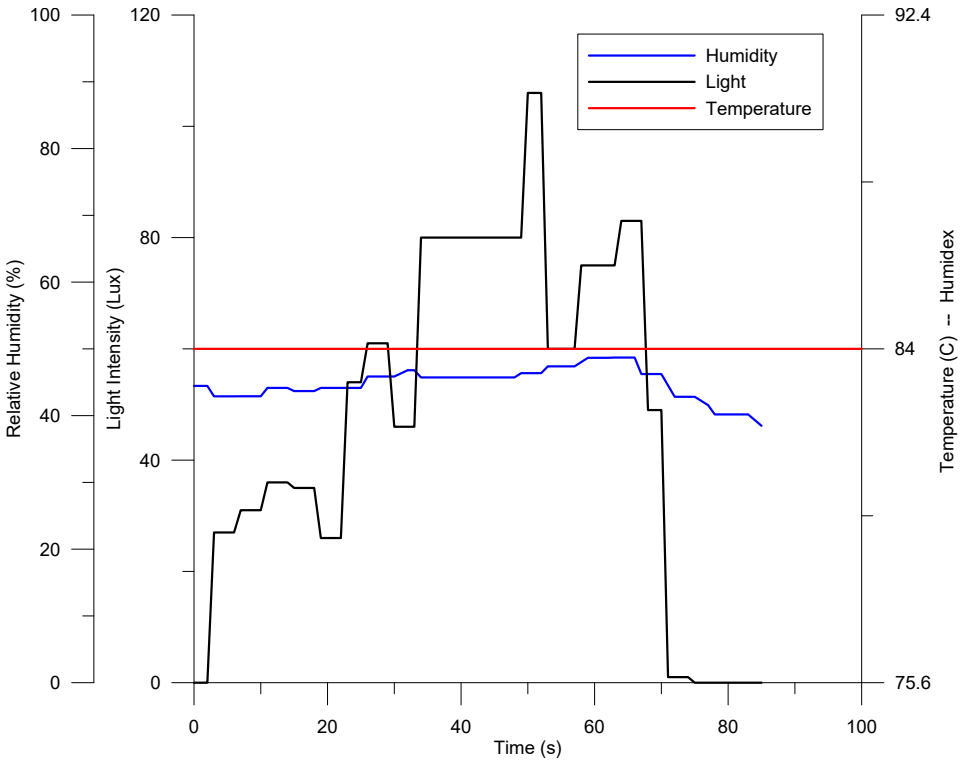


Figure C.155: Test 43 THLP 01

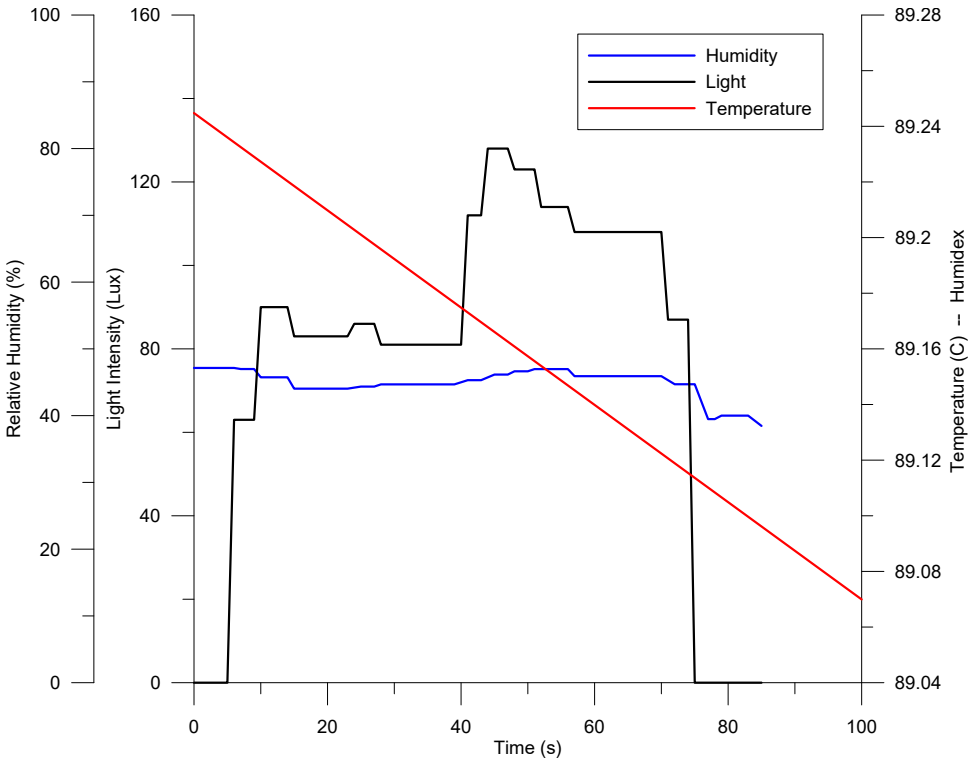


Figure C.156: Test 43 THLP 02

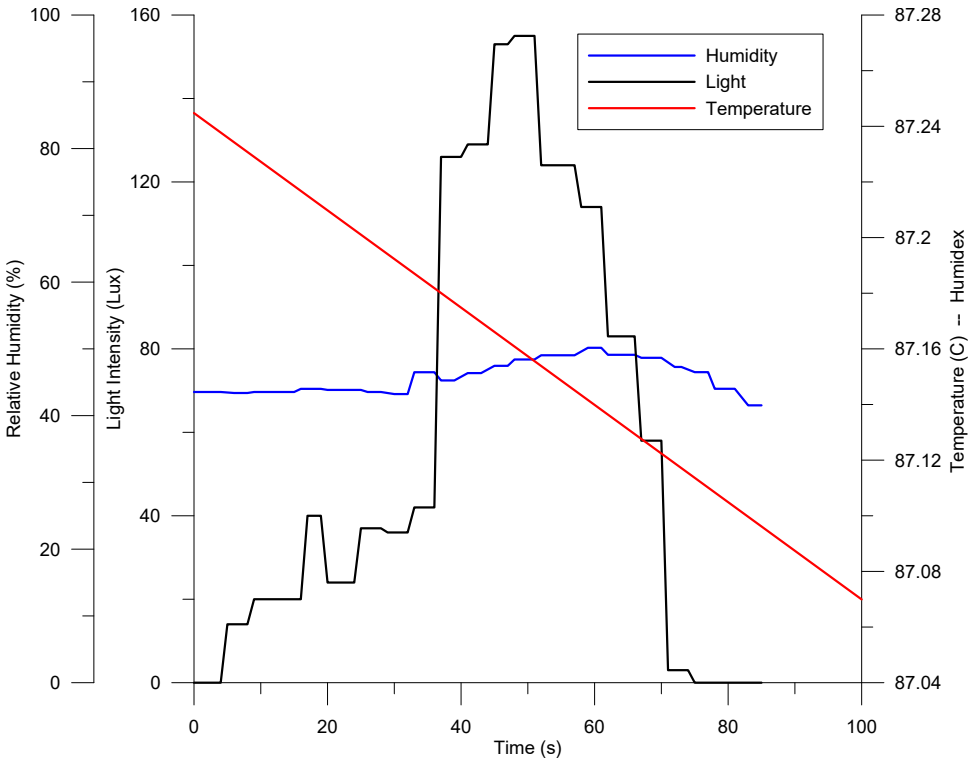


Figure C.157: Test 43 THLP 03

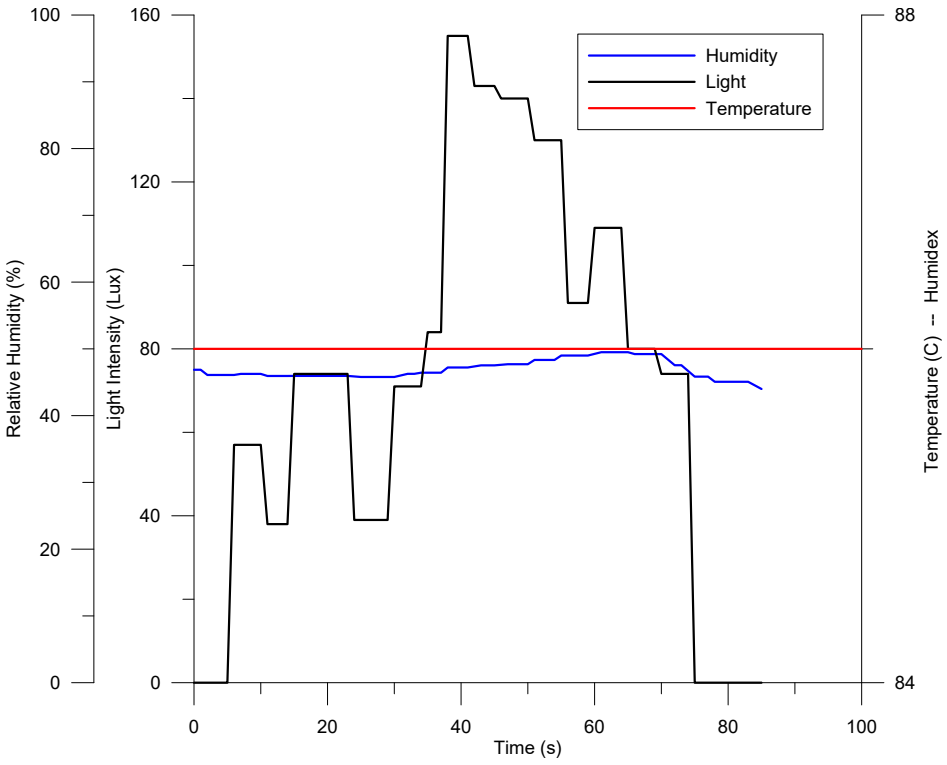


Figure C.158: Test 43 THLP 04

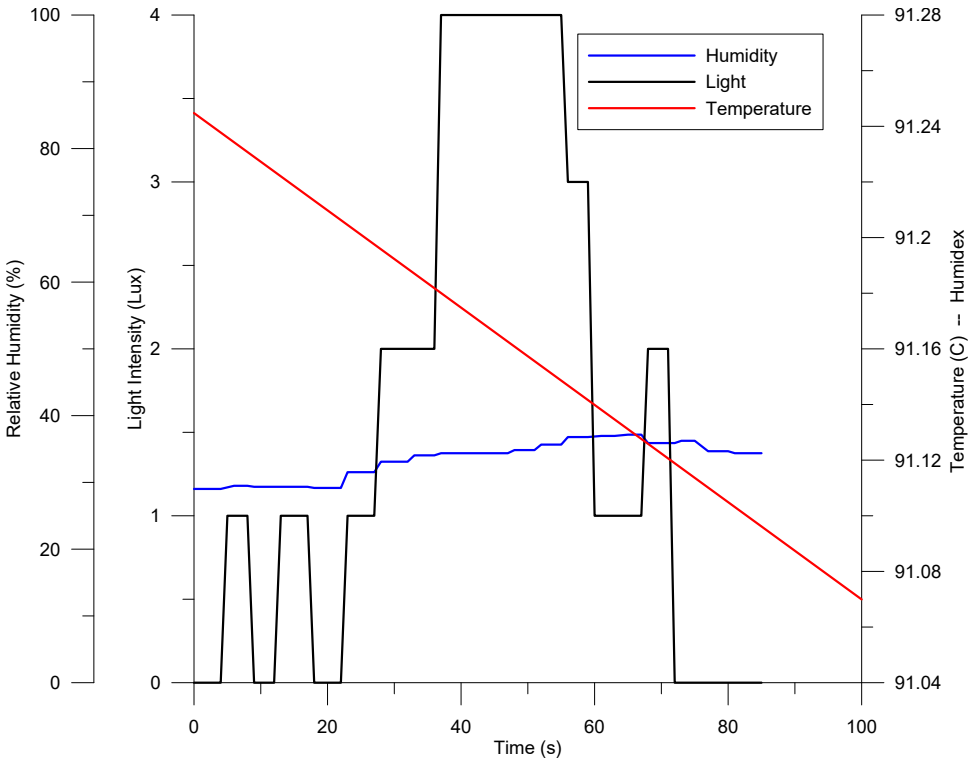


Figure C.159: Test 43 THLP 05

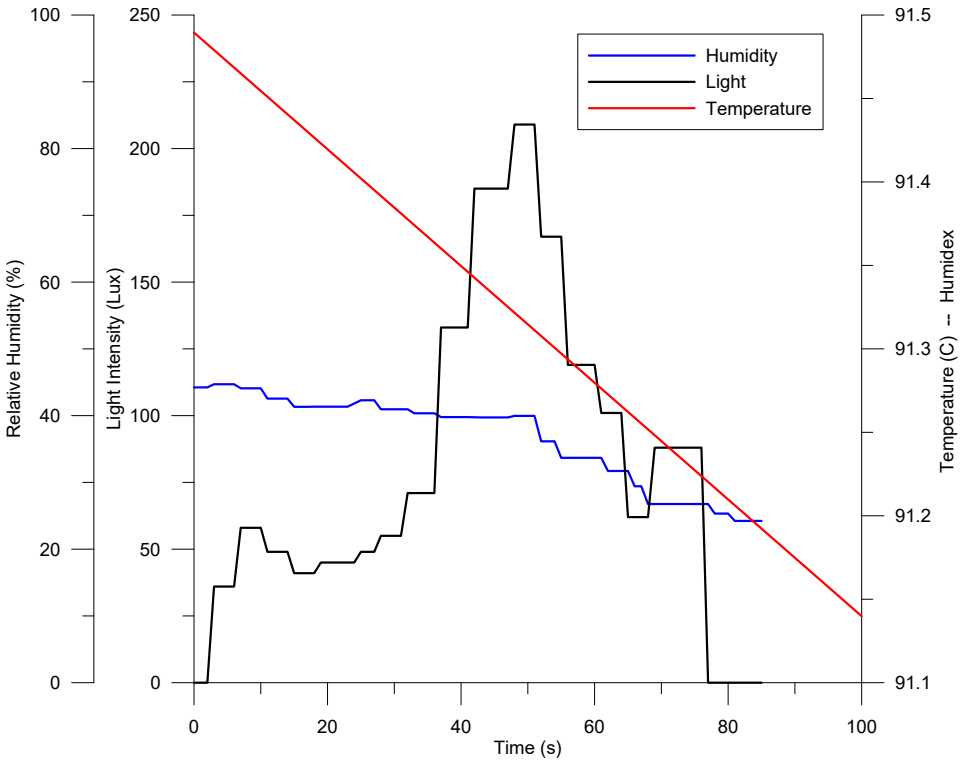


Figure C.160: Test 43 THLP 07

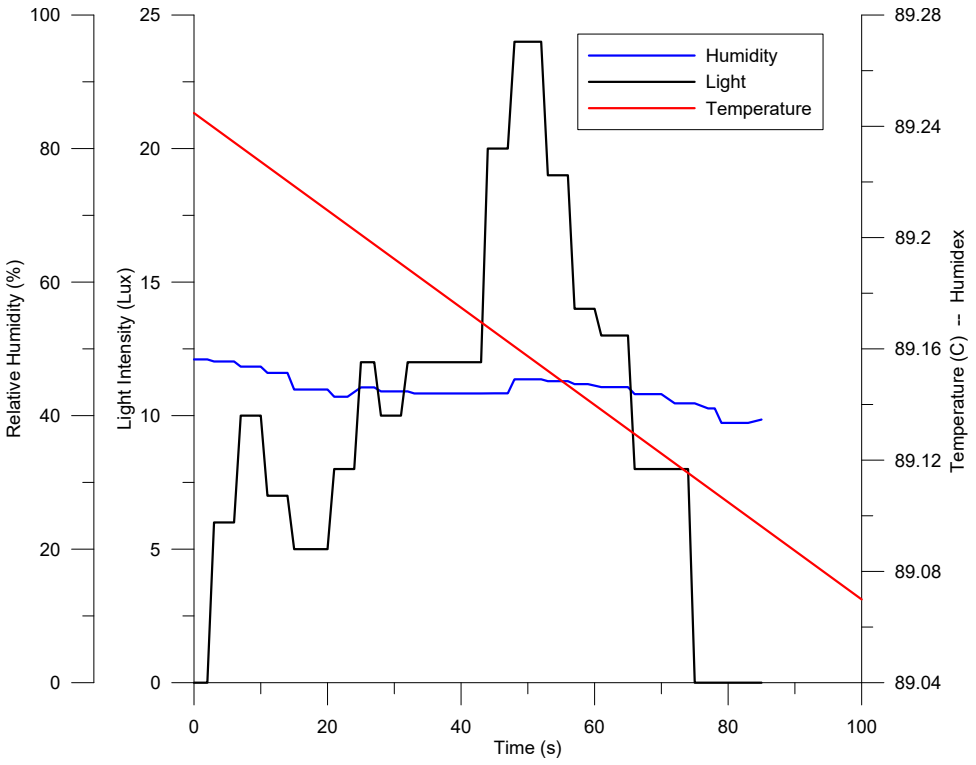


Figure C.161: Test 43 THLP 08

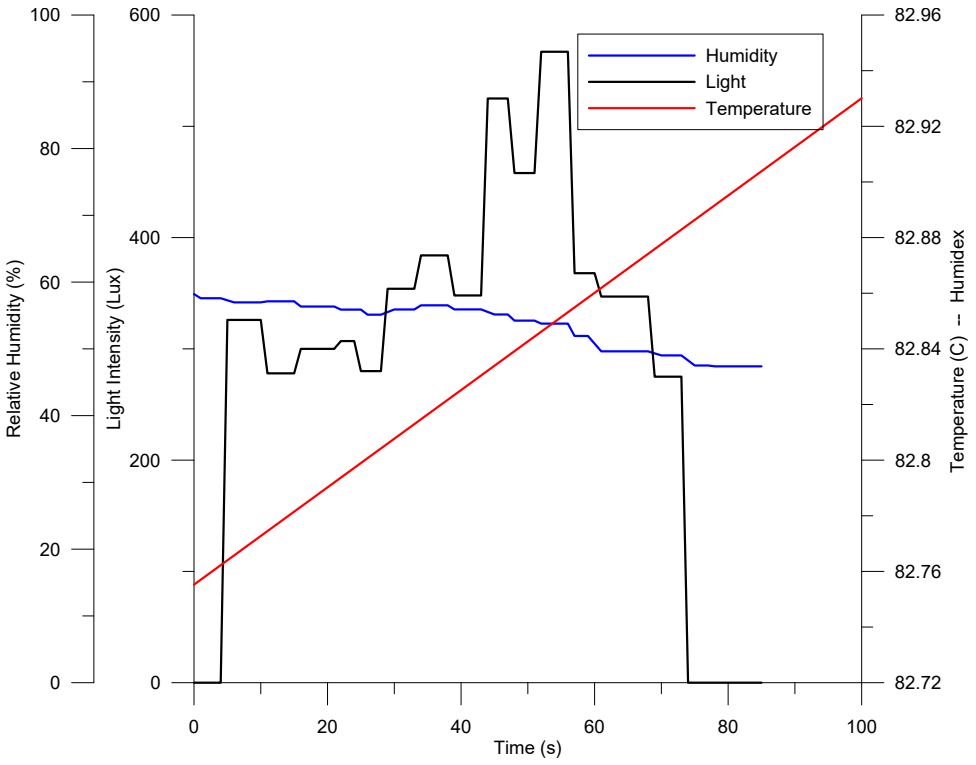


Figure C.162: Test 43 THLP 09

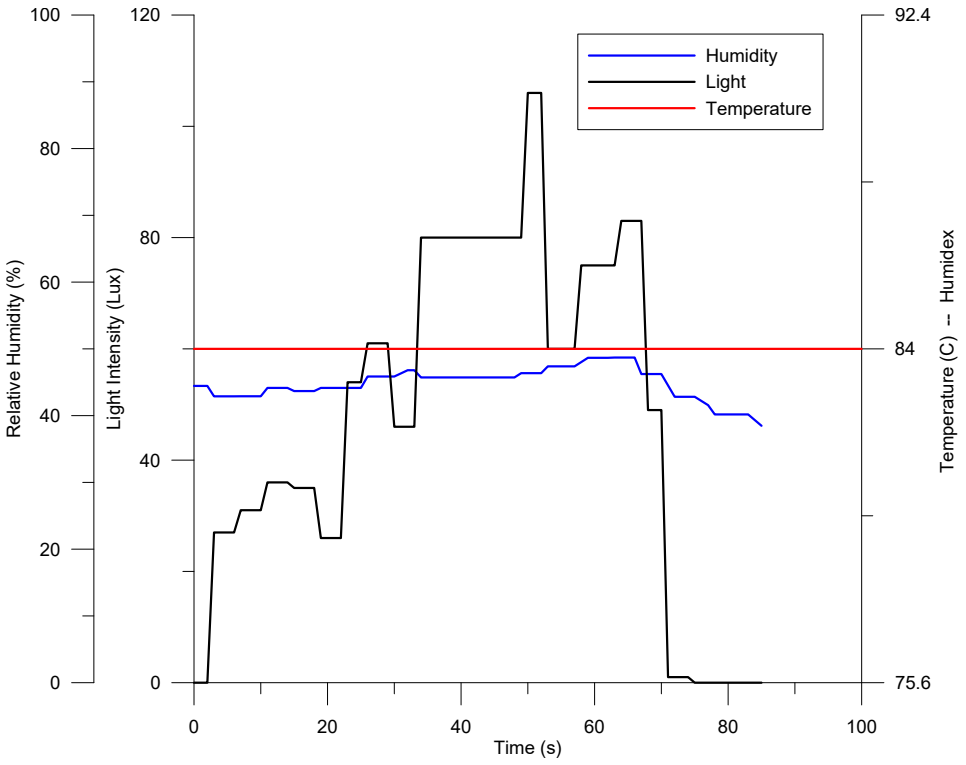


Figure C.163: Test 44 THLP 01

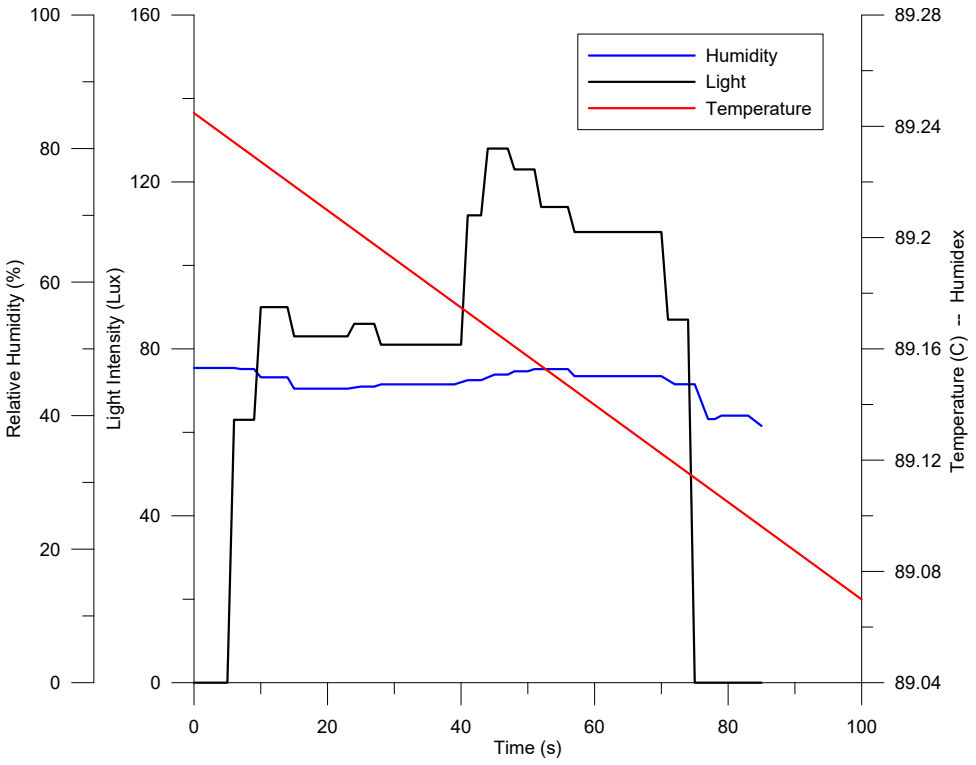


Figure C.164: Test 44 THLP 02

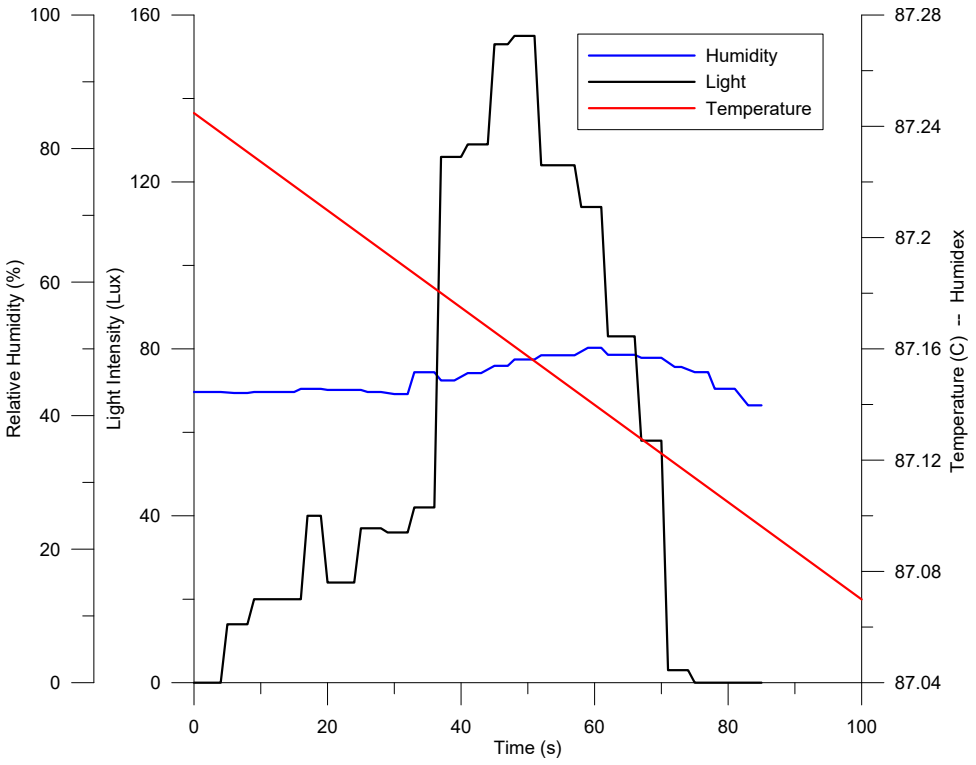


Figure C.165: Test 44 THLP 03

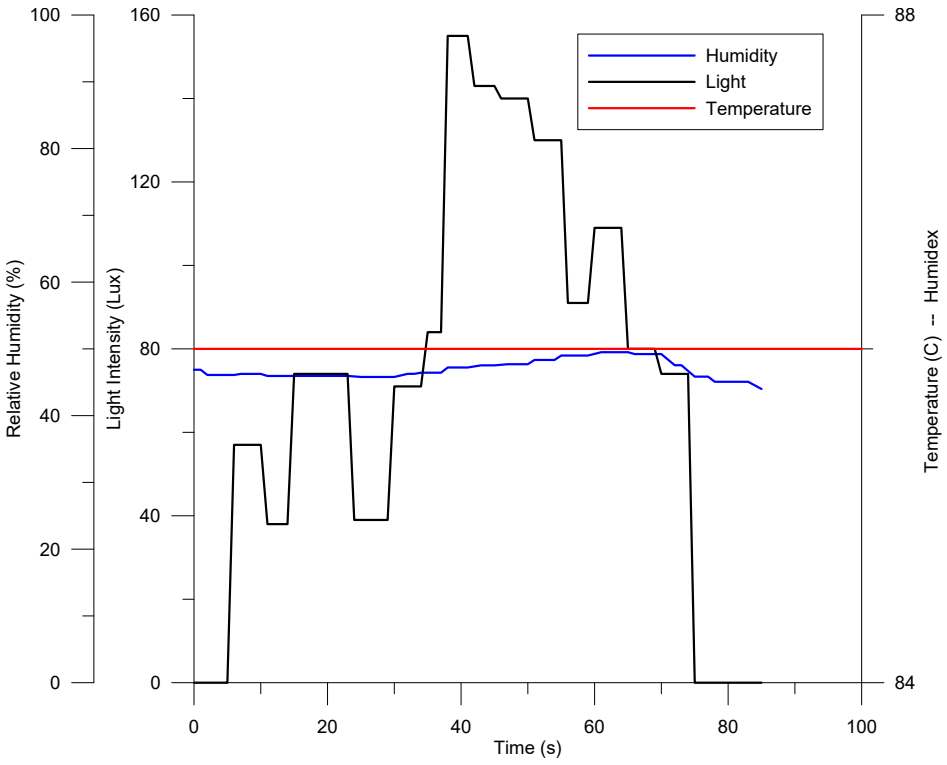


Figure C.166: Test 44 THLP 04

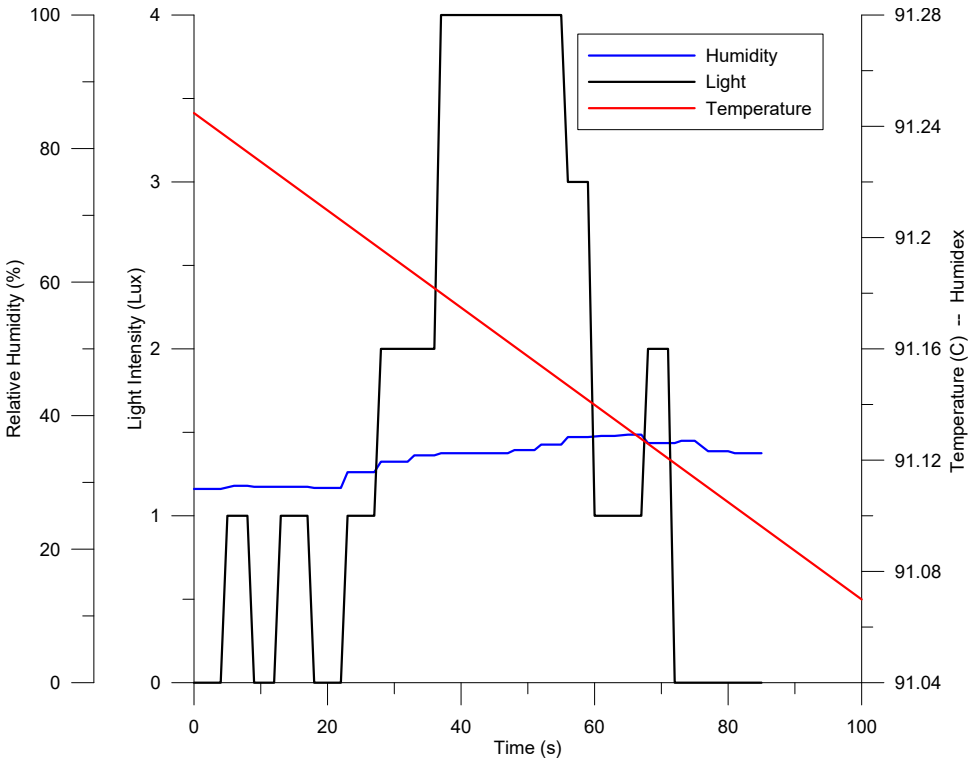


Figure C.167: Test 44 THLP 05

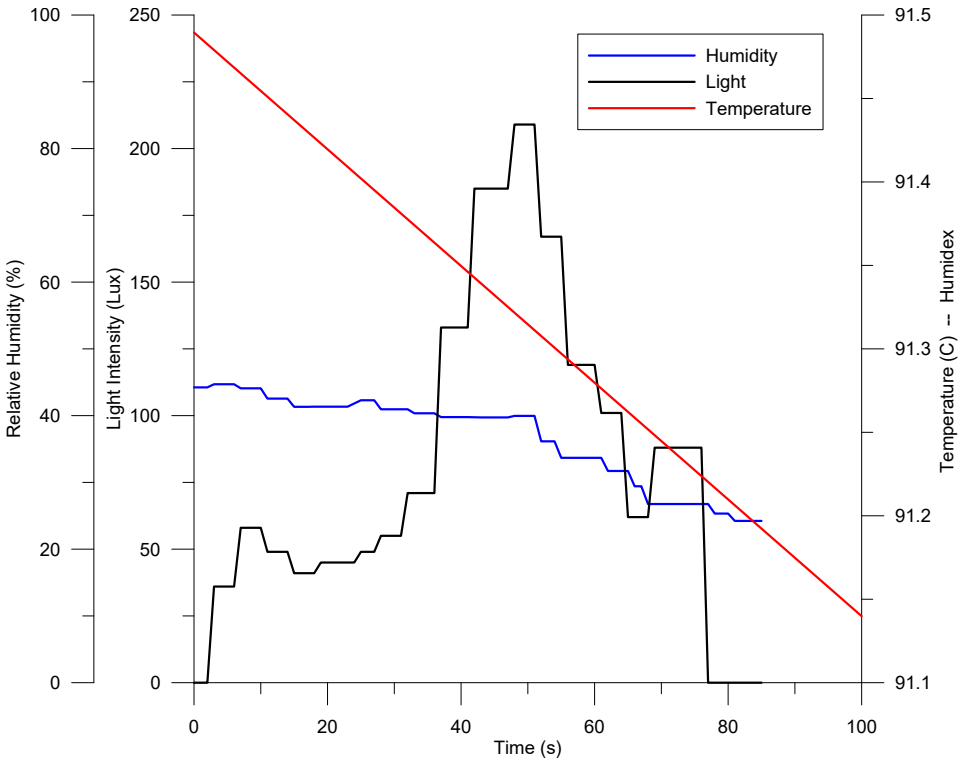


Figure C.168: Test 44 THLP 07

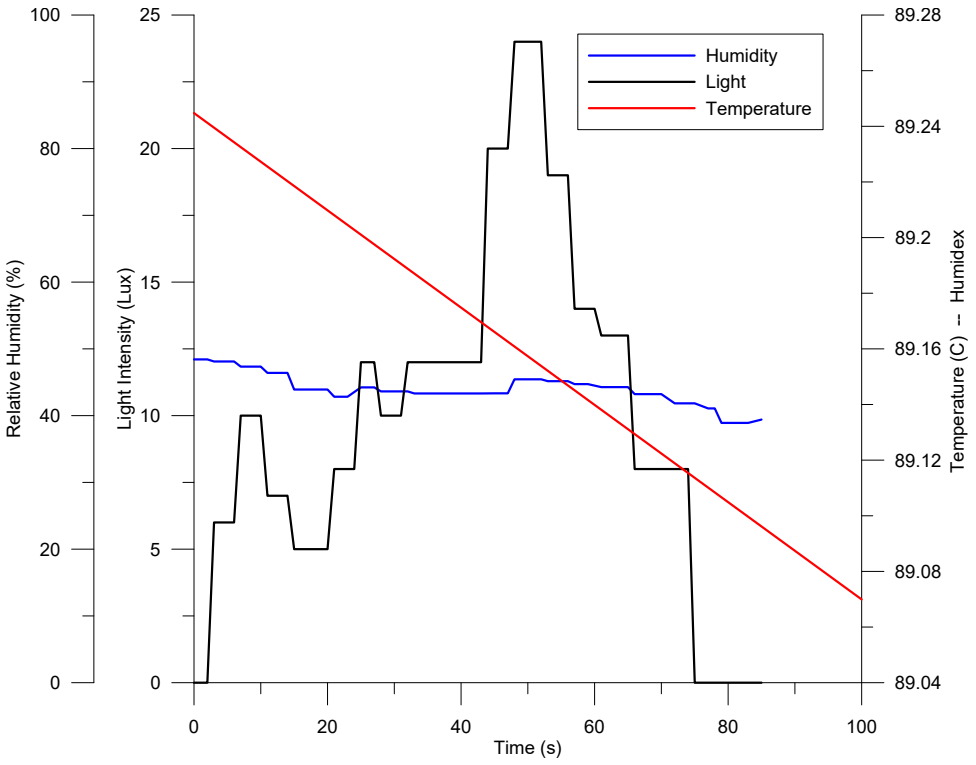


Figure C.169: Test 44 THLP 08

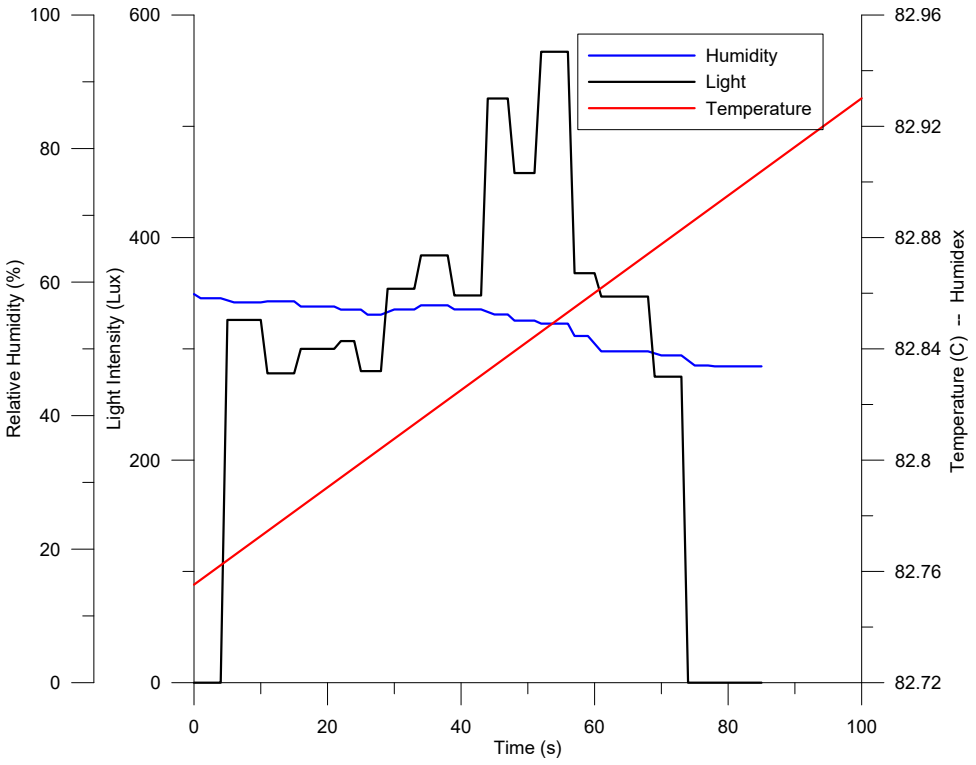


Figure C.170: Test 44 THLP 09

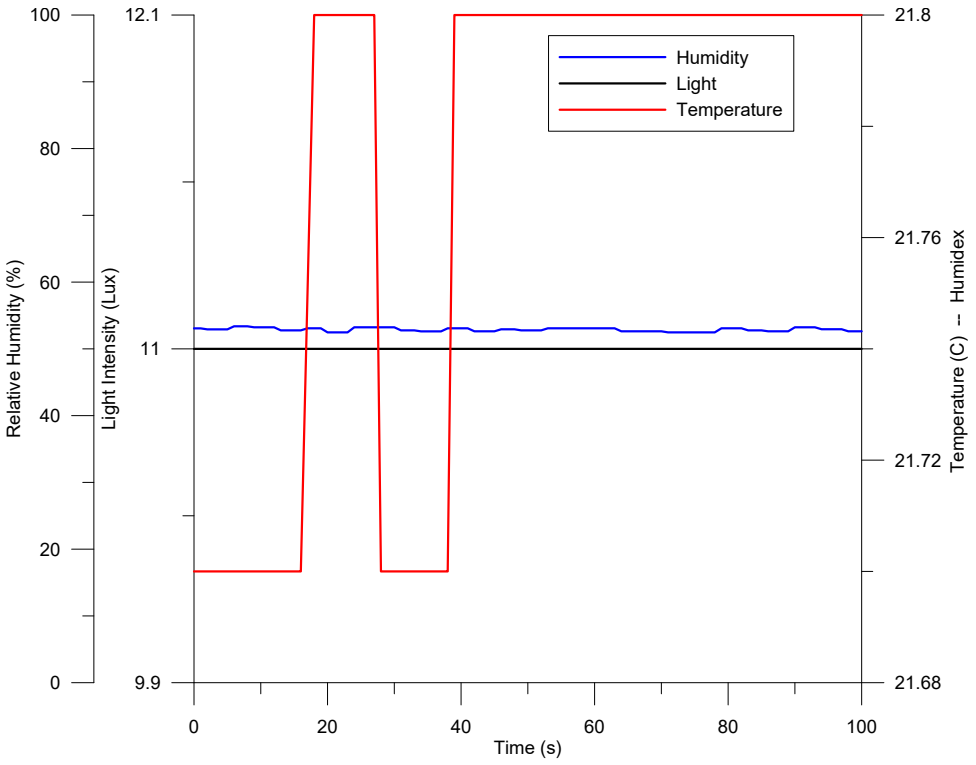


Figure C.171: Test 45 THLP 01

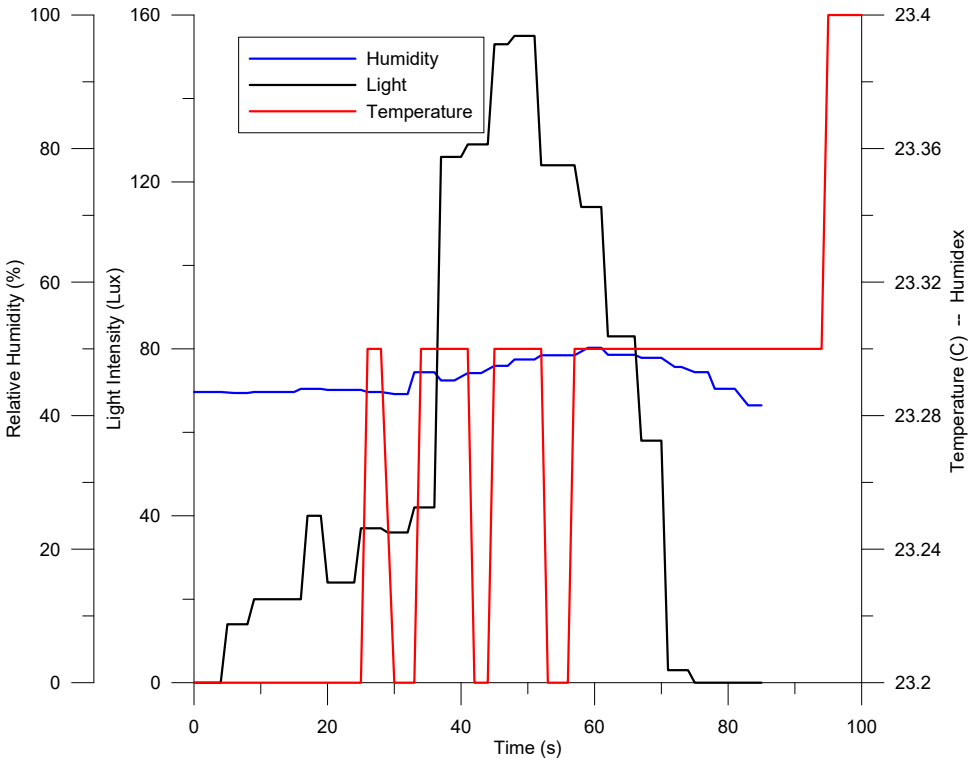


Figure C.172: Test 45 THLP 03

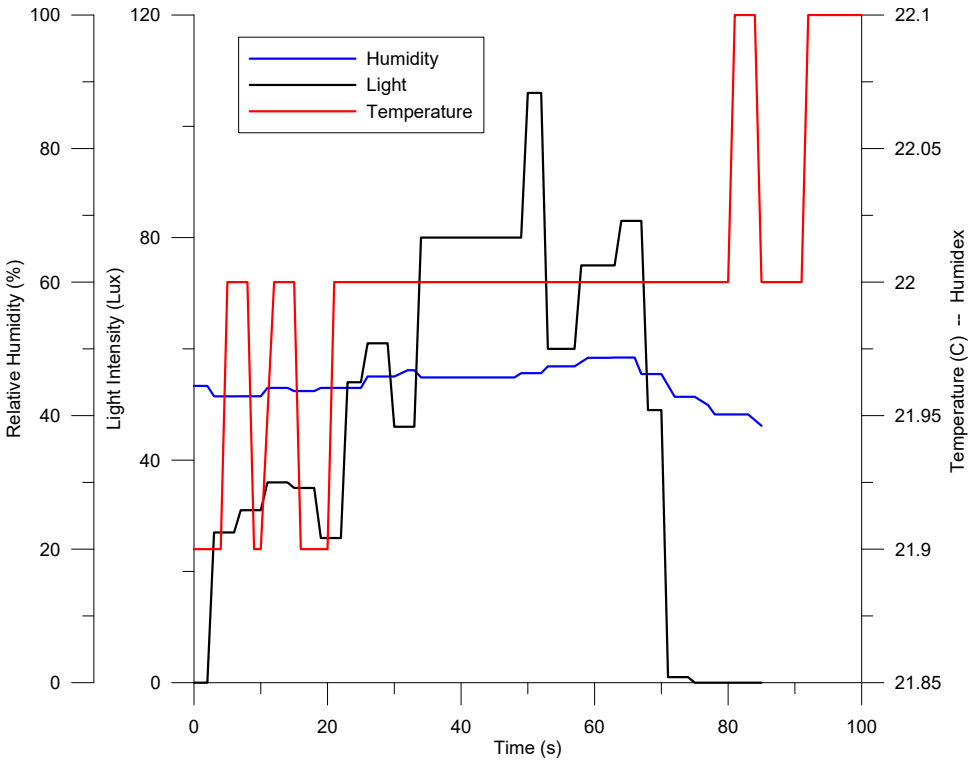


Figure C.173: Test 45 THLP 04

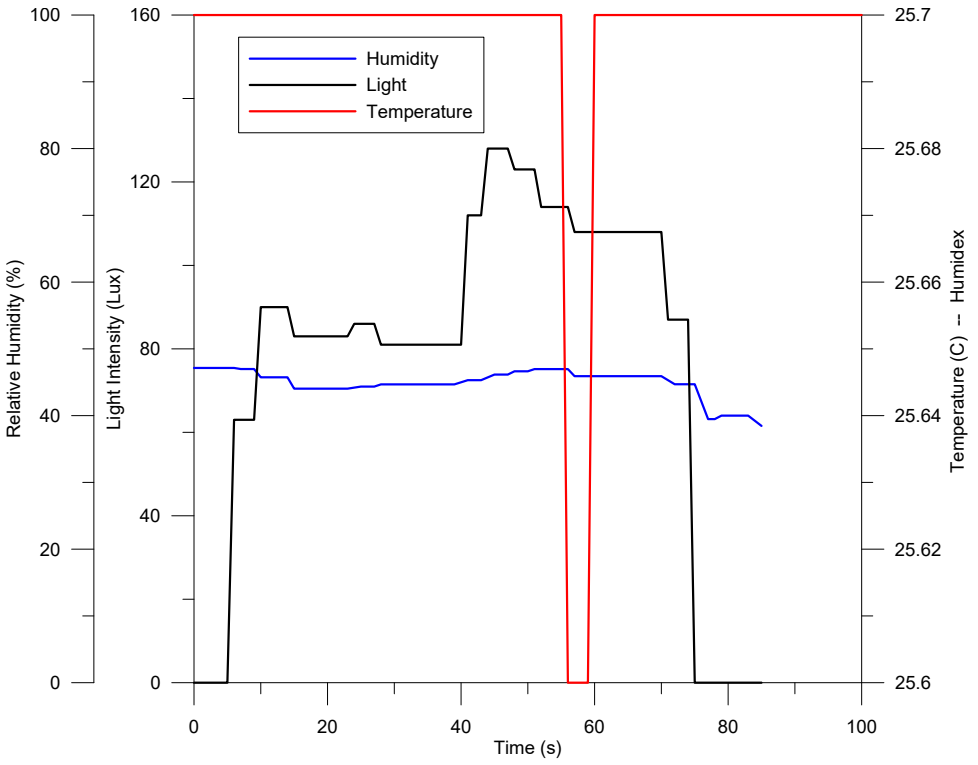


Figure C.174: Test 45 THLP 05

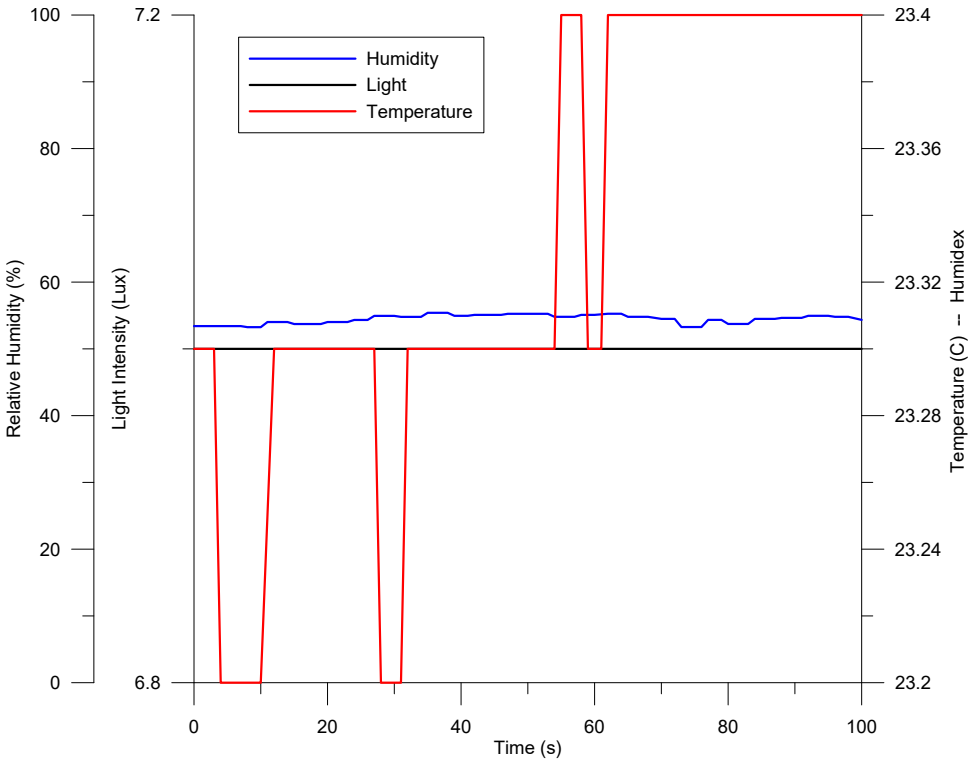


Figure C.175: Test 45 THLP 07

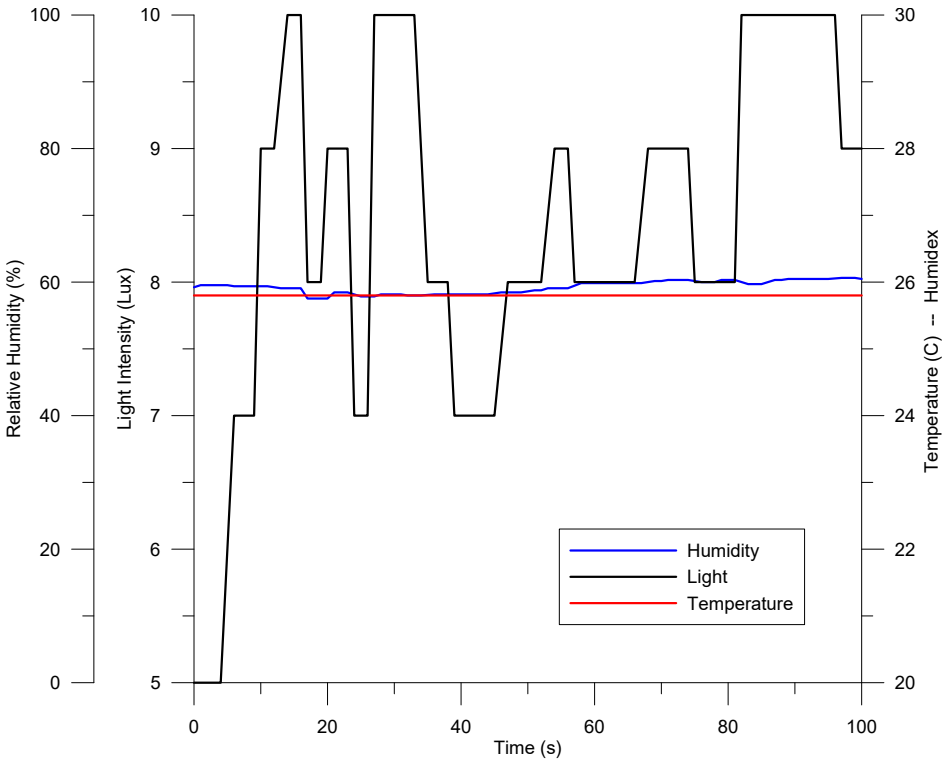


Figure C.176: Test 46 THLP 01

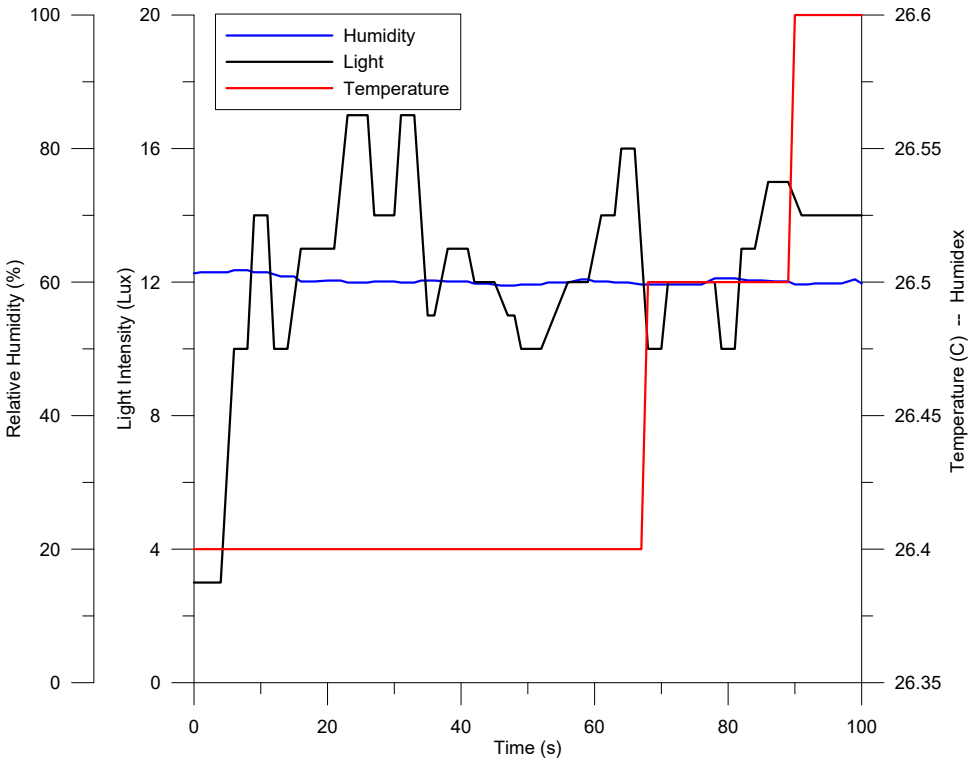


Figure C.177: Test 46 THLP 02

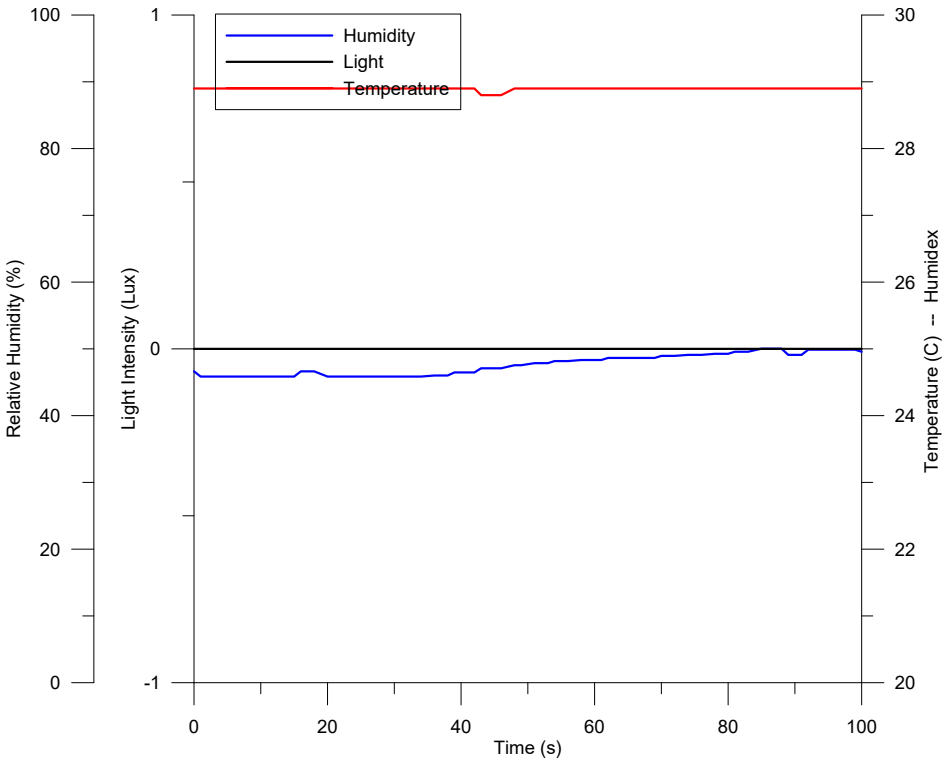


Figure C.178: Test 46 THLP 04

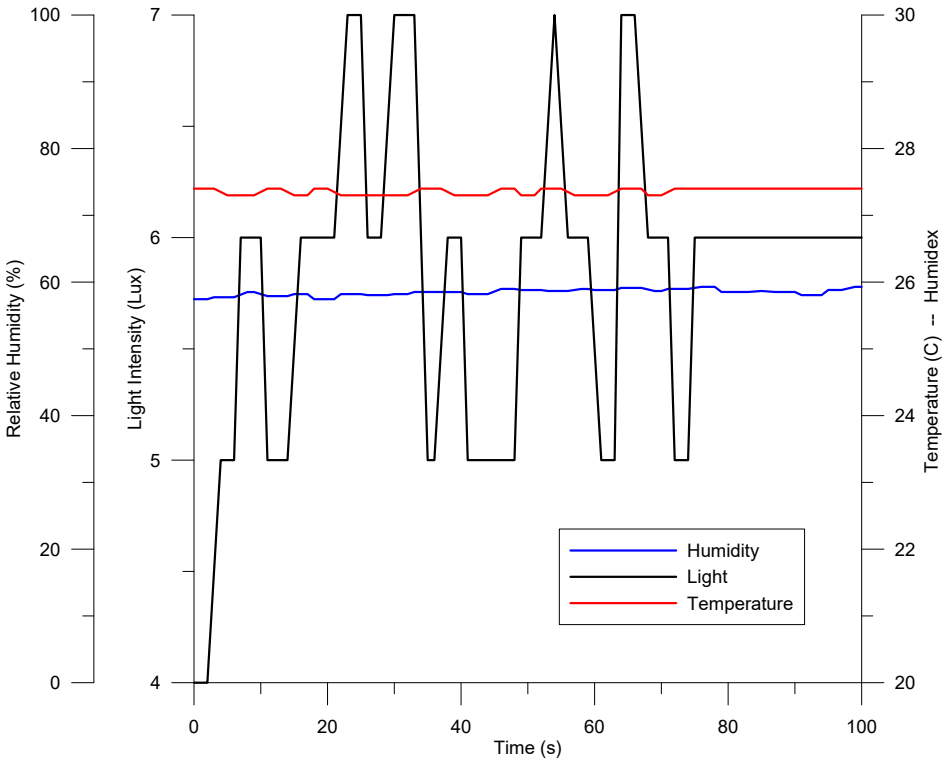


Figure C.179: Test 46 THLP 05

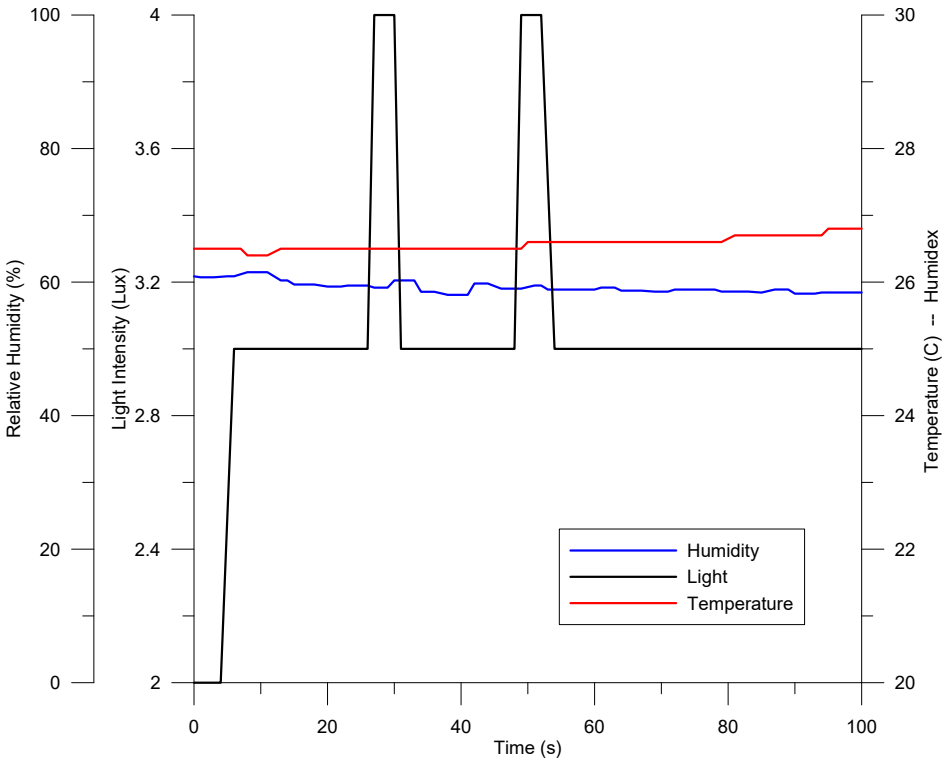


Figure C.180: Test 46 THLP 08

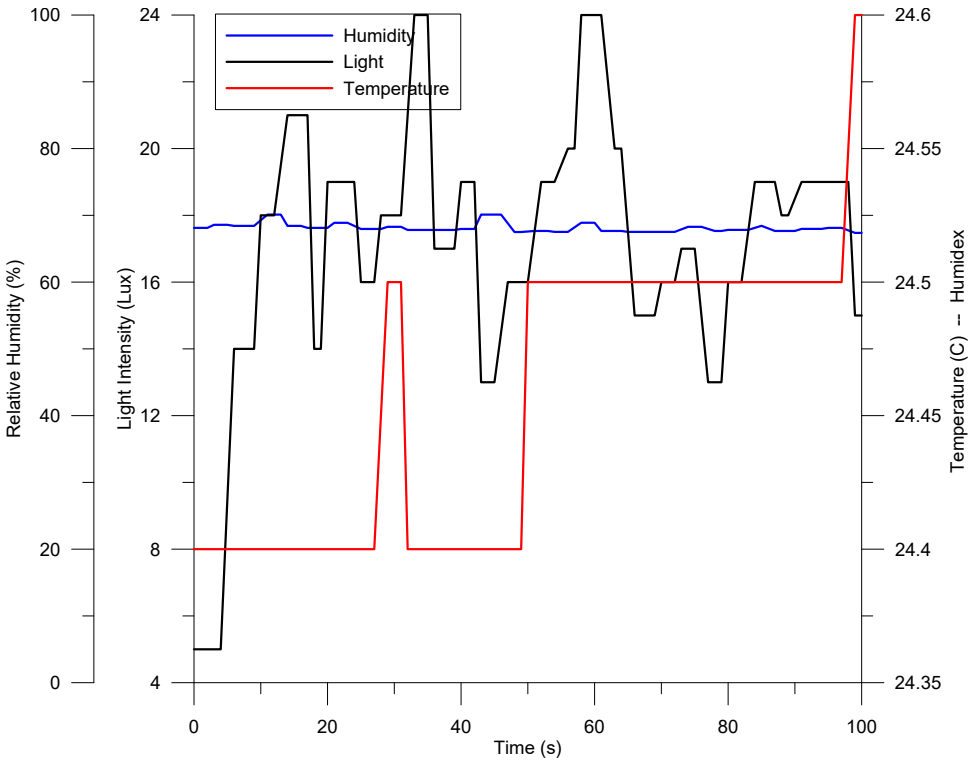


Figure C.181: Test 46 THLP 09

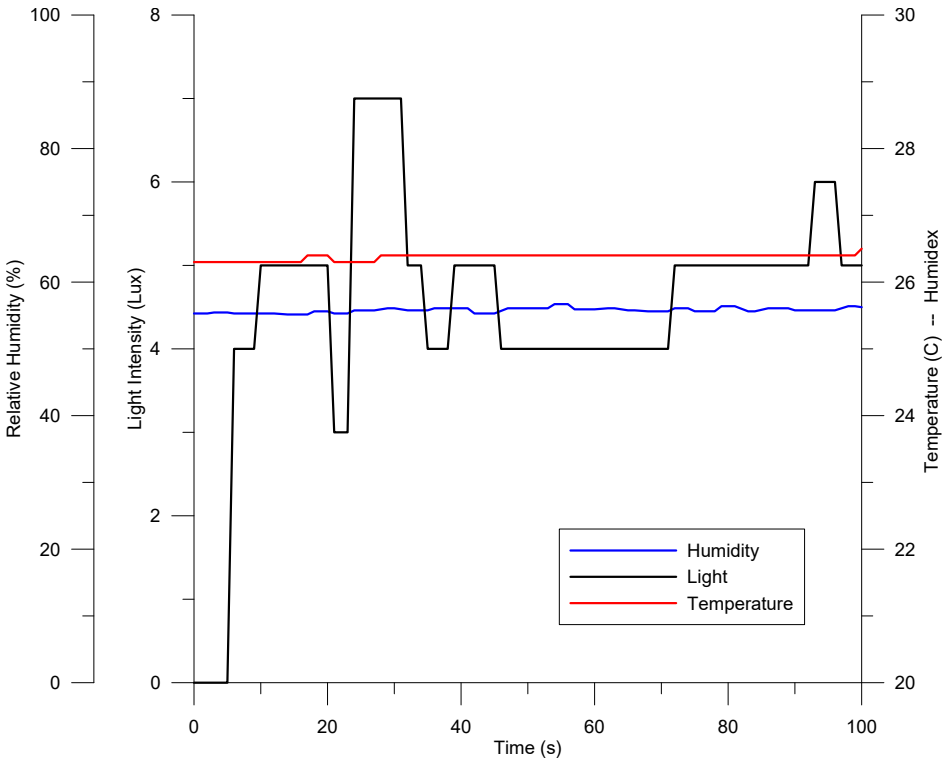


Figure C.182: Test 47 THLP 01

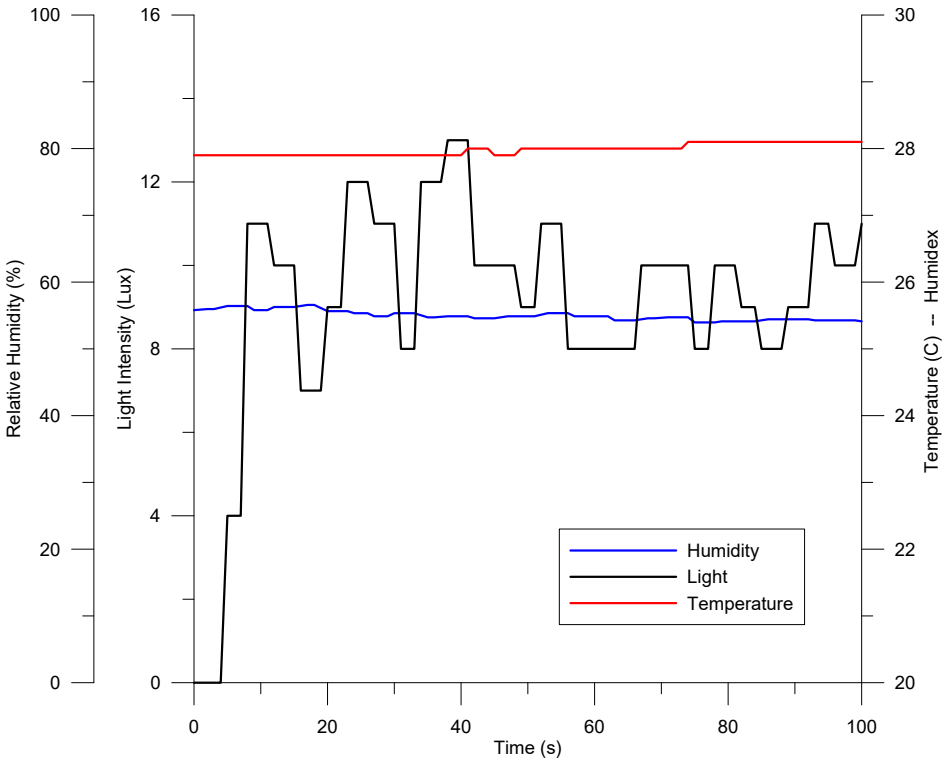


Figure C.183: Test 47 THLP 02

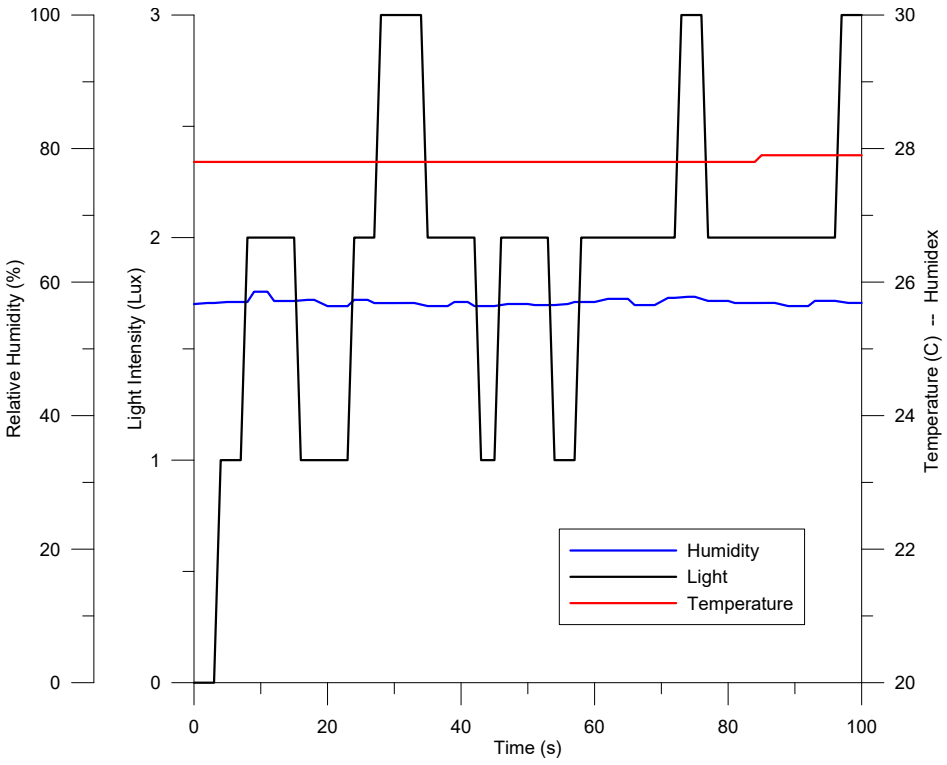


Figure C.184: Test 47 THLP 03

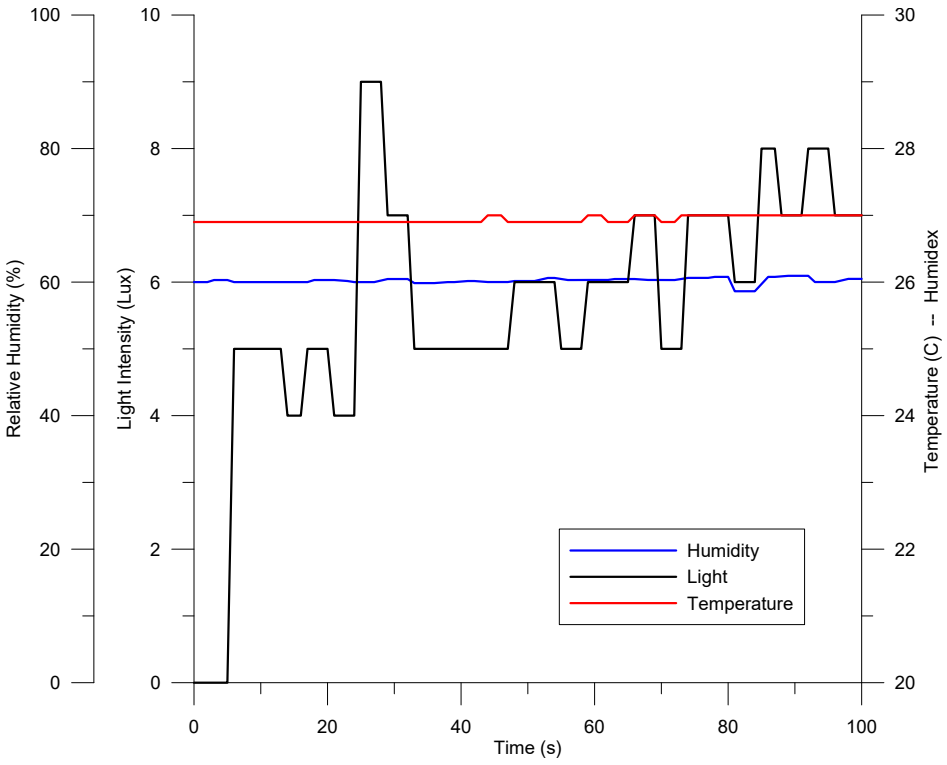


Figure C.185: Test 47 THLP 04

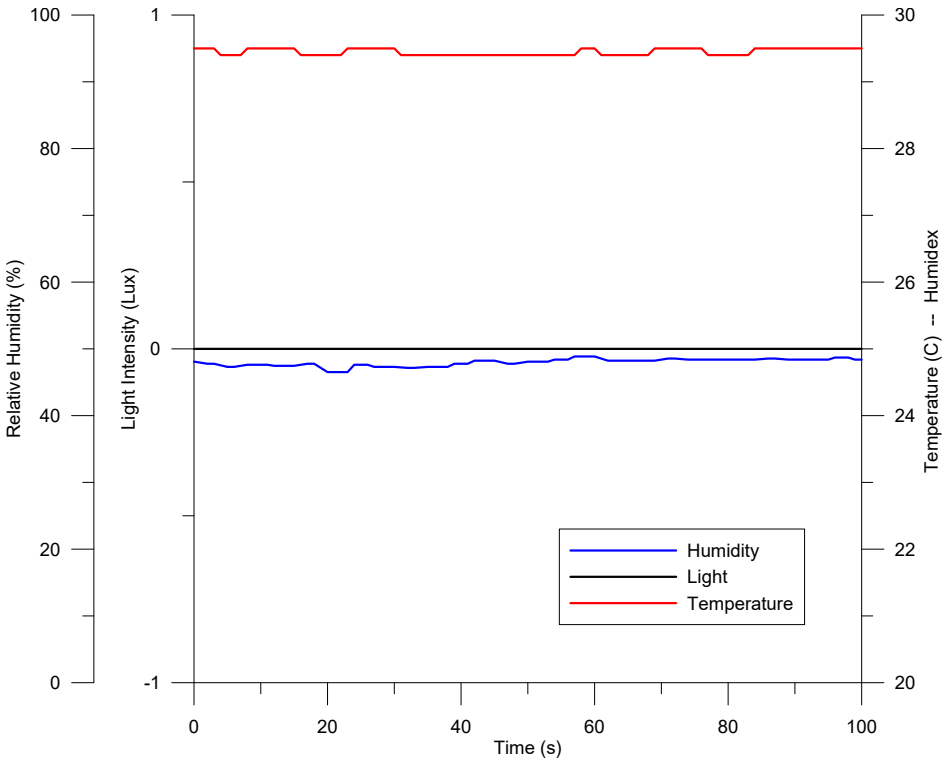


Figure C.186: Test 47 THLP 05

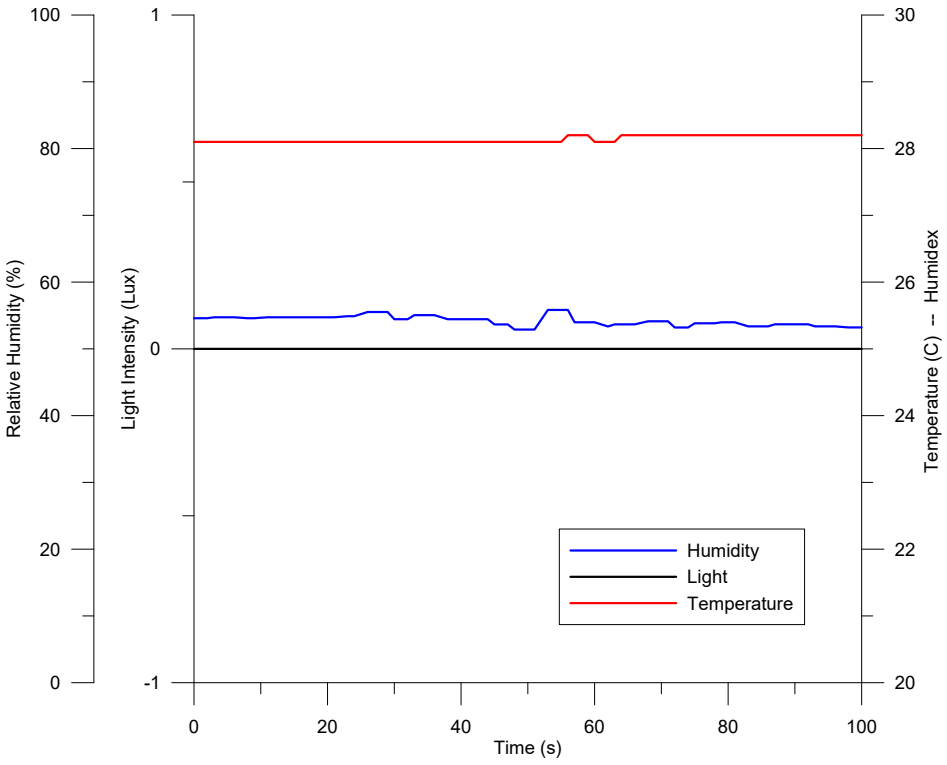


Figure C.187: Test 47 THLP 08

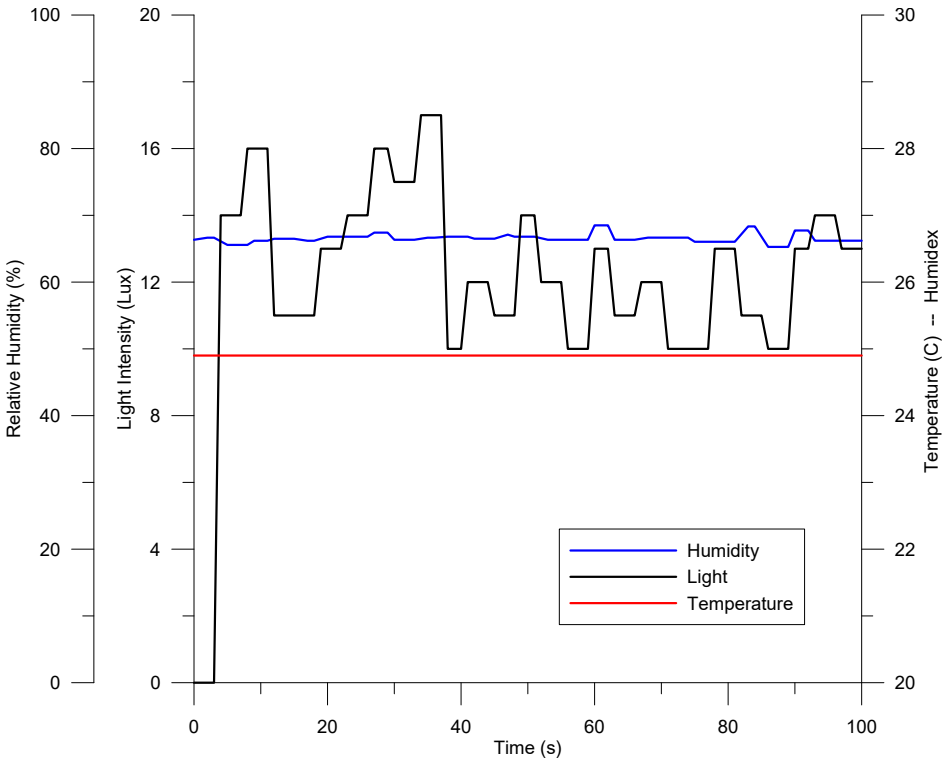


Figure C.188: Test 47 THLP 09

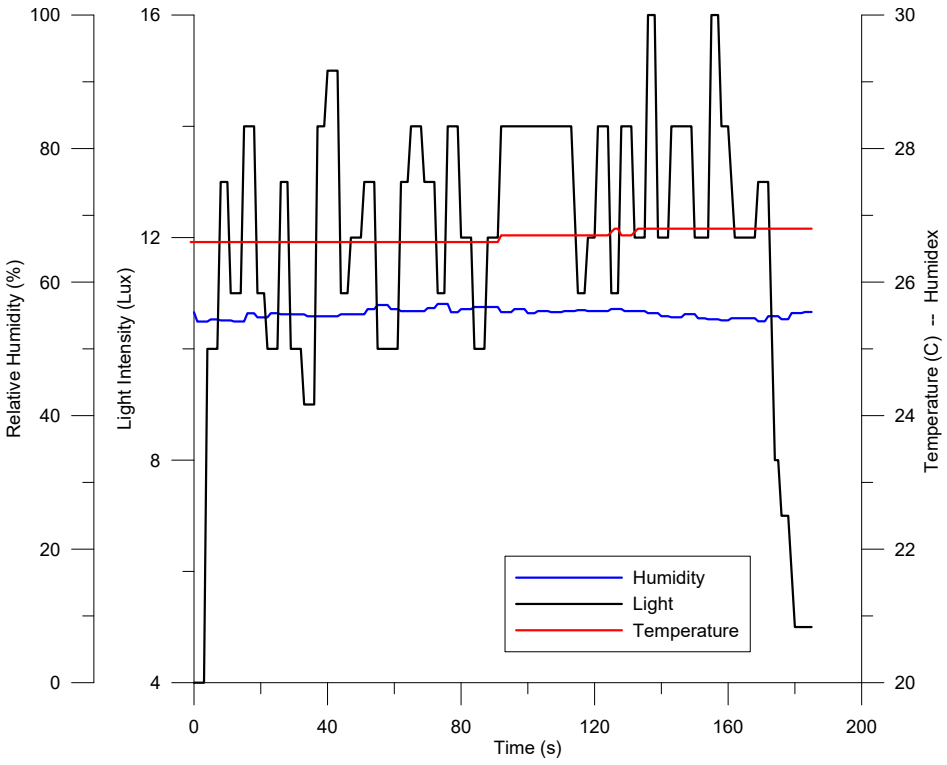


Figure C.189: Test 48 THLP 01

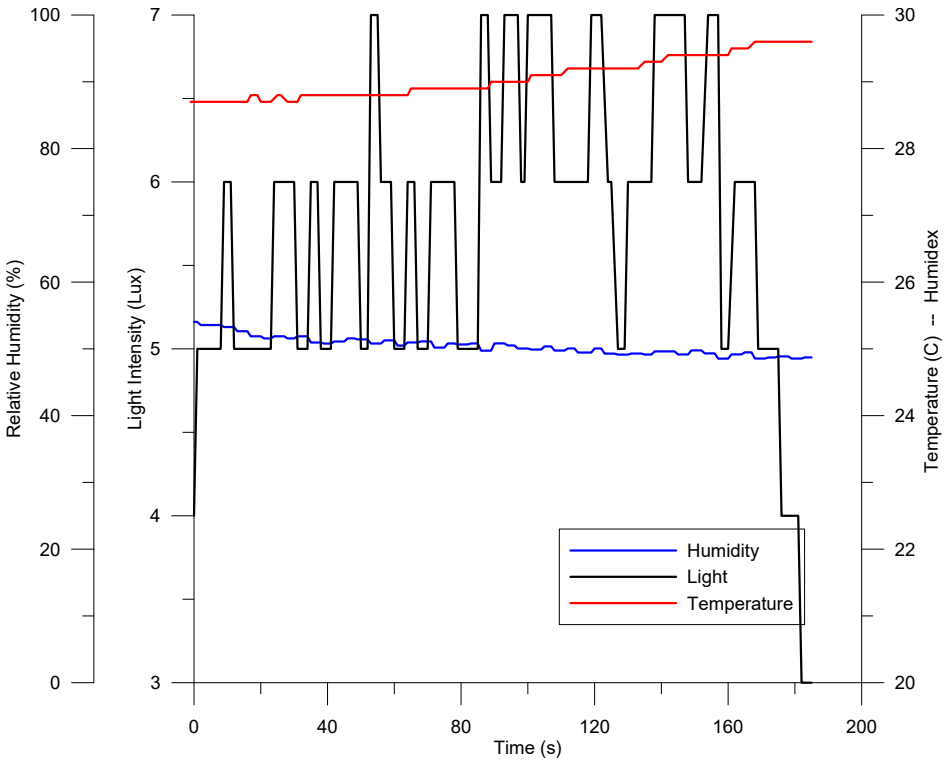


Figure C.190: Test 48 THLP 02

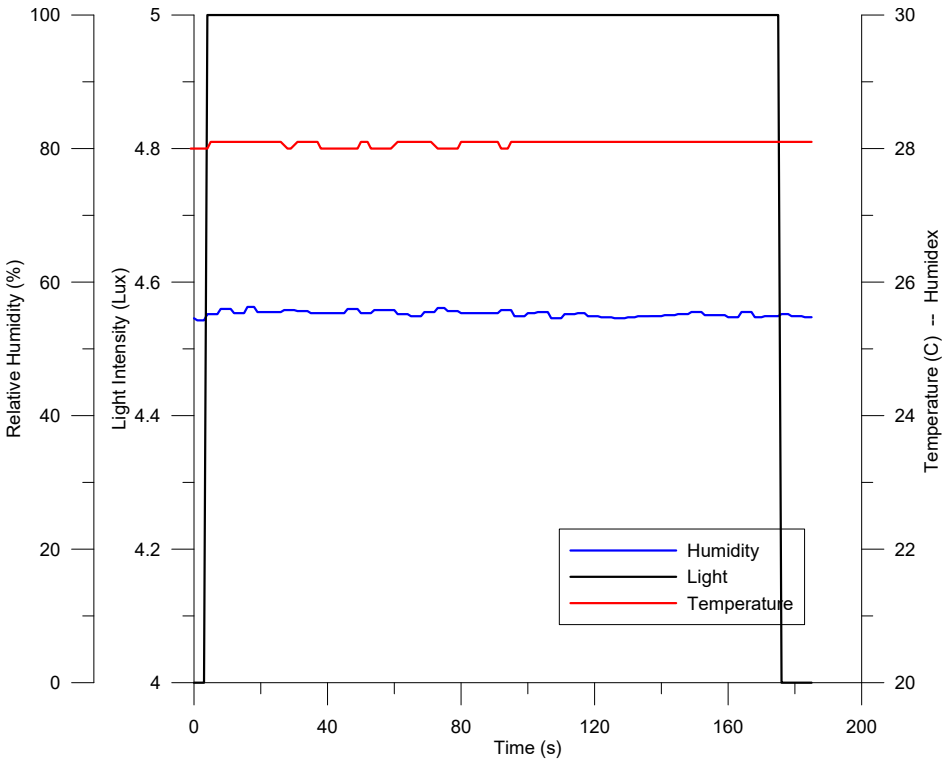


Figure C.191: Test 48 THLP 03

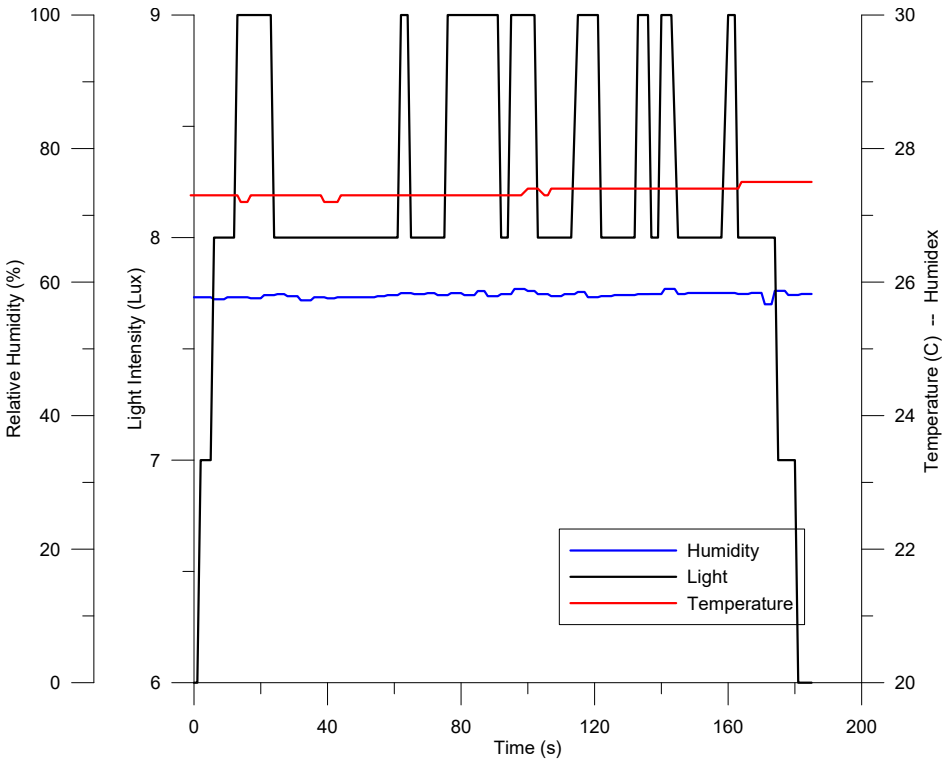


Figure C.192: Test 48 THLP 04

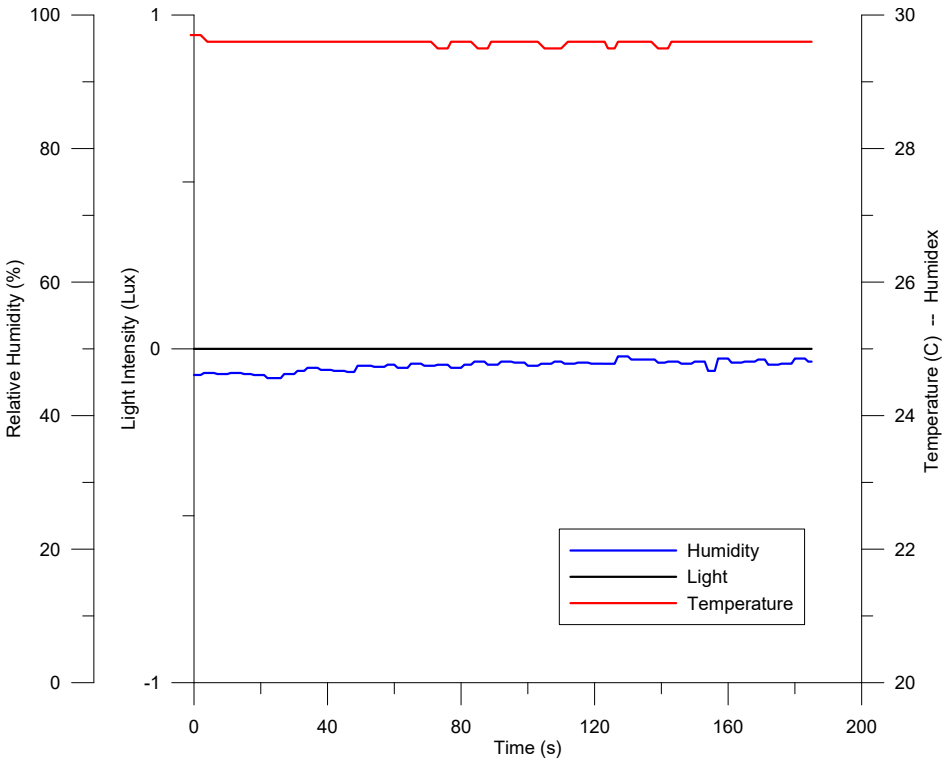


Figure C.193: Test 48 THLP 05

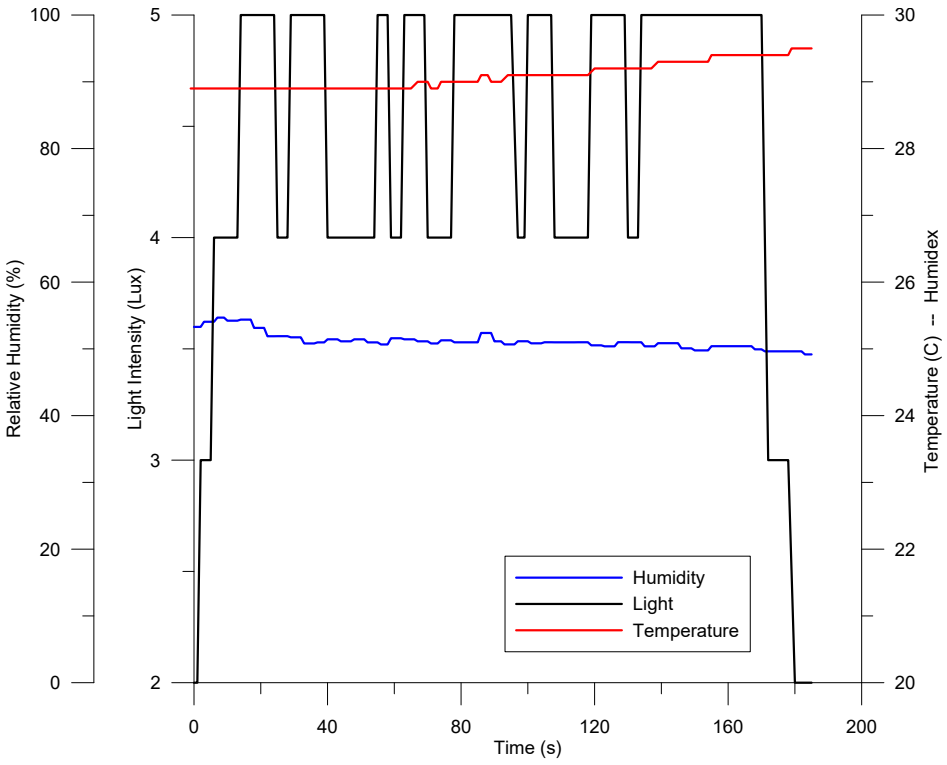


Figure C.194: Test 48 THLP 08

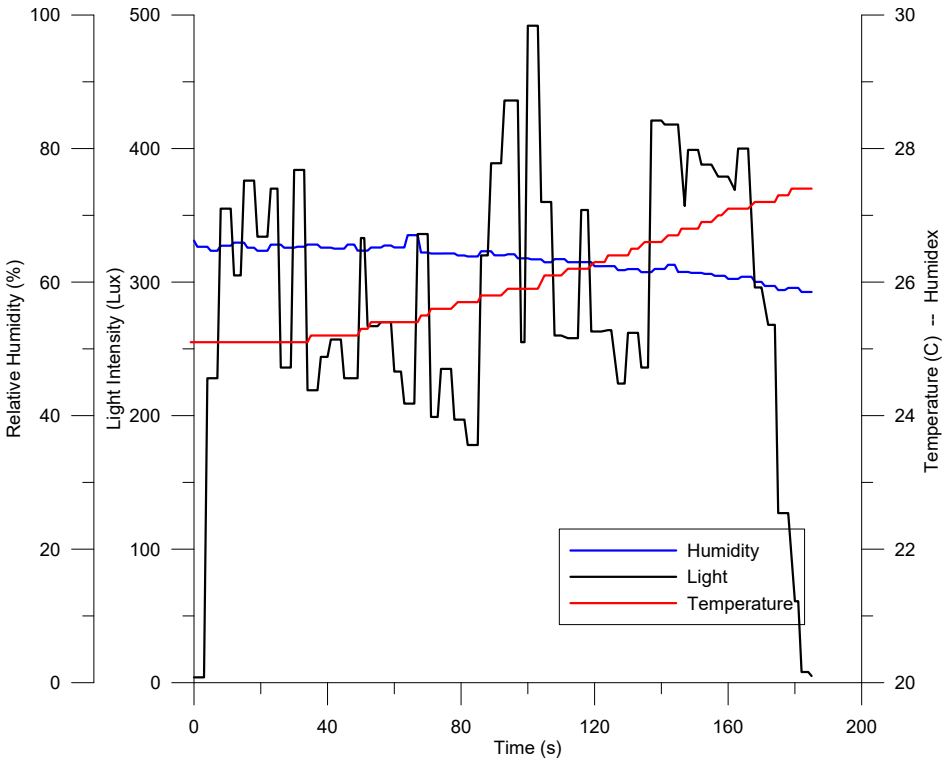


Figure C.195: Test 48 THLP 09

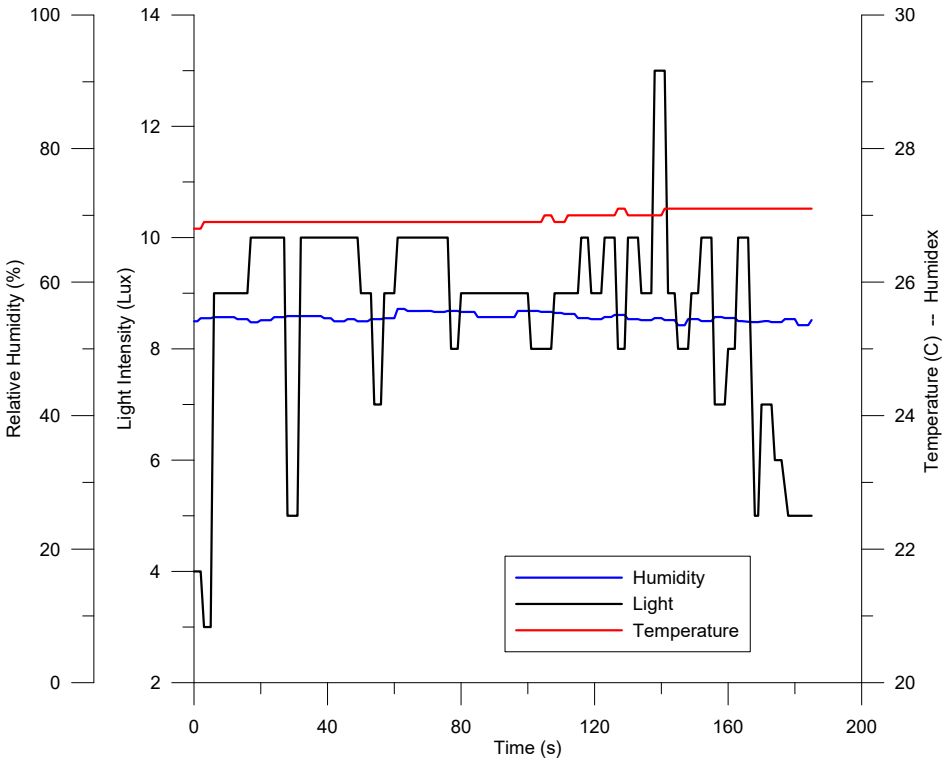


Figure C.196: Test 49 THLP 01

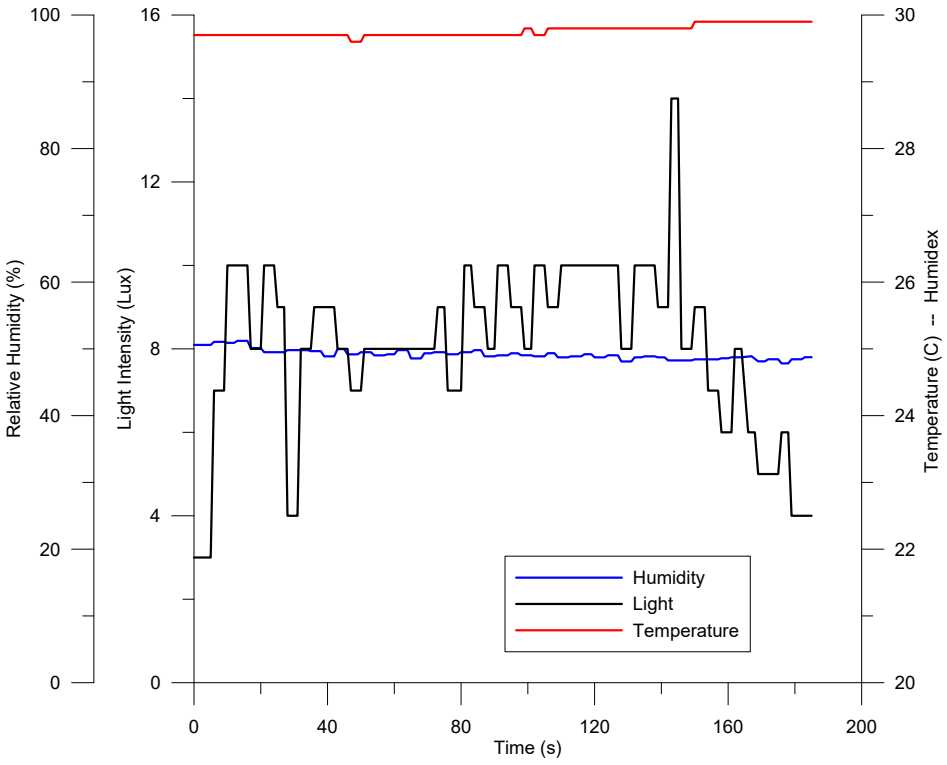


Figure C.197: Test 49 THLP 02

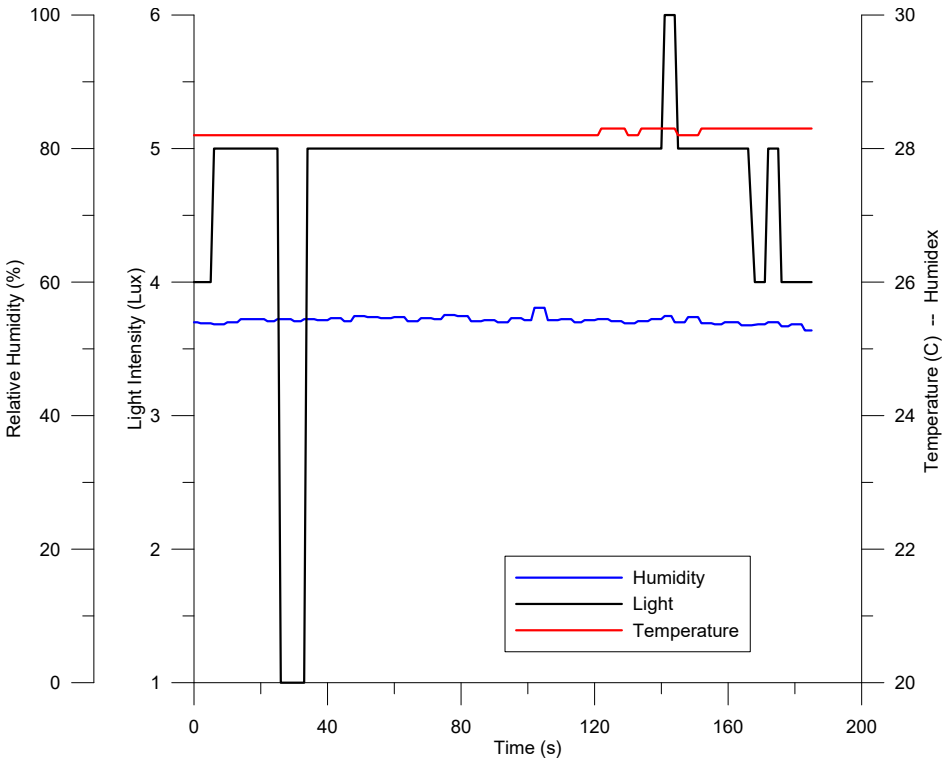


Figure C.198: Test 49 THLP 03

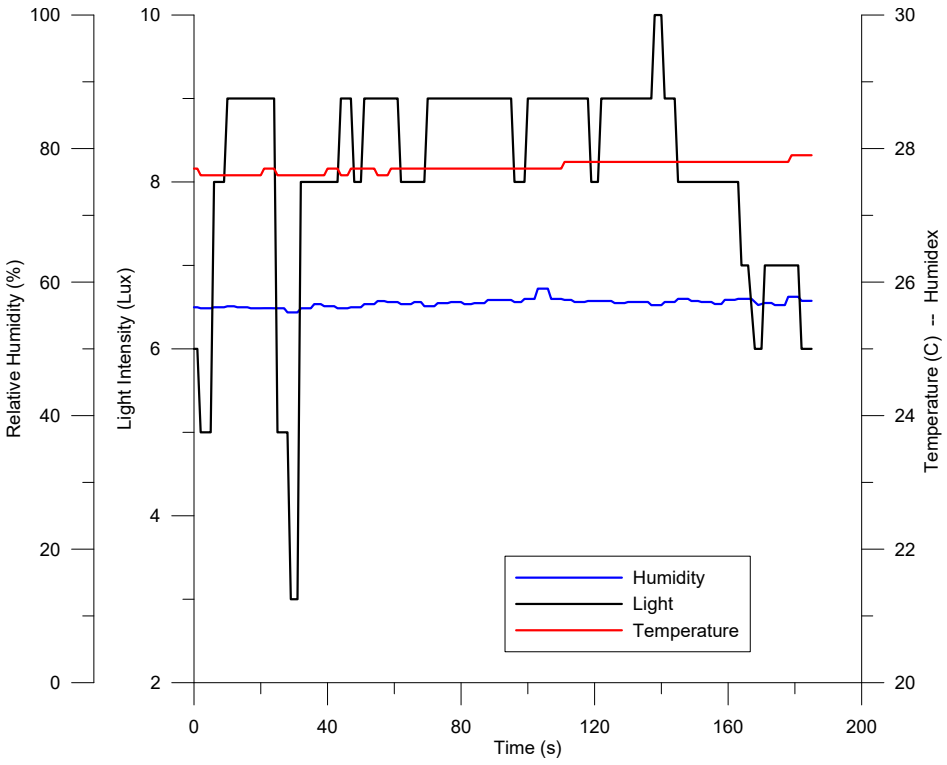


Figure C.199: Test 49 THLP 04

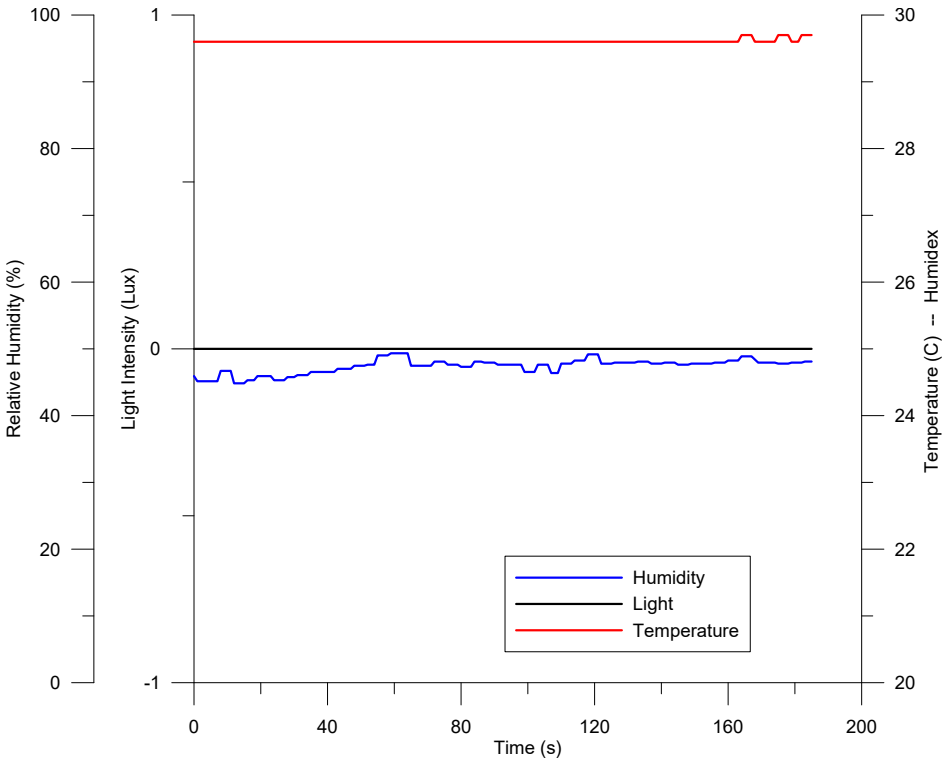


Figure C.200: Test 49 THLP 05

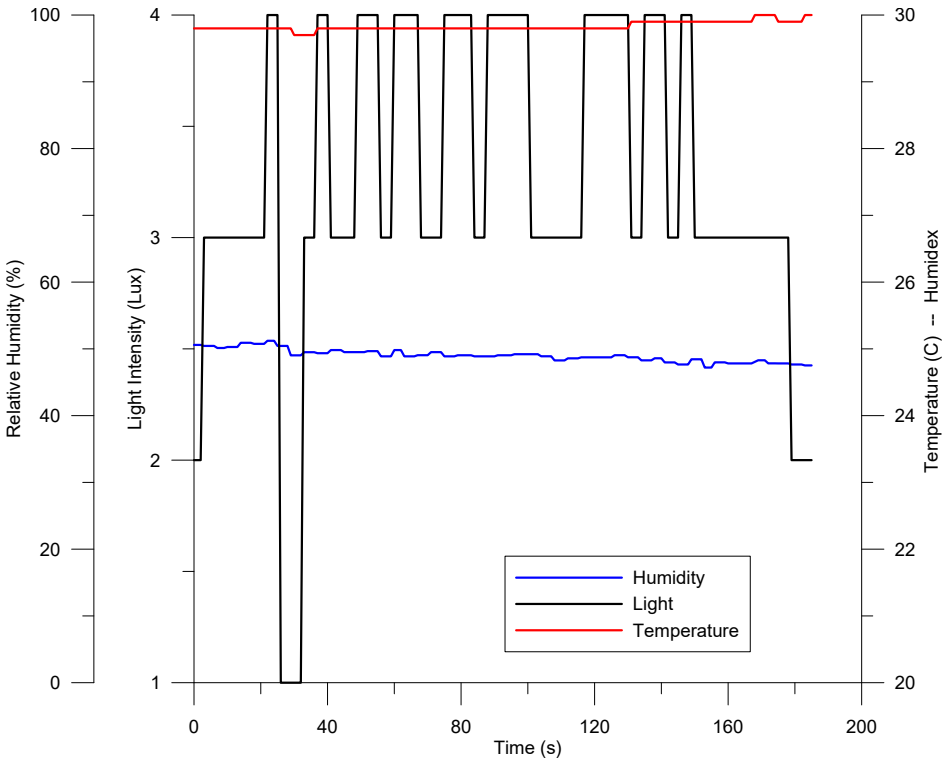


Figure C.201: Test 49 THLP 08

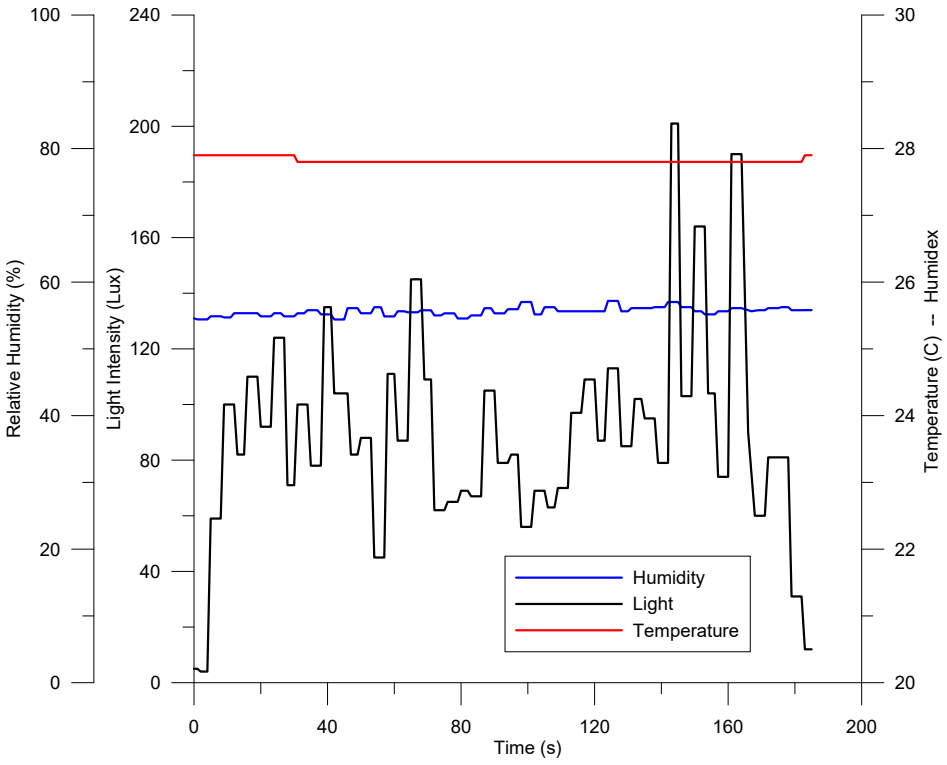


Figure C.202: Test 49 THLP 09

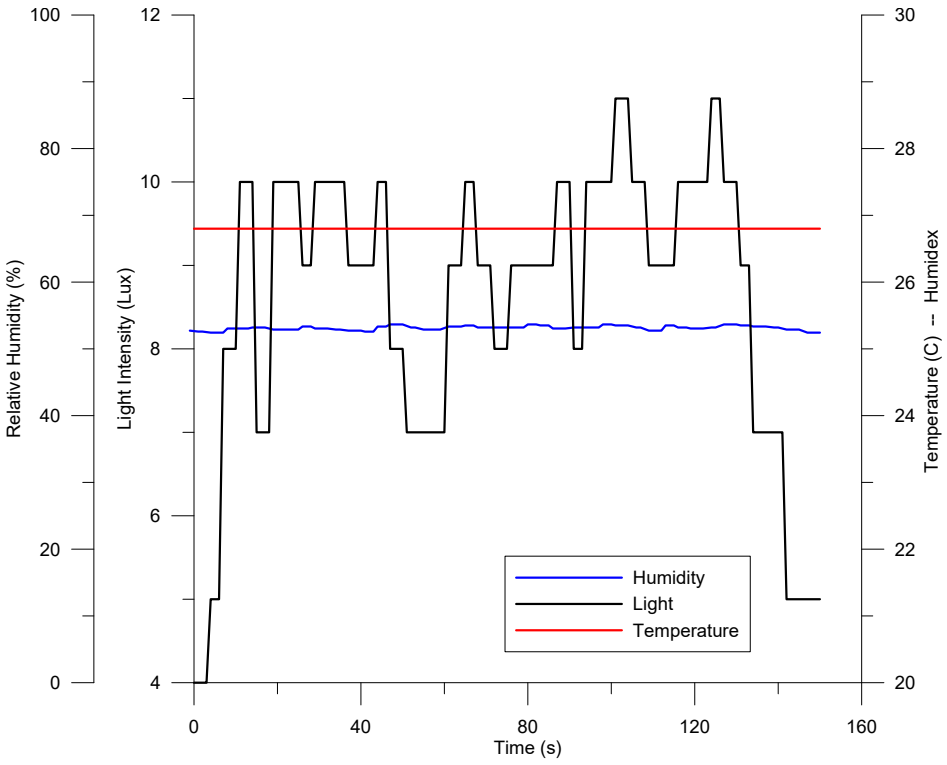


Figure C.203: Test 50 THLP 01

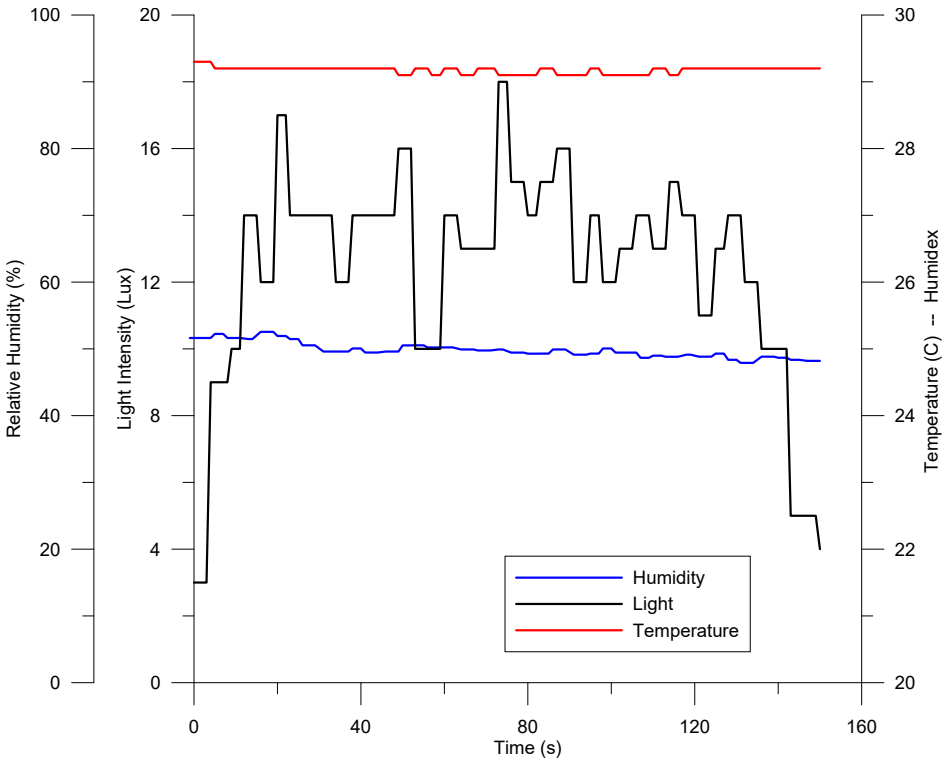


Figure C.204: Test 50 THLP 02

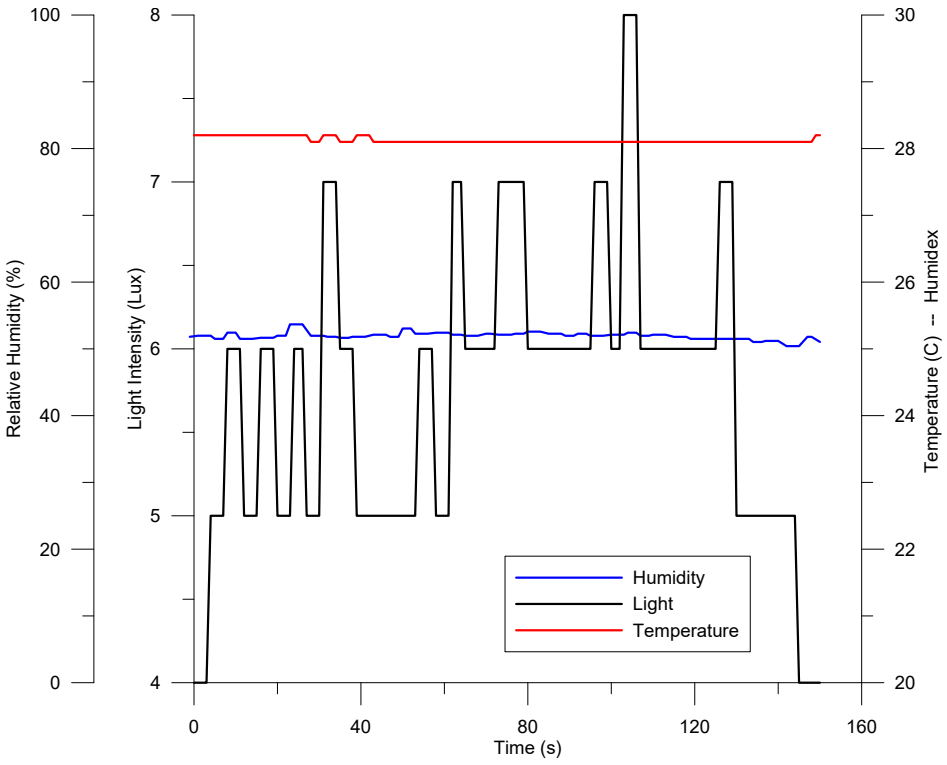


Figure C.205: Test 50 THLP 03

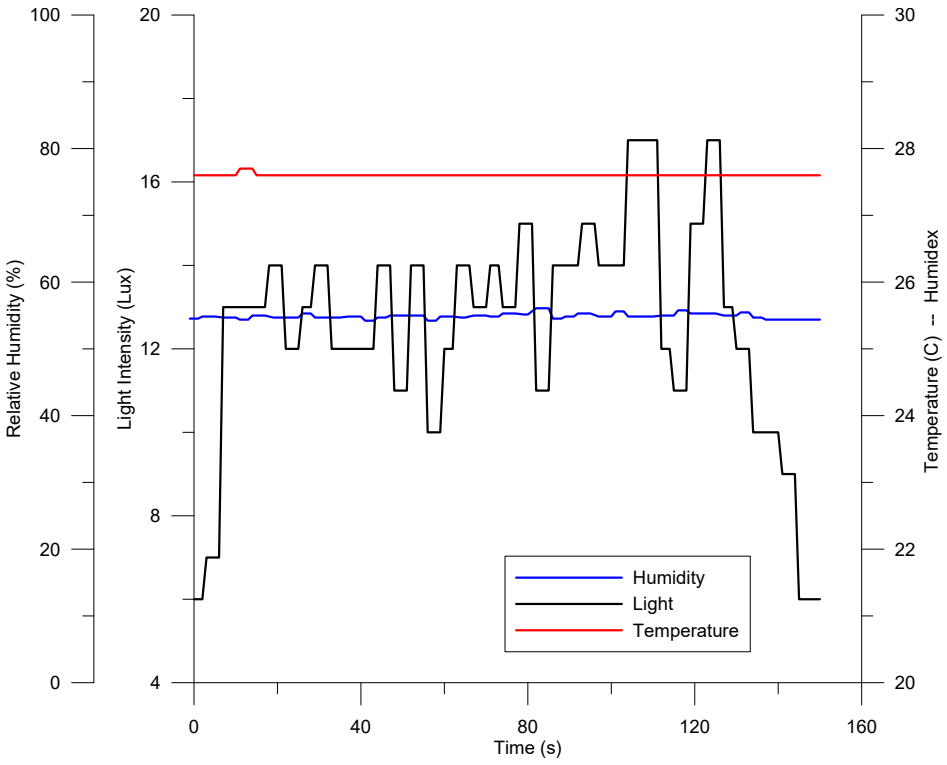


Figure C.206: Test 50 THLP 04

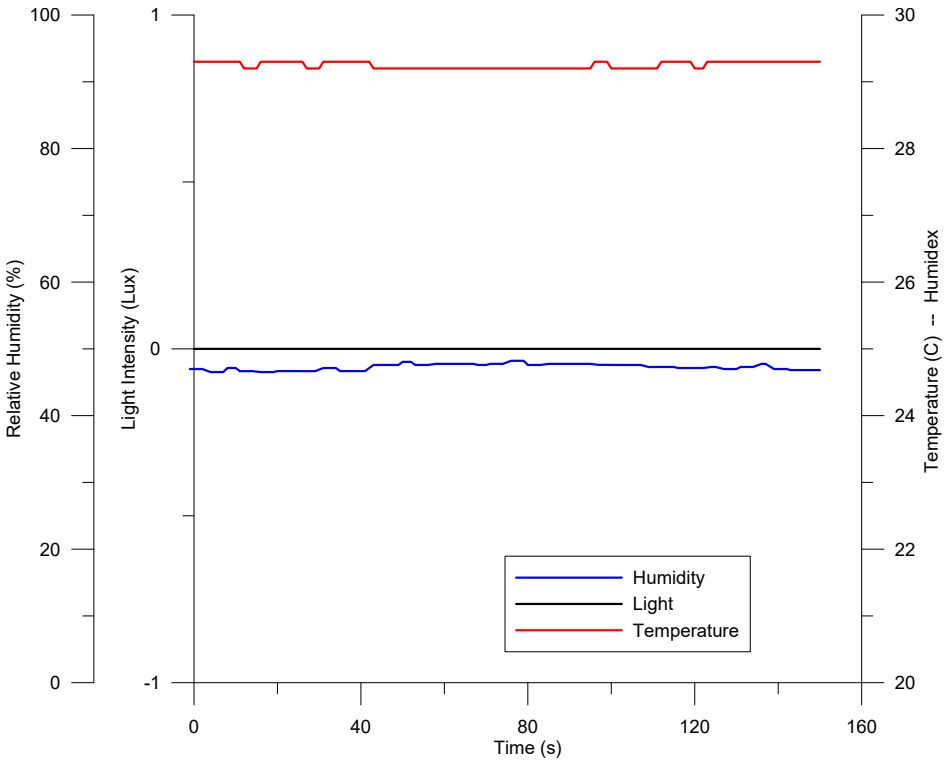


Figure C.207: Test 50 THLP 05

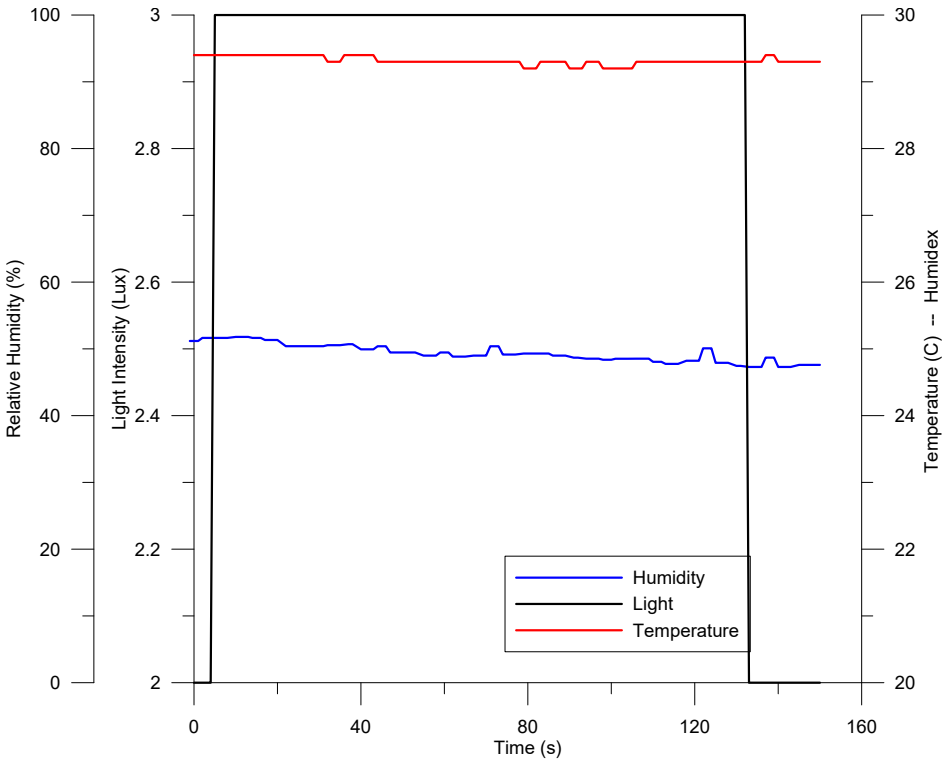


Figure C.208: Test 50 THLP 08

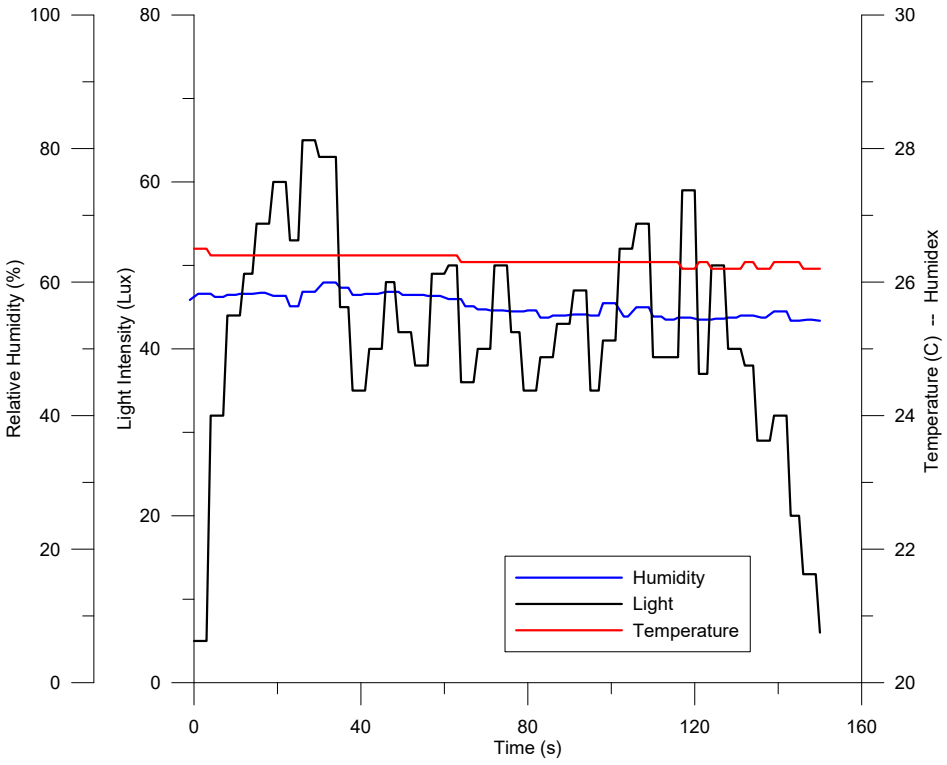


Figure C.209: Test 50 THLP 09

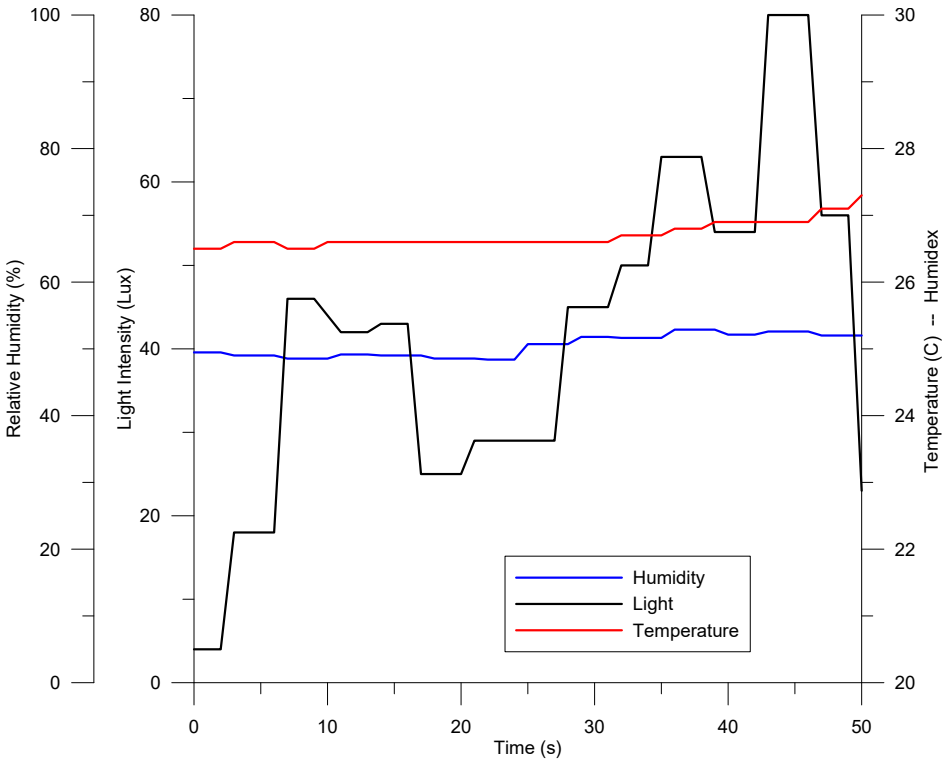


Figure C.210: Test 51 THLP 01

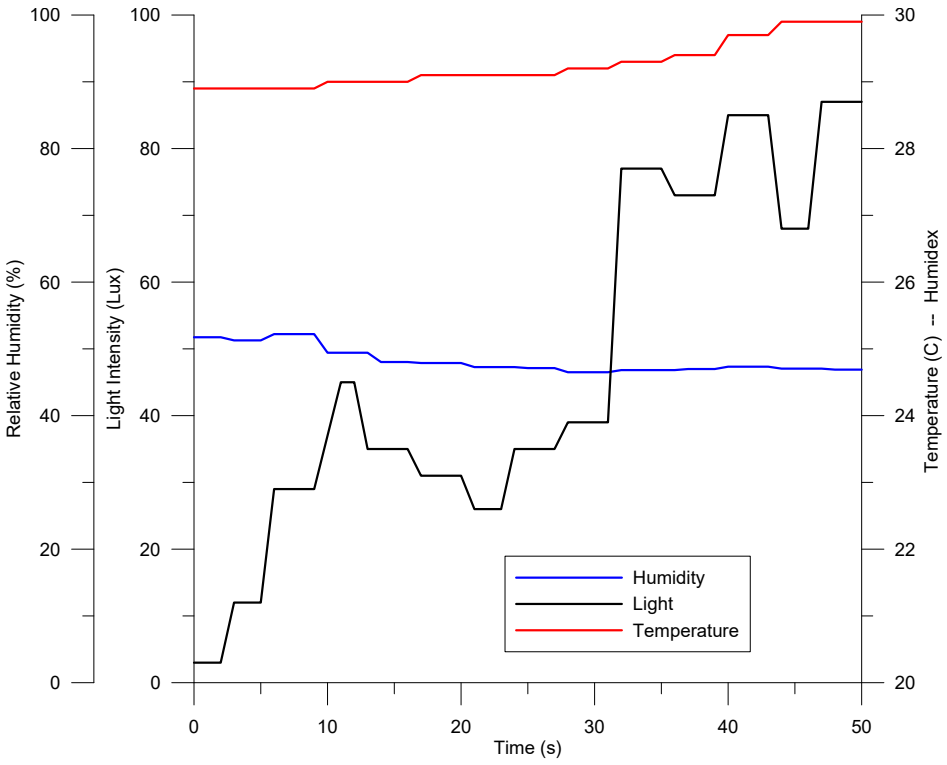


Figure C.211: Test 51 THLP 02

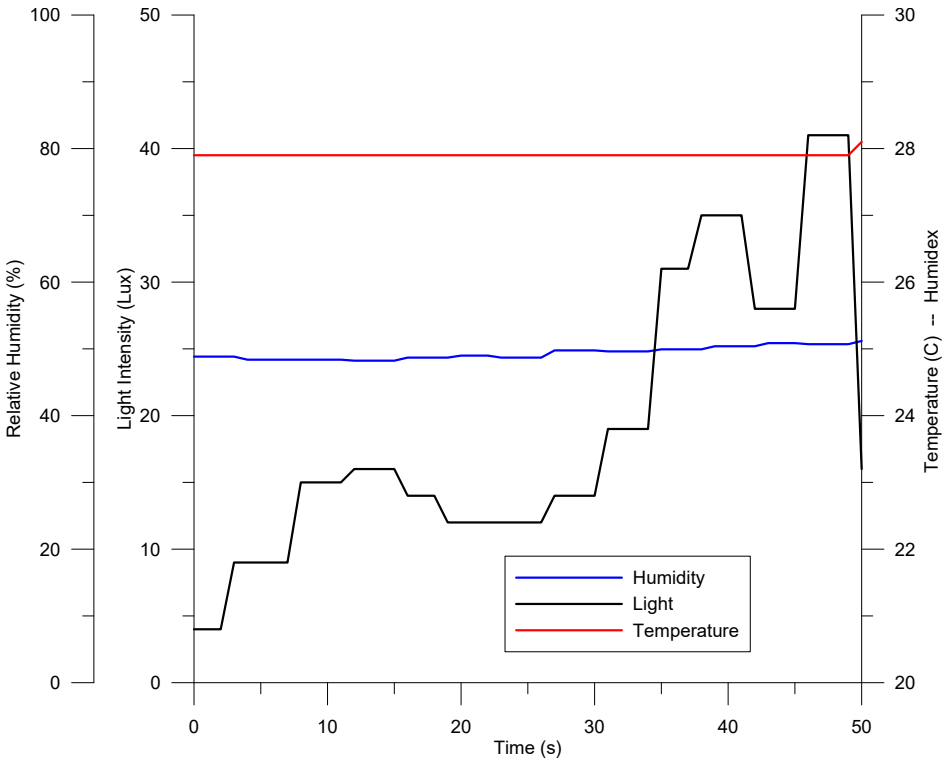


Figure C.212: Test 51 THLP 03

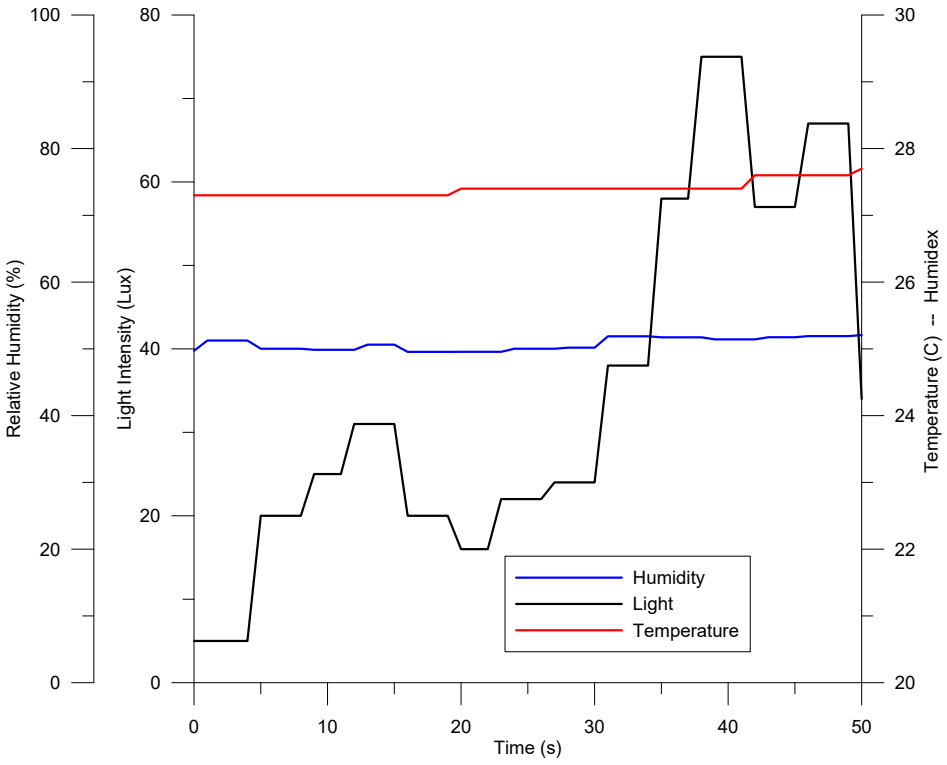


Figure C.213: Test 51 THLP 04

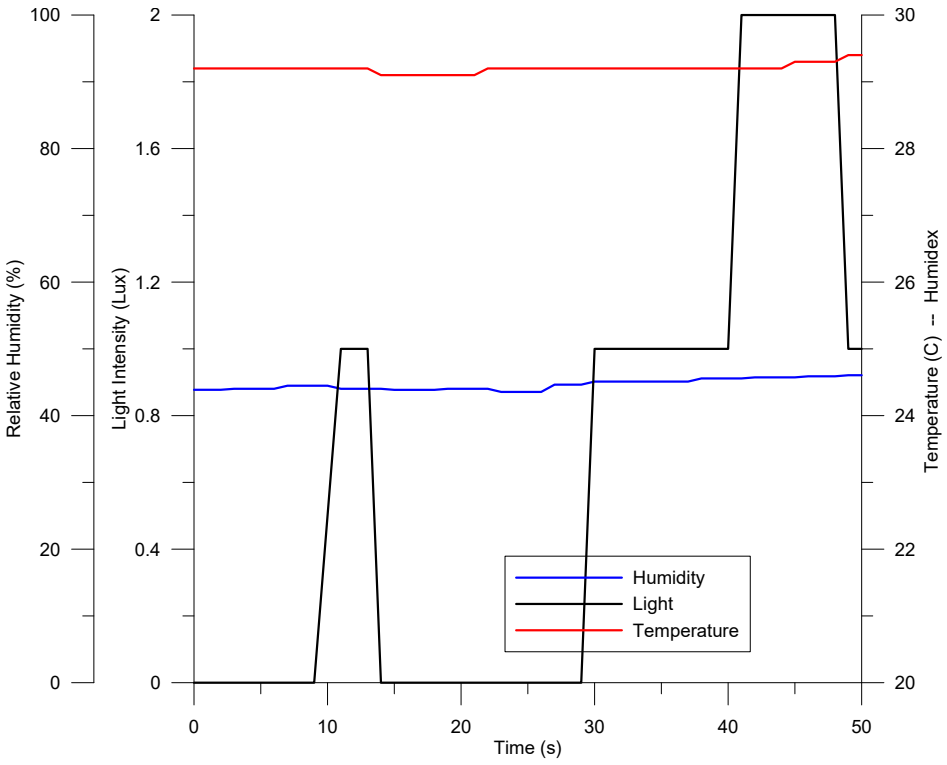


Figure C.214: Test 51 THLP 05

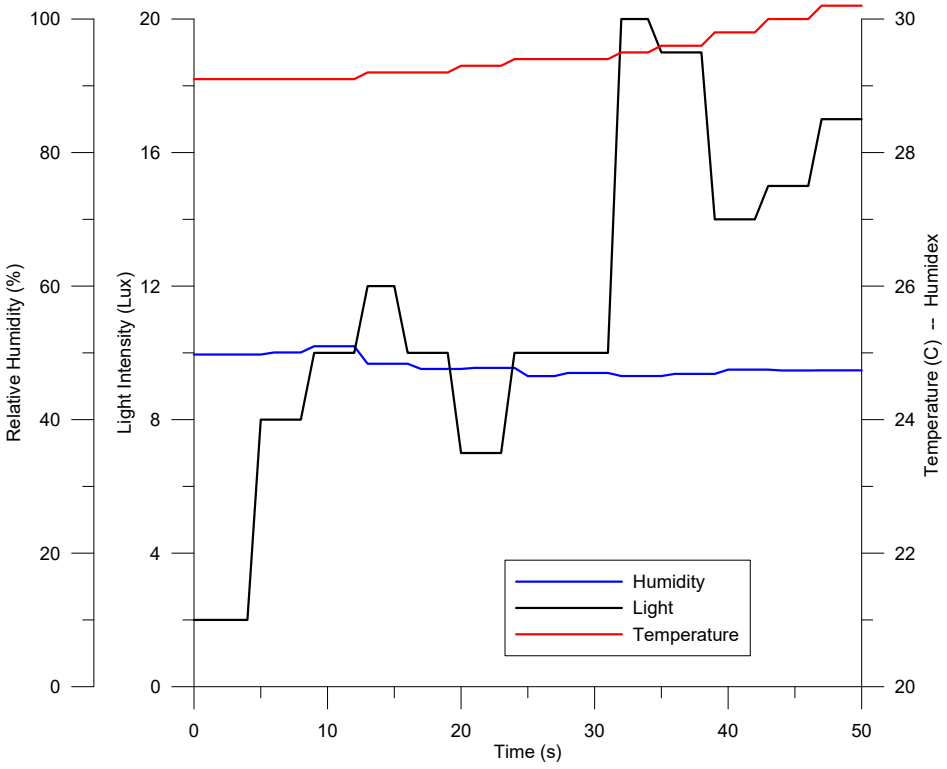


Figure C.215: Test 51 THLP 08

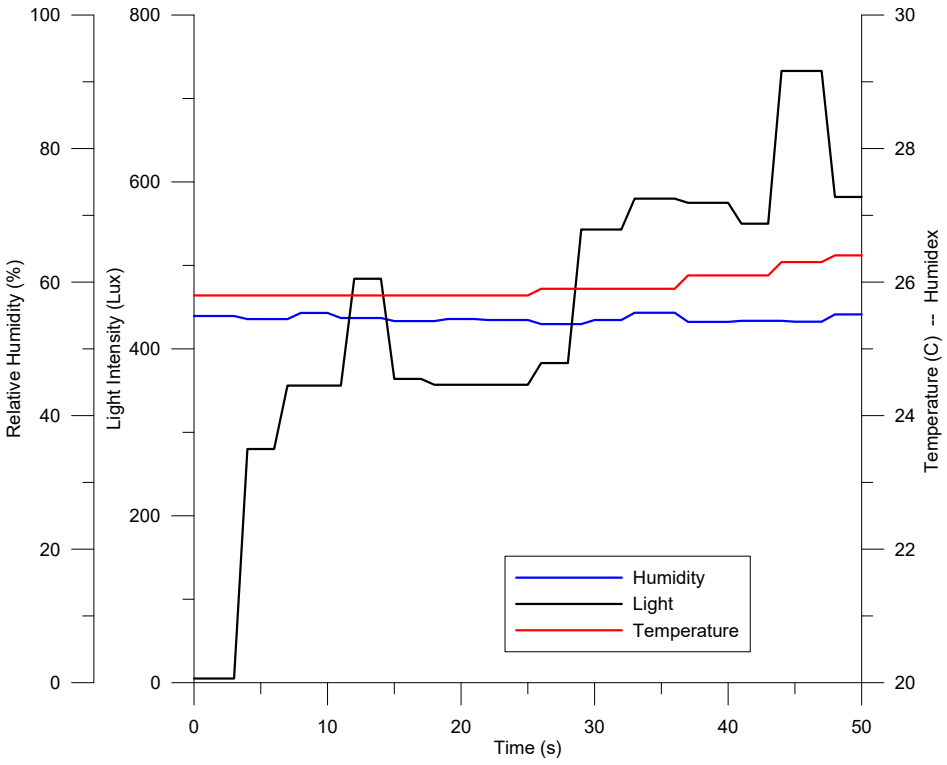


Figure C.216: Test 51 THLP 09

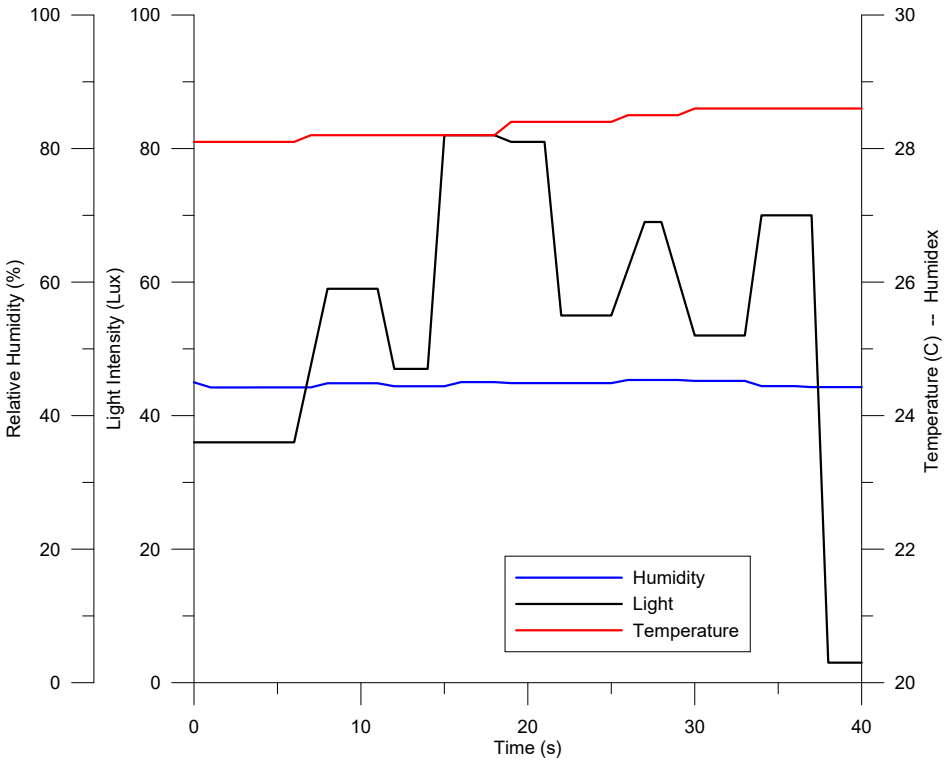


Figure C.217: Test 52 THLP 01

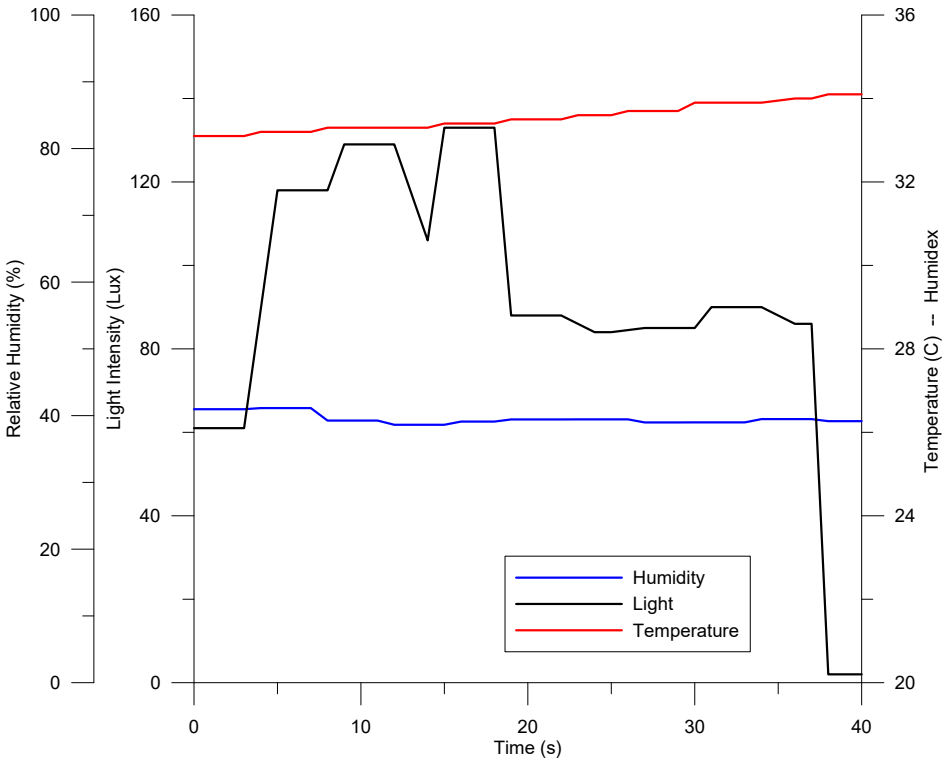


Figure C.218: Test 52 THLP 02

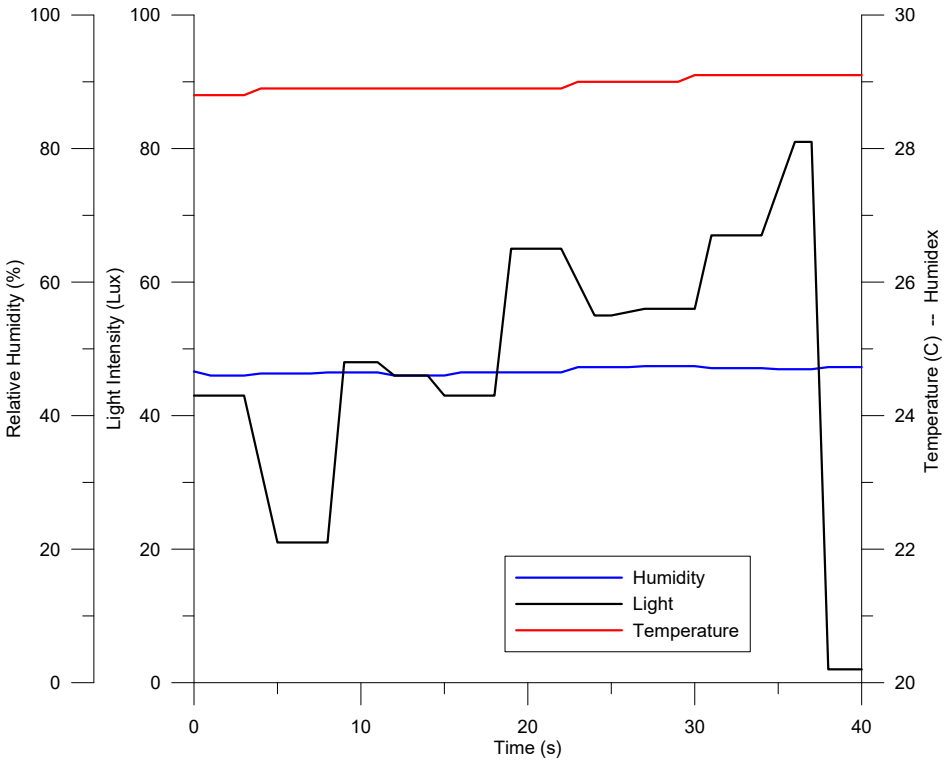


Figure C.219: Test 52 THLP 03

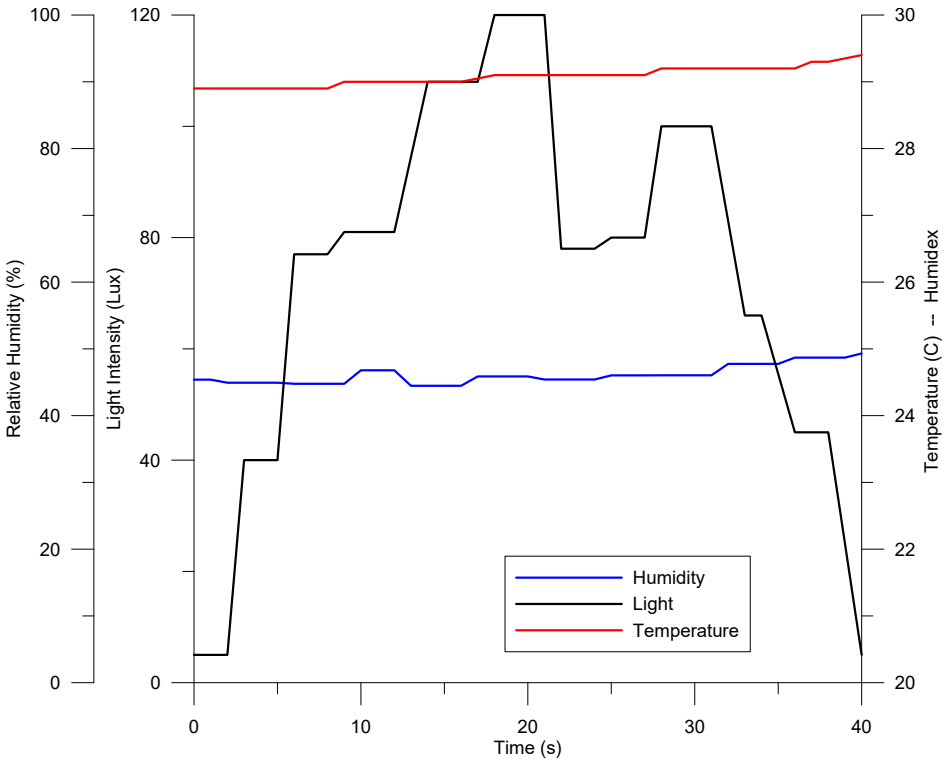


Figure C.220: Test 52 THLP 04

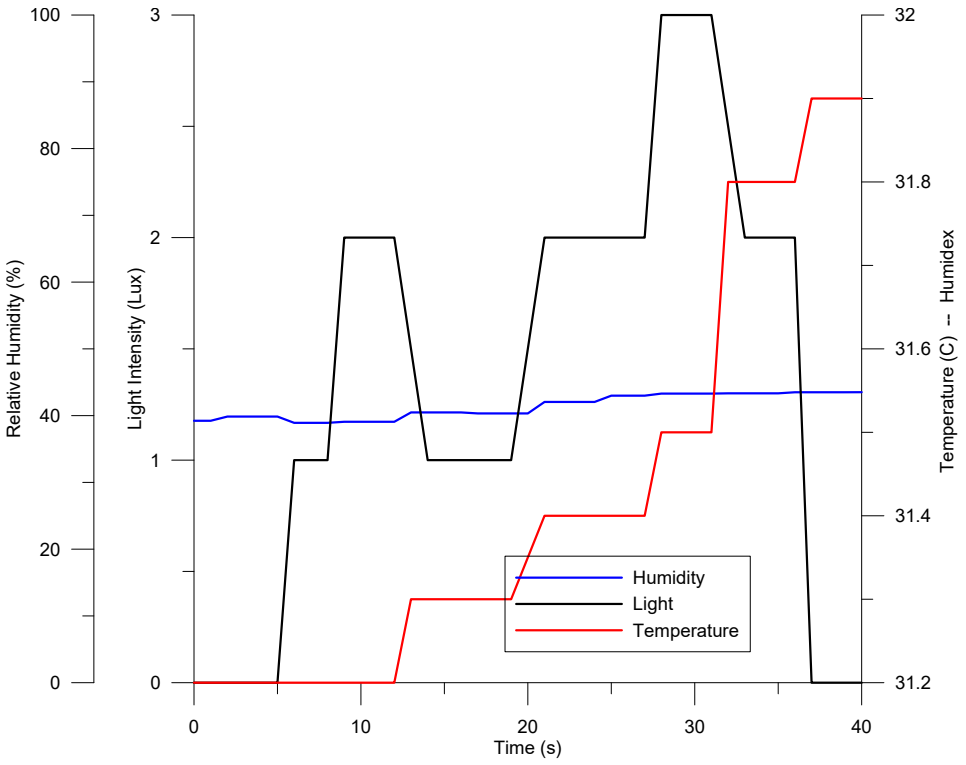


Figure C.221: Test 52 THLP 05

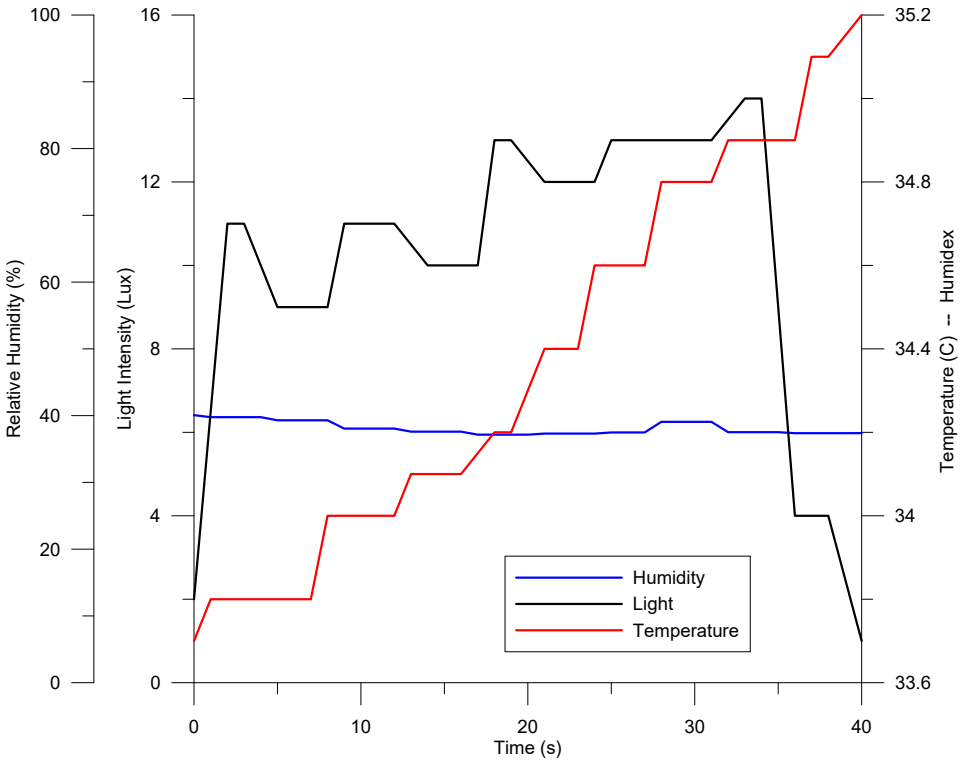


Figure C.222: Test 52 THLP 08

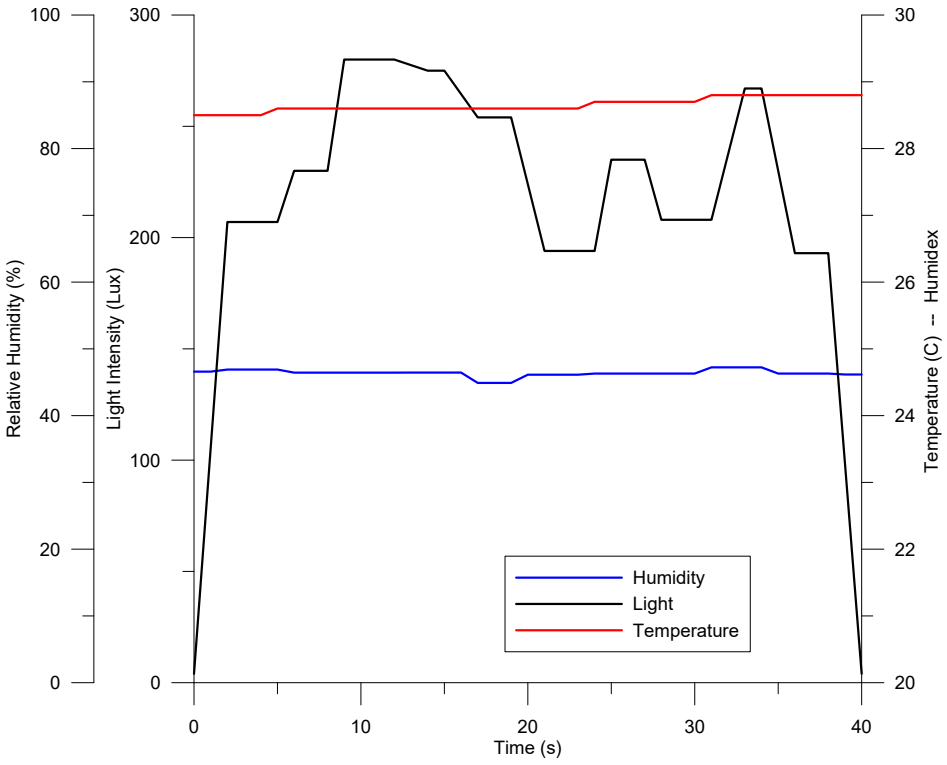


Figure C.223: Test 52 THLP 09

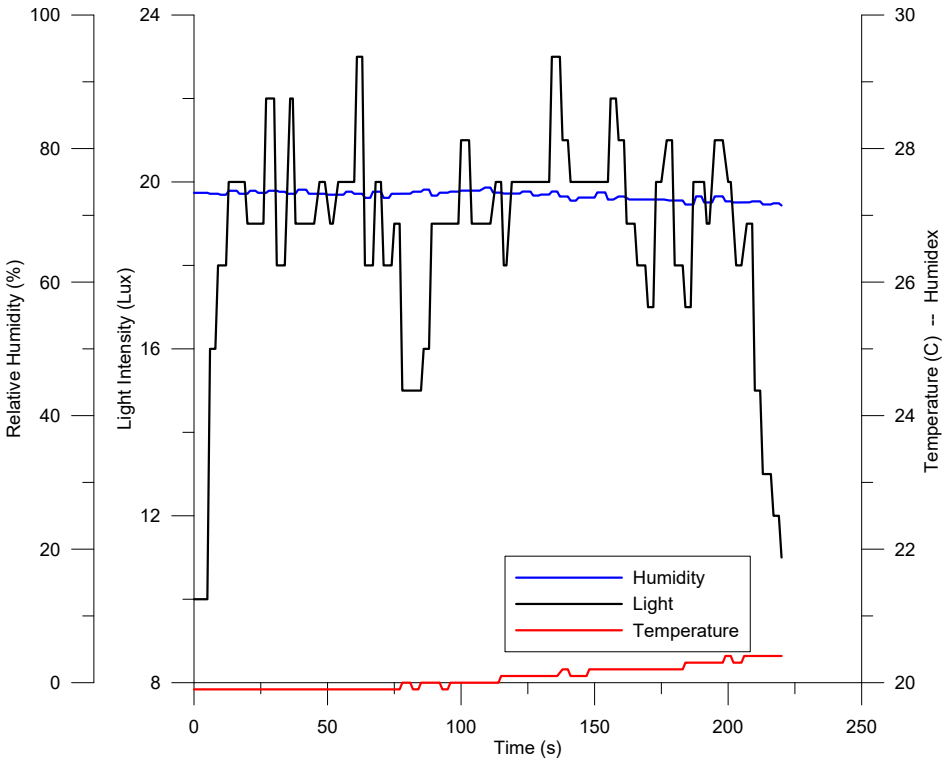


Figure C.224: Test 53 THLP 01

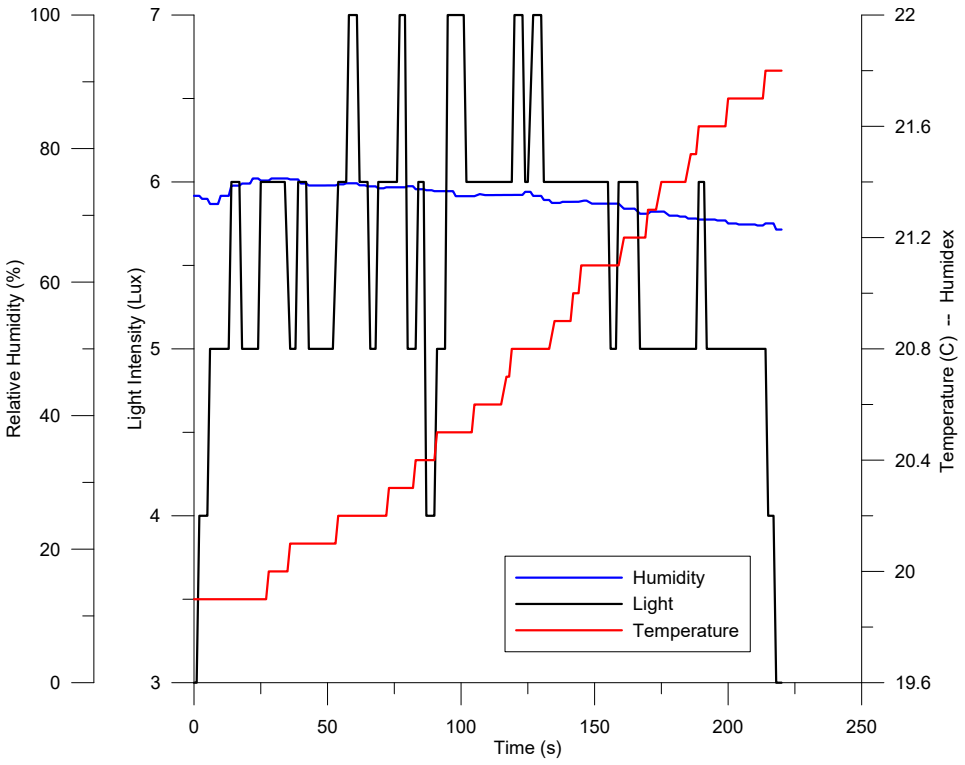


Figure C.225: Test 53 THLP 02

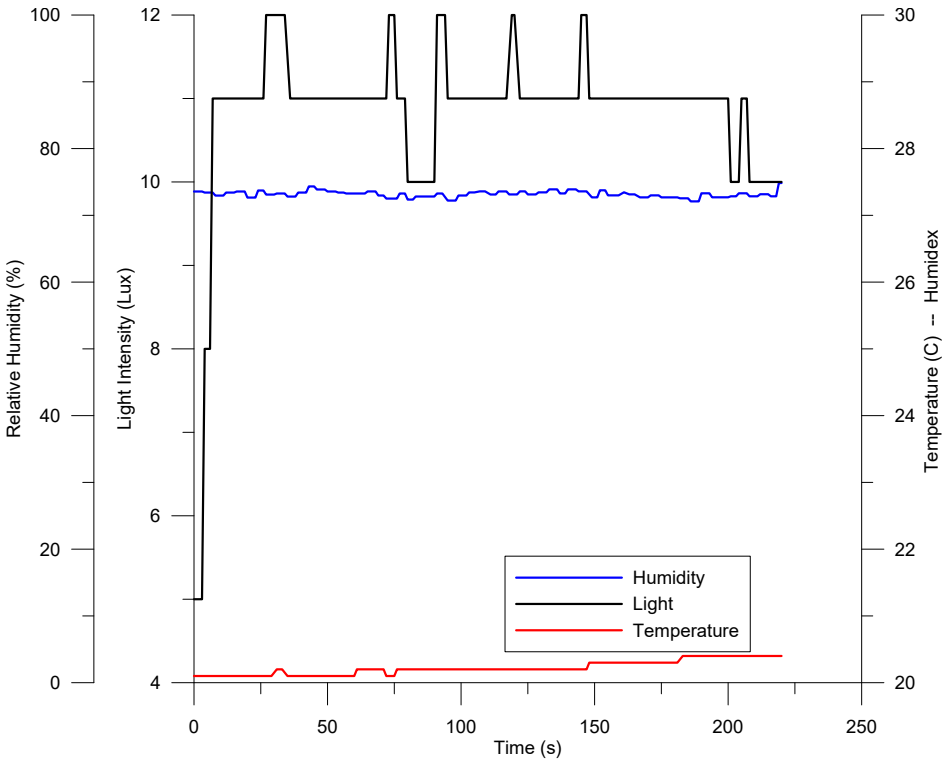


Figure C.226: Test 53 THLP 03

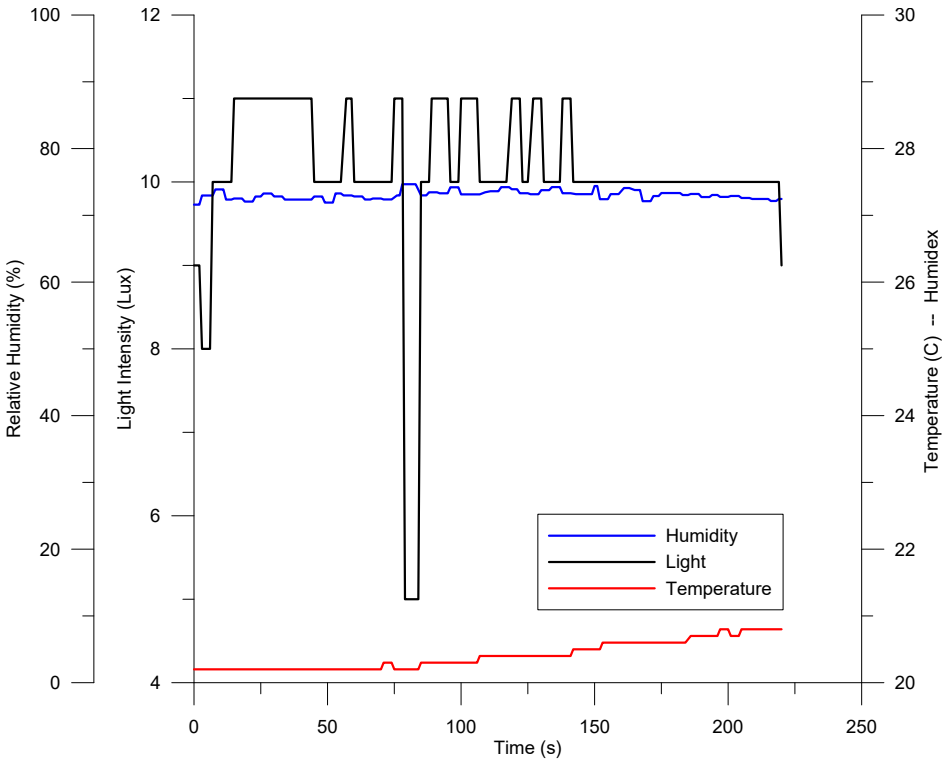


Figure C.227: Test 53 THLP 04

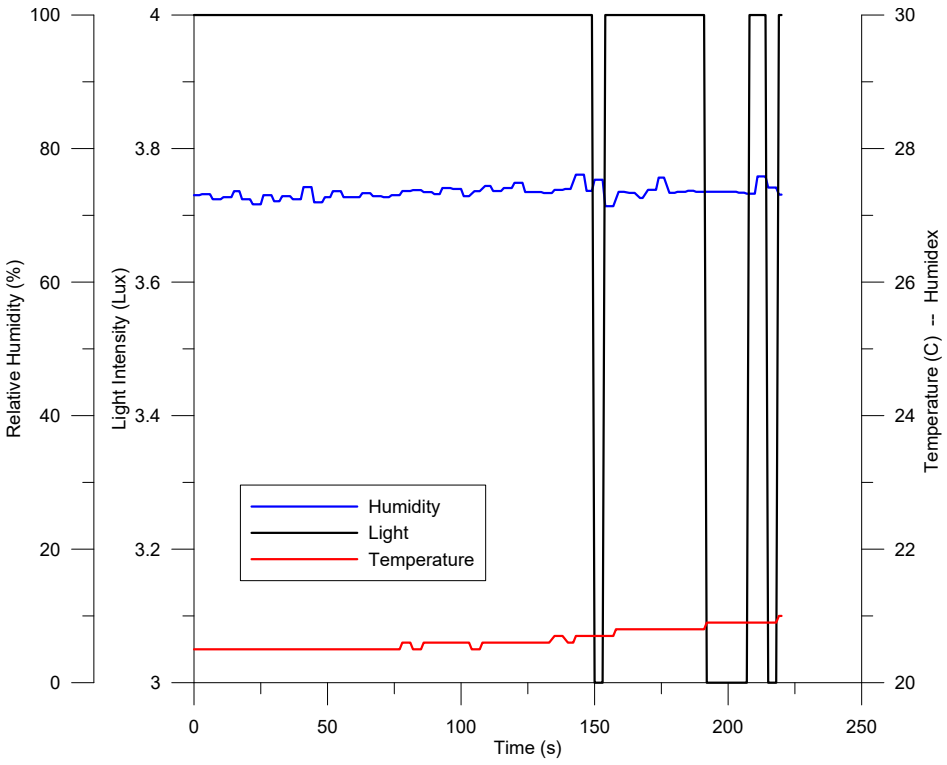


Figure C.228: Test 53 THLP 05

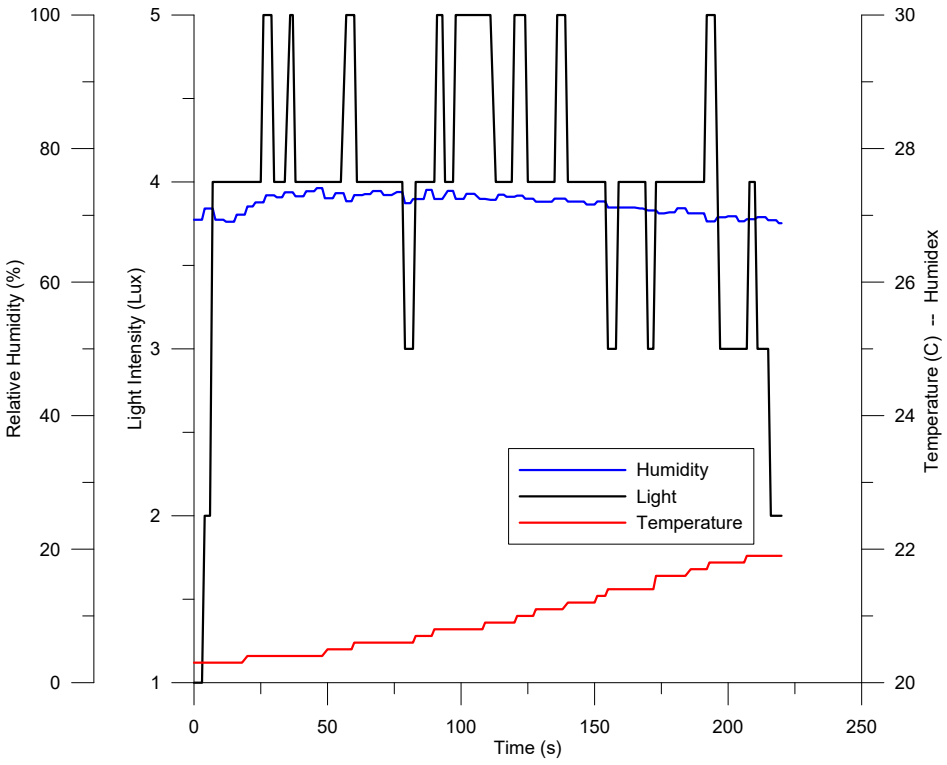


Figure C.229: Test 53 THLP 08

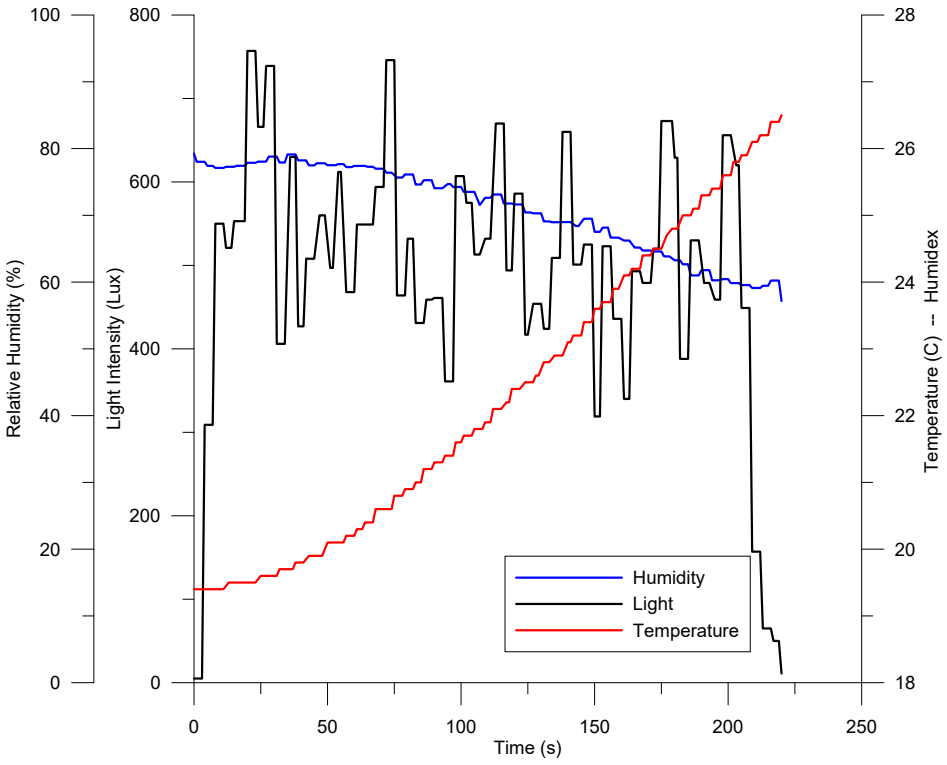


Figure C.230: Test 53 THLP 09

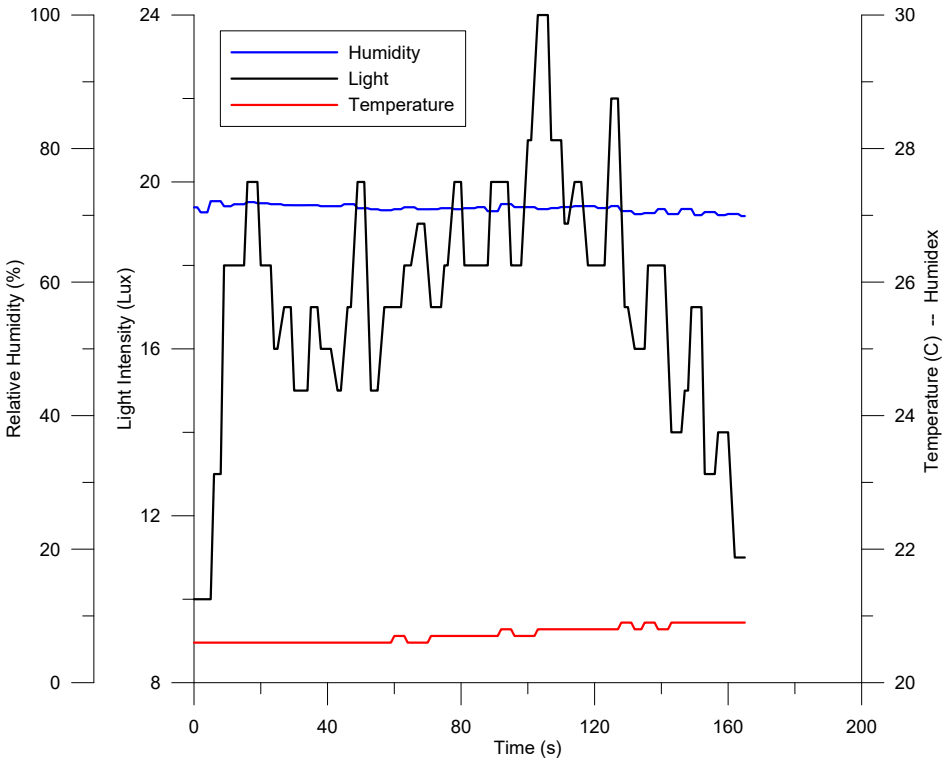


Figure C.231: Test 54 THLP 01

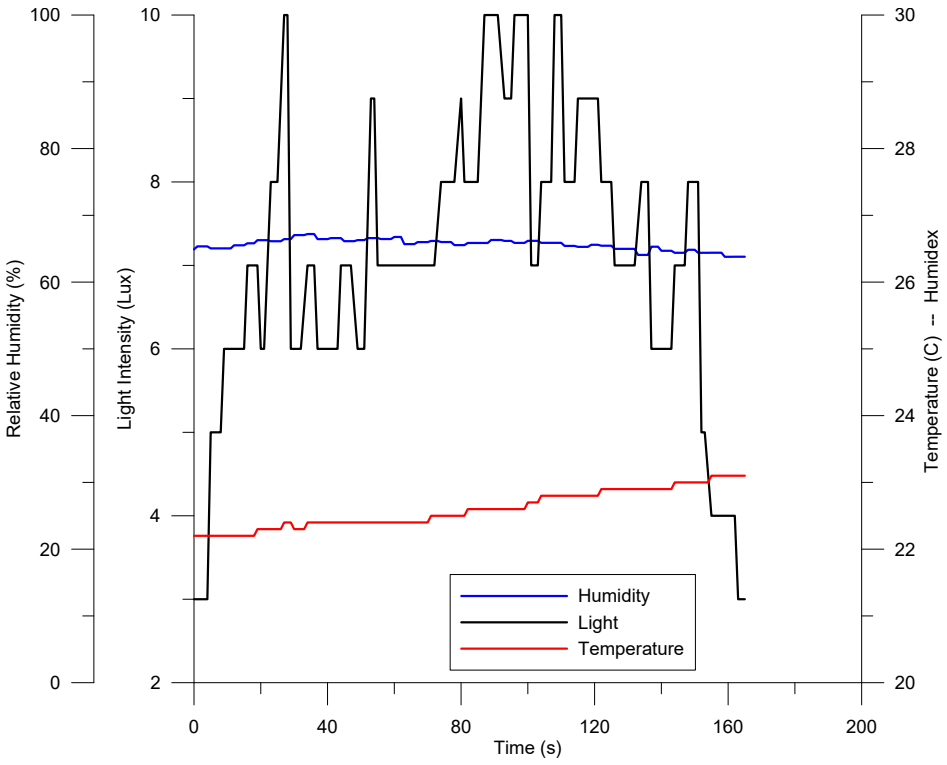


Figure C.232: Test 54 THLP 02

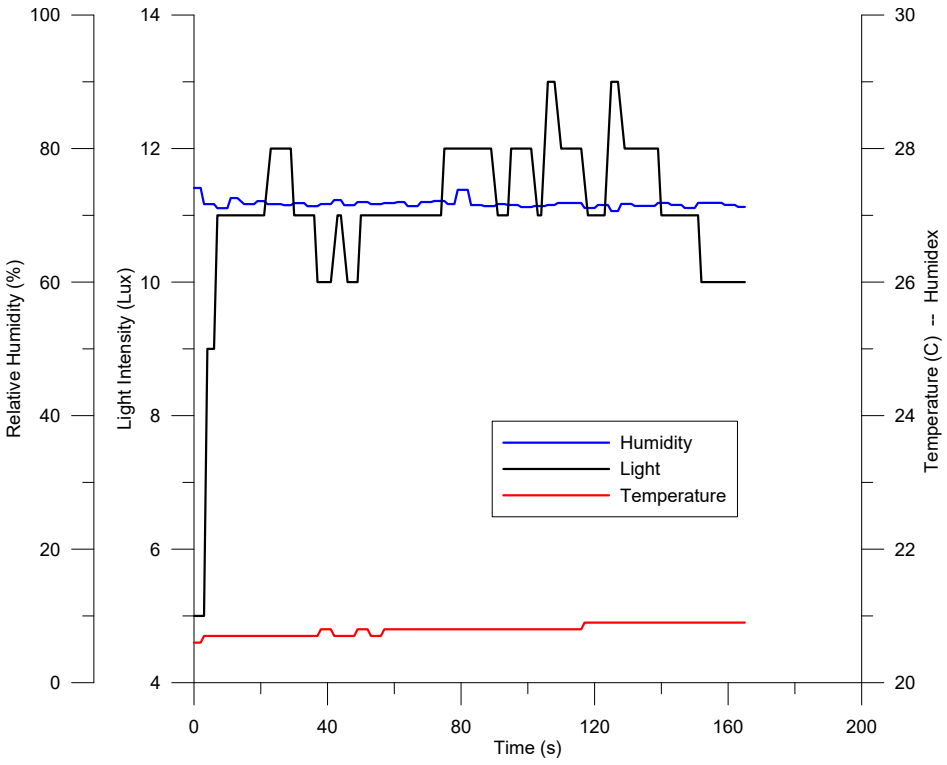


Figure C.233: Test 54 THLP 03

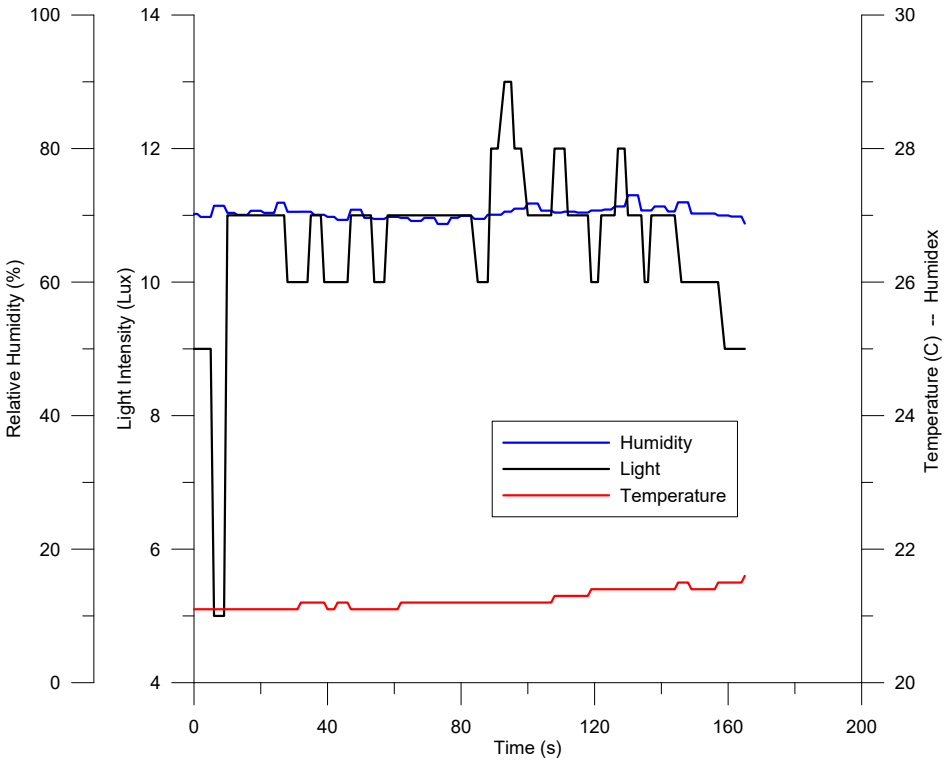


Figure C.234: Test 54 THLP 04

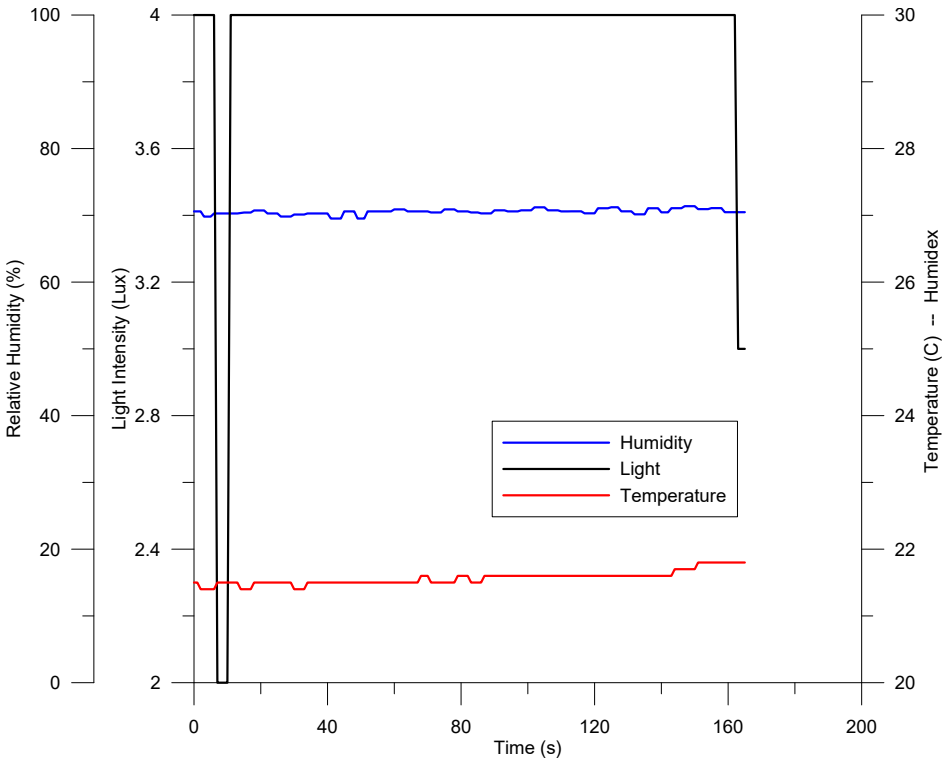


Figure C.235: Test 54 THLP 05

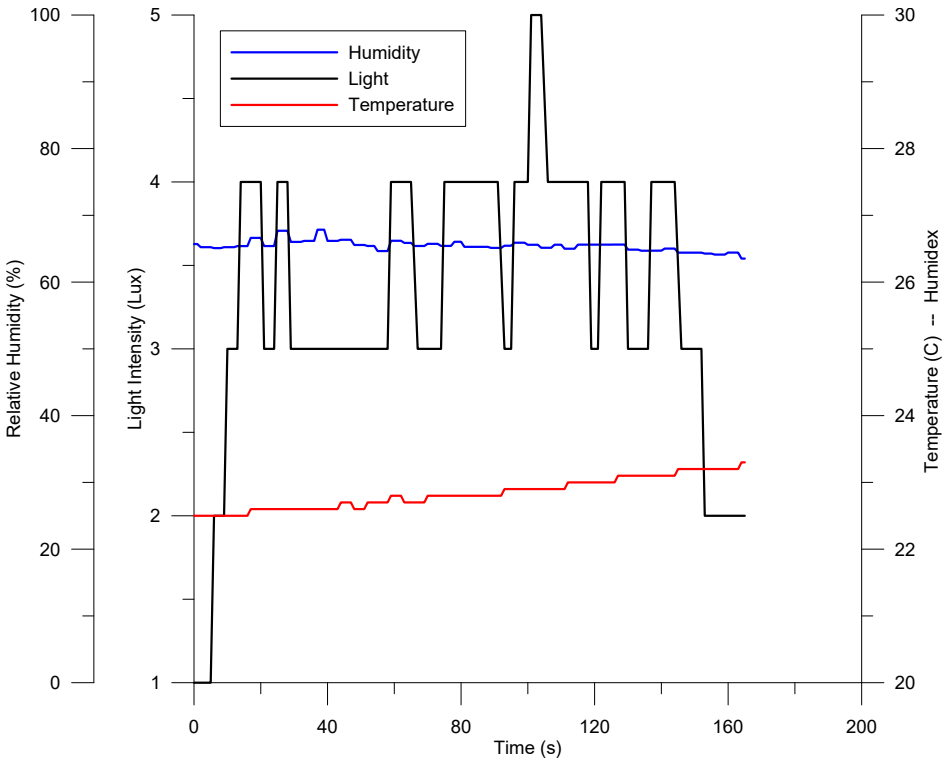


Figure C.236: Test 54 THLP 08

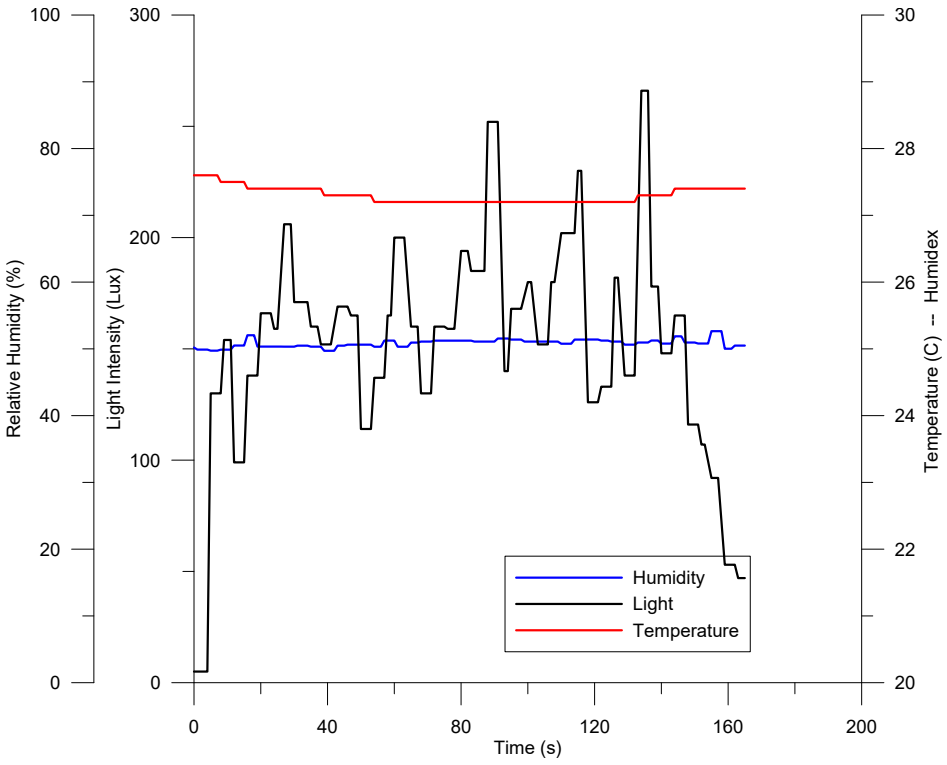


Figure C.237: Test 54 THLP 09

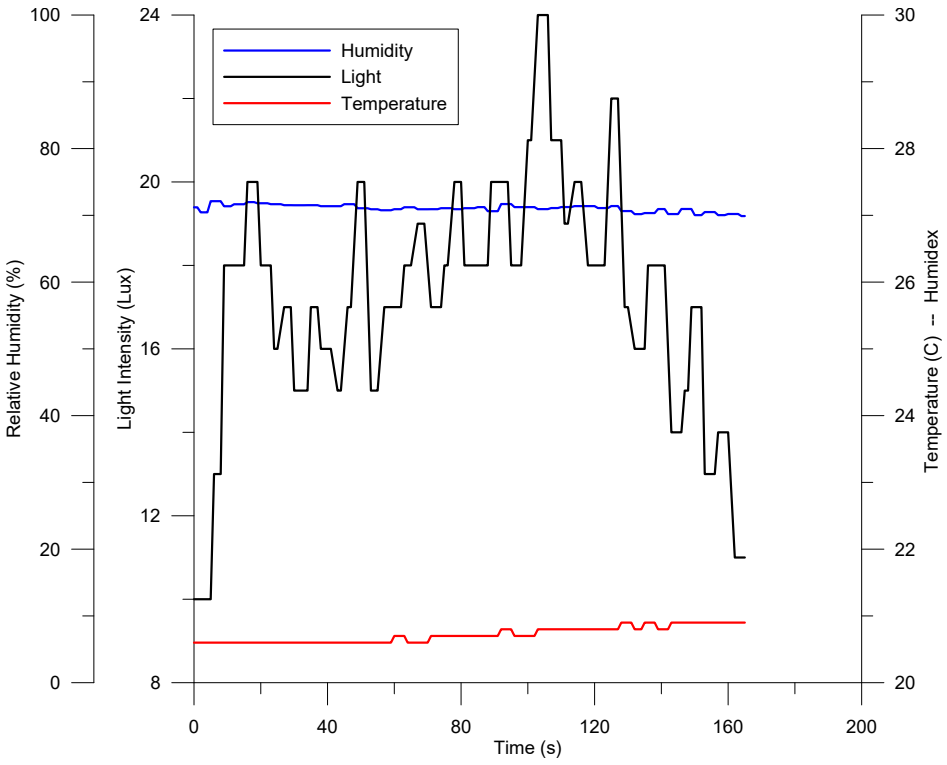


Figure C.238: Test 55 THLP 01

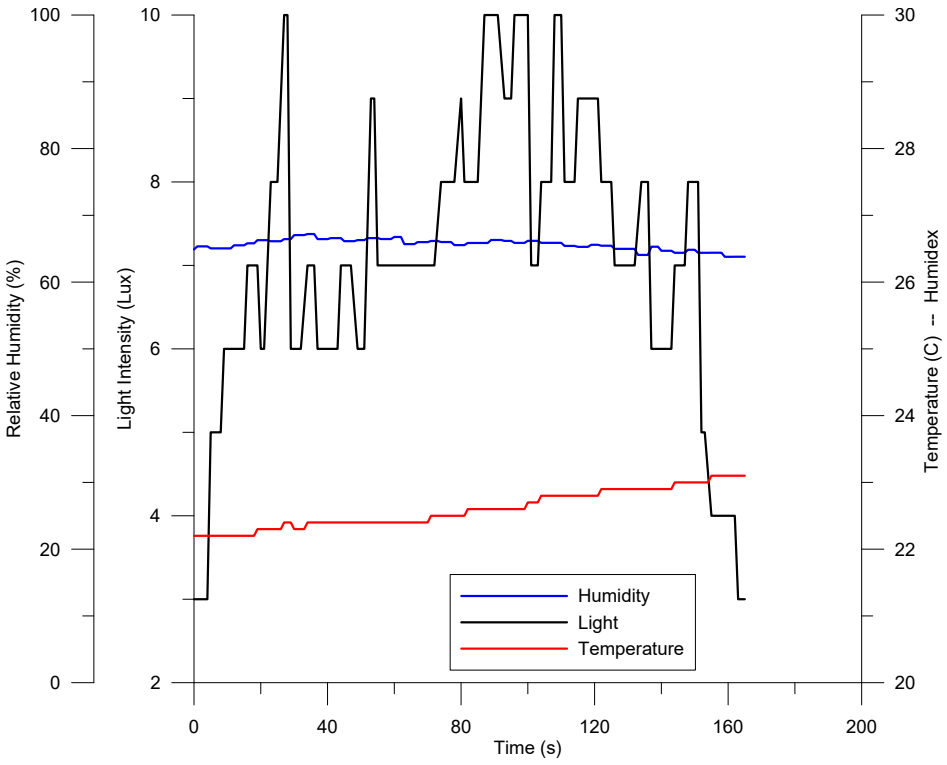


Figure C.239: Test 55 THLP 02

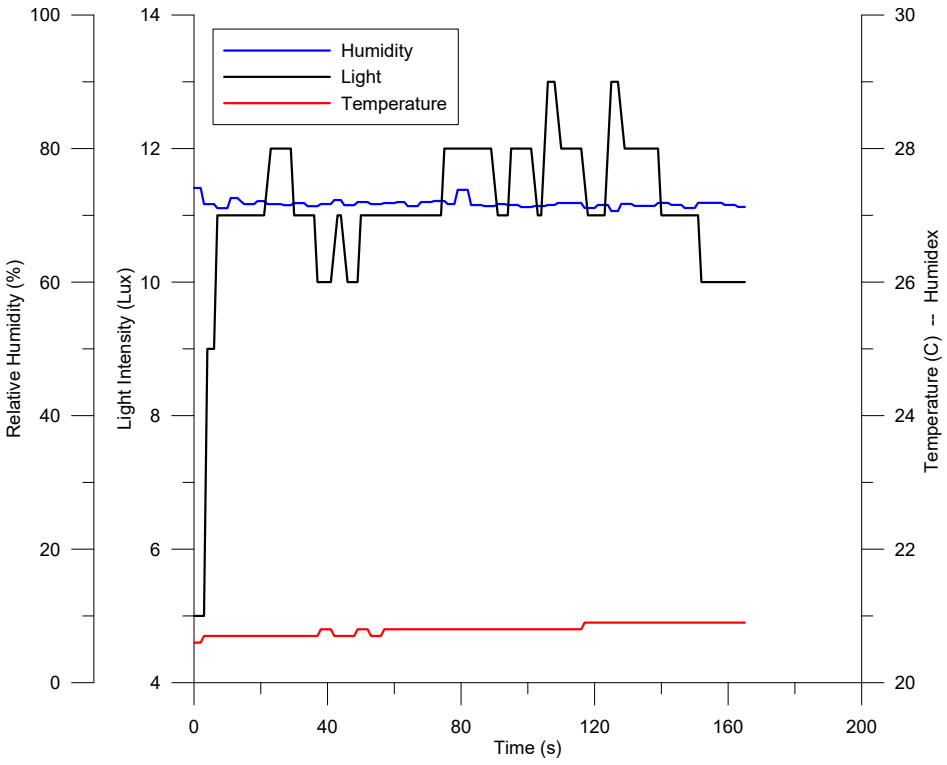


Figure C.240: Test 55 THLP 03

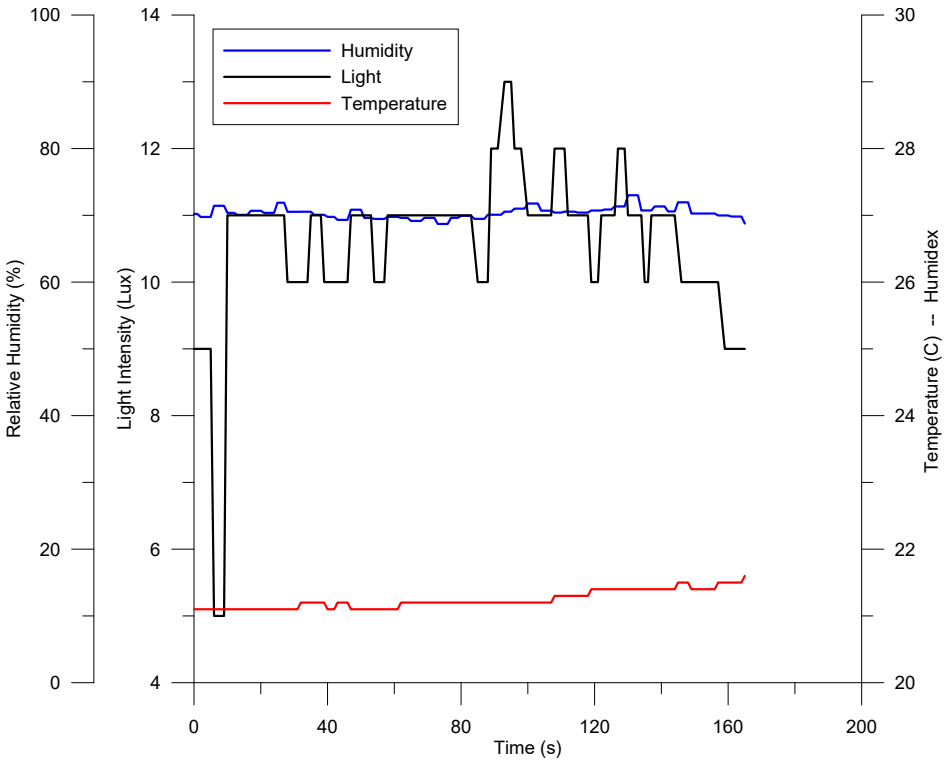


Figure C.241: Test 55 THLP 04

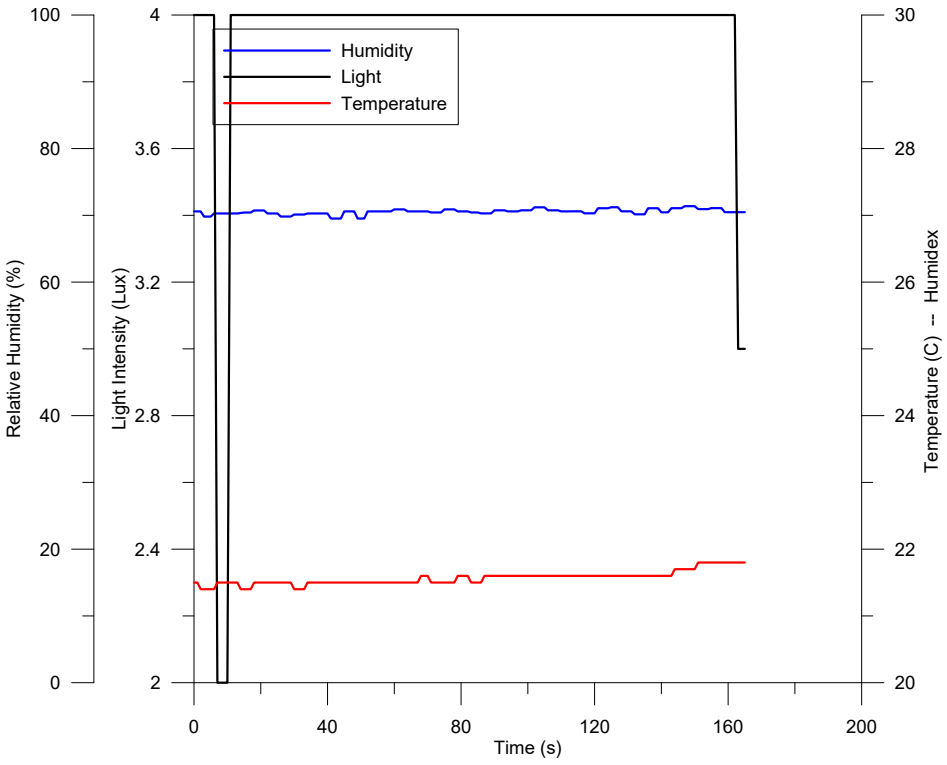


Figure C.242: Test 55 THLP 05

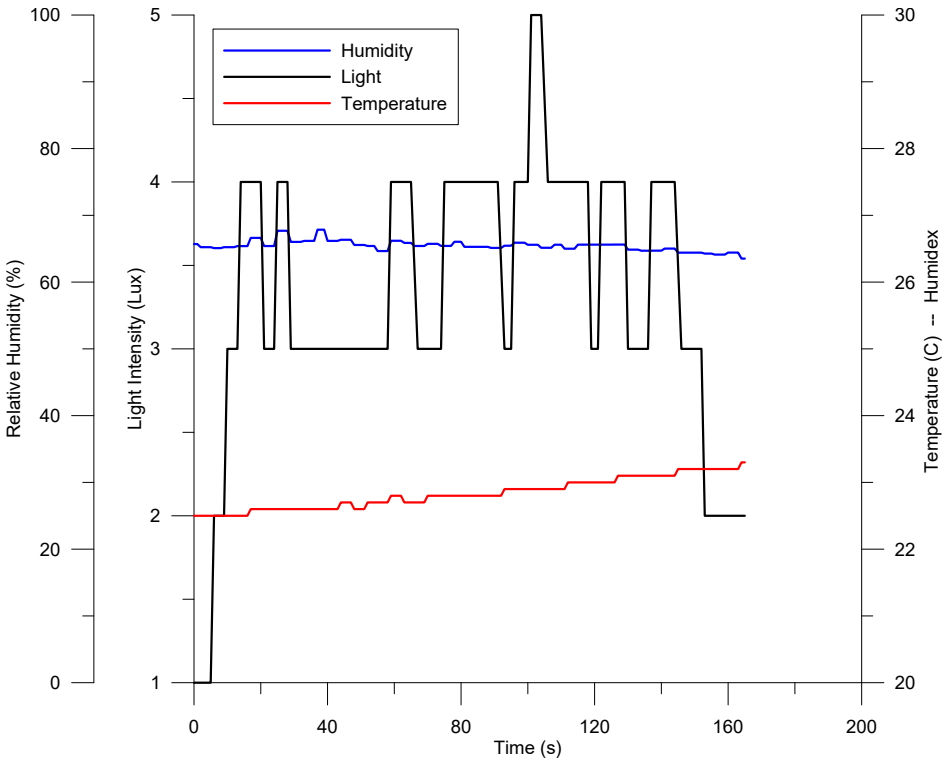


Figure C.243: Test 55 THLP 08

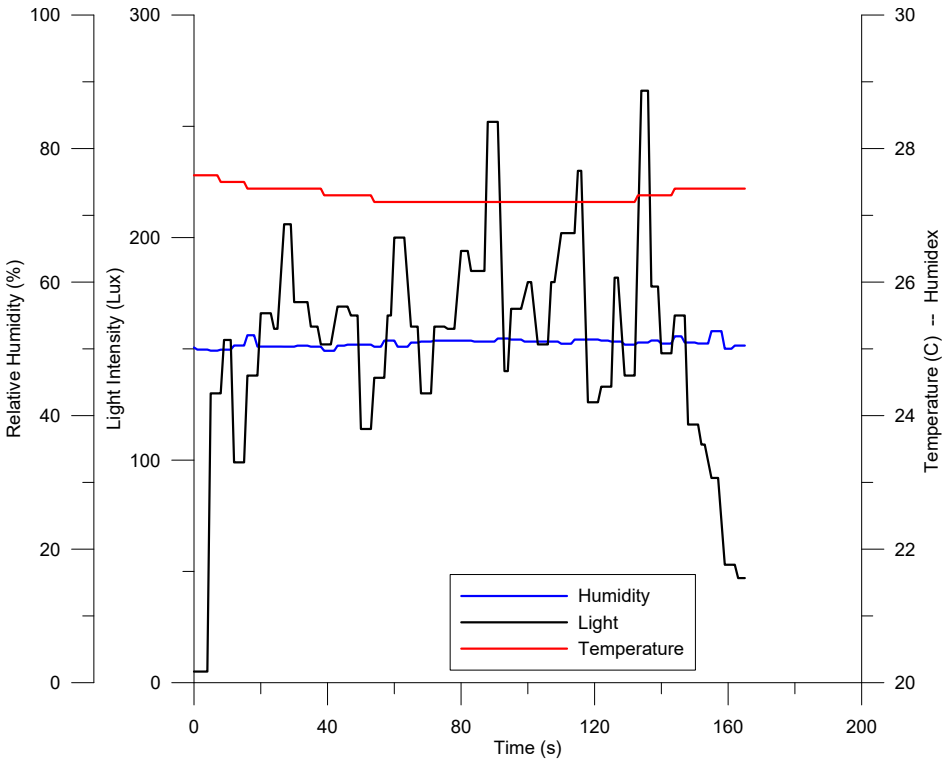


Figure C.244: Test 55 THLP 09

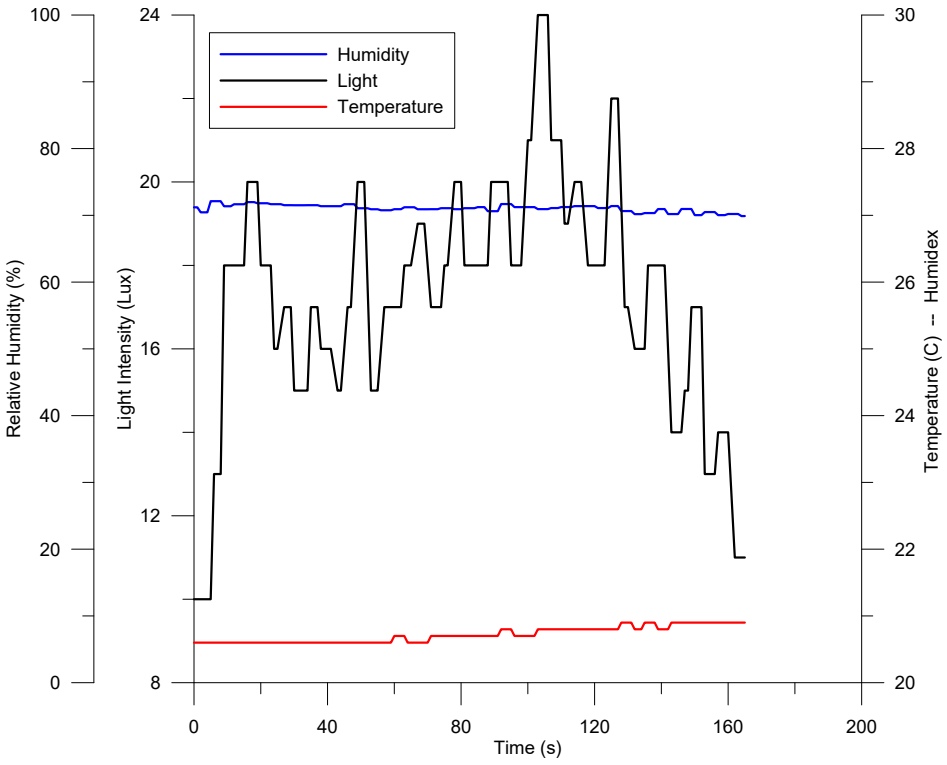


Figure C.245: Test 56 THLP 01

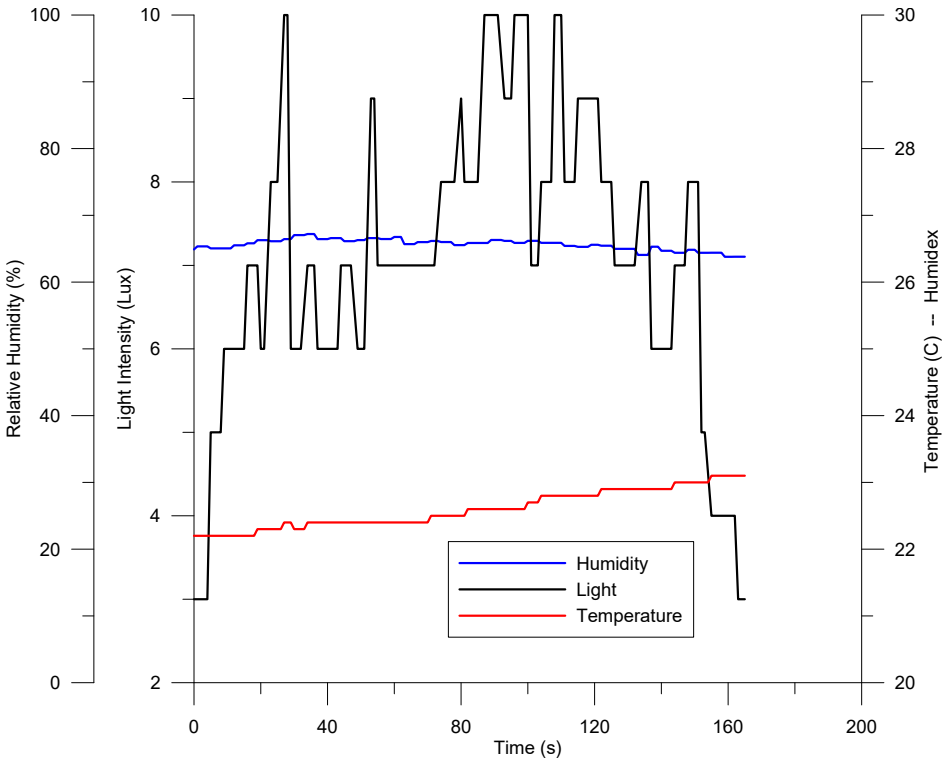


Figure C.246: Test 56 THLP 02

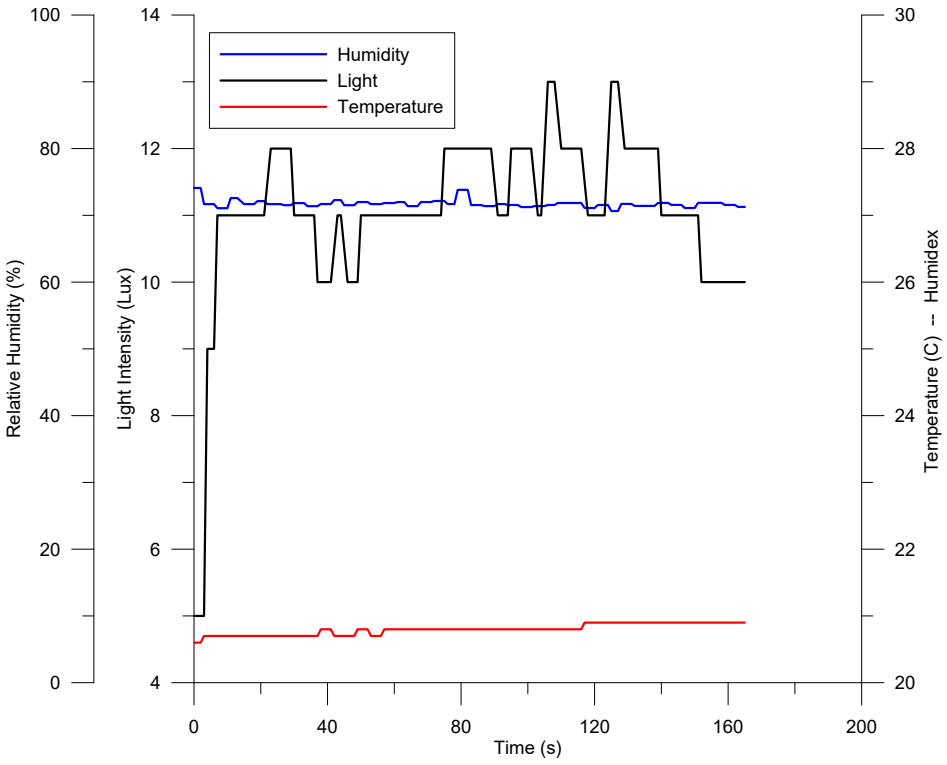


Figure C.247: Test 56 THLP 03

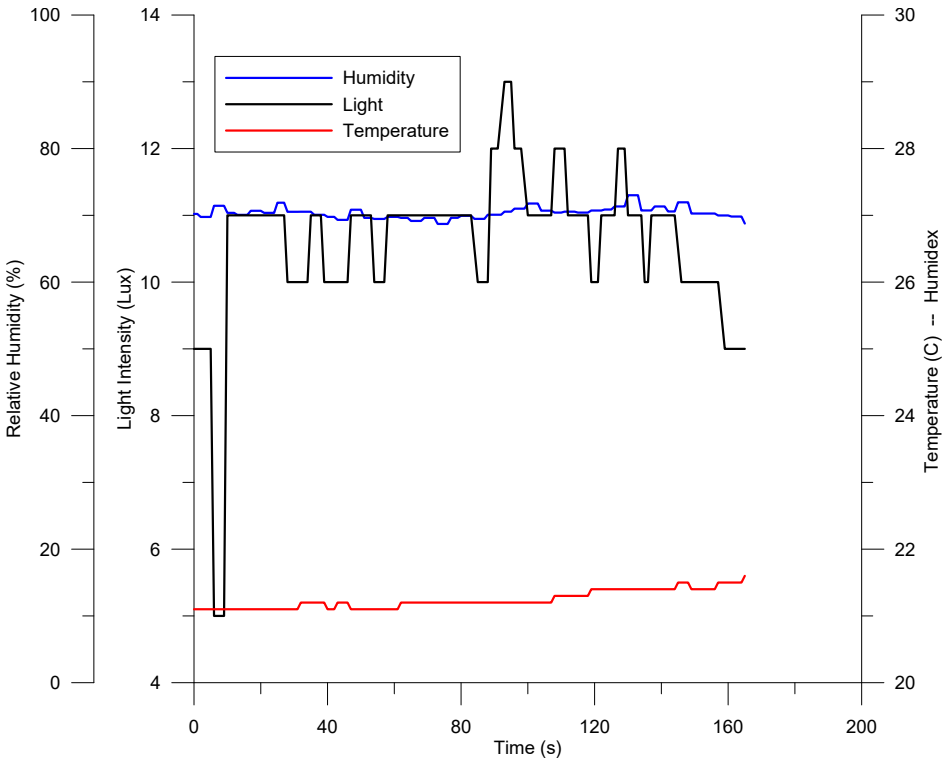


Figure C.248: Test 56 THLP 04

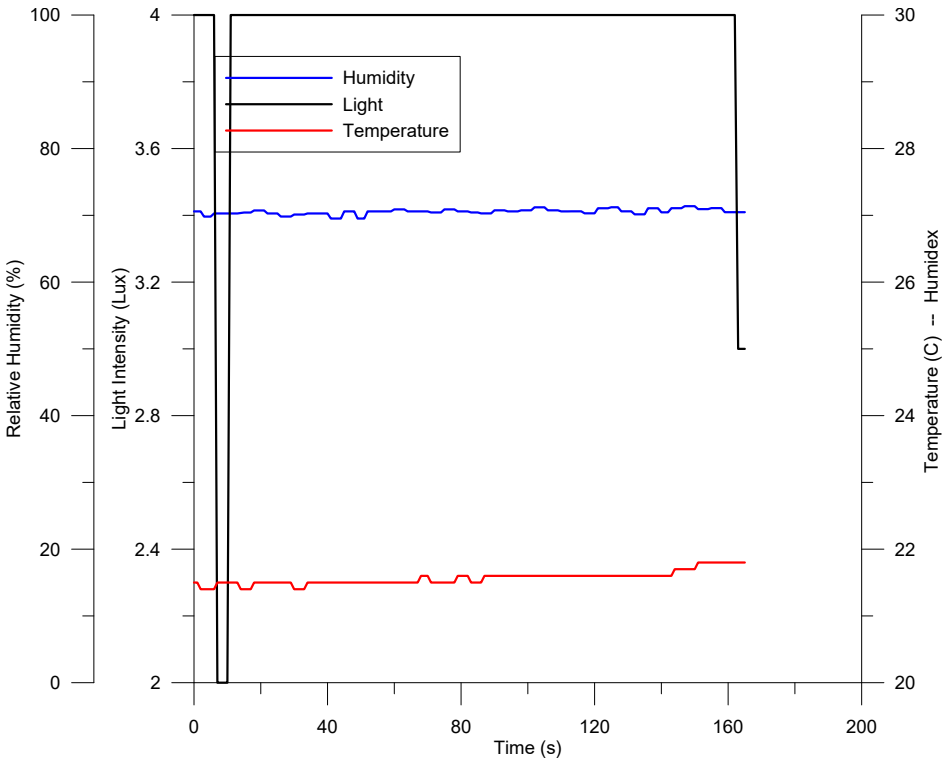


Figure C.249: Test 56 THLP 05

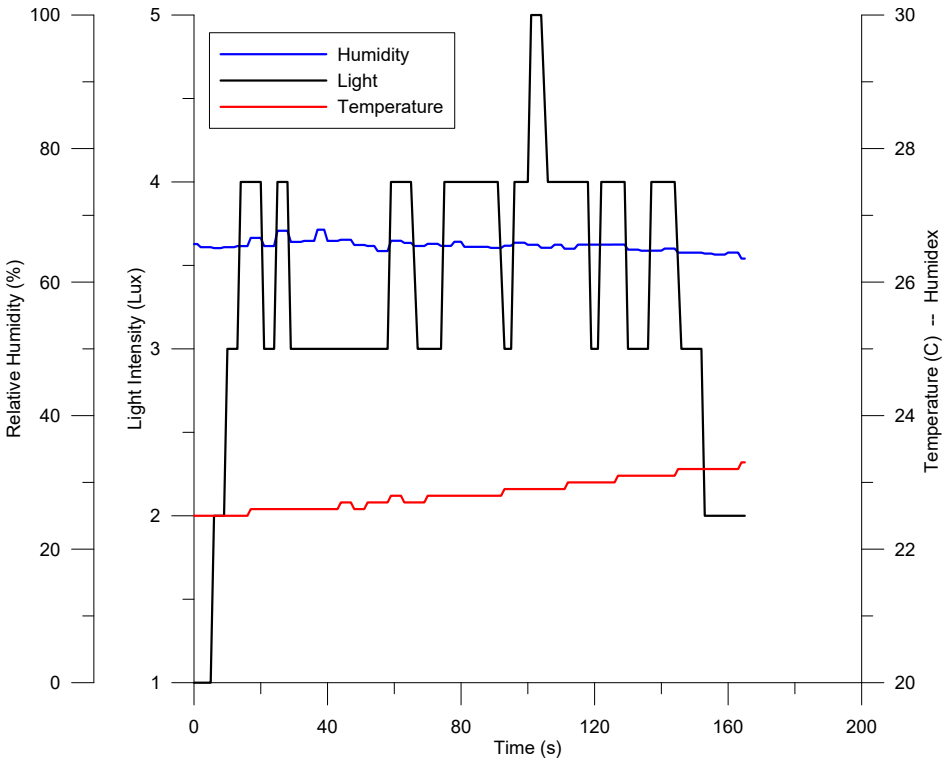


Figure C.250: Test 56 THLP 08

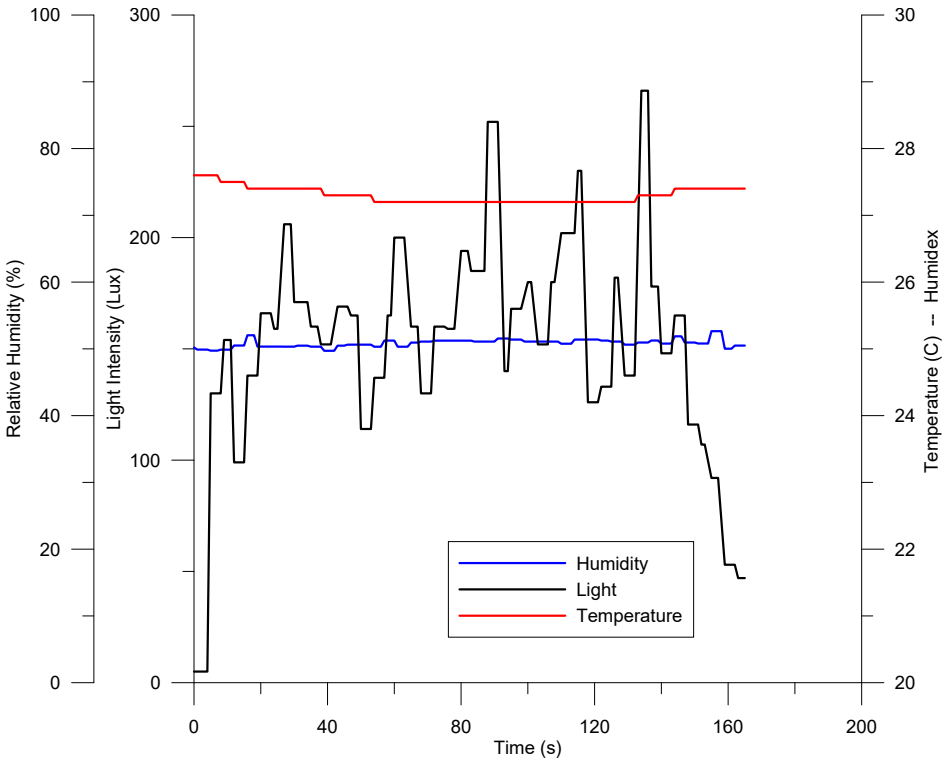


Figure C.251: Test 56 THLP 09

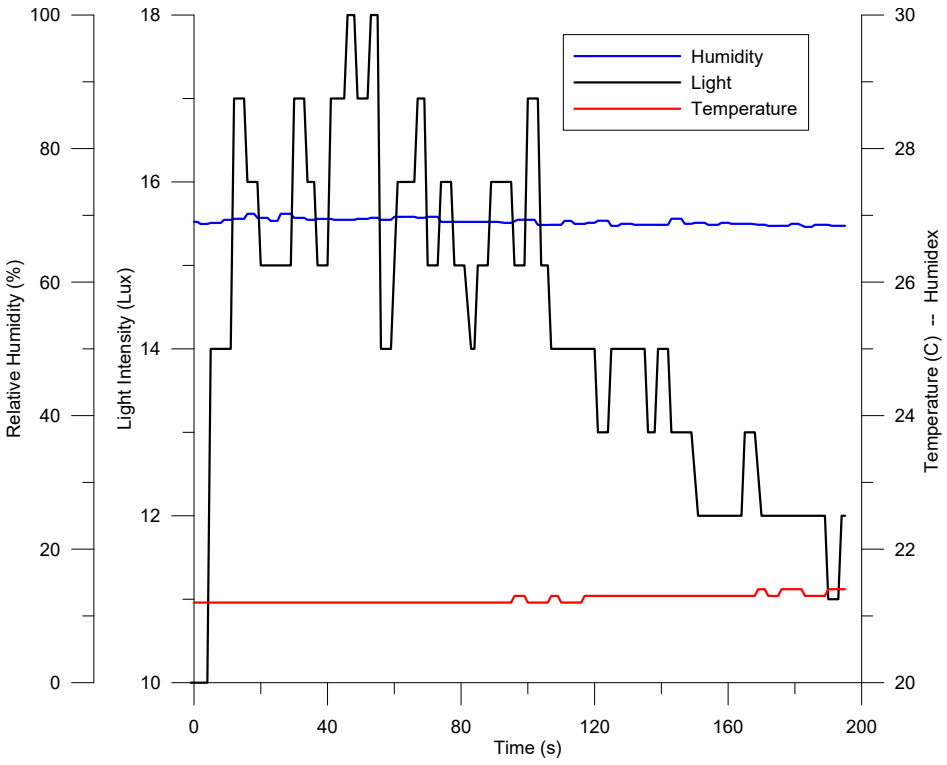


Figure C.252: Test 57 THLP 01

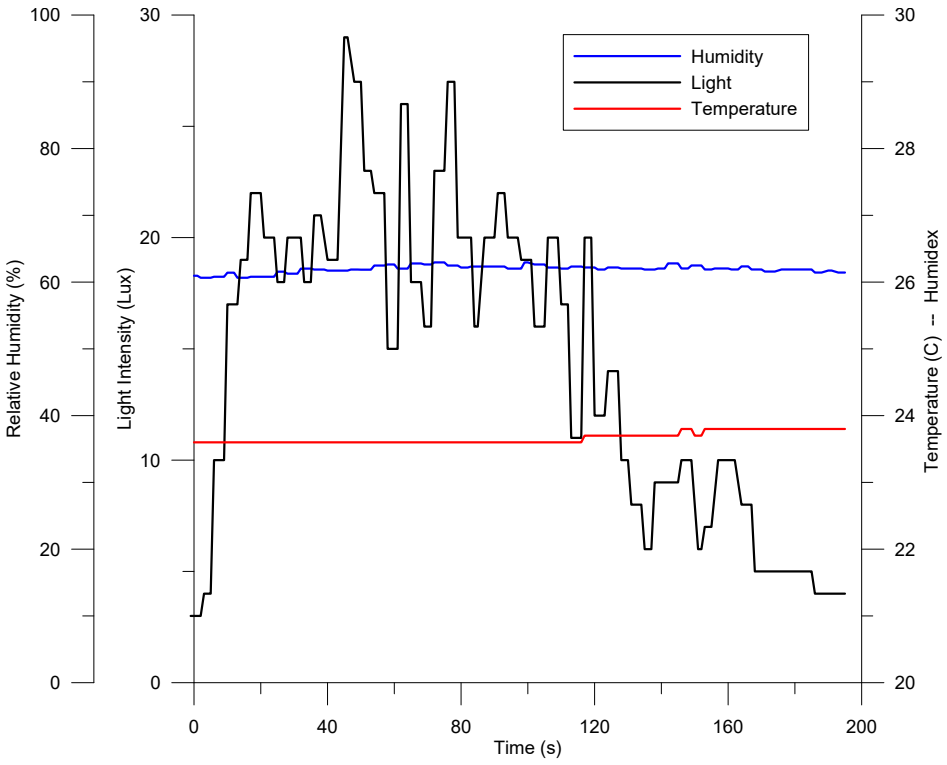


Figure C.253: Test 57 THLP 02

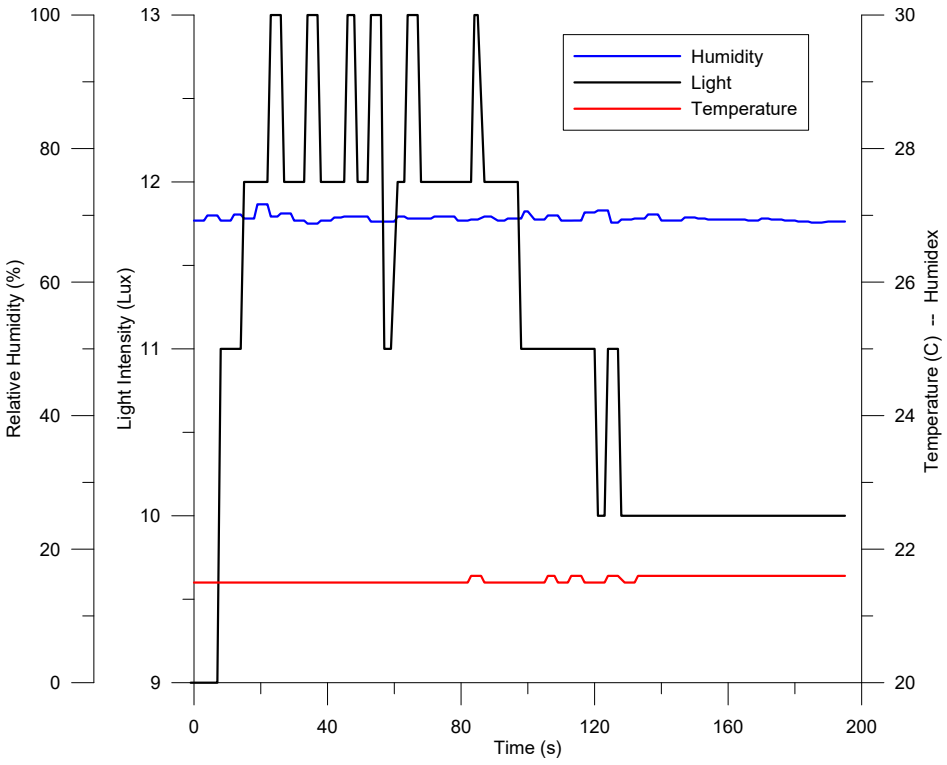


Figure C.254: Test 57 THLP 03

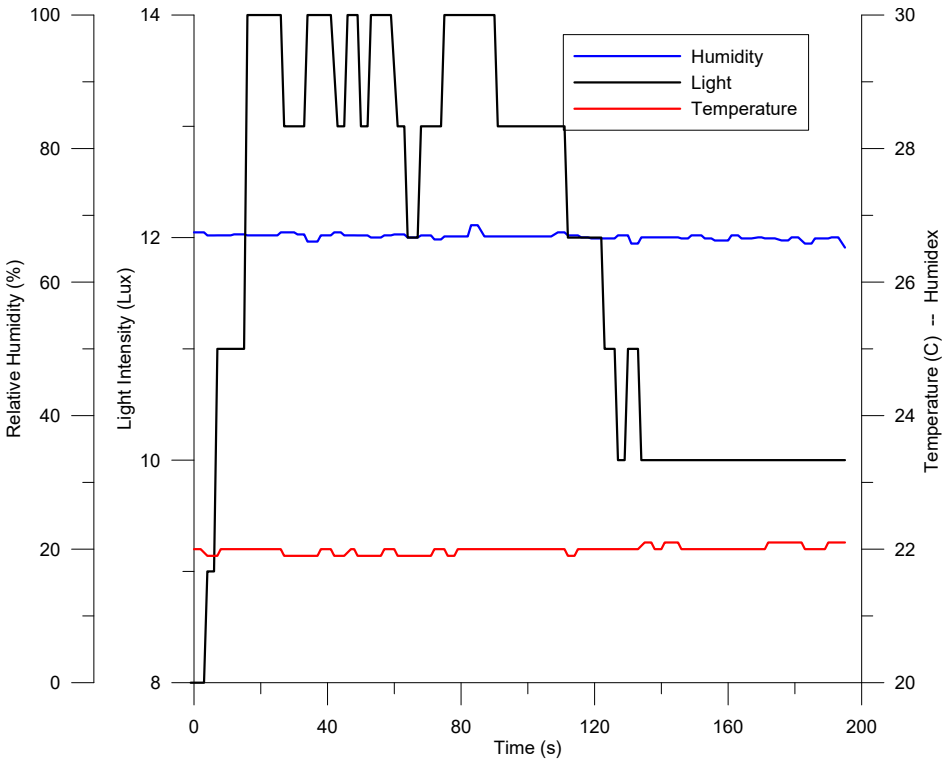


Figure C.255: Test 57 THLP 04

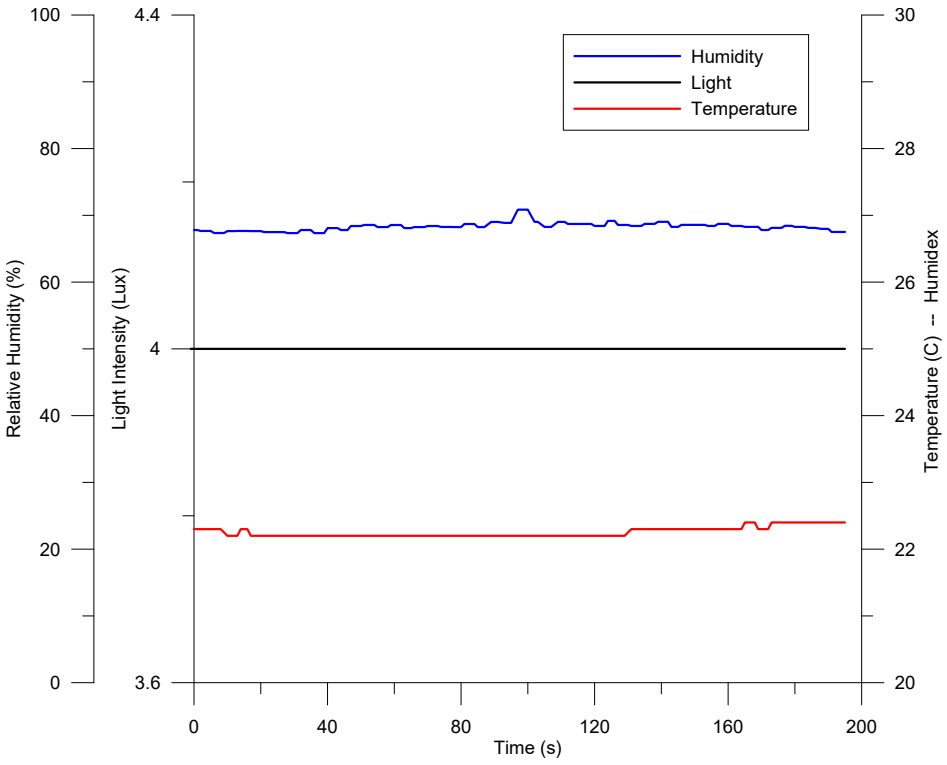


Figure C.256: Test 57 THLP 05

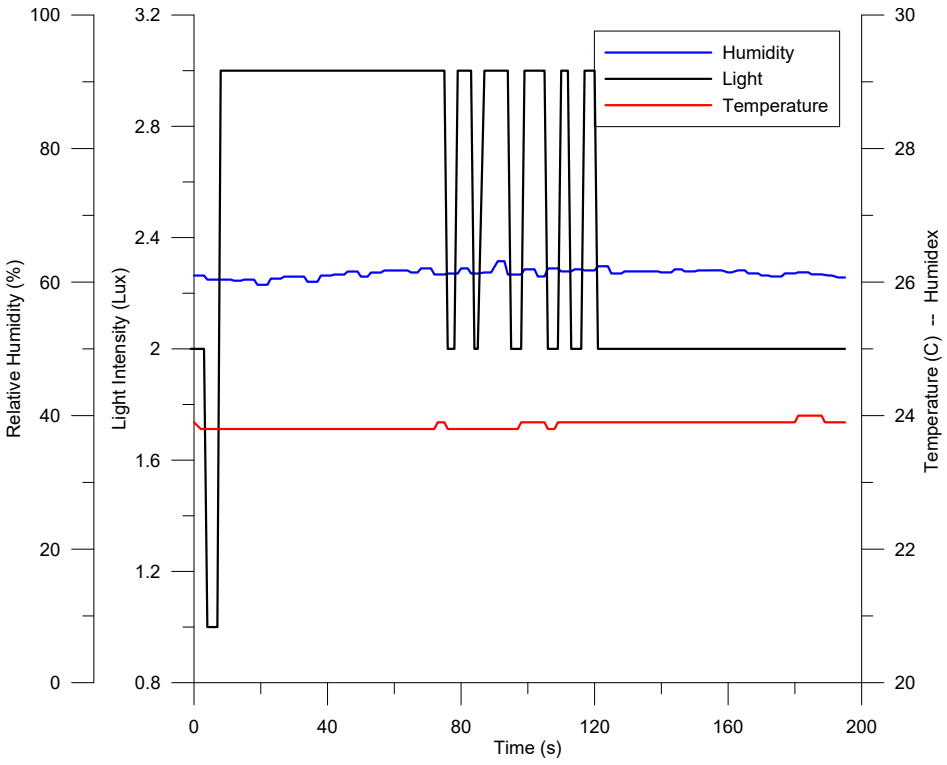


Figure C.257: Test 57 THLP 08

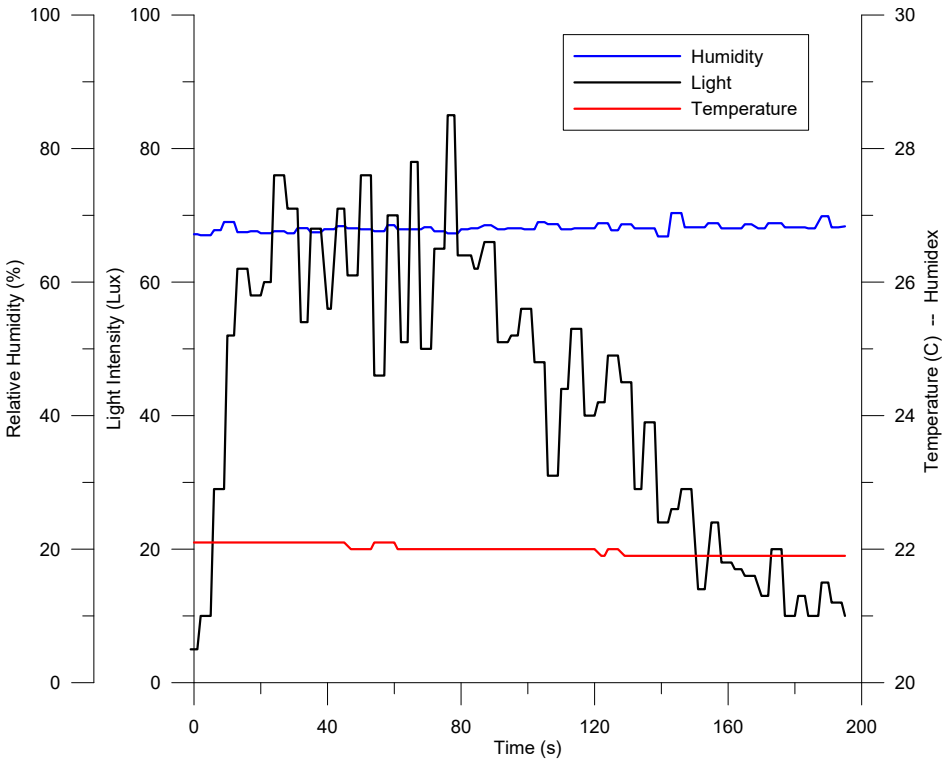


Figure C.258: Test 57 THLP 09

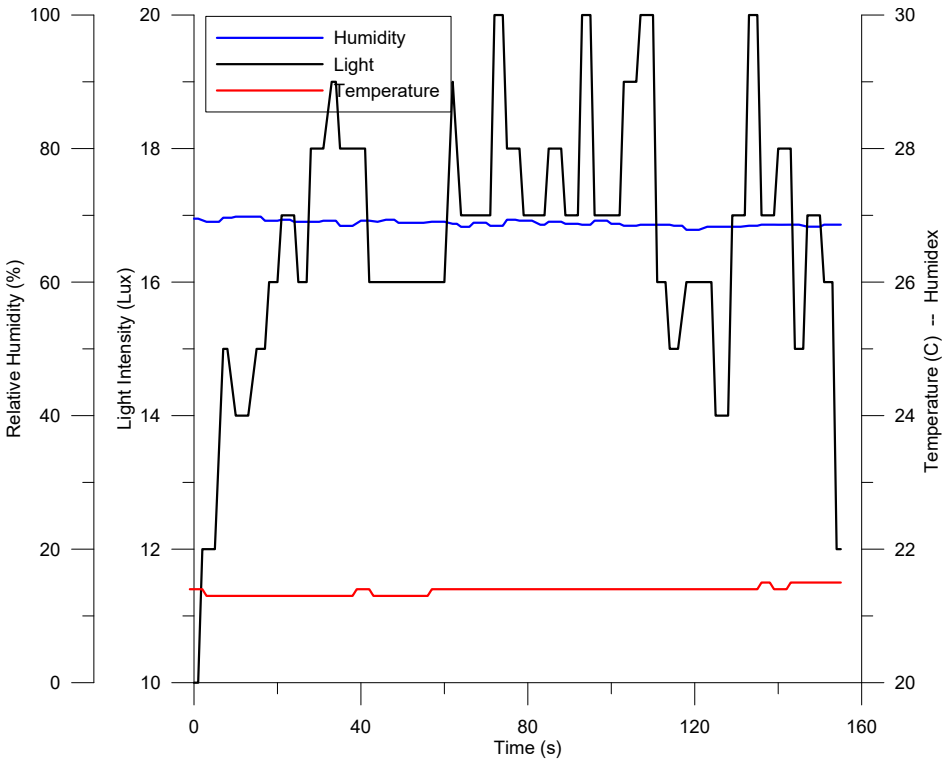


Figure C.259: Test 58 THLP 01

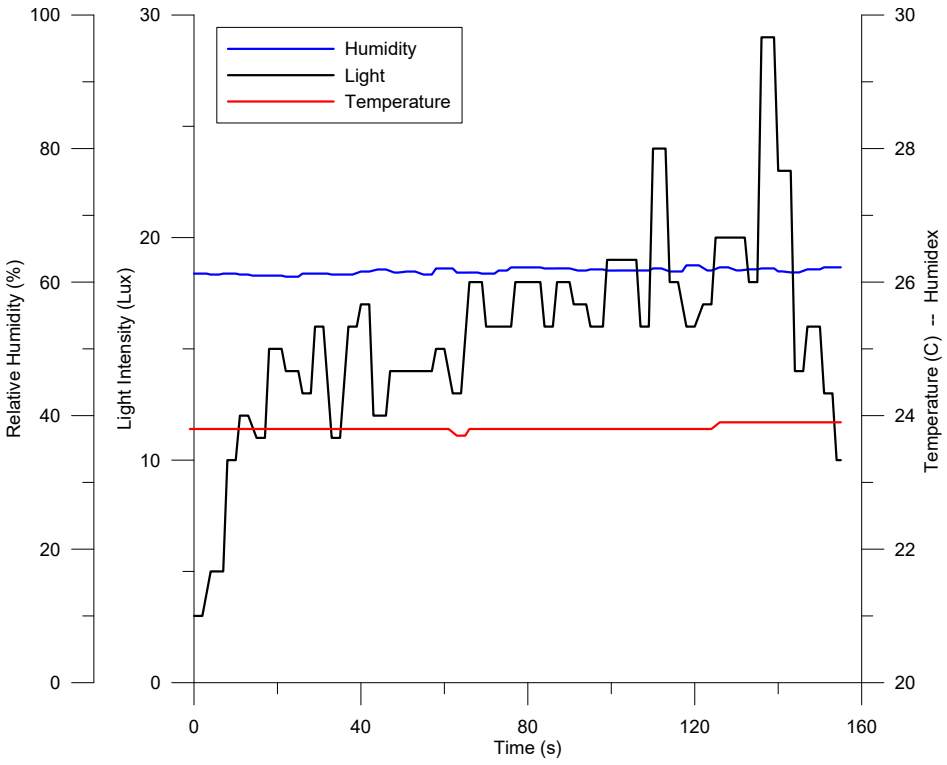


Figure C.260: Test 58 THLP 02

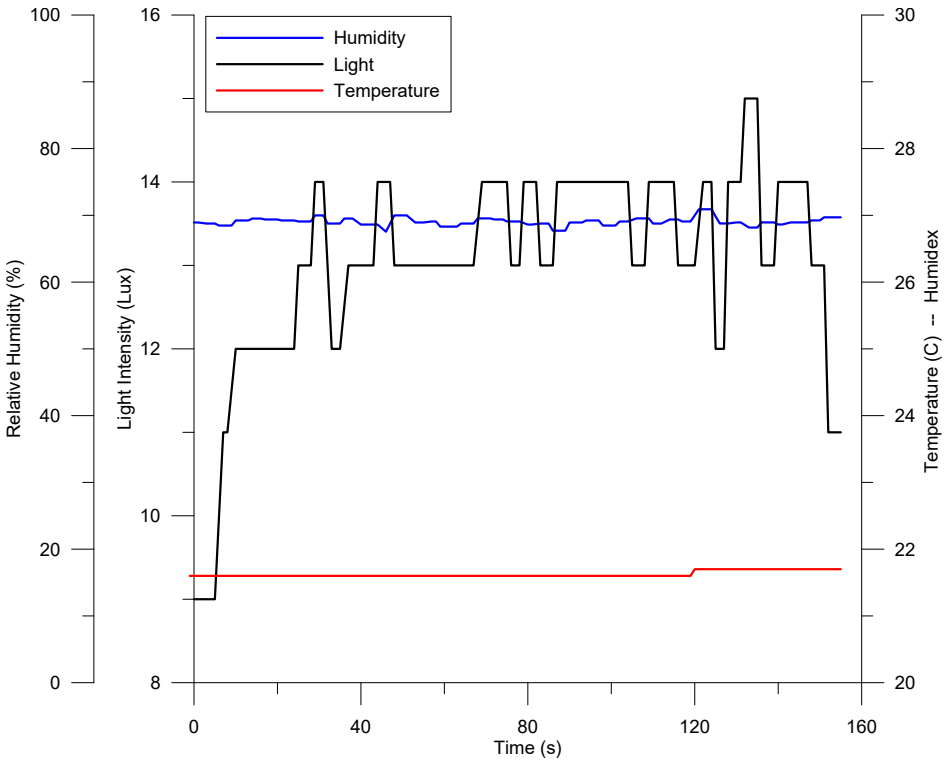


Figure C.261: Test 58 THLP 03

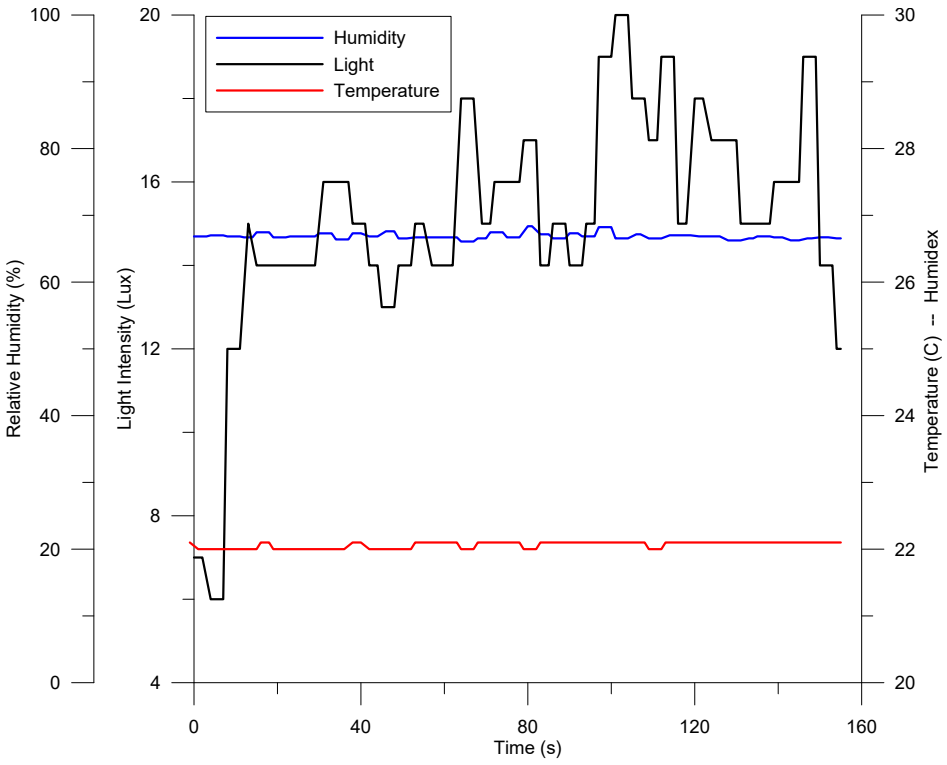


Figure C.262: Test 58 THLP 04

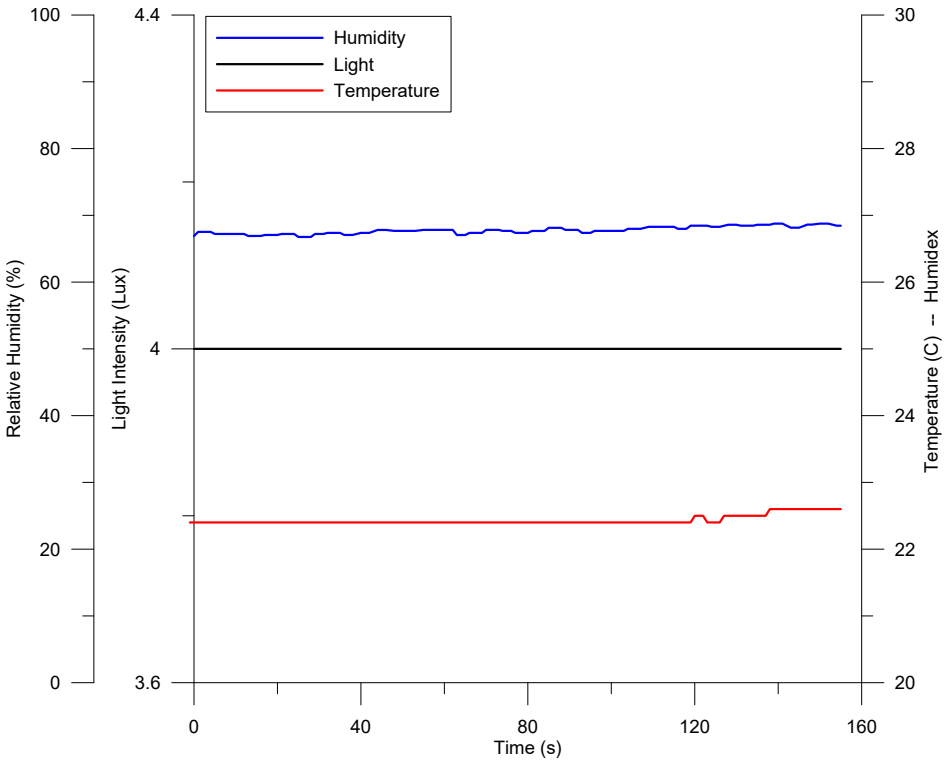


Figure C.263: Test 58 THLP 05

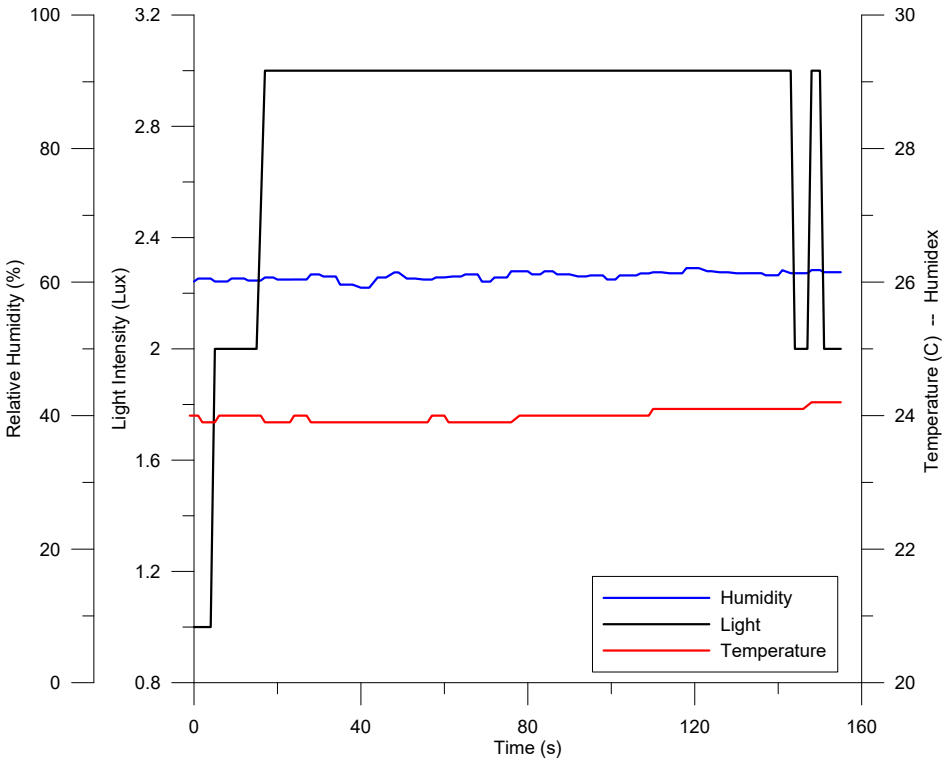


Figure C.264: Test 58 THLP 08

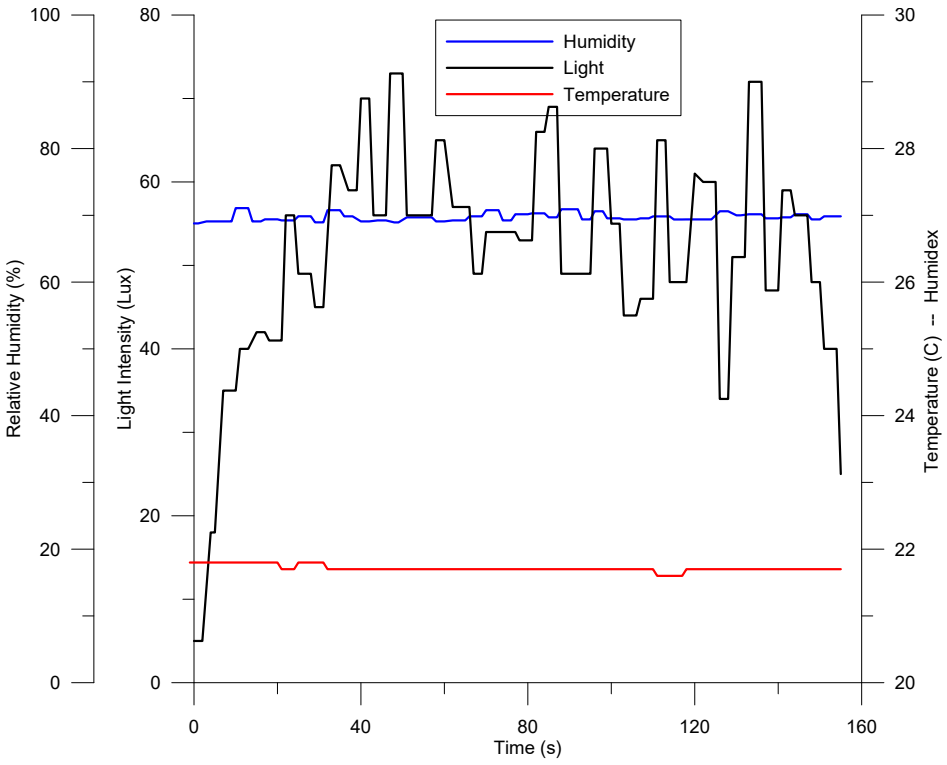


Figure C.265: Test 58 THLP 09

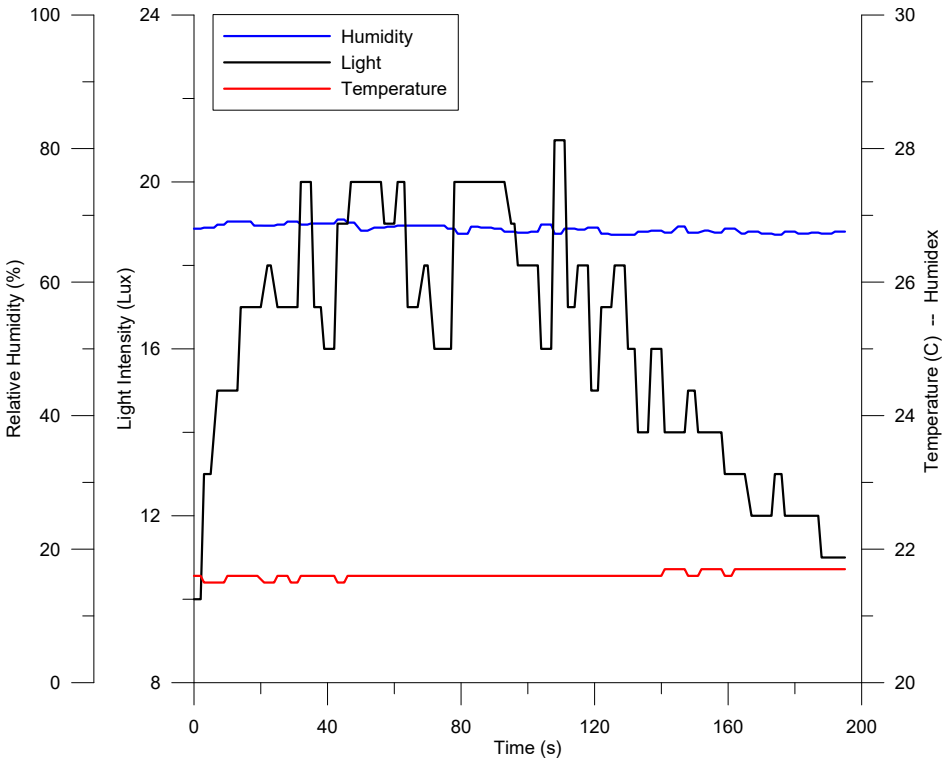


Figure C.266: Test 59 THLP 01

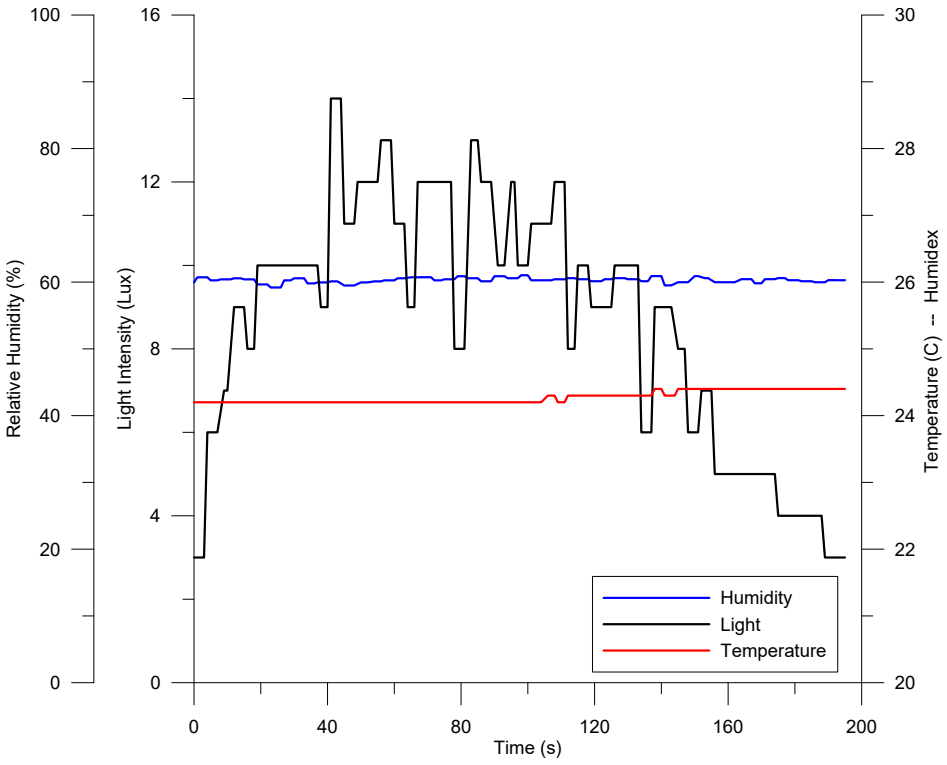


Figure C.267: Test 59 THLP 02

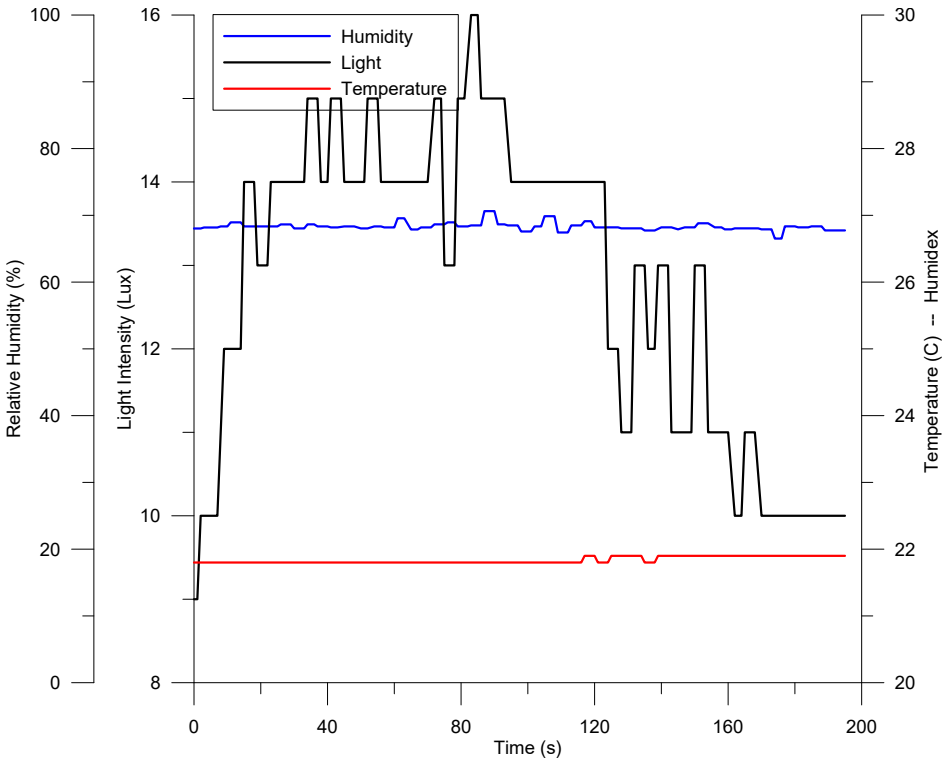


Figure C.268: Test 59 THLP 03

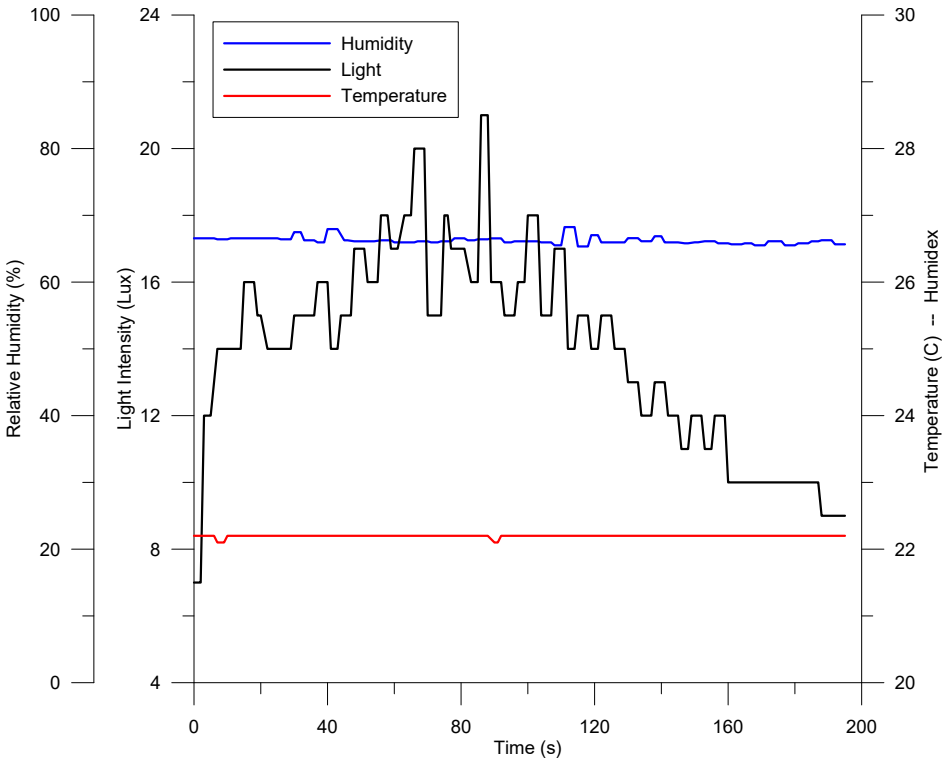


Figure C.269: Test 59 THLP 04

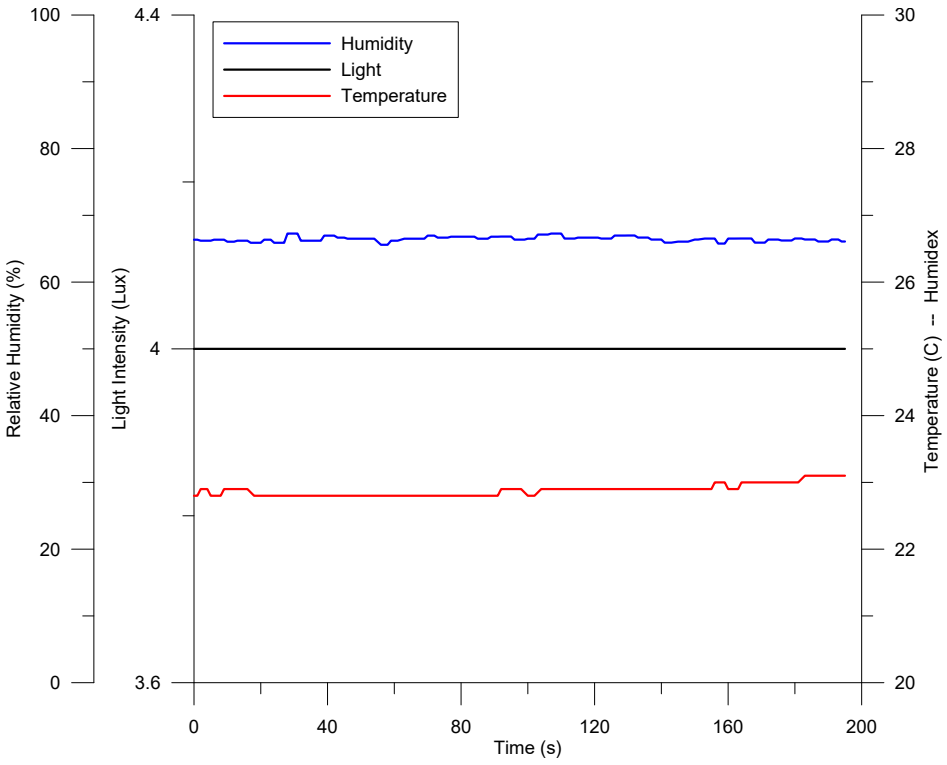


Figure C.270: Test 59 THLP 05

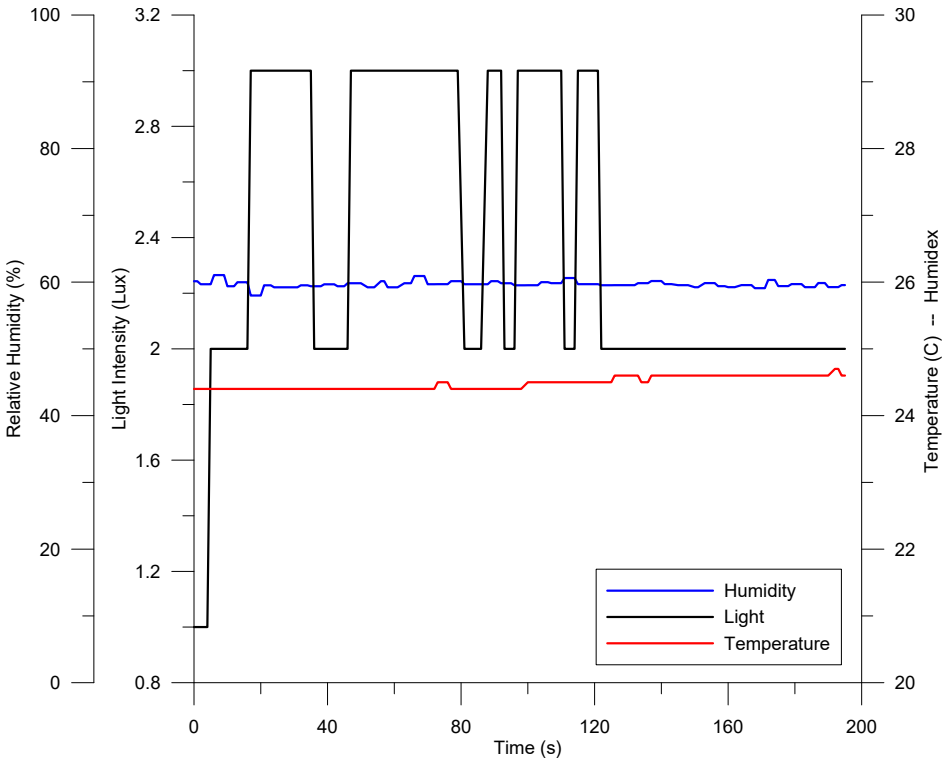


Figure C.271: Test 59 THLP 08

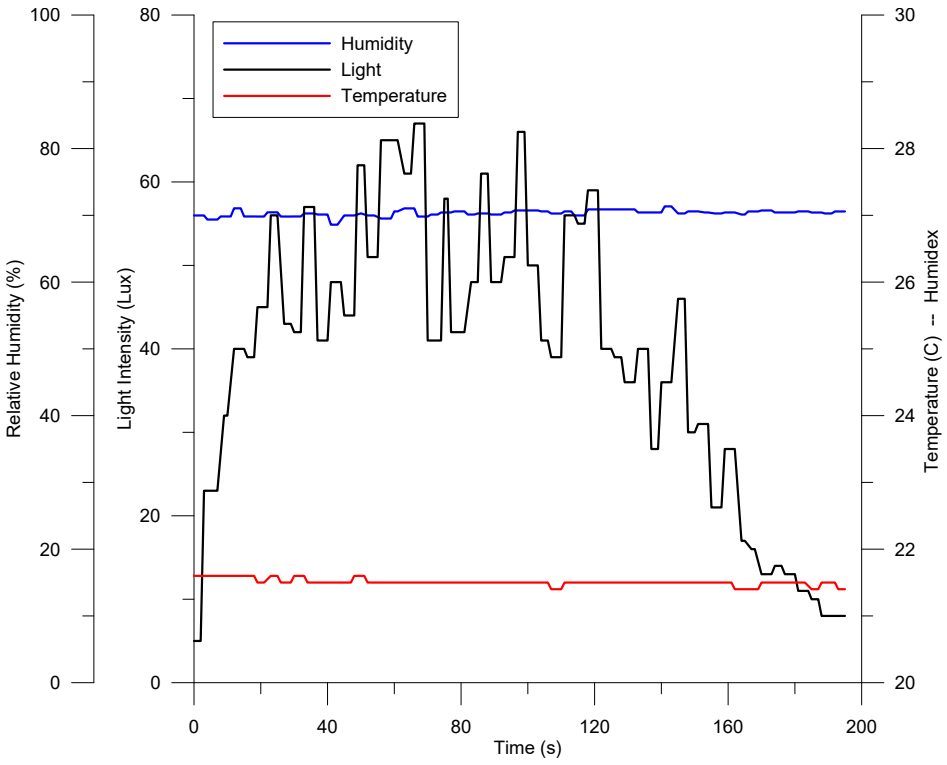


Figure C.272: Test 59 THLP 09

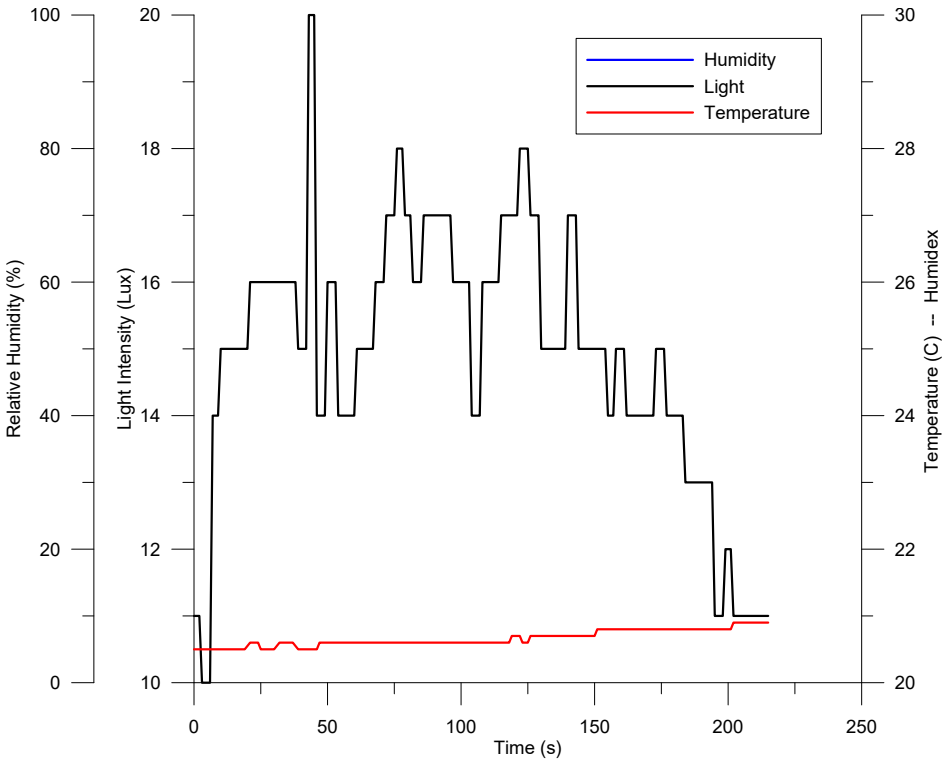


Figure C.273: Test 60 THLP 01

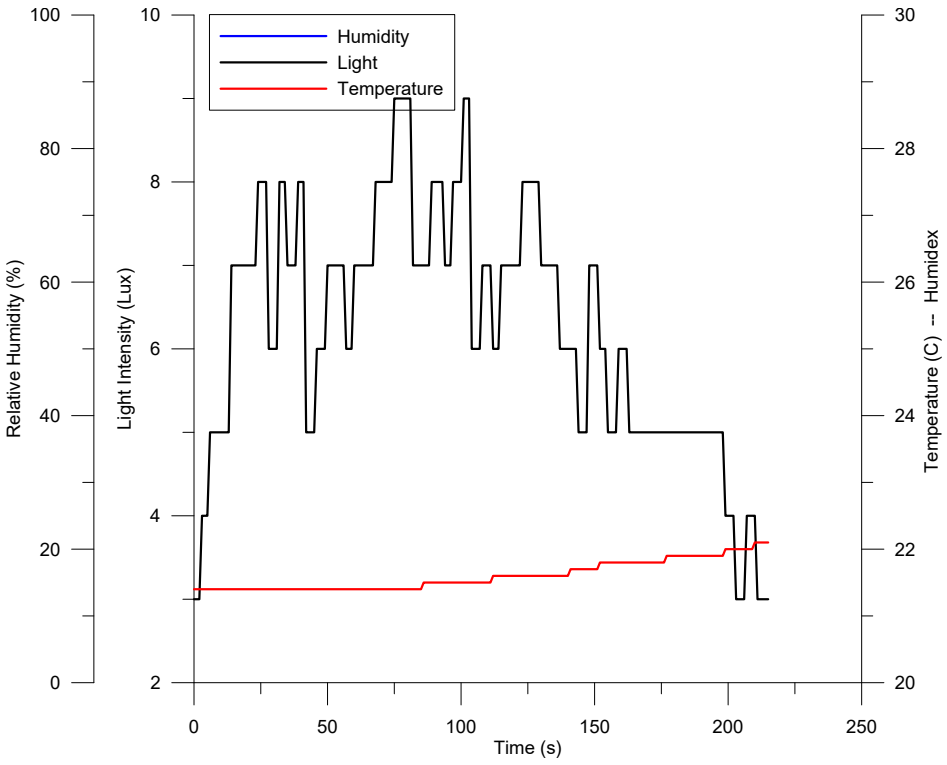


Figure C.274: Test 60 THLP 02

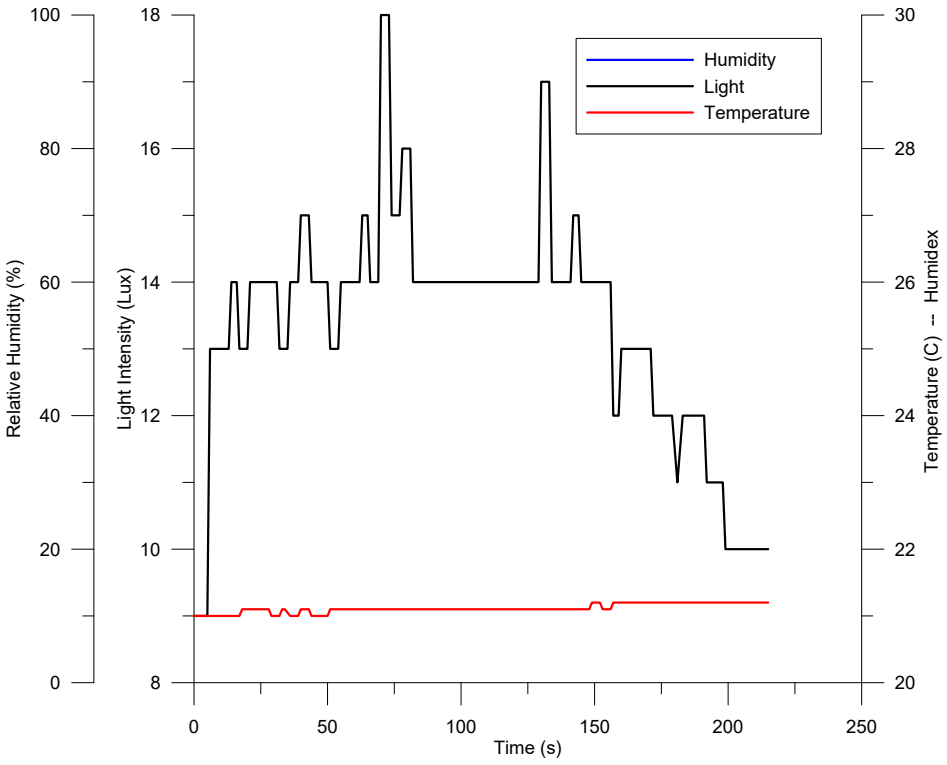


Figure C.275: Test 60 THLP 03

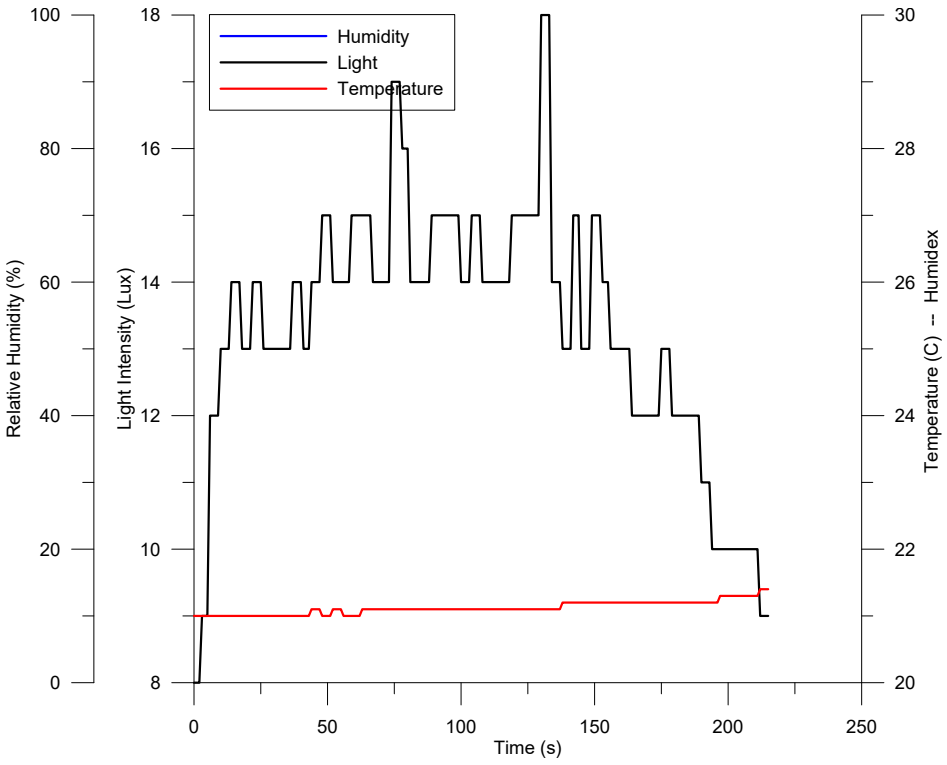


Figure C.276: Test 60 THLP 04

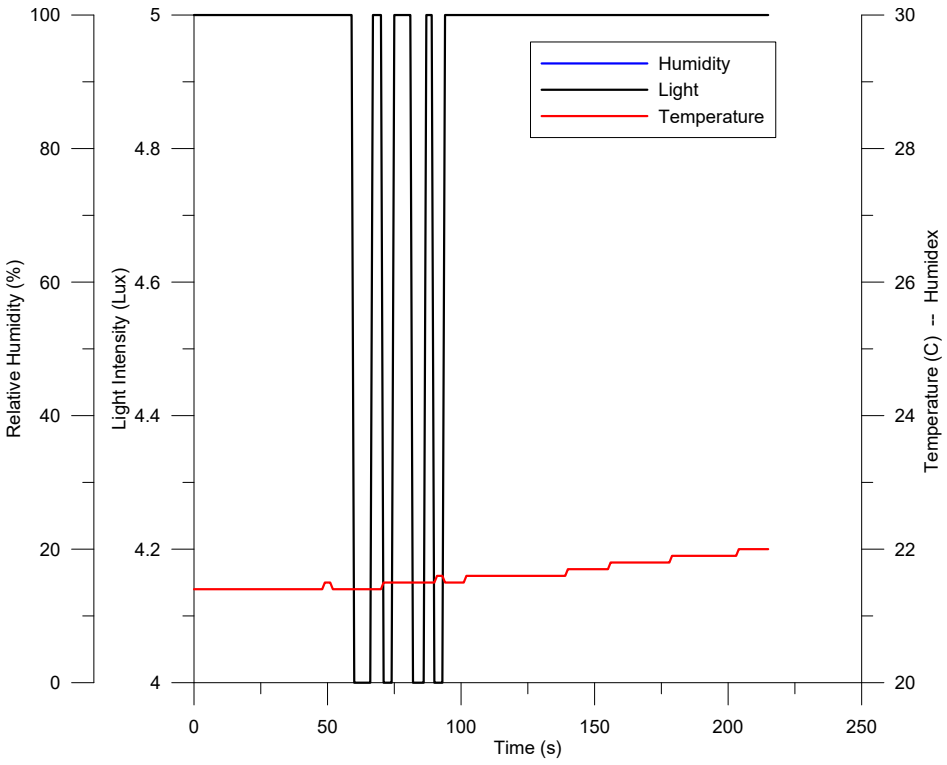


Figure C.277: Test 60 THLP 05

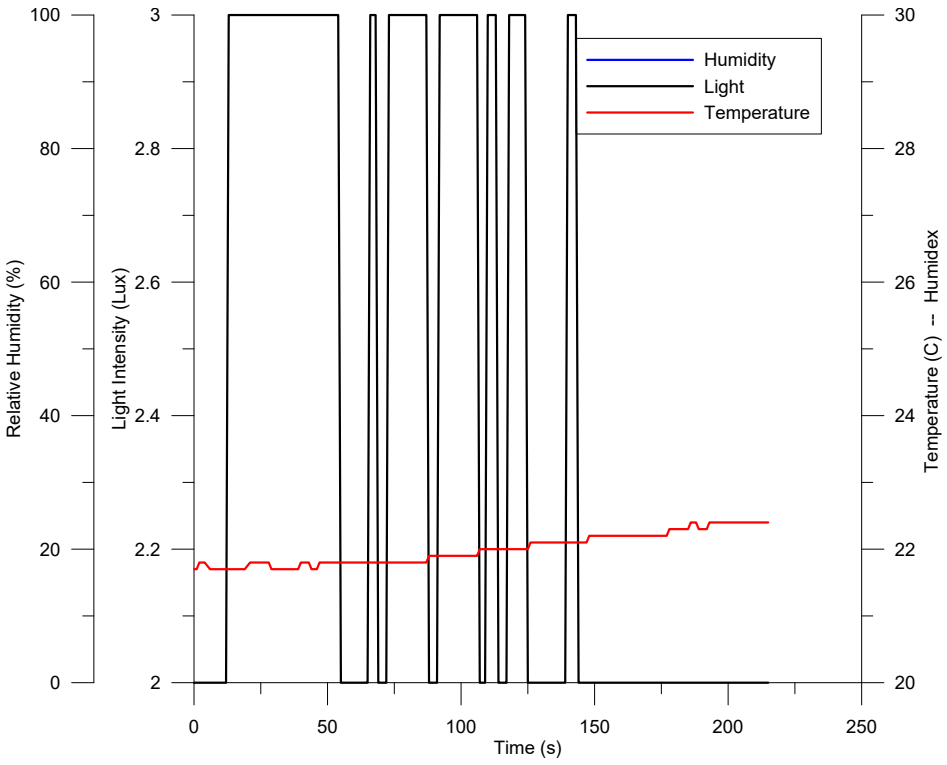


Figure C.278: Test 60 THLP 08

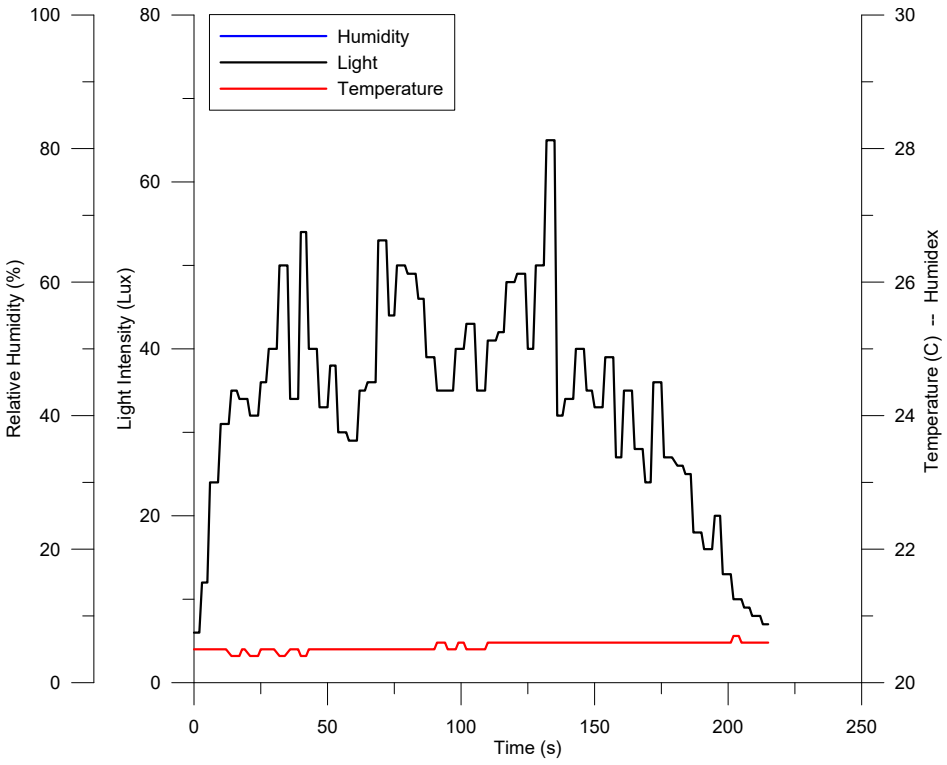


Figure C.279: Test 60 THLP 09

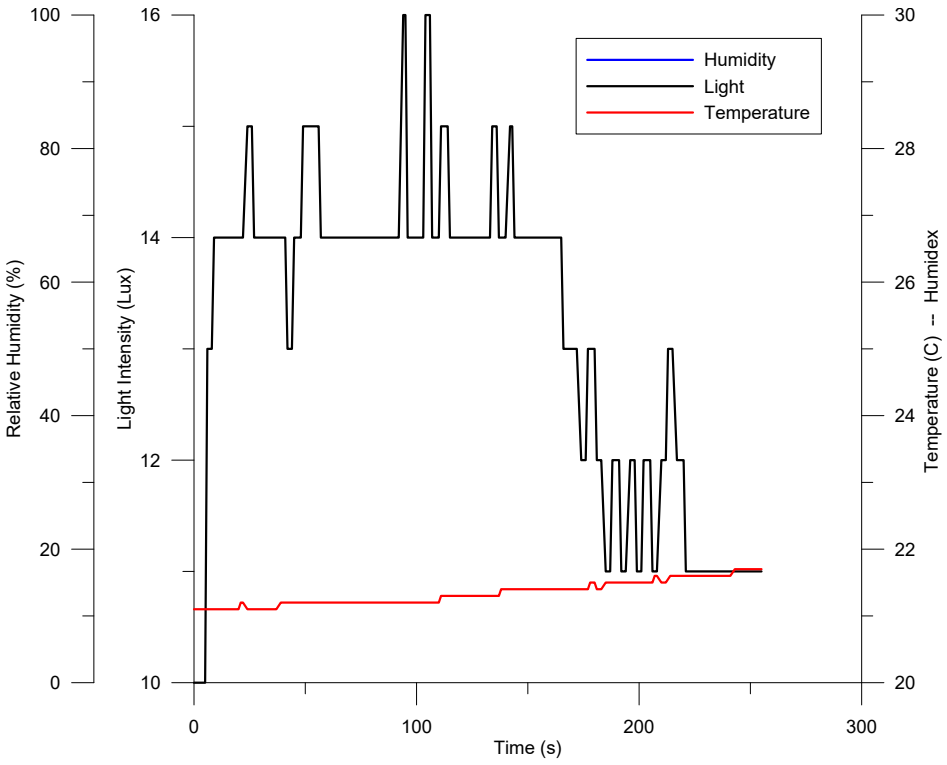


Figure C.280: Test 61 THLP 01

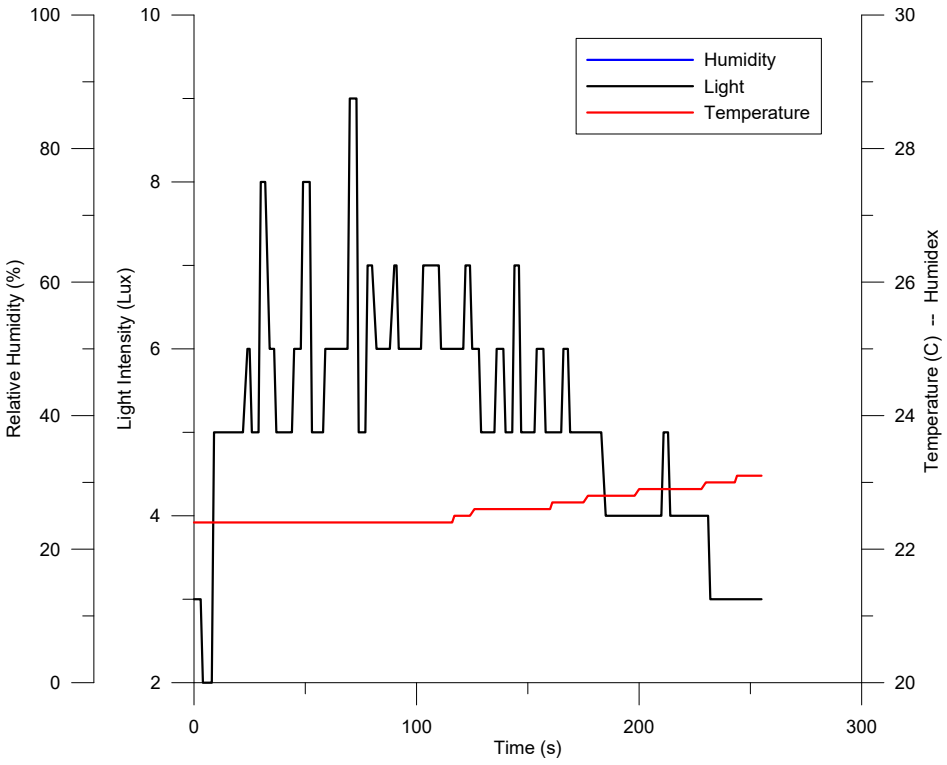


Figure C.281: Test 61 THLP 02

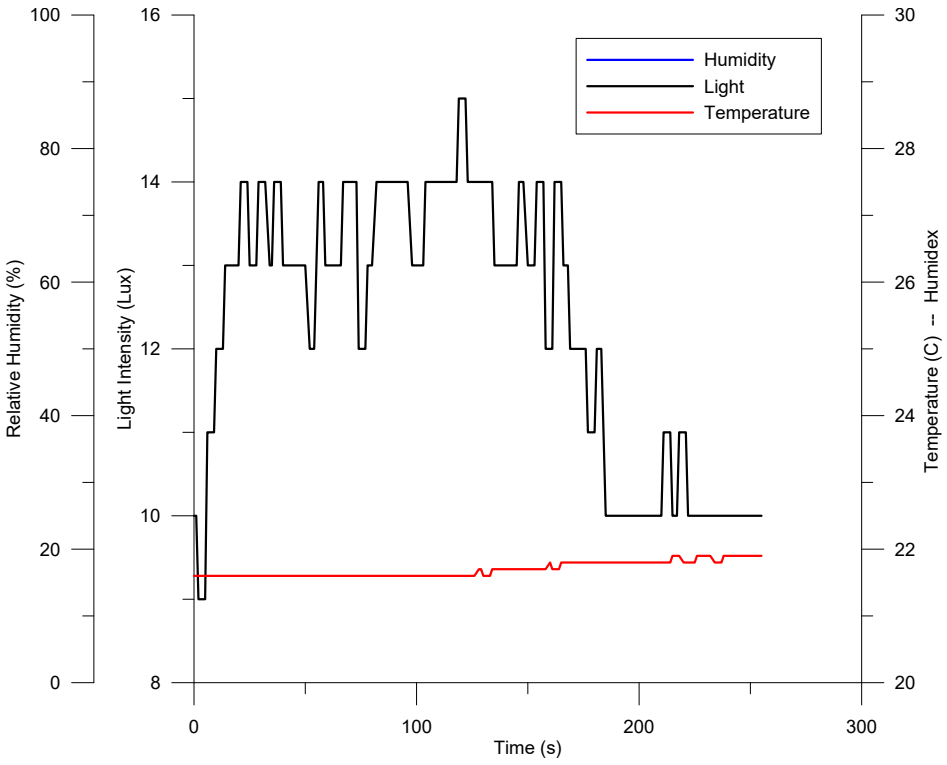


Figure C.282: Test 61 THLP 03

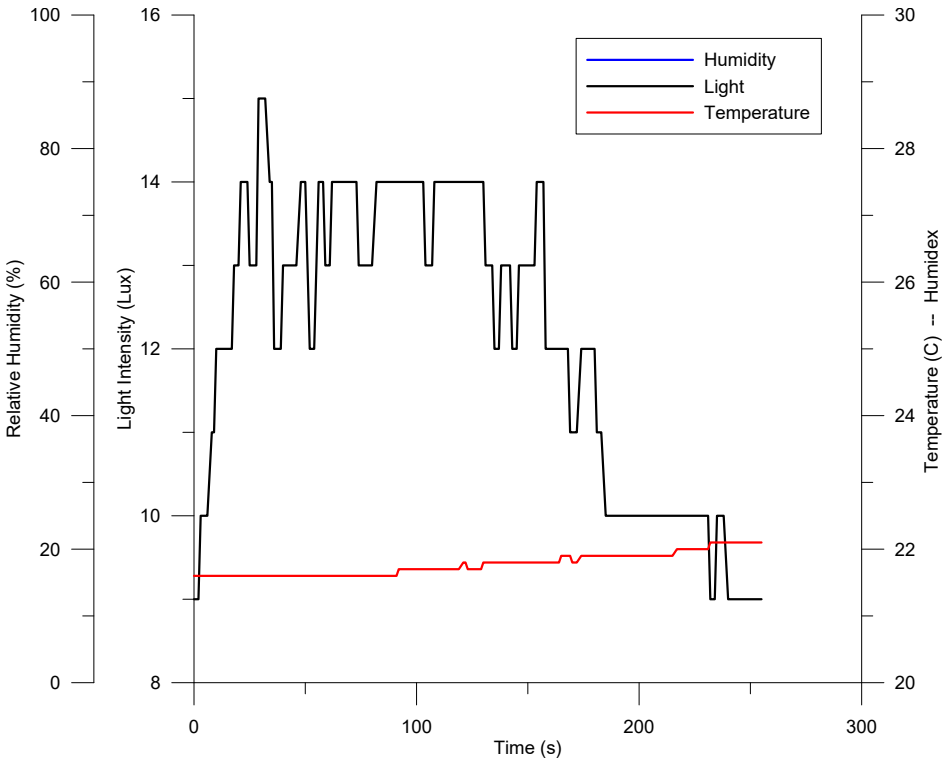


Figure C.283: Test 61 THLP 04

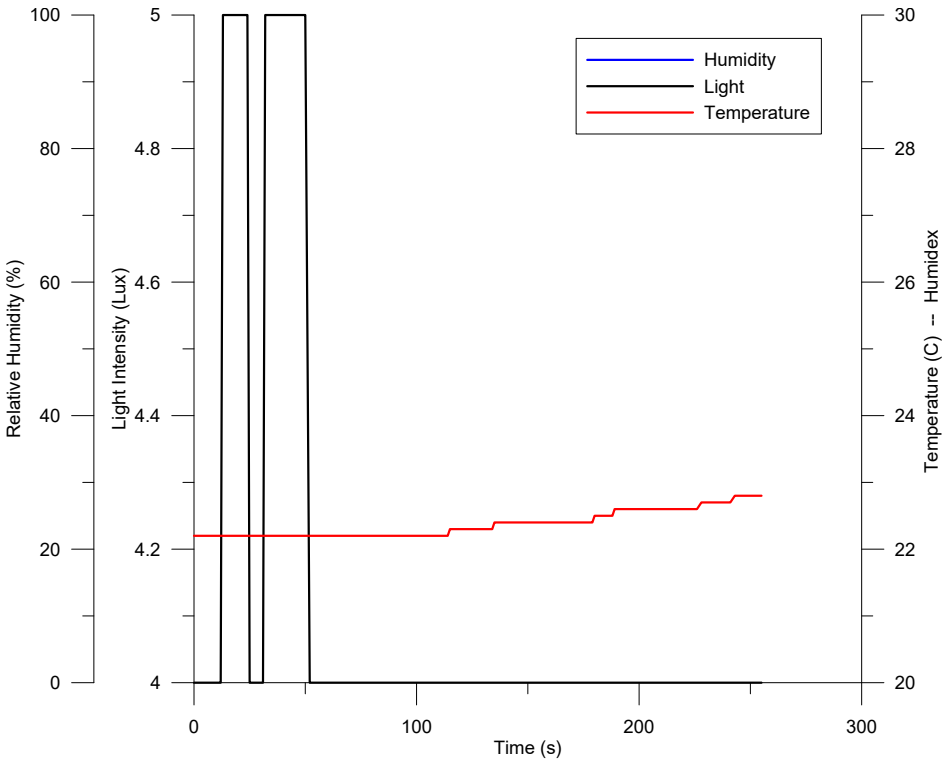


Figure C.284: Test 61 THLP 05

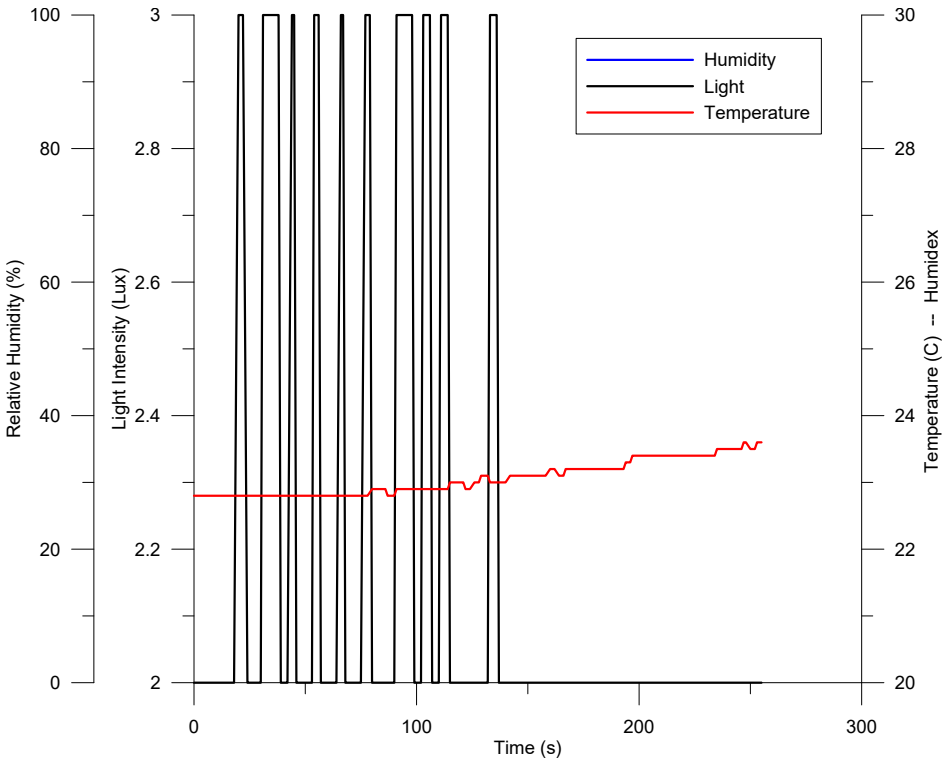


Figure C.285: Test 61 THLP 08

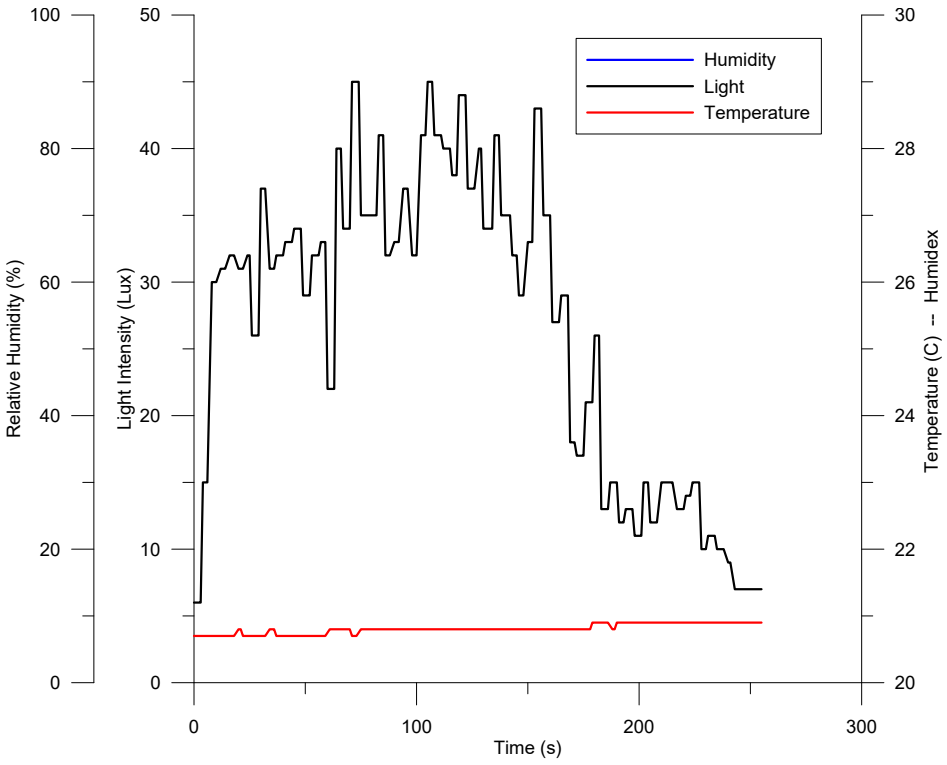


Figure C.286: Test 61 THLP 09

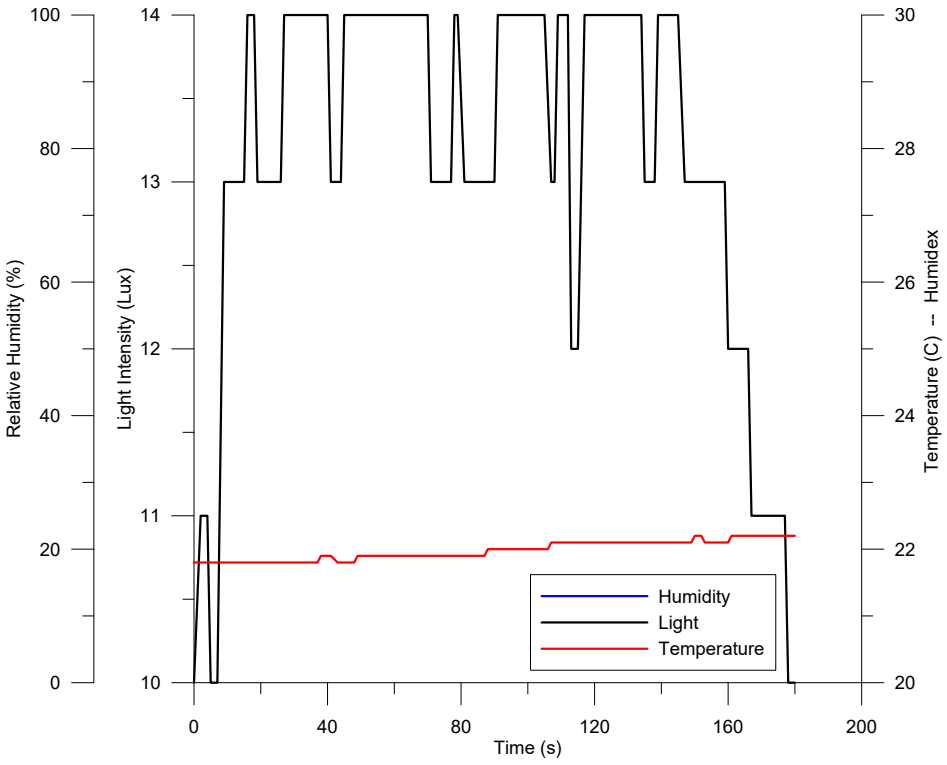


Figure C.287: Test 62 THLP 01

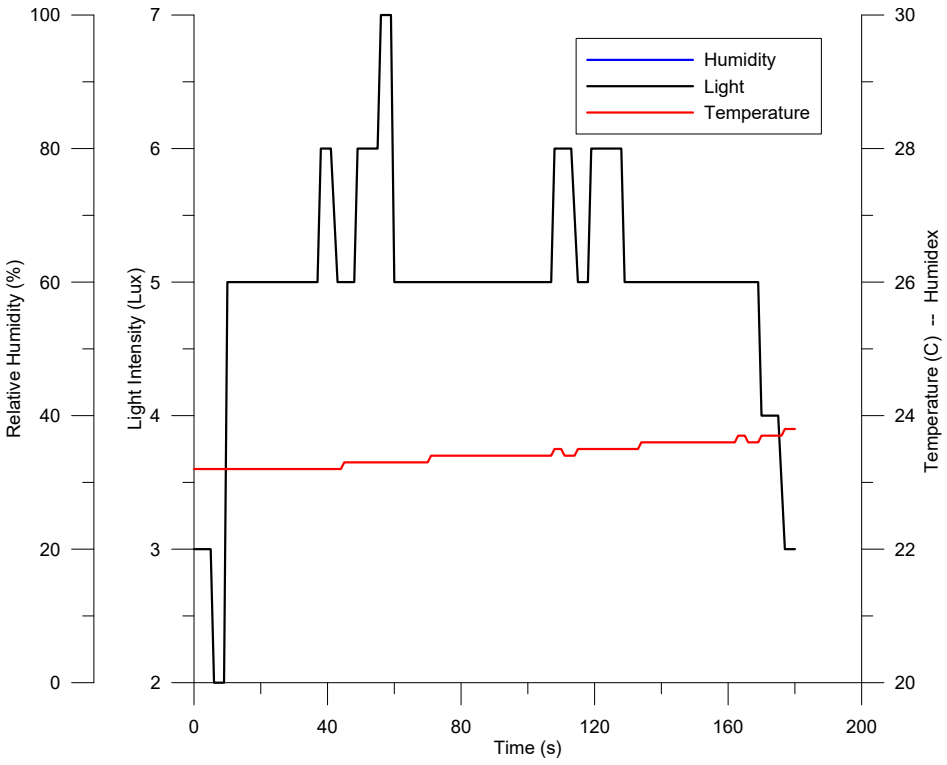


Figure C.288: Test 62 THLP 02

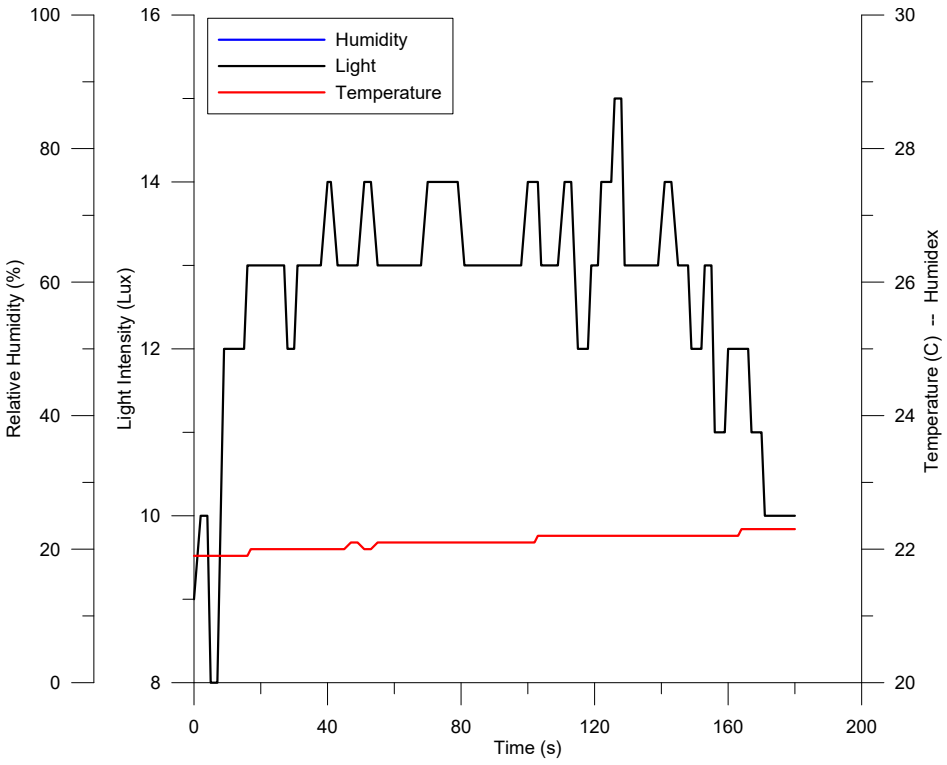


Figure C.289: Test 62 THLP 03

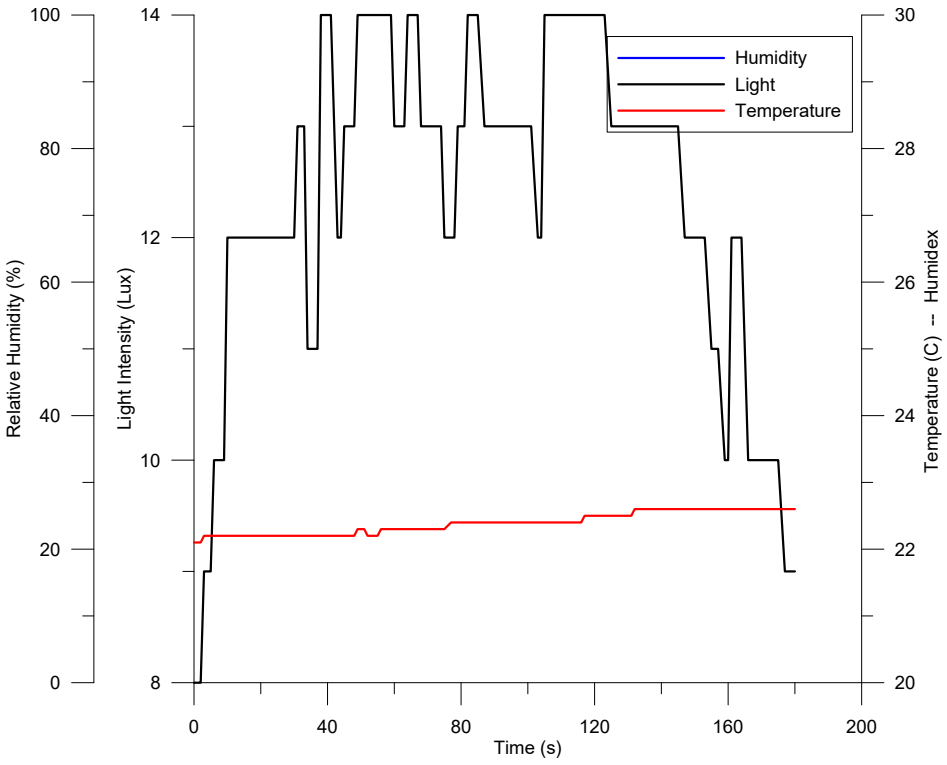


Figure C.290: Test 62 THLP 04

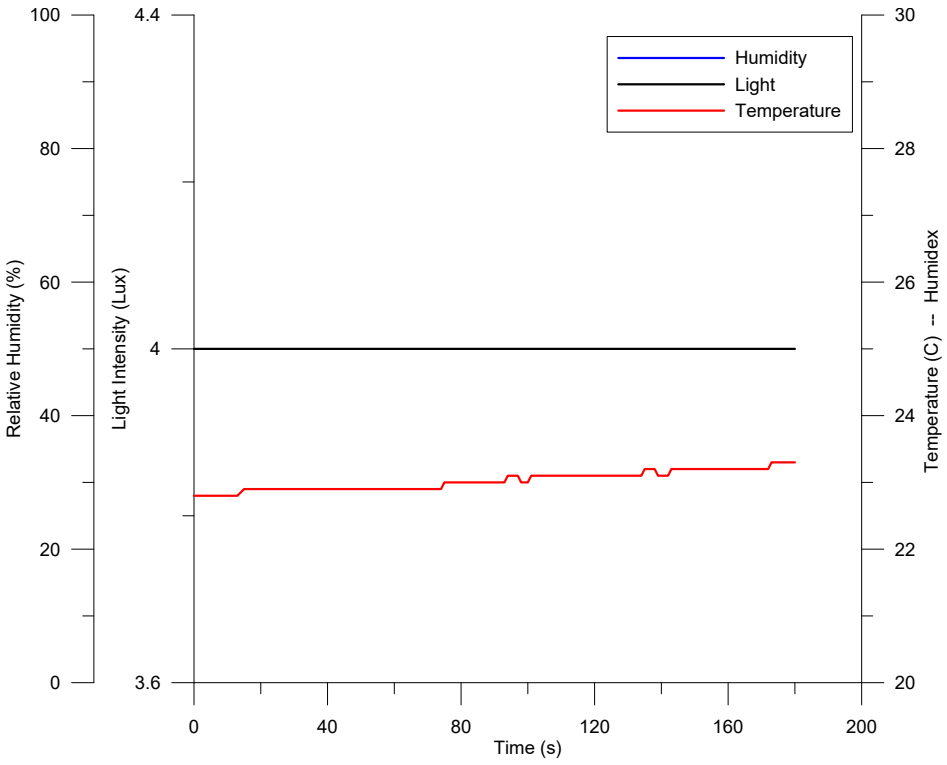


Figure C.291: Test 62 THLP 05

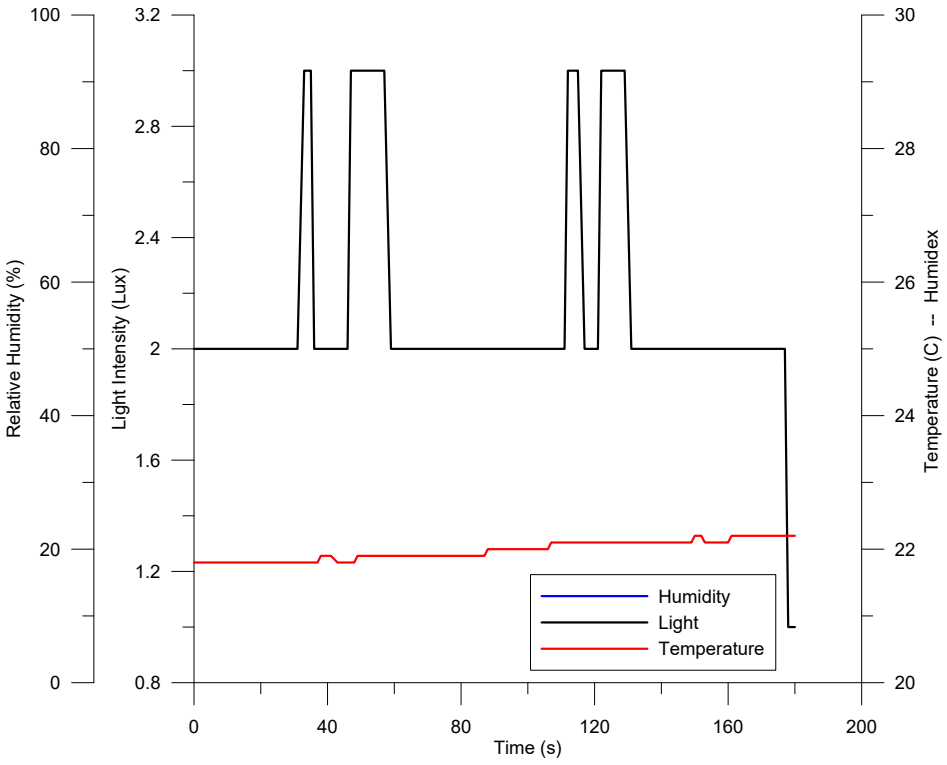


Figure C.292: Test 62 THLP 08

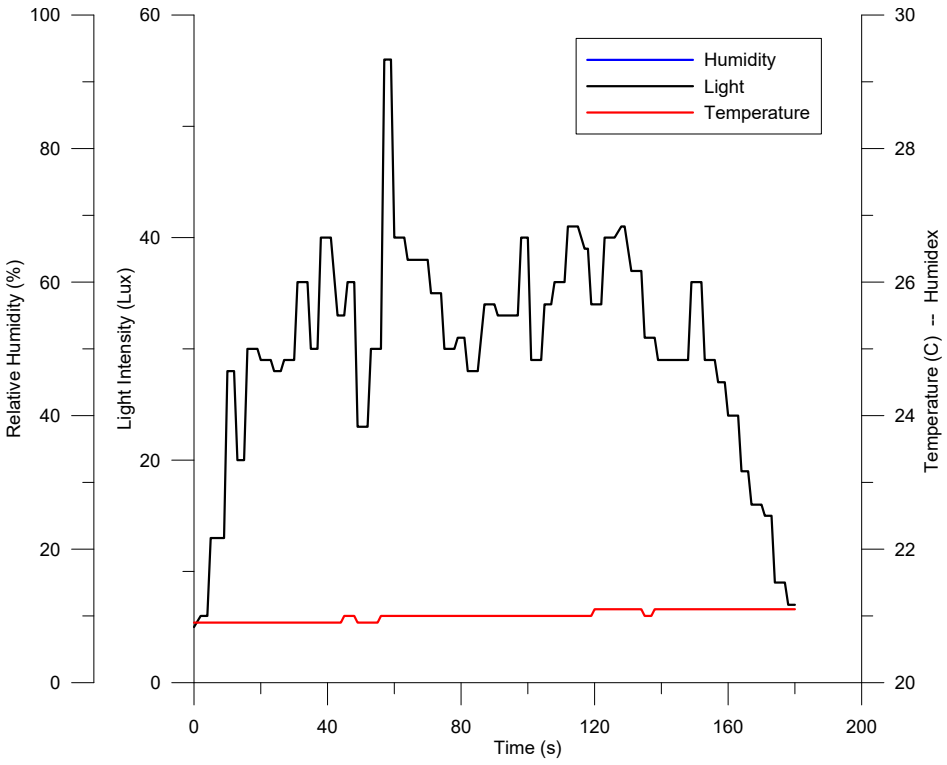


Figure C.293: Test 62 THLP 09

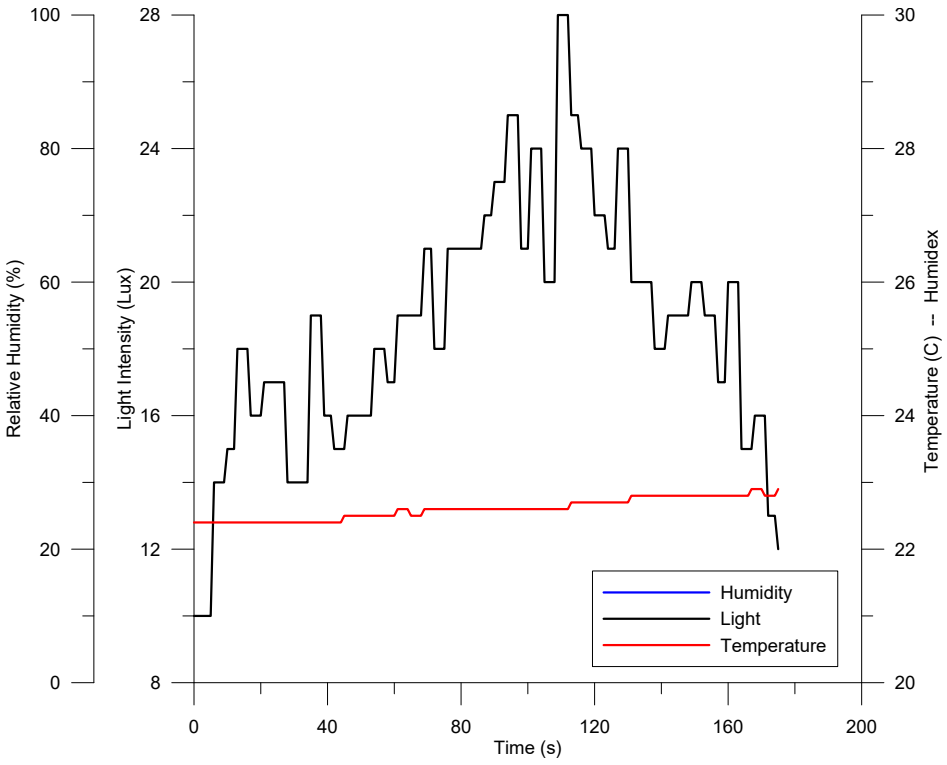


Figure C.294: Test 63 THLP 01

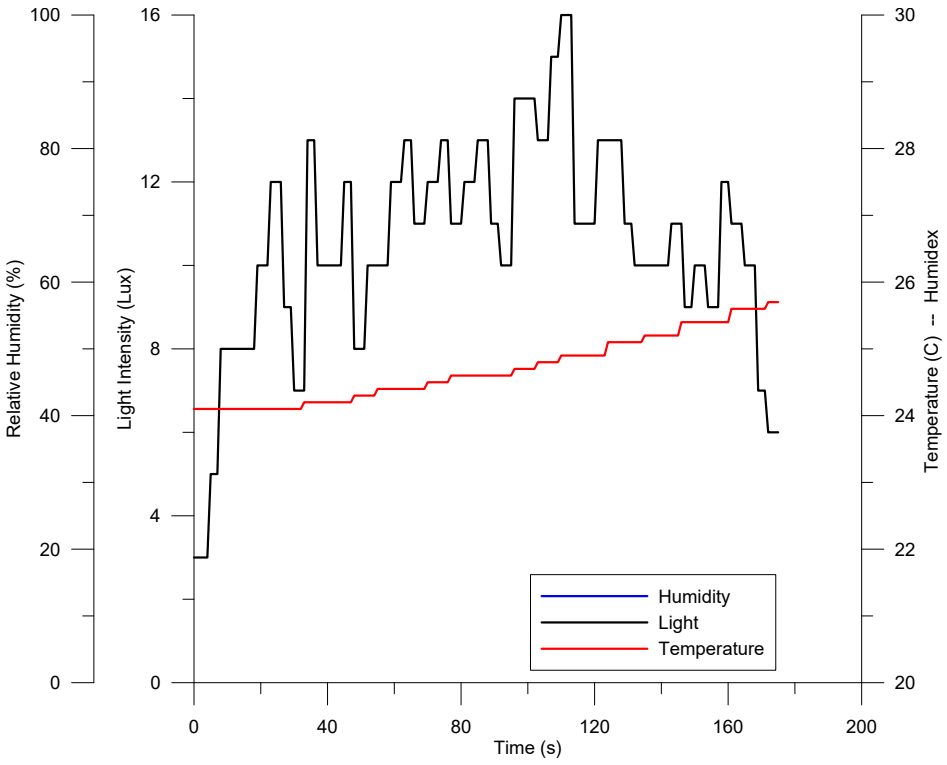


Figure C.295: Test 63 THLP 02

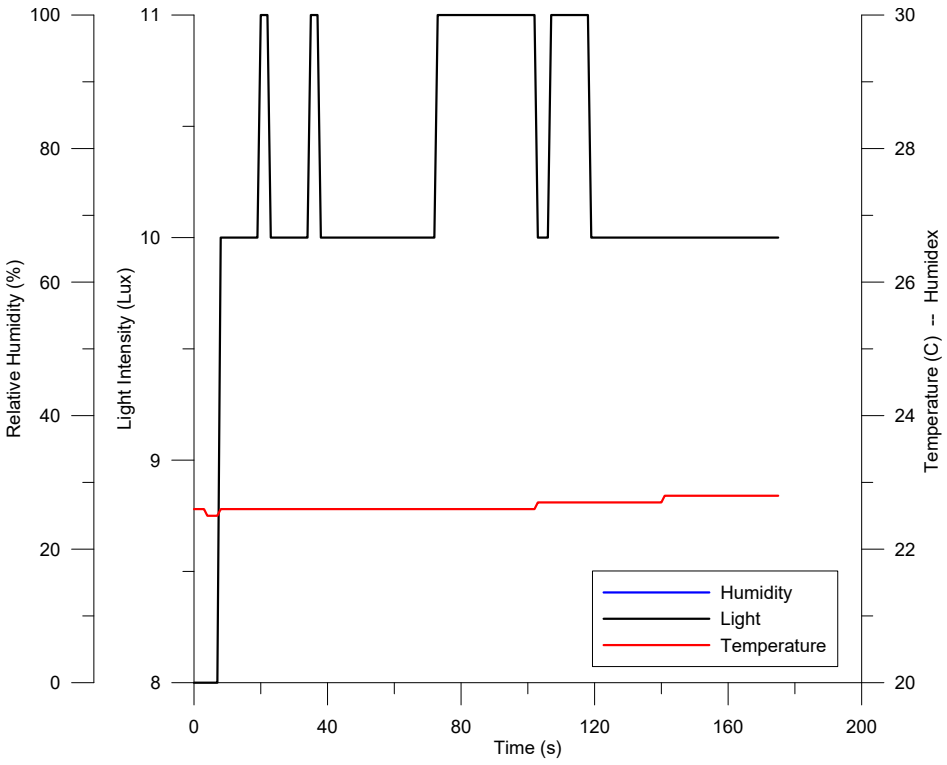


Figure C.296: Test 63 THLP 03

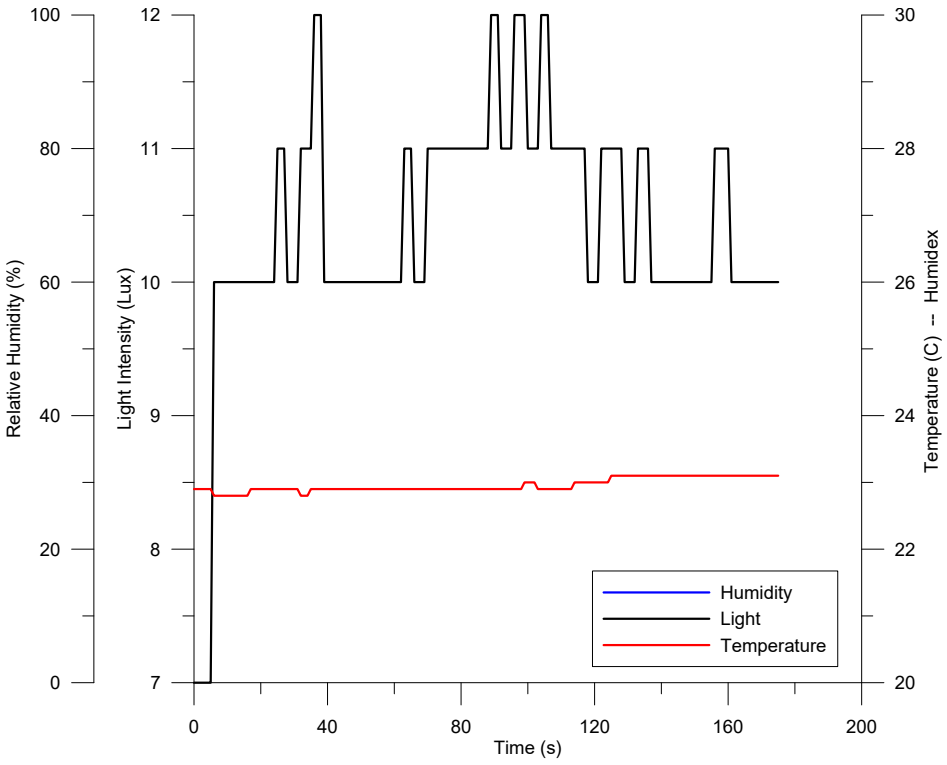


Figure C.297: Test 63 THLP 04

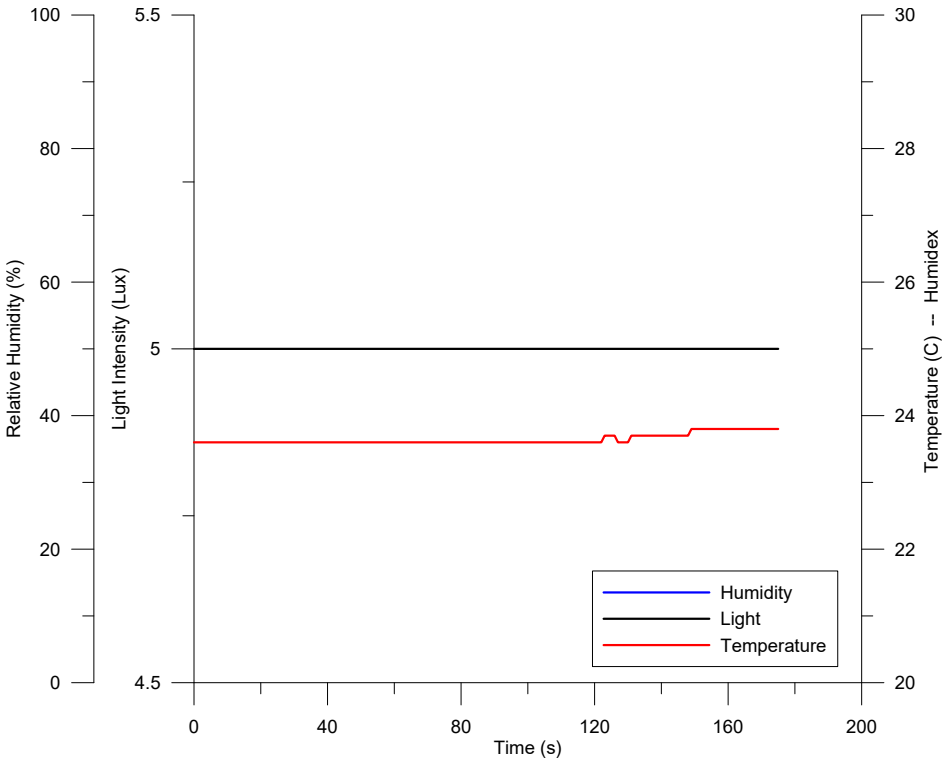


Figure C.298: Test 63 THLP 05

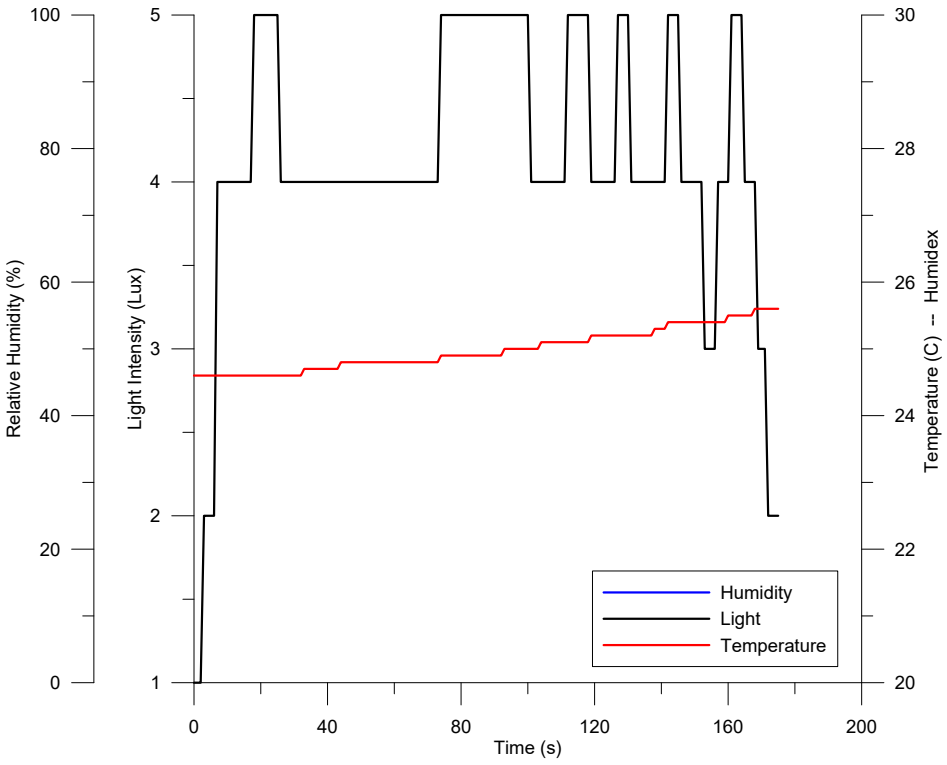


Figure C.299: Test 63 THLP 08

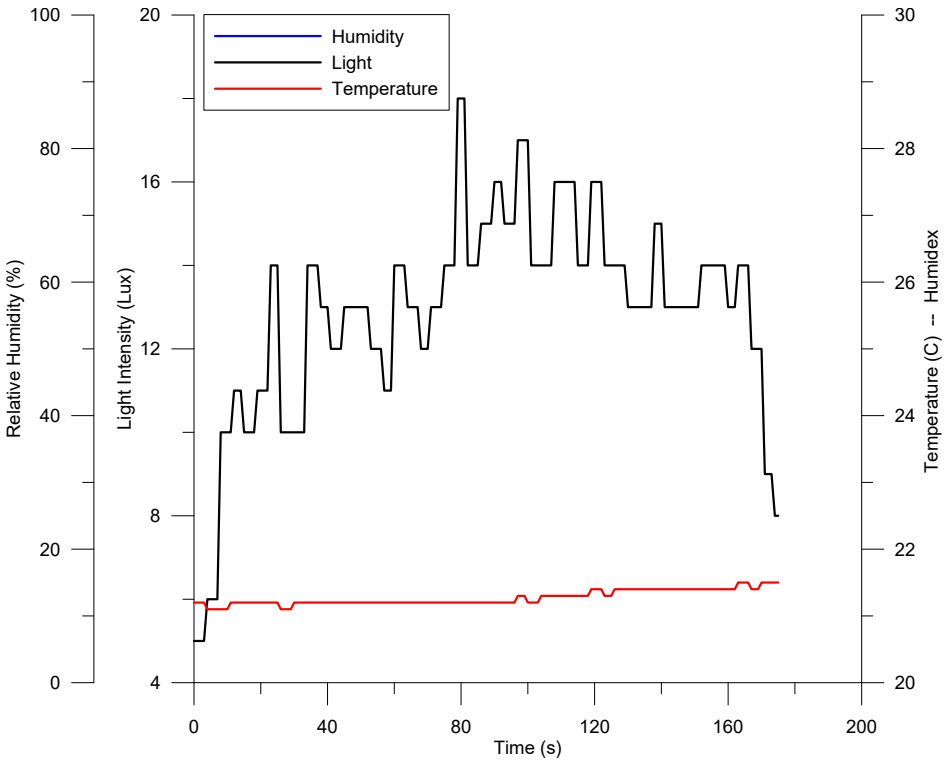


Figure C.300: Test 63 THLP 09

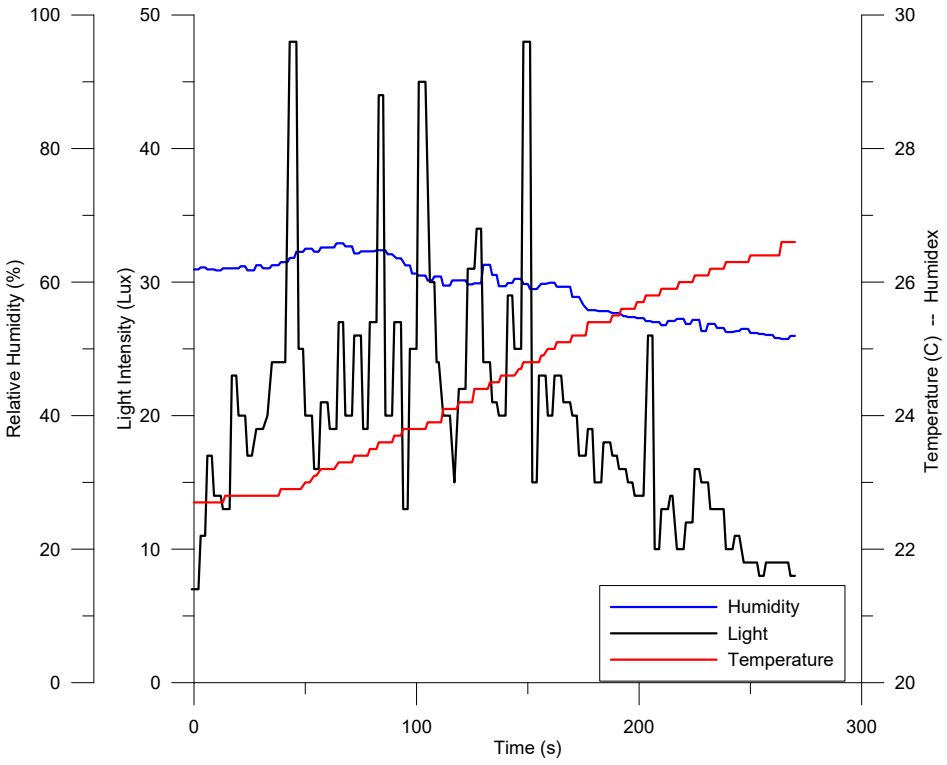


Figure C.301: Test 66 THLP 01

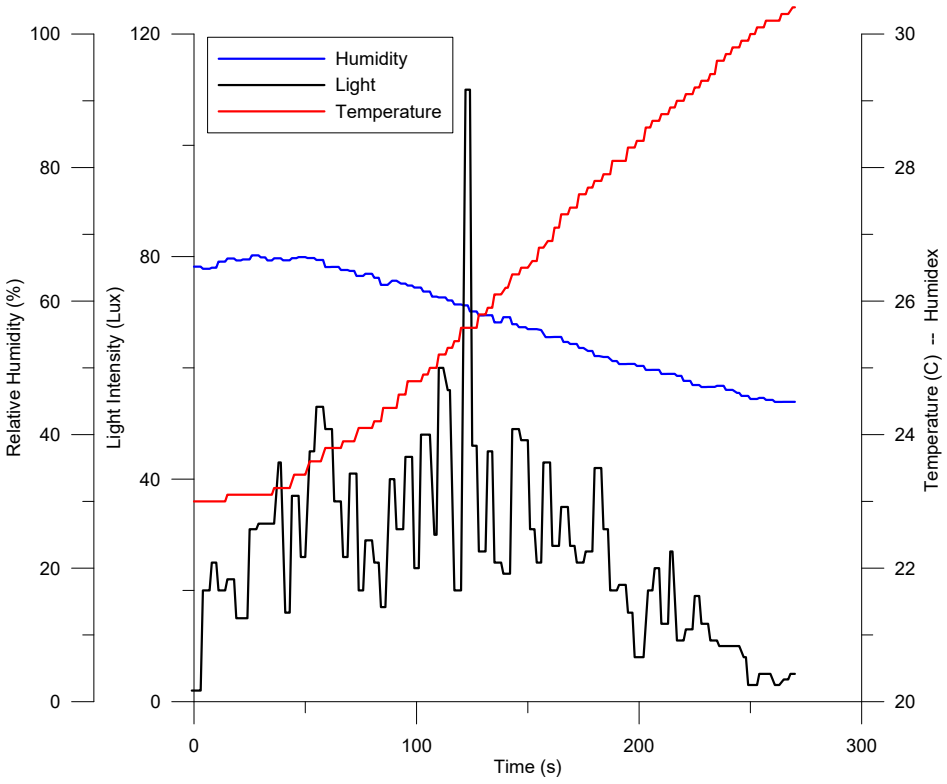


Figure C.302: Test 66 THLP 02

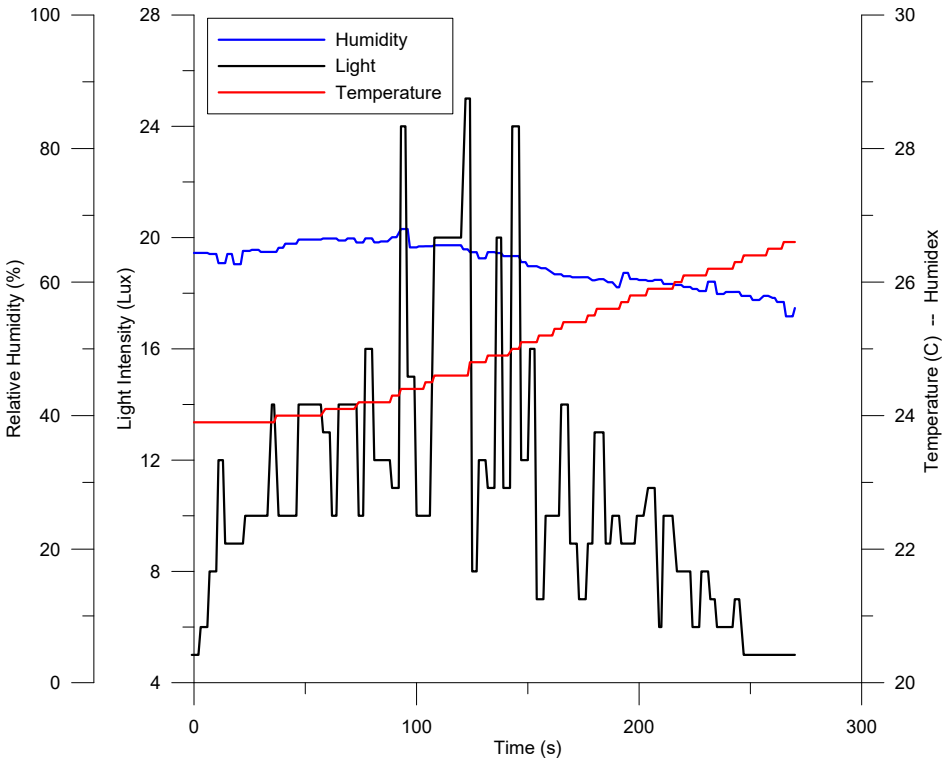


Figure C.303: Test 66 THLP 03

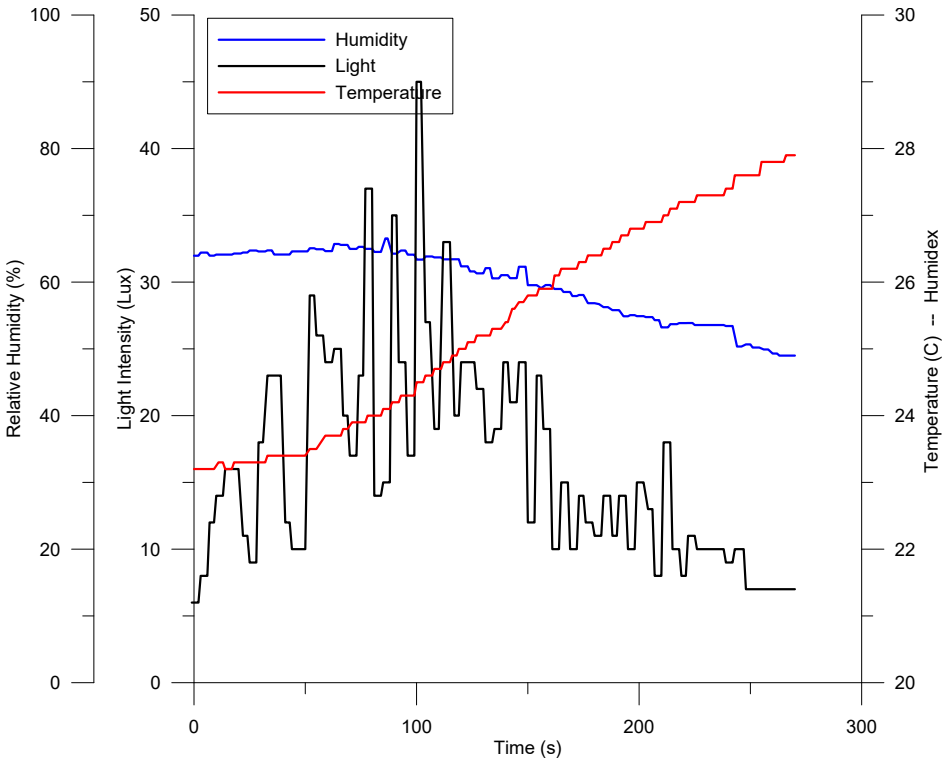


Figure C.304: Test 66 THLP 04

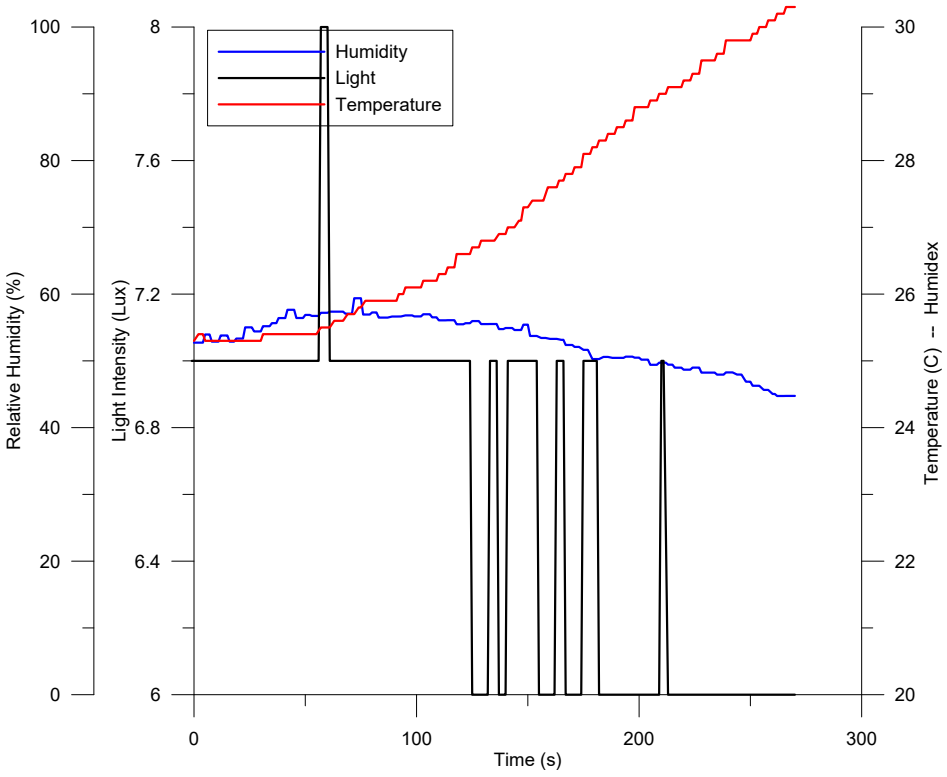


Figure C.305: Test 66 THLP 05

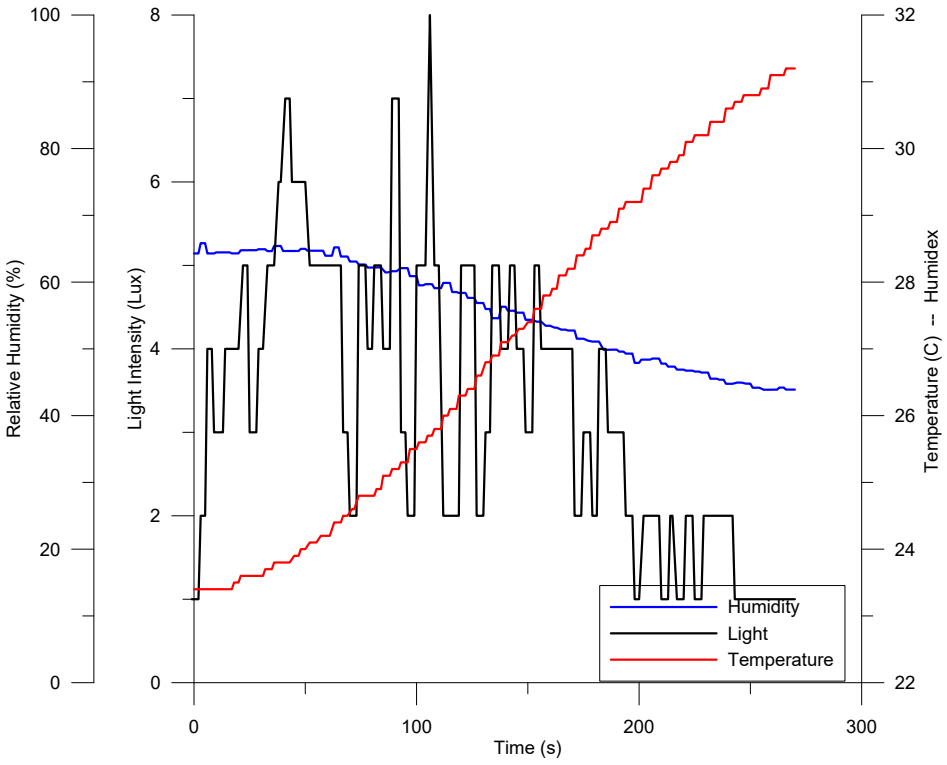


Figure C.306: Test 66 THLP 08

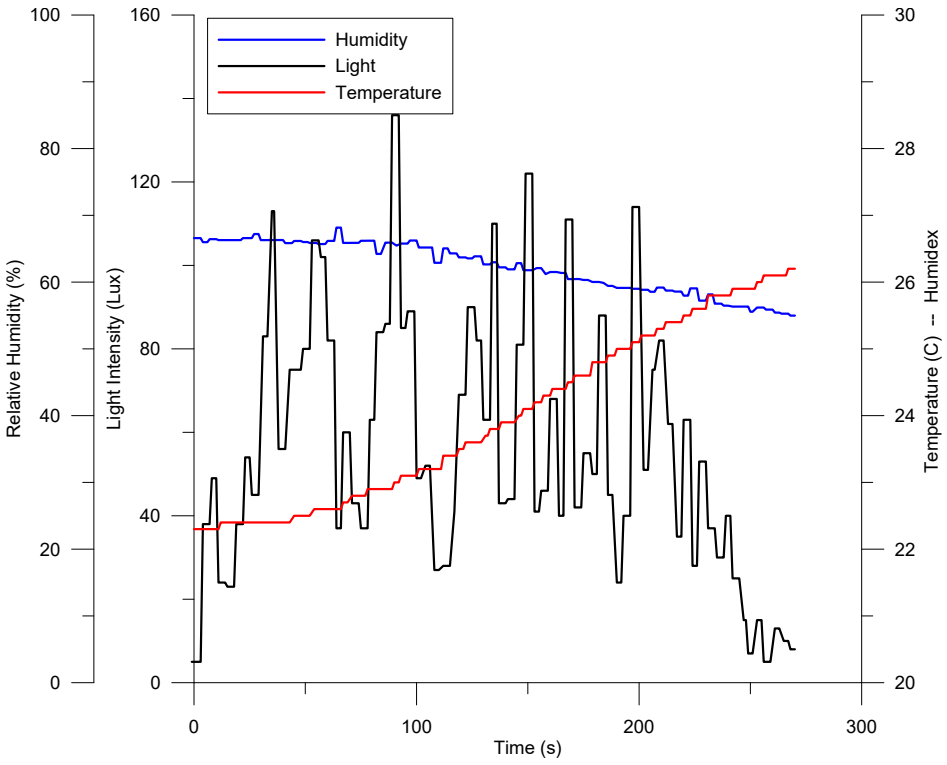


Figure C.307: Test 66 THLP 09

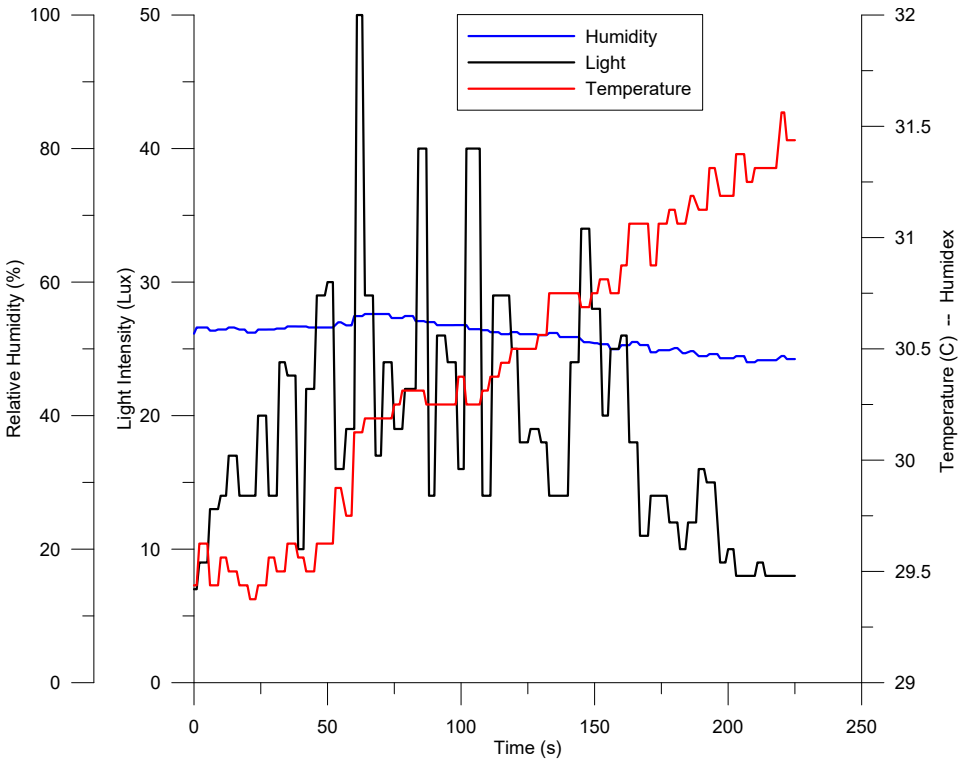


Figure C.308: Test 67 THLP 01

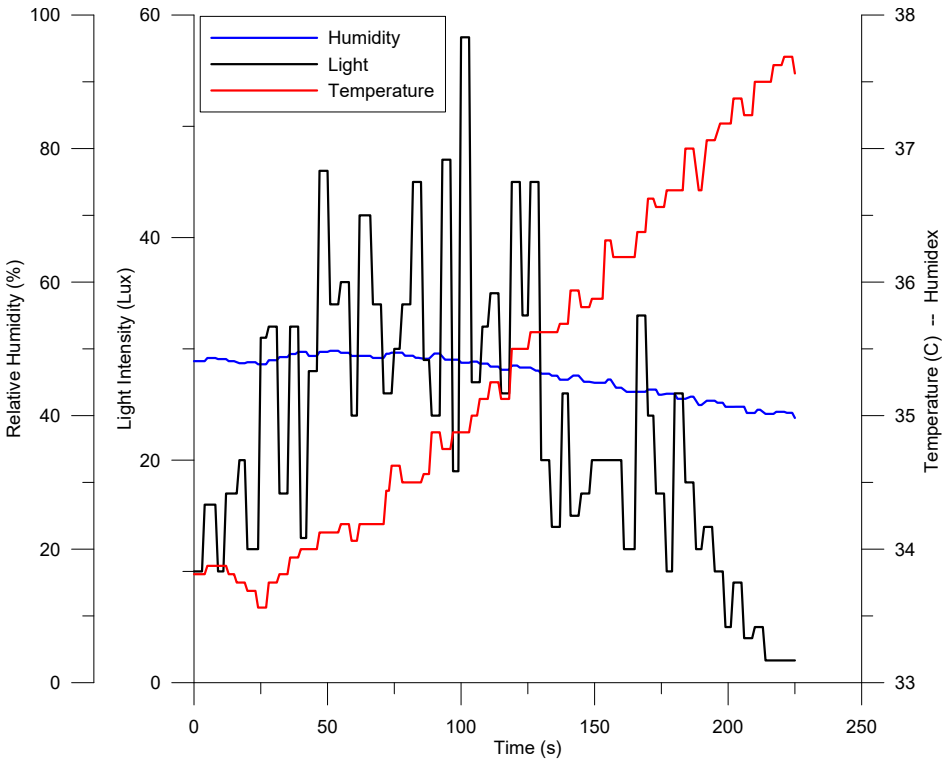


Figure C.309: Test 67 THLP 02

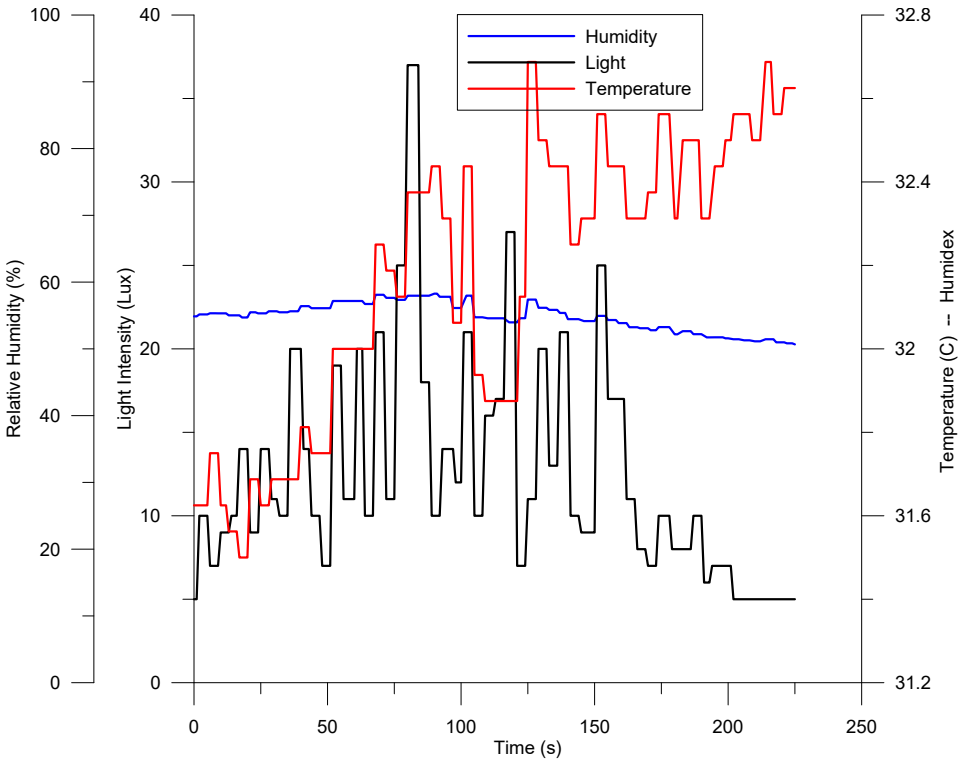


Figure C.310: Test 67 THLP 03

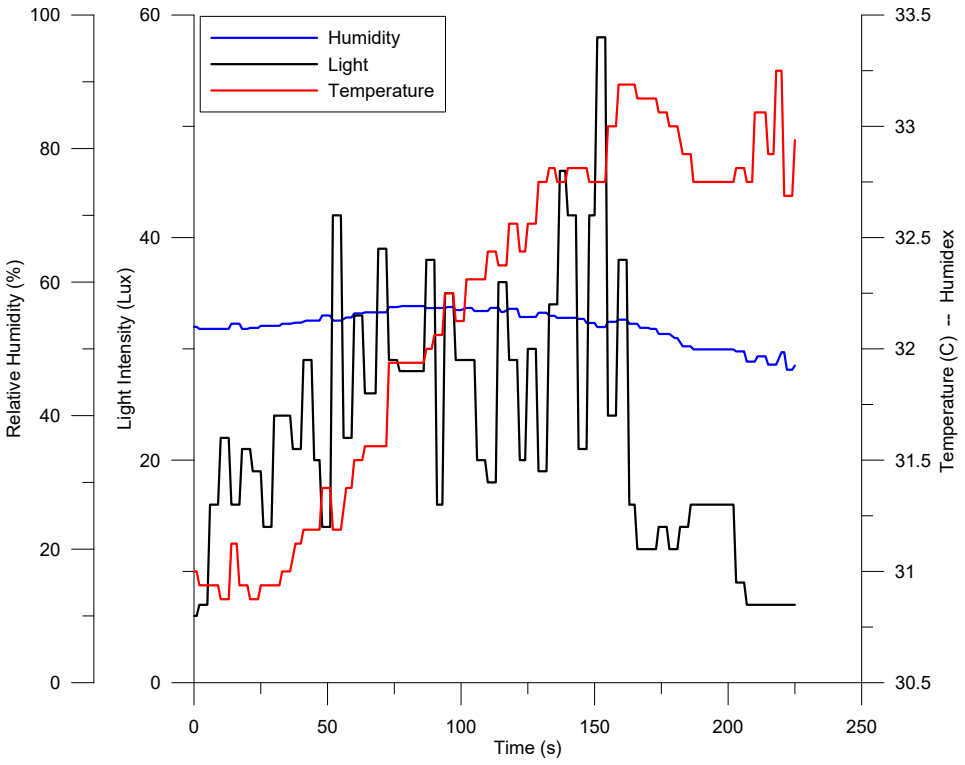


Figure C.311: Test 67 THLP 04

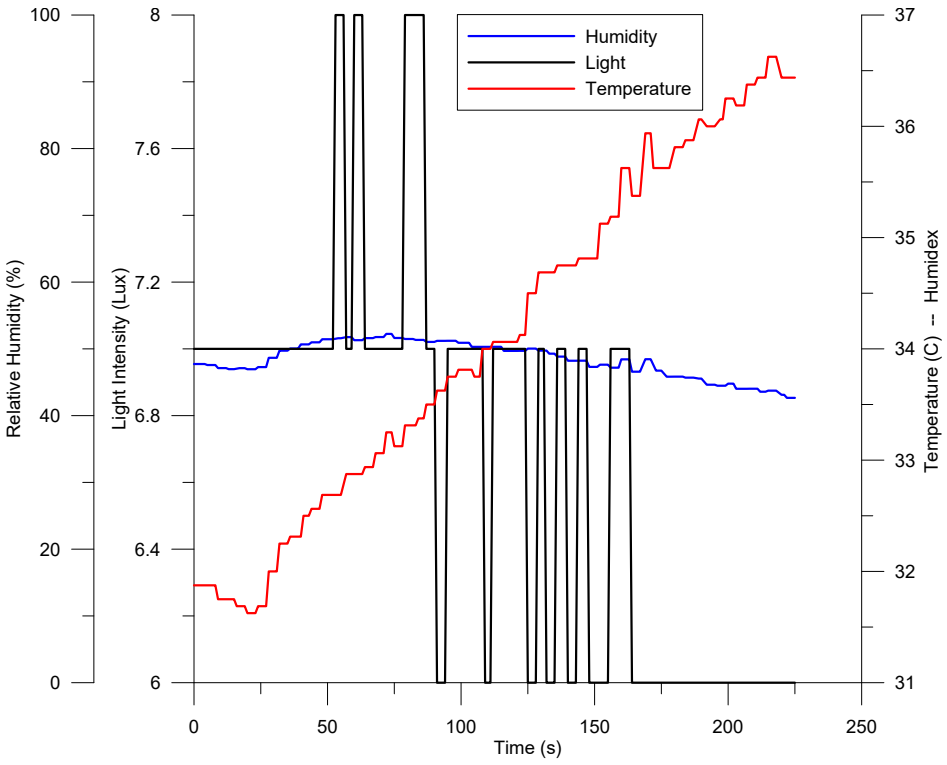


Figure C.312: Test 67 THLP 05

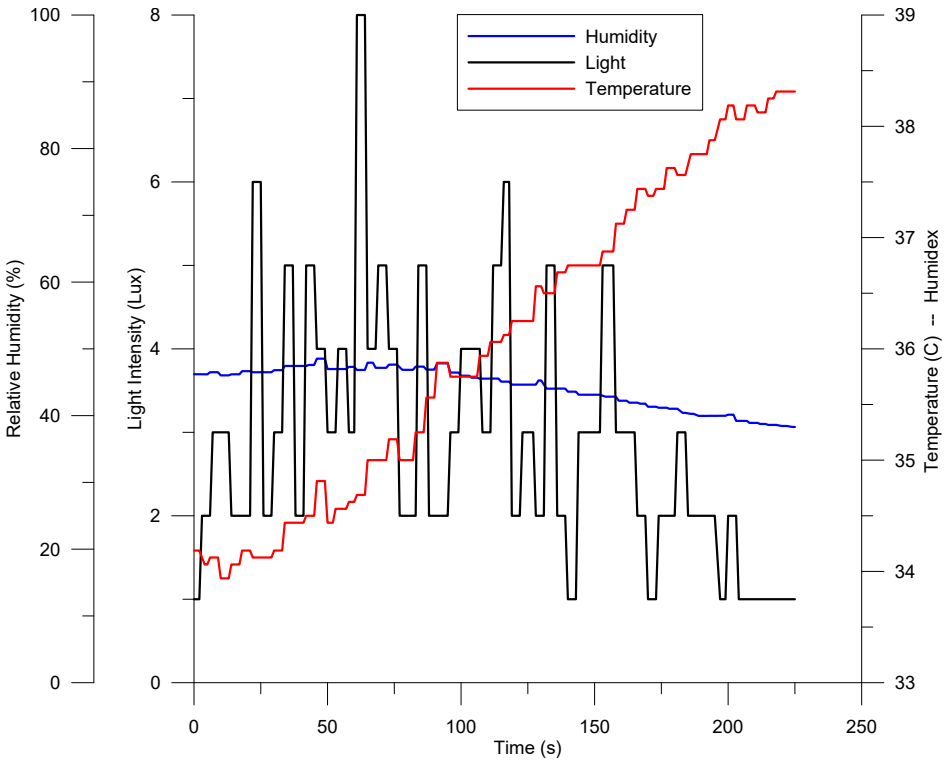


Figure C.313: Test 67 THLP 08

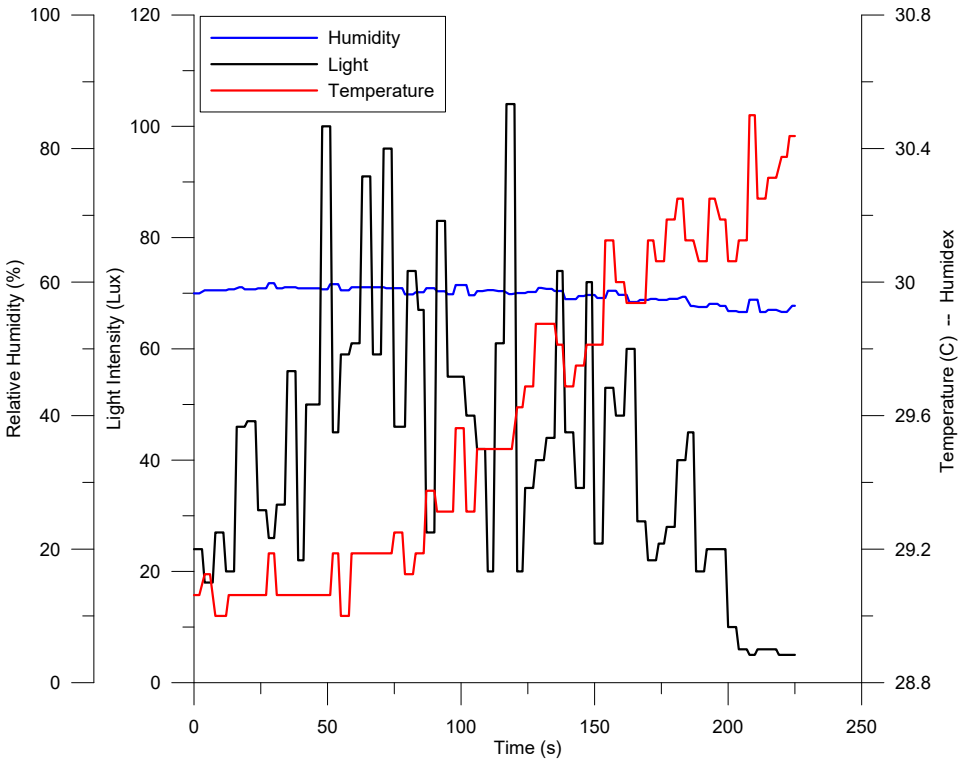


Figure C.314: Test 67 THLP 09

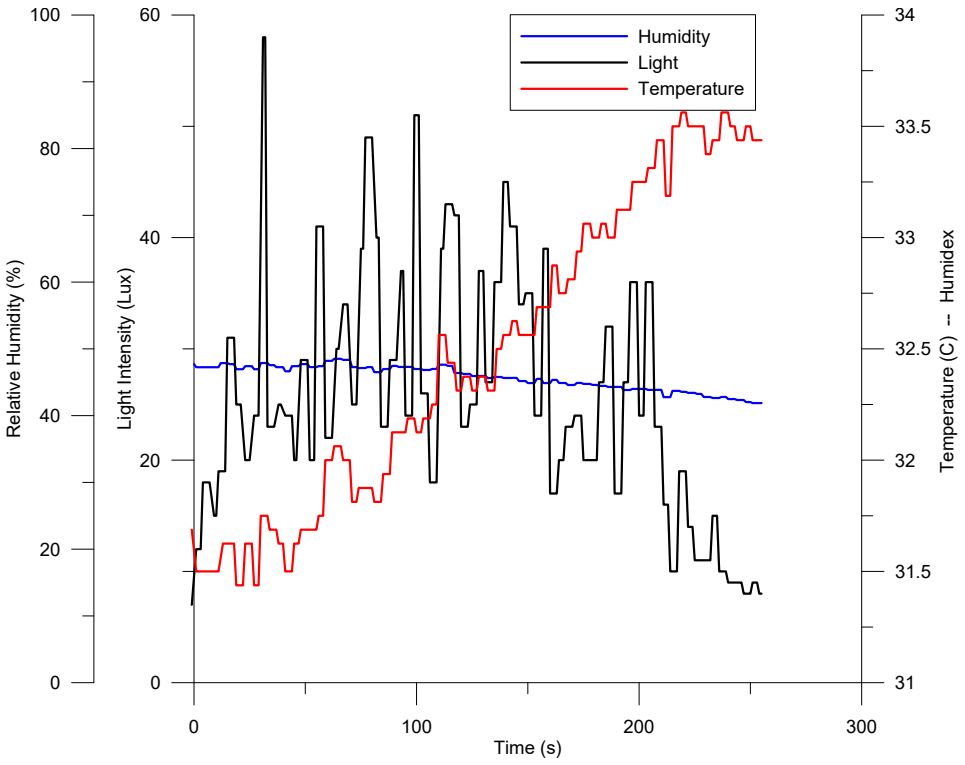


Figure C.315: Test 68 THLP 01

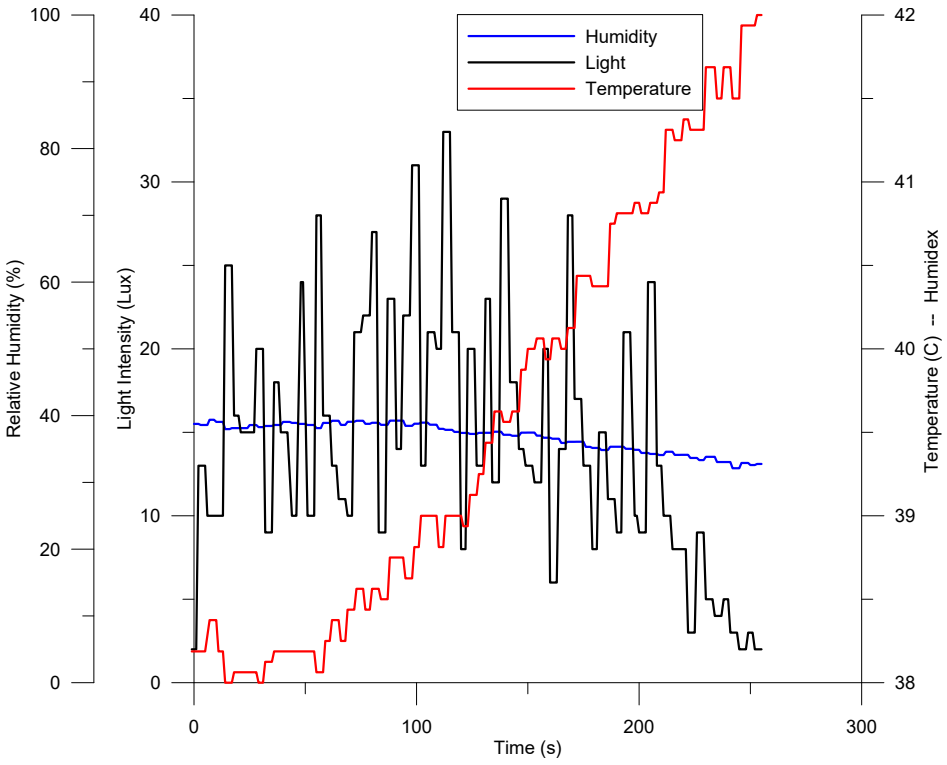


Figure C.316: Test 68 THLP 02

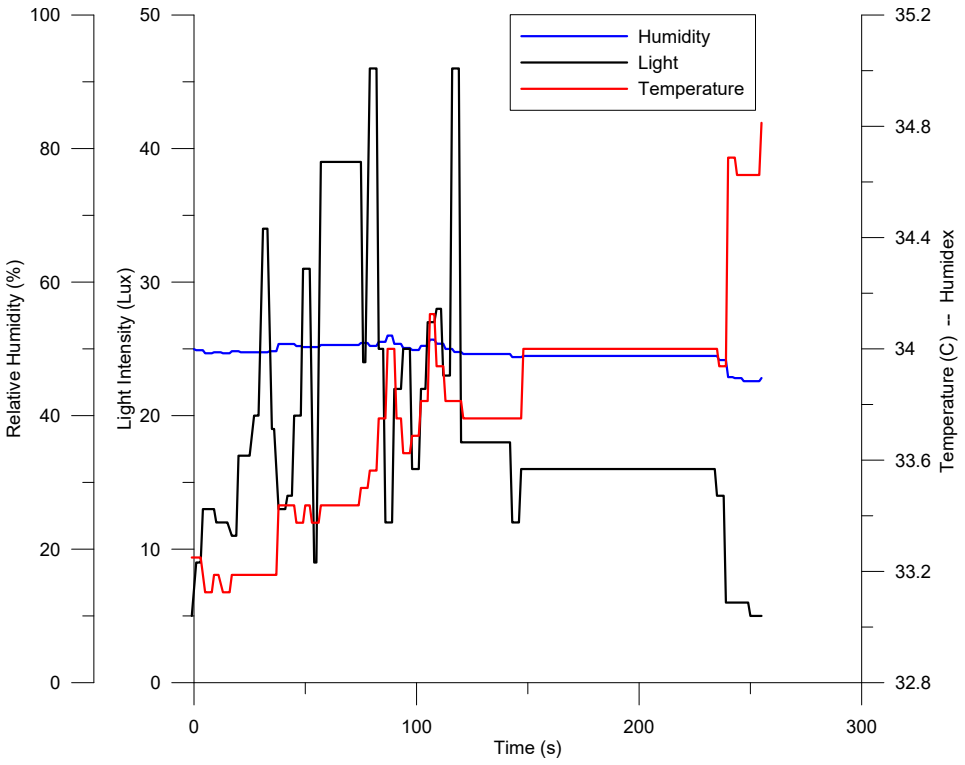


Figure C.317: Test 68 THLP 03

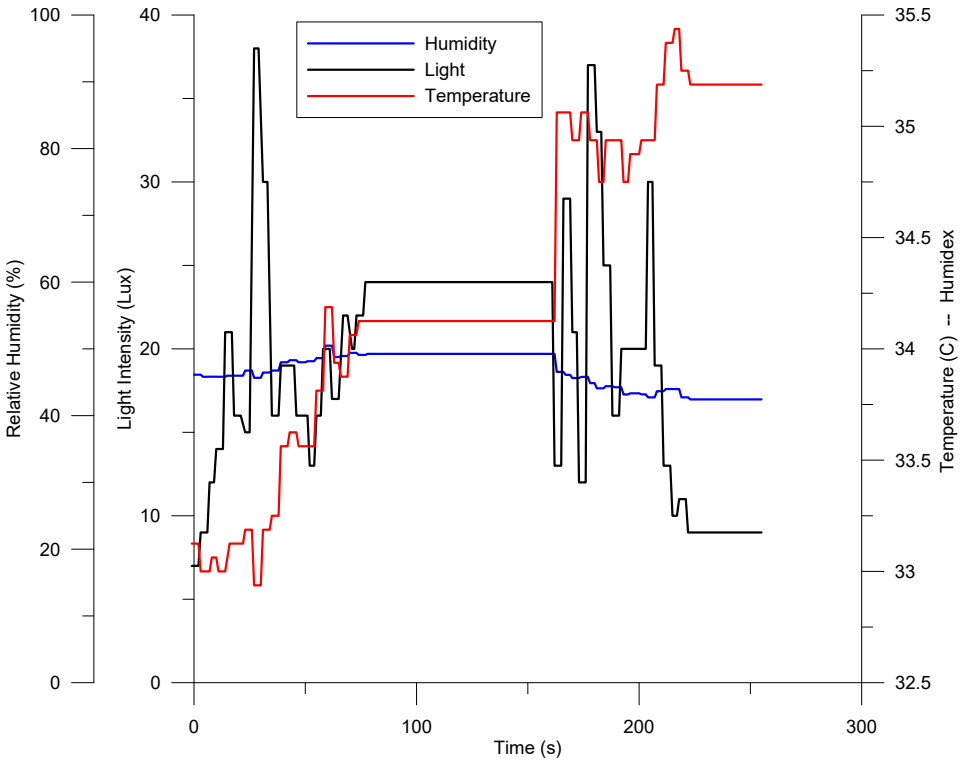


Figure C.318: Test 68 THLP 04

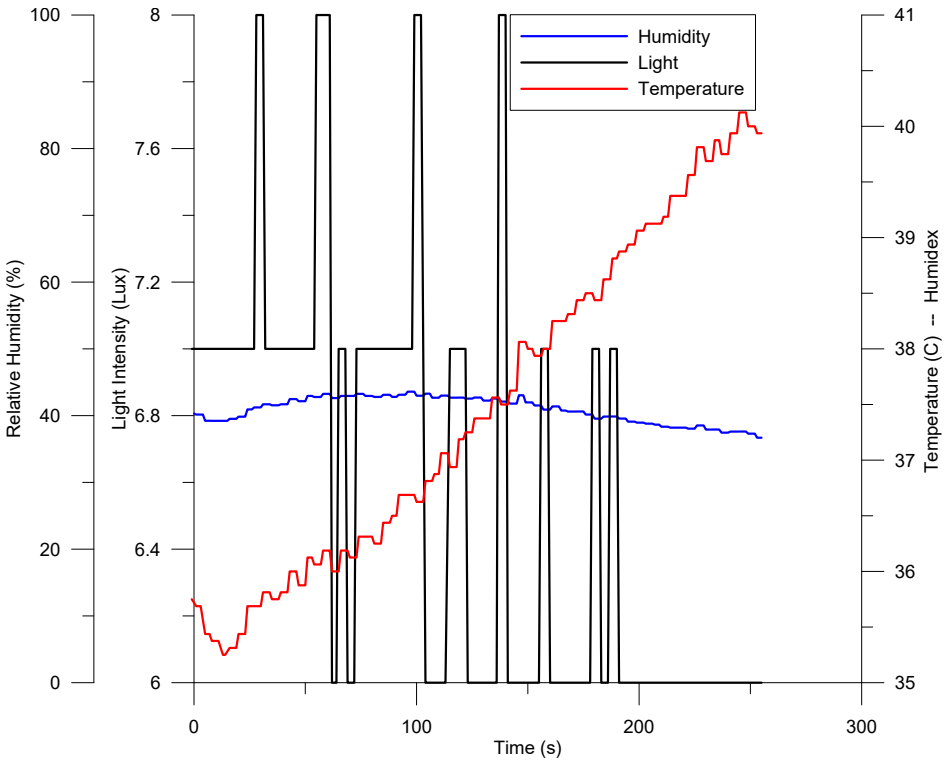


Figure C.319: Test 68 THLP 05

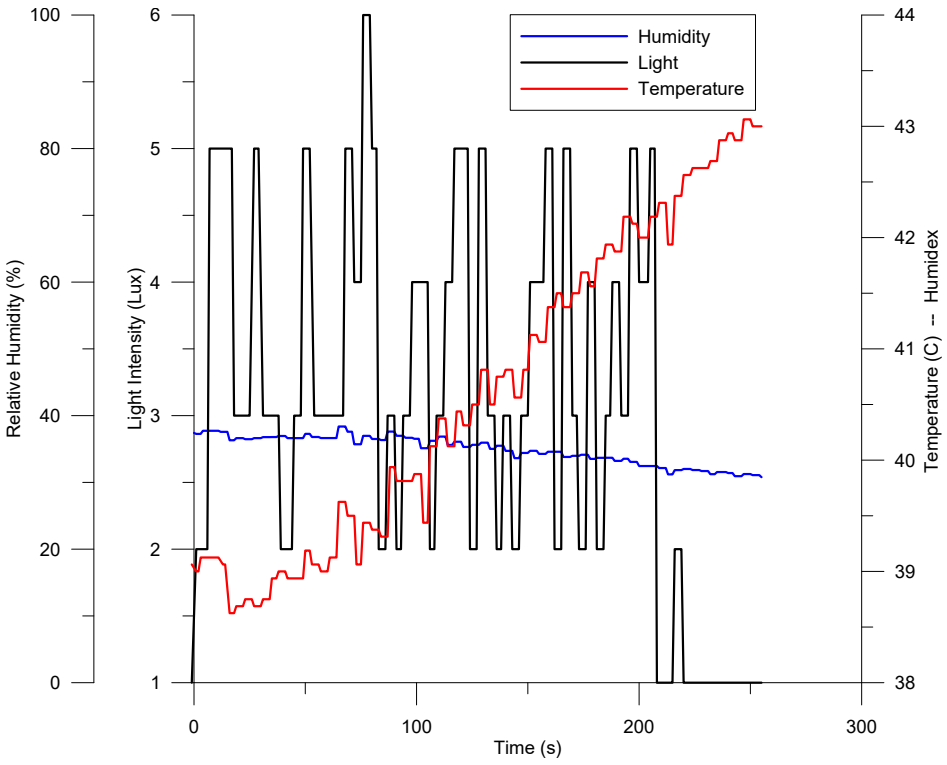


Figure C.320: Test 68 THLP 08

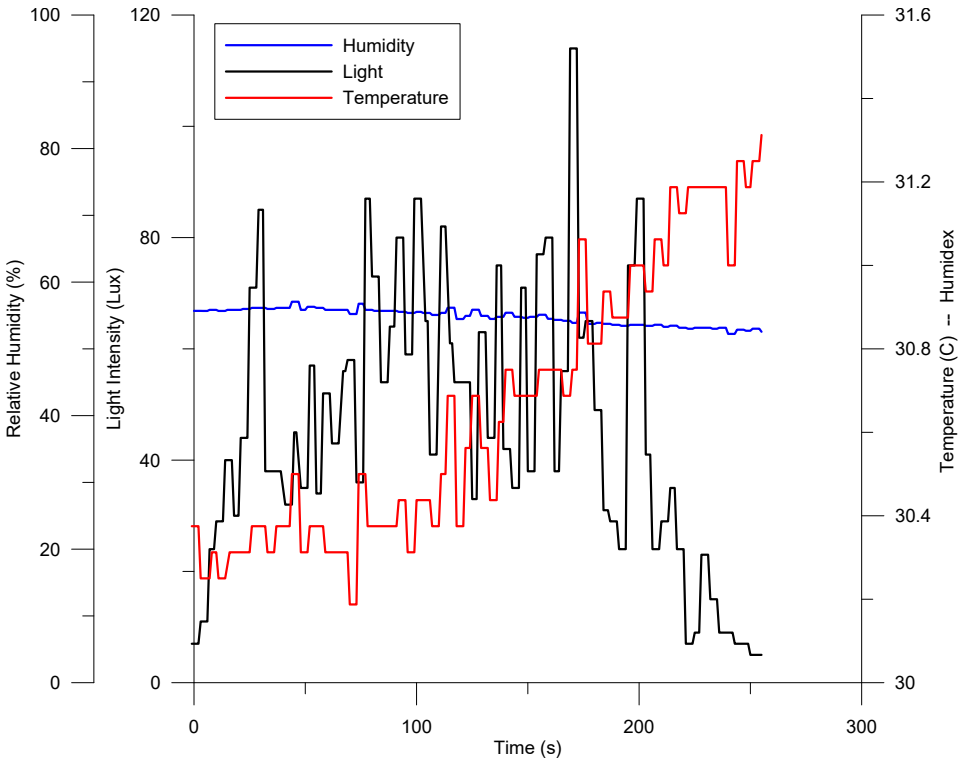


Figure C.321: Test 68 THLP 09

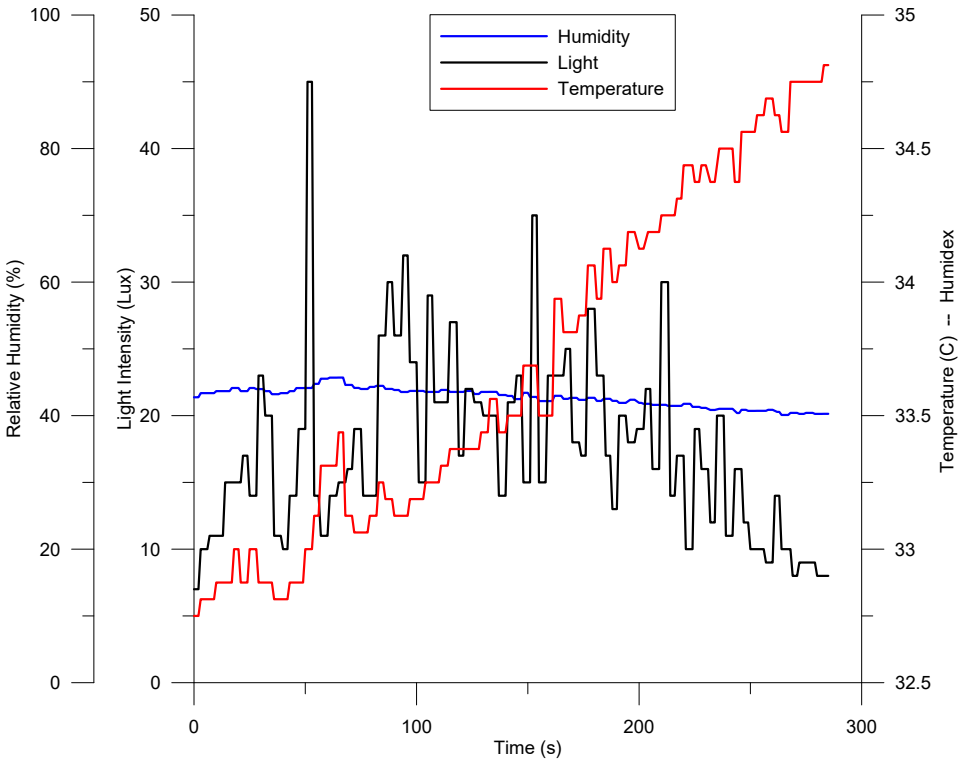


Figure C.322: Test 69 THLP 01

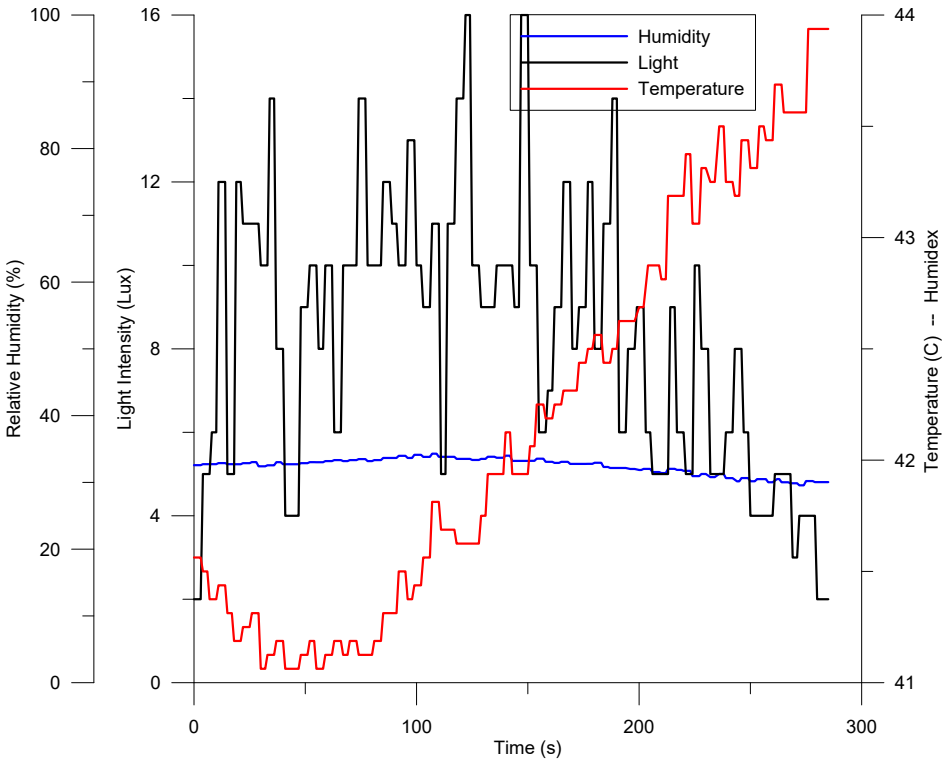


Figure C.323: Test 69 THLP 02

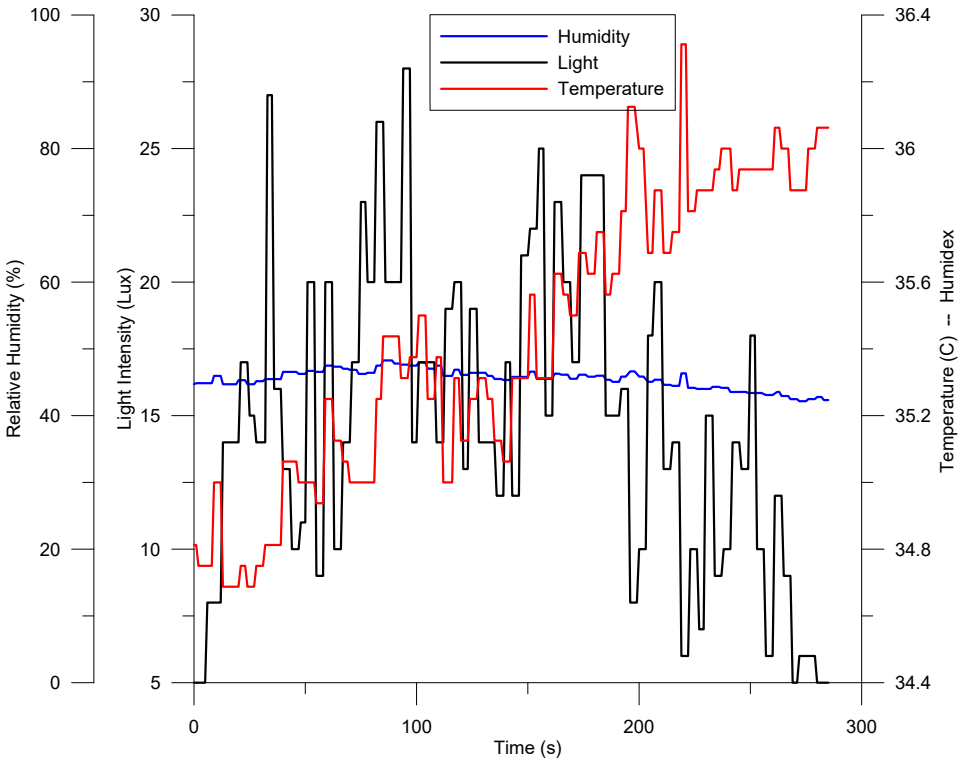


Figure C.324: Test 69 THLP 03

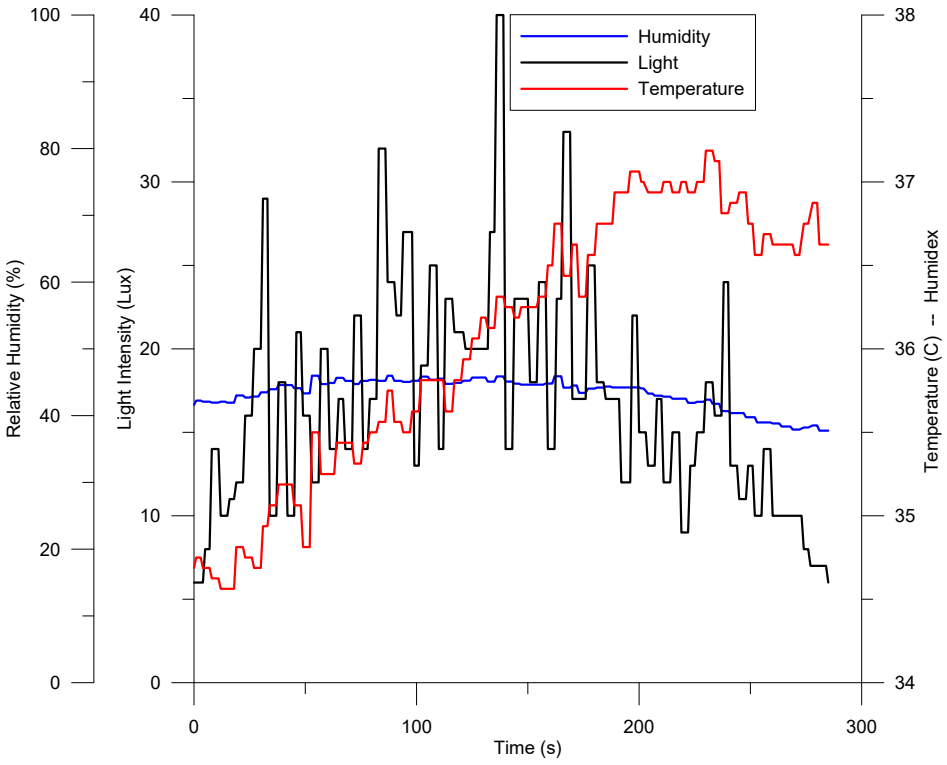


Figure C.325: Test 69 THLP 04

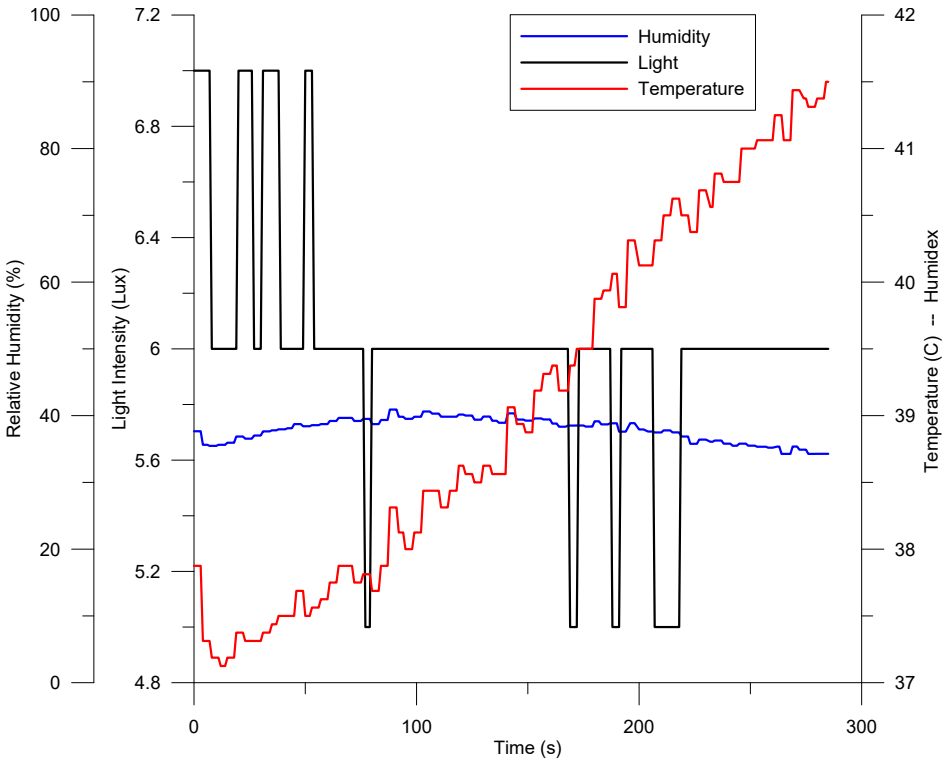


Figure C.326: Test 69 THLP 05

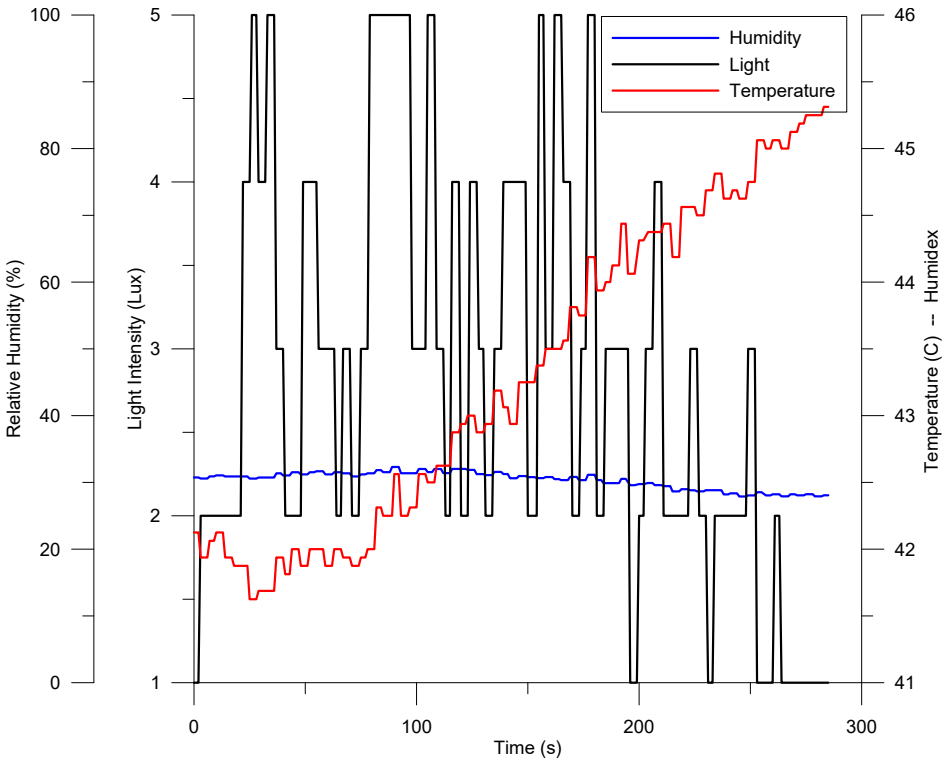


Figure C.327: Test 69 THLP 08

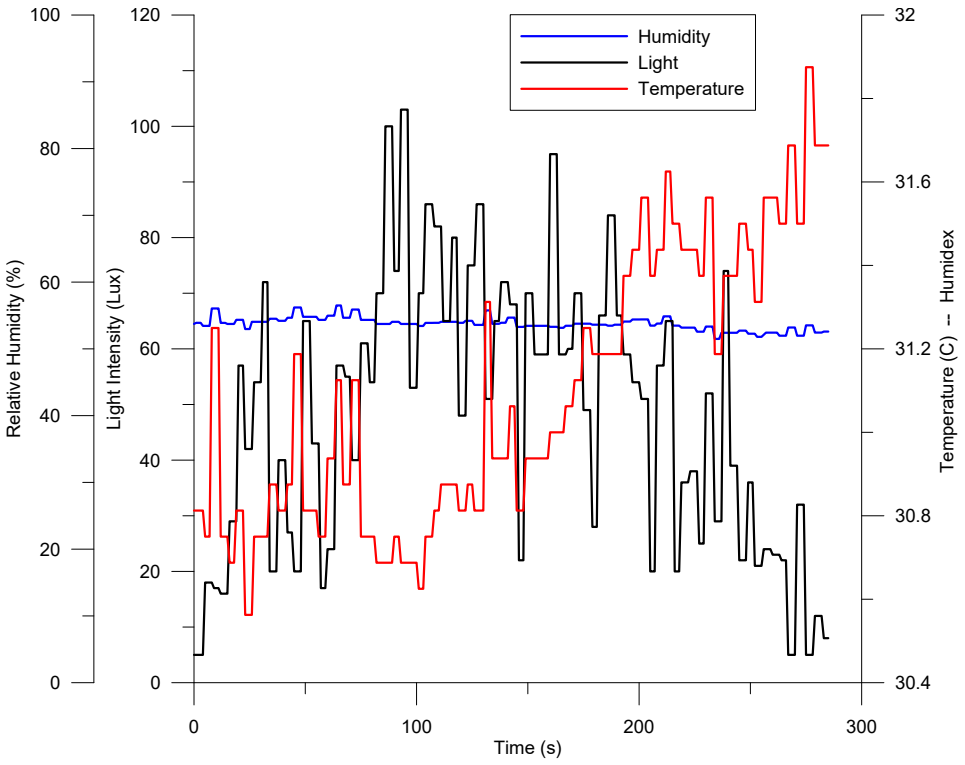


Figure C.328: Test 69 THLP 09

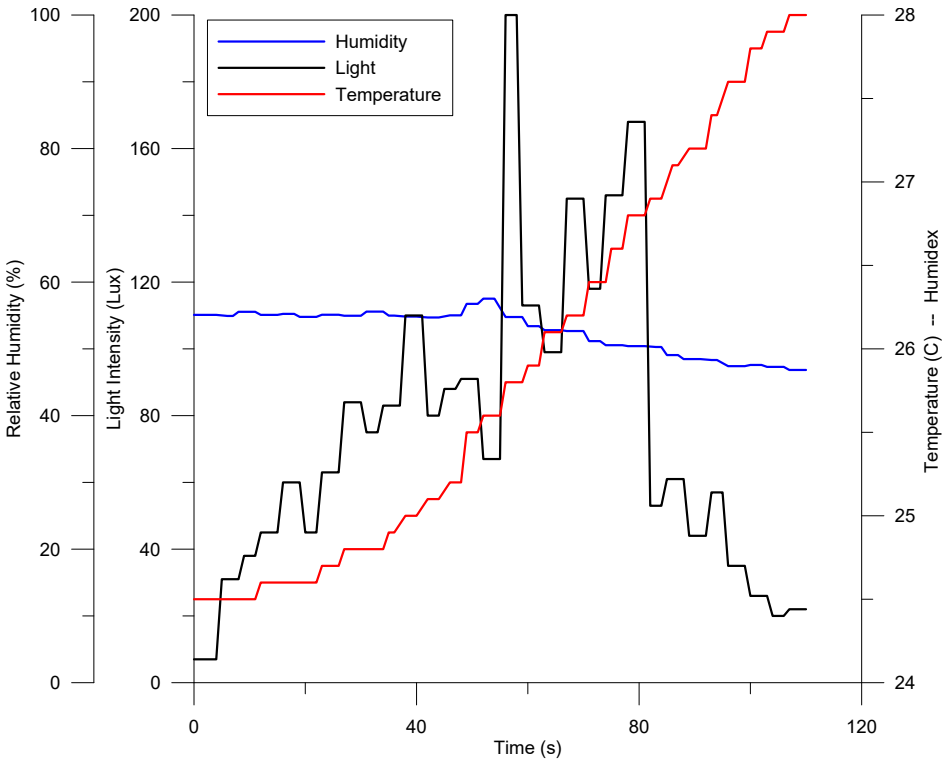


Figure C.329: Test 73 THLP 01

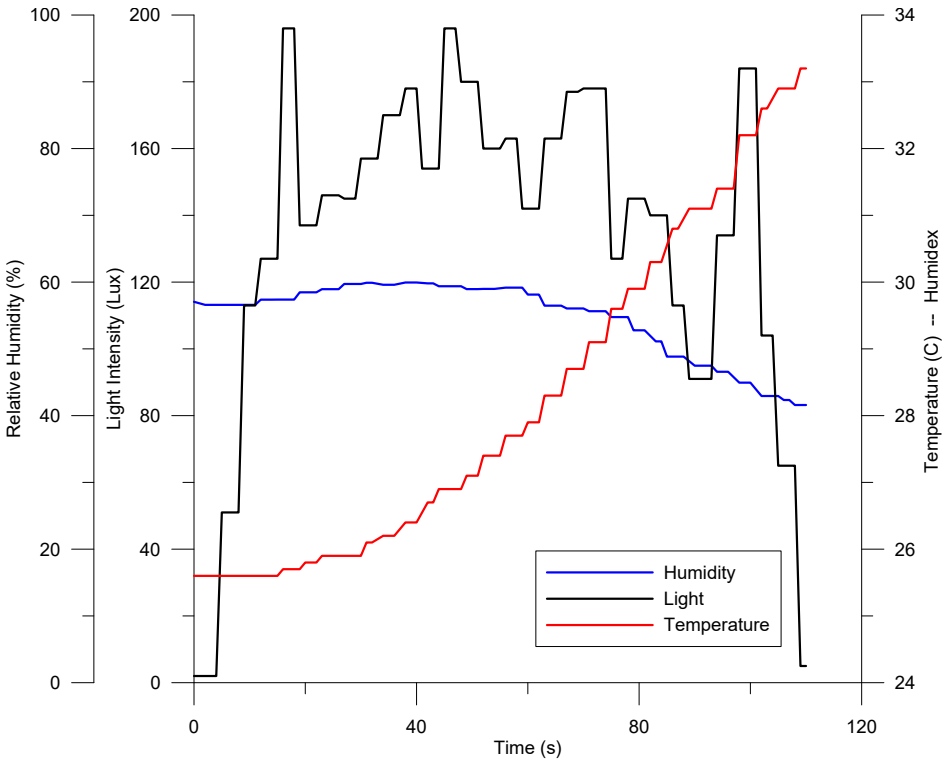


Figure C.330: Test 73 THLP 02

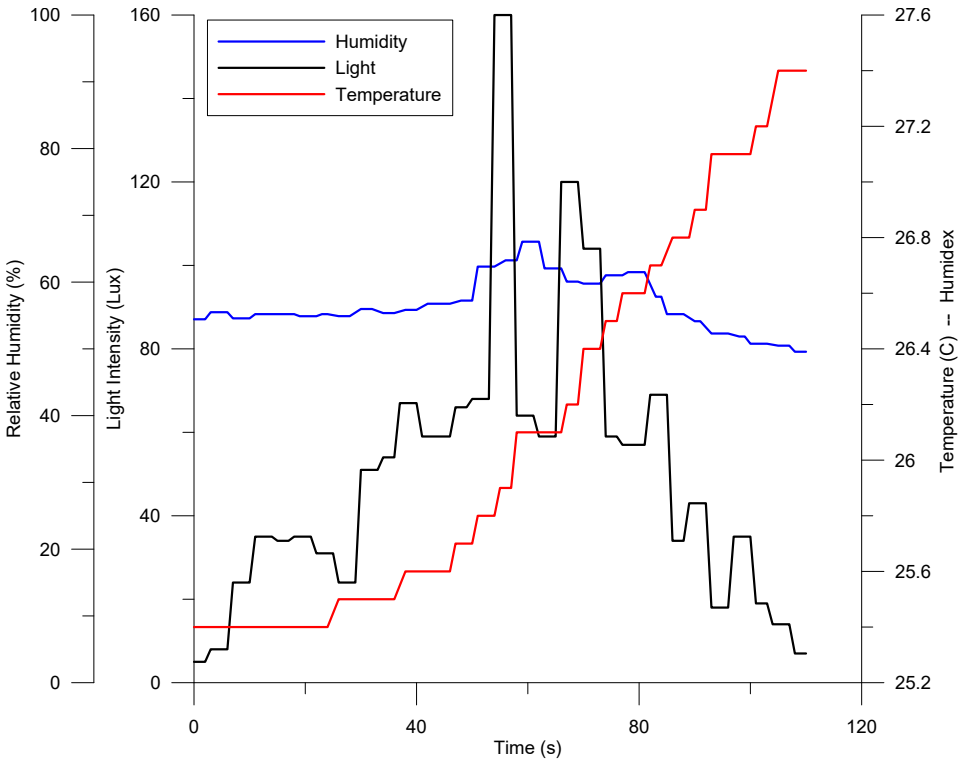


Figure C.331: Test 73 THLP 03

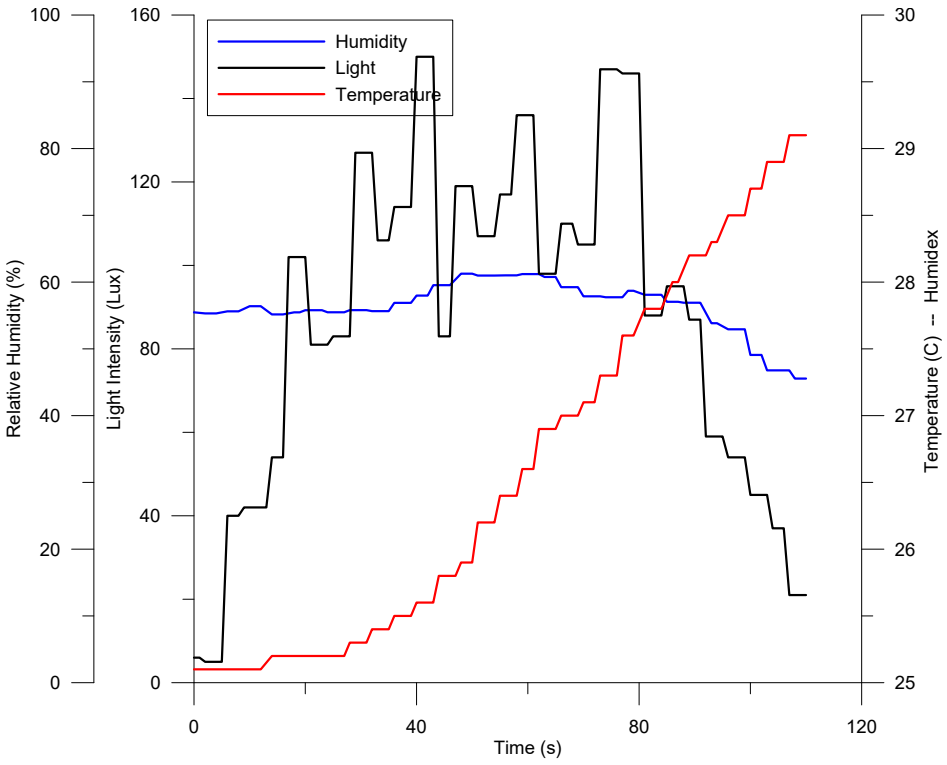


Figure C.332: Test 73 THLP 04

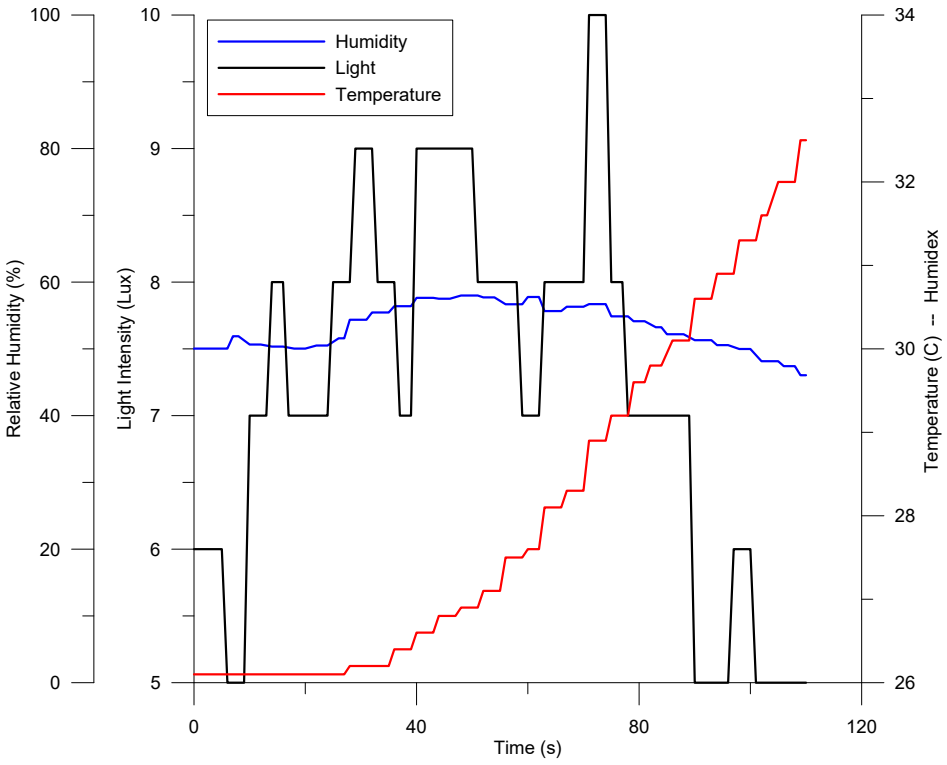


Figure C.333: Test 73 THLP 05

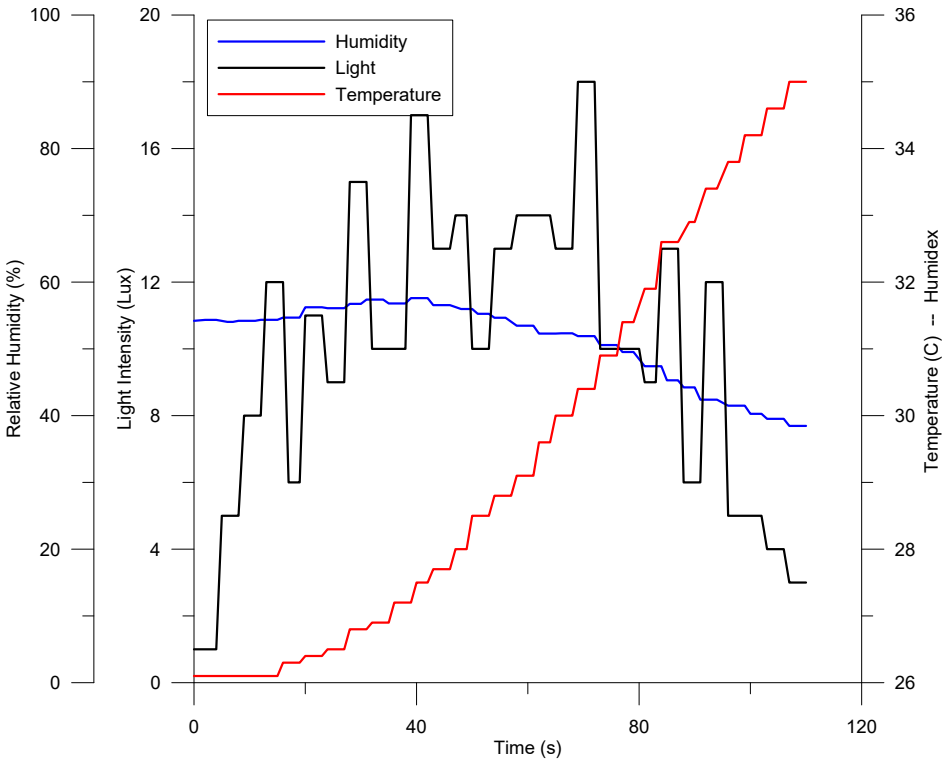


Figure C.334: Test 73 THLP 08

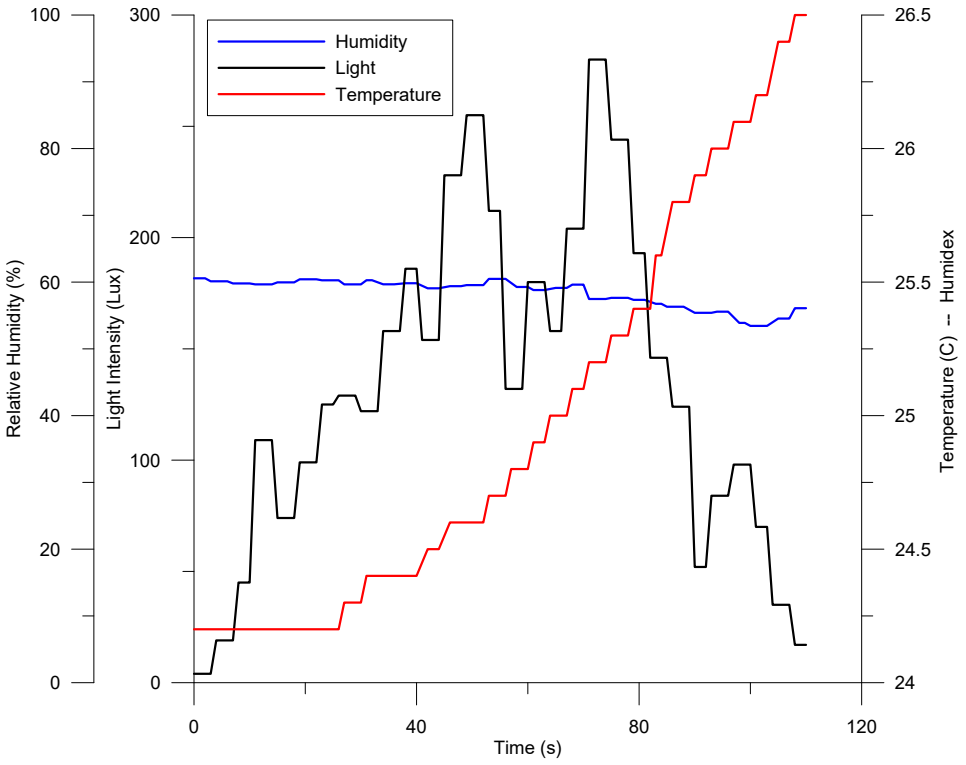


Figure C.335: Test 73 THLP 09

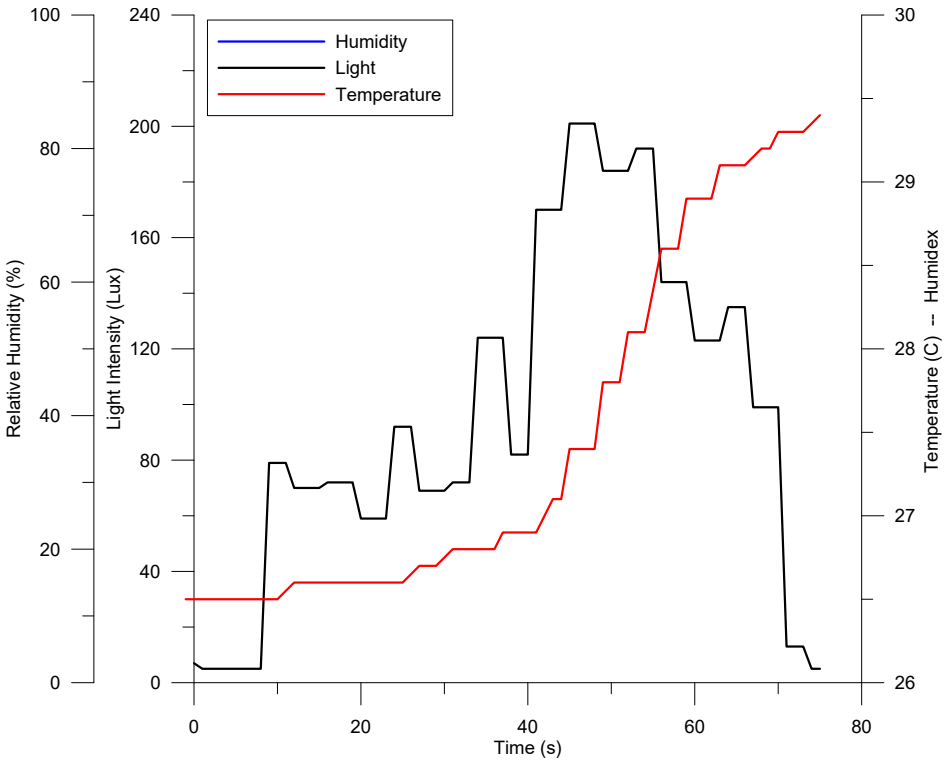


Figure C.336: Test 74 THLP 01

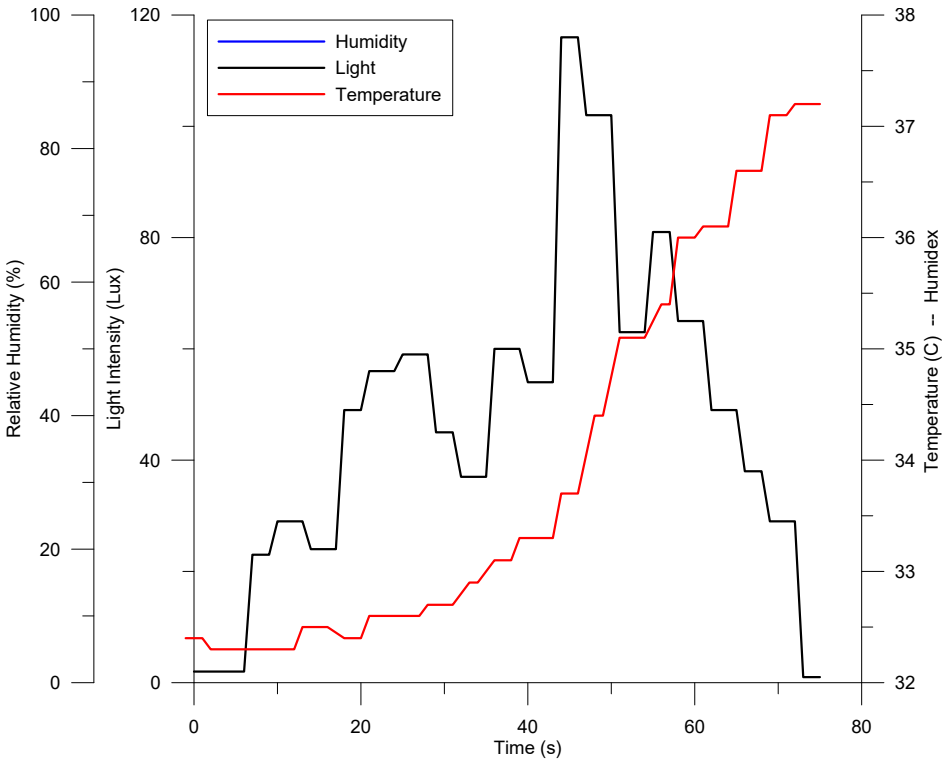


Figure C.337: Test 74 THLP 02

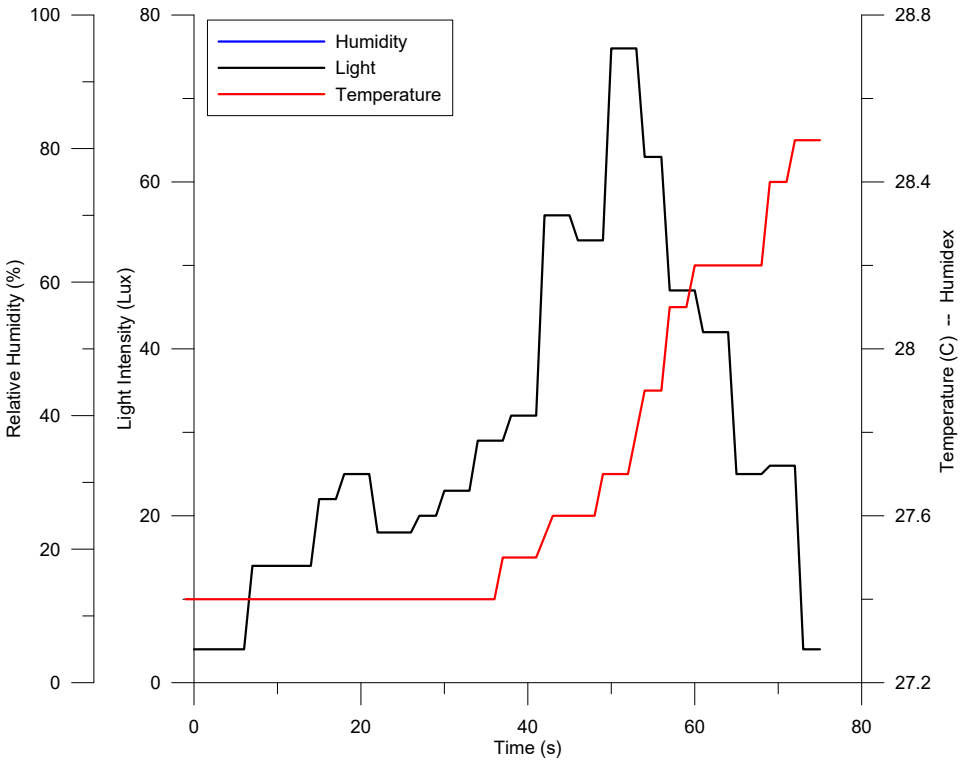


Figure C.338: Test 74 THLP 03

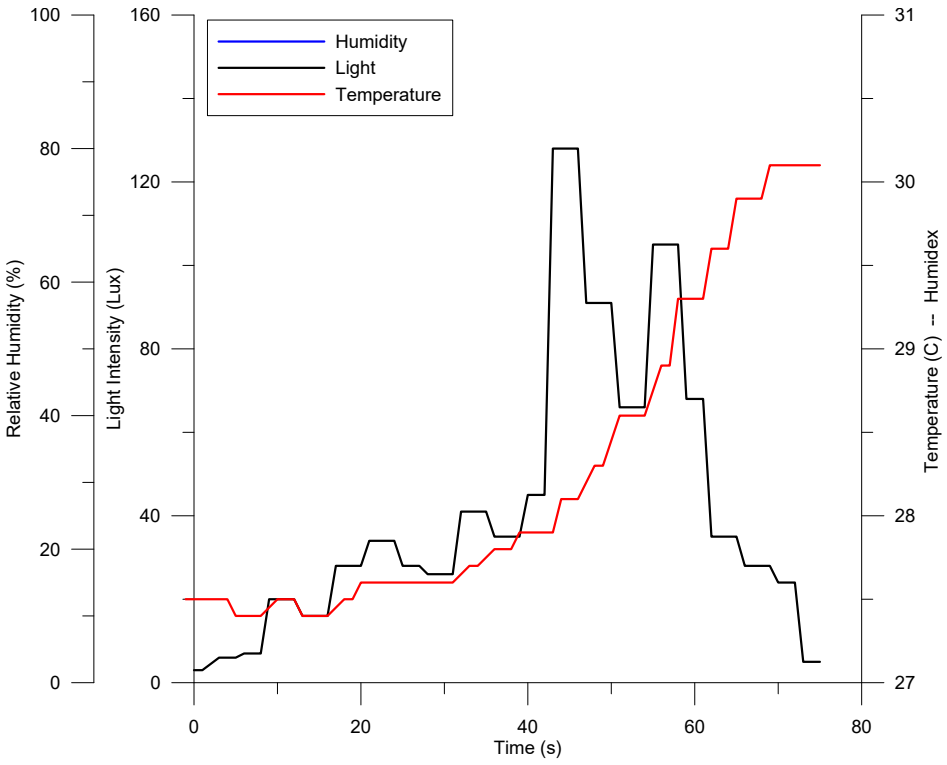


Figure C.339: Test 74 THLP 04

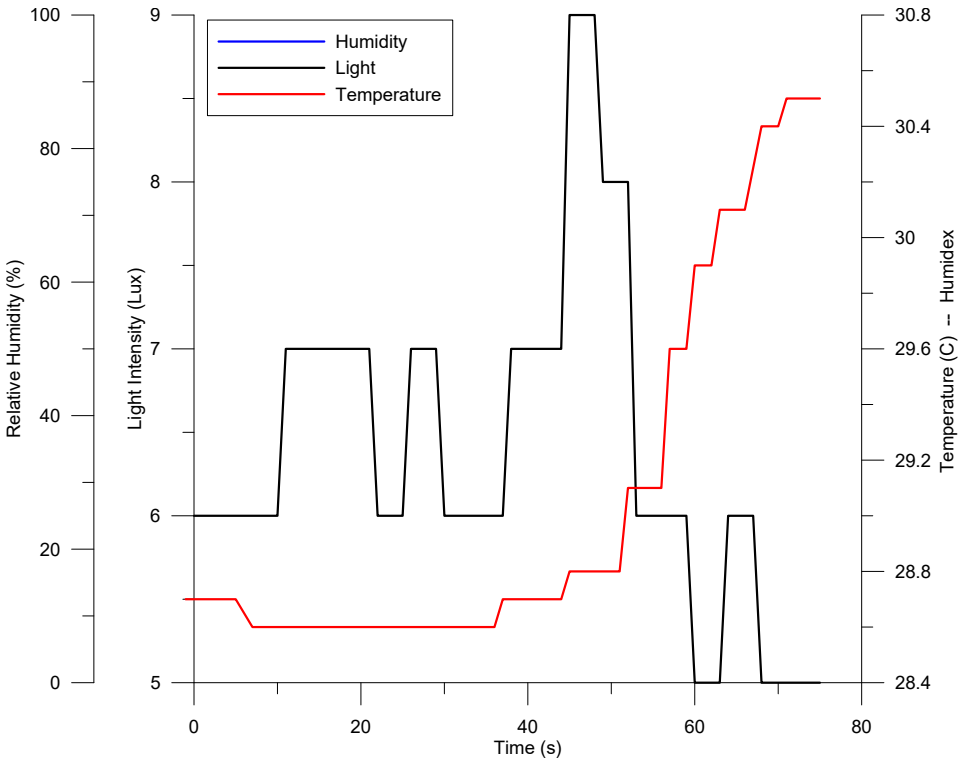


Figure C.340: Test 74 THLP 05

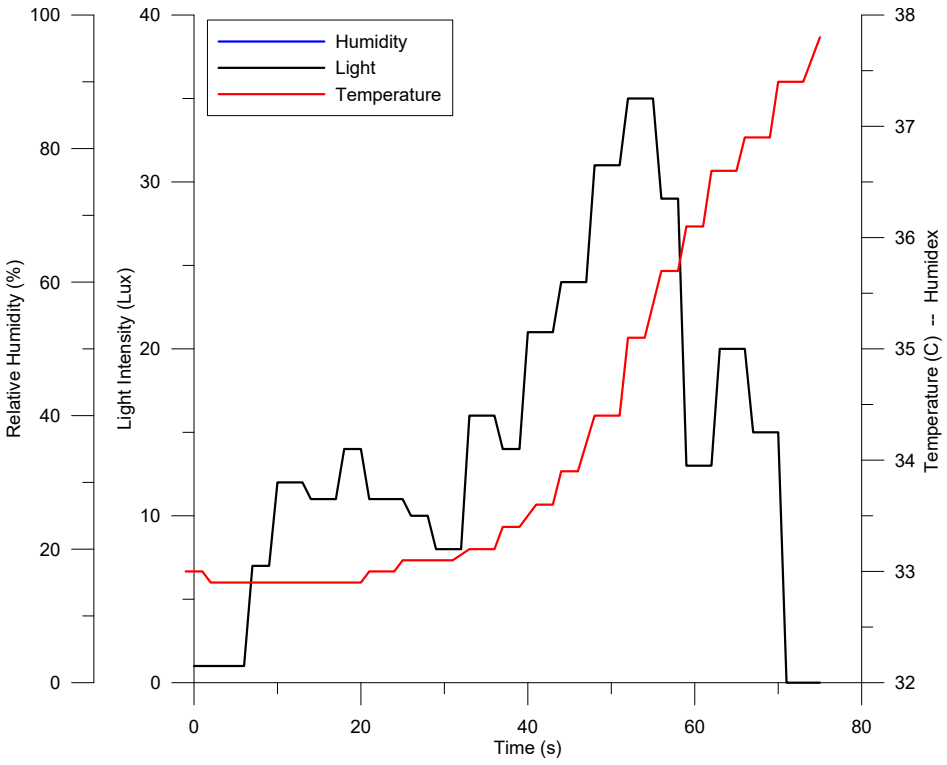


Figure C.341: Test 74 THLP 08

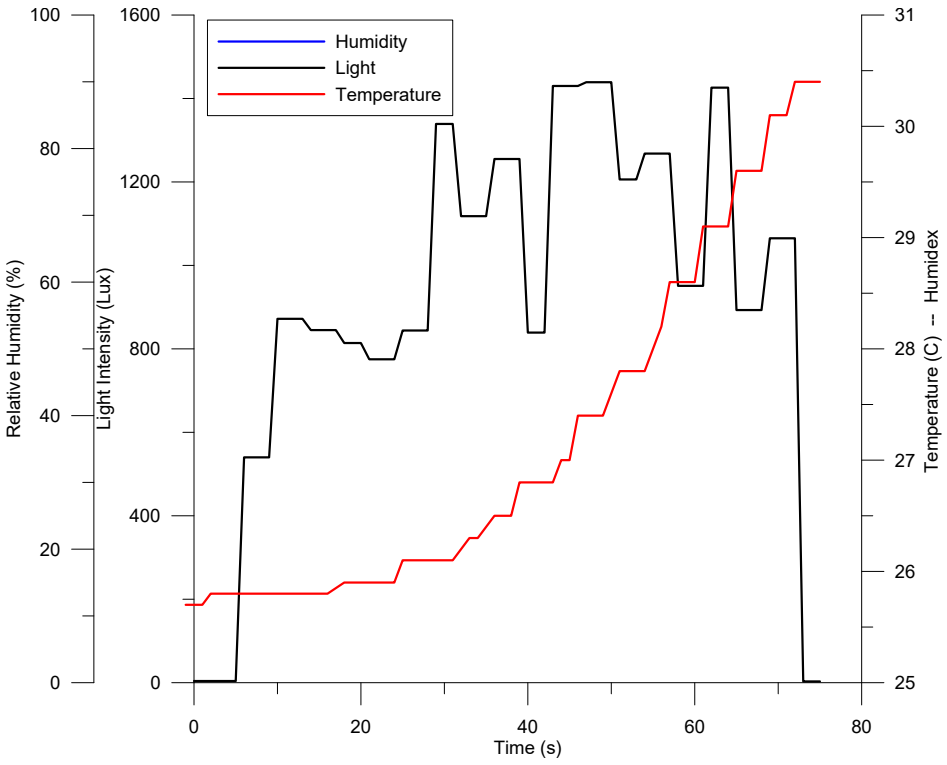


Figure C.342: Test 74 THLP 09

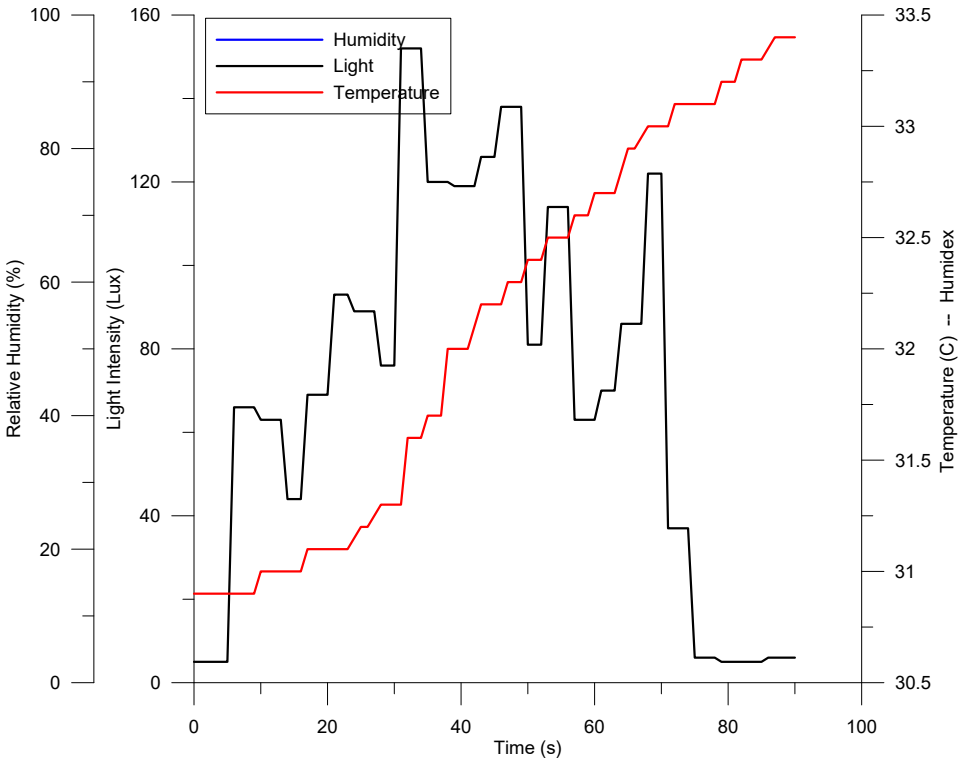


Figure C.343: Test 75 THLP 01

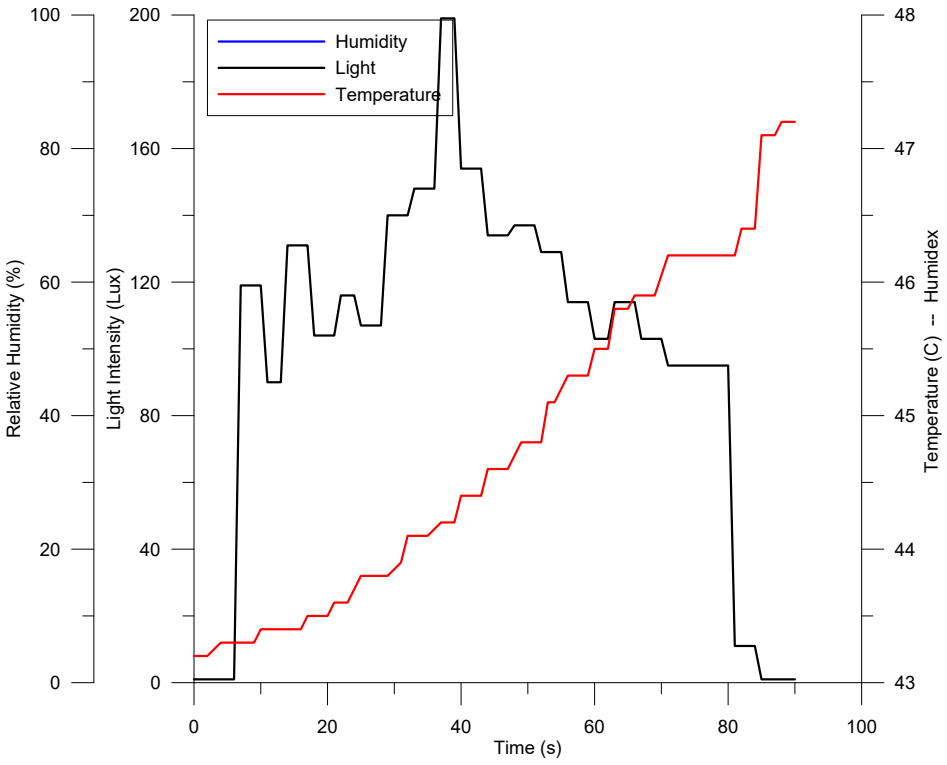


Figure C.344: Test 75 THLP 02

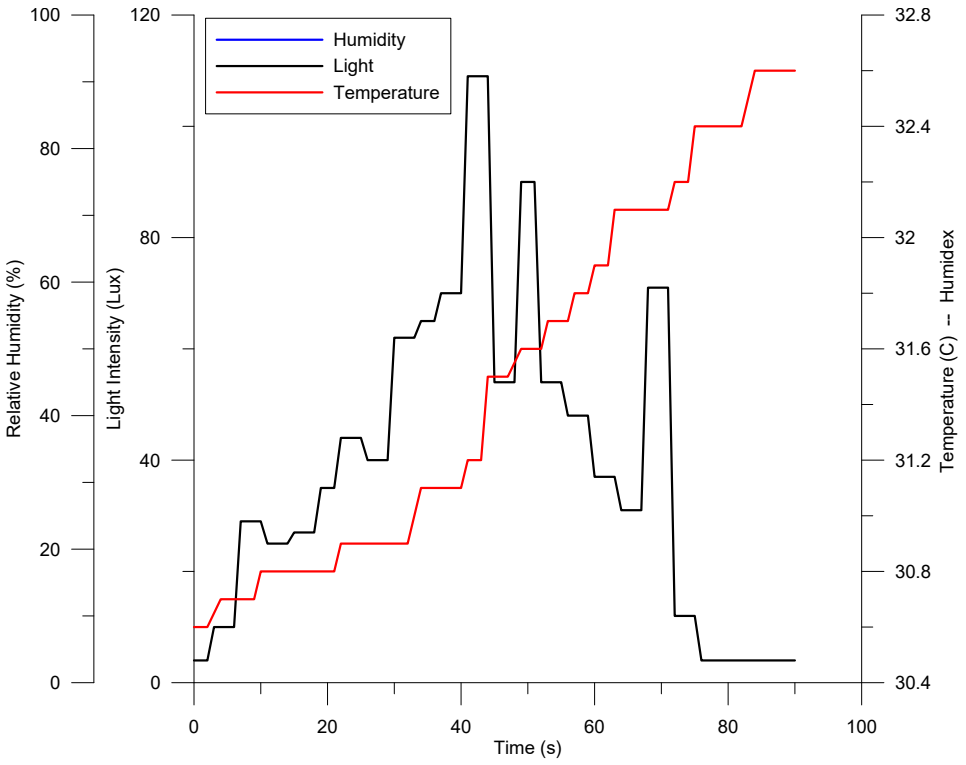


Figure C.345: Test 75 THLP 03

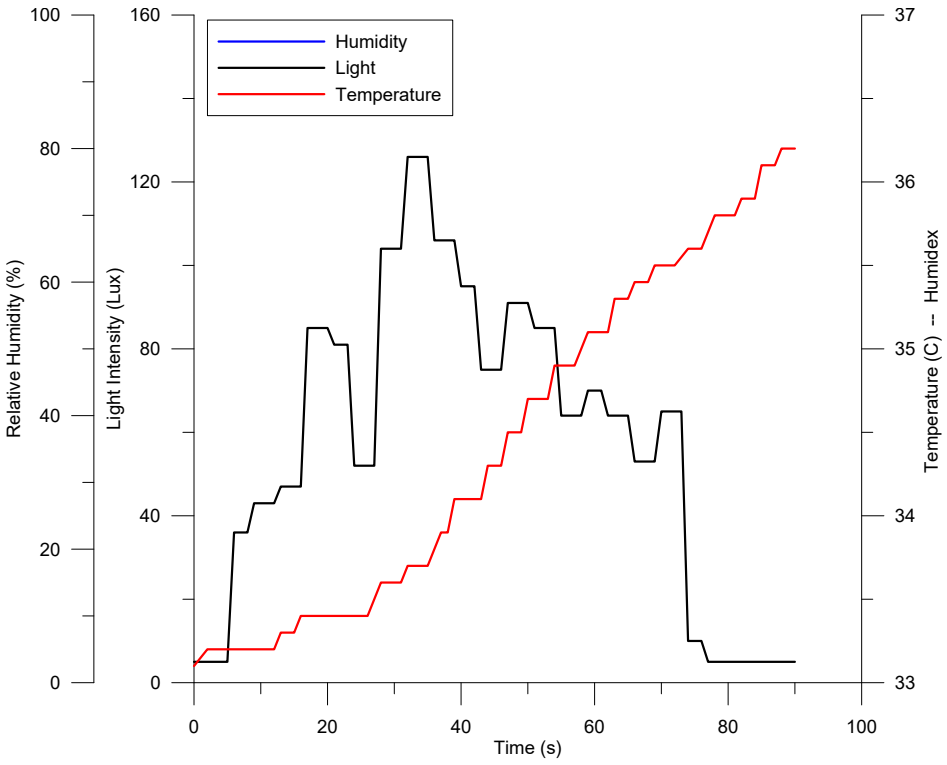


Figure C.346: Test 75 THLP 04

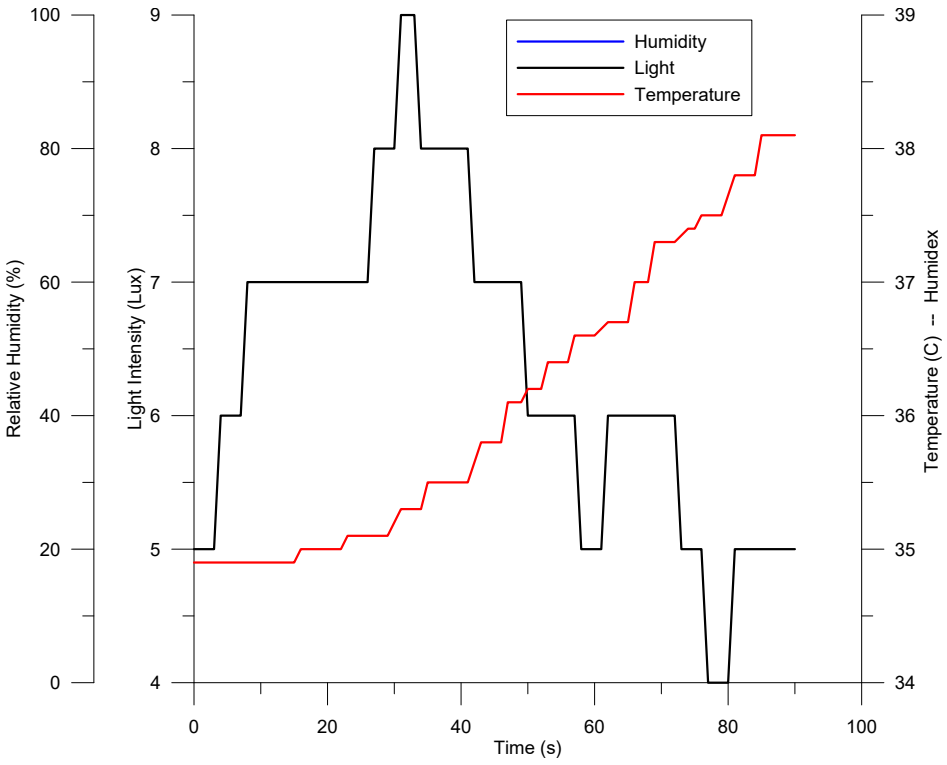


Figure C.347: Test 75 THLP 05

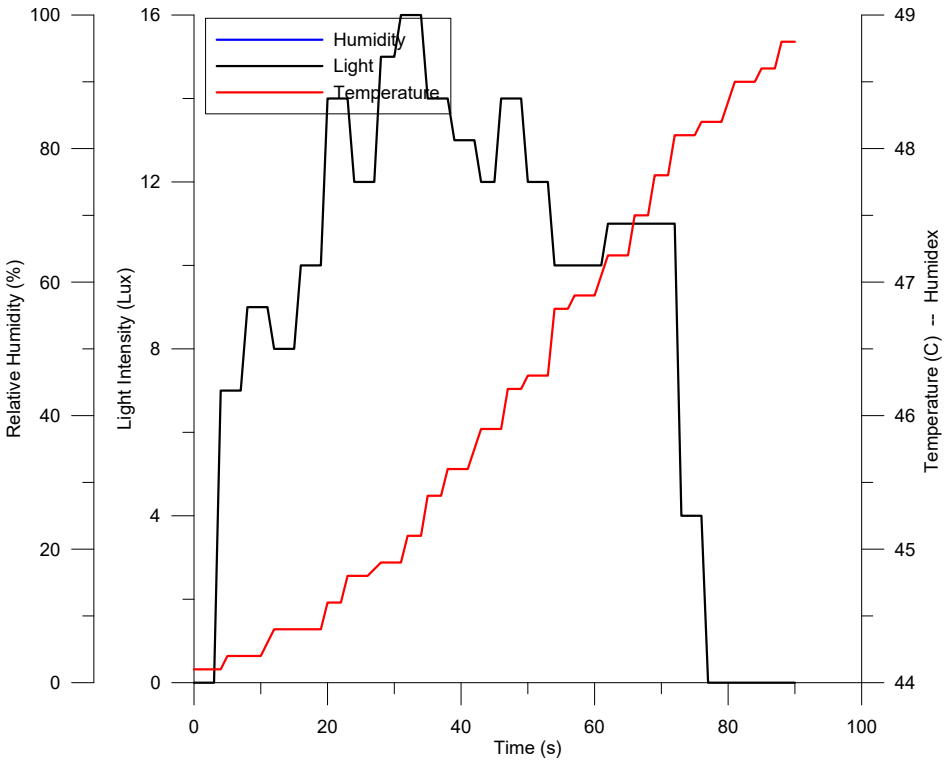


Figure C.348: Test 75 THLP 08

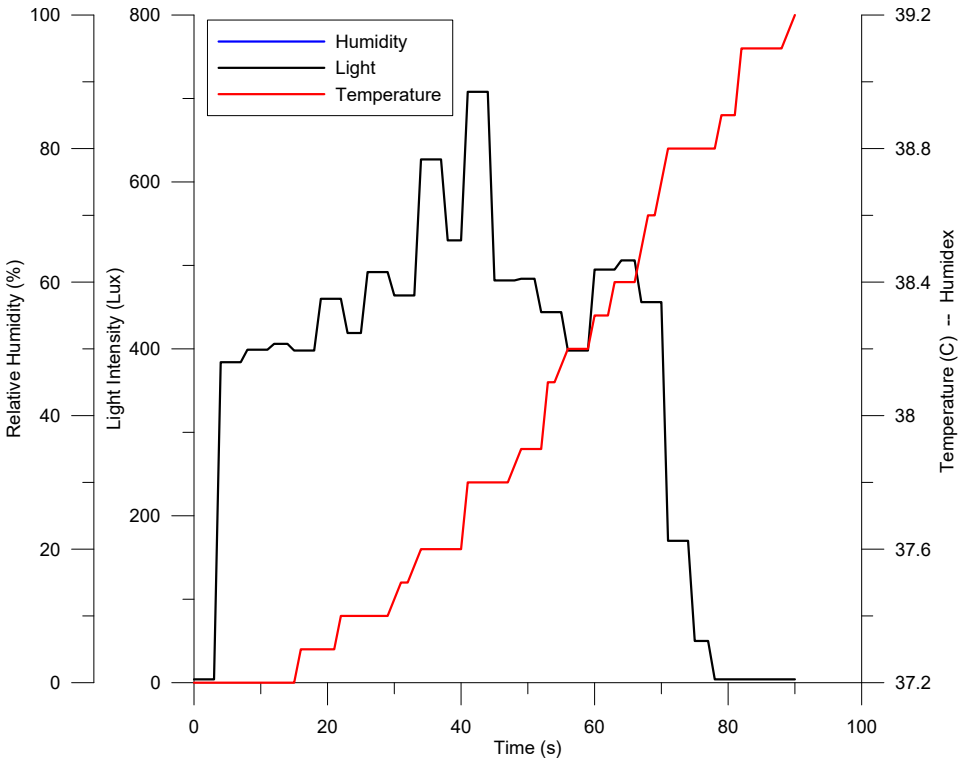


Figure C.349: Test 75 THLP 09

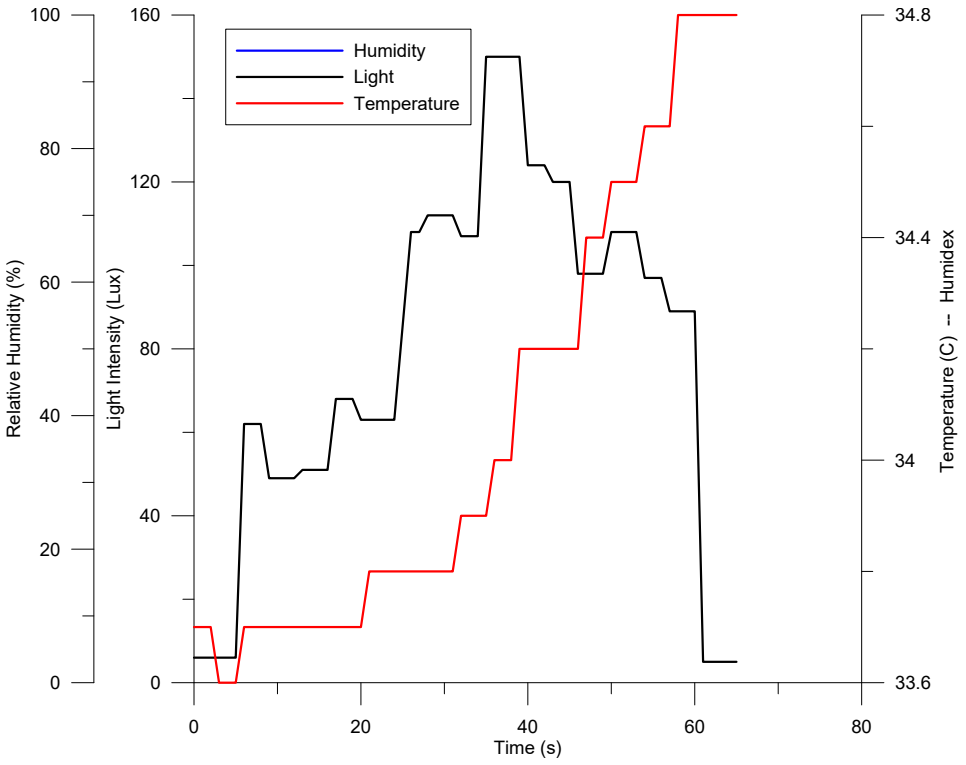


Figure C.350: Test 76 THLP 01

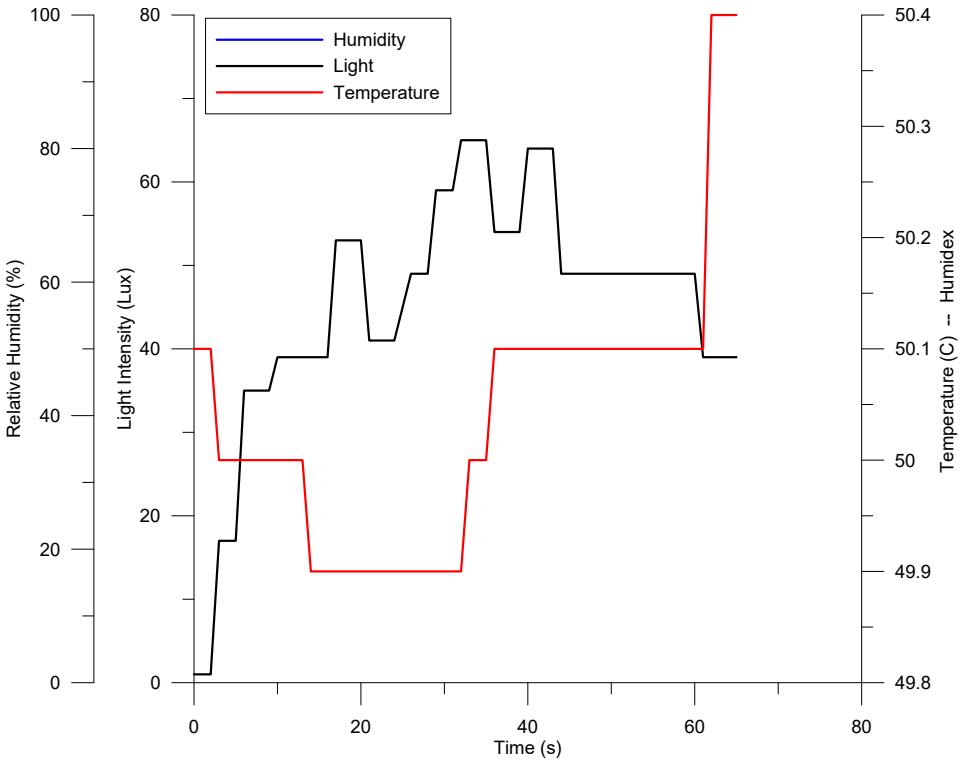


Figure C.351: Test 76 THLP 02

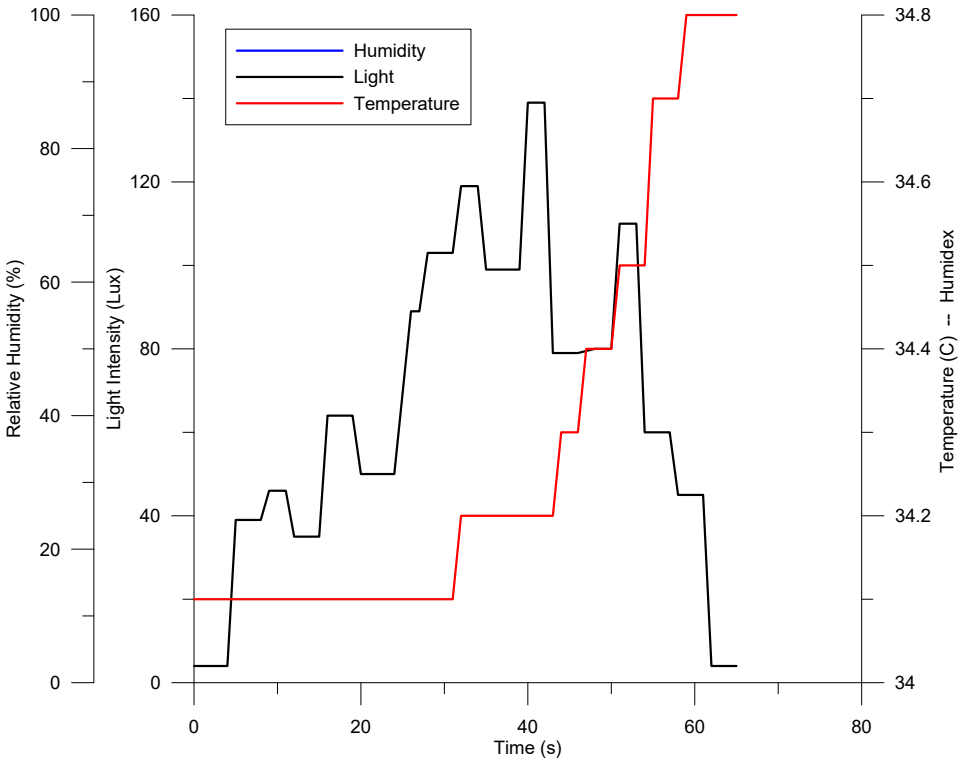


Figure C.352: Test 76 THLP 03

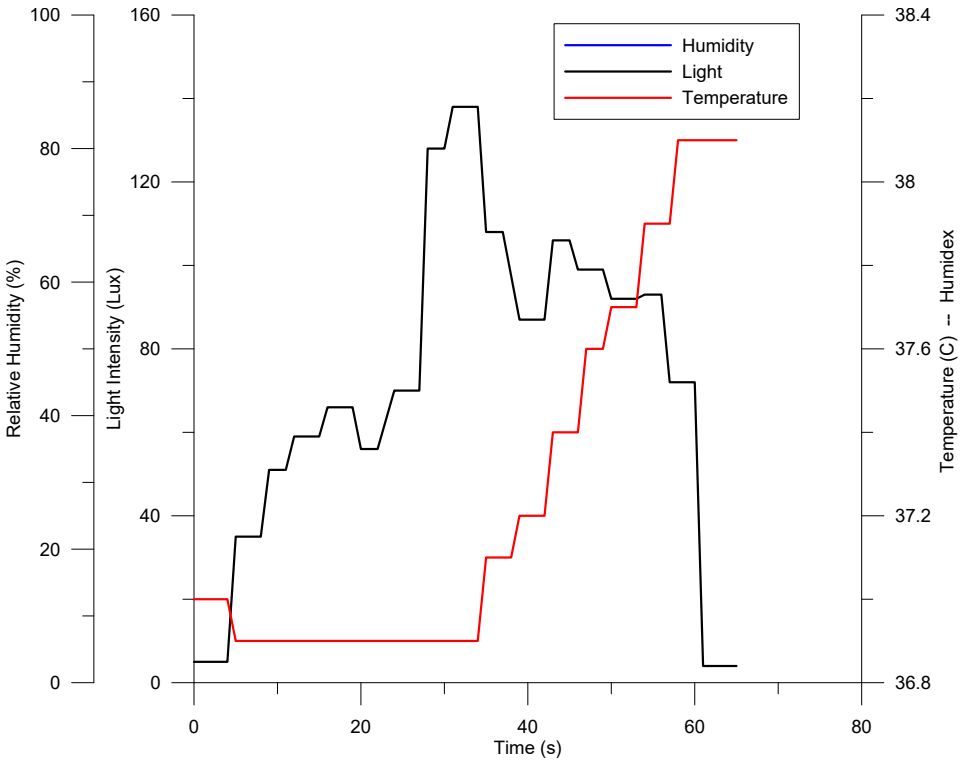


Figure C.353: Test 76 THLP 04

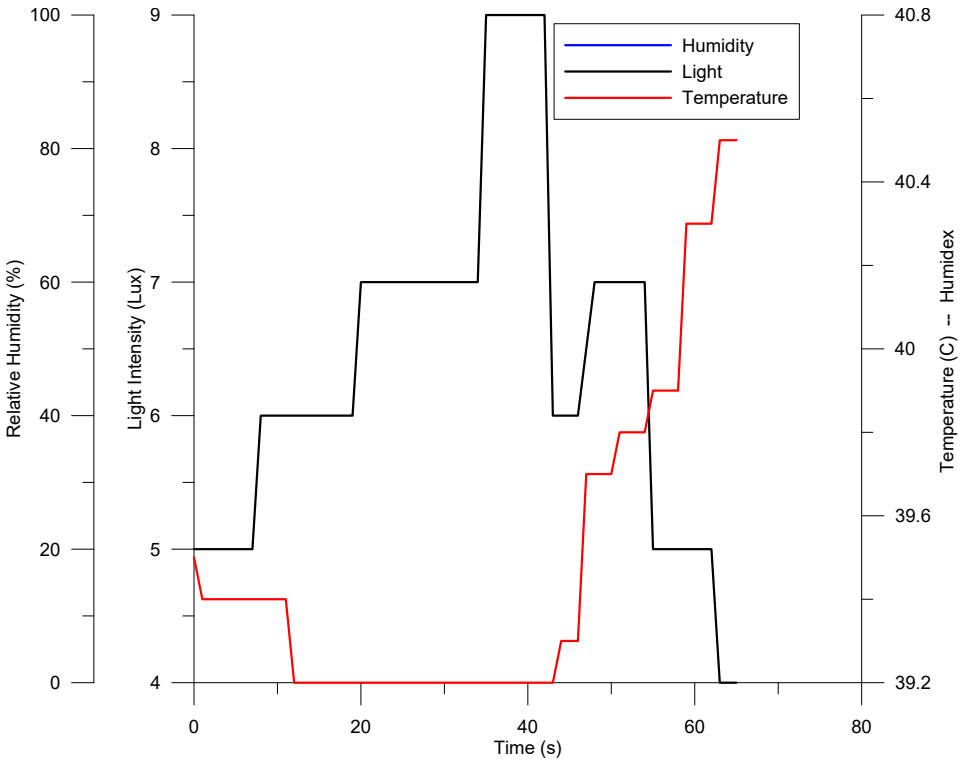


Figure C.354: Test 76 THLP 05

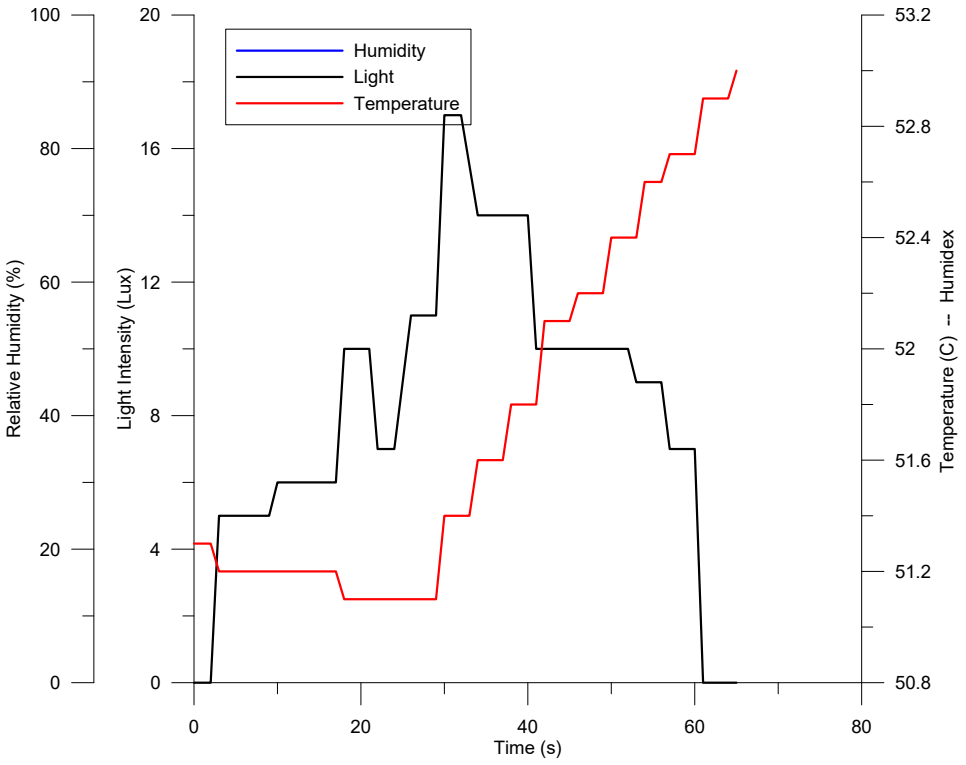


Figure C.355: Test 76 THLP 08

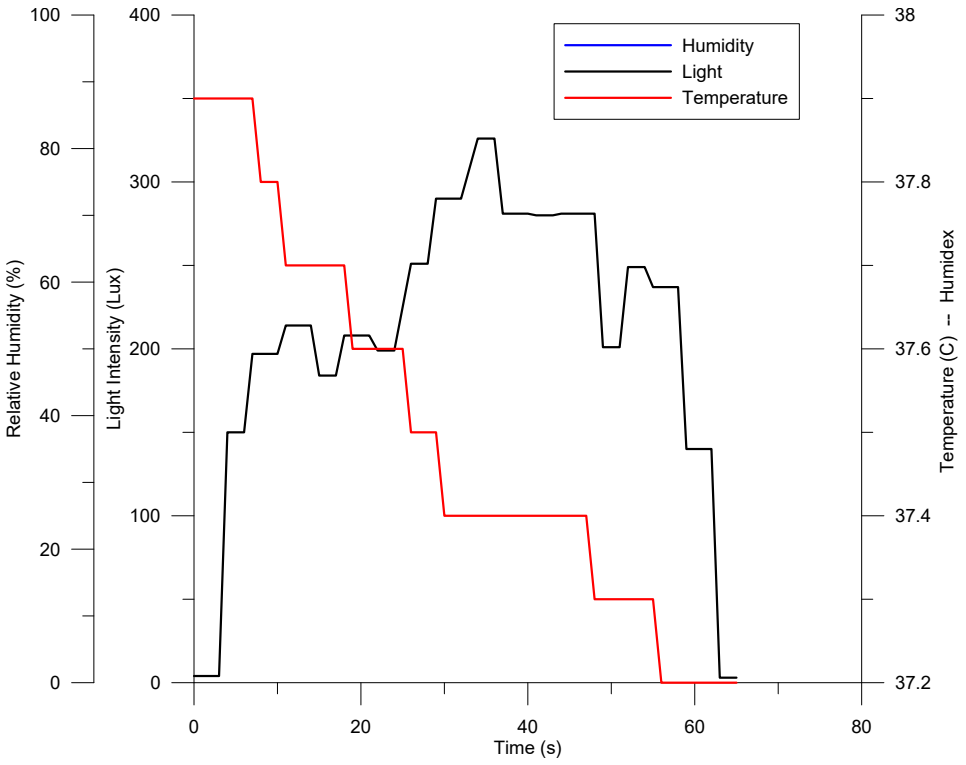


Figure C.356: Test 76 THLP 09

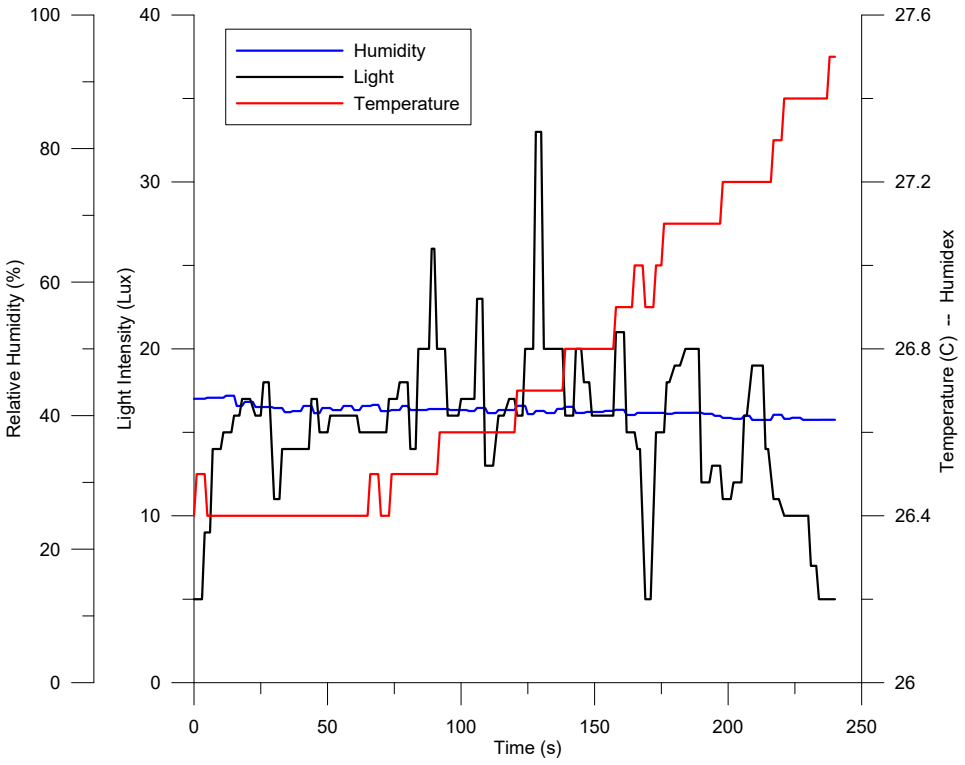


Figure C.357: Test 77 THLP 02

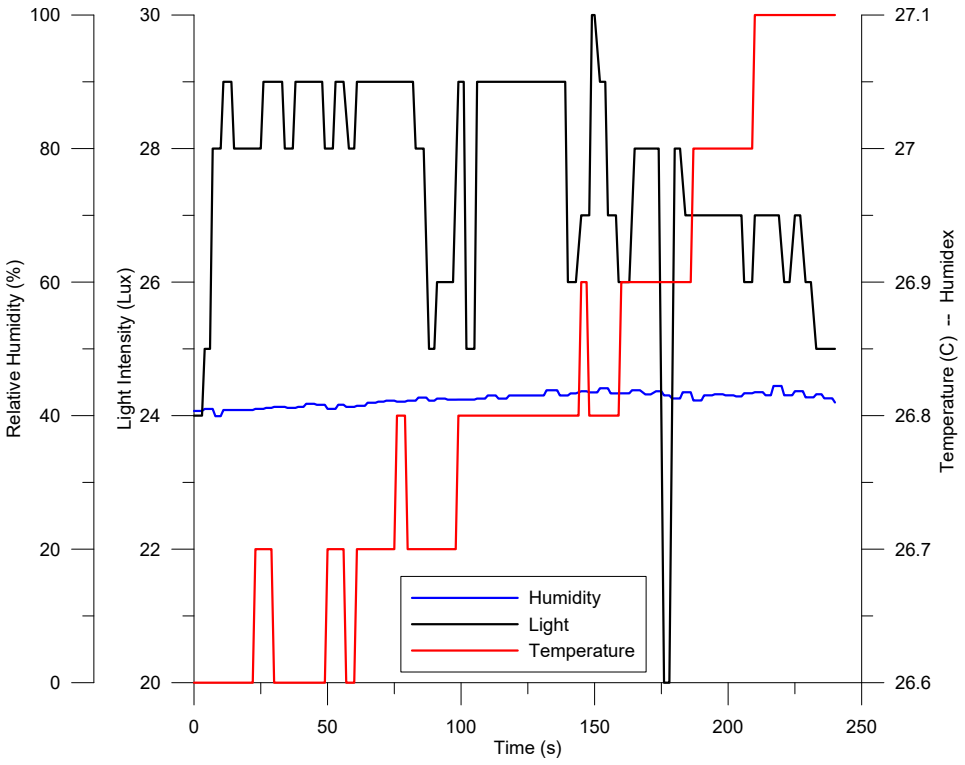


Figure C.358: Test 77 THLP 03

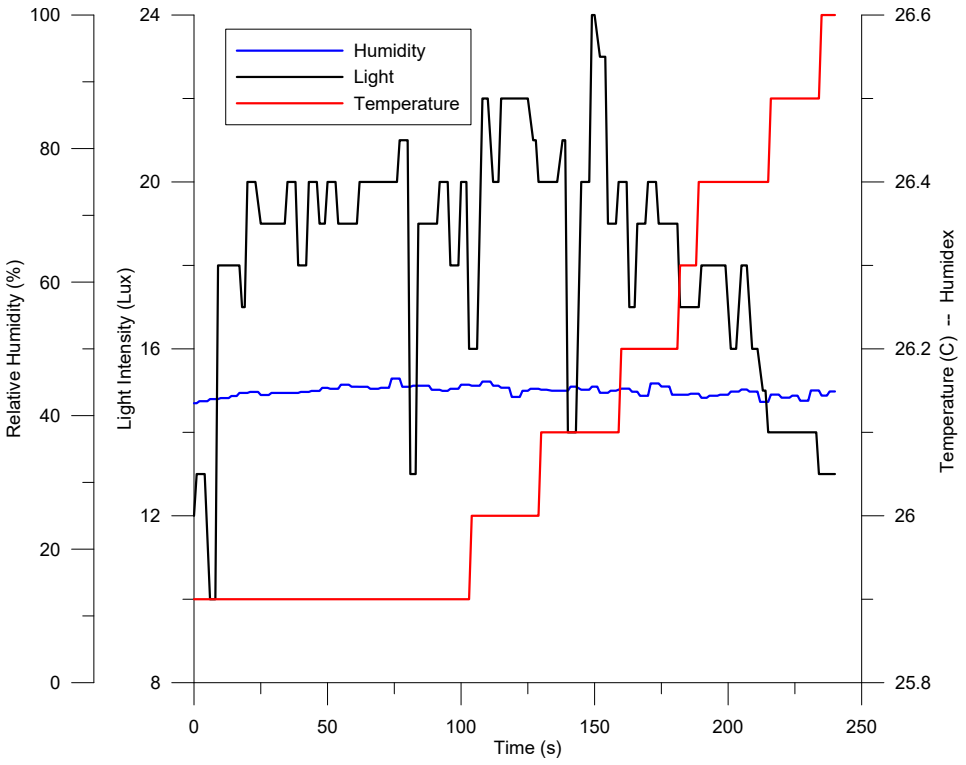


Figure C.359: Test 77 THLP 04

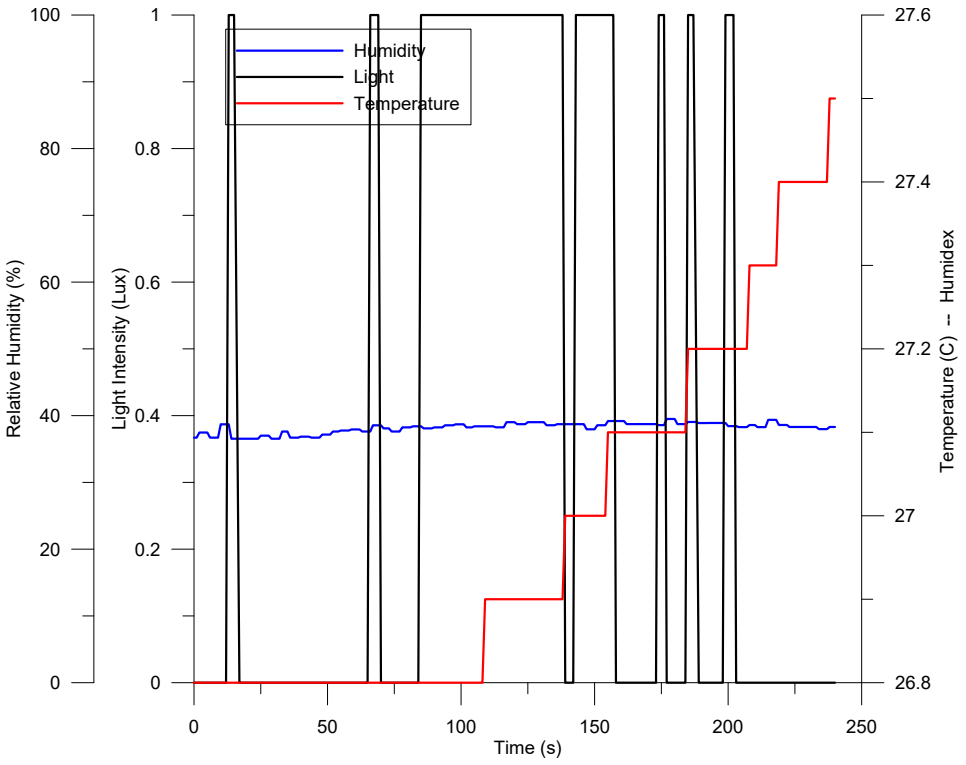


Figure C.360: Test 77 THLP 05

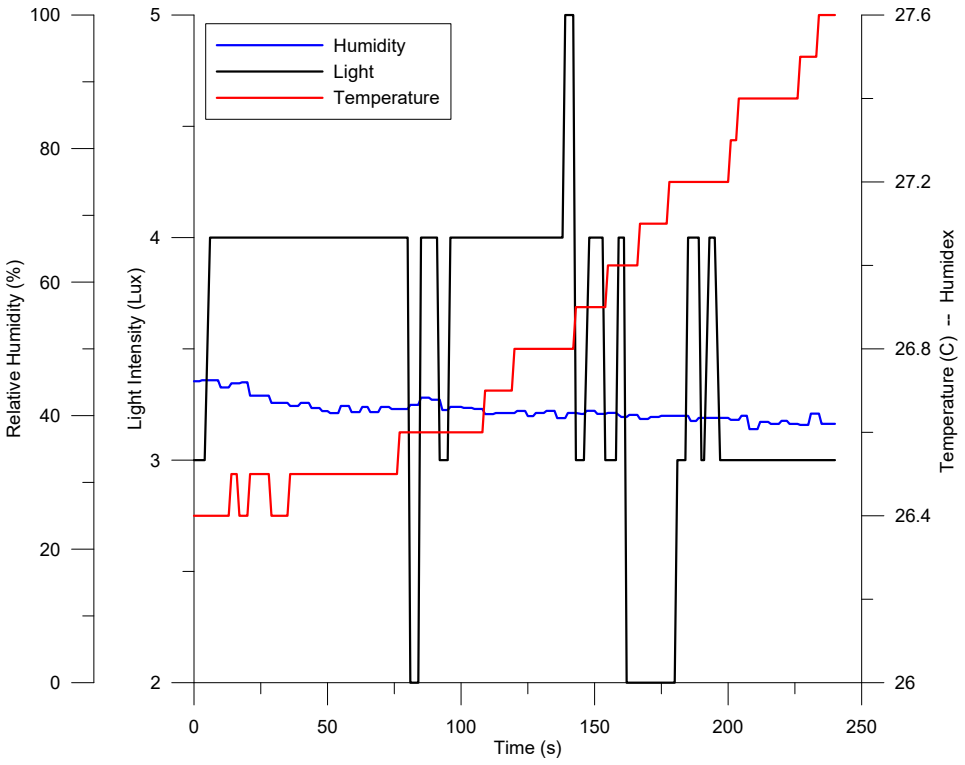


Figure C.361: Test 77 THLP 08

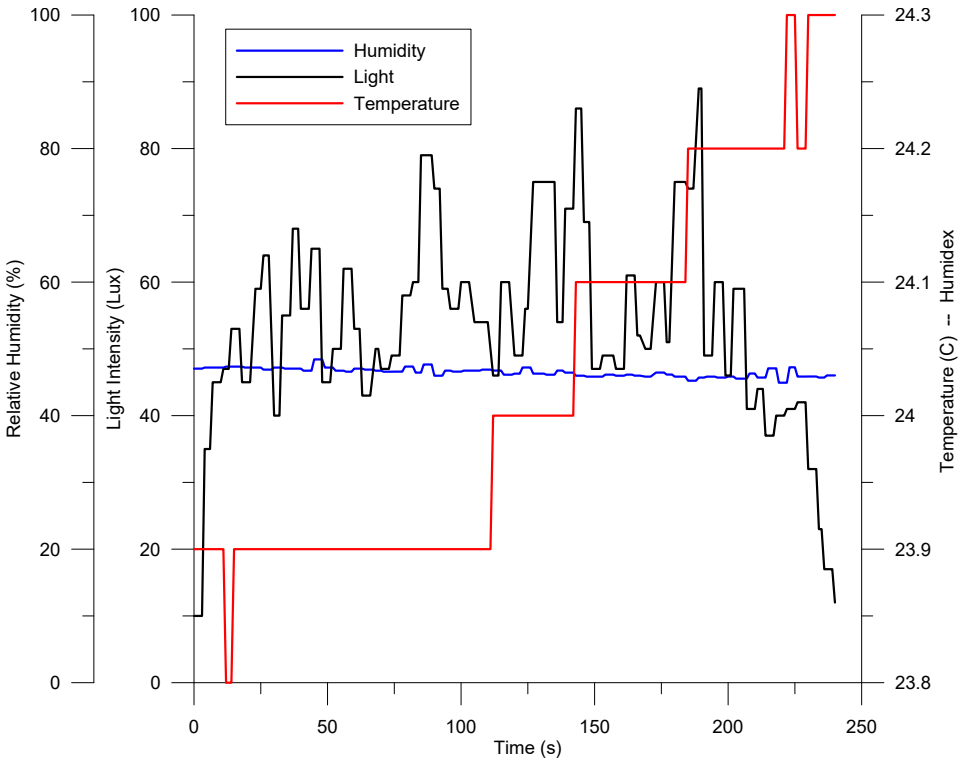


Figure C.362: Test 77 THLP 09

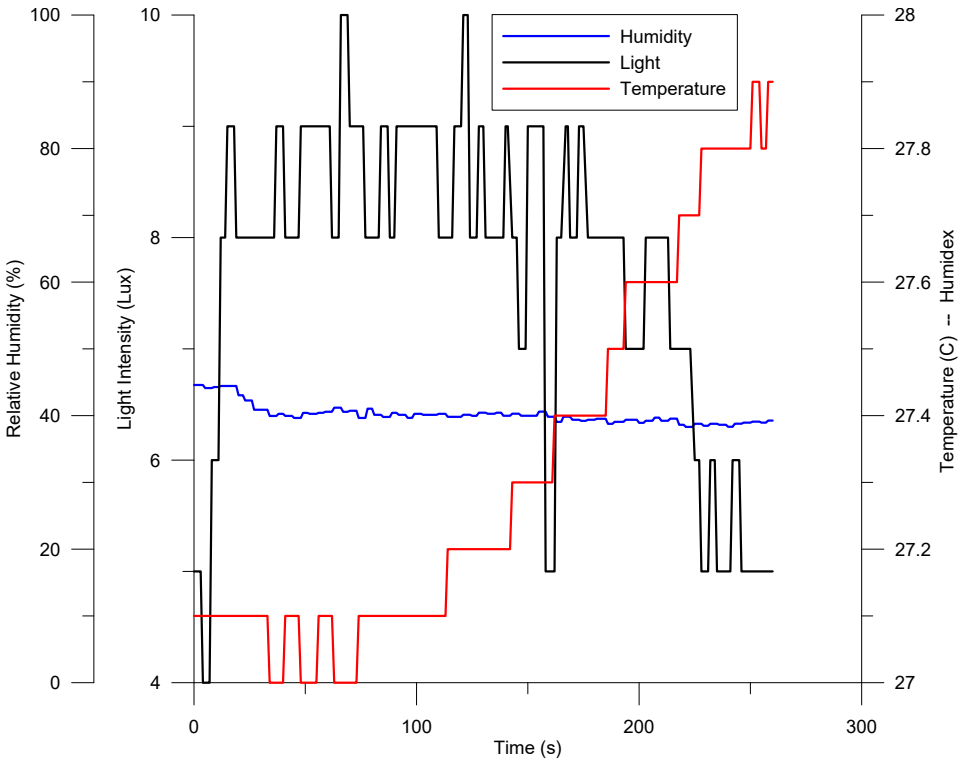


Figure C.363: Test 78 THLP 02

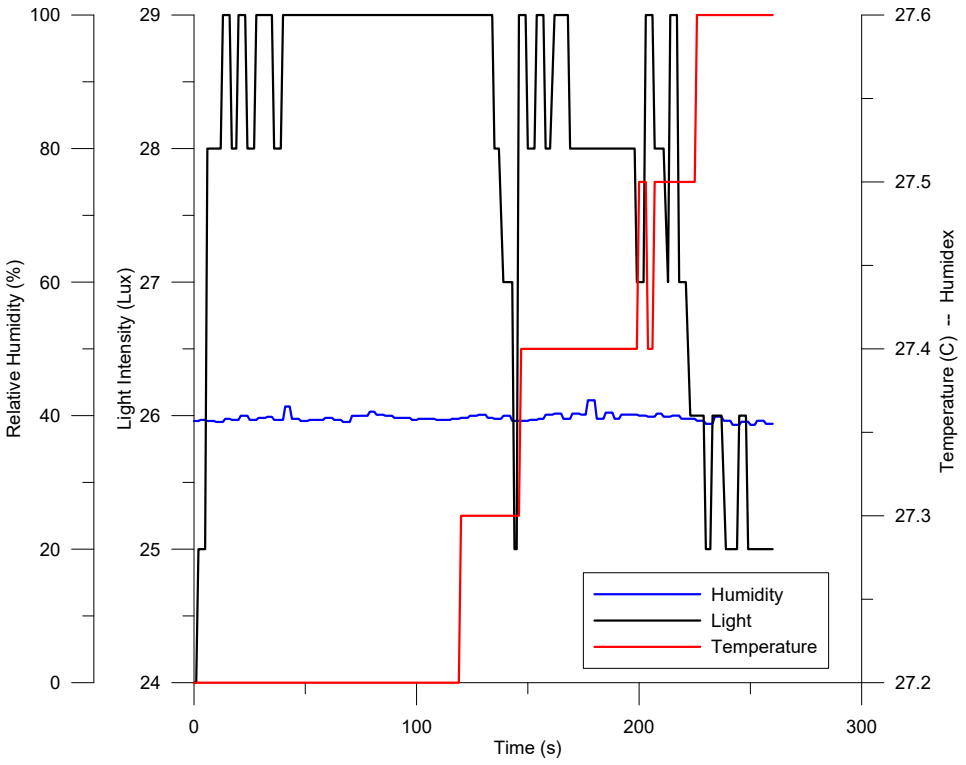


Figure C.364: Test 78 THLP 03

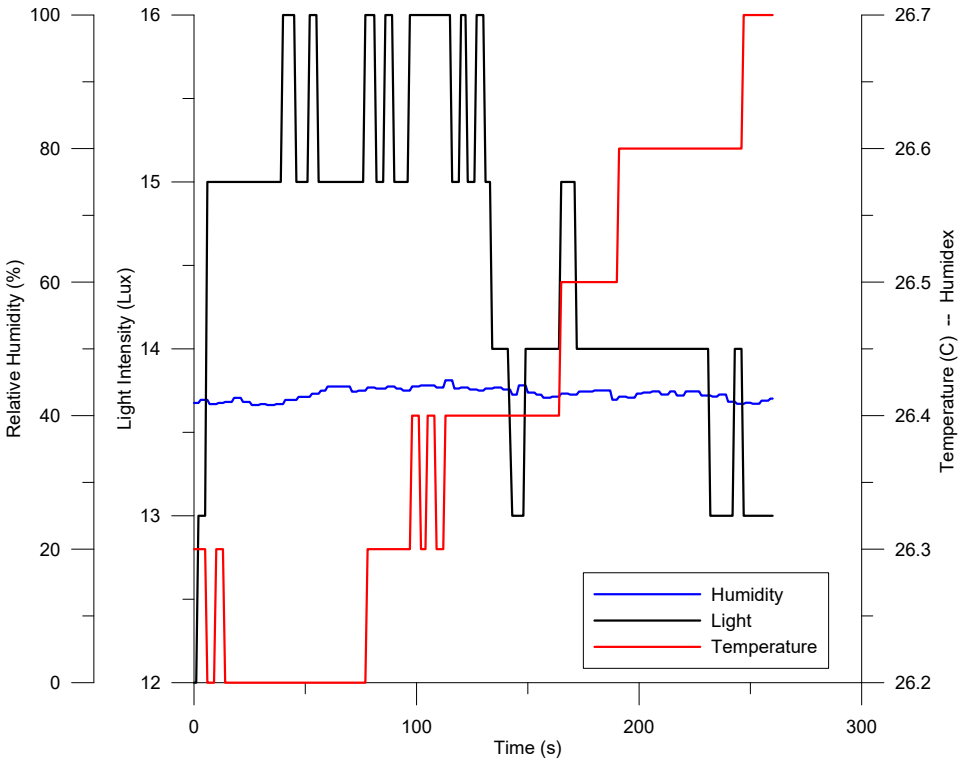


Figure C.365: Test 78 THLP 04

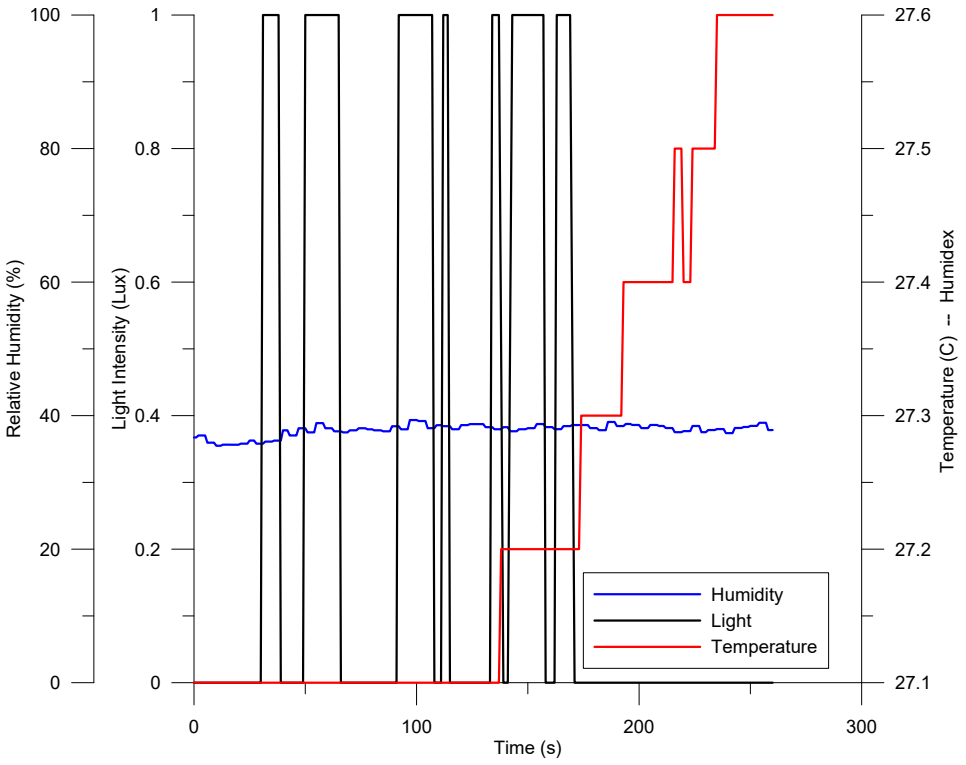


Figure C.366: Test 78 THLP 05

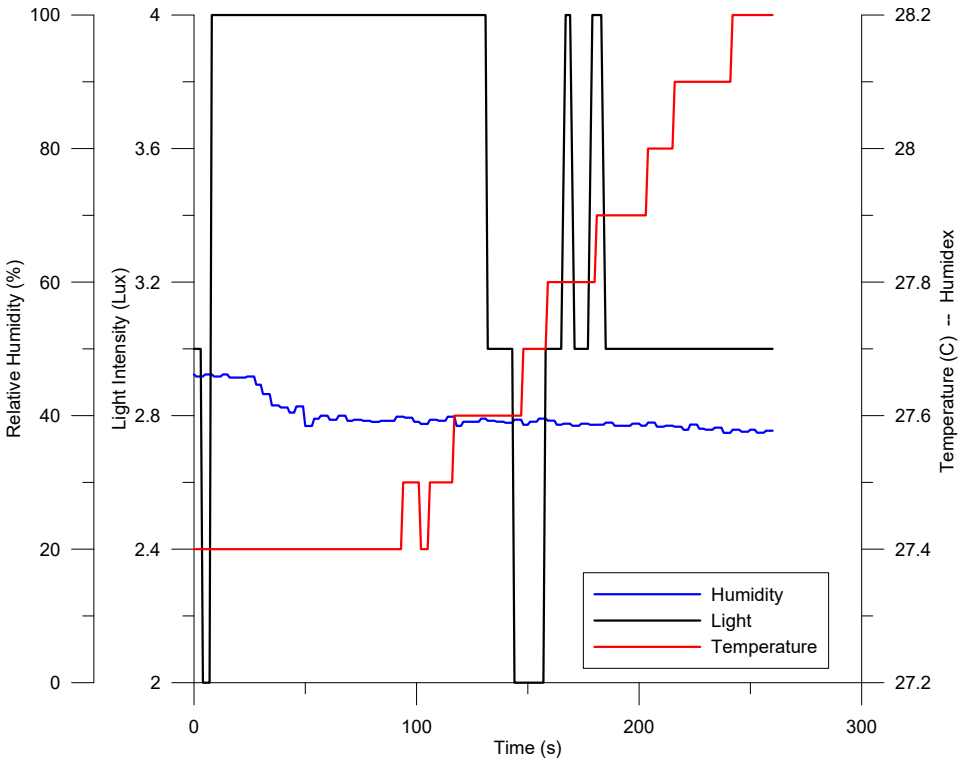


Figure C.367: Test 78 THLP 08

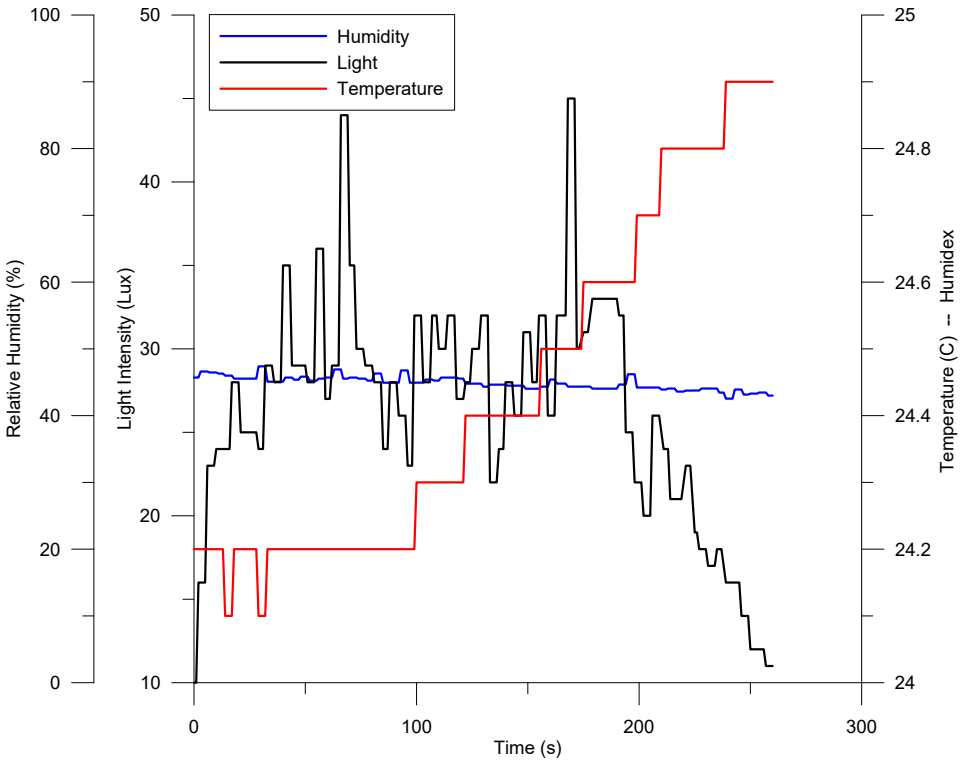


Figure C.368: Test 78 THLP 09

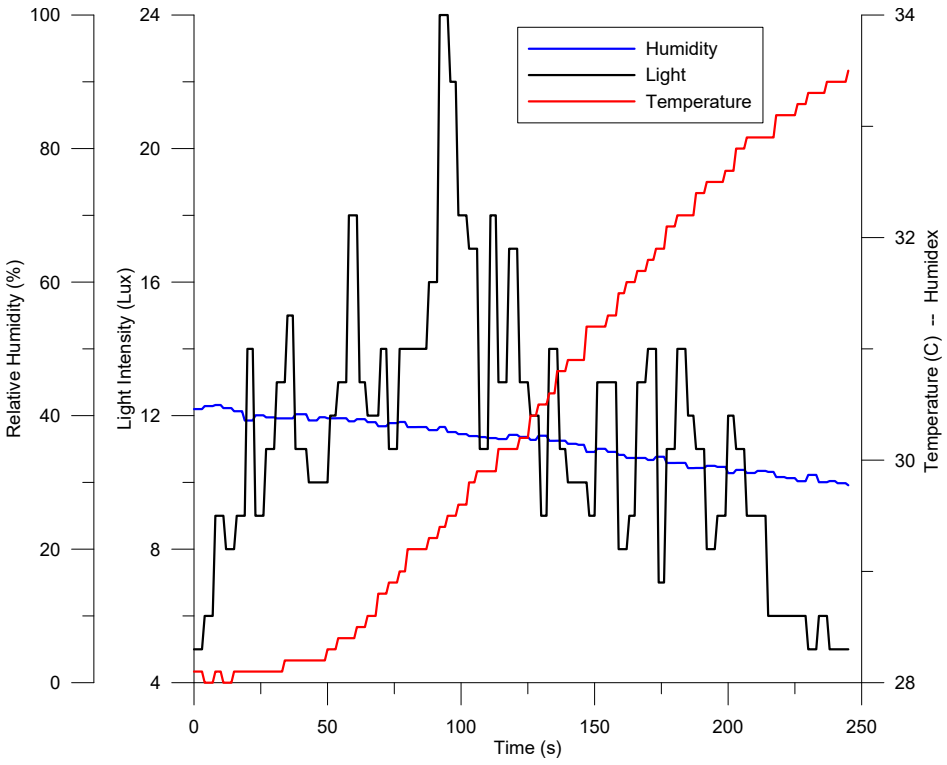


Figure C.369: Test 79 THLP 02

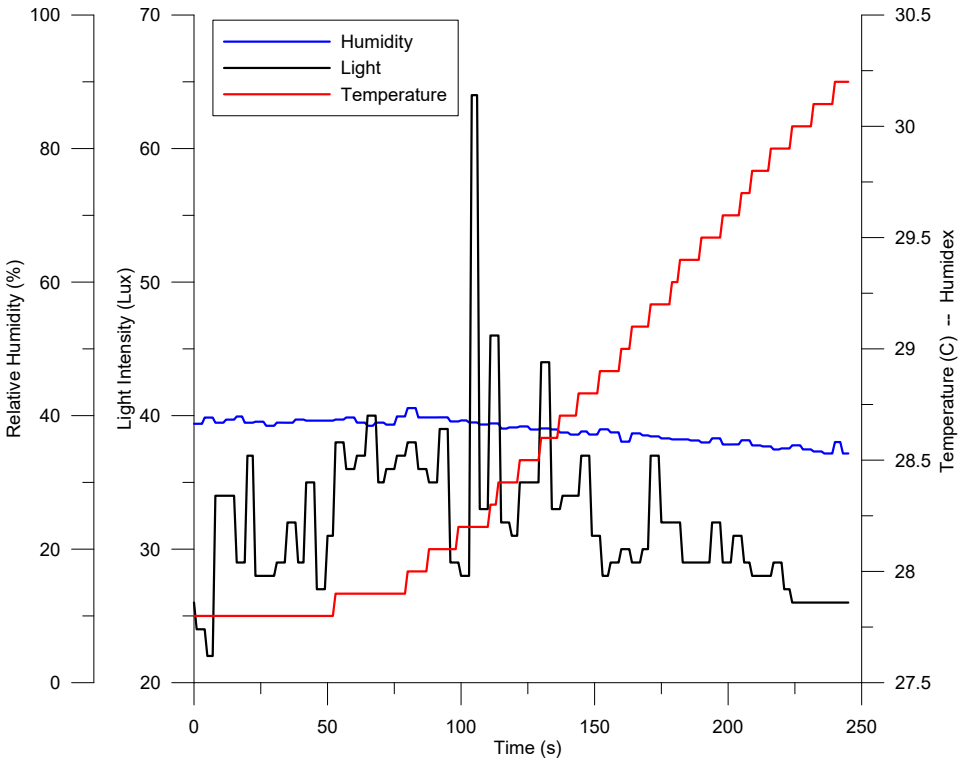


Figure C.370: Test 79 THLP 03

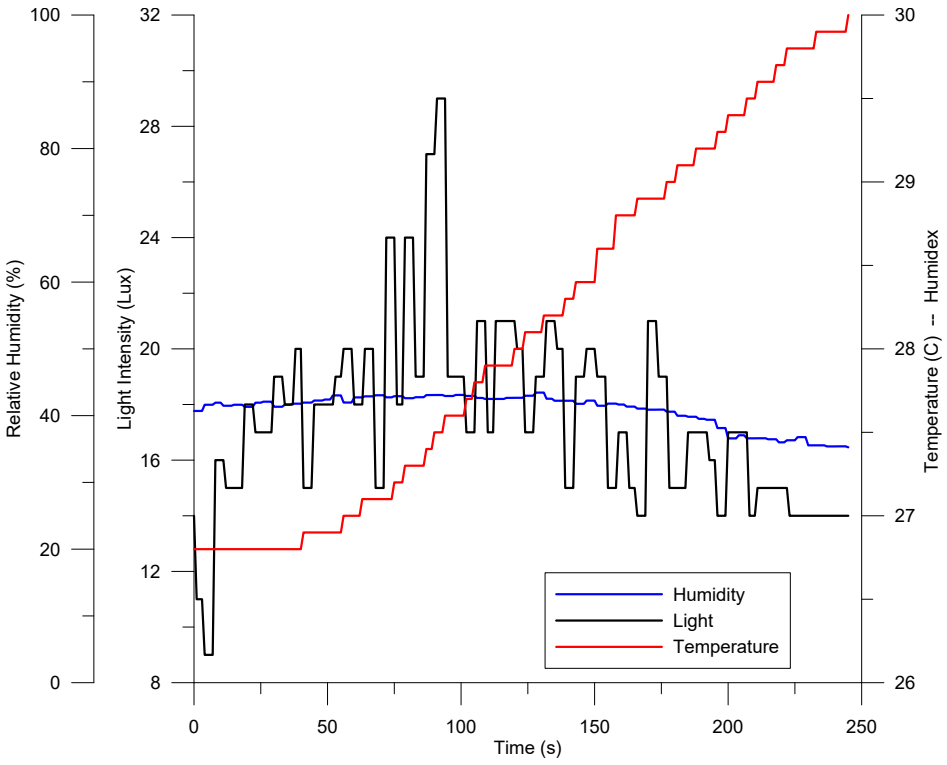


Figure C.371: Test 79 THLP 04

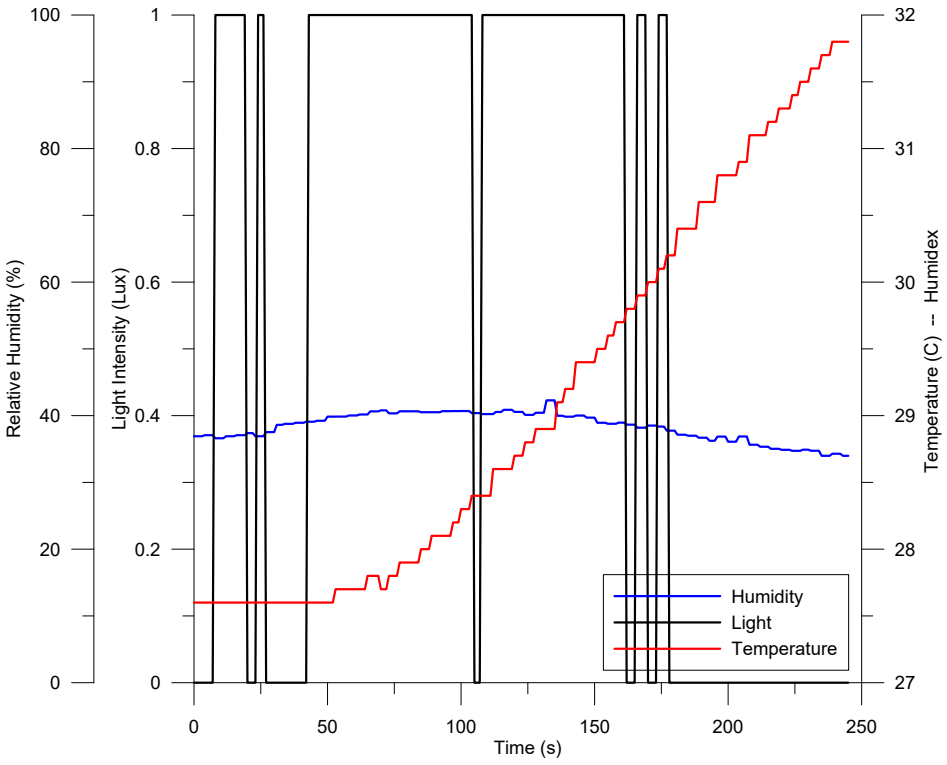


Figure C.372: Test 79 THLP 05

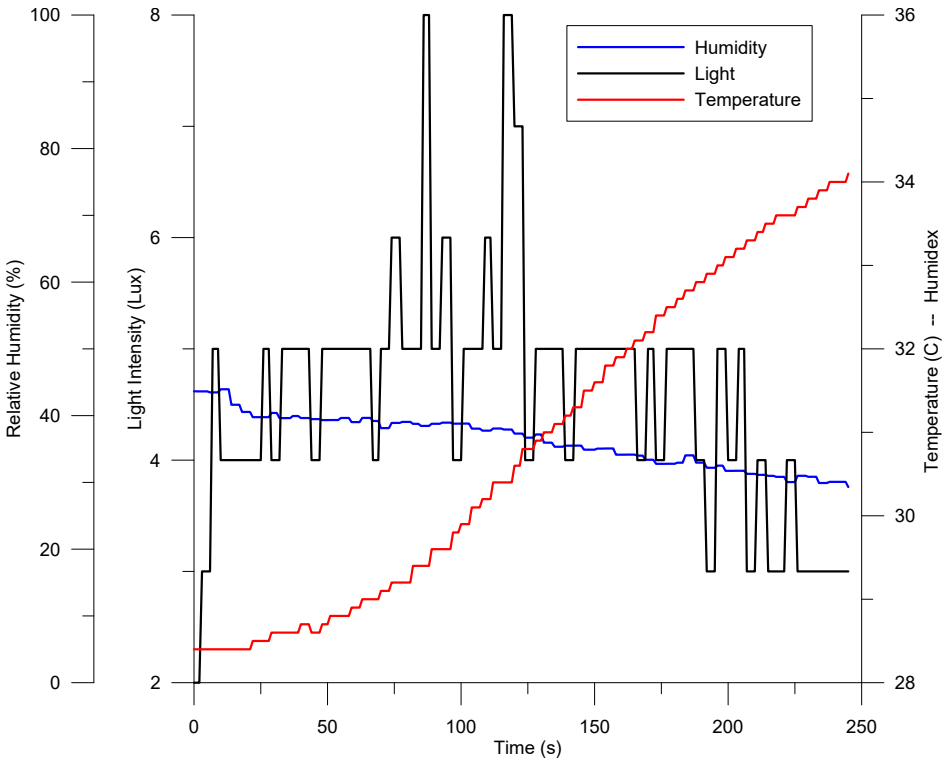


Figure C.373: Test 79 THLP 08

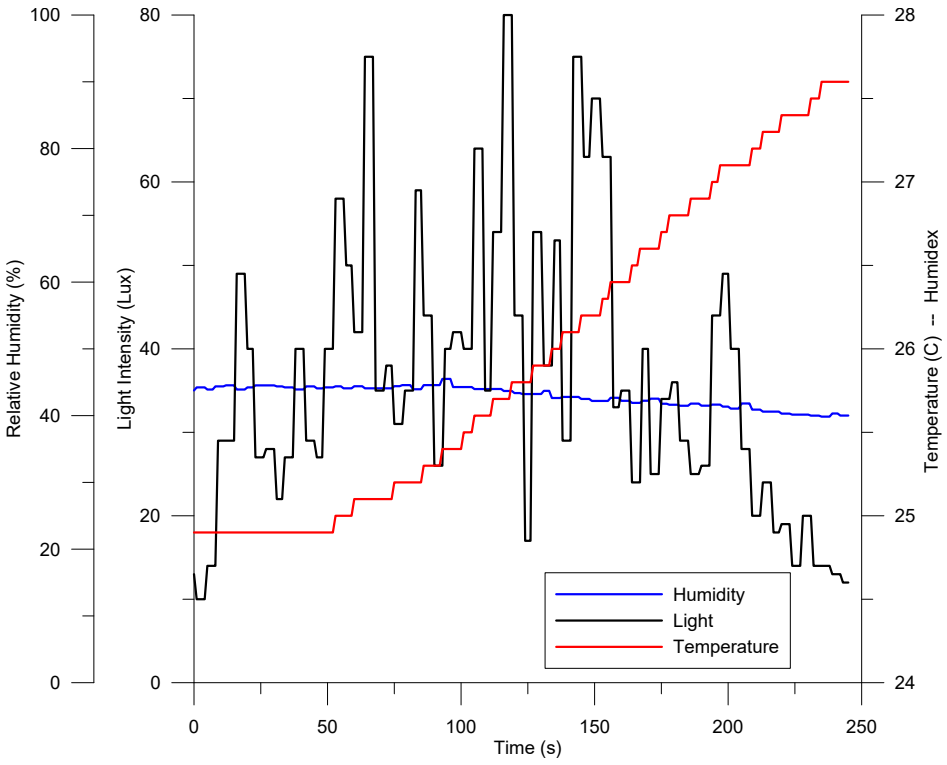


Figure C.374: Test 79 THLP 09

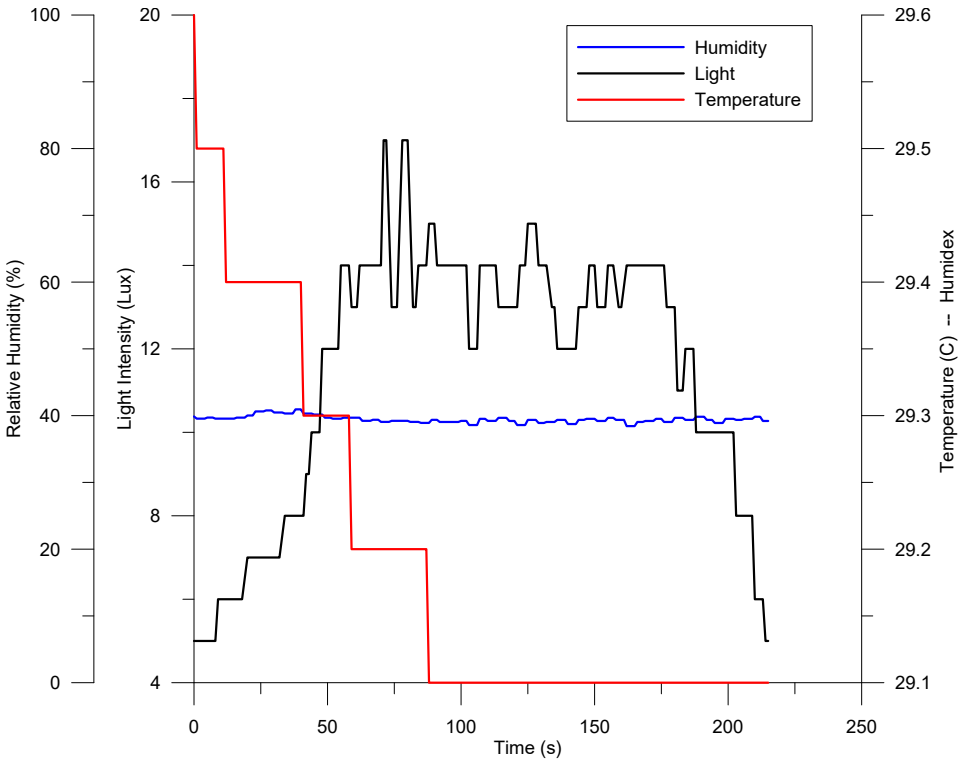


Figure C.375: Test 80 THLP 02

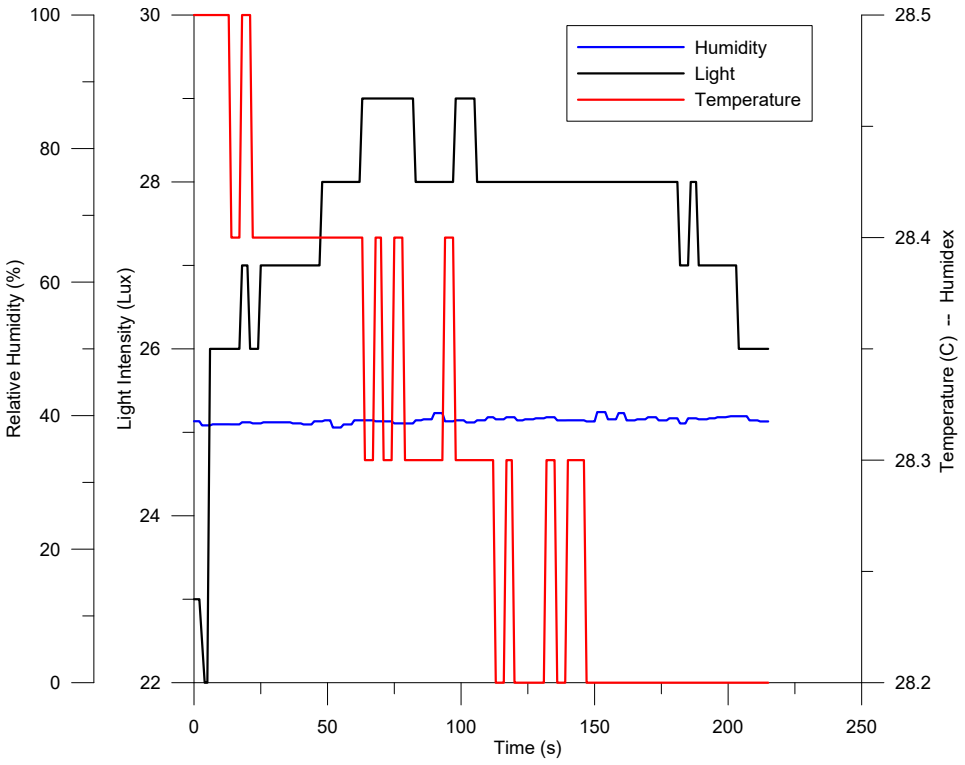


Figure C.376: Test 80 THLP 03

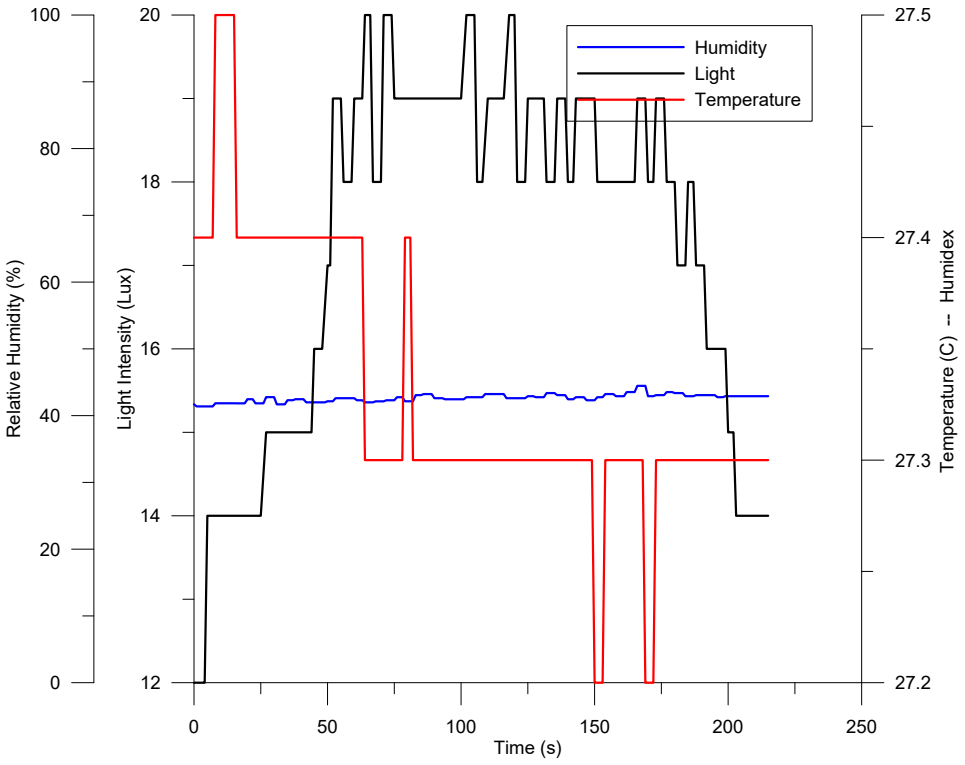


Figure C.377: Test 80 THLP 04

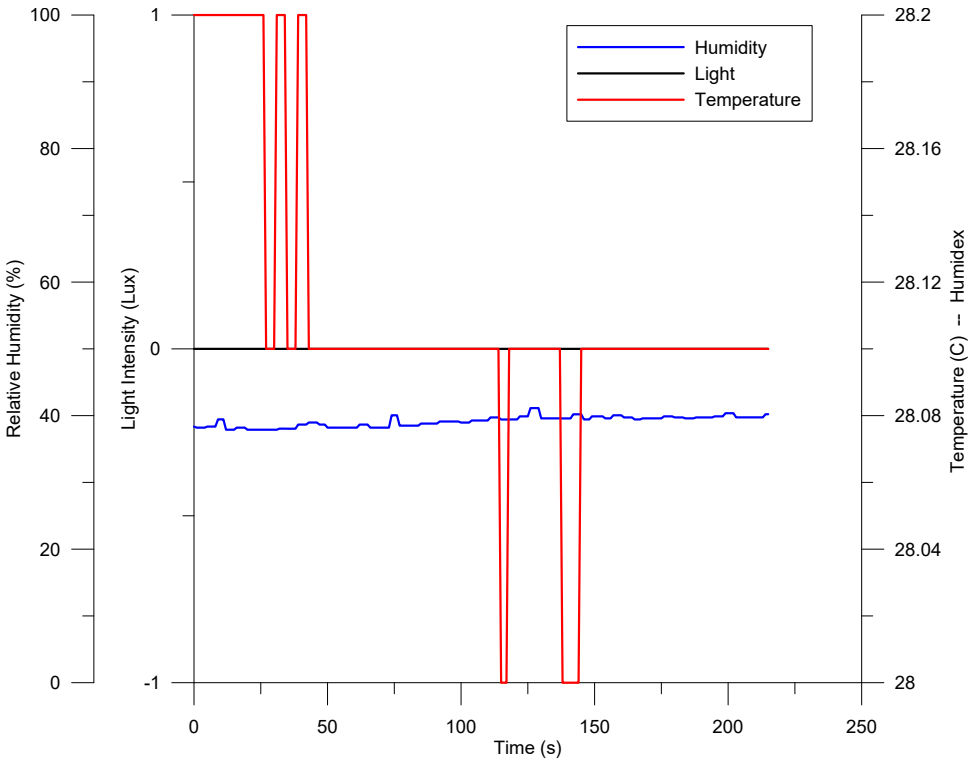


Figure C.378: Test 80 THLP 05

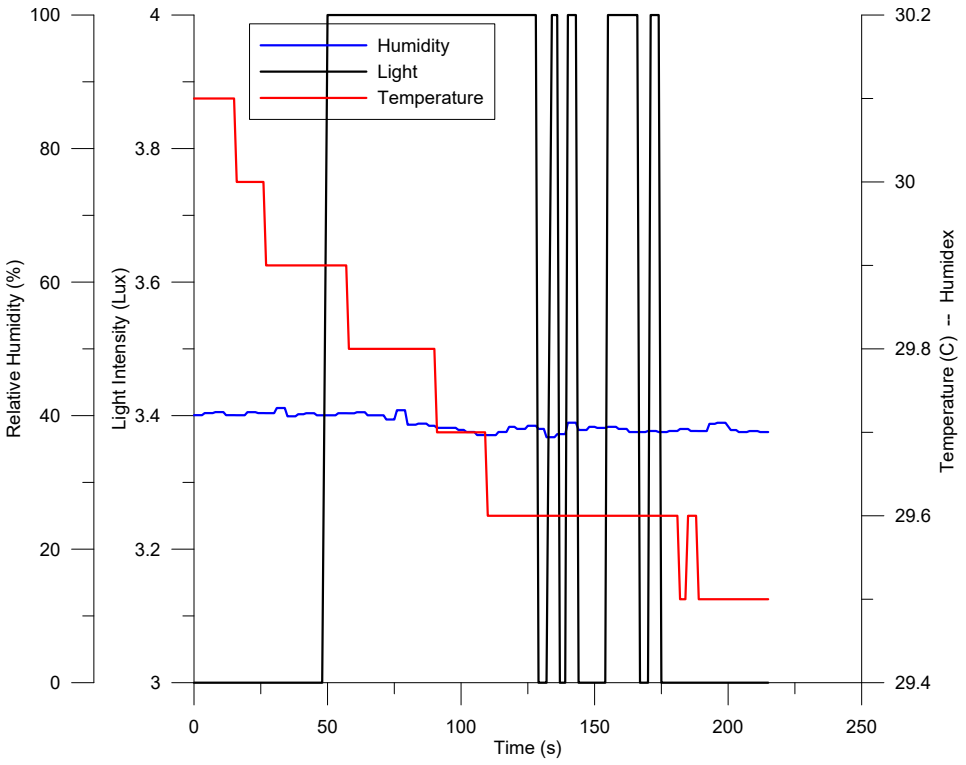


Figure C.379: Test 80 THLP 08

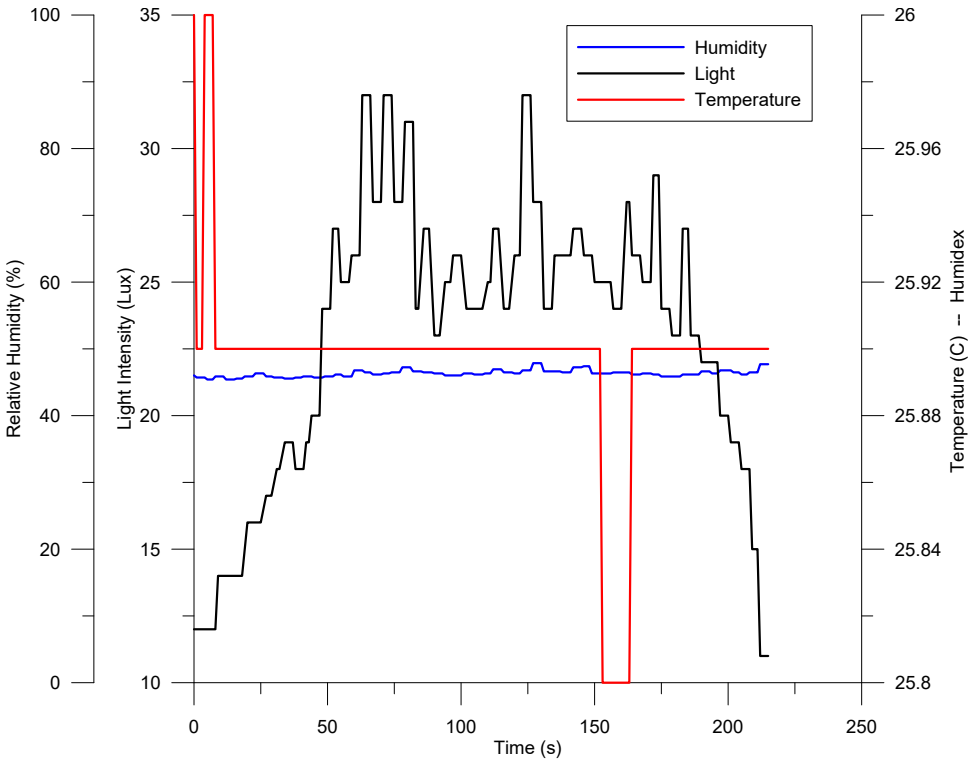


Figure C.380: Test 80 THLP 09

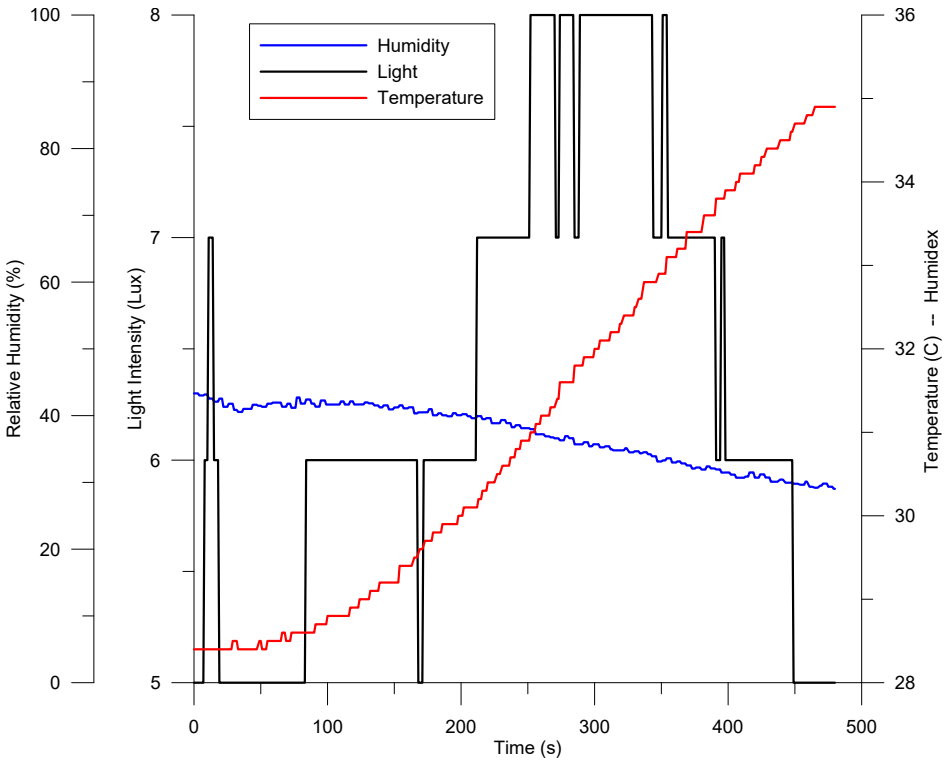


Figure C.381: Test 81 THLP 02

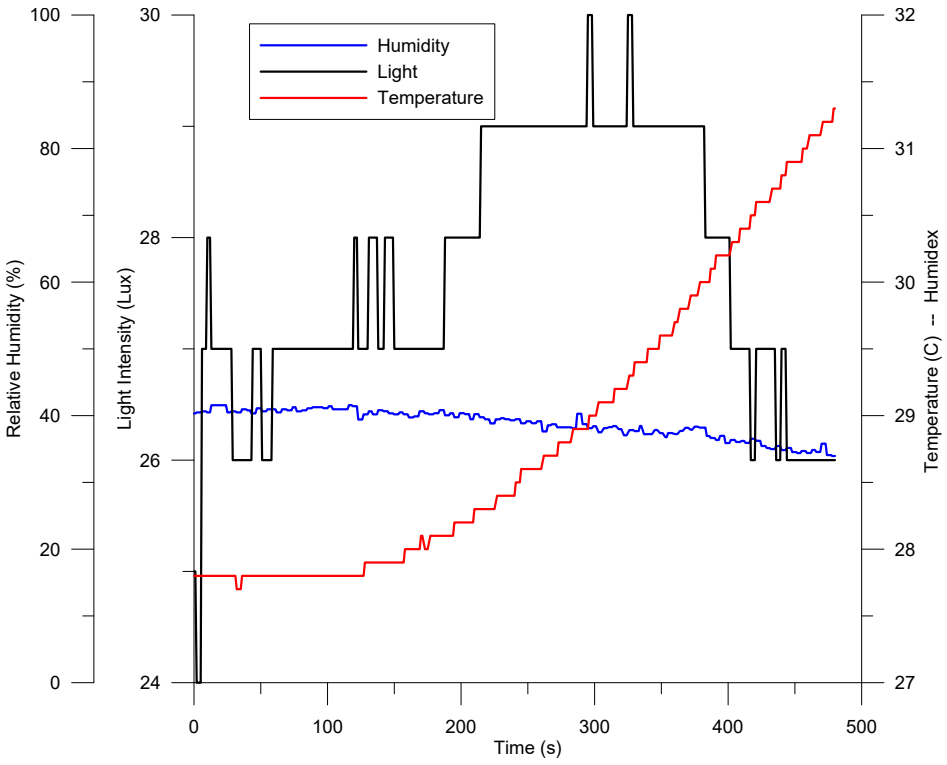


Figure C.382: Test 81 THLP 03

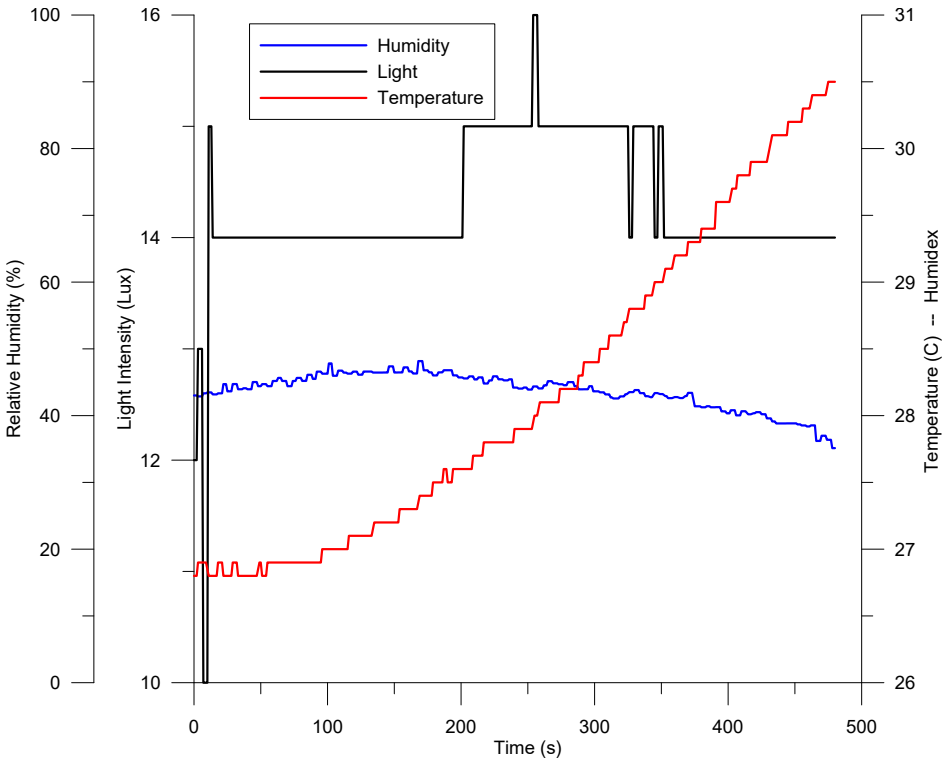


Figure C.383: Test 81 THLP 04

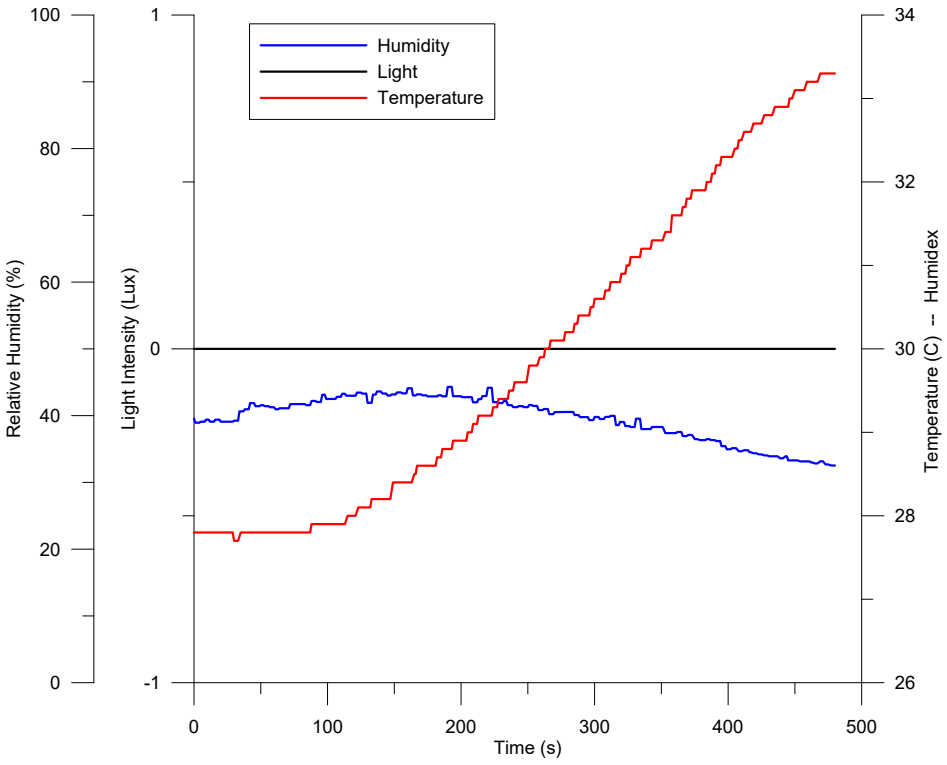


Figure C.384: Test 81 THLP 05

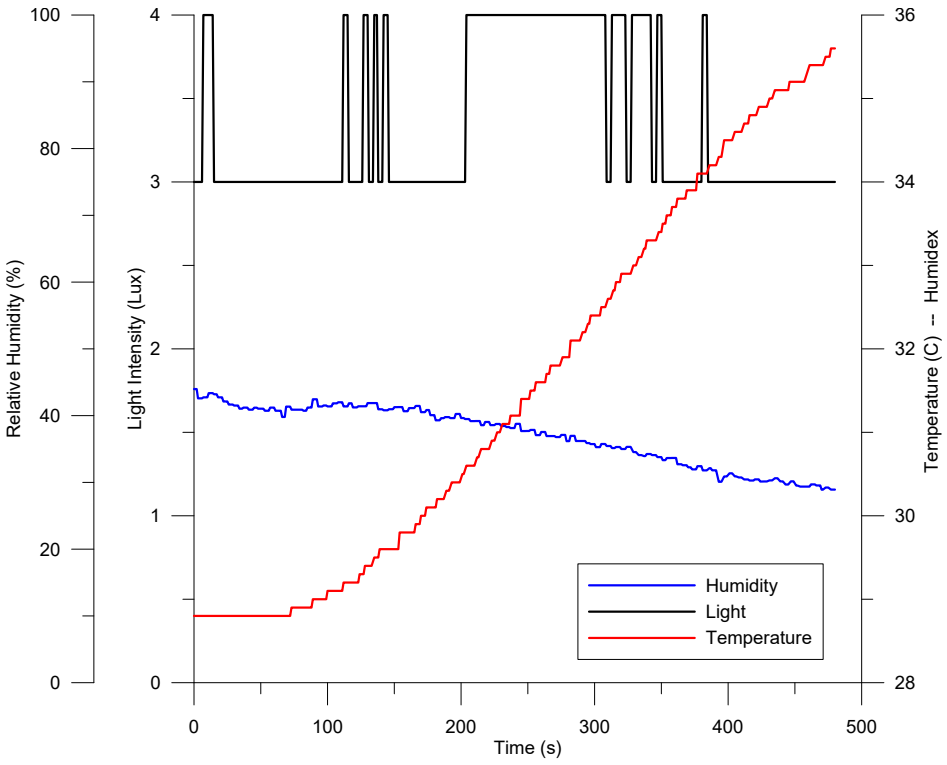


Figure C.385: Test 81 THLP 08

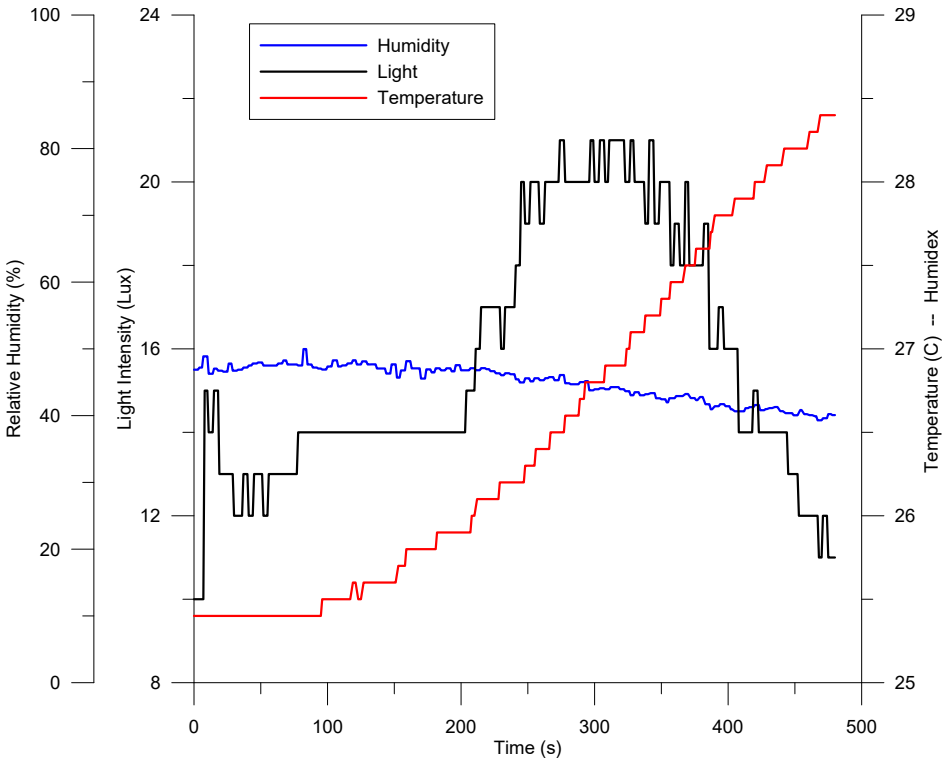


Figure C.386: Test 81 THLP 09

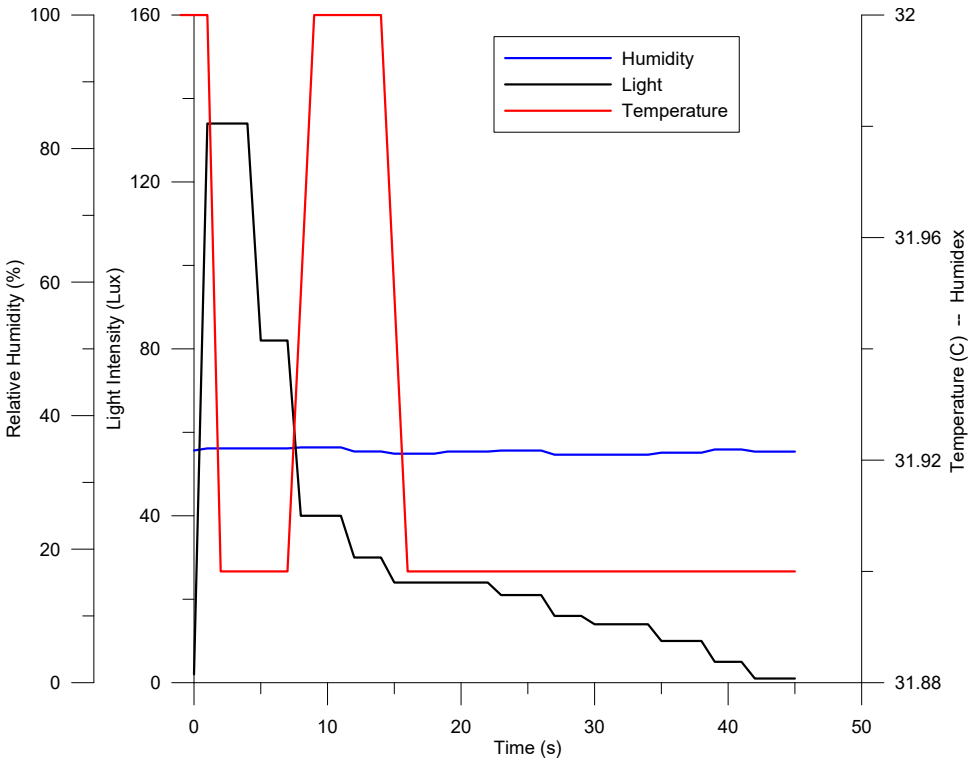


Figure C.387: Test 82 THLP 02

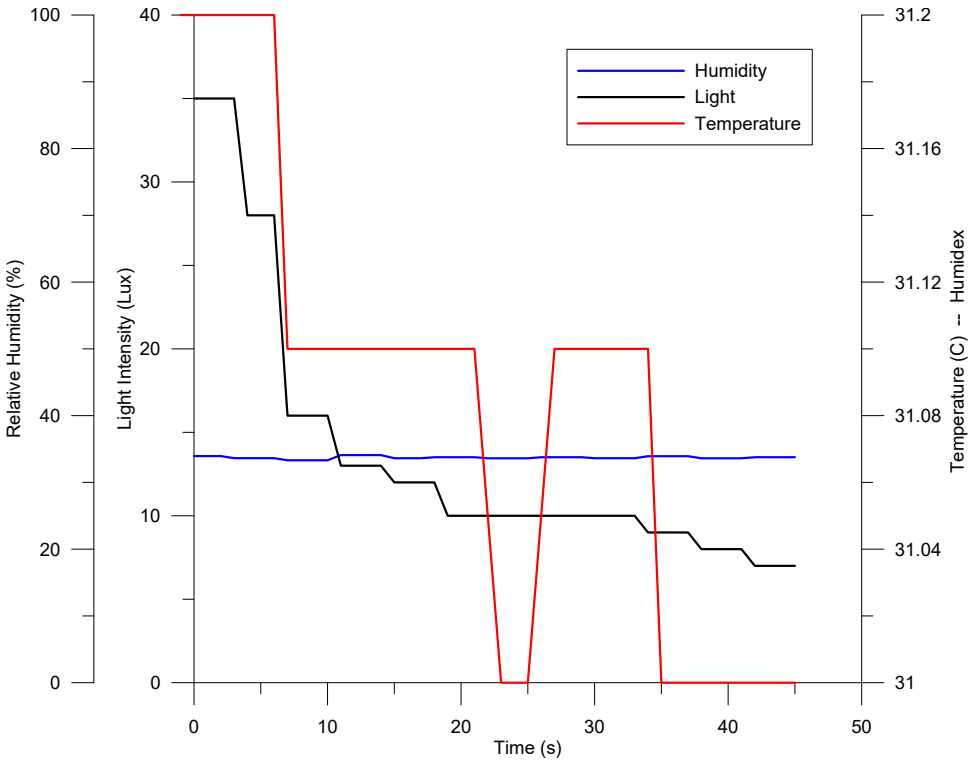


Figure C.388: Test 82 THLP 03

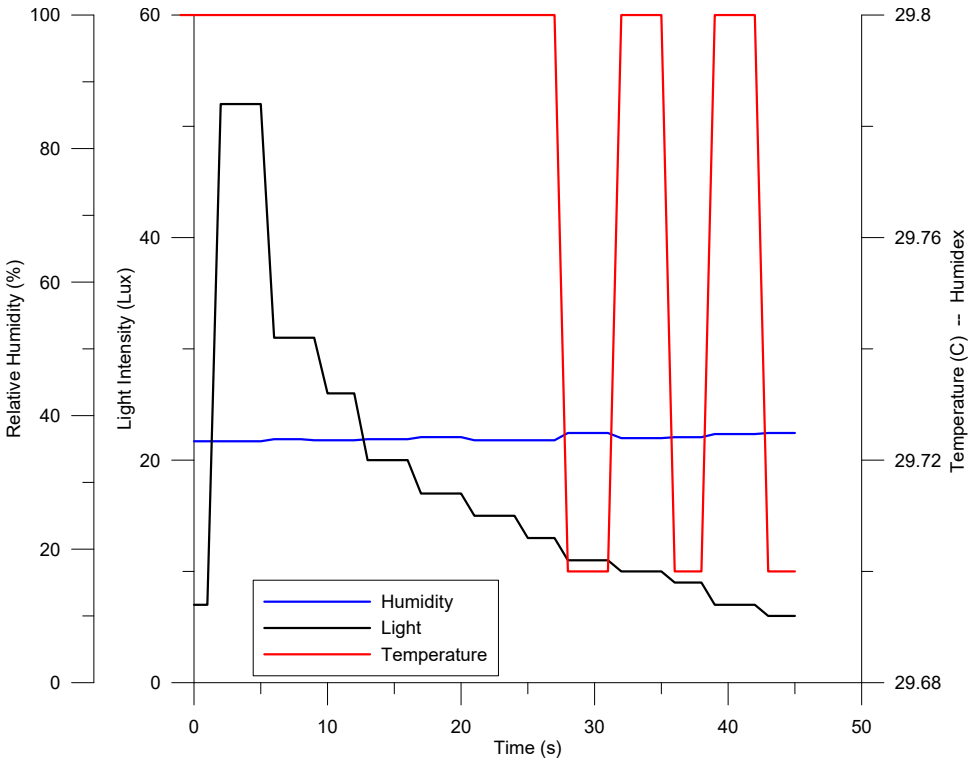


Figure C.389: Test 82 THLP 04

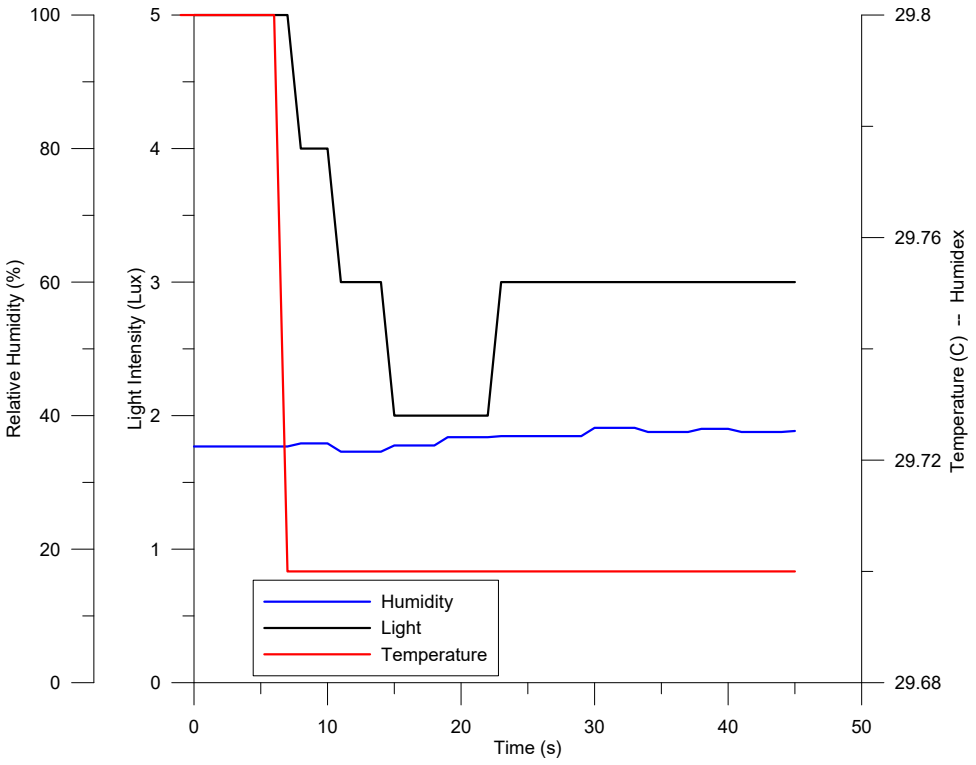


Figure C.390: Test 82 THLP 05

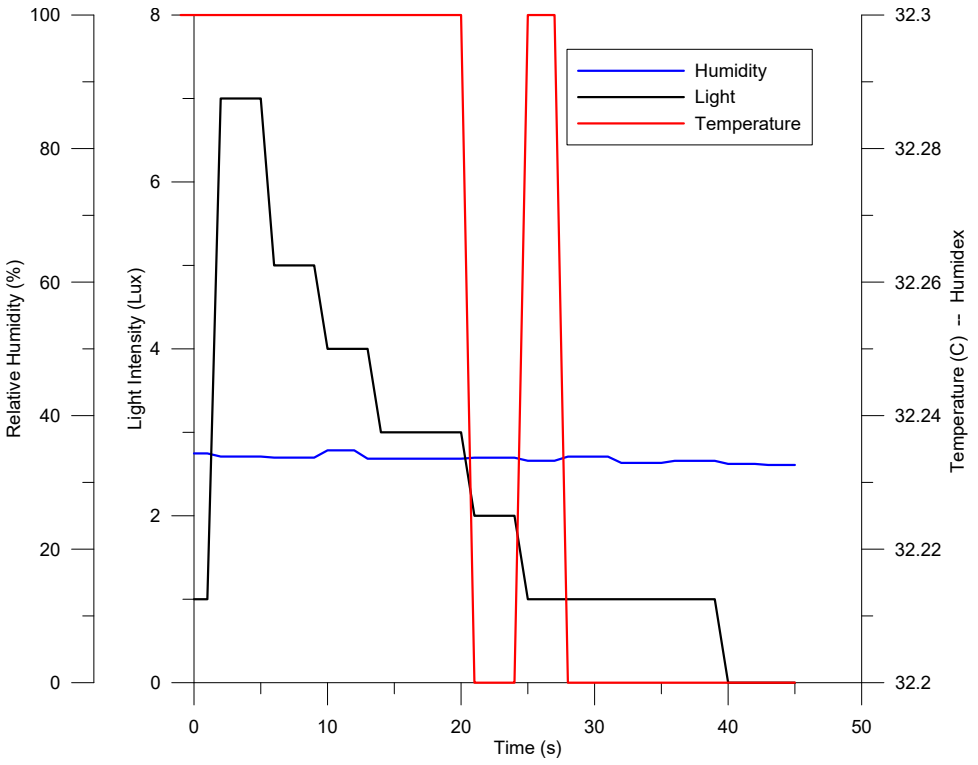


Figure C.391: Test 82 THLP 08

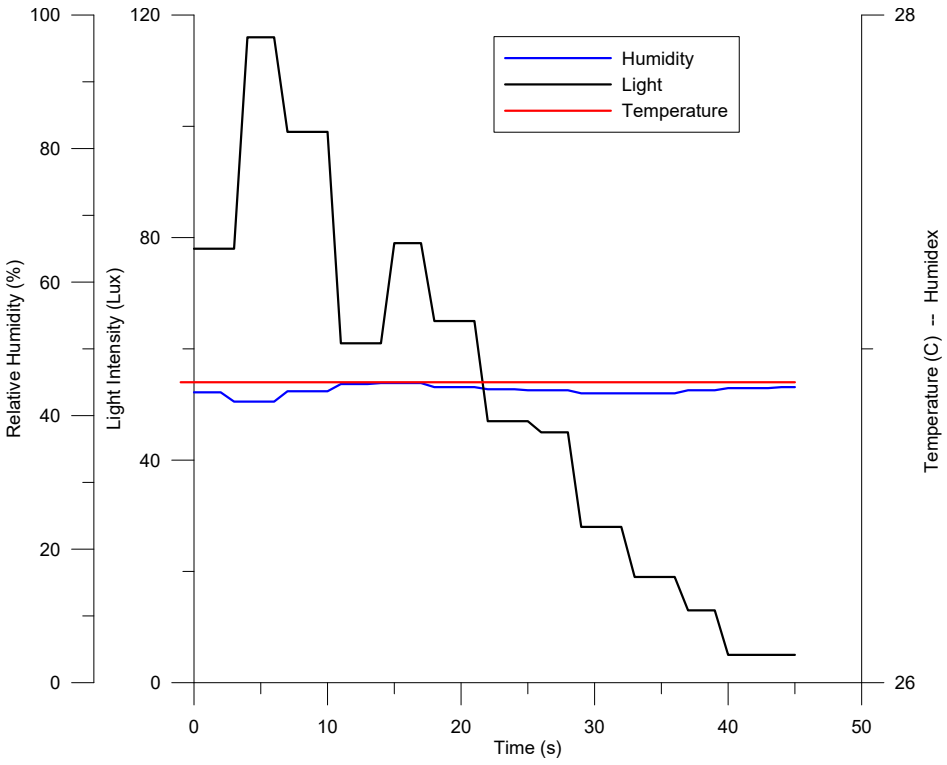


Figure C.392: Test 82 THLP 09

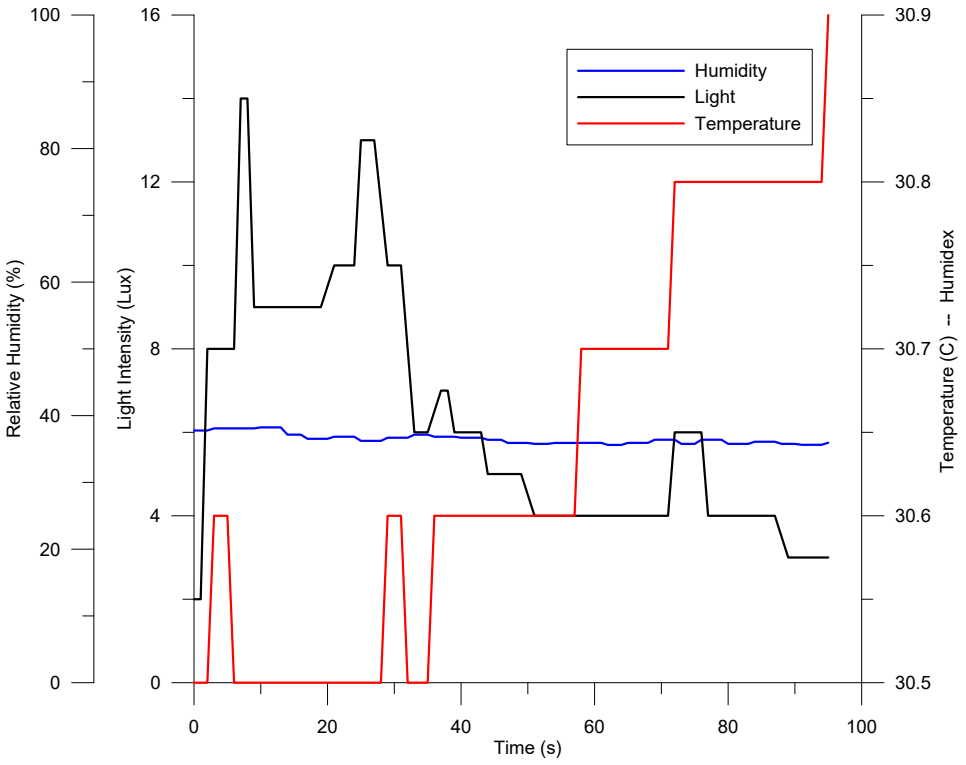


Figure C.393: Test 83 THLP 02

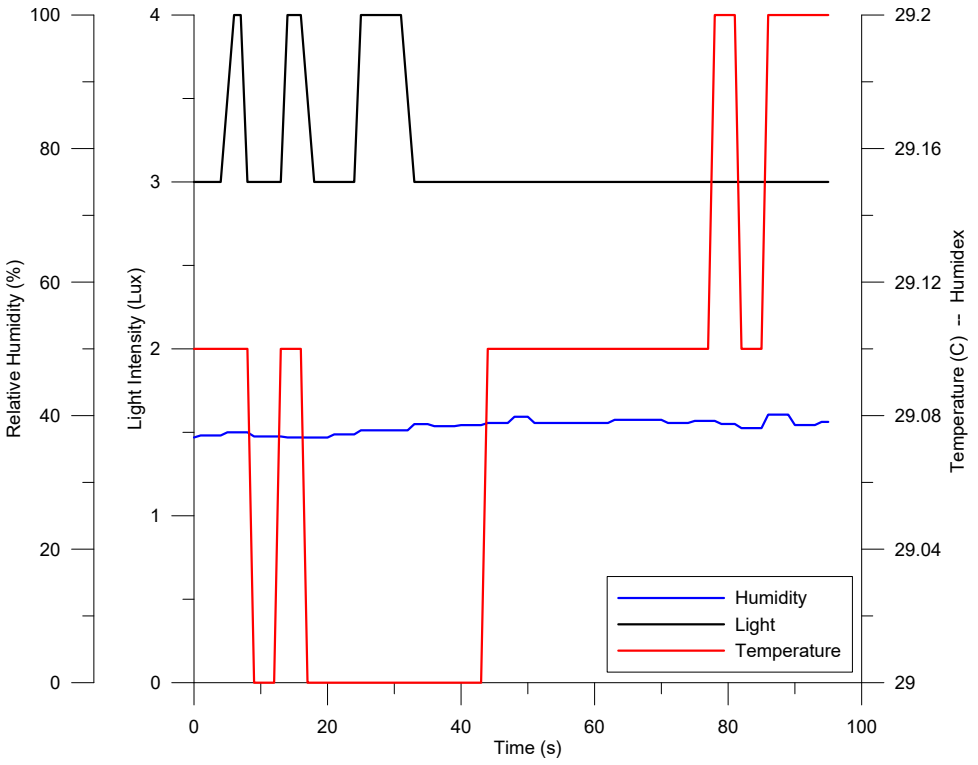


Figure C.394: Test 83 THLP 03

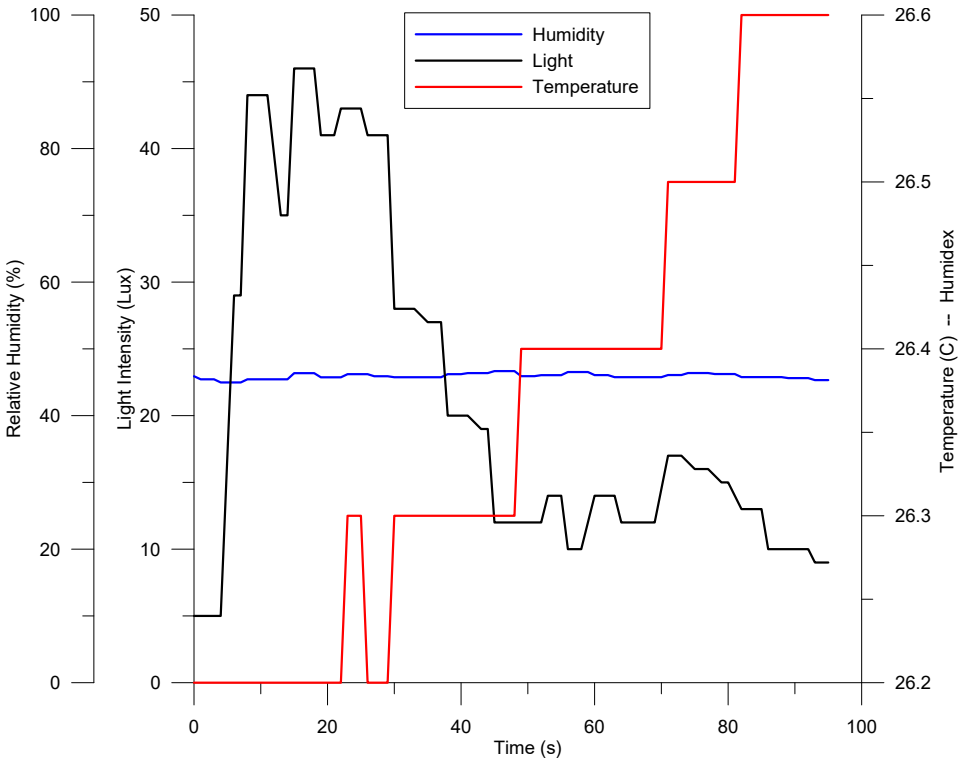


Figure C.395: Test 83 THLP 04

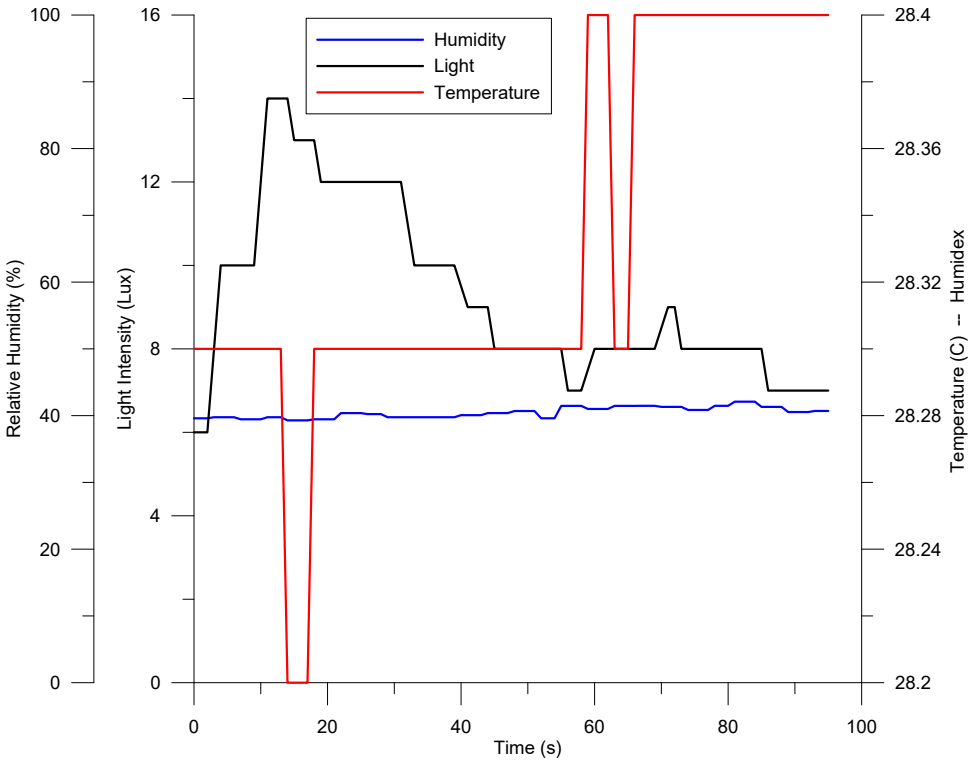


Figure C.396: Test 83 THLP 05

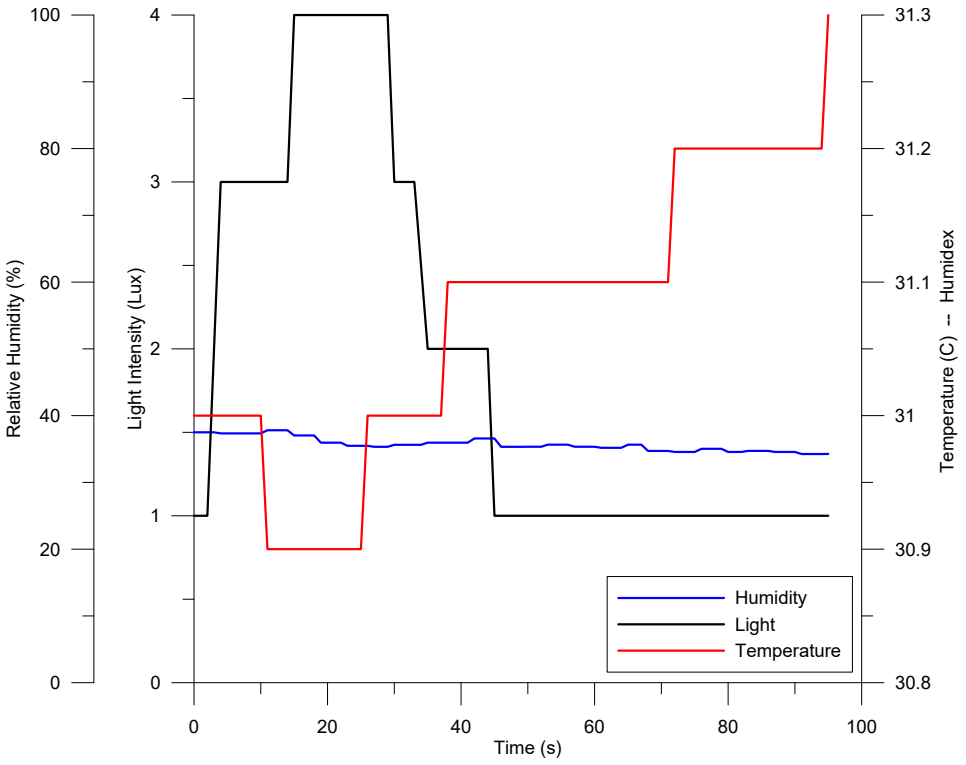


Figure C.397: Test 83 THLP 08

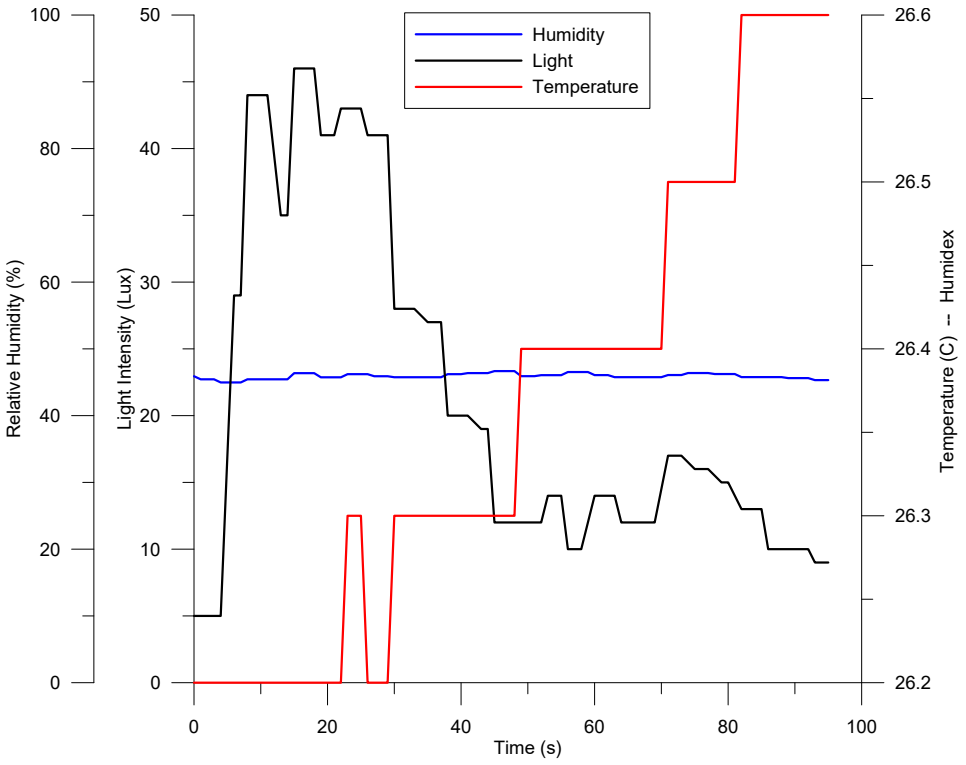


Figure C.398: Test 83 THLP 09

C.2 Living Room Full-Scale Results

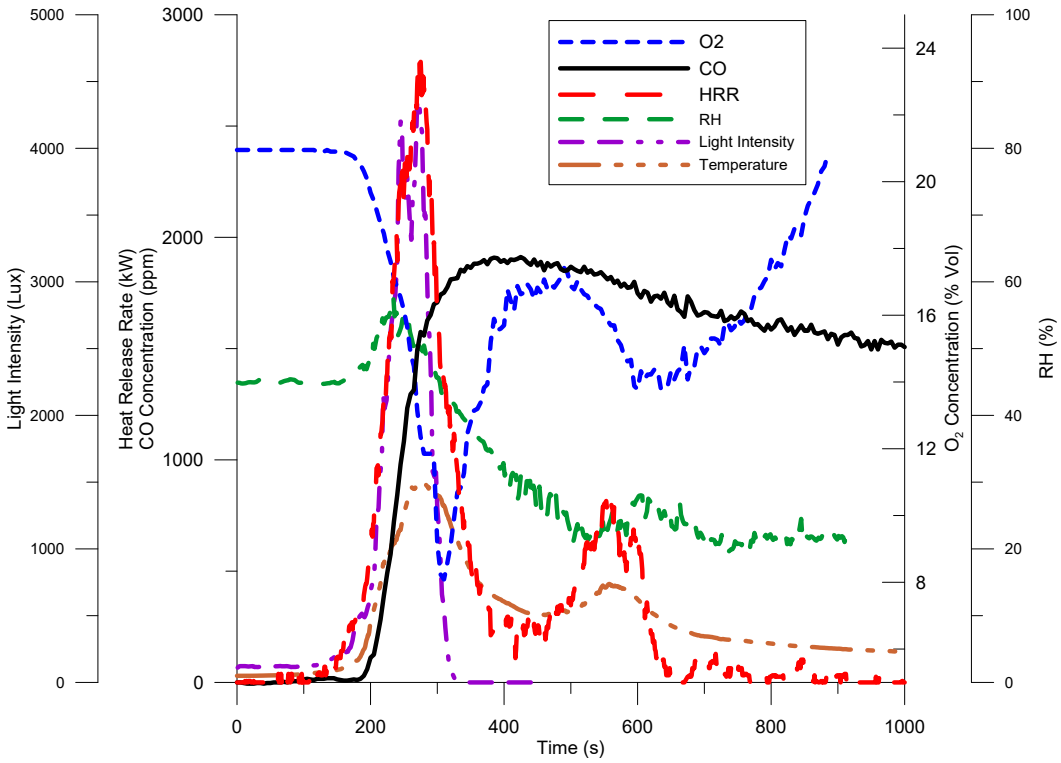


Figure C.399: Heat Release Rate, O_2 and CO Concentration, Relative Humidity, and Light Intensity for Test 2

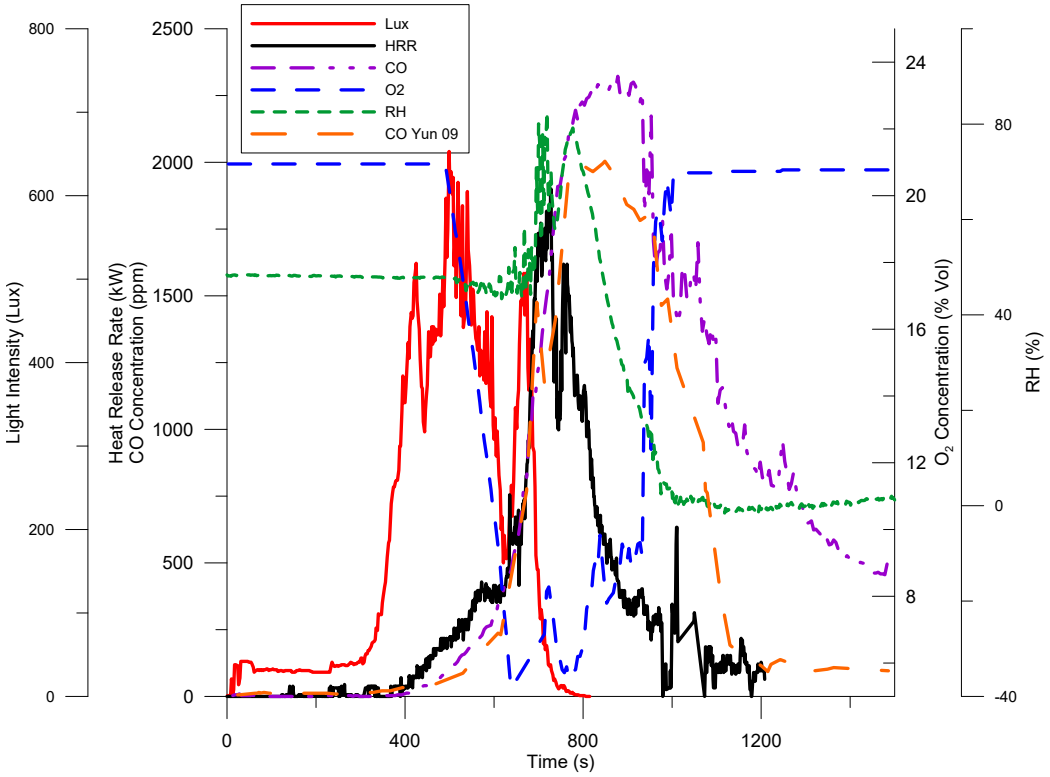


Figure C.400: Heat Release Rate, O_2 and CO Concentration, Relative Humidity, and Light Intensity for Test 3

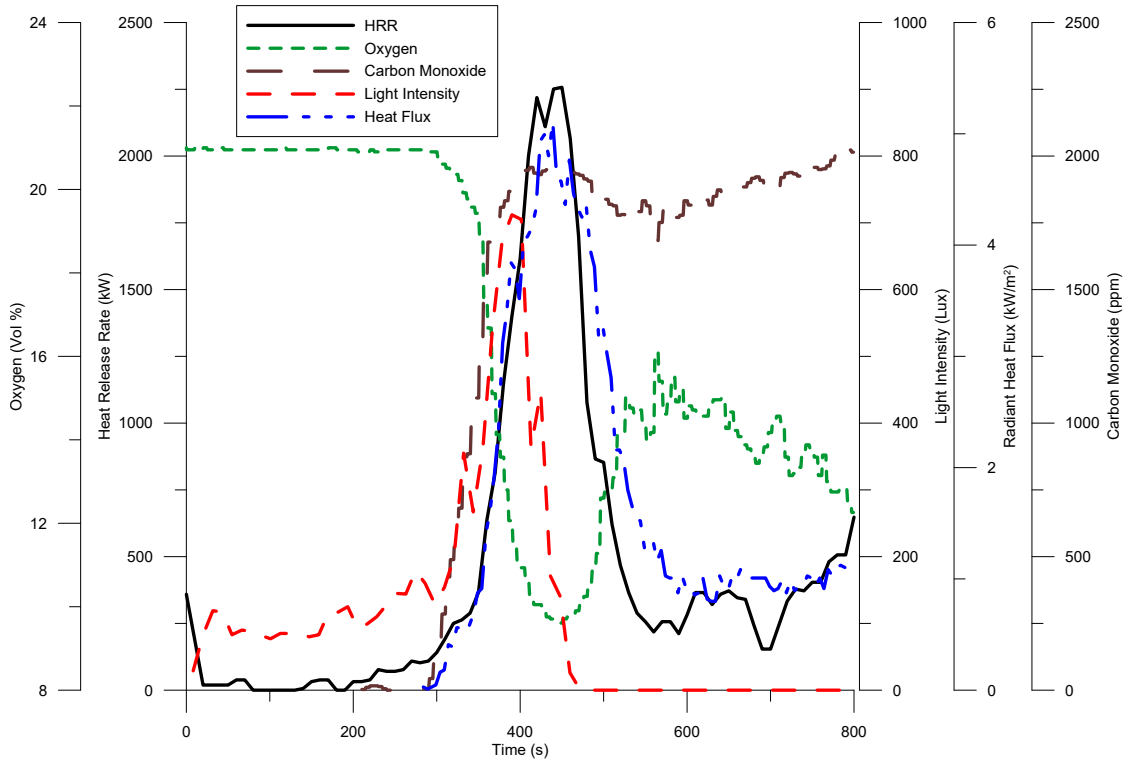


Figure C.401: Heat Release Rate, O_2 and CO Concentration, Heat Flux and Light Intensity for Test 4

Appendix D

Arduino and Linux Programming

The Bridge library enables communication between Arduino and OpenWrt-Yun. The WiFi and Ethernet interfaces, USB host, and SD card are all connected to the AR9331. The Bridge library allows you to work with these devices, as well as run scripts and communicate with web services, Fig.D.1. The Console, based on Bridge, enables you to send information from the Yun to a computer just as you would with the serial monitor, but wirelessly. It creates a secure connection between the Yun and your computer via SSH. Further details on the Yun may be found at http://www.arduino.cc/en/Guide/ArduinoYun.

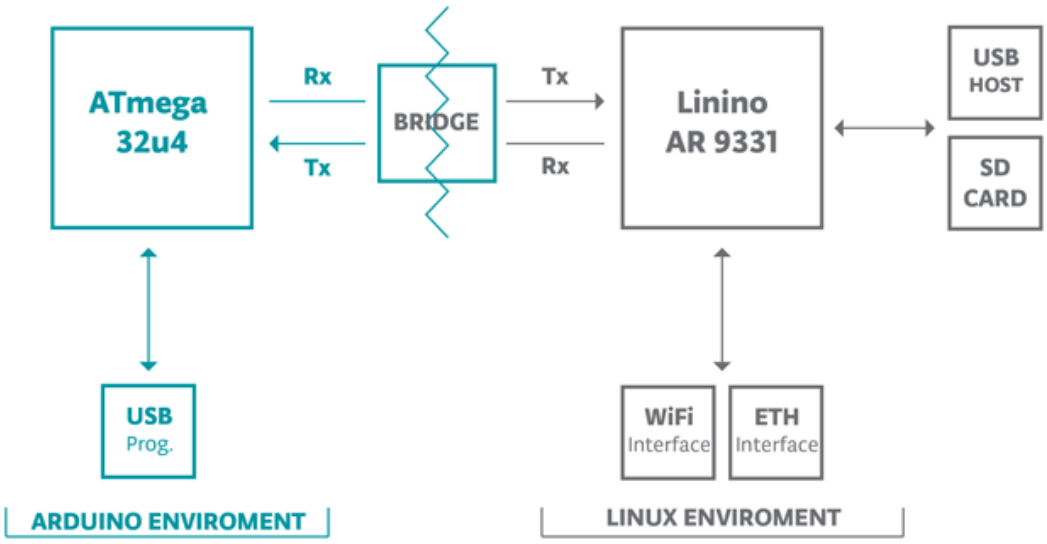


Figure D.1: Block Diagram of Arduino/Linux Interface.

D.1 Arduino Programming

The following code snippet is the Arduino C code which was loaded onto each Yun for the sensor block. The plot.ly keys were modified for each block to record the signal. Specifics on the operation of plot.ly can be found here: http://help.plot.ly/tutorials/.

```
//YUN001

#include <PlotlyYun.h>
#include <YunMessenger.h>
#include <Bridge.h>
#include <Console.h>
#include <Wire.h>
#include <FileIO.h>
#include <HttpClient.h>
#include <Mailbox.h>
#include <Process.h>
#include <YunClient.h>
```

```
#include <YunServer.h>
#include "Adafruit_HTU21DF.h"
#include "TSL2561.h"
#include "Adafruit_TCS34725.h"

// lowest and highest sensor readings:
const int pirMin = 0;      // sensor minimum
const int pirMax = 1024;   // sensor maximum
const int COPin = A3;      // CO Analog input pin
const int CH4Pin = A2;     // CH4 Analog input pin
int COValue = 0;           // value read from the sensor
int CH4Value = 0;          // value read from the sensor

int ledPin = 13;       // choose the pin for the LED
int pirPin = 7;        // choose the input pin (for PIR sensor)
int pirState = LOW;    // we start, assuming no motion detected
int pirval = 0;        // variable for reading the pin status\
//int y = 0;


Adafruit_HTU21DF htu = Adafruit_HTU21DF();
Adafruit_TCS34725 tcs = Adafruit_TCS34725(
   TCS34725_INTEGRATIONTIME_700MS, TCS34725_GAIN_1X);
TSL2561 tsl(TSL2561_ADDR_FLOAT);

// Initialize plotly "plotters" with hardware specific keys

plotly plotter0("0000000000");//Humidity
plotly plotter1("1111111111");//Temperature
plotly plotter2("2222222222");//CH4
plotly plotter3("3333333333");//CO
plotly plotter4("4444444444");//TSL2561-Lux
plotly plotter5("5555555555");//TSL2561-IR
plotly plotter6("6666666666");//TSL2561-Luminosity
plotly plotter7("7777777777");//TCS34725-ColorTemp
plotly plotter8("8888888888");//TCS34725-Lux
plotly plotter9("9999999999");//PIR
```

```
void setup() {


    // start-up the bridge and the console
    Bridge.begin();
    ;

    delay(2000);
    Console.begin();
    while (!Console) {
      ; // wait for Console port to connect.
    }
    Console.buffer(64);
    delay(2000);

   Console.println("Information␣about␣the␣room␣conditions:");

  pinMode(ledPin, OUTPUT);      // declare LED as output
  pinMode(pirPin, INPUT);     // declare sensor as input

  // initialize serial communication @ 9600 baud:
  Serial.begin(9600);

  if (tcs.begin()) {
    Console.println("Found␣TCS34725");
  } else {
    Console.println("No␣TCS34725␣found␣...␣check␣connections")
       ;
    while (1);
  }
    if (tsl.begin()) {
    Console.println("Found␣TSL2561");
  } else {
    Console.println("No␣sensor␣TSL2561␣...␣check␣connnections"
       );
    while (1);
```

```
  }

    Console.println("HTU21D-F␣test");

    if (!htu.begin()) {
    Console.println("No␣sensor␣HTU21D-F␣...␣check␣connnections
       ");
    while (1);
  }
  // You can change the gain on the fly
  //to adapt to brighter/dimmer light situations
  tsl.setGain(TSL2561_GAIN_0X);     //no gain (for bright
     situations)
  //tsl.setGain(TSL2561_GAIN_16X);  //16x gain (for dim
     situations)

  /*Changing the integration time gives you a longer time over
      which to sense light longer timelines are slower, but
     are good in very low light situations*/
  tsl.setTiming(TSL2561_INTEGRATIONTIME_13MS);  // shortest
     integration time (bright light)
  //tsl.setTiming(TSL2561_INTEGRATIONTIME_101MS);  // medium
     integration time (medium light)
  //tsl.setTiming(TSL2561_INTEGRATIONTIME_402MS);  // longest
     integration time (dim light)
}



void loop() {
  // HTU21D-F temperature and humidity sensor
  Console.print("HTU21D-F␣␣");
  Console.print("Temp:␣"); Console.print(htu.readTemperature()
     );
  Console.print("\t\tHum:␣"); Console.println(htu.readHumidity
     ());
     plotter0.plot(htu.readHumidity());
```

```
  plotter1.plot(htu.readTemperature());

// Gas Sensors
  COValue = analogRead(COPin);
  CH4Value = analogRead(CH4Pin);
  Console.println();
  Console.print("CH4␣Sensor␣␣␣");Console.print(CH4Value);
     Console.println("␣ppm");
  Console.print("CO␣Sensor␣␣␣");Console.print(COValue);
     Console.println("␣ppm");

  plotter2.plot(CH4Value);
  plotter3.plot(COValue);

//TCS34725
  uint16_t r, g, b, c, colorTemp, lux;

  tcs.getRawData(&r, &g, &b, &c);
  colorTemp = tcs.calculateColorTemperature(r, g, b);
  lux = tcs.calculateLux(r, g, b);
  Console.print("TCS34725␣␣␣");
  Console.print("Color␣Temp:␣"); Console.print(colorTemp,
     DEC); Console.print("␣K,␣");
  Console.print("Lux:␣"); Console.print(lux, DEC); Console.
     print(",␣");
  Console.print("R:␣"); Console.print(r, DEC); Console.
     print("␣");
  Console.print("G:␣"); Console.print(g, DEC); Console.
     print("␣");
  Console.print("B:␣"); Console.print(b, DEC); Console.
     print("␣");
  Console.print("C:␣"); Console.print(c, DEC); Console.
     print("␣");
  Console.println("␣");

  plotter7.plot(colorTemp);
  plotter8.plot(lux);
```

```
  //TSL2561
    //Simple data read example. Just read the infrared,
       fullspecrtrum diode
    // or 'visible' (difference between the two) channels.
    // This can take 13-402 milliseconds! Uncomment whichever
        of the following you want to read
    //uint16_t x = tsl.getLuminosity(TSL2561_VISIBLE);
    uint16_t x = tsl.getLuminosity(TSL2561_FULLSPECTRUM);
    //uint16_t x = tsl.getLuminosity(TSL2561_INFRARED);
    Console.print("TSL2561␣␣");
    Console.print("Luminosity:␣");Console.print(x, DEC);


  //IR
    uint32_t lum = tsl.getFullLuminosity();
    uint16_t ir, full;
    ir = lum >> 16;
    full = lum & 0xFFFF;
    Console.print("␣␣IR:␣"); Console.print(ir);   Console.
       print("\t\t");
    Console.print("Full:␣"); Console.print(full);   Console.
       print("\t");
    Console.print("Visible:␣"); Console.print(full - ir);
       Console.print("\t");
    Console.print("Lux:␣"); Console.println(tsl.calculateLux(
       full, ir));

    plotter4.plot(tsl.calculateLux(full, ir));
    plotter5.plot(ir);
    plotter6.plot(x);

//PIR motion sensor
    pirval = digitalRead(pirPin);  // read input value
    Console.print("PIR␣Motion:␣␣");
    Console.println(pirval);
```

```
  if (pirval == HIGH) {            // check if the input is
     HIGH
    digitalWrite(ledPin, HIGH);  // turn LED ON
    if (pirState == LOW) {
      // we have just turned on
      Console.println("Motion␣detected!");
          plotter9.plot(pirval);

      // We only want to print on the output change, not state
      pirState = HIGH;
    }
  } else {
    digitalWrite(ledPin, LOW); // turn LED OFF
    if (pirState == HIGH){
      // we have just turned off
      Console.println("Motion␣ended!");
         plotter9.plot(pirval);

     // We only want to print on the output change, not state
      pirState = LOW;
    }


  }


    delay(1000); // Graph 10 points every 10 second
}
```

D.2 Linux Programming

The following code snippet is the Python code to run the script on the OpenWRT Linux system on the Yun, from https://www.arduino.cc/en/Guide/ArduinoYun.

```
#!/usr/bin/python
# -*- coding: utf-8 -*-
```

```
from YunMessenger import Console
import plotly.plotly as py
import json
import traceback
import datetime
import time
from pytz import timezone
import sys
import os

# Initialize a YunMessenger console object
try:
    c = Console.Console(log_filename="/root/Plotly.log")
except IOError as e:
    print("ERROR: The log file directory that you specified
       does not exist")
    raise e

# Load up plotly credentials
config_filename = '/root/config.json'
try:
    with open(config_filename) as config_file:
        config_string = config_file.read()
        # Unicode song-and-dance to convert curly double
           quotes to straight single quotes
        config_unicode = unicode(config_string, 'utf-8')
        punctuation = { 0x2018:0x27, 0x2019:0x27, 0x201C:0x22,
            0x201D:0x22 }
        normalized_config_string = config_unicode.translate(
           punctuation).encode('ascii', 'ignore')
        plotly_user_config = json.loads(
           normalized_config_string)
except IOError as e:
    helpful_msg = "Please place a configuration file at {
       filename}"\
        " with your plotly credentials and try again.\n"\
        "Questions? Need some help? Support@plot.ly".format(
           filename=config_filename)
```

```
    print(helpful_msg)
    c.logger.error(helpful_msg)
    raise e
except ValueError as e:
    helpful_msg = "The␣JSON␣config␣file␣at␣{filename}␣could␣
       not␣be␣decoded,␣"\
        "are␣you␣sure␣that␣it␣is␣in␣the␣right␣format?\n"\
        "Questions?␣Support@plot.ly".format(filename=
           config_filename)
    print(helpful_msg)
    c.logger.error(helpful_msg)
    raise e

# Extract the credentials and settings from the config file
username = plotly_user_config['plotly_username']
api_key = plotly_user_config['plotly_api_key']
stream_tokens = plotly_user_config['plotly_streaming_tokens']
file_option = plotly_user_config['file_option']

if 'show_this_many_points' in plotly_user_config:
    maxpoints = plotly_user_config['show_this_many_points']
else:
    maxpoints = 500

# Make the initializing plotly request
# Pass all stream tokens from the config file into this plot
py.sign_in(username, api_key)

url = py.plot(
    [
        {'x': [], 'y': [], 'stream': {'token': token, '
           maxpoints': maxpoints}}
        for token in stream_tokens
    ],
    filename='Stream␣from␣Yun',
    auto_open=False,
    fileopt=file_option)
```

```
status = "Plot␣initialized␣at:␣{url}\nwith␣token(s):␣{tokens}"
   \
          .format(url=url, tokens=',␣'.join(stream_tokens))
print(status)
c.logger.info(status)


class PlotlyHandler:
    ''' Create a message handler for streams
    that writes to streams that are indexed by token
    '''
    def __init__(self, stream_tokens):
        ''' Store the stream tokens in an object
         so that the message handler can access them
        '''
        self.streams = {}
        for token in stream_tokens:
            self.streams[token] = py.Stream(token)
            self.streams[token].open()

    def handlePlotlyMessages(self, msg):
        ''' Write the msg data to the associated plotly stream
        msg is a json string of the form:
            {"x": 1, "y": 1, "token": "ibagefhdci"}
            or
            {"y": 1, "token": "ibagefhdci", "timezone": "
               America/Montreal"}
        If it's the latter form, we'll compute the time and
           assign that as x
        '''
        data = json.loads(msg)
        if data['token'] in self.streams:
            token = data['token']
            del data['token']
            if 'x' not in data and 'timezone' in data:
                try:
                    tz = timezone(data['timezone'])
```

```
                except:
                    c.logger.warning("Unrecognized␣timezone:␣{
                       timezone}\n"
                        "Defaulting␣to␣America/Montreal".
                           format(timezone=data['timezone']))
                    c.logger.debug(traceback.format_exc())
                    tz = timezone("America/Montreal")
                del data['timezone']
                data['x'] = tz.localize(datetime.datetime.now
                   ())
            self.streams[token].write(data)
            time.sleep(50./1000.)
        else:
            c.logger.warning("Recieved␣the␣token:␣{token}␣
               which␣has␣no␣associated␣stream.\n"\
                "Add␣the␣token␣{token}␣to␣your␣config.json␣
                   file␣to␣register␣this␣stream.".format(token
                   =data['token']))

plotlyHandler = PlotlyHandler(stream_tokens)

# Assign a "subscriber" to 'plotly' messages that are
   transmitted from plotly
c.onMessage['plotly'] = plotlyHandler.handlePlotlyMessages

# Start listening for messages (data) from the Arduino!
c.run()
```

D.3 HTM Programming

The following code snippets are the Python code to run the HTM scripts.

D.3.1 analyze.py

```
import pandas as pd
```

```
import numpy as np
import scipy.stats as st

def stats(df):
    '''
    Returns a DataFrame of summary statistics for each column
    '''
    return df.describe().T

def normalize(df):
    '''
    Normalizes values in each column to a scale of 0 to 1
       using:
         (value - min) / (max - min)
    '''
    norm = lambda x: (x - x.min()) / (x.max() - x.min())
    return df.apply(norm)

def d_dt(df, time_col=None):
    '''
    Takes the first derivative of the data with respect to
       time using a central
    differencing scheme. Time column is assumed to be the
       index by default, and
    assumed to be numeric.
    '''
    if time_col is None:
        times = df.index.values
    else:
        times = df[time_col].values

    t1 = np.roll(times, shift=1)
    t1[0] = t1[1]

    t2 = np.roll(times, shift=-1)
    t2[-1]=t2[-2]

    deriv = lambda x: (x.shift(-1) - x.shift(1)) / (t2 - t1)
```

```
    return df.apply(deriv)

def d_dt2(df, time_col=None):
    '''
    Takes the second derivative of the data with respect to
       time. Time column
    is assumed to be the index by default, and assumed to be
       numeric.
    '''
    if time_col is None:
        times = df.index.values
    else:
        times = df[time_col].values

    t1 = np.roll(times, shift=1)
    t1[0] = t1[1]

    t2 = times

    deriv2 = lambda x: (x.shift(-1) - 2*x + x.shift(1)) / ((t2
        - t1)**2)
    return df.apply(deriv2)

def rel_change(df, bg=10):
    '''
    Calculates the relative change in value from the baseline.
        An optional
    background (bg) parameter changes the number of points
       used to calculate
    the baseline value.
    '''
    change = lambda x: x - np.mean(x[:bg])
    return df.apply(change)

def turning_point(s):
    return (s<s.shift(1)) & (s<=s.shift(-1)) | (s>s.shift(1))
       & (s>=s.shift(-1))
```

```
def steps(s):
    return (s<s.shift(1)) | (s>s.shift(1))

def slope(series, start, stop):
    x = series.index[start:stop]
    y = series[start:stop]
    return st.linregress(x,y)[0]

def _moving_regress(series, window=30):
    half = int(0.5*window)
    end = len(series)
    regress = pd.Series(np.zeros(end),series.index)
    for i in range(end):
        start = max(0, i-half)
        stop = min(i+half, end-1)
        regress[i] = slope(series, start, stop)
    return regress

def moving_regress(df, window=30):
    return df.apply(_moving_regress, window=window)

def _trailing_avg(series, window=10):
    end = len(series)
    avg = pd.Series(np.zeros(end),series.index)
    for i in range(end):
        start = max(0, i-window)
        stop = min(i, end-1)
        avg[i] = series[start:stop].mean()
    return avg

def trailing_avg(df, window=10):
    return df.apply(_trailing_avg, window=window)
```

D.3.2 data.py

```
import pandas as pd
#from pandas import DataFrame#, MultiIndex
```

```
import os
from os.path import basename, abspath

from datetime import datetime

import numpy as np

import matplotlib.pyplot as plt
import matplotlib as mpl

pd.set_option('display.mpl_style','default')
mpl.rc('font',family='sans-serif', size=12.0)

sensors = ('Humidex','Humidity','Light','Pressure','
   Temperature', 'Heat␣Flux')
units = ('--', '%','lux','Pa',u"\u00b0C", "kw/m^2")
verbosity = True

class RawDataFile(object):
    '''
    RawDataFile contains information about, and methods to
       load and clean
    raw sensor data files exported from the multisensor
       detectors.
    '''

    def __init__(self, path):
        self.path = path
        self.directory, self.filename = os.path.split(path)
        self.verbose = verbosity
        self.cleaned = False
        self.raw = None
        self.data = None
        self.col_map = {
            '0004A3FFFE92D1D2':'THLP-01',
            '0004A3FFFE92D2DC':'THLP-02',
            '0004A3FFFEDF293A':'THLP-03',
            '0004A3FFFEDEE121':'THLP-04',
```

```
            '0004A3FFFEDE9AAA':'THLP-05',
            '0004A3FFFEDEB732':'THLP-06',
            '0004A3FFFEDE9C29':'THLP-07',
            '0004A3FFFEDEE150':'THLP-08',
            '0004A3FFFEDE89D8':'THLP-09',
            '0004A3FFFEDEFF3E':'THLP-10'
            }

    @property
    def sensor_type(self):
        ''' Determine the type of data contained in a file
           based on the filename

            Return: The file type as a string
        '''
        for sensor in sensors:
            if sensor.lower() in self.filename.lower():
                return sensor

    def load(self, clean=True):
        '''
        Load a single data file.
        '''
        # Custom date parsing function
        parser = lambda s: datetime.strptime(s, '%y.%m.%d_%I:%
           M.%S')

        if self.verbose:
            print 'importing %s...' % self.path

        self.raw = pd.read_csv(self.path, skiprows=1,
           index_col=0, \
            parse_dates=['Date/Time'], date_parser=parser)

        if clean:
            self.clean()

    def clean(self):
```

```
        '''
        Performing an initial cleaning of the raw data to
           prepare it for
        later analysis, by performing the following operations
           :
            - Remove any duplicate data rows (rows with same
               times)
            - Remove unneeded columns
            - Correct time column (index)
            - Rename columns according col_map

        Returns: None, Sets cleaned attribute to True, if
           successful
        '''
        if self.verbose:
            print 'cleaning␣raw␣data...'

        # Remove rows containing duplicate times
        df = self.raw.copy()
        df['index'] = df.index.values
        df.drop_duplicates(subset='index', inplace=True)

        # remove unnecessary columns
        if 'Uptime' in df.columns.values:
            del df['Uptime']
        del df['index']

        df = self.fix_times(df)

        # rename columns
        df.rename(columns=self.col_map, inplace=True)
        df.name = 'detector'

        self.data = df
        self.cleaned = True

    def fix_times(self, df):
        '''
```

```
        Corrects the time data. The raw data format does not
           distinguish between
        AM and PM, and uses a 12-hour time format. So all
           times before hour 8
        (i.e. 8:00 AM) are assumed to be off by 12 hours.

        Returns: DataFrame with the corrected time index
        '''
        # Identify times in the index with an hour less than 8
        hour = df.index.hour
        selector = (hour < 8)

        # Create two arrays of times:
        #    1. the original times, and
        #    2. times offset by 12 hours
        times = df.index.values
        times12 = times + np.timedelta64(12, 'h')

        # Create a new array of times using np.where to do a
           vectorized 'if'
        new_times = np.where(selector, times12, times)

        # Return the dataset with the corrected times in the
           index
        return df.set_index(new_times)

class RawData(object):

    def __init__(self, data_dir = '.'):
        self.directory = data_dir
        self.verbose = verbosity
        self.test_series= {}

    def _filter_files(self, dirname, names, exts=['csv','txt'
       ]):
        ''' Search a list of files for data files containing
           the requested file
            extensions (exts).
```

```
            Return: A list of full file paths for sensor data
               files.
        '''
        files=[]
        exts = [e.lower() for e in exts]
        # loop through the list of file names provided
        for name in names:
            # loop through each file extension
            for x in exts:
                # Check if filename ends with file extension
                if name.lower().endswith(x):
                    # Check if the filename contains a sensor
                       name
                    for sensor in sensors:
                        if sensor.lower() in name.lower():
                            # Add the filename to the list of
                               data files
                            files.append(os.path.join(dirname,
                                name))
        return files

    def load_dir(self, recursive=True, clean=True):
        '''
        Load all data files from the data directory into a
           dict of DataFrames.
        By default, the data directory will be searched
           recursively for
        additional data files.

        Return: None. Dict of data_frames added to data_frames
        '''
        strip_root = lambda k: basename(abspath(k))

        # walk through the data_dir searching for data files
        for dirpath, dirnames, files in os.walk(self.directory
           ):
            # extract list of data files from list of all
```

```
                files
            files = self._filter_files(dirpath, files)
            series = TestSeries(strip_root(dirpath))

            for f in sorted(files):
                # load the file into a DataFrame
                rd = RawDataFile(f)
                rd.load(clean)
                series.add_file(rd)

            if series.files:
                series.combine()
                self.test_series[series.name] = series

            if not recursive:
                return

class TestSeries(object):

    def __init__(self, name):
        self.verbose = verbosity
        self.name = name
        self.data = {} # dict of combined data, with sensors
            as keys
        self.files = []
        self.tests = []

    def add_file(self, raw_file):
        ''' Adds a RawDataFile to the list of files to the
            test series.'''
        self.files.append(raw_file)

    def combine(self):
        '''
        Combines a RawDataFiles based on the type of sensor
        data contained in each. Data is concatenated to rows
        for sensor types already present in the dict.
```

```
        Return: None. Sets data attribute to dict of combined
           DataFrames
        '''

        combined = {}
        for f in self.files:
            s = f.sensor_type
            if f.sensor_type in combined:
                # existing cols, so add rows (axis = 0)
                combined[s] = pd.concat([combined[s], f.data])
            else:
                combined[s] = f.data
            combined[s].sort_index(inplace=True)

        self.data = combined


    def extract_tests(self, test_info = None):
        slicer = TestSlicer(self, test_info)
        self.tests = slicer.slice()

class TestSlicer(object):
    '''
    Class used to extract, combine, and clean test data for a
       test series.
    '''
    def __init__(self, test_series, test_info=None):
        self.test_series = test_series
        self.test_info = test_info
        self.verbose = verbosity
        # attempt to load test info
        if test_info is None:
            try:
                self.load_test_info()
            except:
                pass

    def load_test_info(self, f='./TestMatrix.csv'):
```

```
        #self.test_info = pd.read_csv(f, parse_dates=['end','
            start'],
        #        infer_datetime_format = True, index_col='test
            ')

        # read the test info from a file
        self.test_info = pd.read_csv(f, parse_dates=['
            StartTime','EndTime'],
                infer_datetime_format = True, index_col='
                    TestID')

        #delete any tests (rows) that don't have a start or
            end time
        self.test_info.dropna(subset=['StartTime','EndTime'],
            inplace=True)


    def _slice_test(self, test_id, data_start, test_start, end
        ):
        '''
        Slices an individual test from the data for a test
            series
        using the start & end timestamps. An elapsed time
            column is
        added and set as the new index of the DataFrame. The
            data is also
        further cleaned to prepare for analysis.
        '''
        # makes sure any sliced test has at least 10% of data
        MIN_LENGTH = (end-data_start).total_seconds() * 0.1

        if test_id == 39: return

        if self.verbose:
            print 'slicing␣data␣for␣test␣%d:' % test_id
            print '\tstarting␣at␣%s' % str(data_start)
            print '\tending␣at␣%s' % str(end)
            print ''
```

```
test = {}
for s, df in self.test_series.data.iteritems():
    # extract the test data for the given sensor
    # (between start and end times)
    temp = df.copy()

    # asof finds the index value closest to requested
       time,
    # asof returns nan if not found.
    new_start = temp.index.asof(data_start)
    new_end = temp.index.asof(end)
    # check to make sure start/end times were found
       before slicing
    if not new_start is np.nan and not new_end is np.
       nan:
        temp = temp[new_start:new_end]

        # add elapsed time to the DataFrame and set it
            as the index
        temp['timestamp'] = temp.index.values  # copy
           the index (times)
        temp['elapsed'] = self._elapsed(temp['
           timestamp'], test_start)
        temp = temp.set_index('elapsed')
        del temp['timestamp']
        if temp.index.size >= MIN_LENGTH:
            test[s] = temp

    else:
        continue


if test != {}:
    # Concatenate the DataFrames of multiple sensors
       into a single large
    # DataFrame for a test with a MultiIndex on the
       columns
```

```
            merged = pd.concat(test, axis=1)
            merged.columns.names = ['sensor','detector']

            # Return a TestData object containing the cleaned
               data for the test
            return TestData(test_id, self._clean(merged))


    def slice(self, test_ids=None):
        '''
        Slices all tests from a test series.

        Returns: List of TestData objects
        '''
        tests = []

        if test_ids is None:
            # Get a list of tests in the test series.
            selector = (self.test_info.Directory == self.
               test_series.name)
            test_ids = self.test_info[selector].index.values.
               astype(int)

        if self.verbose:
            print '%d tests found in Test Series "%s"' % \
                (len(test_ids),self.test_series.name)

        for test_id in test_ids:
            data_start = self.test_info.ix[test_id].
               DataStartTime
            start = self.test_info.ix[test_id].StartTime
            end = self.test_info.ix[test_id].EndTime
            test = self._slice_test(test_id, data_start, start
               , end)
            if not test is None:
                if self.verbose:
                    print 'Test "%s" added.' % test_id
                tests.append(test)
```

```
        return tests

    def _clean(self, df):
        '''
        Clean the sliced test data frame to prepare it for
           analysis, by
        performing the following operations:
            - Force regular 1 second data intervals
            - Fill in any gaps where data is missing (
               interpolate)
            - Sort columns
        '''

        # Create a new series with the same start and end
           times as the
        # DataFrame time index at regular one second intervals
        rng = np.arange(df.index[0], df.index[-1] + 1, 1)
        df = df.reindex(rng)

        # interpolate between missing values
        df = df.interpolate()

        #return the data frame with sorted columns
        df.sort_index(axis=1, inplace=True) #used to be sort
        return df

    def _elapsed(self, time_col, start):
        return np.divide(time_col - start, np.timedelta64(1, '
           s')).astype('int64')


class TestData(object):
    '''
    Class used to extract, combine, and clean test data for a
       test series.
    '''
    def __init__(self, test_id, data):
```

```
        self.test_id = test_id
        self.data = data
        self.verbose = verbosity
        self.test_series = None

    @property
    def sensors(self):
        return np.unique(self.data.columns.get_level_values(0)
            .values)

    @property
    def detectors(self):
        return np.unique(self.data.columns.get_level_values(1)
            .values)

    def select_sensor(self, sensor, replace_index=True):
        '''
        Selects a subset of columns that match a given sensor
            type.
        Sensor names are assumed to be on 1st level of column
            MultiIndex
        By default, removes the MultiIndex level containing
            the sensor

        Returns: DataFrame
        '''
        # create a mask to filter columns by sensor type
        mask = self.data.columns.get_level_values(0) == sensor
        # create a new data frame of only the sensor data
        new = self.data.ix[:,mask]
        if replace_index:
            # remove the multi-index so detector labels appear
                as header
            new.columns = new.columns.get_level_values(1)
        return new

    def select_detector(self, detector, replace_index=True):
        '''
```

```
        Selects a subset of columns that match a given
           detector label.
        Detector names are assumed to be on 2nd level of
           column MultiIndex
        By default, removes the MultiIndex level containing
           the sensor

        Returns: DataFrame
        '''
        # create a mask to filter columns by detector label
        mask = self.data.columns.get_level_values(1) ==
           detector
        # create a new data frame of only the sensor data
        new = self.data.ix[:,mask]
        if replace_index:
            # remove the multi-index so sensor names appear as
                header
            new.columns = new.columns.get_level_values(0)
        return new

    def save_detector(self, detector, directory='./tests/',
       filename=''):
        '''
        Saves data for a given detector to a csv file.
        '''
        det = self.select_detector(detector)
        if not det.empty:
            if not filename:
                filename = 'Test%02d_%s.csv' % (self.test_id,
                   detector)
            p = os.path.join(directory, filename)
            if self.verbose:
                print 'saving %s...' % p
            det.to_csv(p)
        else:
            print "Detector '%s' not found for Test %d." % (
               detector,
                    self.test_id)
```

```
def save_sensor(self, sensor, directory='./tests/',
   filename=''):
    '''
    Saves data for a fiven sensor to a csv file.
    '''
    sens = self.select_sensor(sensor)
    if not sens.empty:
        if not filename:
            filename = 'Test%02d_%s.csv' % (self.test_id,
               sensor)
        p = os.path.join(directory, filename)
        if self.verbose:
            print 'saving %s...' % p
        sens.to_csv(p)
    else:
        print "Sensor '%s' not found for Test %d." % (
           sensor, self.test_id)

def save(self, directory='./tests/', filename=''):
    '''
    Saves all test data for test_id to a csv file.
    '''
    if not filename:
        filename = 'Test%02d.csv' % self.test_id
    p = os.path.join(directory, filename)
    if self.verbose:
        print 'saving %s...' % p
    self.data.to_csv(p)

def plot(self, sensor=None, detector=None, title=''):
    sensor_title = lambda s:'%s (%s)' % (s, sensor_units(s
       ))
    xlabel = 'Time (s)'

    if sensor and detector:
        # single plot of data for specific sensor and
           detector
```

```
            df = self.select_sensor(sensor)
            if not title:
                title = 'Test %s - %s %s' % (self.test_id,
                   detector, sensor)
            ax = df[detector].plot(title=title)
            ax.set_ylabel(sensor_title(sensor))
            ax.set_xlabel(xlabel)
#            ax.set_xlim(left=0)
            ax.legend(loc='best', prop={'size':8})

            ax_or_axes = ax

        elif sensor and not detector:
            # single plot of data for specific sensor from all
                detectors
            df = self.select_sensor(sensor)
            if not title:
                title = 'Test %s - %s' % (self.test_id, sensor
                   )
            ax = df.plot(title=title)
            ax.set_ylabel(sensor_title(sensor))
            ax.set_xlabel(xlabel)
#            ax.set_xlim(left=0)
            ax.legend(loc='best', prop={'size':8})

            ax_or_axes = ax

        elif not sensor and detector:
            # array of plots (axes) for a specific detector.
            # Each sensor in a separate plot (axes).
            df = self.select_detector(detector)

            # create a 3 x 2 array of plots
            fig, axes = plt.subplots(nrows=3,ncols=2, figsize
               =(12,10))

            # add a title to the figure
            if not title:
```

```
                title = 'Test %s - %s' % (self.test_id,
                    detector)
            fig.suptitle(title)

            for sensor, ax in zip(self.sensors, axes.flat):
                df[sensor].plot(ax = ax)
                ax.set_ylabel(sensor_title(sensor))
                ax.set_xlabel(xlabel)
#                ax.set_xlim(left=0)
                ax.legend(loc='best', prop={'size':8})

            # hide the axis for unused plots
            for i in range(len(self.sensors),len(axes.flat)):
                axes.flat[i].axis('off')

            ax_or_axes = axes

        else:
            # array of plots (axes) for all detectors.
            # Each sensor in a separate plot (axes).

            # create a 3 x 2 array of plots
            fig, axes = plt.subplots(nrows=3,ncols=2, figsize
                =(12,10))

            # add a title to the figure
            if not title:
                title = 'Test %s' % (self.test_id)
            fig.suptitle(title)

            for sensor, ax in zip(self.sensors, axes.flat):
                df = self.select_sensor(sensor)
                df.plot(ax = ax)
                ax.set_ylabel(sensor_title(sensor))
                ax.set_xlabel(xlabel)
#                ax.set_xlim(left=0)
                ax.legend(loc='best', prop={'size':8})
```

```
            # hide the axis for unused plots
            for i in range(len(self.sensors),len(axes.flat)):
                axes.flat[i].axis('off')

            ax_or_axes = axes

        return ax_or_axes

def sensor_units(sensor):
    try:
        return units[list(sensors).index(sensor)]
    except:
        return '???'
```

D.3.3 main.py

```
import os
import re
from copy import deepcopy

import pandas as pd
import matplotlib.pyplot as plt

import data
#import fds
from analyze import stats, normalize

#import analyze

def load_raw(data_dir = './data/'):
    '''
    Creates a RawData object and loads all RawDataFiles from
       each TestSeries
    found in the data directory.

    Returns: RawData object
    '''
    raw = data.RawData(data_dir)
```

```
    raw.load_dir()

    return raw

def load_data(data_dir='./data/', test_info = None, from_raw =
    True):
    '''
    Retrieves a list of TestData objects.

    If from_raw is True, data will be imported from raw data
       files. If False,
    data will be loaded from csv files containing TestData
    '''
    if from_raw:
        # Load from raw data files. Clean data and create
           TestData objects from
        #the raw data files.
        if test_info is None:
            test_info = load_test_info()

        raw = load_raw(data_dir)

        tests = []

        for name in sorted(raw.test_series):
            series = raw.test_series[name]
            print 'extracting tests for "%s"' % name
            series.extract_tests(test_info)

            if series.tests:
                tests.extend(series.tests)

    else:
        # Load TestData from CSV files containing processed
           data
        tests = []
        files = []
        regex = re.compile(r"Test(\d+).csv")
```

```
        files += [f for f in os.listdir(data_dir) \
                    if f.endswith('.csv')]

        for f in files:
            # Extract test_id from CSV file name using a
               regular expression
            match = regex.search(f)
            if match:
                test_id = int(match.group(1))
                print 'Loading Test %s from csv...' % test_id

                # import the data from CSV
                path = os.path.join(data_dir,f)
                df = pd.read_csv(path,header=[0,1], skiprows
                   =(2,), index_col=0)

                if not df.empty and not df is None:
                    df.index.name = 'elapsed'
                    # create a TestData object and add it to
                       the list of tests
                    test = data.TestData(test_id, df)
                    tests.append(test)

    return tests

def load_test_info(f='./TestMatrix.csv'):
    ''' Creates a DataFrame containing test information. '''
    # read the test info from a file
    test_info = pd.read_csv(f,
            parse_dates=['DataStartTime','StartTime','EndTime'
               ],
            infer_datetime_format = True, index_col='TestID')

    #delete any tests (rows) that don't have a start or end
       time
    return test_info.dropna(subset=['StartTime','EndTime'])

def load_fds(data_dir='./fds/'):
```

```
    tests = []
    files = []
    regex = re.compile(r"(\w+)_devc.csv")
    files += [f for f in os.listdir(data_dir) \
                if f.endswith('_devc.csv')]

    for f in files:
        # Extract test_id from CSV file name using a regular
           expression
        match = regex.search(f)
        if match:
            test_id = match.group(1)
            print "Loading␣FDS␣Simulation␣'%s'␣from␣csv..." %
               test_id

            # import the data from CSV
            test = fds.fds_to_test(os.path.join(data_dir,f),
               test_id)
            tests.append(test)

    return tests

def save_tests(tests, test_dir='./tests/', file_pattern=''):
    if not os.path.exists(test_dir):
        os.mkdir(test_dir)

    for test in tests:
        if file_pattern:
            test.save(test_dir, file_pattern % test.test_id)
        else:
            test.save(test_dir)

def plot_tests(tests, plot_dir, file_pattern = 'Test%02d_%s'):
    if not os.path.exists(plot_dir):
        os.mkdir(plot_dir)

    for t in tests:
        for s in t.sensors:
```

```
            ax = t.plot(sensor=s)
            fig = ax.get_figure()
            filename = file_pattern % (t.test_id, s)
            save_fig(fig, plot_dir, filename)
            plt.close(fig)

def norm_tests(tests):
    norms = []
    for test in tests:
        # make a deepcopy of the TestData object
        new = deepcopy(test)
        # normalize the data
        new.data = normalize(new.data)
        norms.append(new)
    return norms

def save_stats(tests, stats_dir, file_pattern='Test%02d_stats.
   csv'):
    """
    Save statistics for test data to csv files.
    """
    if not os.path.exists(stats_dir):
        os.mkdir(stats_dir)

    for test in tests:
        # create the filenae and full path to the csv file
        filename = file_pattern % test.test_id
        p = os.path.join(stats_dir, filename)
        print 'saving␣%s...' % p
        # save the stats as a csv file
        stats(test.data).to_csv(p)

def save_fig(figure=None, directory='.', filename='fig',
   format='png', dpi=300):
    """Writes figure to a file in the given format.

    Args:
      figure: Matplotlib Figure object
```

```
      directory: string directory path
      filename: string name of file (without file extension)
      format: string image format for figure (file extension)
      dpi: resolution of saved image
    """
    if figure:
        path = os.path.join(directory, '%s.%s' % (filename,
           format))
        print 'Writing', path
        figure.savefig(path, format=format, dpi=dpi,
           bbox_inches='tight')

def all(root_dir='./'):
    """Run all the primary subroutines for the test data"""
    # load test from the processed csv files
    tests = load_data('./tests/', None, False)
#    tests = load_data()

    # save tests to csv files and plot
    save_tests(tests)
    plot_tests(tests, root_dir + 'tests/plots/')

    # save statistics
    save_stats(tests, root_dir + 'tests/stats/')

#    # create normalized plots of data
#    norms = norm_tests(tests)
#    save_tests(norms, root_dir + 'tests/normalized')
#    plot_tests(norms, root_dir + '/tests/normalized/plots')


def all_fds(root_dir='./fds/'):
    """Run all the primary subroutines for the FDS simulations
       """
    # load FDS simulations from the processed csv files
    tests = load_fds(root_dir)

    # save tests to csv files and plot
```

```
    test_pattern = '%s.csv'
    plot_pattern = '%s_%s'
    save_tests(tests, root_dir + 'tests/', file_pattern =
       test_pattern)
    plot_tests(tests, root_dir + 'tests/plots/', file_pattern
       = plot_pattern)

    # save statistics
    save_stats(tests, root_dir + 'tests/stats/',
               file_pattern = '%s_stats.csv')

    # create normalized plots of data
    norms = norm_tests(tests)
    save_tests(norms, root_dir + 'tests/normalized',
               file_pattern = test_pattern)
    plot_tests(norms, root_dir + 'tests/normalized/plots',
               file_pattern = plot_pattern)
```

D.3.4 nupicanomalyoutput.py

```
# ------------------------------------------------------
# Numenta Platform for Intelligent Computing (NuPIC)
# Copyright (C) 2013, Numenta, Inc.  Unless you have an
   agreement
# with Numenta, Inc., for a separate license for this software
    code, the
# following terms and conditions apply:
#
# This program is free software: you can redistribute it and/
   or modify
# it under the terms of the GNU Affero Public License version
   3 as
# published by the Free Software Foundation.
#
# This program is distributed in the hope that it will be
   useful,
# but WITHOUT ANY WARRANTY; without even the implied warranty
   of
```

```
# MERCHANTABILITY or FITNESS FOR A PARTICULAR PURPOSE.
# See the GNU Affero Public License for more details.
#
# You should have received a copy of the GNU Affero Public
   License
# along with this program.  If not, see http://www.gnu.org/
   licenses.
#
# http://numenta.org/licenses/
# ----------------------------------------------------
"""
Provides a class for writing data out of NuPIC models.
"""
import csv
import os
import math

#from collections import deque
#from abc import ABCMeta, abstractmethod
from nupic.algorithms.anomaly_likelihood import
   AnomalyLikelihood
#import time

## Try to import matplotlib, but we don't have to.
#try:
#  import matplotlib
#  matplotlib.use('TKAgg')
#  import matplotlib.pyplot as plt
##  import matplotlib.gridspec as gridspec
##  from matplotlib.dates import date2num, DateFormatter
#except ImportError:
#  pass

#WINDOW = 300
#HIGHLIGHT_ALPHA = 0.3
#ANOMALY_HIGHLIGHT_COLOR = 'red'
#WEEKEND_HIGHLIGHT_COLOR = 'yellow'
#ANOMALY_THRESHOLD = 0.999
```

```
#class NuPICOutput(object):
#
#  __metaclass__ = ABCMeta
#
#
#  def __init__(self, name, nsensors):
#    self.name = name
#    self.anomalyLikelihoodHelper = anomaly_likelihood.
   AnomalyLikelihood()
#
#
#  @abstractmethod
#  def write(self, timestamp, value, predicted, anomalyScore):
#    pass
#
#
#  @abstractmethod
#  def close(self):
#    pass

class FileOutput(object):


#  def __init__(self, *args, **kwargs):
#      if 'output_dir' in kwargs:
#        out_dir = kwargs.pop('output_dir')
#      else:
#        self.output_dir = list(args).pop()
#      NuPICOutput.__init__(self, *args, **kwargs)
#      self.output_dir = out_dir
  def __init__(self, name, output_dir = '.', sensors = [],
     filelen=5000):
    self.name = name
#    self.output_dir = output_dir
    self.sensors = sensors
```

```
    self.count = 0

    # create anomaly likelihood helper for each sensor
    self.helpers = []
    for s in sensors:
#         print "creating likelihood helper for %s" % s
        self.helpers.append(self._create_likelihood_helper(
          filelen))

    # create header row for output file
    header = ['timestamp']
    header.extend(sensors)
    header.extend(['%s_pred' % s for s in sensors])
    header.extend(['%s_ascore' % s for s in sensors])
    header.extend(['%s_alikelihood' % s for s in sensors])

    self.filename = "%s.csv" % self.name
    self.path = os.path.join(output_dir, self.filename)
    print "Preparing to output data to %s" % (self.path)

    self.outfile = open(self.path, "w")
    self.writer = csv.writer(self.outfile)
    self.writer.writerow(header)

  def write(self, timestamp, actual, predicted, scores):
      likelihoods = []
      if timestamp is not None:
          for i, s in enumerate(self.sensors):
#              likelihoods.append(self.helpers[i].
   anomalyProbability(
#                      actual[i], scores[i]))
              prob = self.helpers[i].anomalyProbability(actual
                 [i], scores[i])
              #likelihoods.append(prob)

              likelihoods.append(AnomalyLikelihood.
                 computeLogLikelihood(prob))
```

```
        # create row of values to output
        row = [timestamp]
        row.extend(actual)
        row.extend(predicted)
        row.extend(scores)
        row.extend(likelihoods)

        self.writer.writerow(row)
        self.count += 1


def close(self):
  self.outputFile.close()
  print "Done. Wrote %i data lines to %s." % (self.count,
     self.filename)


def _create_likelihood_helper(self, filelen):
    # create the anomaly likelihood object
    # from: https://github.com/numenta/NAB/blob/master/nab/
       detectors/numenta/numenta_detector.py
    probationary_period = self._get_probation(filelen)
    learning_period = int(math.floor(probationary_period /
       2.0))
    return AnomalyLikelihood(
            learningPeriod = learning_period,
            estimationSamples = probationary_period -
               learning_period,
            reestimationPeriod = 30
    )

    # Notes of AnomalyLikelihood parameters:
    # learningPeriod: (int) the number of iterations
       required for the algorithm
    #     to learn the basic patterns in the dataset and for
        the anomaly
    #     score to 'settle down'.
    # estimationSamples: (int) the number of reasonable
```

```
        anomaly scores
      #     required for the initial estimate of the Gaussian.
      # reestimationPeriod: (int) how often we re-estimate the
          Gaussian
      #     distribution.

  def _get_probation(self, filelen):
      #Based on:
      #https://github.com/numenta/NAB/blob/master/nab/util.py
      """Return the probationary period index."""
      percent = 0.15
      return min(
              math.floor(percent * filelen),
              percent * 5000)

#def extractAnomalyIndices(anomalyLikelihood):
#  anomaliesOut = []
#  anomalyStart = None
#  for i, likelihood in enumerate(anomalyLikelihood):
#    if likelihood >= ANOMALY_THRESHOLD:
#      if anomalyStart is None:
#        # Mark start of anomaly
#        anomalyStart = i
#    else:
#      if anomalyStart is not None:
#        # Mark end of anomaly
#        anomaliesOut.append((
#          anomalyStart, i, ANOMALY_HIGHLIGHT_COLOR,
   HIGHLIGHT_ALPHA
#        ))
#        anomalyStart = None
#
#  # Cap it off if we're still in the middle of an anomaly
#  if anomalyStart is not None:
#    anomaliesOut.append((
#      anomalyStart, len(anomalyLikelihood)-1,
#      ANOMALY_HIGHLIGHT_COLOR, HIGHLIGHT_ALPHA
#    ))
```

```
#
#  return anomaliesOut



#class NuPICPlotOutput(NuPICOutput):
#
#
#  def __init__(self, *args, **kwargs):
#    raise NotImplemented("Plotting functionality has not been
    implemented")
##    super(NuPICPlotOutput, self).__init__(*args, **kwargs)
##    # Turn matplotlib interactive mode on.
##    plt.ion()
##    self.dates = []
##    self.convertedDates = []
##    self.value = []
##    self.allValues = []
##    self.predicted = []
##    self.anomalyScore = []
##    self.anomalyLikelihood = []
##    self.actualLine = None
##    self.predictedLine = None
##    self.anomalyScoreLine = None
##    self.anomalyLikelihoodLine = None
##    self.linesInitialized = False
##    self._chartHighlights = []
##    fig = plt.figure(figsize=(16, 10))
##    gs = gridspec.GridSpec(2, 1, height_ratios=[3,  1])
##
##    self._mainGraph = fig.add_subplot(gs[0, 0])
##    plt.title(self.name)
##    plt.ylabel('Light')
##    plt.xlabel('Date')
##
##    self._anomalyGraph = fig.add_subplot(gs[1])
##
##    plt.ylabel('Percentage')
```

```
##    plt.xlabel('Date')
##
##    # Maximizes window
##    mng = plt.get_current_fig_manager()
##    mng.resize(*mng.window.maxsize())
##
##    plt.tight_layout()
#
#
#
##  def initializeLines(self, timestamp):
##    print "initializing %s" % self.name
##    anomalyRange = (0.0, 1.0)
##    self.dates = deque([timestamp] * WINDOW, maxlen=WINDOW)
##    self.convertedDates = deque(
##      [date2num(date) for date in self.dates], maxlen=WINDOW
##    )
##    self.value = deque([0.0] * WINDOW, maxlen=WINDOW)
##    self.predicted = deque([0.0] * WINDOW, maxlen=WINDOW)
##    self.anomalyScore = deque([0.0] * WINDOW, maxlen=WINDOW)
##    self.anomalyLikelihood = deque([0.0] * WINDOW, maxlen=
   WINDOW)
##
##    actualPlot, = self._mainGraph.plot(self.dates, self.
   value)
##    self.actualLine = actualPlot
##    predictedPlot, = self._mainGraph.plot(self.dates, self.
   predicted)
##    self.predictedLine = predictedPlot
##    self._mainGraph.legend(tuple(['actual', 'predicted']),
   loc=3)
##
##    anomalyScorePlot, = self._anomalyGraph.plot(
##      self.dates, self.anomalyScore, 'm'
##    )
##    anomalyScorePlot.axes.set_ylim(anomalyRange)
##
##    self.anomalyScoreLine = anomalyScorePlot
```

```
##    anomalyLikelihoodPlot, = self._anomalyGraph.plot(
##      self.dates, self.anomalyScore, 'r'
##    )
##    anomalyLikelihoodPlot.axes.set_ylim(anomalyRange)
##    self.anomalyLikelihoodLine = anomalyLikelihoodPlot
##    self._anomalyGraph.legend(
##      tuple(['anomaly score', 'anomaly likelihood']), loc=3
##    )
##
##    dateFormatter = DateFormatter('%m/%d %H:%M')
##    self._mainGraph.xaxis.set_major_formatter(dateFormatter)
##    self._anomalyGraph.xaxis.set_major_formatter(
  dateFormatter)
##
##    self._mainGraph.relim()
##    self._mainGraph.autoscale_view(True, True, True)
##
##    self.linesInitialized = True
##
##
##
##  def highlightChart(self, highlights, chart):
##    for highlight in highlights:
##      # Each highlight contains [start-index, stop-index,
  color, alpha]
##      self._chartHighlights.append(chart.axvspan(
##        self.convertedDates[highlight[0]], self.
  convertedDates[highlight[1]],
##        color=highlight[2], alpha=highlight[3]
##      ))
##
##
#
#  def write(self, timestamp, value, predicted, anomalyScore):
#    pass
#
##    # We need the first timestamp to initialize the lines at
    the right X value,
```

```
##     # so do that check first.
##     if not self.linesInitialized:
##       self.initializeLines(timestamp)
##
##     anomalyLikelihood = self.anomalyLikelihoodHelper.
   anomalyProbability(
##       value, anomalyScore, timestamp
##     )
##
##     self.dates.append(timestamp)
##     self.convertedDates.append(date2num(timestamp))
##     self.value.append(value)
##     self.allValues.append(value)
##     self.predicted.append(predicted)
##     self.anomalyScore.append(anomalyScore)
##     self.anomalyLikelihood.append(anomalyLikelihood)
##
##     # Update main chart data
##     self.actualLine.set_xdata(self.convertedDates)
##     self.actualLine.set_ydata(self.value)
##     self.predictedLine.set_xdata(self.convertedDates)
##     self.predictedLine.set_ydata(self.predicted)
##     # Update anomaly chart data
##     self.anomalyScoreLine.set_xdata(self.convertedDates)
##     self.anomalyScoreLine.set_ydata(self.anomalyScore)
##     self.anomalyLikelihoodLine.set_xdata(self.convertedDates
   )
##     self.anomalyLikelihoodLine.set_ydata(self.
   anomalyLikelihood)
##
##     # Remove previous highlighted regions
##     for poly in self._chartHighlights:
##       poly.remove()
##     self._chartHighlights = []
##
##     # weekends = extractWeekendHighlights(self.dates)
##     anomalies = extractAnomalyIndices(self.anomalyLikelihood
   )
```

```
##
##    # # Highlight weekends in main chart
##    # self.highlightChart(weekends, self._mainGraph)
##
##    # Highlight anomalies in anomaly chart
##    self.highlightChart(anomalies, self._anomalyGraph)
##
##    maxValue = max(self.allValues)
##    self._mainGraph.relim()
##    self._mainGraph.axes.set_ylim(0, maxValue + (maxValue *
   0.02))
##
##    self._mainGraph.relim()
##    self._mainGraph.autoscale_view(True, scaley=False)
##    self._anomalyGraph.relim()
##    self._anomalyGraph.autoscale_view(True, True, True)
##
##    plt.draw()
##    # plt.pause(0.0001)
##    plt.gcf().canvas.flush_events()
##    time.sleep(0.05)
##
##
##
#
#  def close(self):
#    plt.ioff()
#    plt.show()
#
#
#
#NuPICOutput.register(NuPICFileOutput)
#NuPICOutput.register(NuPICPlotOutput)
```

D.3.5 plotter.py

```
# -*- coding: utf-8 -*-
"""
```

```
import os
#import csv

import numpy as np
import pandas as pd

from main import load_data

ALL_SENSORS = ['Temperature','Humidity','Light']

def extract_all_tests(test_dir = './tests', data_dir = './data
    '):

    tests = load_data(test_dir, from_raw=False)

    #create empty data frame with the correct columns
    reqd_cols = ALL_SENSORS
    empty = pd.DataFrame({c:[] for c in reqd_cols})

    for test in tests:
        for det in test.detectors:
            # create dataframe for this test / detector
            df = test.select_detector(det)
            data = pd.concat([df, empty])[reqd_cols]


#             # save the data file
            filename = 'Test%02d_%s.csv' % (test.test_id, det)
            path = os.path.join(data_dir, filename)
#             data.to_csv(path)

            # get info required for the output file
            fields = ['Time'] + list(data.columns.values)
            n = len(reqd_cols) # data columns (do not include
               id or timestamp)
            types = ['int'] + ['float'] * n
            flags = [''] * (n + 1)
```

```
            fmt = ['%d'] + ['%f'] * n
            all_values = data.reset_index().values

            print 'writing %s...' % filename
            nupic_csv(path, fields, types, flags, all_values,
               fmt)

def extract_all_bg(outfile, sensors=[]):
    dfs = []
    bgs = [4,5,6,7,1,2,3] # order of background files
    for bg in bgs:
        bg_id = 'bg0%d' % bg
        f = './bg/%s.csv' % bg_id
        dfs.append(extract_bg_data(bg_id, f, sensors))

    bg_all = pd.concat(dfs) # combine all bg dataframe

    # get info required for the output file
    fields = list(bg_all.columns.values)
    n = len(bg_all.columns) - 2 # data columns (do not include
        id or timestamp)
    types = ['string','datetime'] + ['float'] * n
    flags = ['S','T'] + [''] * n
    fmt = ['%s'] * 2 + ['%f'] * n

    print 'writing %s...' % outfile
    nupic_csv(outfile, fields, types, flags, bg_all.values,
       fmt)

    return bg_all

def extract_bg_data(bg_id, bg_file, sensors=[]):
    if not sensors:
        sensors = ALL_SENSORS
    cols = ['Timestamp'] + sensors
    df = pd.read_csv(bg_file)
    #df = df[['Timestamp'] + sensors]
    df['id'] = bg_id
```

```
    df = df[['id']+ cols] # reorder columns
    return df


def nupic_csv(filename, fields, types, flags, data, fmt='%f'):

    # check field types
    VALID_TYPES = {'datetime', 'int', 'float','bool','string'}
    # Compare the set of fields to valid field types
    if len(set(types) - VALID_TYPES):
        raise ValueError("Invalid field type. Valid field
           types are:\n %s" % \
            ", ".join(["'%s'" % str(s) for s in sorted(
               VALID_TYPES)]))

    VALID_FLAGS = {'R', 'S', 'T', 'C', '', None}
    # Compare the set of flags to valid flags
    if len(set(flags) - VALID_FLAGS):
        raise ValueError("Invalid flag. Valid flags are:\n %s"
            % \
            ", ".join(["'%s'" % str(s) for s in sorted(
               VALID_FLAGS)]))

    # replace None with ''
    flags = ['' if f is None else f for f in flags]

    # create header
    header = ",".join(fields) + "\n"
    header += ",".join(types) + "\n"
    header += ",".join(flags)

    np.savetxt(filename, data, fmt=fmt, delimiter=',',
               header=header, comments='')

#    with open(filename, 'wb') as csvfile:
#        csv_writer = csv.writer(csvfile)
#
#        # write header
```

```
#         csv_writer.writerow(fields)
#         csv_writer.writerow(types)
#         csv_writer.writerow(flags)
#
#         # write data


if __name__ == "__main__":
    pass
#    fields = ['field1', 'field2', 'field3']
#    types = ['int', 'float','bool']
#    flags = ['R', None, 'S']
#
#    a = np.random.randn(12).reshape((4,3))
#
#    print 'Writing a.csv...'
#    nupic_csv('a.csv', fields, types, flags, a)
```

Appendix E

Sensor Datasheets and Information

EMBEDDED DATA SYSTEMS

MeshNet Environmental Sensor

MN-ENV-THPLR
EDS-1064 through EDS-1068

http://www.EmbeddedDataSystems.com

FEATURES



- Wireless communication over the widely accepted 2.4 GHz frequency band
- Highly accurate Temperature, Humidity and Barometric Pressure sensors
- Calculates dew point, humidex, and heat index
- Discrete Input with Activity Latch and 32 bit pulse counter
- Optional Latching Relay may be controlled independently or by alarm status
- Programmable parameters such as send period and alarms
- Globally unique 64-Bit EUI (Extended Unique Identifier)
- Mesh network topology, which essentially enlarges the wireless network and provides additional transmission routes for the sensor data
- Transmission strength reported on all devices, allowing troubled areas to be identified and addressed proactively (e.g. adding Repeaters)
- Robust Communication protocol includes acknowledgements and retries
- Energy efficient design optimizes battery life
- Applications include thermostatic controls, industrial systems, consumer products, thermometers, or any temperature/humidity/light/barometric pressure sensitive system
- Auto adjusts to comply with EU & USA/CA controllers
- *Complies with FCC, Industry Canada and CE Marking requirements*

DESCRIPTION

The EDS **Environmental Sensor Line**, MN-ENV, offers an innovative way to easily *monitor and control* temperature, humidity, barometric pressure, and/or light in indoor environments. The wall mount sensor features high accuracy temperature, humidity, and barometric pressure sensors. The product also contains a light sensor, a discrete input, an LED, and an optional relay. Together these features offer an efficient and flexible system for monitoring the temperature, humidity, barometric pressure, and light levels and a discrete point at one or more locations within a building.

The internal alarm function allows the Environmental Sensor to identify the alarm status of numerous parameters. Upon alarm, the Sensor will immediately transmit while the LED and/or optional Latching Relay can be configured to react to alarm status. Possible alarm configurations include:

- Activate when an alarm parameter is met and deactivate when the alarm byte is cleared
- Activate when an alarm parameter is met and deactivate when readings return to normal range
- Controlled independent of alarm status.

Since, the EDS Environmental Sensor line's alarm functions can operate independently of the controller the sensor may be used as a standalone thermostat, humidistat, pressurestat and/or light sensor.

Part Numbers:

TEMPERATURE	MN-ENV-T
TEMPERATURE/RELAY	MN-ENV-TR
TEMPERATURE/HUMIDITY	MN-ENV-TH
TEMPERATURE/HUMIDITY/RELAY	MN-ENV-THR
TEMPERATURE/LIGHT	MN-ENV-TL
TEMPERATURE/LIGHT/RELAY	MN-ENV-TLR
TEMPERATURE/BAROMETRIC PRESSURE	MN-ENV-TP
TEMPERATURE/BAROMETRIC PRESSURE/RELAY	MN-ENV-TPR
TEMPERATURE/HUMIDITY/BAROMETRIC PRESSURE/LIGHT	MN-ENV-THPL
TEMPERATURE/HUMIDITY/BAROMETRIC PRESSURE/LIGHT/RELAY	MN-ENV-THPLR

© 2012 Embedded Data Systems, LLC.; 2019 Fortune Drive; Lawrenceburg, KY 40342; Phone/Fax 502-859-5490

INSTALLATION INSTRUCTIONS

1. Remove the Lid of Enclosure - Lightly depress against the two small (0.5”x 0.625”) vented sections on the sides of the enclosure and pull the rear of the enclosure away from the front.
2. Inside will be a screw, which will later be used to secure the enclosure together. Set the screw aside until required.
3. Insert right angle end of the 3.5mm Link Cable into the 3.5mm jack, located to the left of the battery holder. *(NOTE: The Link Cable has a custom pin-out; this cable must be purchased from Embedded Data Systems*)
4. Insert battery into battery holder.
5. Insert the remaining end of the 3.5mm Link Cable into the jack on the face of the MeshNet Controller.
6. Apply Power. The internal 'linking' process takes under 2 seconds; the LED will flash at ½ second rate when complete. If after 5 seconds the LED does not flash at the ½ second rate, repeat the process once again.
7. The LED flashes at the ½ rate, when Power should be removed.
8. Remove the cable from both the Sensor and the Controller.
9. Apply power to both units to verify function.
10. If connections are to be made to the relay or discrete input, remove the battery.
11. Draw the wires through the circular hole in the rear of the enclosure.
12. Mount the rear of the enclosure on the wall using the diagonal slots reserved for the screws. To arrange for the most complete wireless coverage be certain that the + and - symbols on the rear of the enclosure are at the bottom left. This will position the antenna on the radio module in the upper right position.
13. If connections are to be made to the relay or discrete inputs, make connections as described below.
    a. Strip 1/8” of the wires.
    b. Securely attach wires to the corresponding screw-down terminals on the terminal block.
    c. Wiring the discrete input – There are 2 connections to the discrete input, ground and in, which are labeled on the printed circuit board, opposite the 4 connection terminal strip. The input has a threshold of around 0.8 volts between 0 and 1.
    d. Wiring the Relay – There is 2 connections to the relay, common (C) and normally open (NO), which are labeled on the printed circuit board, near the 4 connection terminal strip. Connect the wires to these 2 terminals, making certain the wires are securely fastened
14. Reinsert the battery.
15. Replace the Lid of the Enclosure.
16. Insert the screw into the single screw hole found in the upper left corner of the enclosure.

Parameter	Typical	Units
Relay Voltage Rating (DC)	220	Volts
Relay Current Rating (DC)	2	Amps
Relay Switching Rating (DC - resistive load)	30	Watts
Relay Voltage Rating (AC)	250	Volts
Relay Current Rating (AC)	2	Amps
Relay Switching Rating (AC - resistive load)	62.5	VA

SYSTEM DESCRIPTION

The MeshNet Environmental Sensor is part of the MeshNet Wireless Sensor System, designed to monitor and control real world environmental conditions wirelessly. The system is completed with the Embedded Data Systems MeshNet Controller (MN-CTRL). The controller communicates directly with the Environmental Sensor and presents all data via Ethernet. The Sensor and Controller communicate with each other using a proprietary protocol and are not compatible with other wireless networks. An optional system component is Embedded Data Systems' MeshNet Repeater (MN-RPT) which is used to extend the range of communication between the Controller and Environmental Sensor.

Controller: Each wireless system contains a MeshNet Controller. The Controller interfaces the wireless system to a local area network (LAN) or the Internet via Ethernet. It manages, reads/writes to the wireless devices, presents the data in easy to use formats such as HTTP and XML, and optionally pushes the data on a timed basis to a HTTP Post server.

Repeater: Repeaters are used to extend the distance a Sensor can be located from the Controller. Many Sensors can communicate with the Controller through a single Repeater. Each Controller can manage up to 7 Repeaters, and there can be 1 Repeater between a Controller and Sensor.

Sensor: The MeshNet Environmental Sensors provide the means to monitor and control real world environmental conditions. They are typically battery-powered devices that wake on a timed basis, take readings, send the readings to the controller, confirm successful transmission and check to see if any data is waiting for them.

OPERATION

All data from the MeshNet Environmental Sensor is read using a MeshNet Controller. This can be done through HTTP or SNMP, and an option is provided for pushing the data to a HTTP Post server. All data that is retrieved from the Controller programmatically is in XML form. *See the MeshNet Controller Users Manual for more information.*

Temperature
Last reading, displayed in °C.

Humidity
Last reading, displayed in percent.

Dew Point
Last calculation, displayed in °C. This calculation is made after every temperature and humidity reading.

Humidex
Last calculation, displayed in °C. This calculation is made after every temperature and humidity reading.

Heat Index
Last calculation, displayed in °C. This calculation is made after every temperature and humidity reading

Barometric Pressure
Last reading, displayed in millibars.

Light
Last reading, displayed in Lux.

Battery
Displays voltage of the battery. ***NOTE: In order to conserve power, the battery voltage is read only every 10th time.***

LED
Last read state of the LED; 1 indicates LED is on.

Relay
Last read state of the relay; 1 indicates Relay is on.

Input 1
Input 1 provides a means of reading a discrete state; this parameter displays the most recent input state.

Activity Latch 1
Changes in the input state are detected by hardware, even when the sensor is sleeping. An Activity Latch State of 1 indicates the state has changed at least once since it was last reset. Sending the Activity Latch reset command will reset the Activity Latch. See *Discrete Input* for more details on using this input.

Pulse Counter 1
Changes in the input state are detected by hardware, even when the sensor is sleeping. Counts rising edges at Input 1. This is a 32-bit counter that cannot be reset. It is stored in volatile memory, if power is cycled, the number will return to zero. ***NOTE: Due to hardware limitations, the first pulse after reset is not counted.***

Input Send
If INPUT SEND is set to 0, input changes are sent every time the sensor wakes up to send other sensor information. If set to 1, all sensor data is sent every time the input changes state (rising or falling edge) or a timed transmission is due. Sending data based on input change causes the timed send to restart. For example, if the device is programmed to send data every minute, but the input changed after 20 seconds and Input Send is set to 1, then the data will be send immediately. Then, a minute later the timed send will occur (assuming the input did not change state during that minute).

LED Function and LED State
The LED may operate in any of the following modes:

Mode	Function
On with any alarm, off if no alarms active*	0
On with any alarm, off when clear alarms command received	1
On and Off under command using State parameter	2
Always off	3

* Mode 0 uses hysteresis to avoid rapid changes in the LED and/or relay. The parameter is in alarm when it is greater than the high alarm value (for the high alarm) or less than the low alarm value (for the low alarm). It is out of alarm when it is less (high alarm) than or greater than (low alarm) the threshold value plus:
Temperature - 1 degrees C

Humidity - 1 %

Dew Point - 1 degrees C

Humidex - 1 degrees C

Heat Index - 1 degrees C

BP – 1 millibar

Light - 1 lux

Battery - 0.1v

The state of the LED is stored in non-volatile memory and restored at power-up.

Relay Function and Relay State
The relay and LED may operate in any of the following modes:

Mode	Function
On with any alarm, off if no alarms active*	0
Off with any alarm, on if no alarms active	1
On with any alarm, off when clear alarms command received	2
Off with any alarm, on when clear alarms command received	3
On and Off under command using State parameter	4
Always off	5
Always on	6

* Hysteresis is applied as described above under LED Function

The relay is a latching relay. It retains state when power is lost. **NOTE:** ***Relay will change state if unit is jolted sufficiently*****.**

The state of the relay is stored in non-volatile memory and is restored at power-up. Since the relay is latching, its state remains the same, even when power is removed.

ALARM PARAMETERS

Alarms are calculated every time a reading is taken by the sensor, which is programmed using the *sensor read period* parameter. If the reading is above the high alarm value, the corresponding high alarm bit is set, and if the reading is below the low alarm value, the low alarm bit is set.

The primary use for alarms is to cause the LED and/or relay to activate automatically under the desired conditions. See the section above on the LED and relay.

Alarm States
Will set to 1 if an alarm is active. Alarm states can only be cleared by sending the clear alarms command, which clears ***all*** alarm states; no provision is made to clear individual alarm states.

Alarm Values
Program these values to cause alarms under desired conditions.

	Units	Range	Resolution	High Default	Low Default
Temperature	Centigrade	-40 to 150	1	125	-40
Dew point	Centigrade	-40 to 150	1	125	-40
Humidex	Centigrade	-40 to 150	1	125	-40
Heat index	Centigrade	-40 to 150	1	125	-40
Humidity	Percent	0 to 100	1	100	0
Barometric pressure	Millibars	0 to 2000	0.001	2000.000	0.000
Light	Lux	0 to 500000	1	100000	0
Battery	Volts	0 to 4	0.01	-	2.90

OPERATIONAL PARAMETERS

EUI
The EUI, or Extended Unique Identifier, is a globally unique 64-bit number, represented by 16 hexadecimal digits. This number can be used by software to uniquely identify every MeshNet wireless device.

Controller RSSI
This indicates the strength of the radio signal at the Controller; higher numbers equate to stronger signals. Due to hardware limitations, the highest number that can be displayed is -34 dBm., however the actual signal strength may be much higher.

Device RSSI
This indicates the strength of the radio signal at the Repeater. Due to hardware limitations, the highest number that can be displayed is -34 dBm, however the actual signal strength may be much higher.

Address
This is the address of the repeater, which was assigned by the controller.

Repeater
When the repeater joins the controller, it is assigned a repeater number, which is displayed here. A zero indicates there is no repeater in the communication path.

Health
This is a number ranging from 0 to 7; 0 is not connected and 7 is healthy. The number is incremented when a packet is received from the repeater, and decremented when a packet is not received after a predetermined period of time. Numbers less than 7 indicate a weak wireless link or other problem.

Version
This indicates the firmware version of the sensor.

User Name
The user programmable string used to identify any given Sensor; it may be up to 29 characters long. It is saved in non-volatile memory and so is retained even when power is cycled. The string is best used as a human readable label, which can uniquely identify each MeshNet Environmental Sensor.

Read Counter
Counts the number of times a packet has been sent to the controller. This number has a maximum of 4294967296. When the maximum is reached, the number rolls back to 0 and begins counting up again.

Sensor Read Period
Use to define frequency of sensor readings. Larger periods will conserve battery power. After sensors are read, alarms are checked. If any are found active on this read cycle, they will be sent to the MeshNet Controller immediately.

Each count represents 10 seconds. Maximum number may be 65535. Note that the timer used has a specification of ±15% and is temperature dependent, so there can be a rather large variance between what is programmed and the actual period.

At power up, the device sends data packets every 10 seconds for the first 6 packets, if the read period is not 0. After the first 6 packets are sent, the device reverts to sending packets at the sensor read period duration. This is to facilitate programming in cases where a long read period is desired. Even with very long read periods, simply cycling the power will cause parameters to be written without having to wait for the sensor read period to time out.

Setting	Period
0	4 seconds
1	10 seconds
2	20 seconds
6	1 minute
60	10 minutes
360	1 hour
720	2 hours
8640	1 day
65535	7 days, 14 hours, 2 minutes, 30 seconds

Report Count
Number of sensor read periods to elapse before sending a report to the MeshNet Controller. Zero means send report every time sensors are read.

Setting	Period
0	Send every time the sensors are read
1	Send every other time the sensors are read
2	Send every 2nd time the sensors are read
3	Send every 3rd time the sensors are read

Factory Reset
Write anything to this location to reset parameters to factory defaults. The sensor read counter must be below 20 or the command is ignored. This parameter is not sent from the sensor to the controller so no data is presented.

WRITE PARAMETERS

In order to conserve power, MeshNet sensors sleep when not reading the sensors or sending data. When sleeping, they cannot receive wireless data. Because of this, writes are queued by the MeshNet Controller and sent when the Sensors are awake.

Writes Pending
The number of writes waiting to be sent to the sensor.

Writes Succeeded
The number of writes that have been receive and acknowledged by the sensor.

Writes Failed
The number of writes that were not able to be sent to the sensor or were not acknowledged.

WIRELESS COMMUNICATIONS

The device communicates via an industry standard 802.15.4 wireless link. Wireless packets are acknowledged, all data is checked for errors using CRC and corrupted data is resent.

DIAGNOSTIC PARAMETERS

The following parameters are provided for diagnostic purposes. Wireless communications are acknowledged and retried if no acknowledgment is received. The parameters below can be used to determine link quality.

Connection Counter
Counts the number of connections to the controller. When a device is first powered, it connects to a controller, obtaining a address and thus belonging to the network. If the signal strength is good, and power is not lost at the controller, this number will stay low. A high number could be due to low signal strength, periodic interference or power problems. Maximum is 65535, after which the number rolls over to zero and continues to count up.

Message Attempts
The number of times a packet has been sent. This number is the same as Send Counter, except that it can be reset and has a maximum of 65535, after which it rolls over to zero and continues to count up.

Message Packet Retries
The number of times a packet had to be resent due to no acknowledgment being received. Maximum is 65535, after which it rolls over to zero and continues to count up.

Message Failures
When no acknowledgment is received, the packet is resent. After 4 retries, the message has failed. The counter increments when such a failure has occurred. Maximum is 65535, after which it rolls over to zero and continues to count up.

Message Counter Reset
Used to reset the above 3 message counters to zero.

PROGRAMMABLE PARAMETER SUMMARY

	Units	Range	Resolution	High Default	Low Default
Temperature	Centigrade	-40 to 150	1	125	-40
Dew point	Centigrade	-40 to 150	1	125	-40
Humidex	Centigrade	-40 to 150	1	125	-40
Heat index	Centigrade	-40 to 150	1	125	-40
Humidity	Percent	0 to 100	1	100	0
Barometric pressure	Millibars	0 to 2000	0.001	2000.000	0.000
Light	Lux	0 to 500000	1	100000	0
Battery	Volts	0 to 4	0.01	-	2.90
Report count		0 to 65535	1	0	
Sensor read period		0 to 65535	1	0	
LED function		0 to 3	1	2	
Relay function		0 to 6	1	2	
LED state		0 to 1	1	0	
Relay state		0 to 1	1	0	
Input send		0 to 1	1	0	

BATTERY LIFE

The MeshNet Environmental Sensor spends most if it's time in sleep mode; it wakes up to take readings, send data and see if any packets are in the queue to be received. Battery life can be maximized by reading the sensors and sending the data as infrequently as possible. The programming parameters *Sensor Read Period* and *Report Count* define how often data is sent to the controller.

Battery life is highly variable on a number of parameters.

1. How often data is sent.
2. How often the sensors are read.
3. Extreme temperatures reduce the useful life of the battery.
4. The number of sensors reduces battery life; barometric pressure and light take relatively little power. Humidity takes the most power, followed by temperature.
5. Battery life is reduced if the relay is switched often or the LED is turned on. The LED is the single largest user of power, far exceeding all other operations.
6. The device can be programmed to read the sensors more often than sending the results. If an alarm is generated, the results will be sent when the alarm is discovered, even if a send is not scheduled. This enables the reduction of the number of wireless transmissions and maximizes battery life without sacrificing responsiveness.
7. If the sensor is sending data through a repeater, battery life will be reduced because the sensor has to wait longer for the acknowledgment.
8. If the sensor has to reconnect to the controller frequently, battery life will be reduced. This happens when the signal is low or there is interference.

LINKING PROCEDURE

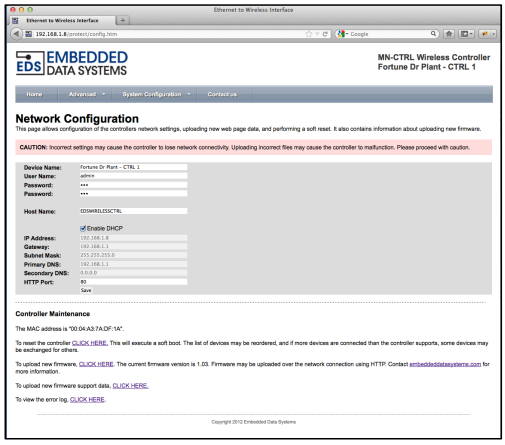
1. **Link a MeshNet Sensor to the MeshNet Controller.** Using the custom "Linking Cable" provided, insert the straight 3.5mm connector end into the jack located on the front of the MeshNet Controller. Insert the right angle 3.5mm connector into the jack located inside the MeshNet Sensor (or Repeater). *(Use only the custom "Linking Cable" provided by EDS or linking will not occur.)* If power is not already applied to all devices, do so now. The internal "linking" process takes under 2 seconds; the LED on the face of the MeshNet Sensor will flash at a 1/2 second rate when complete. Once the LED signals success, power and the "Linking Cable" should be removed. (If after 5 seconds the LED does not flash at the 1/2 second rate, repeat the process)
2. **Apply power to the MeshNet Controller a second time.** The green PWR/ACT LED located on the front of the Controller will begin to flash at one-second intervals, indicating that the product is operating normally. Power must be 5 volts +/- 10% at 400 milliamp.







3. **Connect it to your Network**. Connect a live network cable to the Ethernet Port on the device. The green LED on the Ethernet connector will light, indicating a valid network connection. The yellow LED on the Ethernet connector blinks only when there is network traffic.
4. **Determine the IP address of the MeshNet Controller** by checking your DHCP server logs or using EDS Appliance Scanner Software available from the EDS website. If the MeshNet Controller does not find a DHCP server running on your network, it will default to the following IP address: 169.254.1.1.
5. **Configure your device**. Type the IP address of the MeshNet Controller into your web browser (e.g., http://192.168.1.27) and press enter. Select the menu item "Network" under "System Configuration". When the name and password is requested, enter "**admin**" for the name and "**eds**" for the password. A webpage similar to the one shown to the right will enable you to configure and monitor various aspects of your MeshNet Controller.



CONGRATULATIONS! You have successfully installed a MeshNet Wireless Sensor System. *Please refer to the Web Access section of the Operation Manual to obtain an understanding of the function of each of the web pages served by the MeshNet Controller.*

Some things to keep in mind:

- Support is provided for MeshNet Controller IP address identification only when utilizing the EDS Appliance Scanner Software (http://short.eds.bz/apps-edsscanner). Please consult your network administrator if you cannot locate the DHCP address.
- ***For instructions on appropriate placement of the components of the MeshNet Wireless Sensor System, please refer to Proper Placement section of the Operation Manual.***

EDS ENVIRONMENTAL SENSOR IDS

ID	Features
EDS1064	Temp
EDS1065	Temp, humidity
EDS1066	Temp, barometric pressure
EDS1067	Temp, light
EDS1068	Temp, humidity, barometric pressure and light

EDS REPEATER DEVICE IDS

ID	Features
EDS2101	MeshNet Repeater with high power radio

SPECIFICATIONS

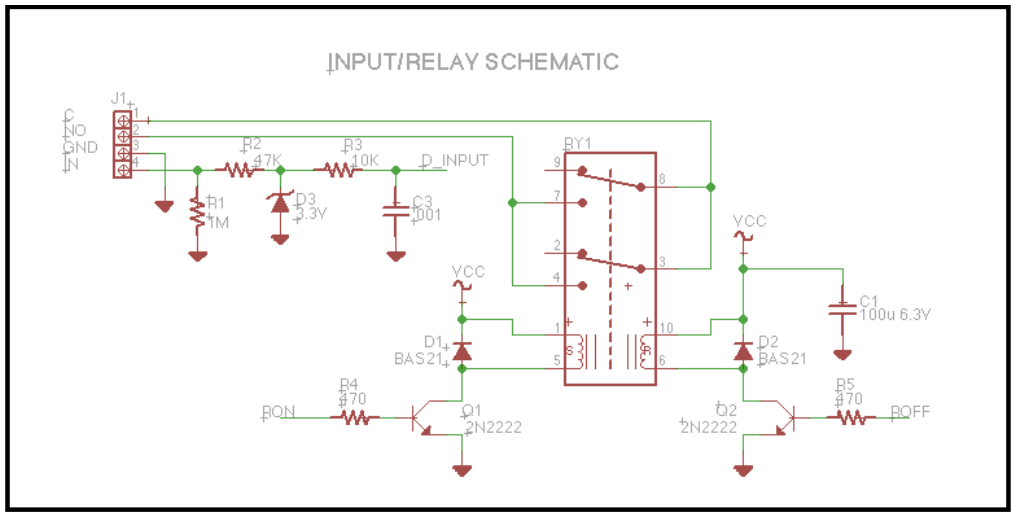
PARAMETER	MIN	TYP	MAX	UNITS
Operating Temperature Range	-40	-	85	°C
Temperature Accuracy -20 to +100°C	-0.5	±0.25	+0.5	°C
Temperature Accuracy -40 to +125°C	-1	±0.25	+1	°C
Temperature Accuracy at 25°C	-0.2	-	0.2	°C
Temperature Resolution	-	0.0625	-	°C
RH Accuracy: 11% RH to 89% RH (note 2)	-5	-	+5	% RH
RH Accuracy: 0-10% RH and 90-100% RH	-7	-	+7	% RH
Pressure Accuracy: 700 to 1,100 hPa at 0 to 65°C (note 2)	-2.5	±1	+2.5	hPa/Millibar
Pressure Accuracy: 300 to 700 hPa at 0 to 65°C	-3	±1	+3	hPa/Millibar
Pressure Accuracy: at -20 to 0°C	-4	±1.5	+4	hPa/Millibar
Pressure Accuracy: 20.67 to 32.48	-0.07	±0.03	+0.07	inHg
Measurement Range	300	-	1,100	hPa/Millibar
Maximum Pressure	-	-	10,000	hPa/Millibar
Light Measurement Range	0	-	65535	Lux
Light Sensitivity	-20	-	+20	%
Relay Voltage Rating (DC)	-	220	-	Volts
Relay Current Rating (DC)	-	2	-	Amps
Relay Switching Power Rating (DC, resistive load)	-	-	30	Watts
Relay Voltage Rating (AC)	-	250	-	Volts
Relay Current Rating (AC)	-	2	-	Amps
Relay Switching Power Rating (AC, resistive load)	-	-	62.5	VA
Supply Voltage	2.9	-	3.6	Volts
Active Current	-	28	-	mA
Sleep Current	-	8.8	-	uA
Battery voltage reading accuracy (note 1)	-1.2	-	+1.2	%
Discrete input voltage	-48	-	+48	Volts
Discrete input low threshold (note 3)	0.435	-	0.54	Volts
Discrete input high threshold (note 3)	1.525	-	1.7	Volts
Pulse counting frequency	-	-	TBD	KHz
Enclosure Dimensions (L x W x H)	80	80	21	mm

Notes:

1. The battery voltage varies depending on how much current is flowing. When the sensor is sleeping, the voltage is higher than when it is awake. The reading is taken when the sensor is awake.
2. These sensors are light sensitive, they should be kept away from bright light or their accuracy will degrade.
3. Discrete input voltages are ratiometric, based on the battery voltage. The input low voltage maximum equation is 0.15 * Vbat, the input high voltage minimum equation is 0.25 * Vbat + 0.8.

Discrete Input

The discrete input circuit can have additional components to suit the intended application. If it is used to monitor contact closure, then it may require a pull up or pull down resistor and capacitor to remove contact bounce. If it is used to count pulses (such as from a flow meter) a capacitor may not be required to remove contact bounce, or if one is required, the value can be modified so the pulses are still present at maximum frequency.



Regulatory Compliance

FEDERAL COMMUNICATIONS COMMISSION (FCC) COMPLIANCE STATEMENT

This device complies with part 15 of the FCC Rules. Operation is subject to the following two conditions: (1) This device may not cause harmful interference, and (2) this device must accept any interference received, including interference that may cause undesired operation.

INDUSTRY CANADA (IC) COMPLIANCE STATEMENT

This Class B digital apparatus complies with Canadian ICES-003.
Cet appareil numérique de la classe B est conforme à la norme NMB-003 du Canada.

EUROPEAN COMMUNITY (EC) DIRECTIVES CONFORMITY

APPLICATION OF COUNCIL DIRECTIVE 2004/108/EC Standard to which Conformity is Declared:

EN 61326-1:2006	(Emmissions)
EN 61326-2-3:2006	(Immunity)
EN 61000-3-2:2006+A1:2009+A2:2009	(Harmonics)
EN 61000-3-3:2008	(Flicker)

CE FC

Caution: *The manufacturer is not responsible for any radio or television interference caused by using other than recommended cables or by unauthorized changes or modifications to this equipment. Unauthorized changes or modifications could void the user's authority to operate this equipment.*